NOVEL APPROACHES TO RAPID DIAGNOSIS AND TREATMENT MONITORING OF ACTIVE TUBERCULOSIS, VOL II

EDITED BY: Xiao-Yong Fan and Hairong Huang
PUBLISHED IN: Frontiers in Microbiology

frontiers Research Topics

frontiers

ISSN 1664-8714
ISBN 978-2-83250-567-0
DOI 10.3389/978-2-83250-567-0

About Frontiers

Frontiers is more than just an open-access publisher of scholarly articles: it is a pioneering approach to the world of academia, radically improving the way scholarly research is managed. The grand vision of Frontiers is a world where all people have an equal opportunity to seek, share and generate knowledge. Frontiers provides immediate and permanent online open access to all its publications, but this alone is not enough to realize our grand goals.

Frontiers Journal Series

The Frontiers Journal Series is a multi-tier and interdisciplinary set of open-access, online journals, promising a paradigm shift from the current review, selection and dissemination processes in academic publishing. All Frontiers journals are driven by researchers for researchers; therefore, they constitute a service to the scholarly community. At the same time, the Frontiers Journal Series operates on a revolutionary invention, the tiered publishing system, initially addressing specific communities of scholars, and gradually climbing up to broader public understanding, thus serving the interests of the lay society, too.

Dedication to Quality

Each Frontiers article is a landmark of the highest quality, thanks to genuinely collaborative interactions between authors and review editors, who include some of the world's best academicians. Research must be certified by peers before entering a stream of knowledge that may eventually reach the public - and shape society; therefore, Frontiers only applies the most rigorous and unbiased reviews.
Frontiers revolutionizes research publishing by freely delivering the most outstanding research, evaluated with no bias from both the academic and social point of view. By applying the most advanced information technologies, Frontiers is catapulting scholarly publishing into a new generation.

What are Frontiers Research Topics?

Frontiers Research Topics are very popular trademarks of the Frontiers Journals Series: they are collections of at least ten articles, all centered on a particular subject. With their unique mix of varied contributions from Original Research to Review Articles, Frontiers Research Topics unify the most influential researchers, the latest key findings and historical advances in a hot research area! Find out more on how to host your own Frontiers Research Topic or contribute to one as an author by contacting the Frontiers Editorial Office: frontiersin.org/about/contact

NOVEL APPROACHES TO RAPID DIAGNOSIS AND TREATMENT MONITORING OF ACTIVE TUBERCULOSIS, VOL II

Topic Editors:
Xiao-Yong Fan, Fudan University Shanghai, China
Hairong Huang, Capital Medical University Beijing, China

Citation: Fan, X.-Y., Huang, H., eds. (2022). Novel Approaches to Rapid Diagnosis and Treatment Monitoring of Active Tuberculosis, Vol II.
Lausanne: Frontiers Media SA. doi: 10.3389/978-2-83250-567-0

Table of Contents

frontiers | Frontiers in Microbiology

TYPE Editorial
PUBLISHED 07 October 2022
DOI 10.3389/fmicb.2022.1044314

OPEN ACCESS

EDITED AND REVIEWED BY
Axel Cloeckaert,
Institut National de recherche pour l'agriculture, l'alimentation et l'environnement (INRAE), France

*CORRESPONDENCE
Xiao-Yong Fan
xyfan008@fudan.edu.cn

SPECIALTY SECTION
This article was submitted to Infectious Agents and Disease, a section of the journal Frontiers in Microbiology

RECEIVED 14 September 2022
ACCEPTED 20 September 2022
PUBLISHED 07 October 2022

CITATION
Hu Z and Fan X-Y (2022) Editorial: Novel approaches to rapid diagnosis and treatment monitoring of active tuberculosis, vol II.
Front. Microbiol. 13:1044314.
doi: 10.3389/fmicb.2022.1044314

Editorial: Novel approaches to rapid diagnosis and treatment monitoring of active tuberculosis, vol II

Zhidong Hu and Xiao-Yong Fan*

Shanghai Public Health Clinical Center, Fudan University, Shanghai, China

KEYWORDS

***Mycobacterium tuberculosis*, molecular diagnoses, biomarker, tuberculosis, latent infection**

Editorial on the Research Topic
Novel approaches to rapid diagnosis and treatment monitoring of active tuberculosis, vol II

Tuberculosis (TB), caused by respiratory *Mycobacterium tuberculosis* (*Mtb*) infection, remains a major global threat to human health. According to the World Health Organization (WHO)'s latest Global Tuberculosis Report, there were an estimated more than 10 million new TB cases and 1.4 million deaths in 2020 (WHO, 2021). Considering TB transmission have already happened before the diagnosis progress of passive case findings, the rapid and reliable test to detect active *Mtb* infections are needed, especially the diagnosis of the emerging drug-resistant strains (Dheda et al., 2019; Gunther et al., 2022). Detection of active TB patients, monitoring of therapy and determination of treatment effect are significant challenge for TB control efforts, the currently routine TB diagnostic tools, including *Mtb* culture, acid-fast staining, tuberculin skin test, chest X-ray, GeneXpert MTB/RIF, etc., all have their limitations (Al-Zamel, 2009; Heyckendorf et al., 2022). This challenge is complicated by the fact that sputum sample collection is not always straightforward to obtain, especially in TB patients with improved symptom, extrapulmonary TB (EPTB) patients, and childhood TB (Norbis et al., 2014; Jonckheree and Furin, 2017). The GeneXpert MTB/RIF sputum assay based on PCR was developed to improve the specificity and speed of diagnosis, but it cannot distinguish between viable and non-viable bacilli, and its sensitivity under low bacterial loads is still waiting to be optimized. The challenges of GeneXpert MTB/RIF assay to monitoring the treatment effect is also existed, especially in patients co-infected with HIV and TB (Denkinger et al., 2014; Detjen et al., 2015; Naidoo and Dookie, 2022).

In this Research Topic, we summarize a number of studies that either investigated novel methods in the diagnosis of TB or optimized the current TB diagnosis assays, and several reviews that focused on different topics and indicated directions for future research.

Jiao et al. determined the diagnostic efficacy of multiple cross displacement amplification (MCDA), which is a DNA amplification strategy on the basis of an isothermal strand-displacement polymerization reaction, and combined it with real-time PCR assay in patients with pulmonary TB. The MCDA assay showed a higher sensitivity than microscopy, culture, or Xpert using sputum samples, with a slight drop in specificity. Thus, MCDA assay might assist in the accurate and rapid diagnosis of TB in settings with platforms of real-time PCR equipment. Quan et al. evaluated the diagnostic efficacy of EasyNAT MTB complex assay (EasyNAT), which is a novel cross-priming amplification-based by using gastric aspirate samples in childhood TB. Compared with Xpert Ultra, EasyNAT yielded similar specificity but a modest lower sensitivity in childhood TB diagnosis using gastric aspirate samples. Thus, EasyNAT might be used as an alternative method for diagnosing childhood TB due to its cost-effectiveness and speed. Wang et al. conducted a prospective, multicenter study of the plasma concentrations of soluble triggering receptors expressed on myeloid cells (sTREM)-1 and sTREM-2 in subjects undergoing 3HP treatment regimen (once-weekly rifapentine plus isoniazid for 3 months) and examined the use of these biomarkers to predict systemic adverse reactions (SARs). The baseline concentrations of sTREM-1 were higher in patients with SARs than those without, and the area under the receiver operating characteristic curves showed that the plasma levels of sTREM-1 and sTREM-2 had modest discriminative power pertaining to the development of SARs during 3HP treatment at day 1. Pan et al. evaluated the performance of a novel *Mtb*-specific *CXCL10* mRNA release assay in TB diagnosis. The *CXCL10* gene encodes the IP-10 protein, which was shown to have potential as a biomarker of *Mtb* infection due to its high expression level after *Mtb* antigen stimulation. Their assay provided a sensitivity of 93.9% and a specificity of 98.0% in the diagnosis of *Mtb* infection, respectively, similar to T-SPOT.TB which gave a sensitivity of 94.5% and a specificity of 100%. Díaz-Fernández et al. compared the capacity of cell surface markers CD27, CD38, HLA-DR, and Ki-67 to distinguish LTBI, active TB, and patients who ended treatment and resolved TB. Their study showed that the percentages of cells bearing $CD27^{-}$, $CD38^{+}$, $HLA\text{-}DR^{+}$, and $Ki\text{-}67^{+}$ on *Mtb*-specific CD4 T cells were increased during the progression of active TB disease, and unbiased multiparametric analyses identified cell clusters based on CD27 or HLA-DR whose abundance can be correlated to treatment efficacy. These novel methods showed potential clinical application.

The study of Antonello et al. determined the performances of in-house droplet digital PCR (ddPCR)-based assays compared to culture using 89 biopsies, including fresh and formalin-fixed and paraffin-embedded (FFPE) samples. Their analysis support a highly accurate, sensitive, and rapid *Mtb* diagnosis with FFPE samples by ddPCR assay, as defined by a high concordance between the IS6110 assay and culture results. The quantitative method of ddPCR assay could differentiate a high bacillary load and disseminated condition from paucibacillary anatomically compartmentalized TB; this might accelerate *Mtb* diagnosis when culture techniques are unavailable. Carrère-Kremer et al. analyzed the cytokines patterns in QuantiFERON Gold Plus assay-positive populations. Their data showed that higher IFN-γ responses, and lower ratios of tube 1/tube 2 IFN-γ concentrations, were measured in the active TB group compared with LTBI. Patients with low ratios of IL-2/IFN-γ, IP-10/IFN-γ, and MIG/IFN-γ were much more likely to have active TB. These features of T cell response may be helpful in low prevalence settings to raise suspicion of ATB in patients who tested positive in IFN-γ release assays. Thus, these studies might optimize the current TB diagnosis assays.

Lin et al. tested the performance of endobronchial ultrasound-guided transbronchial biopsy (EBUS-TBB) in TB diagnosis and showed it to be safe and effective in diagnosing sputum smear-negative pulmonary TB. The EBUS echoic feature was also a predictor of the positive TB culture rate. To improve the efficiency of clinical diagnosis in spinal TB patients by computed tomography (CT), Li et al. developed a novel deep learning method based on three handcrafted features and one convolutional neural network feature. This gave efficient feature fusion for multimodal features. The introduction of these methods into the TB research field provides novel approaches for TB diagnosis.

Rapid TB diagnosis is challenging in EPTB infection due to the small number of mycobacteria and the lack of fresh samples with which to apply culture techniques. Rindi reviewed the current knowledge of the diagnostic performance of the Xpert Ultra assay in EPTB detection. It was shown that the sensitivity of the Xpert Ultra assay differs by specimen types, with high sensitivity among specimens obtained from cerebrospinal and fluid lymph nodes, and low sensitivity when using pleural fluids. Similar challenges are faced in the diagnosis of latent TB and the review by Gong et al. focused on this. Firstly, the authors summarized the concept and expounded on the immunological mechanism of LTBI. Secondly, they outlined novel interferon-gamma release assays and skin tests that have been developed recently. Finally, they summarized the research status, directions, and challenges in LTBI diagnosis, including novel biomarkers, new models/algorithms, omics technologies, and microbiota. The review written by Guo et al. focused on the progress of proteomics in biomarker discovery in TB diagnosis. Firstly, the authors summarized the proteomics research approaches. Secondly, the current status of research on the diagnostic application of proteomic biomarkers for TB was outlined. Finally, they described the prospects of proteomics in the field of TB biomarker discovery for rapid and accurate TB diagnosis. These high-quality reviews gave a thorough and up-to-date summary of their topics and provided directions for future research.

Overall, the manuscripts reviewed within this Research Topic demonstrate that the field of TB diagnosis is now rapidly evolving, providing us with new insights into how we can increase the sensitivity and specificity of TB diagnosis. Novel research approaches are indicated that may further improve the diagnosis of active TB cases, the identification of latent TB, of susceptible and resistant isolates of *Mtb*, and enable better monitoring the efficacy of anti-TB treatment in near future.

Author contributions

ZH and X-YF conceived, designed, and wrote the manuscript. X-YF edited the manuscript with conceptual advice. Both authors contributed to the article and approved the submitted version.

Acknowledgments

We are thankful to the authors who submitted their articles to support this Research Topic, to Prof. Douglas B. Lowrie for his critical polish on the text, and to the grants from the National Natural and Science Foundation of China (82171815, 81873884, and 82171739), National Key Research and Development Program of China (2021YFC2301503), and Shanghai Science and Technology Commission (20Y11903400).

Conflict of interest

The authors declare that the research was conducted in the absence of any commercial or financial relationships that could be construed as a potential conflict of interest.

Publisher's note

All claims expressed in this article are solely those of the authors and do not necessarily represent those of their affiliated organizations, or those of the publisher, the editors and the reviewers. Any product that may be evaluated in this article, or claim that may be made by its manufacturer, is not guaranteed or endorsed by the publisher.

References

Al-Zamel, F. A. (2009). Detection and diagnosis of *Mycobacterium tuberculosis*. *Expert Rev. Anti Infect. Ther.* 7, 1099–1108. doi: 10.1586/eri.09.92

Denkinger, C. M., Schumacher, S. G., Boehme, C. C., Dendukuri, N., Pai, M., and Steingart, K. R. (2014). Xpert MTB/RIF assay for the diagnosis of extrapulmonary tuberculosis: a systematic review and meta-analysis. *Eur. Respir. J.* 44, 435–446. doi: 10.1183/09031936.00007814

Detjen, A. K., DiNardo, A. R., Leyden, J., Steingart, K. R., Menzies, D., Schiller, I., et al. (2015). Xpert MTB/RIF assay for the diagnosis of pulmonary tuberculosis in children: a systematic review and meta-analysis. *Lancet Respir. Med.* 3, 451–461. doi: 10.1016/S2213-2600(15)00095-8

Dheda, K., Gumbo, T., Maartens, G., Dooley, K. E., Murray, M., Furin, J., et al. (2019). The Lancet Respiratory Medicine Commission: 2019 update: epidemiology, pathogenesis, transmission, diagnosis, and management of multidrug-resistant and incurable tuberculosis. *Lancet Respir. Med.* 7, 820–826. doi: 10.1016/S2213-2600(19)30263-2

Gunther, G., Ruswa, N., and Keller, P. M. (2022). Drug-resistant tuberculosis: advances in diagnosis and management. *Curr. Opin. Pulm. Med.* 28, 211–217. doi: 10.1097/MCP.0000000000000866

Heyckendorf, J., Georghiou, S. B., Frahm, N., Heinrich, N., Kontsevaya, I., Reimann, M., et al. (2022). Tuberculosis treatment monitoring and outcome measures: new interest and new strategies. *Clin. Microbiol. Rev.* 2022, e0022721. doi: 10.1128/cmr.00227-21

Jonckheree, S., and Furin, J. (2017). Overcoming challenges in the diagnosis, prevention, and treatment of pediatric drug-resistant tuberculosis. *Expert Rev. Respir. Med.* 11, 385–394. doi: 10.1080/17476348.2017.1309294

Naidoo, K., and Dookie, N. (2022). Can the GeneXpert MTB/XDR deliver on the promise of expanded, near-patient tuberculosis drug-susceptibility testing? *Lancet Infect. Dis.* 22, e121–e127. doi: 10.1016/S1473-3099(21)00613-7

Norbis, L., Alagna, R., Tortoli, E., Codecasa, L. R., Migliori, G. B., and Cirillo, D. M. (2014). Challenges and perspectives in the diagnosis of extrapulmonary tuberculosis. *Expert Rev. Anti Infect. Ther.* 12, 633–647. doi: 10.1586/14787210.2014.899900

WHO (2021). *WHO Global TB Report.*

frontiers in Microbiology

ORIGINAL RESEARCH
published: 13 September 2021
doi: 10.3389/fmicb.2021.727774

Rapid Detection and Quantification of *Mycobacterium tuberculosis* DNA in Paraffinized Samples by Droplet Digital PCR: A Preliminary Study

*Maria Antonello[1†], Rossana Scutari[2†], Calogero Lauricella[3], Silvia Renica[1], Valentina Motta[3], Stefania Torri[4], Cristina Russo[5], Leonarda Gentile[5], Valeria Cento[1], Luna Colagrossi[5], Giordana Mattana[5], Luigi Ruffo Codecasa[6], Chiara Vismara[4], Francesco Scaglione[1,4], Silvio Marco Veronese[3], Emanuela Bonoldi[3], Alessandra Bandera[7,8], Andrea Gori[7,8], Ester Mazzola[4], Carlo Federico Perno[5,9] and Claudia Alteri[1,9]**

[1] Department of Oncology and Hemato-Oncology, University of Milan, Milan, Italy, [2] Department of Experimental Medicine, University of Rome "Tor Vergata," Rome, Italy, [3] Department of Pathology, ASST Grande Ospedale Metropolitano Niguarda, Milan, Italy, [4] Unit of Microbiology, Department of Chemical-Clinical and Microbiology Analyses, ASST Grande Ospedale Metropolitano Niguarda, Milan, Italy, [5] Unit of Microbiology and Diagnostic Immunology, Bambino Gesù Children's Hospital, IRCCS, Rome, Italy, [6] Regional TB Reference Centre, Villa Marelli Institute, ASST Grande Ospedale Metropolitano Niguarda, Milan, Italy, [7] Infectious Disease Unit, Department of Internal Medicine, Fondazione IRCCS Ca' Granda, Ospedale Maggiore Policlinico, Milan, Italy, [8] Department of Pathophysiology and Transplantation, University of Milan, Milan, Italy, [9] Multimodal Medicine Research Area, Bambino Gesù Children's Hospital, IRCCS, Rome, Italy

Background: Rapid and reliable diagnosis of tuberculosis (TB) represents a diagnostic challenge in compartmentalized extrapulmonary TB infection because of the small number of mycobacteria (MTB) and the frequent lack of fresh samples to perform culture. Here, we estimate the performances of homemade droplet digital PCR (ddPCR)-based assays against culture in 89 biopsies, for those fresh and formalin-fixed and paraffin-embedded (FFPE) subsamples were available.

Methods: MTB diagnosis in fresh subsamples was performed by culture. Fresh subsamples were also analyzed for acid-fast bacilli smear-microscopy (AFB) and Xpert® MTB/RIF (Xpert). MTB examination was repeated in blind in the 89 FFPE subsamples by in-house ddPCR assays targeting the IS6110 and rpoB. Analytical sensitivity of ddPCR assays was evaluated using serial dilution of H37Rv strain. Limit of detection (LOD) was calculated by probit analysis. Results were expressed in copies/10^6 cells.

Results: IS6110 and rpoB ddPCR assays showed a good linear correlation between expected and observed values (R^2: 0.9907 and 0.9743, respectively). Probit analyses predicted a LOD of 17 and 40 copies/10^6 cells of MTB DNA for IS6110 and rpoB, respectively. Of the 89 biopsies, 68 were culture positive and 21 were culture negative. Considering mycobacterial culture as reference method, IS6110 assay yielded positive results in 67/68 culture-positive samples with a median interquartile range (IQR) of 1,680 (550–8,444) copies/10^6 cells (sensitivity: 98.5%; accuracy: 98.9). These performances were superior to those reported by the rpoB assay in FFPE subsamples (sensitivity: 66.20%; accuracy: 74.1) and even superior to those reported by Xpert and AFB in

OPEN ACCESS

Edited by:
Xiao-Yong Fan,
Fudan University, China

Reviewed by:
Amit Singh,
All India Institute of Medical Sciences, India
Gerald Mboowa,
Makerere University, Uganda
Allyson Guimarães Costa,
Federal University of Amazonas, Brazil

***Correspondence:**
Claudia Alteri
claudia.alteri@unimi.it

[†]These authors have contributed equally to this work and share first authorship

Specialty section:
This article was submitted to Infectious Diseases, a section of the journal Frontiers in Microbiology

Received: 19 June 2021
Accepted: 16 August 2021
Published: 13 September 2021

Citation:
Antonello M, Scutari R, Lauricella C, Renica S, Motta V, Torri S, Russo C, Gentile L, Cento V, Colagrossi L, Mattana G, Codecasa LR, Vismara C, Scaglione F, Veronese SM, Bonoldi E, Bandera A, Gori A, Mazzola E, Perno CF and Alteri C (2021) Rapid Detection and Quantification of Mycobacterium tuberculosis DNA in Paraffinized Samples by Droplet Digital PCR: A Preliminary Study. Front. Microbiol. 12:727774. doi: 10.3389/fmicb.2021.727774

fresh subsamples (sensitivity: 79.4 and 33.8%, respectively; accuracy: 84.3 and 49.4, respectively). When Xpert and AFB results were stratified according to mycobacterial load detected by rpoB and IS6110 ddPCR, bacterial load was lower in Xpert and AFB negative with respect to Xpert and AFB-positive samples ($p = 0.003$ and 0.01 for rpoB and $p = 0.01$ and 0.11 for IS6110), confirming the poor sensitivity of these methods in paucibacillary disease.

Conclusion: ddPCR provides highly sensitive, accurate, and rapid MTB diagnosis in FFPE samples, as defined by the high concordance between IS6110 assay and culture results. This approach can be safely introduced in clinical routine to accelerate MTB diagnosis mainly when culture results remain unavailable.

Keywords: MTB, ddPCR, MTB diagnosis, *tuberculosis*, extrapulmonary TB

INTRODUCTION

Tuberculosis (TB) is a multisystemic disease caused by *Mycobacterium tuberculosis* complex (MTB). The pathogen primarily infects the lungs (pulmonary TB) but can also affect other structural parts of the human anatomy (extrapulmonary TB), such as lymph nodes, intestines, pleura, skin, and bones (Noussair et al., 2009).

It affects approximately 2 billion people worldwide, especially in developing countries, and stands as the leading cause of death from a single infectious agent [World Health Organization (WHO), 2012].

To reduce the mortality of MTB infection, to prevent its spread, and to start the correct treatment, an early, accurate, and rapid diagnosis is essential.

To date, the conventional approach for MTB diagnosis is mainly based on microscopic detection of acid-fast bacilli in smears (AFB), followed by MTB culture (Ryu, 2015; Caulfield and Wengenack, 2016). While AFB is a laborious method characterized by variable sensitivity (71.4% in lung samples and 24% in extrapulmonary samples) (Karadağ et al., 2013), mycobacterium culture is considered the gold standard method for MTB diagnosis as it has high specificity but requires a long time of incubation, up to 8 weeks for a certain negativity (Forbes et al., 2018).

For these reasons, in the case of extrapulmonary MTB infection, the diagnosis is challenging because of the small amount of MTB present at the sites of the disease and the difficulty of obtaining culture results (Golden, 2005; Noussair et al., 2009). In the case of surgically resected tissues fixed in formalin, mycobacterial culture is not feasible at all, and a correct diagnosis based on pathological features and AFB smear is difficult. Acid-fast staining for MTB on formalin-fixed and paraffin-embedded (FFPE) tissue has indeed a very low sensitivity, ranging between 3 and 60% (Fukunaga et al., 2002; Ahmed et al., 2011; Eshete et al., 2011), and some histological findings, like granuloma and necrosis, typically found in many other diseases including sarcoidosis and fungal infections (El-Zammar and Katzenstein, 2007), make MTB diagnosis particularly challenging.

In the last decade, real-time (RT) PCR assays have been introduced in laboratory routine, thanks to their sensitivity and their shortened turnaround time (Forbes and Hicks, 1993; Marchetti et al., 1998; Moure et al., 2019). Most of these methods are based on the detection of multi-copy insertion sequences (IS, such as IS986, IS987, IS1081, and IS6110), which should increase the sensitivity of the assays (Bisognin et al., 2018; Lin et al., 2021). Among these RT-PCR-based assays, Xpert® MTB/RIF (Cepheid, Sunnyvale, CA, United States) (Xpert) is recommended by the World Health Organization (WHO) as rapid molecular diagnostic test for adults and children also in the case of extrapulmonary and FFPE specimens [Lee et al., 2011; Mazzola et al., 2016; Yang et al., 2017; Moure et al., 2019; Nyaruaba et al., 2019; World Health Organization (WHO), 2020], although it has a low diagnostic accuracy in paucibacillary disease (Allahyartorkaman et al., 2019).

Among other molecular platforms, droplet digital PCR (ddPCR) is a highly sensitive method widely used for the detection of a variety of pathogens, thanks to its ability to reliably detect down to a few copies of genomes (Caviglia et al., 2018; Alteri et al., 2020; Chen et al., 2021; Malin et al., 2021). Currently, two reports suggested that homemade ddPCR assays might provide a valid alternative for detecting MTB in extrapulmonary and/or FFPE samples (Yang et al., 2017; Cao et al., 2020), but as far as we know no study has defined the concordance between these molecular assays and the reference culture method.

Here, to evaluate the ddPCR-based method as suitable alternative for routine clinical diagnoses of MTB in FFPE samples, the performances of two MTB ddPCR-based assays were compared with the gold-standard culture methods and with the conventional AFB and Xpert in a set of tissues, for those fresh and FFPE subsamples were available.

MATERIALS AND METHODS

Clinical Sample Collection

A total of 89 consecutive biopsies from different anatomical districts of patients with a clinical suspect of TB were retrospectively collected at ASST Grande Ospedale

Metropolitano Niguarda (Milan, Italy) between 2013 and 2019. Samples were selected according to clinical suspect of MTB based on radiology findings, cytology reports, and/or medical history of patients including previous MTB treatment [World Health Organization (WHO), 2013]. The distribution of samples against year of collection is reported in **Supplementary Table 1**. Biopsies were subdivided in two subsamples by trained medical personnel. One fresh subsample was immediately tested for MTB diagnosis by culture methods, using both solid (Lowenstein–Jensen) and liquid (MGIT 960; Becton Dickinson Biosciences, Sparks, MD, United States) media [European Centre for Disease Prevention and Control (ECDC), 2018; Riccardi et al., 2020]. Fresh subsamples were also analyzed for AFB microscopy and Xpert® MTB/RIF (Cepheid, Sunnyvale, CA, United States) (Tortoli et al., 2012). As required by WHO and ECDC guidelines [World Health Organization (WHO), 2012; European Centre for Disease Prevention and Control (ECDC), 2018], all these procedures took place in a Biosafety Level 3 (BSL3) laboratory, with limited access, using required personal protective equipment and following control measures and all procedures to minimize aerosol and droplet formation. The residual sample was stored as formalin fixed and paraffin embedded (FFPE) (Slaoui and Fiette, 2011; Sadeghipour and Babaheidarian, 2019) for alternative diagnosis by histopathological examination and archived in a biobank for later use.

The study was conducted in accordance with the principles of the 1964 Declaration of Helsinki. The related information of the samples was processed by maintaining anonymization measures. Due to the non-interventional nature of the study and according to the applicable relevant national legislation and local rules, approval of the local Research Ethics Committee and informed consent were not mandatory.

DNA Extraction and *Mycobacteria tuberculosis* Detection in Formalin-Fixed and Paraffin-Embedded Samples

MTB detection was repeated in blind in the stored FFPE samples by using ddPCR homemade assays. In brief, after sample deparaffinization (Fu et al., 2016), total DNA was extracted using Maxwell CSC DNA FFPE kit (Promega, Madison, WI, United States) following the instruction of the manufacturer (Sarnecka et al., 2019).

MTB DNA was quantified by means of the QX200^{TM} Droplet Digital PCR System (Biorad) using homemade assays targeting the multicopy gene *IS6110* (Forward: 5′-ATCTGGAC CCGCCAA-3′; Reverse: 5′-CCTATCCGTATGGTGGATAA-3′, and HEX Probe: 5′-AGGTCGAGTACGCCTT-3′) and the single-copy gene *rpoB* (Forward: 5′-GGAGCGCCAAACCG-3′; Reverse: 5′-AGTCCCGGAACCTCAA-3′, and FAM Probe: 5′-TTCGCTAAGCTGCGC-3′). The human albumin was used as housekeeping gene (ddPCR^{TM} Copy Number Assay: ALB, Human, dHsaCNS864404398).

The cycling condition was the following: 95°C (10 min), 39 cycles of 94°C (30 s), and 56°C (1 min), 98°C (10 min), 4°C (∞). A sample was considered "positive and quantifiable" if at least two droplets (in *IS6110* or *rpoB* assay) were observed.

MTB DNA (copies/reaction) was then normalized into number copies/10^6 cells. In detail, raw data obtained were converted into copies/10^6 cells according to the following formula: [MTB-DNA (copies/10^6 cells) = MTB-DNA raw data × 10^6 cells/(housekeeping gene copies/2)].

Accuracy and Limit of Detection of Droplet Digital PCR Assay

To verify the correct performance of MTB detection and quantification, the laboratory-cultured H37Rv strain (previously inactivated by incubation at 95°C for 20 min and sonication at room temperature for 15 min) served as quantitation standards in two independent runs. Five serial dilutions were prepared in order to deposit 10^4, 10^3, 10^2, 10, and 1 copy(ies) of the MTB genome (1 ng = 168,100 copies) in 3 μg of human genomic DNA, corresponding to 10^6 cells. The first three dilutions were repeated in duplicate, while the remaining ones were in triplicate. To determine the specificity and cross-reactivity of the MTB ddPCR-based assays, the DNA of cultured non-tuberculous strains [*M. abscessus* subsp. *abscessus* (MBABAB) and *M. abscessus* subsp. *bolletii* (MBABBO)], and negative controls (n = 20) were also added in each run. The negative controls belonged to FFPE samples from subjects without clinical and bacteriological signs of MTB infection [World Health Organization (WHO), 2013].

Coefficient of determination (R^2) of MTB quantification was assessed for both *IS6110* and *rpoB* by linear regression analysis by plotting the measured copies of the standards and comparing them with expected values of serial dilutions. The coefficient of variation (CV) was calculated as the standard deviation (SD) of copies/10^6 cells divided by replicate mean.

The lower limit of blank (LoB) was determined by testing the replicates of the 20 negative controls, according to the following formula: LoB = mean of blank + 1.645 × (SD of blank) (Armbruster and Pry, 2008). The limit of detection (LoD) was determined by probit regression analysis.

Statistical Analyses

Sensitivity and specificity of ddPCR, Xpert, and AFB in terms of the ability to correctly diagnose MTB in tissue samples (pulmonary and extrapulmonary) were evaluated against culture results.

Reproducibility of quantification methods was assessed by intra- and inter-run tests using serial standard dilutions, and the differences between the expected and observed values were expressed as the mean ± SD *IS6110* and *rpoB* copy numbers.

Descriptive statistics were expressed as median values and interquartile range (IQR) for continuous variables and absolute number and frequency (percentage) for categorical variables. To assess significant differences, Fisher exact or Kruskal–Wallis test and Wilcoxon rank sum test were used for categorical and continuous variables, respectively. A p-value < 0.05 was considered statistically significant. All statistical analyses were performed with SPSS software package for Windows (version 25.0, SPSS INC., Chicago, IL, United States).

RESULTS

Study Population

The demographic and clinical characteristics of the population included in the study are reported in **Table 1**. Samples were retrieved mainly by male (57.3%) with a median age of 36 years (IQR: 27–53). As expected, extrapulmonary samples were the majority (85, 95.5%) and mainly from lymphatic system (52, 58.4%) followed by pleural samples (17, 19.1%). Sixty-eight samples (76.4%) were MTB positive because of the positive mycobacterial culture from the fresh sample [median (IQR) days for culture positivity: 11 (13–16)]. The remaining 21 samples were MTB negative because of the negative culture and subsequent different diagnosis. Most of the positive samples (94.1%) belonged to patients receiving their first TB diagnosis at the time of the biopsy, and only 5.9% belonged to patients with a previously MTB-positive known condition.

No differences were found between MTB-positive and -negative samples, with the sole exception of patients aged below 40 years, most frequently found among MTB-positive samples (**Table 1**). Viral coinfections were quite rare (9.0%) and prevalently found in patients with positive MTB culture (4.5%, no significant data).

Performance of Droplet Digital PCR-Based Assays

Assay Linearity and Limit of Detection

The linearity of the ddPCR assays was tested by quantifying serial dilutions of a known amount of MTB DNA. Our method showed a good linear correlation between expected and observed MTB DNA quantification, for both *IS6110* (R^2 = 0.9907) and *rpoB* (R^2 = 0.9743) (**Figures 1A,B**). No signal was detected in any of the 20 certainly negative samples tested, nor in the non-tuberculous extract (MBABAB and MBABBO) added in each run (**Supplementary Figure 1**). An example of Quantasoft panel for *IS6110* and *rpoB* obtained by the positive MTB DNA control, four positive samples, and a negative sample are also reported in **Supplementary Figure 2**.

Intra-run and Inter-run Reproducibility

Intra-run reproducibility analysis confirmed the high reliability of the methods (**Figures 1C,D**). The mean (±SD) differences between the expected and observed MTB copy number per 10^6 cells (expressed as $\log_{10}$) were for *IS6110* assay: -0.363 ± 0.07 for 10^5, -0.338 ± 0.02 for 10^4, -0.338 ± 0.05 for 10^3, -0.340 ± 0.06 for 10^2, -0.338 ± 0.12 for 10 copies, -0.348 ± 0.04 for one copy; for *rpoB* assay: 0.898 ± 0.10 for 10^5, 0.840 ± 0.05 for 10^4, 0.802 ± 0.08 for 10^3, 0.602 ± 0.02 for 10^2, -0.060 ± 0.40 for 10 copies, -0.348 ± 0.04 for one copy. Mean CVs of the two experiments were 3.48 for *IS6110*, and 7.85 for *rpoB*.

The analysis of inter-run reproducibility confirmed the above results. The mean (±SD) differences between the expected and observed MTB copy number per 10^6 cells (expressed as $\log_{10}$) were for *IS6110* assay: -0.292 ± 0.17 for 10^5, -0.317 ± 0.03 for 10^4, -0.367 ± 0.04 for 10^3, -0.307 ± 0.05 for 10^2, -0.176 ± 0.33 for 10, and -0.584 ± 0.1 for one copy; for *rpoB* assay: 0.899 ± 0.10 for 10^5, 0.824 ± 0.02 for 10^4, 0.764 ± 0.05 for 10^3, 0.611 ± 0.01 for 10^2, 0.523 ± 0.67 for 10, -0.090 ± 0.16 for one copy. Mean CV was 9.04 and 24.61 for *IS6110* and *rpoB*, respectively.

Sensitivity and Specificity of Droplet Digital PCR-Based Assays Against Culture

All the DNA extracts obtained by the 89 FFPE samples were of high quality and quantity as confirmed by human albumin quantification [median (IQR): 1,760 (1,228–2,200) copies/μl; **Supplementary Figure 3**].

The overall sensitivity of the ddPCR assays was 98.5 (95.6–100.0) for *IS6110* and 66.2 (54.9–77.4) for *rpoB*. No false-positive results were highlighted among the 21 culture-negative FFPE samples (**Table 2**).

Among the 68 positive mycobacterial cultures, ddPCR yielded 67/68 (98.5%) positive results for *IS6110* with a median (IQR) of 1,680 (550–8,444) copies/10^6 cells, and 45/68 (66.2%) positive results for *rpoB* with a median (IQR) of 308 (99–1,419) copies/10^6 cells. One sample was negative for both *rpoB* and *IS6110*, 45 samples were positive for both *IS6110* and *rpoB* (double positive), and 22 were positive only for *IS6110* (single positive). Double-positive with respect to single-positive samples were characterized by higher mycobacterial loads [*IS6110* copies/10^6 cells, median (IQR): 3,578 (1,352–11,983) vs. 308 (99–1,419), p = 0.001], but not by a shorter time to positive culture [days, median (IQR): 13 (11–16) vs. 12 (10–15), p = 0.687].

Sensitivity and Specificity of Xpert and Acid-Fast Bacilli Against Culture

When used in fresh subsamples, Xpert and AFB had a sensitivity of 79.4% (69.8–89.0) and 33.8% (22.6–45.1), respectively, lower than that observed with ddPCR in FFPE subsamples. As for ddPCR, no false-positive results were highlighted (**Table 2**). To define if the bacterial load can influence the sensitivity of Xpert and AFB, qPCR and smear results were stratified according to *rpoB* and *IS6110* load detected by ddPCR-assays. As expected, *rpoB* and *IS6110* loads were significantly lower in Xpert-negative with respect to Xpert-positive samples [*rpoB* load, median (IQR): 107 (97–210) vs. 414 (110–2,651), p = 0.003; *IS6110* load, median (IQR): 941 (361–1,412) vs. 2,892 (552–10,709), p = 0.01, **Figures 2A,B**]. Superimposable data were found for smear results (**Figures 2C,D**). No significant differences in the *IS6110* or *rpoB* loads were found against time of the first MTB diagnosis, anatomical districts, age, or sex of patients (**Supplementary Figures 4A–H**).

DISCUSSION

Results of this preliminary study clearly revealed that the ddPCR-based assay was non-inferior to the reference culture method for the detection of MTB in tissue biopsies, even when FFPE samples were considered. Moreover, the performances of *IS6110* ddPCR assay in detecting MTB in FFPE subsamples were superior to

TABLE 1 | Demographic and clinical data of the sampled population.

	Overall	Culture positive (*N* = 68)	Culture negative (*N* = 21)	*p*-Value[a]
Male, *n* (%)	51 (57.3)	41 (60.3)	10 (47.6)	0.325
Age, median (IQR)	36 (27–53)	35 (26–45)	54 (35–71)	**0.006**
<40, *n* (%)	54 (60.7)	47 (69.1)	7 (33.3)	**0.005**
≥40, *n* (%)	35 (39.3)	21 (30.9)	14 (66.7)	
TB classes				
New case of TB, *n* (%)	64 (71.9)	64 (94.1)	–	–
Case of previously diagnosticated TB, *n* (%)	4 (4.5)	4 (5.9)	–	–
Viral coinfections, *n* (%)	8 (9)	7 (10.3)	1 (4.8)	0.675
HIV co-infection, *n* (%)	4 (4.5)	4 (5.9)	0 (0.0)	0.569
Anatomical districts				
Pulmonary site, *n* (%)	4 (4.5)	1 (1.5)	3 (14.3)	**0.039**
Extrapulmonary site, *n* (%)	85 (95.5)	67 (98.5)	18 (85.7)	
Lymphatic system, *n* (%)	52 (58.4)	44 (64.7)	8 (38.1)	**0.043**
Pleura, *n* (%)	17 (19.1)	15 (22.0)	2 (9.5)	0.341
Musculoskeletal apparatus, *n* (%)	4 (4.5)	1 (1.5)	3 (14.3)	**0.039**
Gastrointestinal tract, *n* (%)	4 (4.5)	4 (5.9)	0 (0.0)	0.569
Others[b], *n* (%)	8 (9.0)	3 (4.4)	5 (23.8)	**0.016**
Previous MTB results[c]				
Smear positive test, *n* (%)	23 (25.8)	23 (33.8)	0 (0.0)	–
Xpert MTB/RIF positive test, *n* (%)	54 (60.7)	54 (79.4)	0 (0.0)	–

IQR, interquartile range; TB, tuberculosis; MTB, Mycobacterium tuberculosis.
[a]Fisher exact test and Wilcoxon rank sum test were used for categorical and continuous variables, respectively. Statistically significant differences (p-values < 0.05) are highlighted in bold.
[b]Soft tissue biopsy (n = 4); hearth biopsy (n = 2); spinal cord biopsy (n = 1), nasal biopsy (n = 1).
[c]Performed on fresh subsamples.

the standard Xpert® MTB/RIF and AFB microscopy used for tuberculosis case detection in fresh subsamples, as well as defined by the sensitivities obtained in the 89 in-blind analyzed biopsies (sensitivity: 98.5 vs. 79.4 vs. 33.8%, respectively).

Due to the low sensitivity and specificity of AFB microscopy when compared with culture method (Karadağ et al., 2013; Molicotti et al., 2014; Pk et al., 2017; Bahr et al., 2018), molecular methods (as Xpert® MTB/RIF assay) were introduced to improve the speed and specificity of TB diagnosis mainly in the context of extrapulmonary and FFPE samples, when bacterial load is low, and culture is not even possible. Sensitivities of Xpert® MTB/RIF and its ultra version reported in fresh non-FFPE clinical samples, so far, are always higher than 60% (Tortoli et al., 2012; Sauzullo et al., 2016; Lee et al., 2017; Bahr et al., 2018; Dorman et al., 2018; Sarfaraz et al., 2018; Sulis et al., 2018; Aydemir et al., 2019; Kohli et al., 2021) and can reach more than 90% only in some body districts (Mazzola et al., 2016). The few data available regarding the Xpert assay performances in FFPE samples are based on a few clinical biopsies and reported a wide range of sensitivities, which were not even concordant (from 97.6% in the case of the Ultra version to 53.2% in the case of the first MTB/RIF assay) (Seo et al., 2014; Du et al., 2019; Njau et al., 2019; Budvytiene and Banaei, 2020; Huang et al., 2020). Some of these reports also suggest different sensitivities against the sites of biopsies (i.e., lymph node vs. non-lymph nodes sites) (Polepole et al., 2017).

Hence, performing an accurate, quantitative, and sensitive MTB diagnosis is still a challenge. ddPCR is a third-generation PCR technology that allows an absolute quantification of nucleic acid molecules. This methodology is widely used to diagnose infectious diseases for its good accuracy, sensitivity, and specificity (Caviglia et al., 2018; Alteri et al., 2020; Chen et al., 2021; Malin et al., 2021), and has been successfully applied in different samples and clinical settings like SARS-CoV-2 (Alteri et al., 2020), HPV (Malin et al., 2021), HBV (Caviglia et al., 2018), or HIV (Strain et al., 2013), as some examples.

To the best of our knowledge, this is the first study that compared the performances of ddPCR with the MTB culture, recognized to be the gold standard for the MTB diagnosis, thanks to the availability of one fresh and one FFPE subsamples from the same biopsy.

In brief, we defined the performances of two duplex ddPCR assays targeting the multi-copy MTB gene *IS6110* or the single-copy MTB gene *rpoB*, respectively, and the human albumin as housekeeping gene. Introducing a reference gene in the MTB ddPCR assay was helpful in measuring and reducing the errors from variations among the samples, defining efficiency of DNA extraction and amplifications. The use of the reference gene was also important for normalizing and providing accurate quantification of MTB copy numbers, expressed in our study as per 10^6 human cells.

By comparing the performances of *IS6110* and *rpoB* ddPCR assays, we confirmed that targeting a multicopy gene like *IS6110* guarantees a sensitive and reliable MTB detection (LOD 17 vs. 40 copies/10^6 human cells) (Bahador et al., 2005; Kolia-Diafouka et al., 2019). According to the approach by Armbruster and Pry (2008), the LoB were 0 copies/reaction for both *IS6110* and *rpoB*.

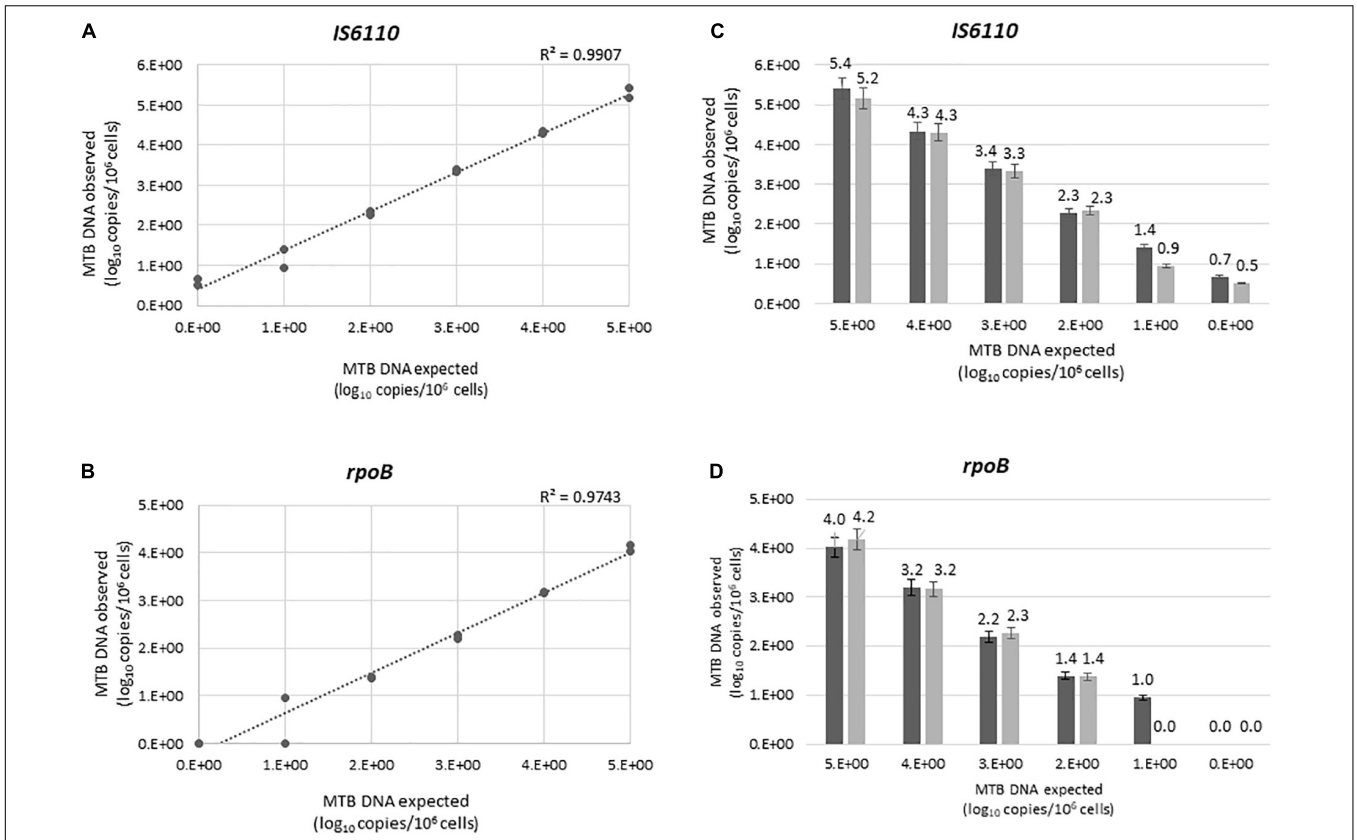

FIGURE 1 | Linear correlations between the expected and the observed *IS6110* **(A)** and *rpoB* **(B)** load, expressed as $\log_{10}$ copies/10^6 cells. *IS6110* **(C)** rpoB **(D)** load in the first and second experiment were shown in dark and light gray, respectively. Each value was tested in two independent experiments, each led in duplicate. Bars represent mean (+SD).

TABLE 2 | Performances of homemade ddPCR assays, Xpert® MTB/RIF molecular assay, and AFB against MTB culture.

Method	Sensitivity (%) (95% CI)	Specificity (%) (95% CI)	PPV (%) (95% CI)	NPV (%) (95% CI)	Accuracy
IS6110 ddPCR assay[a]	98.5 (95.6–100.0)	100.0 (86.3–100.0)	100.0 (95.7–100.0)	95.5 (82.3–100.0)	98.9
rpoB ddPCR assay[a]	66.2 (54.9–77.4)	100.0 (82.8–100.0)	100.0 (92.0–100.0)	47.7 (32.9–62.5)	74.1
Xpert® MTB/RIF molecular assay[b]	79.4 (69.8–89.0)	100.0 (83.2–100.0)	100.0 (93.5–100.0)	60.0 (43.77–76.23)	84.3
AFB[b]	33.8 (22.6–45.1)	100.0 (83.0–100.0)	100.0 (84.5–100.0)	31.8 (20.6–43.1)	49.4

CI, confidence interval; NPV, negative predicted value; PPV, positive predicted value, AFB acid-fast bacilli microscopy.
[a] *Performed on FFPE subsamples.*
[b] *Performed on fresh subsamples.*

Probit analysis predicted a LoD of 14 copies/10^6 cells for *IS6110* and 40 copies/10^6 cells for *rpoB*.

This ddPCR assay was non-inferior to the reference culture method, failing to find bacilli in only one 12-day culture-positive biopsy. This biopsy resulted in MTB negative by both Xpert and AFB methods, suggesting the presence of a paucibacillary TB disease. In line with this hypothesis, the negative ddPCR result could be caused by the absence of MTB inclusions in the FFPE subsample.

Both ddPCR assays allow to detect MTB where AFB and Xpert failed. Indeed, when the rpoB and IS6110 loads detected by ddPCR were reported against AFB and Xpert results, the copies of bacilli were lower in AFB/Xpert-negative samples with respect to AFB/Xpert-positive samples, thus, highlighting the high efficiency of ddPCR assay in diagnosing also low bacterial loads.

About paucibacillary TB disease, maintaining two mycobacterial targets like *rpoB* and *IS6110* might allow to easily discriminate between high (characterized by double positive results) and low (characterized by single positive result) mycobacteria loads. This approach can also be used as a proxy measure for monitoring anti-TB treatment efficacy over time.

No difference in sensitivity and specificity of the ddPCR-based assays was found between patients with and without a history of

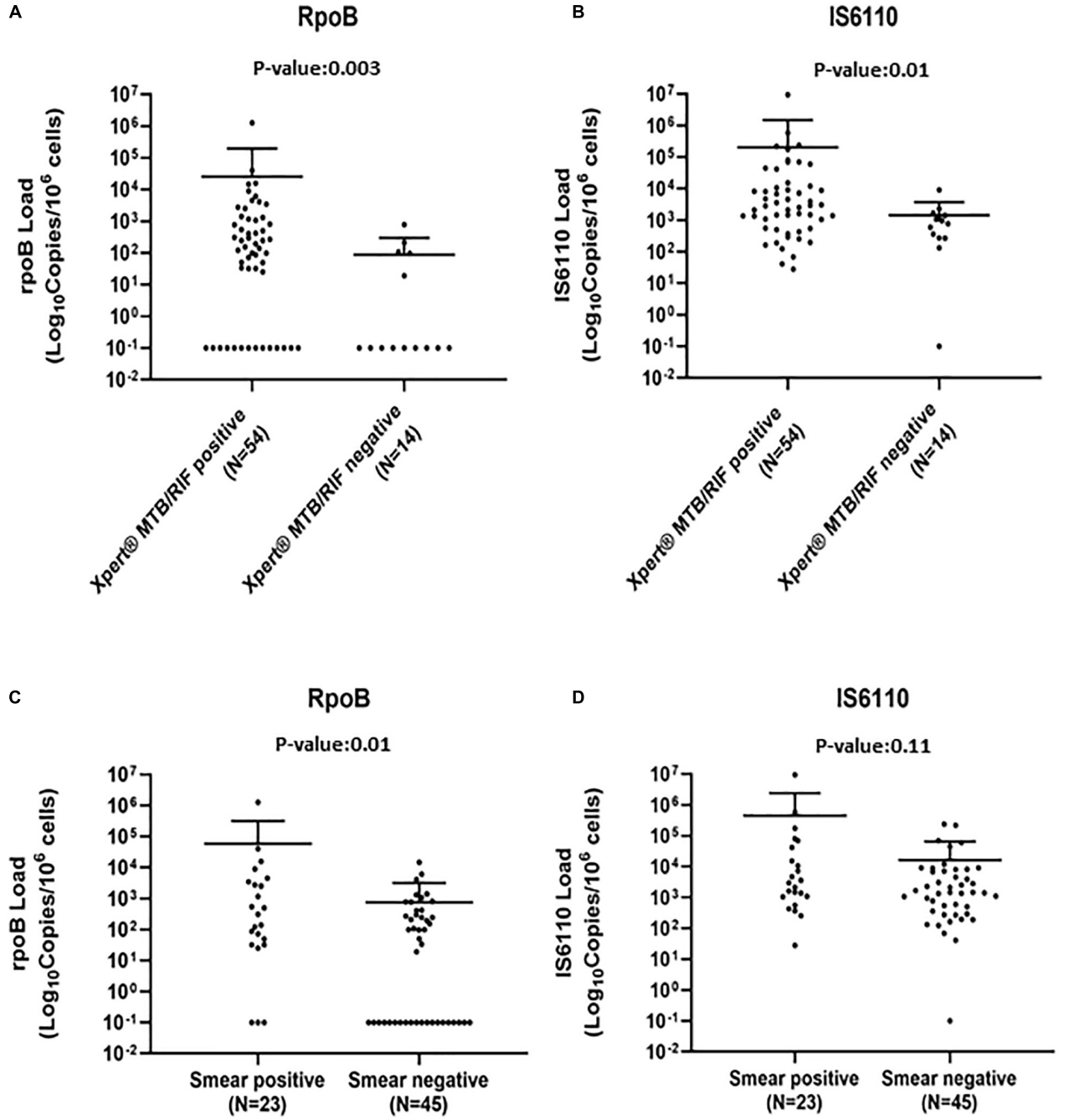

FIGURE 2 | *Mycobacteria tuberculosis* (MTB) *rpoB* and *IS6110* load against Xpert **(A,B)** and acid-fast bacilli (AFB) smear **(C,D)** results. Each value was represented by a dot; bars represent median and interquartile range (IQR). *p*-Values were calculated by Wilcoxon rank sum test and Kruskal–Wallis where necessary.

tuberculosis, nor a difference was found against sex, age, or site of biopsies. Both assays maintain the ability to rule out MTB from culture-negative samples (specificity: 100%).

Our results are consistent with other published papers (Patterson et al., 2018; Song et al., 2018; Cho et al., 2020) reporting the rapid detection of MTB DNA in clinical or cultural samples by ddPCR system. In 2017, Yang et al. (2017) used a *IS6110* ddPCR assay to quantify MTB DNA in the whole blood of patients with pulmonary and extrapulmonary TB, proving that this technique can have the potential to be included in TB routine diagnosis. Two years later, Nyaruaba et al. (2019) stated that ddPCR technology offers enormous advantages for MTB diagnosis, such as unparalleled sensitivity, high precision, and absolute quantification, over common molecular diagnostic platforms like the qPCR. In 2020, Cao et al. (2020) used a homemade *IS6110* ddPCR assay for MTB diagnosis in FFPE

samples. Recently, a single dye duplex ddPCR protocol targeting two different MTB IS demonstrates the superiority of this system with respect to qPCR in the detection of MTB in different culture isolates (Nyaruaba et al., 2020).

This preliminary study has some limitations that need to be discussed. First, the monocentric nature of the study prevented us to collect a large number of clinical samples by different body districts, limiting the possibility to draw certain statements. A multicenter study with larger sample size could be helpful and supportive in confirming the results obtained, including the sensitivity and the specificity here reported. Moreover, the Xpert method was only performed on fresh subsamples. This avoided the possibility to compare the performances of ddPCR assay and Xpert method in FFPE subsamples. Ultra-version of the Xpert® MTB/RIF, developed to improve the detection of paucibacillary disease, was not available at the time of the study, and thus, its performance on both fresh and FFPE samples was not assessed. No clinical follow-up was available, and thus, no correlation between mycobacteria load and clinical outcome can be performed. In addition, the negative control population was not selected against other diseases like HIV, asthma, *Leishmania*, toxoplasma, diabetes, and neither this information was retrospectively available. Even if in this study all positive ddPCR results were confirmed to be positive by culture, these molecular assays are unable to discriminate between viable or non-viable bacilli.

Moreover, some disadvantages of ddPCR over other molecular methods need to be mentioned: (1) the system is not widely available; (2) ddPCR implementation is more complex than other standard molecular methods and needs specialized personnel; and (3) the cost per ddPCR reaction is not cheaper than other standard molecular methods (Hindson et al., 2013; Campomenosi et al., 2016).

In spite of these limitations, our study showed preliminary evidence regarding the highly sensitive, accurate, and rapid MTB diagnosis in FFPE samples by ddPCR methods, as defined by the high concordance between IS6110 assay and culture results. The quantitative approach of ddPCR and its performances independent of body districts make this system able to differentiate high bacillary load multisystemic disseminated condition from paucibacillary anatomically compartmentalized TB. Considering these results, the ddPCR approach can be safely introduced in the clinical routine to accelerate MTB diagnosis with respect to culture, as well as to provide reliable results when culture remains unavailable, like in the case of FFPE samples.

DATA AVAILABILITY STATEMENT

The original contributions presented in the study are included in the article/**Supplementary Material**, further inquiries can be directed to the corresponding author.

AUTHOR CONTRIBUTIONS

CA, MA, RS, CFP, and EM contributed to the conception and design of the study. ST, CV, FS, SMV, EB, and EM provided the samples. MA and RS designed and conducted the experiments with the help of CL, SR, VM, ST, LG, LC, and GM. CR, VC, CV, LRC, AB, and AG helped with the clinical characterization of the patients. MA, RS, and CA analyzed and interpreted the data and wrote the manuscript. CA, CFP, EM, AB, and AG critically revised the manuscript. All authors contributed to the article and approved the submitted version.

FUNDING

This research was funded by the Italian "Ministero dell'Istruzione, dell'Università e della Ricerca" (Grant No. ARS01_00530).

SUPPLEMENTARY MATERIAL

The Supplementary Material for this article can be found online at: https://www.frontiersin.org/articles/10.3389/fmicb.2021.727774/full#supplementary-material

Supplementary Figure 1 | Quantasoft panel for *IS6110* (green) and *rpoB* (blue) of all 20 negative samples, 2 non-tuberculous extracts [*M. abscessus* subsp. *abscessus* (MBABAB) and *M. abscessus* subsp. *bolletii* (MBABBO)], and 1 positive control.

Supplementary Figure 2 | Quantasoft panel for *IS6110* (green) and *rpoB* (blue) of positive control (Pos Ctrl; H37Rv), four positive samples (repeated in duplicate), and a negative sample (repeated in duplicate).

Supplementary Figure 3 | Human albumine quantification in the 89 samples, expressed as copies/μl. Dots represent MTB positive culture samples, while triangles represent MTB negative culture samples; bars represent median and interquartile range (IQR).

Supplementary Figure 4 | MTB *rpoB* and *IS6110* load against new and past MTB diagnoses **(A,B)**, sex **(C,D)**, age **(E,F)**, and anatomical compartments **(G,H)**. Each value was represented by a dot; bars represent median and interquartile range (IQR). *p*-Values were calculated by Wilcoxon rank sum test and Kruskal–Wallis where necessary.

REFERENCES

Ahmed, H. G. E., Nassar, A. S., and Ginawi, I. (2011). Screening for tuberculosis and its histological pattern in patients with enlarged lymph node. *Patholog. Res. Int.* 2011, 1–4. doi: 10.4061/2011/417635

Allahyartorkaman, M., Mirsaeidi, M., Hamzehloo, G., Amini, S., Zakiloo, M., and Nasiri, M. J. (2019). Low diagnostic accuracy of Xpert MTB/RIF assay for extrapulmonary tuberculosis: A multicenter surveillance. *Sci. Rep.* 9:55112. doi: 10.1038/s41598-019-55112-y

Alteri, C., Cento, V., Antonello, M., Colagrossi, L., Merli, M., Ughi, N., et al. (2020). Detection and quantification of SARS-CoV-2 by droplet digital PCR in real-time PCR negative nasopharyngeal swabs from suspected COVID-19 patients. *PLoS One* 15:236311. doi: 10.1371/journal.pone.0236311

Armbruster, D. A., and Pry, T. (2008). Limit of blank, limit of detection and limit of quantitation. *Clin. Biochem. Rev.* 29(Suppl. 1), S49–S52.

Aydemir, O., Karakece, E., Koroglu, M., Altindis, M., and Terzi, H. A. (2019). Comparison of the GeneXpert® MTB/RIF test and conventional methods in the diagnosis of mycobacterium tuberculosis. *Clin. Lab.* 65, 1–6. doi: 10.7754/Clin.Lab.2018.180613

Bahador, A., Etemadi, H., Kazemi, B., Ghorbanzadeh, R., Nakhjavan, F. A., and Nejad, Z. A. (2005). Performance Assessment of IS1081-PCR for direct detection of tuberculous pleural effusion:compared to rpoB-PCR. *Res. J. Agric. Biol. Sci.* 2005, 142–145.

Bahr, N. C., Nuwagira, E., Evans, E. E., Cresswell, F. V., Bystrom, P. V., Byamukama, A., et al. (2018). Diagnostic accuracy of Xpert MTB/RIF Ultra for tuberculous meningitis in HIV-infected adults: a prospective cohort study. *Lancet Infect. Dis.* 18, 68–75. doi: 10.1016/S1473-3099(17)30474-7

Bisognin, F., Lombardi, G., Lombardo, D., Carla Re, M., and Dal Monte, P. (2018). Improvement of Mycobacterium tuberculosis detection by Xpert MTB/RIF Ultra: A head-to-head comparison on Xpert-negative samples. *PLoS One* 13:201934. doi: 10.1371/journal.pone.0201934

Budvytiene, I., and Banaei, N. (2020). Simple processing of formalin-fixed paraffin-embedded tissue for accurate testing with the xpert MTB/RIF assay. *J. Clin. Microbiol.* 58:19. doi: 10.1128/JCM.01905-19

Campomenosi, P., Gini, E., Noonan, D. M., Poli, A., D'Antona, P., Rotolo, N., et al. (2016). A comparison between quantitative PCR and droplet digital PCR technologies for circulating microRNA quantification in human lung cancer. *BMC Biotechnol.* 60:2927. doi: 10.1186/s12896-016-0292-7

Cao, Z., Wu, W., Wei, H., Gao, C., Zhang, L., Wu, C., et al. (2020). Using droplet digital PCR in the detection of Mycobacterium tuberculosis DNA in FFPE samples. *Int. J. Infect. Dis.* 99, 77–83. doi: 10.1016/j.ijid.2020.07.045

Caulfield, A. J., and Wengenack, N. L. (2016). Diagnosis of active tuberculosis disease: From microscopy to molecular techniques. *J. Clin. Tuberc. Other Mycobact. Dis.* 4, 33–43. doi: 10.1016/j.jctube.2016.05.005

Caviglia, G. P., Abate, M. L., Tandoi, F., Ciancio, A., Amoroso, A., Salizzoni, M., et al. (2018). Quantitation of HBV cccDNA in anti-HBc-positive liver donors by droplet digital PCR: A new tool to detect occult infection. *J. Hepatol.* 69, 301–307. doi: 10.1016/j.jhep.2018.03.021

Chen, B., Jiang, Y., Cao, X., Liu, C., Zhang, N., and Shi, D. (2021). Droplet digital PCR as an emerging tool in detecting pathogens nucleic acids in infectious diseases. *Clin. Chim. Acta* 517, 156–161. doi: 10.1016/j.cca.2021.02.008

Cho, S. M., Shin, S., Kim, Y., Song, W., Hong, S. G., Jeong, S. H., et al. (2020). A novel approach for tuberculosis diagnosis using exosomal DNA and droplet digital PCR. *Clin. Microbiol. Infect.* 26:942. doi: 10.1016/j.cmi.2019.11.012

Dorman, S. E., Schumacher, S. G., Alland, D., Nabeta, P., Armstrong, D. T., King, B., et al. (2018). Xpert MTB/RIF Ultra for detection of Mycobacterium tuberculosis and rifampicin resistance: a prospective multicentre diagnostic accuracy study. *Lancet Infect. Dis.* 18, 76–84. doi: 10.1016/S1473-3099(17)30691-6

Du, W. L., Song, J., Wang, J. G., Liu, Z. C., Li, K., Wang, Y. X., et al. (2019). Performance of xpert MTB/RIF Ultra and Xpert MTB/RIF for the diagnosis of tuberculosis through testing of formalin-fixed Paraffin-embedded Tissues. *Biomed. Environ. Sci.* 32, 922–925. doi: 10.3967/bes2019.115

El-Zammar, O. A., and Katzenstein, A. L. A. (2007). Pathological diagnosis of granulomatous lung disease: a review. *Histopathology* 50, 289–310. doi: 10.1111/j.1365-2559.2006.02546.x

Eshete, A., Zeyinudin, A., Ali, S., Abera, S., and Mohammed, M. (2011). M. tuberculosis in Lymph node biopsy paraffin-embedded sections. *Tuberc. Res. Treat.* 2011, 1–5. doi: 10.1155/2011/127817

European Centre for Disease Prevention and Control (ECDC) (2018). *Handbook on tuberculosis laboratory diagnostic methods in the European Union*. Solna Municipality: ECDC.

Forbes, B. A., and Hicks, K. E. S. (1993). Direct detection of Mycobacterium tuberculosis in respiratory specimens in a clinical laboratory by polymerase chain reaction. *J. Clin. Microbiol.* 31, 1688–1694. doi: 10.1128/jcm.31.7.1688-1694.1993

Forbes, B. A., Miller, M. B., Banaei, N., Brown-Elliott, B. A., Das, S., Salfinger, M., et al. (2018). *Laboratory Detection and Identification of Mycobacteria. M48-A. 2nd ed*. Annapolis Junction, MD: CLSI.

Fu, Y. C., Liao, I. C., Chen, H. M., and Yan, J. J. (2016). Detection of Mycobacterium tuberculosis complex in paraffin-embedded tissues by the new automated Abbott RealTime MTB Assay. *Ann. Clin. Lab. Sci.* 46, 412–417.

Fukunaga, H., Murakami, T., Gondo, T., Sugi, K., and Ishihara, T. (2002). Sensitivity of acid-fast staining for Mycobacterium tuberculosis in formalin-fixed tissue. *Am. J. Respir. Crit. Care Med.* 166, 994–997. doi: 10.1164/rccm.2111028

Golden, M. P. (2005). *Extrapulmonary tuberculosis: an overview. Am. Fam. Physician* 72, 1761–1768

Hindson, C. M., Chevillet, J. R., Briggs, H. A., Gallichotte, E. N., Ruf, I. K., Hindson, B. J., et al. (2013). Absolute quantification by droplet digital PCR versus analog real-time PCR. *Nat. Methods* 2013, 1003–1005. doi: 10.1038/nmeth.2633

Huang, S., Qin, M., Shang, Y., Fu, Y., Liu, Z., Dong, Y., et al. (2020). Performance of Xpert MTB/RIF in diagnosis of lymphatic tuberculosis from fresh and formaldehyde-fixed and paraffin embedded lymph nodes. *Tuberculosis* 124:101967. doi: 10.1016/j.tube.2020.101967

Karadağ, A., Usta, E., Bilgin, K., Güney, A. K., Eroğlu, C., and Günaydin, M. (2013). Comparison of culture, real-time DNA amplification assay and Ehrlich-Ziehl-Neelsen for detection of Mycobacterium tuberculosis. *Balkan Med. J.* 30, 13–15. doi: 10.5152/balkanmedj.2012.061

Kohli, M., Schiller, I., Dendukuri, N., Yao, M., Dheda, K., Denkinger, C. M., et al. (2021). Xpert MTB/RIF Ultra and Xpert MTB/RIF assays for extrapulmonary tuberculosis and rifampicin resistance in adults. *Cochrane Database Syst. Rev.* 2021:CD012768. doi: 10.1002/14651858.CD012768.pub3

Kolia-Diafouka, P., Carrère-Kremer, S., Lounnas, M., Bourdin, A., Kremer, L., Van de Perre, P., et al. (2019). Detection of Mycobacterium tuberculosis in paucibacillary sputum: performances of the Xpert MTB/RIF ultra compared to the Xpert MTB/RIF, and IS6110 PCR. *Diagn. Microbiol. Infect. Dis.* 94, 365–370. doi: 10.1016/j.diagmicrobio.2019.02.008

Lee, H. S., Park, K. U., Park, J. O., Chang, H. E., Song, J., and Choe, G. (2011). Rapid, sensitive, and specific detection of Mycobacterium tuberculosis complex by real-time PCR on paraffin-embedded human tissues. *J. Mol. Diagnostics* 13, 390–394. doi: 10.1016/j.jmoldx.2011.02.004

Lee, J., Choi, S. M., Lee, C. H., Lee, S. M., Yim, J. J., Yoo, C. G., et al. (2017). The additional role of Xpert MTB/RIF in the diagnosis of intrathoracic tuberculous lymphadenitis. *J. Infect. Chemother.* 23, 381–384. doi: 10.1016/j.jiac.2017.03.001

Lin, C. R., Wang, H. Y., Lin, T. W., Lu, J. J., Hsieh, J. C. H., and Wu, M. H. (2021). Development of a two-step nucleic acid amplification test for accurate diagnosis of the Mycobacterium tuberculosis complex. *Sci. Rep.* 11:5750. doi: 10.1038/s41598-021-85160-2

Malin, K., Louise, B. M., Gisela, H., Mats, K. G., and Gabriella, L.-L. (2021). Optimization of droplet digital PCR assays for the type-specific detection and quantification of five HPV genotypes, including additional data on viral loads of nine different HPV genotypes in cervical carcinomas. *J. Virol. Methods* 294:114193. doi: 10.1016/j.jviromet.2021.114193

Marchetti, G., Gori, A., Catozzi, L., Vago, L., Nebuloni, M., Rossi, M. C., et al. (1998). Evaluation of PCR in detection of Mycobacterium tuberculosis from formalin-fixed, paraffin-embedded tissues: Comparison of four amplification assays. *J. Clin. Microbiol.* 36, 1512–1517. doi: 10.1128/jcm.36.6.1512-1517.1998

Mazzola, E., Arosio, M., Nava, A., Fanti, D., and Gesu, G. (2016). Performance of real-time PCR Xpert ® MTB/RIF in diagnosing extrapulmonary tuberculosis. *Infez. Med.* 4, 304–309.

Molicotti, P., Bua, A., and Zanetti, S. (2014). Cost-effectiveness in the diagnosis of tuberculosis: Choices in developing countries. *J. Infect. Dev. Ctries.* 8, 24–38. doi: 10.3855/jidc.3295

Moure, Z., Castellví, J., Sánchez-Montalvá, A., Pumarola, T., and Tórtola, M. T. (2019). The role of molecular techniques for the detection of mycobacterium tuberculosis complex in paraffin-embedded biopsies. *Appl. Immunohistochem. Mol. Morphol.* 27, 77–80. doi: 10.1097/PAI.0000000000000533

Njau, A. N., Gakinya, S. M., Sayed, S., and Moloo, Z. (2019). Xpert® MTB/RIF assay on formalin-fixed paraffin-embedded tissues in the diagnosis of extrapulmonary tuberculosis. *Afr. J. Lab. Med.* 8:748. doi: 10.4102/ajlm.v8i1.748

Noussair, L., Bert, F., Leflon-Guibout, V., Gayet, N., and Nicolas-Chanoine, M. H. (2009). Early diagnosis of extrapulmonary tuberculosis by a new procedure combining broth culture and PCR. *J. Clin. Microbiol.* 47, 1452–1457. doi: 10.1128/JCM.00066-09

Nyaruaba, R., Mwaliko, C., Kering, K. K., and Wei, H. (2019). Droplet digital PCR applications in the tuberculosis world. *Tuberculosis* 117, 85–92. doi: 10.1016/j.tube.2019.07.001

Nyaruaba, R., Xiong, J., Mwaliko, C., Wang, N., Kibii, B. J., Yu, J., et al. (2020). Development and evaluation of a single dye duplex droplet digital PCR assay for the rapid detection and quantification of mycobacterium tuberculosis. *Microorganisms* 8:8050701. doi: 10.3390/microorganisms8050701

Patterson, B., Morrow, C., Singh, V., Moosa, A., Gqada, M., Woodward, J., et al. (2018). Detection of bacilli in Mycobacterium tuberculosis bio-aerosols from untreated TB patients. *Gates Open Res.* 1:11. doi: 10.12688/gatesopenres.12758.2

Pk, M., Mp, N., and Dn, M. (2017). Performance of GeneXpert assay in detecting pulmonary tuberculosis and rifampicin resistance in patients attending kitui county hospital, kenya. *J. Tropical Dis. Public Health* 2017:246. doi: 10.4172/2329-891X.1000246

Polepole, P., Kabwe, M., Kasonde, M., Tembo, J., Shibemba, A., O'Grady, J., et al. (2017). Performance of the Xpert MTB/RIF assay in the diagnosis of tuberculosis in formalin-fixed, paraffin-embedded tissues. *Int. J. Mycobacteriol.* 6, 87–93. doi: 10.4103/2212-5531.201892

Riccardi, N., Ferrarese, M., Castellotti, P., Mazzola, E., Sozzi, F., Rigatti, P., et al. (2020). A rare case of multi-focal human TB after BCG instillation for non-muscle-invasive bladder cancer. *Urol. J.* 87, 199–202. doi: 10.1177/0391560319860396

Ryu, Y. J. (2015). Diagnosis of pulmonary tuberculosis: Recent advances and diagnostic algorithms. *Tuberc. Respir. Dis.* 78, 64–71. doi: 10.4046/trd.2015.78.2.64

Sadeghipour, A., and Babaheidarian, P. (2019). Making formalin-fixed, paraffin embedded blocks. *Methods Mol. Biol.* 1897, 253–268. doi: 10.1007/978-1-4939-8935-5_22

Sarfaraz, S., Iftikhar, S., Memon, Y., Zahir, N., Hereker, F. F., and Salahuddin, N. (2018). Histopathological and microbiological findings and diagnostic performance of GeneXpert in clinically suspected tuberculous lymphadenitis. *Int. J. Infect. Dis.* 76, 73–81. doi: 10.1016/j.ijid.2018.08.020

Sarnecka, A. K., Nawrat, D., Piwowar, M., Ligęza, J., Swadźba, J., and Wójcik, P. (2019). DNA extraction from FFPE tissue samples – a comparison of three procedures. *Wspolczesna Onkol.* 23, 52–58. doi: 10.5114/wo.2019.83875

Sauzullo, I., Maria Rodio, D., Facchinetti, S., Puggioni, G., De Angelis, M., Goldoni, P., et al. (2016). Diagnostic accuracy of Xpert MTB/RIF versus smear microscopy in the early diagnosis of tuberculosis in the real life of the "Umberto I" Hospital in Rome. *New Microbiol.* 39, 304–306.

Seo, A. N., Park, H. J., Lee, H. S., Park, J. O., Chang, H. E., Nam, K. H., et al. (2014). Performance characteristics of nested polymerase chain reaction vs real-time polymerase chain reaction methods for detecting mycobacterium tuberculosis complex in paraffin-embedded human tissues. *Am. J. Clin. Pathol.* 142, 384–390. doi: 10.1309/AJCP2QZRH4ZNPRDD

Slaoui, M., and Fiette, L. (2011). Histopathology procedures: from tissue sampling to histopathological evaluation. *Methods Mol. Biol.* 691, 69–82. doi: 10.1007/978-1-60761-849-2_4

Song, N., Tan, Y., Zhang, L., Luo, W., Guan, Q., Yan, M. Z., et al. (2018). Detection of circulating Mycobacterium tuberculosis-specific DNA by droplet digital PCR for vaccine evaluation in challenged monkeys and TB diagnosis article. *Emerg. Microbes. Infect.* 7:76. doi: 10.1038/s41426-018-0076-3

Strain, M. C., Lada, S. M., Luong, T., Rought, S. E., and Gianella, S. (2013). Highly precise measurement of HIV DNA by droplet digital PCR. *PLoS One* 8:55943. doi: 10.1371/journal.pone.0055943

Sulis, G., Agliati, A., Pinsi, G., Bozzola, G., Foccoli, P., Gulletta, M., et al. (2018). Xpert MTB/RIF as add-on test to microscopy in a low tuberculosis incidence setting. *Eur. Respir. J.* 51:2017. doi: 10.1183/13993003.02345-2017

Tortoli, E., Russo, C., Piersimoni, C., Mazzola, E., Dal Monte, P., Pascarella, M., et al. (2012). Clinical validation of Xpert MTB/RIF for the diagnosis of extrapulmonary tuberculosis. *Eur. Respir. J.* 40, 442–447. doi: 10.1183/09031936.00176311

World Health Organization (WHO). (2012). *Tuberculosis laboratory biosafety manual*.Geneva: WHO.

World Health Organization (WHO). (2013). *Definitions and reporting framework for tuberculosis*. Geneva: WHO.

World Health Organization (WHO). (2020). *Global tuberculosis report 2020*. Geneva: WHO.

Yang, J., Han, X., Liu, A., Bai, X., Xu, C., Bao, F., et al. (2017). Use of digital droplet PCR to detect Mycobacterium tuberculosis DNA in whole blood-derived DNA samples from patients with pulmonary and extrapulmonary tuberculosis. *Front. Cell. Infect. Microbiol.* 7:369. doi: 10.3389/fcimb.2017.00369

Conflict of Interest: The authors declare that the research was conducted in the absence of any commercial or financial relationships that could be construed as a potential conflict of interest.

Publisher's Note: All claims expressed in this article are solely those of the authors and do not necessarily represent those of their affiliated organizations, or those of the publisher, the editors and the reviewers. Any product that may be evaluated in this article, or claim that may be made by its manufacturer, is not guaranteed or endorsed by the publisher.

frontiers in Microbiology

ORIGINAL RESEARCH
published: 22 September 2021
doi: 10.3389/fmicb.2021.735166

Dihydroartemisinin-Loaded Chitosan Nanoparticles Inhibit the Rifampicin-Resistant *Mycobacterium tuberculosis* by Disrupting the Cell Wall

Xiujuan Gu[1,2], Qi Cheng[3], Ping He[4], Yan Zhang[2], Zhengfang Jiang[2] and Yali Zeng[2]**

[1] Department of Clinical Laboratory, Affiliated Hospital of Southwest Medical University, Luzhou, China, [2] Department of Clinical Laboratory, Sichuan Mianyang 404 Hospital, Mianyang, China, [3] Respiratory Medicine, Chengdu Seventh People's Hospital, Chengdu, China, [4] School of Materials Science and Engineering, Southwest University of Science and Technology, Mianyang, China

OPEN ACCESS

Edited by:
Xiao-Yong Fan,
Fudan University, China

Reviewed by:
Anima Nanda,
Sathyabama Institute of Science and Technology, India
Xiuzhu Dong,
Institute of Microbiology, Chinese Academy of Sciences, China

***Correspondence:**
Zhengfang Jiang
2375351899@qq.com
Yali Zeng
631734429@qq.com

Specialty section:
This article was submitted to Infectious Diseases, a section of the journal Frontiers in Microbiology

Received: 02 July 2021
Accepted: 23 August 2021
Published: 22 September 2021

Citation:
Gu XJ, Cheng Q, He P, Zhang Y, Jiang ZF and Zeng YL (2021) Dihydroartemisinin-Loaded Chitosan Nanoparticles Inhibit the Rifampicin-Resistant Mycobacterium tuberculosis by Disrupting the Cell Wall. Front. Microbiol. 12:735166. doi: 10.3389/fmicb.2021.735166

Tuberculosis (TB) caused by *Mycobacterium tuberculosis* (MTB) is a deadly infection, and increasing resistance worsens an already bad scenario. In this work, a new nanomedicine antibacterial agent, based on dihydroartemisinin (DHA) and chitosan (CS), has been successfully developed to overcome MTB's drug-resistant. To enhance DHA's solubility, we have prepared nanoparticles of DHA loaded CS by an ionic crosslinking method with sodium tripolyphosphate (STPP) as the crosslinking agent. The DHA-CS nanoparticles (DHA-CS NPs) have been fully characterized by scanning electron microscopy, Fourier transforms infrared spectroscopy, dynamic light scattering, and ultraviolet spectrophotometry. DHA-CS NPs show an excellent antibacterial effect on the rifampicin (RFP)-resistant strain (ATCC 35838) and, at a concentration of 8.0 μg/ml, the antibacterial impact reaches up to 61.0 ± 2.13% (n = 3). The results of Gram staining, acid-fast staining, auramine "O" staining and electron microscopy show that the cell wall of RFP-resistant strains is destroyed by DHA-CS NPs (n = 3), and it is further verified by gas chromatography-mass spectrometry. Since all the metabolites identified in DHA-CS NPs treated RFP-resistant strains indicate an increase in fatty acid synthesis and cell wall repair, it can be concluded that DHA-CS NPs act by disrupting the cell wall. In addition, the resistance of 12 strains is effectively reduced by 8.0 μg/ml DHA-CS NPs combined with RFP, with an effective rate of 66.0%. The obtained results indicate that DHA-CS NPs combined with RFP may have potential use for TB treatment.

Keywords: ***Mycobacterium tuberculosis*, rifampin-resistance, dihydroartemisinin, chitosan, nanoparticle, gas chromatography-mass spectrometry, metabolomics**

INTRODUCTION

Caused by *Mycobacterium tuberculosis* (MTB), tuberculosis (TB) is a chronic infectious disease with high mortality rate. TB incidence has been gradually increasing in recent years, and it has become a significant global public health problem (Stein et al., 2008). According to the worldwide progress report on tuberculosis elimination 2020, TB still accounts for the highest mortality from

any infectious diseases worldwide, causing 1.5 million deaths in 2018. In addition, approximately half a million new cases of rifampicin (RFP)-resistant TB were reported with 78.0% multidrug-resistant TB (MDR-TB) in 2018 (Harding, 2020). According to the global tuberculosis report 2019, the latest treatment data has shown that the treatment success rate of MDR-TB is 56.0%, and extensively severe drug-resistant TB (XDR-TB) is almost impossible to incurable. Both MDR-TB and XDR-TB are resistant to RFP. Therefore, developing anti-TB new drugs is a practical approach to the treatment of RFP-resistant TB (Dheda et al., 2014; Maitre et al., 2017).

Artemisinin is one of sesquiterpene lactone peroxides isolated from the Chinese plant *Artemisia annua* L. Multiple derivatives with active metabolite dihydroartemisinin (DHA) have been developed with improved pharmacological features (Zhu, 2014). The pharmacological effects of DHA mainly include antimalarial, antitumoral, antischistosomal, and antibacterial activities (Meshnick et al., 1993; Want et al., 2015). Recent studies have confirmed that artemisinin derivatives have bacteriostatic effects on MTB (Zhang et al., 2014; Beg et al., 2017; Upadhyay et al., 2017; Wais et al., 2017). However, artemisinin derivatives have also disadvantages such as poor water solubility, low bioavailability, short duration of effective blood drug concentration and rapid excretion (Jin, 2020). Nowadays, no in-depth studies have been conducted on the application of artemisinin drugs for TB prevention.

Nanomedicine refers to the use of nanotechnology to prepare drugs and corresponding carriers into a new class of pharmaceuticals with a particle size ranging from 1 to 1,000 nm (Satalkar et al., 2016). It can improve drug absorption and drug efficacy, increase drug stability, enhance drug targeting, and reduce drug toxicity (Rani et al., 2018; Kumari et al., 2019; Martinelli et al., 2019; Wang et al., 2019). CS is a natural polymer with peculiar benefits, such as biocompatibility, biodegradability, non-toxicity, mucoadhesion and antibacterial properties, and can activate macrophages to increase the bactericidal activity (Hou and Zhao, 2006; Kucukoglu et al., 2019; Radwan-Pragłowska et al., 2019). MTB can persist in an immune-competent host via several immune evasion strategies, such as altered antigen presentation to prevent the recognition of infected macrophages by T cells, thereby evading macrophage killing mechanisms (Sia and Rengarajan, 2019). Therefore, chitosan is expected to become an effective carrier for the treatment of TB.

In this work, DHA-CS nanoparticles (DHA-CS NPs) were prepared using CS as the drug carrier to investigate the antibacterial activity of DHA-CS NPs on RFP-resistant strains and the mechanism of action. It would lay a substantial foundation for the clinical application of DHA-CS NPs.

MATERIALS AND METHODS

Bacterial Culture

Eighteen clinical drug-resistant strains and one RFP-resistant MTB strain (ATCC 35838) were obtained from Mianyang Centers for Disease Control and Prevention (CDC), China, and stored in a refrigerator at −80°C. The information about strains is shown in **Table 1**. MTB strains were inoculated on L-J medium (Shanghai Yiheng Scientific Instruments Co., Ltd., Shanghai, China) and cultured at 37∘C in a 5% CO_2 incubator (Zhou et al., 2017).

Materials

DHA was purchased from Ron Reagent Company (Shanghai, China). CS with molecular weight 50–190 kDa (degree of deacetylation > 95.0%) was purchased from Guanghan Hengyu New Materials Co., Ltd. (Chengdu, China). Sodium tripolyphosphate (STPP) was provided by Southwest University of Science and Technology, Sichuan, China.

Preparation of DHA-CS NPs

DHA-CS NPs were produced using ionic-gelation methods with STPP. 50.0 mg CS was dissolved in 50 ml 1.0% acetic acid solution. 10.0 mg DHA and 10.0 mg STPP were dissolved in 10 ml absolute ethanol. Then, DHA-STPP ethanol solution was slowly dripped into the CS solution with magnetic stirring at 1,000 rpm and stirred at 60°C for 2 h. CS NPs were prepared with the same method.

Morphology and Particle Size and FTIR Spectrum

DHA-CS NPs were diluted to 0.50 μg/ml using distilled water. The morphology of DHA-CS NPs was observed by scanning electron microscope (SEM) (Ultra 55, ZEISS, Heidenheim, Germany). Particle sizes and dispersion index of DHA-CS NPs were analyzed using a laser particle size analyzer (90 plus, Brookhaven, Waltham, MS, United States). Fourier transform infrared (FTIR) spectrometer (Nicolet 6700, Thermo Fisher Scientific, Waltham, MA, United States) was used to identify the chemical compounds of samples.

TABLE 1 | Information on strains.

Serial number	Name	Source	Drug-resistance
1	Clinical isolates	Mianyang CDC	RFP
2	Clinical isolates	Mianyang CDC	RFP
3	Clinical isolates	Mianyang CDC	RFP
4	Clinical isolates	Mianyang CDC	RFP, INH, EMB
5	Clinical isolates	Mianyang CDC	RFP, INH
6	Clinical isolates	Mianyang CDC	RFP
7	Clinical isolates	Mianyang CDC	RFP, INH, EMB
8	Clinical isolates	Mianyang CDC	RFP
9	Clinical isolates	Mianyang CDC	RFP
10	Clinical isolates	Mianyang CDC	RFP
11	Clinical isolates	Mianyang CDC	RFP, INH
12	Clinical isolates	Mianyang CDC	RFP
13	Clinical isolates	Mianyang CDC	RFP
14	Clinical isolates	Mianyang CDC	RFP
15	Clinical isolates	Mianyang CDC	RFP
16	Clinical isolates	Mianyang CDC	RFP, INH
17	Clinical isolates	Mianyang CDC	RFP
18	Clinical isolates	Mianyang CDC	RFP, INH
19	ATCC35838	Mianyang CDC	RFP

Entrapment Efficiency and Drug Loading

10.0 mg DHA was added into a 100 ml volumetric flask and made up to 100 ml with 2.0% NaOH aqueous solution and ethanol (4:1, v/v). The DHA solution was incubated for 2 h to obtain a 100.0 μg/ml standard solution. 0.20, 0.60, 1.0, 1.4, 1.8 ml standard solutions were put into different volumetric flasks (10 ml) and then heated in a water bath at 60°C for 30 min. The absorbance of sample solutions was measured in the wavelength range of 200–400 nm by an ultraviolet spectrophotometer (Evolution 300, Thermo Fisher Scientific, Waltham, MA, United States). Then, the linear regression of DHA concentration (C) with DHA absorbance (A) was obtained.

500 μl DHA-CS NPs were placed into an ultrafiltration centrifuge tube (Beijing Cedoris Scientific Instruments Co., Ltd., Beijing, China) and centrifuged at 3,340 *g* (TGL-18M, BIOBASE, Lu Xiangyi Centrifuge Co., Ltd., Shanghai, China) for 15 min. Equal amounts of ultrafiltration solutions and non-centrifuged DHA-CS NPs were placed into different volumetric flasks (10 ml) and made up to 10 ml with 2.0% NaOH aqueous solution and ethanol (4:1, v/v). The two volumetric flasks were incubated in a water bath at 60°C for 30 min. Finally, the absorbance of free DHA in centrifuged and non-centrifuged DHA-CS NPs solutions was measured. The entrapment efficiency and drug loading of DHA-CS NPs were calculated as follows:

Entrapment efficiency (%) = (total mass of DHA—mass of free DHA)/total mass of DHA × 100% (1)

Drug loading (%) = (total mass of DHA—mass of free DHA)/total mass of nano-DHA composite × 100% (2)

Preparation of Bacterial Suspension

3–4 drops of 0.50% Tween 80 and resistant MTB colonies grown on L-J medium for 3–4 weeks were placed into a thick large glass tube. After grinding, 6–8 drops of physiological saline were dropped into the tube and then stood to precipitate large particles of bacteria. Finally, supernatants were aspirated, and Middlebrook 7H9 Broth Base (Sigma, San Francisco, California, United States) was used to adjust the supernatants to 3.0×10^8 CFU/ml.

Optimal Concentration of DHA-CS NPs

The antimicrobial effect of 0.50–256.0 μg/ml drugs on ATCC 35838 MTB was detected by bacterial dead/live ratio testing, and an appropriate drug concentration was selected for the other experiment. Different concentrations (0.50, 1.0, 2.0, 4.0, 8.0, 16, 32, 64, 128, 256 μg/ml) of drugs (DHA-CS NPs, CS NPs, and DHA) and bacterial solutions [diluted to 3.0×10^7 CFU/ml, referenced MTB liquid drug sensitivity kit instructions (Autobio, Shanghai, China)] were added at 100.0 μl/well in 96-well plates (Kangborui Biological Technology Co., Ltd., Chengdu, China). Three parallel holes were set up for each concentration. Negative and blank control groups were established simultaneously and incubated in an incubator at 37°C for 6 days. Then, samples were stained according to the instructions of LIVE/DEADTM BacLight^{TM} Bacterial Viability Kit reagent (Invitrogen, San Francisco, California, United States). The FSC LOG and SSC LOG parameters were selected to establish FSC LOG VS. SSC LOG scatter plots, and the gain and voltage were adjusted to make sure all events are in the plot. Sterile 7H9 solution was used as a blank control to deduct the background noise. Then we used individually stained live bacteria and dead bacteria to adjust the FL1, FL3 voltages, and appropriate compensation value. Finally, the flow cytometry (FC500, Beckman, Waltham, MA, United States) scheme was formulated, and live and dead bacteria areas were delimited (Wu, 2015).

Antibacterial rates were calculated as follows: Antibacterial rate (%) = (number of live bacteria in the control group − number of live bacteria in the experimental group)/number of live bacteria in the control group × 100%.

Then, the optimal concentration for the next experiments was selected by bacterial live/dead ratio testing.

Group-wise differences were tested by one-way ANOVA or *t*-test using SPSS 17.0, and p-value < 0.05 was considered to be statistically significant.

Auramine "O" Staining, Acid-Fast Staining and Gram Staining

Auramine "O" staining, acid-fast staining and Gram staining (Baso, Zhuhai, China) methods were used to observe the number and morphology of ATCC 35838 MTB in the presence and absence of drugs. DHA-CS NPs, CS NPs, and free DHA with the final concentration of 8.0 μg/ml were separately added to bacterial suspensions (3.0×10^8 CFU/ml), and three parallel trials were set up for each drug. The negative control group was established simultaneously. Then, samples were incubated at 37°C in a 5% CO_2 incubator for 6 days. After that, the suspension was centrifuged for 10 min at 4,000 *g* to remove excess supernatant and retain only 20 μl. After mixing, precipitates were placed on different slides and smeared as a 2 cm diameter circular film. After UV irradiation for 2 h, MTB was subjected to staining. Finally, MTB of auramine "O" staining was observed using a fluorescence microscope at 400× magnification (E 100, Nikon, Tokyo, Japan). MTB of acid-fast staining and Gram staining was observed at 1,000× magnification by oil immersion technique (BX 43, Olympus, Tokyo, Japan).

SEM

SEM was used to observe ATCC 35838 MTB's structure in the presence and absence of drugs. DHA-CS NPs, CS NPs and free DHA with the final concentration of 8.0 μg/ml were added to bacterial suspensions (3.0×10^8 CFU/ml), and three parallel trials were set up. The negative control group was established simultaneously. Then samples were cultured at 37°C in a 5% CO_2 incubator for 6 days.

After centrifuged for 13 min at 300 *g*, supernatants were discarded. 50 μl residues were placed on glass slides and fixed with 3% glutaraldehyde for 30 min, then washed three times with dH_2O. The slides were air-dried and dehydrated by a graded series of ethanol (30, 50, 70, 80, 90, and 95%) for 15 min at each step, and finally dehydrated two times by absolute ethanol for 20 min. After that, samples were dried ambiently, and the morphology of MTB was observed using field emission SEM.

Metabolomics Analysis

The influence of DHA-CS NPs on MTB metabolic pathway was detected by metabolic omics method. ATCC 35838 RFP-resistant strain was suspended to approximately 1.0×10^7 colony-forming units CFU/ml (van Breda et al., 2015; Koen et al., 2018). Cell suspensions (2.0 ml) and DHA-CS NPs (final concentrations of 0.0 and 8.0 μg/ml) were added to each 5.0 ml EP tubes. They were incubated at 37°C for 24 h. The three samples containing no DHA-CS NPs and four samples containing 8.0 μg/ml DHA-CS NPs were centrifuged at 10,000 *g* for 1 min, and sediments were collected. 10.0 mg of each sample was placed into an EP tube and extracted with chloroform, methanol and water in a ratio of 1:3:1. Samples were repeatedly placed in liquid nitrogen freeze-thaw 5 times (2 min each time) and sonicated for 30 min in an ice bath, then centrifuged at 10,000 g for 1 min at 4°C. The supernatants were transferred to different sample bottles, and 2.0 μl of 3-phenyl butyric acid (Kangbo Rui Biotechnology Co., Ltd., Chengdu, China) was added as an internal standard (1.75 μg/ml). After freeze-drying, the samples were redissolved in 80 μl methoxyamine hydrochloride in pyridine solution (20.0 mg/ml), and the oximation reaction was performed in a water bath at 50°C for 90 min. Then, methoxyamine hydrochloride-(trimethylsilyl)-trifluoroacetamide (Shanghai Xinyu Biological Technology Co., Ltd., Shanghai, China) derivatization reagent containing 1.0% trimethylchlorosilane (Shanghai Xinyu Biological Technology Co., Ltd., Shanghai, China) was added to each sample. After that, the derivatization reaction was carried out in a 50°C water bath for 90 min (Wang et al., 2015).

Samples (1.0 μl) were analyzed in a random sequence by gas chromatography-mass spectrometer (GC-MS) (TQ8050, Shimadzu Corporation, Tokyo, Japan). Shimadzu HP-5 capillary column (30 m × 250 μm × 0.25 μm) was used for GC separation of compounds. High-purity helium was used as the carrier gas with a carrier gas flow rate of 1.0 ml/min. Interface temperature was 280°C, and inlet temperature was 270°C; initial temperature of column was set to 70°C for 4 min, then raised to 133°C at the rate of 3°C/min, heated to 200°C at the rate of 2°C/min, increased to 220°C and finally heated to 260°C at the rate of 5°C/min. The ionization mode was electron bombardment with an electron energy of 70 eV and a temperature of 230°C. A mass range of 85∼500 m/z was used for the mass spectra.

Mass spectrometry deconvolution, peak alignment and peak identification were carried out on the raw data by GC-MS Solution software (version 2.1). The qualitative analysis was performed by matching with the National Institute of Standards and Technology (NIST). The data were analyzed with SIMCA-P (version 13.0), including principal component analysis (PCA), partial least squares discriminant analysis (PLS-DA) and orthogonal partial least squares discriminant analysis (OPLS-DA). SPSS 17.0 was used to perform *t*-test on the data, and p-value < 0.05 was considered statistically significant.

DHA-CS NPs Combined With RFP

Solid drug sensitivity testing was used to detect whether the combination of DHA-CS NPs and RFP could reduce the resistance of clinical RFP-resistant strains. Bacterial suspensions of eighteen clinical resistant strains (serial number: 1–18) were diluted to 3.0×10^6 CFU/ml and 3.0×10^4 CFU/ml with 0.90% NaCl solution. DHA-CS NPs with final concentrations of 8.0 μg/ml was added to diluted suspensions, and then they were placed at 37°C in a 5% CO_2 incubator for 24 h. Negative control groups were established at the same time (without DHA-CS NPs). Afterward, bacterial suspensions were inoculated on the surface of drug-sensitive solid culture media (Zhuhai Bezo Biotechnology Co., Ltd, Sichuan, China) at 20.0 μl/well, and placed at 37°C in a 5% CO_2 incubator for 1 month.

The tangible medium is a plate with multiple culture wells (**Supplementary Figure 1**). Each culture plate has two wells ("a" and "b") without drugs, and the remaining wells contain anti-tuberculosis drugs. The wells of "c" and "d" are embedded with isoniazid (INH), "e" and "f" wells are embedded with ethambutol (EMB), "g" and "h" wells are embedded with RFP (in this work, only RFP was concerned). Bacterial suspensions of negative control groups were inoculated in "a" and "b" wells, and the DHA-CS NPs drug groups were inoculated in other wells.

RESULTS

Morphology, Particle Size Distribution and Dispersion Index of DHA-CS NPs

To determine the morphology and particle size of DHA-CS NPs, SEM, and laser particle size analyzer were used. The average particle size of DHA-CS NPs was 217.0 ± 8.12 nm, and the dispersion index was 0.342 ± 0.01 ($n = 3$). SEM results showed that the DHA-CS NPs formed a uniform quasi-spherical shape with low polydispersity, and the diameter was consistent with the above particle size measurement results (**Figure 1**).

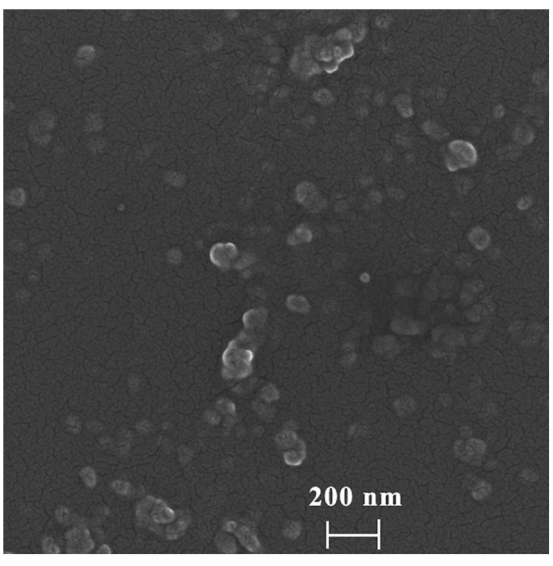

FIGURE 1 | SEM of DHA-CS NPs.

FTIR Assayed DHA Loading on CS NPs

FTIR analysis was used to confirm whether DHA was loaded on CS. DHA, CS NPs, and DHA-CS NPs were aqueous solutions, so the results of FTIR were significantly affected by the characteristic peaks of water. In **Figure 2**, the bands near 3354.0 cm^{-1} and 1639.0 cm^{-1} are ascribed to the characteristic hydroxyl peaks of adsorbed water (Dinache et al., 2020). The absorption peak intensity of CS NPs and DHA-CS NPs near 1639.0 cm^{-1} was significantly stronger than that of DHA and presented the stretching vibration of C = O in amide bond, indicating the successful crosslinking interaction between TPP and the amino groups of CS within CS NPs (Ye et al., 2015). In addition, compared with CS NPs, two new peaks of DHA-CS NPs near 1326.0 cm^{-1} and 1282.0 cm^{-1} were due to the crosslinking interaction between DHA and TPP, indicating that DHA was successfully loaded on CS NPs.

Encapsulation Efficiency and Drug Loading Capacity of DHA-CS NPs

The measured optical densities (ODs) of DHA standard solutions were 0.111, 0.259, 0.404, 0.552, and 0.676, and the OD curve was fitted by the regression equation C = 28.01A–1.22 (R^2 = 0.9992, n = 5). A good linear correlation was found between DHA concentration (C) and OD (A) in the range of 2.0–18.0 μg/ml (**Figure 3**).

According to Equations (1) and (2), the encapsulation efficiency of DHA-CS NPs was calculated to be (76.4 ± 4.53)%, and the drug loading capacity was (7.9 ± 0.12)% (n = 3). The results above indicated the successful preparation of DHA-CS NPs.

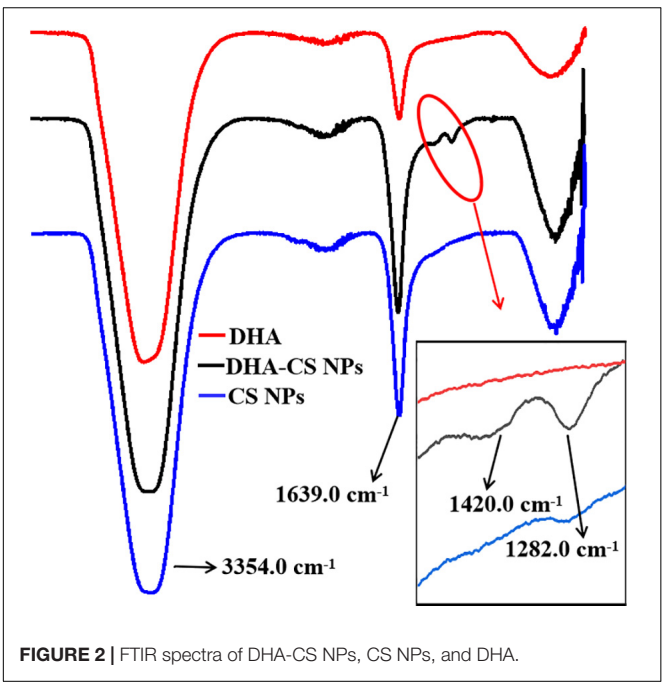

FIGURE 2 | FTIR spectra of DHA-CS NPs, CS NPs, and DHA.

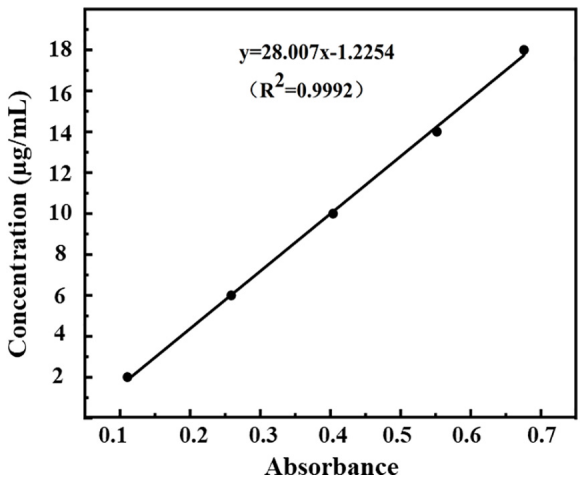

FIGURE 3 | Standard curve of absorbance-concentration of DHA measured at 238 nm by UV-VIS spectroscopy.

DHA-CS NPs Had Antibacterial Activity Against MTB

To detect the antibacterial effect and select DHA-CS NPs concentration, the antibacterial rate curves were drawn using the bacterial dead/live ratio testing. The antibacterial rate curve in **Figure 4** showed that enhanced antibacterial activity of DHA was observed with increasing the concentration at the range of 32.0–256.0 μg/ml, and the highest value was obtained at 256.0 μg/ml. However, the DHA concentration of 256.0 μg/ml had no clinical application value (Li et al., 2020).

CS is a broad-spectrum antibacterial agent and has certain antibacterial effects against *Escherichia coli*, *Pseudomonas aeruginosa*, *Enterococcus faecalis*, and *Staphylococcus saprophyticus* (Andres et al., 2007). In this work, CS also showed anti-Mycobacterial results. The highest antibacterial effect of CS NPs was obtained at 16.0 μg/ml with a value of (54.4 ± 1.93)%. Compared with CS NPs, the antibacterial effect of DHA-CS NPs enhanced (p < 0.05), and it could be due to an additive antibacterial effect of DHA and CS (Jøraholmen et al., 2020). The antibacterial effect of DHA-CS NPs (0.5–256.0 μg/ml) was highest at 8.0 μg/ml with a value of (61.0 ± 2.13)%. Therefore, the optimal concentration of DHA-CS NPs was selected as 8.0 μg/ml for the next experiments.

Morphology and Quantity of MTB Changed After DHA-CS NPs Treatment

Three staining experiments were used to detect the morphology and quantity of MTB after drug treatment. In the negative control group and DHA group, acid-fast staining and auramine "O" staining of MTB in **Figure 5** showed that bacteria were slightly curved, long rod-shaped, chain-shaped, branched aggregated, and grown. The results of the DHA-CS NPs group and CS NPs group showed that MTB was short rod-shaped and arranged individually; the number of MTB was significantly reduced.

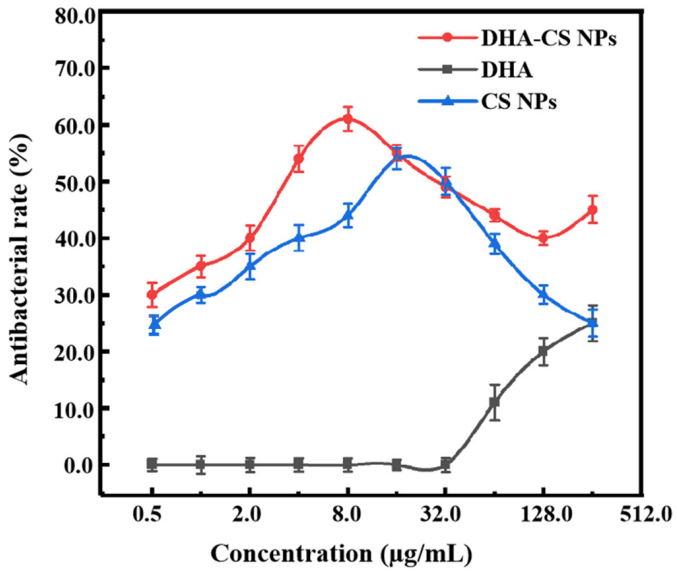

FIGURE 4 | Antibacterial rate curves of MTB treated with 0.50–256 μg/ml drugs for 6 days (n = 3).

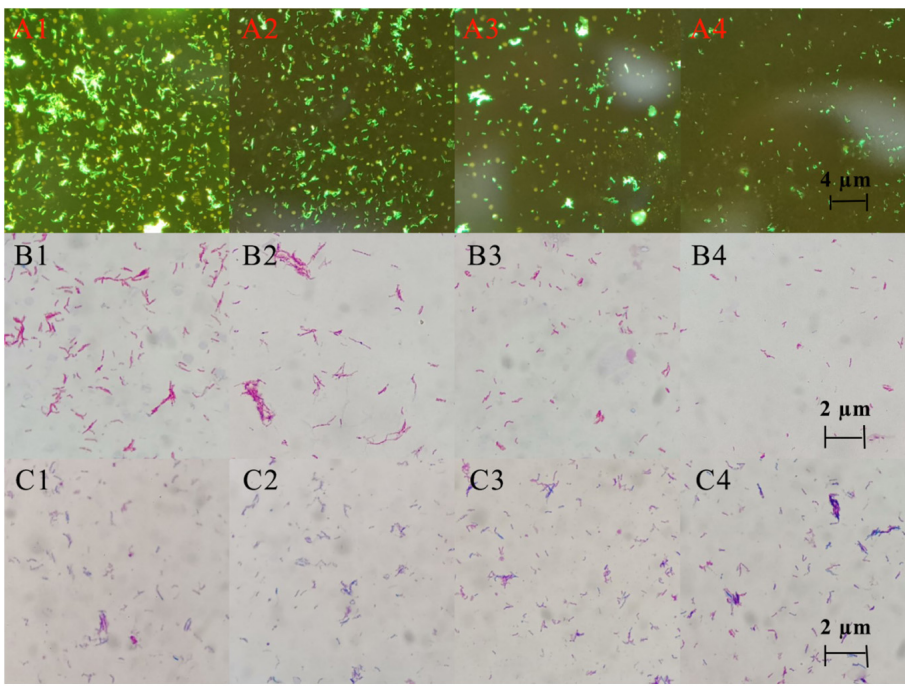

FIGURE 5 | Auramine "O" staining, acid-fast staining, and gram staining pictures of MTB after 6 days treatment with 8.0 μg/ml DHA-CS NPs (n = 3). **(A1–4)** auramine "O" staining, **(B1–4)** acid-fast staining, **(C1–4)** Gram staining, **(A1,B1,C1)** Negative control group, **(A2,B2,C2)** DHA drug group, **(A3,B3,C3)** 8.0 μg/ml CS NPs drug group, **(A4,B4,C4)** 8.0 μg/ml DHA-CS NPs drug group.

The Gram staining results of MTB showed that it was not easy to stain, and the outline of bacteria was not clear. Compared with the negative control group and the DHA group, Gram staining results showed that the outline of MTB treated with DHA-CS NPs and CS NPs was clear and easily stained.

Bacterial Wall and Membrane Integrity Was Destroyed by DHA-CS NPs

SEM was used to detect the structure of MTB after DHA-CS NPs treatment. As shown in **Figure 6**, the MTB of the negative control group and DHA drug group showed typical long rod-shaped structures with a smooth surface and an intact cell wall.

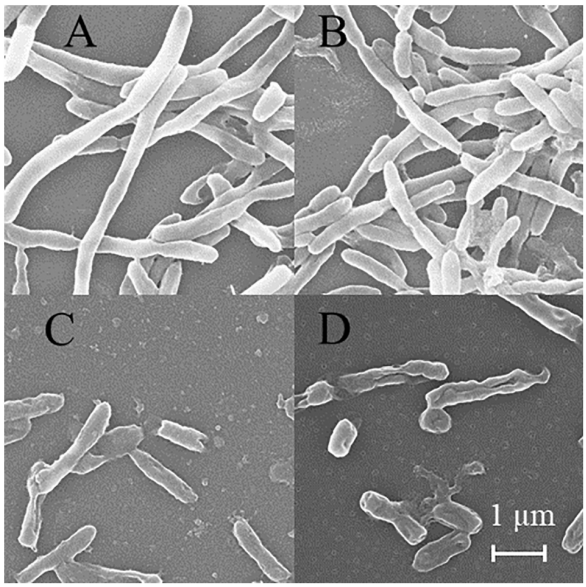

FIGURE 6 | SEM of MTB treated by 8.0 μg/ml DHA-CS NPs for 6 d (n = 3). **(A)** Negative control group, **(B)** 8.0 μg/ml free DHA drug group, **(C)** 8.0 μg/ml CS NPs drug group, **(D)** 8.0 μg/ml DHA-CS NPs drug group.

In the DHA-CS NPs group and CS NPs group, the damaged cell morphology of the tested pathogens showed large surface collapse, abnormal cell breakage, and wrinkled cell walls. At present, some works clarified the destructive effect of CS on bacterial cell walls (Arkoun et al., 2017; Verlee et al., 2017) and there were no reports about DHA-CS NPs, so we chose GC-MS experiment to verify it.

MTB Upregulated Fatty Acid Synthesis Pathway After DHA-CS NPs Treatment

Using PCA to analyze the two groups of samples, the results showed significant differences between individually cultured MTB samples in the presence and absence of DHA-CS NPs. The PCA score scatter plot in **Figure 7** showed that the contribution rates of the two principal components were 78.0 and 9.0%, which could explain 95.0% of the data difference. Subsequently, based on the successful verification of the OPLS-DA and PLS-DA models, the metabolites with Variable Importance in Projection (VIP) value > 1.00, reliability correlation [p(corr)] value > 0.500 in the (V + S) scatter plot in **Figure 8**, and t-test p-value < 0.0500 were considered to be the differential metabolites with the most contribution (**Table 2**). Twelve differential metabolites obtained by the above multivariate statistical analysis were shown in **Figure 9** in bold. These metabolites were related to MTB fatty acid synthesis pathway, glucose metabolism and glycerolipid metabolism.

DHA-CS NPs Combined With RFP Effectively Reduced MTB Resistance

The above results confirmed that DHA-CS NPs had a significant antibacterial effect on RFP-resistant strains. Next, we selected eighteen clinical isolates with known drug-resistant types to test whether DHA-CS NPs combined RFP can reduce the resistance.

The testing was divided into two batches. In 1–9 plates, the concentration of the bacterial solution inoculated in "a" and "g" wells was 3.0×10^6 CFU/ml, "b" and "h" with was 3.0×10^4 CFU/ml, while the 10–18 plates were opposite. In **Figure 10**, the yellow colonies were MTB colonies. Colonies grew in the holes of the negative control groups. Still, no colonies grew in the high/low concentration inoculation holes of the drug groups, indicating that the drug resistance of the strain was reduced. Compared with the initial resistance to RFP, the resistance of 12 strains (1, 2, 4, 5, 6, 9, 10, 11, 13, 14, 15, and 17) was reduced by 8.0 μg/ml DHA-CS NPs combined with RFP, with an effective rate of 66.0%.

DISCUSSION

The DHA-CS NPs complex has the characteristics of DHA and CS. CS is particularly interesting as the broad spectrum of antibacterial activity of CS is well known and documented, offering the possibility of synergistic effects with antimicrobial drugs (Fu, 2018; Yin et al., 2019). DHA also has anti-MTB activity at a certain concentration (Kalani et al., 2019; Morake et al., 2019). In the bacterial live/dead testing, both CS and DHA have antibacterial effects on RFP-resistant MTB, and DHA-CS NPs have the best antibacterial action. Therefore, the significant antibacterial activity of DHA-CS NPs may be an additive effect of DHA and CS. However, its antibacterial effect is not positively related to the concentration. Appropriate low concentration of DHA-CS NPs has the most substantial antibacterial ability. The high concentration of CS probably can cause a certain amount of positive charge on the surface of the bacteria to keep the bacteria in suspension. In addition, due to the high concentration and high viscosity of CS, it has also coated the bacterial surface to prevent leakage of intracellular components. Therefore, the antibacterial effect of a high concentration of CS is achieved by isolating nutrients. Appropriate low concentration of CS may neutralize the negative charge on the surface of the MTB and make the bacteria glue together. In this way, DHA-CS NPs can easily penetrate the bacteria to disturb the cell membrane and cause cell death due to leakage of intracellular components (Sudarshan et al., 1992; Yang et al., 2007).

In a nutrient-rich environment, MTB is long rod-shaped and chain-shaped. After DHA-CS NPs treatment, acid-fast staining and auramine "O" staining has shown that the RFP-resistant MTB is short rod-shaped. It indicated that MTB growth is inhibited. The outer layer of the MTB cell wall is rich in lipid content, accounting for about 60.0% of dry weight. The thick lipid layer impedes penetration of Gram staining solution (Casabon et al., 2013; Vilchèze et al., 2014; Dong et al., 2016; Thompson et al., 2016; Zhou et al., 2016), which makes MTB challenging to stain. MTB of DHA-CS NPs group is easily stained, indicating that the DHA-CS NPs destroy the lipid structure of the outer layer of the MTB cell wall, making the Gram-dye solution enter it easier.

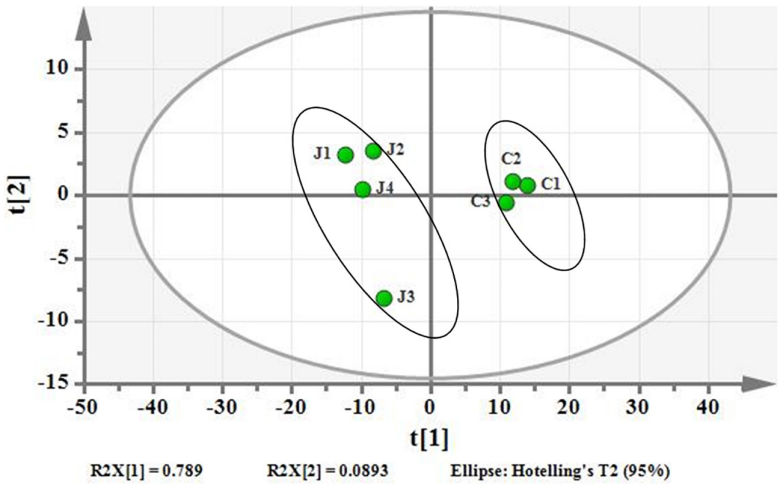

FIGURE 7 | PCA differentiation using the GC-MS whole metabolome analyzed data of the individually cultured MTB in the absence (C) and presence (J) of 8.0 μg/ml DHA-CS NPs.

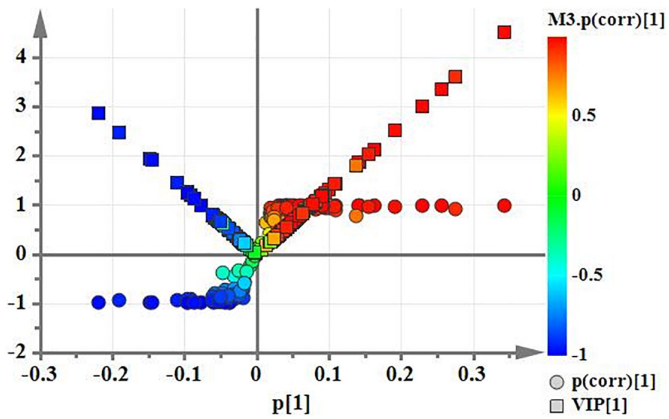

FIGURE 8 | (V+S) plot of OPLS-DA model analysis selecting the differential metabolites of the individually cultured MTB in the absence and presence of 8.0 μg/ml DHA-CS NPs.

Metabolomics is an emerging "omics" science evolved from proteomics, genomics, and transcriptomics. It is based on dynamic changes in low molecular weight metabolites in organisms and has been applied in clinical research, human nutrition, medical research, and development, microbiology metabolism and mechanism researches. This experiment used metabolomics to confirm that RFP-resistant MTB fatty acid synthesis and cell wall repair increased after DHA-CS NPs treatment. Twelve differential metabolisms are identified by GC-MS technology, and 10 of these metabolites are directly related to MTB fatty acid synthesis, including palmitic acid, octadecenoic acid, octadecanoic acid, erucic acid, and so on. These metabolites can form methyl-branched chain fatty acids and eventually form mycolic acid, which is a crucial component of MTB cell wall (Preez and Loots, 2012; Koen et al., 2018). The elevation of these metabolites suggests that MTB upregulates the cell wall synthesis pathway, based on the increased concentration of alkanes (eicosane, octacosane, 2-methyl octadecane, 2-methyl eicosane) and fatty acid amides (oleamide and octadecanamide). Considering that MTB treated with DHA-CS NPs requires more energy to preferably utilize fatty acids toward cell wall repair, MTB will use glucose as a primary energy substrate to obtain energy (Carvalho et al., 2010). In this work, the increase in glucose concentration confirmed it. In addition, the intermediate product of glycolysis can also be used as a substrate for MTB fatty acid biosynthesis, such as 3P-glyceric acid, which can be confirmed by the increase in the concentration of 1-monopalmitin.

At present, although there is no report on the anti-MTB mechanism of DHA-CS NPs, studies have reported that artemisinin drugs and CS can destroy the cell wall structure of bacteria or parasites. Artemisinin and its derivatives can generate free radicals under the mediation of Fe^{2+} and destroy the cell membrane of Plasmodium (Clark et al., 1984; Meshnick, 2002; Antoine et al., 2014). Therefore, the rupture of DHA-CS NPs peroxy bridge may also generate free radicals to attack the

TABLE 2 | Metabolite markers that best explain the variance between the individually cultured samples in the absence and presence of DHA-CS NPs.

Name	[a]OPLS-DA (VIP)	[b]OPLS-DA [p (corr)]	[c]*t*-test (*p*-value)
Palmitic acid	4.50	0.984	0.0030
Octadecanoic acid	3.61	0.915	0.0060
Octadecenoic acid	3.00	0.991	0.0010
Oleamid	2.51	0.972	0.0010
1-monopalmitin	2.13	0.990	0.0010
Erucic acid	2.03	0.952	0.0010
Glucose	1.86	0.992	0.0010
2-methyl eicosane	1.43	0.988	0.0010
Eicosane	1.43	0.899	0.0060
Octadecane	1.42	0.952	0.0030
Octadecanamide	1.19	0.968	0.0020
2-methyl octadecane	1.05	0.927	0.0070

[a]*OPLS-DA (VIP): VIP-value > 1.00 are considered to be the differential metabolites with the most contribution.*
[b]*OPLS-DA [p (corr)]: correlation coefficient value > 0.500 are considered to be the differential metabolites with the most contribution.*
[c]*t-test (p-value): p-value < 0.0500 indicates that the difference was statistically significant.*

bacterial cell wall. CS is an N-deacetylation product of chitin and is the positively charged polyelectrolyte in polysaccharides (Guo, 2007; Tantala et al., 2019). Studies have shown that it can combine with negatively charged cell walls, thereby exerting a broad-spectrum antibacterial effect (Fu, 2018; Yin et al., 2019). Because the cell wall of MTB is negatively charged, DHA-CS NPs can bind to it and interfere with cell wall synthesis. In summary, the antibacterial mechanism of DHA-CS NPs on RFP-resistant MTB may be that it interferes with cell wall synthesis and generates free radicals to damage the cell wall.

The results of DHA-CS NPs combined with anti-tuberculosis drugs have shown that 8.0 μg/ml DHA-CS NPs can reduce MTB resistance. Currently, there are some reports of DHA reduce bacterial resistance. Wu et al. (2013) have shown that the combination of DHA and ampicillin can reduce the resistance of *E. coli*. Lv et al. (2009) have found that artemisinin combined with cefoxitin can reduce the resistance of *Staphylococcus aureus*. Recent studies have demonstrated that efflux pumps of MTB provide a crucial mechanism in the drug-resistant development of anti-TB drugs (Parumasivam et al., 2016). The above results confirm that DHA-CS NPs can destroy the MTB cell wall, so the accumulation of RFP in the cell may be one reason for the decreased resistance. RNA polymerase (RNA-PA) is an essential enzyme required for bacterial transcription. RFP can inhibit gene transcription by binding to the beta subunit of the DNA-dependent RNA-PA, encoded by the *rpoB* gene. When *ropB* gene is mutated, the binding site of RFP and RNA-PA disappears, leading to MTB resistance. In previous experiments, gene chip results have shown that DHA-CS NPs decrease the *ropB* mutant gene level (Zhang, 2013). It also may be the reason for the reduced resistance to RFP.

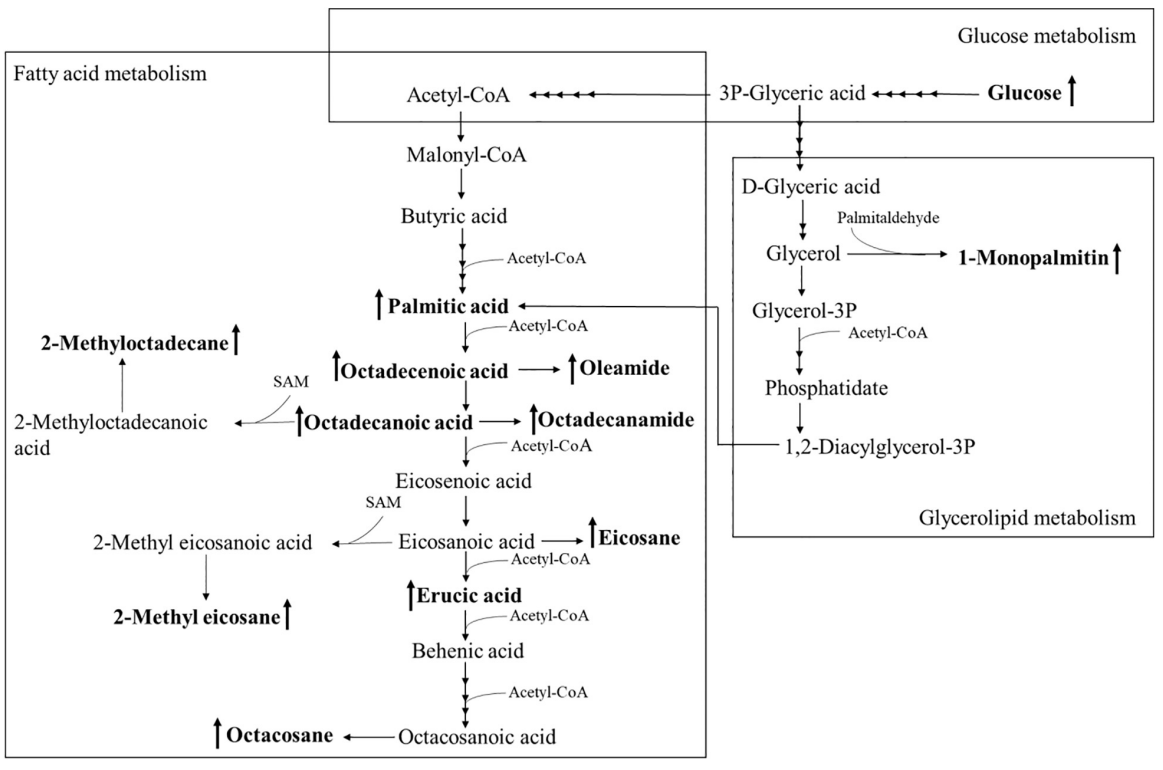

FIGURE 9 | Altered MTB metabolome induced by treatment with 8.0 μg/ml DHA-CS NPs. The schematic representation indicates the 12 metabolite markers in bold, and increases in the metabolite markers are indicated by ↑.

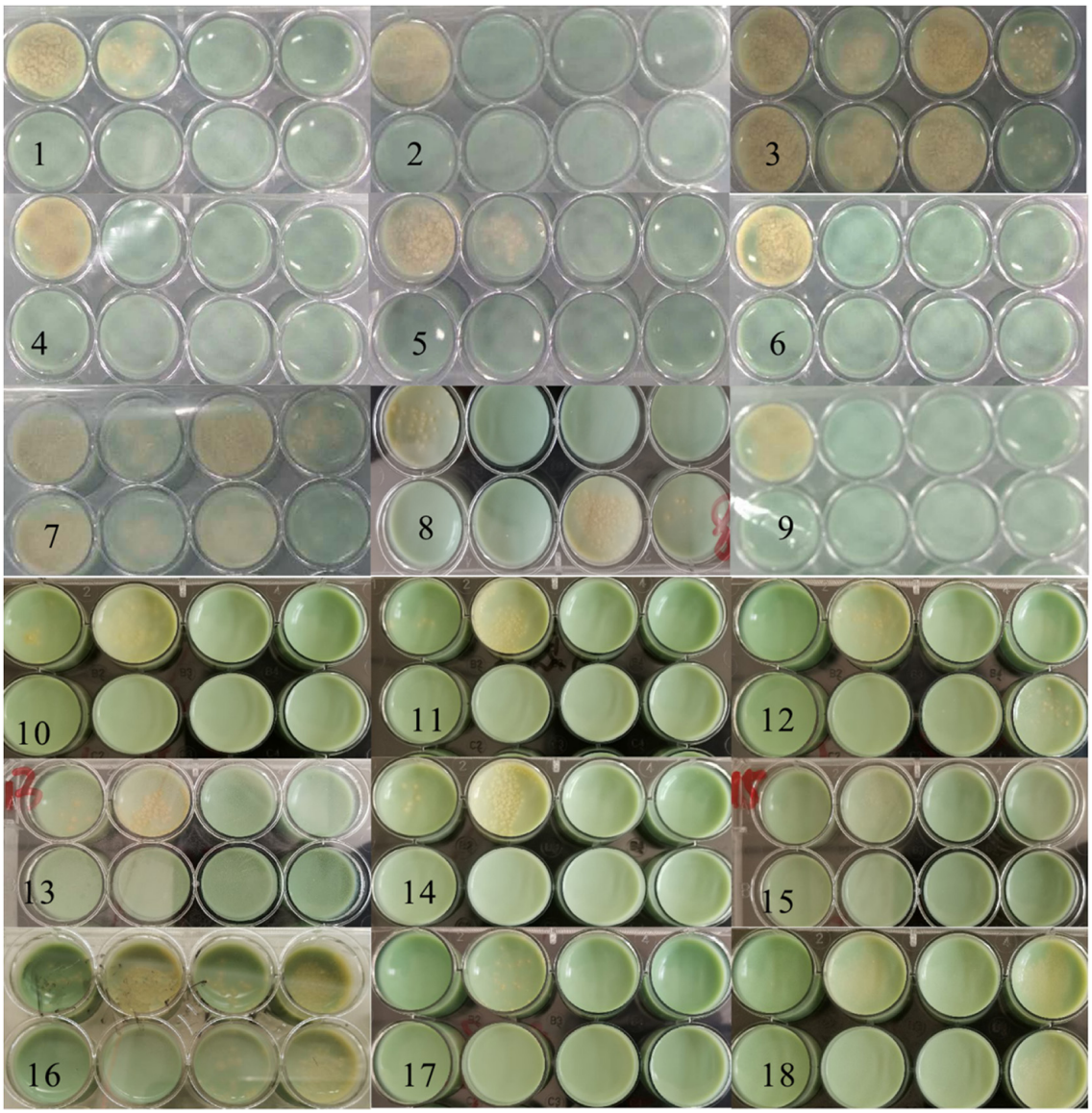

FIGURE 10 | Solid medium drug susceptibility testing of 8.0 μg/ml CS-DHA NPs combined with anti-TB drugs (n = 18).

Overall, DHA-CS NPs reduced the resistance of MTB to RFP, possibly because it reduced the *ropB* mutant gene level or damaged MTB cell wall to increased RFP intake. Therefore, the combination of DHA-CS NPs and the classic anti-tuberculosis drugs RFP is expected to constitute an effective treatment for TB.

CONCLUSION

In conclusion, DHA-CS NPs showed enhanced antibacterial activity compared with free DHA and CS, which was based on the additive effect of DHA-CS NPs by effectively destroying the cell wall of MTB. Furthermore, at effective concentrations, DHA-CS NPs can reduce the RFP resistance, making it a potential anti-TB drug worthy of further investigation.

DATA AVAILABILITY STATEMENT

The original contributions presented in the study are included in the article/ **Supplementary Material**, further inquiries can be directed to the corresponding author/s.

AUTHOR CONTRIBUTIONS

XG: conceptualization, data curation, software, and writing–original draft preparation. QC: methodology. YanZ and XG: validation. YalZ: formal analysis, investigation, resources, and project administration. PH: writing–review and editing. ZJ: visualization and supervision. All authors have read and agreed to the published version of the manuscript.

FUNDING

This research was funded by the Key Project of Sichuan Science and Technology Department (Grant No. 2019YFS0090) and the Project of Mianyang Science and Technology Bureau (Grant No. 150170).

ACKNOWLEDGMENTS

We thank the Sichuan Science and Technology Department and the Project of Mianyang Science and Technology Bureau for providing financial assistance to this article. We appreciate the help of the Mianyang Center for Disease Control.

SUPPLEMENTARY MATERIAL

The Supplementary Material for this article can be found online at: https://www.frontiersin.org/articles/10.3389/fmicb.2021.735166/full#supplementary-material

Supplementary Figure 1 | MTB solid drug-sensitive culture plate.

REFERENCES

Andres, Y., Giraud, L., Gerente, C., and Le Cloirec, P. (2007). Antibacterial effects of chitosan powder: mechanisms of action. *Environ. Technol.* 28, 1357–1363. doi: 10.1080/09593332808618893

Antoine, T., Fisher, N., Amewu, R., O'Neill, P. M., Ward, S. A., and Biagini, G. A. (2014). Rapid kill of malaria parasites by artemisinin and semi-synthetic endoperoxides involves ROS-dependent depolarization of the membrane potential. *J. Antimicrob. Chemother.* 69, 1005–1016. doi: 10.1093/jac/dkt486

Arkoun, M., Daigle, F., Heuzey, M. C., and Ajji, A. (2017). Antibacterial electrospun chitosan-based nanofibers: a bacterial membrane perforator. *Food Sci. Nutr.* 5, 865–874. doi: 10.1002/fsn3.468

Beg, S., Saini, S., Imam, S., Rahman, M., Swain, S., and Hasnain, M. S. (2017). Nanoemulsion for the effective treatment and management of anti-tubercular drug therapy. *Recent Pat. Antiinfect. Drug Discov.* 12, 85–94. doi: 10.2174/1574891x12666170504094330

Carvalho, L. P. S., Fischer, S. M., Marrero, J., Nathan, C., Ehrt, S., and Rhee, K. Y. (2010). Metabolomics of *Mycobacterium tuberculosis* reveals compartmentalized co-catabolism of carbon substrates. *Chem. Biol.* 17, 1122–1131. doi: 10.1016/j.chembiol.2010.08.009

Casabon, I., Zhu, S. H., Otani, H., Liu, j, Mohn, W. W., and Eltis, L. D. (2013). Regulation of the KstR2 regulon of *Mycobacterium tuberculosis* by a cholesterol catabolite. *Mol. Microbiol.* 89, 1201–1212. doi: 10.1111/mmi.12340

Clark, I. A., Hunt, N. H., Cowden, W. B., Maxwell, L. E., and Mackie, E. J. (1984). Radical-mediated damage to parasites and erythrocytes in Plasmodium vinckei infected mice after injection of t-butyl hydroperoxide. *Clin. Exp. Immunol.* 56, 524–530.

Dheda, K., Gumbo, T., Gandhi, N. R., Murray, M., Theron, G., Udwadia, Z., et al. (2014). Global control of tuberculosis: from extensively drug-resistant to untreatable tuberculosis. *Lancet Respir. Med.* 2, 321–338. doi: 10.1016/s2213-2600(14)70031-1

Dinache, A., Tozar, T., Smarandache, A., Andrei, I. R., Nistorescu, S., Nastasa, V., et al. (2020). Spectroscopic characterization of emulsions generated with a new laser-assisted device. *Molecules* 25:1729. doi: 10.3390/molecules25071729

Dong, N., Fu, Y. R., and Yin, Z. J. (2016). Research progress on abnormal lipid metabolism induced by mycobacterium tuberculosis infection and its mechanisms. *Chin. J. Tuberc. Respir. Dis.* 39, 548–550.

Fu, J. F. (2018). Preparation of green antimicrobial agent based on chitosan-antimicrobial peptide conjugate. *NEPU*

Guo, Z. Y. (2007). Effect of substitution groups and amino positive electricity of water-soluble chitosan derivatives on antibacterial activity. *IACOS*

Harding, E. (2020). WHO global progress report on tuberculosis elimination. *Lancet Respir. Med.* 8:19. doi: 10.1016/s2213-2600(19)30418-7

Hou, L. N., and Zhao, L. H. (2006). Study on the mechanism of chitooligosaccharide binding and activating macrophages. *J. China Med. Univ.* 35, 124–127.

Jin, L. X. (2020). Research and clinical application of nano-drug carriers. *Chin. J. Tissue Eng. Res.* 14, 1429–1432.

Jøraholmen, M. W., Bhargava, A., Julin, K., Johannessen, M., and Škalko-Basnet, N. (2020). The antimicrobial properties of chitosan can be tailored by formulation. *Mar. Drugs* 18:96. doi: 10.3390/md18020096

Kalani, K., Chaturvedi, V., Trivedi, P., Sudeep, T., and Santosh, K. S. (2019). Dihydroartemisinin and its analogs: a new class of antitubercular agents. *Curr. Top. Med. Chem.* 19, 594–599. doi: 10.2174/1568026619666190304142802

Koen, N., Van Breda, S. V., and Loots, D. T. (2018). Elucidating the antimicrobial mechanisms of colistin sulfate on *Mycobacterium tuberculosis* using metabolomics. *Tuberculosis* 111, 14–19. doi: 10.1016/j.tube.2018.05.001

Kucukoglu, V., Uzuner, H., Kenar, H., and Karadenizli, A. (2019). In vitro antibacterial activity of ciprofloxacin loaded chitosan microparticles and their effects on human lung epithelial cells. *Int. J. Pharm.* 569:118578. doi: 10.1016/j.ijpharm.2019.118578

Kumari, P., Luqman, S., and Meena, A. (2019). Application of the combinatorial approaches of medicinal and aromatic plants with nanotechnology and its impacts on healthcare. *Daru* 27, 475–489. doi: 10.1007/s40199-019-00271-6

Li, L., Wu, J. G., Weng, S. F., Yang, L. M., Wang, H. Z., Xu, Y. Z., et al. (2020). Fourier transform infrared spectroscopy monitoring of dihydroartemisinin-induced growth inhibition in ovarian cancer cells and normal ovarian surface epithelial cells. *Cancer Manag. Res.* 12, 653–661. doi: 10.2147/cmar.s240285

Lv, P., Qin, Y. H., Wang, S. M., Lu, X., Cen, Y., Li, J., et al. (2009). Antimicrobial activity of artesunate against methicillin-resistant *Staphylococcus aureus* in vitro. *J. Chin. Pract. Diagn. Ther.* 25–26.

Maitre, T., Aubry, A., Jarlier, V., Robert, J., Veziris, N., and Cnr-MyRMA. (2017). Multidrug and extensively drug-resistant tuberculosis. *Med. Mal. Infect.* 47, 3–10.

Martinelli, C., Pucci, C., and Ciofani, G. (2019). Nanostructured carriers as innovative tools for cancer diagnosis and therapy. *APL Bioeng.* 3:011502. doi: 10.1063/1.5079943

Meshnick, S. R. (2002). Artemisinin: mechanisms of action, resistance and toxicity. *Int. J. Parasitol.* 32, 1655–1660. doi: 10.1016/s0020-7519(02)00194-7

Meshnick, S. R., Yang, Y. Z., Lima, V., Kuyperset, F., Kamchonwongpaisan, S., and Yuthavong, Y. (1993). Iron-dependent free radical generation from the antimalarial agent artemisinin (qinghaosu). *Antimicrob. Agents Chemother.* 37, 1108–1114. doi: 10.1128/aac.37.5.1108

Morake, M., Coertzen, D., Ngwane, A., Johannes, F., Ho, N. W., Frans, J. S., et al. (2019). Preliminary evaluation of artemisinin-cholesterol conjugates as potential drugs for the treatment of intractable forms of malaria and tuberculosis. *ChemMedChem* 13, 67–77. doi: 10.1002/cmdc.201700579

Parumasivam, T., Chan, J. G. Y., Pang, A., Quan, D. H., Triccas, J. A., and Britton, W. J. (2016). In vitro evaluation of inhalable verapamil-rifapentine particles for tuberculosis therapy. *Mol. Pharm.* 13, 979–989. doi: 10.1021/acs.molpharmaceut.5b00833

Preez, I. D., and Loots, D. T. (2012). Altered fatty acid metabolism due to rifampicin-resistance conferring mutations in the rpoB gene of *Mycobacterium tuberculosis*: mapping the potential of pharmaco-metabolomics for global health and personalized medicine. *OMICS* 16, 596–603. doi: 10.1089/omi.2012.0028

Radwan-Pragłowska, J., Piątkowski, M., Deineka, V., Janus, Ł, Korniienko, V., Husak, E., et al. (2019). Chitosan-based bioactive hemostatic agents with antibacterial properties-synthesis and characterization. *Molecules* 24:2629. doi: 10.3390/molecules24142629

Rani, S., Gothwal, A., Khan, I., Pachouri, P. K., Bhaskar, N., Gupta, U. D., et al. (2018). Smartly engineered PEGylated di-block nanopolymeric micelles: duo

delivery of isoniazid and fifampicin against *Mycobacterium tuberculosis*. *AAPS PharmSciTech* 19, 3237–3324. doi: 10.1208/s12249-018-1151-8

Satalkar, P., Elger, B. S., and Shaw, D. M. (2016). Defining nano, nanotechnology and nanomedicine: why should it matter? *Sci. Eng. Ethics* 22, 1255–1276. doi: 10.1007/s11948-015-9705-6

Sia, J. K., and Rengarajan, J. (2019). Immunology of *Mycobacterium tuberculosis* infections. *Microbiol. Spectr.* 7:10.

Stein, C. M., Zalwango, S., Malone, L. S. L., Won, S., Mayanja-Kizza, H., Mugerwa, R. D., et al. (2008). Genome scan of *M. tuberculosis* infection and disease in Ugandans. *PLoS One* 3:e4094. doi: 10.1371/journal.pone.0004094

Sudarshan, N. R., Hoover, D., and Knorr, D. (1992). Antibacterial action of chitosan. *Food Biotechnol.* 6, 257–272. doi: 10.1080/08905439209549838

Tantala, J., Thumanu, K., and Rachtanapun, C. (2019). An assessment of antibacterial mode of action of chitosan on Listeria innocua cells using real-time HATR-FTIR spectroscopy. *Int. J. Biol. Macromol.* 135, 386–393. doi: 10.1016/j.ijbiomac.2019.05.032

Thompson, A. P., Stericki, L. M., Wegener, K. L., Lu, W., Zhu, L. M., Booker Grant, W., et al. (2016). New research direction of biotin-antituberculosis drugs. *Jiangsu J. Prevent. Med.* 27, 257–261.

Upadhyay, S., Khan, I., Gothwal, A., Pachouri, P. K., Bhaskar, N., Gupta, U. D., et al. (2017). Conjugated and entrapped HPMA-PLA nano-polymeric micelles based dual delivery of first line anti TB drugs: improved and safe drug delivery against sensitive and resistant *Mycobacterium tuberculosis*. *Pharm. Res.* 34, 1944–1955. doi: 10.1007/s11095-017-2206-3

van Breda, S. V., Buys, A., Apostolides, Z., Nardell, E. A., and Stoltz, A. C. (2015). The antimicrobial effect of colistin methanesulfonate on *Mycobacterium tuberculosis* in vitro. *Tuberculosis* 95, 440–446. doi: 10.1016/j.tube.2015.05.005

Verlee, A., Mincke, S., and Stevens, C. V. (2017). Recent developments in antibacterial and antifungal chitosan and its derivatives. *Carbohydr. Polym.* 164, 268–283. doi: 10.1016/j.carbpol.2017.02.001

Vilchèze, C., Molle, V., Carre're-Kremer, S., Leiba, J., Mourey, L., Shenai, S., et al. (2014). Phosphorylation of KasB regulates virulence and acid-fastness in *Mycobacterium tuberculosis*. *PLoS Pathog* 10:e1004115. doi: 10.1371/journal.ppat.1004115

Wais, M., Aqil, M., Goswami, P., Agnihotri, J., and Nadeem, S. (2017). Nanoemulsion-based transdermal drug delivery system for the treatment of tuberculosis. *Recent Pat. Antiinfect. Drug Discov.* 12, 107–119. doi: 10.2174/1574891x12666170602075733

Wang, H. B., Yang, H. J., Yang, J. H., Wang, Y. S., and Lu, F. P. (2015). A comparative study of pre-treatment methods for bacillus subtilis metabolomics samples. *Nanl. Chem.* 43, 1169–1174.

Wang, L., Feng, M., Li, Q., Qiu, C., and Chen, R. (2019). Advances in nanotechnology and asthma. *Ann. Transl. Med.* 7:180.

Want, M. Y., Islamuddin, M., Chouhan, G., Ozbak, H. A., Hemeg, H. A., Dasgupta, A. K., et al. (2015). Therapeutic efficacy of artemisinin-loaded nanoparticles in experimental visceral leishmaniasis. *Clloids Surf. B Biointerfaces* 130, 215–221. doi: 10.1016/j.colsurfb.2015.04.013

Wu, C., Liu, J., Pan, X. C., Xian, W. Y., Li, B., Peng, W., et al. (2013). Design: synthesis and evaluation of the antibacterial enhancement activities of amino dihydroartemisinin derivatives. *Molecules* 18, 6866–6882. doi: 10.3390/molecules18066866

Wu, D. (2015). *Experimental Study on Detection of Isoniazid Resistance of Mycobacterium tuberculosis by Flow Cytometry*. Guangzhou: Guangzhou Medical University (guang zhou yi ke da xue).

Yang, S., Feng, X. Q., Fu, G. Q., Wang, Y. P., Su, Z. X., and Li, X. F. (2007). The inhibitory effect of water-soluble chitosan on several common bacteria and its mechanism. *Zhong guo niang zao* 15–18.

Ye, Y. J., Wang, Y., Lou, K. Y., Chen, Y. Z., Chen, R., and Gao, F. (2015). The preparation, characterization, and pharmacokinetic studies of chitosan nanoparticles loaded with paclitaxel/dimethyl-β-cyclodextrin inclusion complexes. *Int. J. Nanomedicine* 10, 4309–4319.

Yin, M. L., Wang, Y. F., and Ren, X. H. (2019). Preparation of modified chitosan antibacterial nanospheres. *Chem. J. Chinese Univ.* 40, 181–187.

Zhang, Y. (2013). Antibacterial effect and mechanism of nano-drugs on drug-resistant *Mycobacterium tuberculosis*. *Lu Zhou Yi Xue Yuan*

Zhang, Z. R., Dong, E. D., Wu, L., Zhang, Q., Lu, W. Y., Jiang, W., et al. (2014). Research status and frontier direction of biomacromolecule drug delivery system. *Chin. Basic Sci.* 16, 3–8.

Zhou, N., Du, X. B., Yang, L., Xu, Y., Sun, B., and Zhang, Q. (2016). Study on plasma metabolomics of tuberculosis patients with different course of disease. *J. Spectrosc.* 8, 224–225.

Zhou, S. Y., Yang, S. B., and Huang, G. L. (2017). Design, synthesis and biological activity of pyrazinamide derivatives for anti-*Mycobacterium tuberculosis*. *J. Enzyme Inhib. Med. Chem.* 32, 1183–1186.

Zhu, F. P. (2014). In vitro stability and time-dependent pharmacokinetics of dihydroartemisinin. *Shandong Univ.*

Conflict of Interest: The authors declare that the research was conducted in the absence of any commercial or financial relationships that could be construed as a potential conflict of interest.

Publisher's Note: All claims expressed in this article are solely those of the authors and do not necessarily represent those of their affiliated organizations, or those of the publisher, the editors and the reviewers. Any product that may be evaluated in this article, or claim that may be made by its manufacturer, is not guaranteed or endorsed by the publisher.

frontiers in Microbiology

REVIEW
published: 22 October 2021
doi: 10.3389/fmicb.2021.745592

Differential Diagnosis of Latent Tuberculosis Infection and Active Tuberculosis: A Key to a Successful Tuberculosis Control Strategy

*Wenping Gong and Xueqiong Wu**

Tuberculosis Prevention and Control Key Laboratory/Beijing Key Laboratory of New Techniques of Tuberculosis Diagnosis and Treatment, Senior Department of Tuberculosis, The 8th Medical Center of PLA General Hospital, Beijing, China

As an ancient infectious disease, tuberculosis (TB) is still the leading cause of death from a single infectious agent worldwide. Latent TB infection (LTBI) has been recognized as the largest source of new TB cases and is one of the biggest obstacles to achieving the aim of the End TB Strategy. The latest data indicate that a considerable percentage of the population with LTBI and the lack of differential diagnosis between LTBI and active TB (aTB) may be potential reasons for the high TB morbidity and mortality in countries with high TB burdens. The tuberculin skin test (TST) has been used to diagnose TB for > 100 years, but it fails to distinguish patients with LTBI from those with aTB and people who have received Bacillus Calmette–Guérin vaccination. To overcome the limitations of TST, several new skin tests and interferon-gamma release assays have been developed, such as the Diaskintest, C-Tb skin test, EC-Test, and T-cell spot of the TB assay, QuantiFERON-TB Gold In-Tube, QuantiFERON-TB Gold-Plus, LIAISON QuantiFERON-TB Gold Plus test, and LIOFeron TB/LTBI. However, these methods cannot distinguish LTBI from aTB. To investigate the reasons why all these methods cannot distinguish LTBI from aTB, we have explained the concept and definition of LTBI and expounded on the immunological mechanism of LTBI in this review. In addition, we have outlined the research status, future directions, and challenges of LTBI differential diagnosis, including novel biomarkers derived from *Mycobacterium tuberculosis* and hosts, new models and algorithms, omics technologies, and microbiota.

Keywords: tuberculosis, latent TB infection (LTBI), tuberculin skin test (TST), interferon-gamma release assays (IGRAs), biomarkers, differential diagnosis

OPEN ACCESS

Edited by:
Xiao-Yong Fan,
Fudan University, China

Reviewed by:
Alasdair Leslie,
Africa Health Research Institute (AHRI), South Africa
Pooja Vir,
Uniformed Services University of the Health Sciences, United States

***Correspondence:**
Xueqiong Wu
xueqiongwu@139.com

Specialty section:
This article was submitted to Infectious Agents and Disease, a section of the journal Frontiers in Microbiology

Received: *22 July 2021*
Accepted: *24 September 2021*
Published: *22 October 2021*

Citation:
Gong W and Wu X (2021) Differential Diagnosis of Latent Tuberculosis Infection and Active Tuberculosis: A Key to a Successful Tuberculosis Control Strategy. Front. Microbiol. 12:745592. doi: 10.3389/fmicb.2021.745592

Abbreviations: Ala-DH, alanine dehydrogenase; ARI, annual risk in infection; aTB, active tuberculosis; AUCs, areas under the curve; BCG, Bacillus Calmette–Guérin; CFP-10, culture filtrate protein 10; CLIA, chemiluminescent immunoassay; CTL, cytotoxic T lymphocytes; DCs, dendritic cells; DC-SIGN, DC-specific intercellular adhesion molecule-3 grabbing nonintegrin; DosRs, dormancy survival regulon antigens; EGF, epidermal growth factor; ELISA, enzyme-linked immunosorbent assay; ELISpot, enzyme-linked immunospot; ESAT-6, early secreted antigenic target 6; GM-CSF, granulocyte macrophage colony-stimulating factor; HCs, health controls; HCWs, healthcare workers; HLAs, human leukocyte antigens; IFN-γ, interferon-γ; IGRAs, interferon-gamma release assays; IL, interleukin; IP-10, interferon-gamma-inducible protein 10; IS, ImmunoScore; LTBI, latent tuberculosis infection; MIP-1β, macrophage inflammatory protein 1β; NS, nutrition starvation; NTM, non-tuberculous mycobacteria; OT, old tuberculin; PPD, purified protein derivative; PPRs, pattern recognition receptors; QFT-GIT, QuantiFERON-TB Gold In-Tube; QFT-Plus, QuantiFERON-TB Gold-Plus; RAs, reactivation antigens; RD, region of difference; RPF, resuscitation-promoting factor; TAS, toxin–antitoxin system-associated antigens; TB, tuberculosis; Th, helper T lymphocytes; TLR, toll-like receptor; TNF-α, tumor necrosis factor-α; Tregs, regulatory T cells; T-SPOT.TB, T-cell spot of TB assay; TST, tuberculin skin test; VEGF, vascular endothelial growth factor; WHO, World Health Organization.

INTRODUCTION

Tuberculosis (TB) is one of the top 10 causes of death and is the leading cause of death from a single infectious agent worldwide (Gong et al., 2018; WHO, 2020). According to the Global Tuberculosis Report 2020 released by the World Health Organization (WHO), more than 10 million new TB cases and 1.4 million deaths were reported to the WHO in 2019 (WHO, 2020).

To reverse the long-term unfavorable situation of TB prevention and treatment, the WHO formulated an ambitious End TB Strategy in 2015. The aim of this strategy was to reduce the mortality and incidence rates of TB by 90% and 80%, respectively, in 2025 from those reported in 2015 and aim for further reduction by 95% and 90% in 2035, respectively (Stop TB Partnership, 2015). Currently, the global incidence of TB is declining at an average rate of about 2% per year, which is not fast enough to reach the target of a 17% annual decline from 2025 to 2035 set by the End TB Strategy (Stop TB Partnership, 2015; Chaw et al., 2020).

A reason for this gap may be that the source of infection has not been effectively controlled, resulting in a large percentage of the population being infected with latent TB infection (LTBI). A previous study indicated that 23% of the world's population (equivalent to 1.7 billion people) was estimated to be latently infected with *Mycobacterium tuberculosis*, and cases from three WHO regions (Southeast Asia, Western-Pacific, and Africa), which had the highest LBTI burdens, accounted for approximately 80% of all LTBI cases (Houben and Dodd, 2016). Although countries with high TB burdens pay great importance to the prevention, diagnosis, and treatment of active TB (aTB), the same cannot be said in terms of their emphasis on LTBI.

It has been reported that 5–10% of patients with LTBI will progress to aTB during their lifetime (Hauck et al., 2009; Chee et al., 2018; WHO, 2018). However, the risk is higher in immunocompromised individuals, such as in people living with human immunodeficiency virus (HIV), people with diabetes, people with coronavirus disease, infants, and young children (aged < 5 years) (Chee et al., 2018; Gong and Wu, 2020; WHO, 2020; Aspatwar et al., 2021). In 2019, the number of new TB cases in countries with high TB burdens accounted for 86.9% of the global number of new TB cases (WHO, 2020). The latest data indicate that China has the heaviest burden of LTBI worldwide, with about 350 million people latently infected with *M. tuberculosis* (Cui et al., 2020). These data indicate that a significant percentage of the population with LTBI and lack of differential diagnosis of LTBI and aTB may be potential reasons for the high TB morbidity and mortality in countries with a high TB burden. Therefore, countries with high TB burdens should consider increasingly emphasizing LTBI-related research and taking action to accelerate progress toward global milestones and targets for reductions in the burden of TB set for 2025, 2030, and 2035 (Floyd et al., 2018). Accurately identifying and intervening in cases of TB from the population, especially cases of LTBI, are key to reducing morbidity and mortality. Reaching the milestones of the End TB Strategy is also urgent. Eliminating TB is not feasible if there is no isolation of patients with bacterium-positive TB and as long as a large number of people with LTBI exist (Godoy, 2021).

In this review, we first clarified the concept and definition of LTBI and then explained the immunological mechanism of LTBI. We also reviewed the current technologies and methods for LTBI differential diagnosis, such as the tuberculin skin test (TST) and interferon-gamma release assays (IGRAs), by comparing their advantages and disadvantages. Finally, we have outlined the current research status, future directions, and challenges for LTBI differential diagnosis in the future, including novel biomarkers derived from *M. tuberculosis* and its host, new models, algorithms, omics technologies, and microbiota.

CONCEPT AND IMMUNOLOGICAL MECHANISMS OF LATENT TUBERCULOSIS INFECTION

Evolutionary History of the Definition of Latent Tuberculosis Infection

With developments in science and technology, the understanding of the definition of LTBI has been deepening continuously over a long period. The evolution of the definition of LBTI can be divided into three stages—macropathology, bacteriology, and immunology. In the early 19th century, Louis (1825) and Laennec (1826) found tubercles upon autopsy of asymptomatic patients who had no clinical manifestations of TB before death, and they used the term "latent" TB to describe this condition for the first time. Behr et al. (2021) summarized the definition of LTBI in the 19th century as "Latent TB is a postmortem diagnosis referring to a host with tuberculous pathology in the absence of symptoms." In the 20th century, the definition of LTBI began to shift from a pathological description to bacteriological identification. As early as 1956, when McCune et al. (1956) identified the effect of pyrazinamide on mice, they accidentally found that the disappearance of *M. tuberculosis* in the organs of mice did not mean that *M. tuberculosis* was completely eliminated. In contrast, *M. tuberculosis* can still be identified in approximately one-third of mice treated with pyrazinamide for 90 days. The bacteriological concept of LTBI was first proposed as follows: "the infection is present but is hidden beyond the limits of diagnostic reach" or "the presence of tubercle bacilli in the animal tissues can no longer be demonstrated by the most elaborate techniques of microscopy, culture, or animal inoculation" (McCune et al., 1956; Mc, 1959). However, this description is only a clinical and bacteriological definition but does not reflect the nature of LTBI. Behr et al. (2021) summarized the definition of LTBI in the 20th century as "Latent TB remains a postmortem diagnosis but now referring to the tubercle bacilli recovered from autopsy tissue without TB pathology." In the 21st century, the definition of LTBI has changed from postmortem pathological diagnosis in the 19th century and bacterial diagnosis in the 20th century to host immunological diagnosis. In 1999, the American Thoracic Society (ATS) issued guidelines for the treatment of TB and specifically addressed "latent tuberculosis

infection" (ATS, 2000). For the first time, TB immunoreactivity tests such as the TST were used to diagnose latent tuberculosis infection. Eight years later, these guidelines were updated, and the definition of LTBI was modified to include "a state of persistent immune response to stimulation by *M. tuberculosis* antigens with no evidence of clinically manifest active TB" (Lewinsohn et al., 2017). This definition of LTBI was recognized by the WHO in their Guidelines on the Management of Latent Tuberculosis Infection (WHO, 2015). On July 15, 2021, Behr et al. (2021) summarized the evolution of the definition of LTBI in the 21st century as follows: "Latent TB refers to a host who is TB immunoreactive in the absence of TB disease."

As mentioned above, the understanding of LTBI has gone through three stages: anatomical diagnosis in the 19th century, bacteriological diagnosis in the 20th century, and immunological diagnosis in the 21st century. However, currently, there is no distinction between a "latent infection" and "immunological memory" in the absence of TB infection. A previous study has found that most TB-immunoreactive individuals retain immunological memory after clearing *M. tuberculosis* infection, indicating TB immunoreactivity can persist after curative treatment (Behr et al., 2018, 2019). It was estimated that 24.4% of individuals with *M. tuberculosis* infection could self-clear mycobacteria within 10 years and 73.1% over a lifetime (Emery et al., 2021). Therefore, the number of people harboring live *M. tuberculosis* may be substantially lower than previously reported (Behr et al., 2021). The population with positive results of TST and IGRAs includes not only individuals with LTBI but also individuals with persistent TB immunoreactivity after curative treatment. Furthermore, individuals with LTBI are at risk of progression to active TB. Therefore, they are a potential source of future transmission and may benefit from treatment. In contrast, individuals with immunological memory but no *M. tuberculosis* infection are not at risk of progression to active TB. Therefore, they are not a source of future transmission from the initial exposure and would not benefit from treatment. Thus, these concerns should be overcome in the future.

In this review, we adopt the definition of LTBI from an article published by Chee et al. (2018) in 2018: "LTBI is a subclinical condition of *M. tuberculosis* infection, characterized by a complex and heterogeneous state resulting from the interaction between the immune response of the organism and the host." In other words, we believe that LTBI is governed by a process of dynamic balance between host immunity and the invasiveness of *M. tuberculosis*. Once the balance is disrupted, *M. tuberculosis* infection can result in three outcomes (**Figure 1A**).

Immunological Mechanisms of Latent Tuberculosis Infection

Host bactericidal immune responses play a central role in the progression from LTBI to aTB (Pan et al., 2017). To better understand the relationship between host immune responses and mycobacteria, we briefly reviewed the immunological mechanisms of LTBI (**Figure 1B**). As a paradigmatic intracellular pathogen, *M. tuberculosis* first invades the alveolar epithelial cells (pneumocytes I and II) after host inhalation of droplets containing bacteria *via* airborne transmission (Chai et al., 2020). The role of alveolar epithelial cells has been well documented in numerous studies since the 1990s (Kanai et al., 1979; Rodrigues et al., 2020). These cells play a crucial role in the pathogenesis of TB as replicative niches in the spread of infection *via* cellular death due to TB infection and play immunomodulatory roles through the expression of cytokines and chemokines (Scordo et al., 2016; Rodrigues et al., 2020). Macrophages are one of the first responders in host defense against *M. tuberculosis*. Inhaled *M. tuberculosis* is recognized and phagocytosed into phagosomes for clearance by resident alveolar macrophages mainly through their well-equipped pattern recognition receptors (PRRs), which can be blocked by some reactive proteins of *M. tuberculosis* (Westphalen et al., 2014). In addition, in response to *M. tuberculosis* infection, alveolar macrophages secrete a series of pro-inflammatory cytokines and chemokines, such as tumor necrosis factor-α (TNF-α), interleukin-1β (IL-1β), IL-6, IL-23, and granulocyte macrophage colony-stimulating factor (GM-CSF) (Chai et al., 2020). Lung-resident dendritic cells (DCs) are another group of sentinel cells that migrate to the surface of the trachea and alveoli to detect invading pathogens in time. Monocyte-derived DCs can recognize *M. tuberculosis* in collaboration with DC-specific intercellular adhesion molecule-3 grabbing non-integrin (DC-SIGN) and toll-like receptor (TLR) and kill *M. tuberculosis* by upregulating IL-1α, IL-1β, IL-10, and inducible nitric oxide synthase (iNOS) (Tailleux et al., 2003; Mayer-Barber et al., 2011; Chai et al., 2020). After phagocytosis *of M. tuberculosis*, DCs migrate to the surrounding lymph nodes and present the antigens of *M. tuberculosis* to prime $CD4^+$ T lymphocytes (Chai et al., 2020).

Unlike macrophages and DCs, neutrophils do not recognize and phagocytose mycobacteria at the original infection sites. Neutrophils are important responders in host defense against *M. tuberculosis*, but they have been neglected until recently. Neutrophil recruitment occurs at an early stage of granuloma formation. In granulomas, the dying macrophages infected with *M. tuberculosis* release signals to recruit neutrophils to phagocytose them and *M. tuberculosis* (Yang et al., 2012). Previous studies revealed that neutrophils contribute to immune resistance to TB by producing antimicrobial peptides, facilitating the migration of DCs, and exerting protective effects on the oxidative killing of mycobacteria in TB granulomas (Martineau et al., 2007; Yang et al., 2012). Furthermore, accumulating evidence shows that B cells, natural killer (NK) cells, and mucosal-associated invariant T (MAIT) cells also play an important role in the immune response against *M. tuberculosis* by interacting with various immune cells, such as macrophages, T cells, and neutrophils (Achkar et al., 2015; Allen et al., 2015; Gong et al., 2021; Sakai et al., 2021).

However, the adaptive immune response is not triggered immediately; it has an interval of 2–3 weeks, which may be conducive to *M. tuberculosis* colonization (Jasenosky et al., 2015). Subsequently, T lymphocytes are activated and differentiate into interferon-γ-positive (IFN-γ^+) Th1 cells ($CD4^+$ T cells), cytotoxic T lymphocytes ($CD8^+$ T cells), Th17 cells, Th2 cells, and regulatory T cells (Tregs) (Chai et al., 2020). These activated

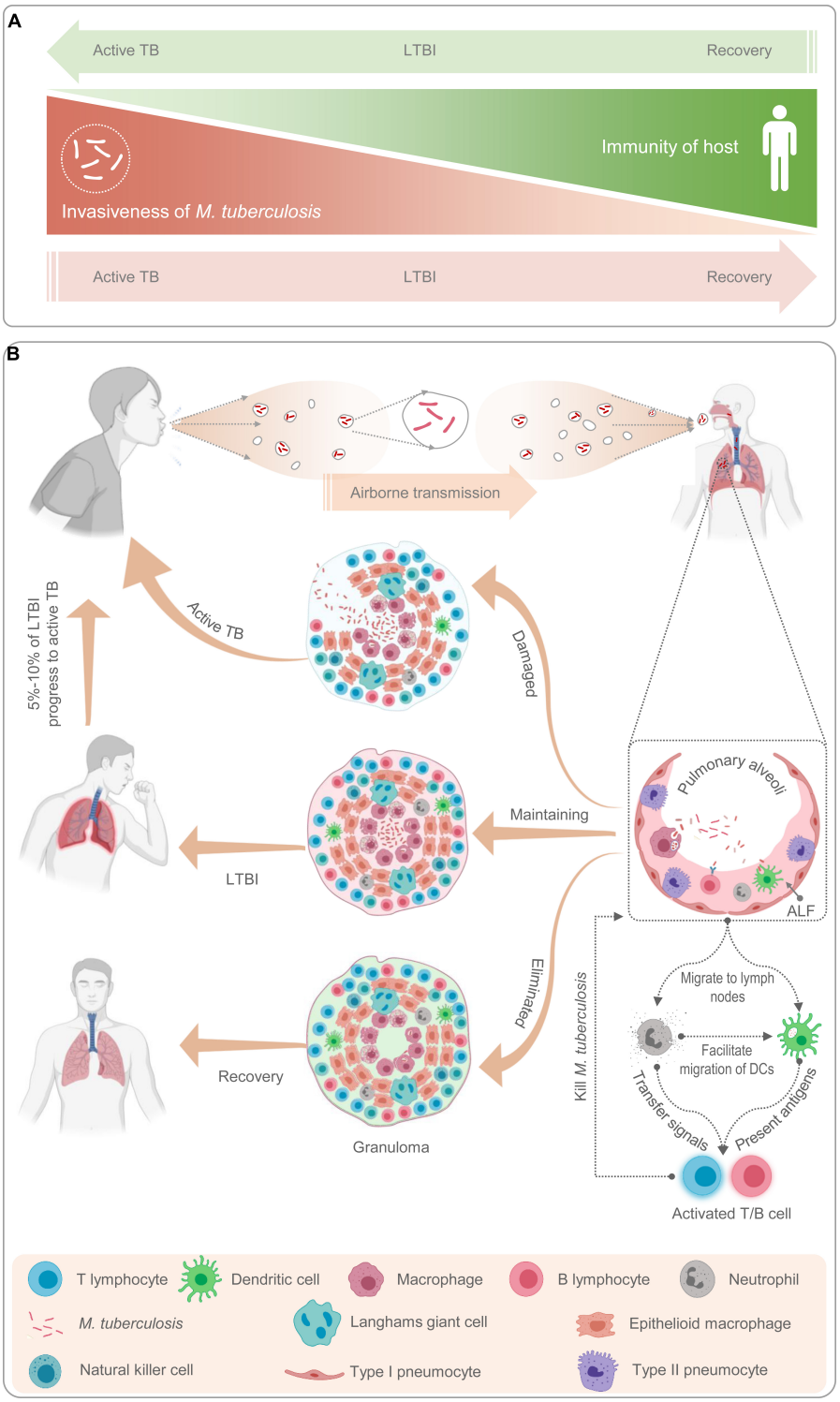

FIGURE 1 | Schematic diagram of latent tuberculosis infection and its mechanism. Latent tuberculosis infection (LTBI) is a balance between immunity of host and invasiveness of *M. tuberculosis*; any tilt would upset the balance **(A)**. The *M. tuberculosis* excreted from patients with active TB is inhaled by healthy people through airborne transmission and recognized and phagocytized by antigen-presenting cells such as macrophages, neutrophils, natural killer cells, and B lymphocytes **(B)**. Then, neutrophils release cytokines to activate and recruit T lymphocytes to gather at the place where *M. tuberculosis* invades to form granulomas **(B)**. If the host immunity is strong, *M. tuberculosis* will be cleared by immune cells and the host recovers; If the host immunity is weak, *M. tuberculosis* will reproduce in the granulomatous tissue and breaks through the granulomatous restriction to cause active TB; If the immunity of host and invasiveness of *M. tuberculosis* is balanced, the host will be latently infected **(A,B)**.

effector cells enter the blood circulation, migrate to the site of *M. tuberculosis* infection, and participate in local anti-TB immunity. At this stage, granulomas begin to form, and TST and IGRA results may be positive. The formation of tuberculous granulomas is a dynamic process between growth and decline. TB granulomas are the main battlefields for host immune cells and *M. tuberculosis*. The dying immune cells expose the hidden *M. tuberculosis* to the external environment to be phagocytosed and killed by the new immune cells. This process changes with the strength of the two belligerents, and the result directly affects the outcome of TB infection (Marino et al., 2015).

CURRENT METHODS USED TO DIAGNOSIS LATENT TUBERCULOSIS INFECTION

It has been reported that approximately one-fourth of the global population is latently infected with *M. tuberculosis* and that 5–15% of them may progress to aTB within 2 years, while the remaining individuals with LTBI are at a constant risk of reactivation (Houben and Dodd, 2016; Pai and Behr, 2016). The differential diagnosis of individuals with LTBI can not only promote an understanding of the pathogenesis of TB but also reduce the risk of progression of LTBI to aTB through preventive treatment. However, there is no specific gold standard test for diagnosing LTBI thus far (Chee et al., 2018). Currently, the diagnosis of LTBI mainly depends on the host's positive immune response to the antigens of *M. tuberculosis* and the clinical manifestations of the host. Currently, two methods are endorsed by the WHO as tests for TB infection—the century-old TST and IGRAs, which have been introduced since 2005 (Zellweger et al., 2020). The characteristics of the TST and IGRAs are listed in **Table 1**.

Skin Tests

Conventional Tuberculin Skin Test

The TST is a diagnostic method performed through subcutaneous injection of old tuberculin (OT) or purified protein derivative (PPD) as an antigen (Mosavari et al., 2021). It has been applied in the screening, diagnosis, and epidemiological studies of primary infection with *M. tuberculosis* for more than 100 years and is the main diagnostic test for LTBI. The TST is widely used to screen and detect TB owing to its advantages of being affordable, being simple to perform, and the requirement of minimal laboratory equipment. However, its disadvantages cannot be neglected, such as its requirement for a second visit after 48–72 h, inability to distinguish LTBI from aTB, false positives with Bacillus Calmette–Guérin (BCG) vaccination, cross-reactivity with non-tuberculous mycobacteria (NTM), and false negatives in immunosuppression and deficiency (Pourakbari et al., 2019).

Novel Emerging Skin Tests

In addition to the conventional TST, three novel strategies for the diagnosis of TB have been developed in recent years—Diaskintest (Generium Pharmaceutical, Moscow, Russia), C-Tb skin test (Statens Serum Institut, Copenhagen, Denmark), and EC-Test (Zhifei Longcom Biologic Pharmacy Co., Anhui, China) (Steffen et al., 2020; WHO, 2020). The Diaskintest is a new effective way to identify the initial presentation of TB and developed based on a fusion protein of the early secreted antigenic target 6 (ESAT-6) and culture filtrate protein 10 (CFP-10) antigens present in virulent strains of *M. tuberculosis*, which are absent in the BCG strain and in most NTMs. Recently, a meta-analysis based on 61 articles and 3,777,083 patients was conducted to evaluate the sensitivity and accuracy of the Diaskintest, and the results indicated that the overall diagnostic specificity, sensitivity, and accuracy of the Diaskintest were 98.0, 86.0, and 95.1%, respectively (Starshinova et al., 2020). However, the C-terminal of the fusion protein used in the Diaskintest contains 11 amino acids (including six histidine (HIS) labels) on the vector sequence other than the target gene, which does not conform to the "Technical Guiding Principles for Quality Control of Recombined DNA Products for Human Use" issued by the China Food and Drug Administration. The novel C-Tb skin test is based on a mixture of antigens ESAT-6 and CFP10. It combines the advantages of the field friendliness of TST and the high specificity of IGRAs. Two phase III clinical trials have investigated the safety and efficacy of the C-Tb skin test, QuantiFERON-TB Gold In-Tube (QFT-GIT), and TST, suggesting that C-Tb and QFT-GIT results were concordant in 94% of participants and that the safety profile of the C-Tb skin test was similar to that of the TST and QFT-GIT in HIV-negative adults and children as well as HIV-positive individuals with active or latent *M. tuberculosis* infection (Ruhwald et al., 2017; Aggerbeck et al., 2018). The EC-Test is the latest skin test for the diagnosis of aTB and LTBI. Similar to the Diaskintest and C-Tb skin test, the EC-Test is also developed based on ESAT-6 and CFP10 antigens of *M. tuberculosis*. Currently, clinical phase I, II, and III trials of the EC-Test have been completed. A phase I clinical trial and a phase IIa clinical trial indicated that the median maximum induration diameter of the EC-Test was similar to that of the TST and that a single dose of the EC-Test (1, 5, 10, or 20 μg/ml) was well tolerated and safe, with its diagnostic accuracy superior to that of the TST (Li et al., 2016a,b). A phase III clinical trial conducted in 1,559 participants found that the EC-Test and IGRAs have fairly high specificity and consistency (88.77%) (Chinese Antituberculosis Association et al., 2020).

Taken together, these three new tests are designed to detect immune responses stimulated with recombinant ESAT-6 and CFP-10 antigens to help address the problem of false-positive TST results that occur in patients who have received BCG vaccination (Ruhwald et al., 2016). Their specificity may be higher than that of the TST and may be more accurate, acceptable, and cheaper alternatives to IGRAs (Ruhwald et al., 2017). These skin tests have the advantages of the TST and IGRAs, which are characterized by simple operation, low cost, and easy reading of results, making it possible to apply them in countries with a high burden of TB and in poverty-stricken areas, especially in countries implementing universal BCG vaccination. Furthermore, increasingly emerging studies have demonstrated that these new skin tests show similar test positivity rates, safety profiles, and specificities to those of IGRAs and provide

TABLE 1 | The characteristics of the skin tests and IGRAs.

Terms	Skin tests				IGRAs				
	Conventional TST	**Diaskintest**	**C-Tb skin test**	**EC-Test**	**T-SPOT.TB**	**QFT-GIT**	**QFT-Plus**	**LIAISON QFT-Plus**	**LIOFeron TB/LTBI**
Manufacturer	Multiple manufacturers	Generium Pharmaceutical, Russia	Statens Serum Institut, Denmark	Zhifei Longcom, China	Oxford Immunotec, United Kingdom	QIAGEN, Hilden, Germany	Qiagen, MD, United States	DiaSorin S.p.A., Italy	LIONEX GmbH, Braunschweig, Germany
Time	> 100 years	2009	2010	2020	1990s	1980s	2015	2017	2019
Antigens	PPD	ESAT-6 and CFP10	ESAT-6 and CFP10	ESAT-6 and CFP10	ESAT-6 and CFP10	ESAT-6, CFP-10, and TB7.7 (p4)	ESAT-6 and CFP10	ESAT-6 and CFP10	ESAT-6, CFP-10, TB7.7, Ala-DH
Tubes	NA	NA	NA	NA	One tube	Nil tube, Antigen tube, and Mitogen tube	Nil tube, TB1 tube, TB2 tube, and Mitogen tube	Nil tube, TB1 tube, TB2 tube, and Mitogen tube	PC tube, TB-A tube, TB-B tube, and NC tube
Technological platform	NA	NA	NA	NA	ELISPOT	ELISA	ELISA	CLIA	ELISA
Sample	NA	NA	NA	NA	PBMCs	Whole blood	Whole blood	Whole blood	Whole blood
Sample transport and storage temperature	Refrigerate at 4°C	Refrigerate at 4°C	Refrigerate at 4°C	Refrigerate at 4°C	Indoor temperature, do not refrigerate or freeze	Indoor temperature, do not refrigerate or freeze	Indoor temperature, do not refrigerate or freeze	Indoor temperature, do not refrigerate or freeze	Indoor temperature, do not refrigerate or freeze
Outcome measure	Millimeters of induration	Millimeters of induration	Millimeters of induration	Millimeters of induration	Number of IFN-γ-producing T cells	Serum concentration of IFN-γ produced by CD4+ T cells	Serum concentration of IFN-γ produced by CD4+ and CD8+T cells	Serum concentration of IFN-γ produced by CD4+ and CD8+T cells	Serum concentration of IFN-γ produced by CD4+ and CD8+T cells
Positive internal control	No	No	No	No	PHA	Mitogen	Mitogen	Mitogen	Unknown
Need for return visit	Yes	Yes	Yes	Yes	No	No	No	No	No
Time required for results	48–72 h	48–72 h	48–72 h	48–72 h	16–20 h	16–24 h	16–24 h	Unknown	16–24 h
in vivo/in vitro	*in vivo*	*in vivo*	*in vivo*	*in vivo*	*in vitro*	*in vitro*	*in vitro*	*in vitro*	*in vitro*
Interpretation of result	Subjective (operator-based)	Subjective (operator-based)	Subjective (operator-based)	Subjective (operator-based)	Objective (instrument-based)	Objective (instrument-based)	Objective (instrument-based)	Objective (instrument-based)	Objective (instrument-based)
False positives with BCG vaccination	Yes	No	No	No	No	No	No	No	No
Cross-reactivity with NTMs	High	Low	Low	Low	Low, but can be influenced by infections of *M. kansasii*, *M. szulgai*, *M. marinum*, and *M. gordonae**	Low, but can be influenced by infections of *M. kansasii*, *M. szulgai*, and *M. marinum* (Andersen et al., 2000)	Low, but can be influenced by infections of *M. kansasii*, *M. szulgai*, and *M. marinum* (Andersen et al., 2000)	Unknown	Low
False positives with immunosuppression and deficiency	High	Low	Low	Low	Low	Low	Low#	Unknown	Unknown
Specificity	62% (BCG vaccinated) and 95% (BCG unvaccinated) (Ruhwald et al., 2016)	98% (Starshinova et al., 2020)	99.3% (Aggerbeck et al., 2013)	98% (Steffen et al., 2020)	76.2% (Yang et al., 2021)	99%§	95% (Sotgiu et al., 2019)	Unknown	98% in aTB and 97% in LTBI (Della Bella et al., 2020)
Sensitivity	75% (Aggerbeck et al., 2018)†	86% (Starshinova et al., 2020)	73.9% (Hoff et al., 2016)	86% (Steffen et al., 2020)	83.5% (Yang et al., 2021)	89%§and 73% (Aggerbeck et al., 2018)†	91% (Sotgiu et al., 2019)	Unknown	90% in aTB and 94%in LTBI (Della Bella et al., 2020)
Accuracy	Unknown	95.1% in total population and 92.4% in HIV-positive patients (Starshinova et al., 2020)	Unknown	87%	88.5% (Yang et al., 2021)	Unknown	Unknown	Unknown	Unknown

(Continued)

TABLE 1 | (Continued)

Terms	Skin tests			IGRAs				
	Conventional TST	Diaskintest	C-Tb skin test	EC-Test	T-SPOT.TB	QFT-GIT	QFT-Plus	LIAISON QFT-Plus	LIOFeron TB/LTBI
Limitations	Relatively low specificity, lacks sensitivity in immunosuppressed individuals and requires two clinic visits	Requires two clinic visits	Requires two clinic visits	Requires two clinic visits, Safety need further observed, Data on LTBI high-risk populations and infants are lacking.	Results should be evaluated in conjunction with clinical and other tests, and a negative result does not rule out the possibility of infection with M. tuberculosis	Results must be used in conjunction with individual's epidemiological history, current medical status, and other diagnostic evaluations	Results must be used in conjunction with risk assessment, radiography, and other medical and diagnostic evaluations	Need to define a borderline range based on clinical diagnostics criteria	Results must be used in conjunction with risk assessment, radiography, and other medical and diagnostic evaluations
Discrimination of LTBI from active TB (Hong et al., 2019; Della Bella et al., 2020; WHO, 2020)	No	No	No	No	No	No	No	No	No

CLIA, chemiluminescence immunoassay; ELISPOT, enzyme-linked ImmunoSpot; IGRAs, interferon-gamma release assays; LTBI, latent tuberculosis infection; NA, not applicable; NC, negative control; NTMs, non-tuberculous mycobacteria; PBMCs, peripheral blood mononuclear cells; PC, positive control; PHA, phytohemagglutinin; PPD, protein-purified derivative; TST, tuberculin skin test.

⋆ These data were obtained from T-SPOT.TB official web (http://tspot.com.cn) and T-SPOT.TB ELISPOT Package Insert. PI-TB8-IVD-CN Rev. 05. September 2019. Accessed May 6, 2021.

§These data were obtained from QuantiFERON official web (https://www.quantiferon.com/products/quantiferon-tb-gold/) and QuantiFERON-TB Gold (QFT) ELISA Package Insert. 1075115 Rev. 07. June 2018. Accessed May 6, 2021.

 # Theoretically, the inclusion of peptides for stimulation of $CD8^+$ T-cells can improve performance in immunocompromised conditions that affect $CD4^+$ T-cell responses and improve discrimination of LTBI from active TB.

†Data are limited in children and HIV-infected persons.

comparable results in terms of diagnosing patients with TB living with HIV and children infected with *M. tuberculosis* (**Table 1**; Litvinov et al., 2009; Aggerbeck et al., 2013; Hoff et al., 2016; Ruhwald et al., 2017; Aggerbeck et al., 2018; Steffen et al., 2020).

Nevertheless, the potential drawbacks of these three new skin tests are worth noting. First, these skin tests have insufficient diagnostic foundations for the differential diagnosis of LTBI. Second, vaccines based on recombinant ESAT6-CFP10 protein for prevention of LTBI may affect the diagnostic value of these skin tests in the future. Finally, these three novel skin tests should be validated in larger clinical trials in children, elderly individuals, and special populations such as in HIV-infected persons, immunosuppressant drug users, and people with malnutrition.

Interferon-Gamma Release Assays

To overcome the deficiencies of the TST, IGRAs have been developed as an alternative immunodiagnostic approach. Thus far, there are five commercialized IGRA kits, including the T-cell spot of the TB assay (T-SPOT.TB, Oxford Immunotec, Abingdon, UK), QuantiFERON-TB Gold In-Tube (QFT-GIT, Qiagen GmbH, Hilden, Germany), QuantiFERON-TB Gold-Plus (QFT-Plus, Qiagen, MD, United States), LIAISON QuantiFERON-TB Gold Plus (LIAISON QFT-Plus, DiaSorin S.p.A., Italy), and LIOFeron TB/LTBI (LIONEX GmbH, Braunschweig, Germany) (De Maertelaere et al., 2020; Della Bella et al., 2020; Altawallbeh et al., 2021; Hamada et al., 2021). In addition, there are five products in development—T-Track (R) TB (Lophius Biosciences GmbH), VIDAS TB-IGRA (bioMérieux), Access QuantiFERON-TB (Boditech Med Inc.), ichroma^{TM} IGRATB (Boditech Med Inc.), and IP-10 IGRA elisa/lateral flow (rBioPharm) (WHO, 2020).

T-cell Spot of the Tuberculosis Assay, QuantiFERON-Tuberculosis Gold In-Tube Test, and QuantiFERON-Tuberculosis Gold-Plus

T-cell spot of the TB assay is an enzyme-linked immunospot (ELISpot) assay developed by Prof. Lalvani in collaboration with his colleagues in the late 1990s (Lalvani et al., 2001). T-SPOT.TB detects the immune responses of peripheral blood-derived IFN-γ-secreting T cells stimulated with peptides from ESAT-6 and CFP10 antigens. The QFT-GIT assay is based on stimulating IFN-γ release from $CD4^+$ T cells in a single TB antigen tube with three antigens of *M. tuberculosis*, including ESAT-6, CFP-10, and TB7.7. Antigens ESAT-6 and CFP-10 are encoded within the *M. tuberculosis* region of difference 1 (RD1) locus, which eliminates interference from BCG and NTMs (Saracino et al., 2009). The QFT-Plus assay is designed to stimulate $CD4^+$ T cells using ESAT-6 and CFP-10 antigens in tube 1 (TB1) and elicit IFN-γ release from both $CD4^+$ and $CD8^+$ T cells using a cocktail of peptides derived from ESAT-6 and CFP-10 antigens in TB2 (Rozot et al., 2013). Compared with the QFT-GIT assay based on $CD4^+$ T-cell immune responses, the biggest improvement in the QFT-Plus assay is the addition of $CD8^+$ T-cell responses. It has been reported that the $CD8^+$ T-cell response in patients with aTB is higher than that in patients with LTBI (Theel et al., 2018). A systematic review and meta-analysis demonstrated

that QFT-Plus is more sensitive than QFT-GIT for detecting *M. tuberculosis* infection (Sotgiu et al., 2019), which is consistent with the results of another meta-analysis (Pourakbari et al., 2019). These data suggest that QFT-Plus is more sensitive than QFT-GIT in detecting *M. tuberculosis* infection, which may be due to $CD8^+$ T-cell immune responses in the TB2 tube. Therefore, QFT-Plus was approved by the United States Food and Drug Administration in 2017 to replace QFT-GIT (Theel et al., 2018). In 2019, Venkatappa et al. (2019) evaluated the agreement between QFT-Plus, QFT-GIT, T-SPOT.TB, and the TST in 506 participants at a high risk of LTBI and/or progression to TB disease. Their results showed that there was 94% agreement between QFT-Plus and QFT-GIT, 77% agreement between QFT-Plus or QFT-GIT and the TST, 92% agreement between QFT-Plus and SPOT.TB, and 91% agreement between QFT-GIT and T-SPOT.TB. These results indicated a high degree of agreement between QFT-GIT and QFT-Plus in a direct comparison and that all tests were in agreement with the TST and T-SPOT.TB.

LIAISON QuantiFERON- Tuberculosis Gold-Plus

The LIAISON QFT-Plus test, developed by DiaSorin in collaboration with Qiagen, is a whole blood-based QuantiFERON technology that offers efficient and high-throughput detection with QFT-Plus. The LIAISON QFT-Plus test is a fourth-generation technology for detecting LTBI. It is an improved version of the QFT-Plus test, in which the enzyme-linked immunosorbent assay (ELISA) in QFT-Plus has been replaced by a chemiluminescent immunoassay (CLIA) (Altawallbeh et al., 2021). A recent study evaluated the diagnostic performance of LIAISON QFT-Plus by comparing it with that of QFT-Plus test in 329 participants, showing 92.8, 97.9, and 97.8% agreement with the QFT-Plus test among patients with aTB, low-risk cohort, and mixed risk cohort participants, respectively (Altawallbeh et al., 2021). Furthermore, LIAISON QFT-Plus test can save time and labor and be a potentially useful addition to streamline LTBI screening (Kadkhoda et al., 2020). Moreover, these findings suggest that the automated LIAISON QFT-Plus test has a diagnostic performance comparable to that of the QFT-Plus test and can be applied for LTBI diagnosis. However, given that it is a newly emerging technology, the LIAISON QFT-Plus test requires more studies with large sample sizes to prove its sensitivity and specificity in the future.

LIOFeron Tuberculosis/Latent Tuberculosis Infection Assay

The LIOFeron TB/LTBI assay, developed by Lionex GmbH (Braunschweig, Germany) in 2019, is a novel IGRA test for diagnosing LTBI and TB (LIONEX, 2021). The LIOFeron TB/LTBI assay contains two components—human blood stimulation tubes (component 01) and human IFN-γ ELISA (component 02). Component 01 contains a positive control tube, a negative control tube, and TB antigen tubes. Compared with other IGRAs, the LIOFeron TB/LTBI assay contains not only ESAT-6, CFP-10, and TB7.7 but also a new antigen of *M. tuberculosis*, alanine dehydrogenase (Ala-DH). Previous studies have reported that Ala-DH is absent in BCG, induces major histocompatibility complex (MHC) class I-restricted T $CD8^+$ lymphocytes to produce IFN-γ, and participates in the adaptation of *M. tuberculosis* to the anaerobic dormant stage in LTBI (Jungblut et al., 1999; Dong et al., 2004; Agren et al., 2008). Recently, the sensitivity and specificity of the novel test were evaluated, and a comparison between its accuracy and that of the QFT-PLUS assay was performed in patients with aTB and LBTI (Della Bella et al., 2020). The results demonstrated that the sensitivity and specificity of the LIOFeron TB/LTBI assay was 90% and 98% for diagnosing aTB and 94% and 97% for diagnosing LTBI and that the LIOFeron TB/LTBI assay showed higher sensitivity than the QFT-Plus test for LTBI detection (Della Bella et al., 2020). However, like other IGRAs, the LIOFeron TB/LTBI assay cannot differentiate between LTBI and aTB.

RESEARCH STATUS, FUTURE DIRECTIONS, AND CHALLENGES FOR LATENT TUBERCULOSIS INFECTION DIFFERENTIAL DIAGNOSIS

Current methods such as the Diaskintest, C-Tb skin test, EC-Test, and T-SPOT.TB, QFT-GIT, QFT-Plus, and LIAISON QFT-Plus have greatly improved the accuracy, sensitivity, and specificity of *M. tuberculosis* infection detection, but they are still unable to distinguish LTBI from aTB. Since LTBI is a complicated heterogeneous state reflecting the interaction between *M. tuberculosis* and the host's immune response, the development of a better diagnostic technology that can differentiate LTBI from aTB requires a deep understanding of both the mycobacteria and its host (Chee et al., 2018). Herein, we will start from these two aspects to outline a possible blueprint for the technology exploration of LTBI differential diagnosis in hopes of pointing out directions and laying the foundation for future research on the topic.

Novel Biomarkers Derived From *Mycobacterium tuberculosis*

Antigens

Mycobacterium tuberculosis proteins encoded by RDs are feasible candidate biomarkers for differentiating *M. tuberculosis* infection from BCG vaccination (Al-Khodari et al., 2011). As mentioned above, the Diaskintest, C-Tb skin test, EC-Test, and T-SPOT.TB, QFT-GIT, QFT-Plus, and LIAISON QFT-Plus were designed based on RD1-encoded antigens, such as ESAT-6 and CFP-10. After reading the literature, we found 129 RD-associated antigens within the 16 RDs of *M. tuberculosis* (Ren et al., 2018). Additionally, although four antigens (Rv1737c, Rv1736c, Rv2031c, and Rv2626c) were excluded from the RD regions, previous studies have shown that these antigens show significant differences between the BCG strain and *M. tuberculosis* (Geluk et al., 2007; Honaker et al., 2008; Ji et al., 2015; Pena et al., 2015). Therefore, all 133 RD-associated antigens should be taken into consideration for developing new methods for the differential diagnosis of LTBI, with detailed information found in **Supplementary Table 1**. As mentioned above, none of these

seven novel methods can distinguish LTBI from aTB, suggesting that the differential diagnosis method of LTBI should contain not only RD-associated antigens but also latency-associated *M. tuberculosis* antigens.

Herein, we suggest that IGRAs should be further improved by the application of multiple antigens derived from RD-associated and latency-associated antigens of *M. tuberculosis*. Numerous studies have aimed to identify latency-associated antigens from *M. tuberculosis* as potential candidates for inclusion in immunodiagnostic tests for LTBI. A total of 124 latency-associated antigens were found in six categories—54 dormancy survival regulon antigens (DosRs), seven nutrition starvation (NS)-associated antigens, 20 reactivation antigens (RAs), five resuscitation-promoting factor (RPF) antigens, eight toxin–antitoxin system-associated antigens (TAS), and 30 other antigens associated with LTBI (**Supplementary Table 2**; Gordon et al., 2001; Chen et al., 2009; Ji et al., 2015; Meier et al., 2018).

Antigens belonging to both latency and RDs are the most novel and promising targets for LTBI differential diagnosis. Thus, we identified 21 LTBI-RD-related antigens from 133 RD-associated antigens and 124 latency-associated antigens of *M. tuberculosis*, including Rv1736c, Rv1737c, Rv2031c, Rv2626c, Rv2653c, Rv2654c, Rv2656c, Rv2657c, Rv2658c, Rv2659c, Rv2660c, Rv1511, Rv1978, Rv1980c, Rv1981c, Rv3872, Rv3873, Rv3878, Rv3879c, Rv3425, and Rv3429 (**Figure 2**). Detailed information on these 21 LTBI-RD-related antigens is summarized in **Table 2**. In brief, (1) There are four antigens derived from DosRs and RD-others, including Rv1736c, Rv1737c, Rv2031c, and Rv2626c. Honaker et al. (2008) reported that Rv1736c and Rv1737c were induced by *M. tuberculosis* rather than 13 BCG strains or *M. bovis*, suggesting that both antigens can be used to differentially diagnose latent infection even in BCG-vaccinated individuals. Rv1737c induced higher frequencies of IFN-γ^+ $CD8^+$ T cells and IFN-γ^+ TNF-α^+ $CD4^+$ T cells with a $CD45RO^+$ $CD27^+$ phenotype in long-term LTBI than pulmonary TB (PTB) (Arroyo et al., 2016), and the levels of the five cytokines [IL-10, transforming growth factor (TGF)-α, TNF-α, IL-12 (p40), and epidermal growth factor (EGF)] stimulated by Rv1737c were significantly higher in patients with TB than in household contacts (Chegou et al., 2012). For the Rv2031c antigen, it has been indicated that it could induce significantly higher IFN-γ production in the TST^-/$RD1^+$ and TST^+/$RD1^+$ groups than in the aTB group (Araujo et al., 2015). Furthermore, in patients with long-term LTBIs, higher percentages of IFN-γ^+ TNF-α^+ $CD8^+$ T cells were found in response to Rv2031c protein in comparison with PPD^- controls, with the most frequent memory phenotype of these cells being effector memory ($CCR7^-$ $CD45RA^-$) T cells, followed by effector ($CCR7^-$ $CD45RA^+$) T cells (Commandeur et al., 2011), which is consistent with an essential role of $CD8^+$ T cells in defending the host from *M. tuberculosis* infection (Bruns et al., 2009). The Rv2626c antigen induced significantly higher levels of IFN-γ in QFT^+ individuals or healthy household contacts than in QFT^- individuals or patients with TB and had the ability to differentiate individuals with LTBI from healthy controls and patients with TB, with 78.95% sensitivity and 83.02% specificity (Prabhavathi et al., 2015; Amiano et al., 2020), which is consistent with the sensitivity

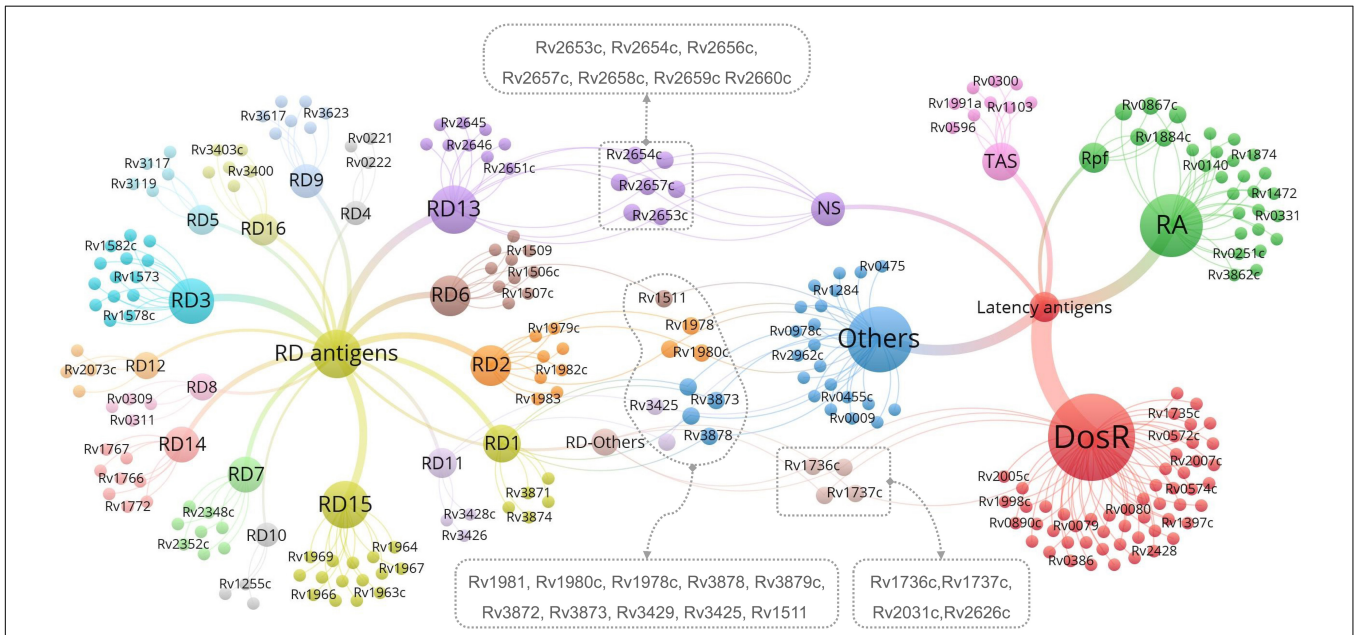

FIGURE 2 | The most promising LTBI-RD-related antigens for differential diagnosis of latent tuberculosis infection (LTBI) in the future. LTBI-related antigens are divided into six subtypes, including DosR, TAS, RA, NS, Rpf, and Others. RD-related antigens are divided into 16 subtypes, including RD1-RD15 and Others. Each subtype contains several antigens, each antigen is represented by a bubble, and different subtypes are represented by different colors. The size of the bubble represents the number of antigens in the subtype, and the line thickness represent the strength of the connection. The LTBI-RD-related antigens were identified by using a visualization and exploration software Graph (version 0.9.2, https://gephi.org/) and highlighted with dotted box. Each dot presents an antigen, limited to the space, some antigens' names were not shown in this figure, the detailed information can be found in **Supplementary Tables 1, 2**.

TABLE 2 | Summary of the most important LTBI-RD related antigens for LTBI differential diagnosis.

Antigens[a]	Types[a]		Product [b]	Function[b]	Functional category[b]	LTBI differential diagnosis	References
	LTBI	RD					
Rv1736c	DosR	Others	Probable nitrate reductase NarX	Involved in nitrate reduction, and in the persistence in the host	Intermediary metabolism and respiration	Induced by *M. tuberculosis* rather than 13 BCG strains or *M. bovis*	Honaker et al., 2008
Rv1737c	DosR	Others	Possible nitrate/nitrite transporter NarK2	Involved in excretion of nitrite, produced by the dissimilatory reduction of nitrate, across the membrane. Responsible for the translocation of the substrate across the membrane.	Cell wall and cell processes	(1) Higher TNF-α^+ $CD4^+$ T cells and IFN-γ^+ TNF-α^+ $CD4^+$ T cells in LTBI vs. PTB. (2) Higher IFN-γ^+ TNF-α^+ $CD8^+$ T cells in LTBI vs. HC	Chegou et al., 2012; Arroyo et al., 2016
Rv2031c	DosR	Others	Heat shock protein HspX	Has a proposed role in maintenance of long-term viability during latent, asymptomatic infections, and a proposed role in replication during initial infection.	Virulence, detoxification, adaptation	(1) Higher IFN-γ^+ TNF-α^+ $CD8^+$ T cells in LTBI vs. HCs (2) Higher concentrations of IFN-γ in LTBI vs. aTB vs. HC (3) Lower IFN-γ, IL-10, TNF-α in LTBI vs. aTB and HCs	Commandeur et al., 2011; Araujo et al., 2015; Belay et al., 2015
Rv2626c	DosR	Others	Hypoxic response protein 1 Hrp1	Unknown	Conserved hypotheticals	(1) 91% of CC QFT^- subjects secreted low levels of IFN-γ, but 43% of HCWs QFT^- people produced elevated IFN-γ, 69% of CC QFT^+ subjects didn't produce IFN-γ to Rv2626c (2) Higher IFN-γ producing T cells in CC vs. aTB and HC (3) IFN-γ response to Rv2626c has shown positivity of 88.57% in CC and 7.5% in PTB (4) Sensitivity and specificity of Rv2626c in aTB was of 77.1% and 85.1%	Ashraf et al., 2014; Prabhavathi et al., 2015; Amiano et al., 2020
Rv2653c	NS	RD-13	Possible PhiRv2 prophage protein	Unknown	Insertion seqs and phages	Less reactive DTH skin responses in *M. tuberculosis*-sensitized guinea pigs vs. PPD, but elicited no response in BCG-vaccinated guinea pigs.	Kasempimolporn et al., 2019
Rv2654c	NS	RD-13	Possible PhiRv2 prophage protein	Unknown	Insertion seqs and phages	(1) Higher IFN-γ levels TB vs. HC, had a high overall agreement (98.0%) with T-SPOT.TB, the combination of Rv2645 and CFP10-ESAT6 increased sensitivity and specificity of 96.0% and 98.2%, respectively. (2) Peptide $Rv2654c_{51-65}$ boosted the quantitative performance of the QFT-GIT assay from 1.83 IU/ml to 2.83 IU/ml	Luo et al., 2015; Horvati et al., 2016
Rv2656c	NS	RD-13	Possible PhiRv2 prophage protein	Unknown	Insertion seqs and phages	Unknown	-
Rv2657c	NS	RD-13	Probable PhiRv2 prophage integrase	Unknown	Insertion seqs and phages	Rv2657c react with the sera from LTBI Guinea pigs but not healthy Guinea pigs, SFCs of HCWs was significantly higher in HCWs vs. aTB	Yang, 2018
Rv2658c	NS	RD-13	Possible prophage protein	Unknown	Insertion seqs and phages	Unknown	-
Rv2659c	NS	RD-13	Probable PhiRv2 prophage integrase	Sequence integration. Integrase is necessary for integration of a phage into the host genome by site-specific recombination	Insertion seqs and phages	Higher IFN-γ producing T cells in LTBI vs. aTB and HC	Bai, 2015
Rv2660c	NS	RD-13	Hypothetical protein	Unknown	Conserved hypotheticals	(1) Higher number of IFN-γ producing cells and the levels of cytokines (IFN-γ, IL-2, IL-10, and MIP-1621299821α 621299821) in LTBI vs. TB, and higher ratio of IFN-γ+ CD4+ T cells in LTBI vs. TB or HCs (2) A component of vaccine H56:IC31 and will affect the diagnosis of Rv2660c once the vaccine is available	He et al., 2015; Luabeya et al., 2015
Rv1511	Others	RD-6	GDP-D-mannose dehydratase GmdA	Unknown, probably involved in nucleotide-sugar metabolism	Intermediary metabolism and respiration	Unknown	-
Rv1978	Others	RD-2	Conserved protein	Unknown	Conserved hypotheticals	ELISPOT of Rv1978 achieved sensitivities of 59% in aTB and specificities of 94% in BCG-vaccinated HC.	Chen et al., 2009
Rv1980c	Others	RD-2	Immunogenic protein Mpt64	Unknown	Cell wall and cell processes	Sensitivity and specificity were 0.92 and 0.95, respectively, sensitivity of the MPT64 test was significantly higher in TB infected children than in adults.	Cao et al., 2021
Rv1981c	Others	RD-2	Ribonucleoside-diphosphate reductase (beta chain) NrdF1	Involved in the DNA replication pathway.	Information pathways	ELISPOT of Rv1981c achieved sensitivities of 60% in aTB and specificities of 90% in BCG-vaccinated HC.	Chen et al., 2009

(Continued)

TABLE 2 | (Continued)

Antigens[a]	Types[a]		Product [b]	Function[b]	Functional category[b]	LTBI differential diagnosis	References
	LTBI	RD					
Rv3872	Others	RD-1	PE family-related protein PE35	Unknown	Pe/ppe	(1) Sensitivity and specificity of PE35 for detecting LTBI in children were 76% and 80%. (2) Elicited stronger immunoreactivity and could discriminate TB from HC vaccinated with BCG (better than Rv3878).	Mukherjee et al., 2007; Mahmoudi et al., 2017
Rv3873	Others	RD-1	PPE family protein PPE68	Unknown	Pe/ppe	Sensitivity and specificity of PE68 for detecting LTBI in children were 73% and 75%.	Mahmoudi et al., 2017
Rv3878	Others	RD-1	ESX-1 secretion-associated protein EspJ	Unknown	Cell wall and cell processes	Elicited stronger immunoreactivity and could discriminate TB from HC vaccinated with BCG.	Mukherjee et al., 2007
Rv3879c	Others	RD-1	ESX-1 secretion-associated protein EspK	Unknown	Cell wall and cell processes	The immunodominance of Rv3879c is higher than that of Rv3878 and Rv3873 in aTB and LTBI subjects.	Hinks et al., 2009
Rv3425	Others	RD-11	PPE family protein PPE57	Unknown	Pe/ppe	(1) Rv0310c-E coupled with Rv3425 (sensitivity: 87.30%, specificity: 73.68%) had the strongest performance for diagnostics of aTB. (2) Rv3425 has the promising potential to distinguish aTB from HC vaccinated with BCG.	Zhang et al., 2007; Wang et al., 2013; Luo et al., 2017
Rv3429	Others	RD-11	PPE family protein PPE59	Unknown	Pe/ppe	ELISPOT of Rv3429 achieved sensitivities of 47% in aTB and specificities of 93% in BCG-vaccinated HC.	Chen et al., 2009

[a]*These antigens were included in both LTBI and RD.*

[b]*The information of Product, Function, and Functional category of each antigen was obtained from mycobrowser database (https://mycobrowser.epfl.ch/) on April 26, 2021.*

aTB, active TB; CC, TB close contacts (subjects exposed to M. tuberculosis for less than three months); DTH, delayed-type hypersensitivity; DosR, Dormancy survival regulon antigens; HCs, health controls; HCWs, healthcare workers (individuals exposed to M. tuberculosis at least 2 years); NS, nutrition starvation-associated antigens; PPD, purified protein derivative; PTB, pulmonary TB; QFT, QuantiFERON; RD, Region of Difference; TB, tuberculosis.

(77.1%) and specificity (85.1%) of Rv2626c reported in another study (Ashraf et al., 2014).

(2) Seven antigens belonging to both NS-associated antigens and RD13 exhibit considerable potential, including Rv2653c, Rv2654c, Rv2656c, Rv2657c, Rv2658c, Rv2659c, and Rv2660c. Among the seven antigens, Rv2654c and Rv2660c were the most studied antigens. A previous study showed that Rv2654c induced a higher IFN-γ level in patients with TB than in healthy controls (HCs) and had a high overall agreement with T-SPOT.TB (98.0%) (Luo et al., 2015). An additional study reported that peptide $Rv2654c_{51-65}$ boosted the quantitative performance of the QFT-GIT assay from 1.83 IU/ml to 2.83 IU/ml (Horvati et al., 2016). Rv2660c is one of the most promising antigens for the differential diagnosis of LTBI. He et al. (2015) found that Rv2660c induced a significantly higher number of IFN-γ-producing cells and levels of cytokines [IFN-γ, IL-2, IL-10, and macrophage inflammatory protein 1-alpha (MIP-1α)] in patients with LTBI than in patients with TB and a higher ratio of IFN-γ^+ $CD4^+$ T cells in the LTBI group than in the aTB or HC group. Moreover, it is important to note that although Rv2660c induced a stronger immune response in LTBI than in aTB, it is a component of vaccine H56:IC31, which affects the differential diagnosis of Rv2660c once the vaccine is available (Luabeya et al., 2015). Rv2653c was used as a diagnostic skin test reagent in comparison with a standard PPD, and it was found that this antigen stimulated less of a delayed-type hypersensitivity (DTH) reaction in *M. tuberculosis*-sensitized guinea pigs, but no response was observed in BCG-vaccinated guinea pigs (Kasempimolporn et al., 2019), suggesting that this antigen can eliminate the interference of BCG vaccination with test results. Our previous study showed that Rv2657c reacted with the sera from LTBI guinea pigs but not those of healthy guinea pigs and that the number of IFN-γ-producing cells induced by Rv2657c and Rv2659c was significantly higher in patients with LTBI than in patients with aTB or HCs (Bai, 2015; Yang, 2018), indicating that Rv2657c and Rv2659c might be promising antigens for the differential diagnosis of LTBI. Additionally, the roles of Rv2656c and Rv2658c in the differential diagnosis of LTBI are unknown.

(3) Ten antigens belong to both LTBI others and RDs, including four antigens in LTBI others-RD1 (Rv3872-Rv3879), three antigens in LTBI others-RD2 (Rv1978, Rv1980c, and Rv1981c), one antigen in LTBI others-RD6 (Rv1511), and two antigens in LTBI others-RD11 (Rv3425 and Rv3429). Among them, the antigen that is most frequently studied is Rv3872. Previous studies have reported that the sensitivity and specificity of Rv3872 for detecting LTBI in children were 76% and 80%, respectively, which could elicit a stronger immunoreactivity for discriminating TB from HCs in patients who have received BCG vaccination (Mukherjee et al., 2007; Mahmoudi et al., 2017). In contrast, the remaining antigens (Rv3879, Rv1978, Rv1980c, Rv1981c, Rv3425, and Rv3429) were only tested between patients with TB and HCs with BCG vaccination or LTBI and HCs with BCG vaccination (Mukherjee et al., 2007; Zhang et al., 2007; Chen et al., 2009; Hinks et al., 2009; Wang et al., 2013; Luo et al., 2017; Mahmoudi et al., 2017; Cao et al., 2021). Hinks et al. (2009) compared the responses to a range of RD1-encoded antigens (ESAT-6, CFP-10, Rv3879c, Rv3878, Rv3873, and Rv2031c) and

defined a similar hierarchy of immunodominance for these antigens in both aTB and LTBI subjects: CFP-10 > ESAT-6 > Rv3879c > Rv3878 > Rv3873 > Rv2031c. Furthermore, Rv3425 has been evaluated as a candidate for the development of a vaccine for TB control, which may affect its accuracy in detecting LTBI (Wang et al., 2008).

Our findings suggest that these 21 LTBI-RD-associated antigens are promising alternatives to diagnostic biomarkers for discriminating LTBI from aTB and HCs in patients who have received BCG vaccination. By analyzing the above research results, it is not difficult to find that the intensity of the immune response induced by these LTBI-RD-related antigens was always higher in the LTBI group than in the aTB group. However, the ESAT-6/CFP10 responses, which are not dormancy related, were also much higher in the LTBI group than in the aTB group; thus, the relative advantages of these LTBI-RD-related antigens are unclear. The reason for this may be as follows: the immunity of patients with aTB is weakened and the responses of T cells are usually suppressed (**Figure 1A**). Therefore, the sensitivity and specificity of these LTBI-RD-related antigens need to be validated in further studies with larger sample sizes and broader population coverage in the future. In addition, there are also problems in the differential diagnosis of LTBI-RD-associated antigens: (1) the immunogenicity of these antigens is significantly lower than that of proliferative antigens; (2) the population coverage rate of the immune responses induced by these antigens is low; (3) most of the *M. tuberculosis* in the macrophages of patients with LTBI are in a state of latent infection, but a small part of them is in a state of irregular proliferation; and (4) not all *M. tuberculosis* in patients with active TB are in a proliferative state and are influenced by the immune state of the host and the treatment of chemotherapy drugs, with some *M. tuberculosis* possibly also being in a latent state.

Peptides

The LTBI-RD-associated antigens derived from *M. tuberculosis* constitute a potential source of specific antigens for immunodiagnosis and vaccine development for LTBI. Screening the diagnostic potential of specific T- or B-cell epitopes from LTBI-RD-associated antigens and verifying their peptides in different populations are a new concept for the differential diagnosis of LTBI. Currently, most of the studies on peptides derived from LTBI-RD-related antigens in differentiating LTBI from aTB and HCs are still in their initial stages. Only a few studies have screened immunodominant peptides of latency and/or RD-related antigens in animal models and humans, such as Rv1985c$_{pool2}$, Rv1985c$_{pool4}$, Rv3425$_{pool1}$ (Wang et al., 2013), Rv1733c$_{57-84}$ (Coppola et al., 2015), Rv2654c$_{51-65}$ (Horvati et al., 2016), peptide pools from RD1 antigens (Rv3871 to Rv3878) (Mustafa et al., 2002), T-cell epitopes of Rv3872 and Rv3873 (Hanif et al., 2011; Jiang et al., 2016), and Rv3425$_{118-126}$ (LIASNVAGV) (Chen et al., 2012). However, most of these mapped and identified peptides can only discriminate aTB from HCs with BCG vaccination and fail to distinguish LTBI from aTB.

The limitation of these studies is that they only focused on epitopes singly identified from $CD4^+$ T lymphocytes [helper T lymphocytes (Th)] or $CD8^+$ T lymphocytes (CTLs) rather than epitopes synchronously identified from Th cells, CTL cells, and B cells. Although the traditional view is that the host clearance and killing of *M. tuberculosis* mainly depend on $CD4^+$ T lymphocytes and $CD8^+$ T lymphocytes, accumulated data show that B lymphocytes also play an irreplaceable role in fighting against *M. tuberculosis* (Gong et al., 2018, 2021; Watson et al., 2021). Therefore, peptides binding to Th cells, CTL cells, and B cells should be considered when designing new candidate biomarkers based on epitopes for distinguishing LTBI from aTB and BCG-vaccinated HCs.

Furthermore, MHC molecules affect the efficacy of peptide-based vaccines and diagnosis (Gong et al., 2021; Jia et al., 2021). It is well known that recognition peptides produced by $CD4^+$ or $CD8^+$ T cells are mostly restricted to MHC-II or MHC-I molecules, respectively. Human leukocyte antigens (HLAs) are highly polymorphic; thus, the selection of peptides that can be recognized by multiple HLAs will increase the population coverage of peptide-based diagnosis (Bui et al., 2006). As the frequency of HLA expression varies greatly among different ethnicities, the problem of population coverage related to MHC polymorphisms becomes more complicated. Thus, without careful consideration, peptide-based vaccines or diagnostic candidates will result in ethnically biased population coverage.

Novel Biomarkers Derived From Hosts

Our previous research and other large amounts of data show that TB is not only an infectious disease but also an immune disease (Gong et al., 2018, 2020, 2021; Li et al., 2020; Liang et al., 2021; Rambaran et al., 2021). The pathogenesis of TB is closely related to the host's immune response. Therefore, to promote the development of sensitive methods for the detection and treatment of LTBI, it is particularly urgent to understand the host responses involved in the establishment and maintenance of LTBI (Banerjee et al., 2021).

Cytokines

Cytokines are small molecular polypeptides or glycoproteins synthesized and secreted by immune cells (such as monocytes, macrophages, T cells, B cells, and NK cells) and some non-immune cells (such as endothelial cells, epidermal cells, and fibroblasts) after stimulation. Cytokines have a variety of biological functions, such as regulation of cell growth, differentiation and maturation, immune response, inflammation, wound healing, tumor growth, and function maintenance. Levels of host cytokines vary in the different stages of *M. tuberculosis* infection, which may serve as biomarkers for differentiating LTBI from aTB (Luo et al., 2019).

Detection of IFN-γ stimulated by specific antigens of *M. tuberculosis* is a common practice in most IGRA experiments. Won et al. (2017) measured the levels of 29 cytokines in 48 patients with aTB, 15 LTBI, and 13 HCs and found that eight cytokines [GM-CSF, IFN-γ, IL-1RA, IL-2, IL-3, IL-13, interferon-gamma-inducible protein 10 (IP-10), and MIP-1β] in the TB-infected group were significantly different from those of the HCs, and that eight cytokines [EGF, GM-CSF, IFN-γ, IL-2, IL-5, IL-10, TNF-α, and vascular endothelial growth factor (VEGF)] were significantly different between aTB and LTBI. However, the

limitation of this study is its small sample size, with its results needing to be further verified through another study with a large sample size. In 2018, Meier et al. (2018) performed a systematic review to summarize the cytokines measured in 34 included studies, with as many as 26 cytokines used as biomarkers in these studies, including IFN-γ, TNF-α, IL-2, IL-10, IL-17, IL-8, IL-6, IP-10, IL-1β, monocyte chemoattractant protein-1 (MCP-1), IL-12, IL-12p40, MCP-2, fractalkine, granzyme B, GM-CSF, IFN-α2, sIL-2Ra, IL-4, IL-5, IL-13, MIP-1β, Regulated upon Activation, Normal T cell Expressed and presumably Secreted (RANTES), sCD40L, TGF-α, and VEGF. Among these 26 cytokines, the top 5 cytokines used as biomarkers for discriminating between LTBI and patients with aTB were IFN-γ (34 publications), TNF-α (15 publications), IL-2 (12 publications), IL-10 (10 publications), and IL-17 (9 publications) (**Supplementary Figure 1**).

Although IFN-γ and TNF-α are still the most popular cytokines in the differential diagnosis of LTBI, studies on IL-2, IL-10, IP-10, and VEGF have been increasing in recent years. To understand the latest research progress on these cytokines for discriminating between LTBI and aTB, we searched publications related to them in the Web of Science database. We found that the number of publications related to IFN-γ, TNF-α, IL-2, IL-10, IP-10, and VEGF were 1,419, 418, 136, 62, 96, and 18, respectively (**Figure 3**). The co-authorship map of IFN-γ (**Figure 3A**), TNF-α (**Figure 3B**), IL-2 (**Figure 3C**), IL-10 (**Figure 3D**), IP-10 (**Figure 3E**), and VEGF (**Figure 3F**) cytokines based on bibliographic data showed similar trends and popularity to the systematic review. In 2020, two meta-analyses were conducted to evaluate candidate cytokines as biomarkers to distinguish LTBI infection from aTB. A systematic meta-analysis by Sudbury et al. (2020) measured 100 cytokines among 56 included studies and found that the most frequently studied cytokines were IFN-γ, IL-2, TNF-α, IP-10, IL-10, and IL-13. A meta-analysis by Qiu et al. (2020) evaluated seven cytokines, including IFN-γ, TNF-α, IP-10, IL-2, IL-10, IL-12, and VEGF, suggesting that cytokines IL-2, IFN-γ, and VEGF can be utilized as promising biomarkers to distinguish LTBI from aTB. Furthermore, compared to IFN-γ, the level of IP-10 was higher and was released independently of age, suggesting that IP-10 may be a candidate biomarker in the pediatric population (Alsleben et al., 2012).

Although individual cytokines provide considerable potential for use in the differential diagnosis of LTBI, for most cytokines, findings were heterogeneous among studies. These differences in results or even diametrically opposite conclusions may be related to differences in study design, experimental methods, statistical methods, individual genetic backgrounds, antigen types, sample sizes, and environmental factors (Rambaran et al., 2021). Therefore, reducing or even eliminating the heterogeneity between different research results is a limitation that needs to be overcome. Recent studies have found that a combination of cytokines may be an alternative to solve this problem. Wang et al. (2018) identified a six-cytokine biosignature (including IFN-γ, IL-10, IL-1Ra, IP-10, VEGF, and IL-12p70) to discriminate between aTB and LTBI, resulting in a sensitivity of 88.2% and a specificity of 92.1% in a biomarker validation cohort (n = 216) and a sensitivity of 85.7% and a specificity of 91.3% in a prospectively recruited clinical validation cohort (n = 194), respectively. Coincidentally, Korma et al. (2020) evaluated the sensitivity, specificity, and accuracy of the combination of seven cytokines (IFN-γ, IP-10, IL-2R, C-X-C Motif Chemokine Ligand 9 (CXCL-9), IL-10, IL-4, and TNF-α) based on gene expression in differentiating between aTB and LTBI. They demonstrated that the combination of IL-10, IP-10, and IL-4 could differentiate pulmonary patients with TB from latent patients with TB with a sensitivity and specificity of 77.1% and 88.1%, respectively (Korma et al., 2020). Luo et al. (2019) identified potential biomarkers from 38 plasma cytokines to discriminate among the different stages of *M. tuberculosis* infection in its study participants, who were composed of 78 patients with aTB, 73 patients with LTBI, and 76 HCs. They found that the combination of five cytokines (IP-10, MCP-1, IL-1α, IL-10, and TNF-α) had an excellent performance in diagnosing LTBI, with 94% sensitivity and 81.25% specificity, and that the combination of three cytokines (eotaxin, macrophage-derived chemokine (MDC), and MCP-1) had a 0.94 area under the curve (AUC) in differentiating ATB from LTBI with 87.76% sensitivity and 91.84% specificity, respectively (Luo et al., 2019). The above data show that the combination of multiple cytokines can significantly improve specificity and sensitivity, which also points out the direction of future research.

Antibodies

Antibody responses are a major form of defense against microbes (Vinuesa et al., 2016). *M. tuberculosis* infection has been reported to induce antibody responses, but it is still unclear whether patients with aTB or those with LTBI produce protective antibodies, as well as which antigens these target (Feng et al., 2013; Loxton and van Rensburg, 2021). With the emerging evidence regarding immune modulation, the complete characterization of B cells and humoral immunity could be of significant value (Dubois Cauwelaert et al., 2016). In 2013, Feng et al. (2013) developed a novel 38F-64F indirect ELISA (including 38 kDa, ESAT-6, CFP10, Mtb8.4, MPT64, TB16.3, and Mtb8) method to detect TB and LTBI, and the results showed that the sensitivity of the 38F-64F indirect ELISA was much higher than that of the sputum culture test (86.91% vs. 50.62%), with the sensitivity of the sputum smear test (78.64% vs. 47.57%) accounting for 74.16% and 37.14% of patients with TB and patients with LTBI, respectively. Five years later, a study screened serum biomarkers of 40 serum samples from patients with LTBI and aTB using a proteome microarray containing 4,262 antigens, and the results suggested that specific IgG levels of 152 *M. tuberculosis* antigens were significantly higher in patients with aTB than in LTBI (Cao et al., 2018). However, any single antigen-specific antibody is not enough to be used to cover the antibody profiles of all patients with TB. Therefore, the combination of antigen-specific antibodies may be an alternative for increasing sensitivity and specificity. Yan et al. (2018) reported that the sensitivity and specificity of individual antigen-specific antibodies are relatively low in detecting patients with TB not infected with the bacteria, but the combination of six antigen-specific antibodies (LAM, 38KD, MPT32, EspC, MPT64, and Mtb81) increased sensitivity and specificity to 69.6% and 77.0%, respectively. Similarly, another study also demonstrated that

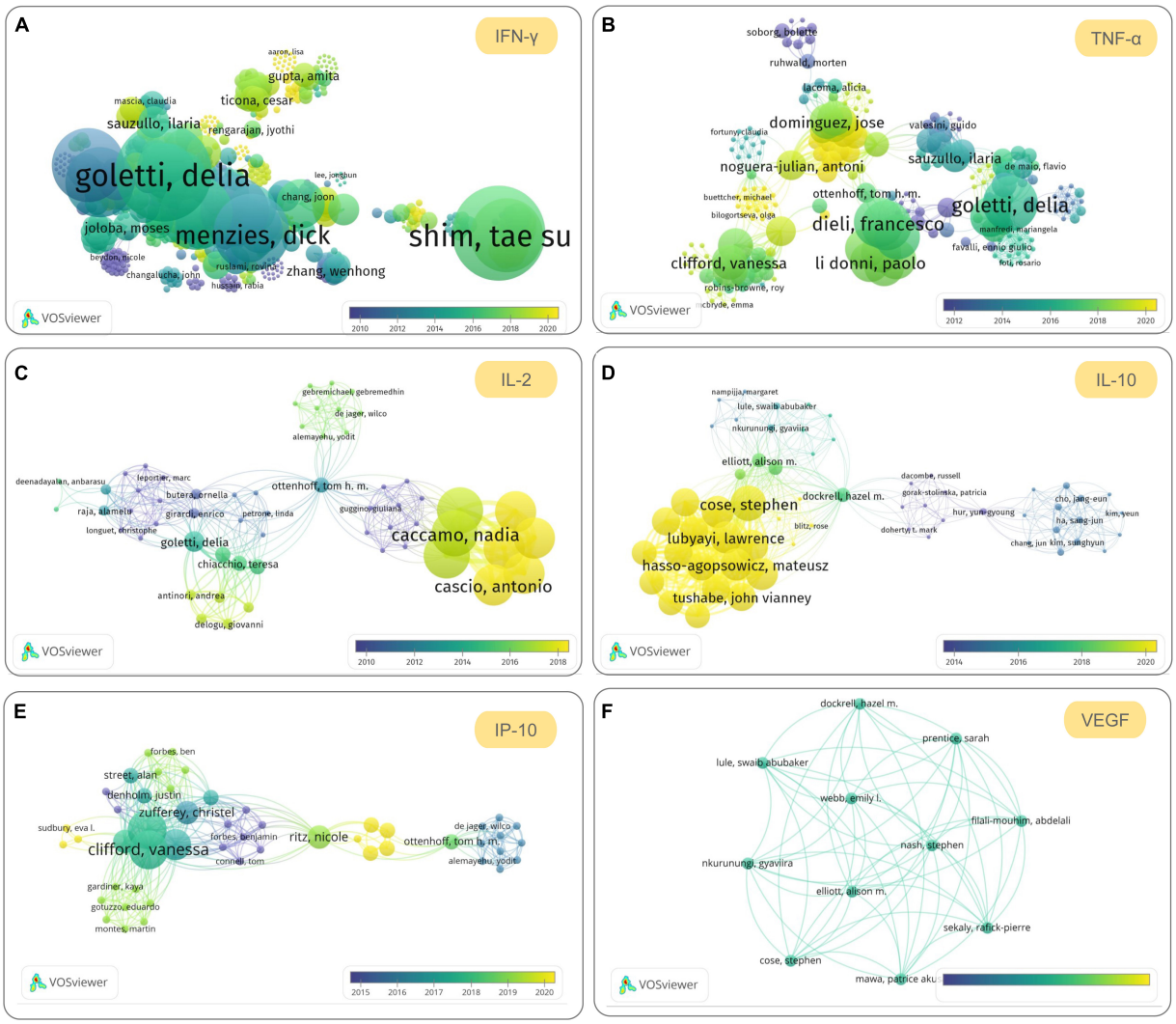

FIGURE 3 | The most promising cytokines to be used to differentiate and diagnose latent tuberculosis infection (LTBI) in the future. The co-authorship maps of interferon (IFN)-γ **(A)**, tumor necrosis factor (TNF)-α **(B)**, interleukin (IL)-2 **(C)**, IL-10 **(D)**, interferon-gamma-inducible protein 10 (IP-10) **(E)**, and vascular endothelial growth factor (VEGF) **(F)** cytokines based on bibliographic data obtained from Web of Science were visualized by using VOSviewer version 1.6.16 (developed by Nees Jan van Eck and Ludo Waltman at Leiden University's Centre for Science and Technology Studies CWTS). The search terms used in Web of Science are "LTBI" and cytokine name (topic terms), the Timespan was set from 1900 to 2021, the database was set "All databases," and other parameters are default values. The parameters in VOSviewer were set as below: Type of analysis, Co-authorship; Unit of analysis, Authors; Counting method, Full counting; Normalization method, Association strength; Layout, Attractions 2, Repulsion-1; Clustering, Resolution 1.00, Min. cluster size 1; other parameters are default values.

the sensitivity (96.6%) and specificity (92.3%) of IgA/IgG of a fused MT10.3:MPT64 protein were significantly higher than those of single antigens in pleural TB cases (da Silva et al., 2019). These results suggest that combining multiple antigen-specific antibodies can significantly improve the sensitivity and specificity of a single antigen-specific antibody, which will help in the diagnosis of TB and LTBI, but the current data are insufficient and further research is needed.

Markers of Immune Cells

As mentioned above, TB is a heterogeneous disease with a wide range of infectious and immunological profiles. It is well-known that the immunological markers of T-lymphocyte subsets and NK cell surfaces correlate with cell differentiation, latency/disease status, and outcome, making these cell surface markers potential targets for TB diagnosis and treatment (Petruccioli et al., 2016).

$CD4^+$ T lymphocytes play a fundamental role in controlling *M. tuberculosis* infection, and the biomarker expression profiles of $CD4^+$ T cell surfaces are associated with bacterial loads at different infection stages. Assessment of CD27 and/or CCR4 expression on $CD4^+$ T cells has been reported to be a robust biomarker for discriminating among TB stages. A previous study analyzed the expression of CD27 and CCR4 biomarkers in IFN-γ^+CD4^+ T cells collected from patients with aTB and patients with LTBI and found that the proportion of $CD27^-$IFN-γ^+CD4^+ T cells or $CCR4^+$ IFN-γ^+CD4^+ T cells

was significantly higher in patients with aTB than in those with LTBI in response to PPD or ESAT-6/CFP-10 recombinant proteins and that the proportion of $CD27^{-}CCR4^{+}IFN\text{-}\gamma^{+}CD4^{+}$ T cells was significantly associated with aTB. Furthermore, other studies also found that the $CD38^{+}CD27^{-}TNF\text{-}\alpha^{+}CD4^{+}$ T-cell subset is a potential biomarker for diagnosing TB with 96.15% specificity and 90.16% sensitivity (Acharya et al., 2021), with $IFN\text{-}\gamma^{+}CD27^{low}CD4^{+}$ T cells described as aTB biomarkers (Latorre et al., 2018). These findings suggest that the loss of CD27 and the increase in CD38 and CCR4 biomarkers could be associated with uncontrolled *M. tuberculosis* infection. In addition, innate T cells, such as MAIT and invariant NK T (iNKT) cells, play roles in recognizing *M. tuberculosis*-infected cells. Accumulating evidence highlights the importance of both MAIT and iNKT cells in controlling TB infection (Ruibal et al., 2021). It has been reported that the number of both cell types was significantly higher in subjects with LTBI than in patients with aTB or uninfected individuals, and that iNKT cells from patients with LTBI showed lower PD-1 expression than those from patients with aTB (Paquin-Proulx et al., 2018).

New Models and Algorithms

As mentioned above, the immunological methods that are frequently used, such as skin tests and IGRAs, are intrinsically unable to discriminate LTBI from aTB. Recently, with the development of artificial intelligence (AI) and bioinformatics, new strategies have been introduced to improve diagnostic performance in distinguishing LTBI from aTB, such as the ImmunoScore (IS) model, Cox proportional hazards model, expectation maximization algorithm, silico mapping algorithm, and random forest algorithm (Villate et al., 2006; Zhou et al., 2017; Ndzi et al., 2019; Wu et al., 2019; Rambaran et al., 2021). IS is a novel and promising prognostic tool that is widely used in tumors. It has been reported that the IS model can effectively distinguish aTB from LTBI, with a sensitivity of 95.7% and a specificity of 92.1% (Zhou et al., 2017). The Cox proportional hazards model was applied to estimate the survival experience and risk factors among patients with TB, and these studies observed that associations were stronger in the Cox proportional hazards model, suggesting that the impact of behavioral and clinical variables affected TB outcome (Tolosie and Sharma, 2014; Abedi et al., 2019; Rambaran et al., 2021). Villate et al. (2006) analyzed infection data of LTBI and *M. avium* using the expectation maximization algorithm, and their results confirmed that the mixture models using the expectation maximization algorithm can better estimate the probability of LTBI in the presence of other NTM and BCG vaccinations. Ndzi et al. (2019) developed a silico mapping algorithm to discriminate LTBI from aTB and found that people with the $QFT\text{-}GIT^{+}$ and $DRB1^{*}10\text{-}DQB1^{*}02\ haplotype^{+}$ may have a higher chance of developing LTBI and that those with the $QFT\text{-}GIT^{+}$ and $DRB1^{*}10\text{-}DQB1^{*}02\ haplotype^{-}$ may progress to aTB. Wu et al. (2019) also developed a random forest algorithm to discriminate between aTB and LTBI based on the test data of T-SPOT.TB, and the results indicated that the sensitivity and specificity of this algorithm were 82.87% and 88.03%, respectively, which were higher than those of T-SPOT.TB (82.80% and 70.00%, respectively), TB (82.80% and 74.20%), and QFT-GIT (71.40% and 81.00%). Although these innovative strategies are still in their initial development stages with only a few studies conducted on them, they still provide valuable information for a comprehensive understanding of TB and allow for new insights on differential diagnosis of LTBI and aTB to be gained.

Omics Technologies

In recent years, advances in multiplexing and information technology have enabled researchers to perform more comprehensive analyses of complete genomes, transcriptomes, proteomes, and metabolomes. The use of these omics techniques has provided valuable insights for understanding the transcriptomic, proteomic, and metabolomic changes of *M. tuberculosis* during dormancy and reactivation.

Transcriptomics

The complete genome sequencing of the *M. tuberculosis* H37Rv strain in 1998 allowed for improvement in our understanding of *M. tuberculosis* (Cole et al., 1998). Transcriptome analysis provides insights into the expression profiles of genes in human samples (such as blood) during the different stages of *M. tuberculosis* infection. As early as 2007, Jacobsen et al. (2007) compared the gene expression signature of peripheral blood mononuclear cells (PBMCs) collected from patients with aTB, individuals with LTBI, and HCs by microarray analysis and found that three genes (*Ras-associated GTPase 33A, lactoferrin*, and *CD64*) were sufficient for classifying these three groups of individuals. Almost at the same time, Mistry et al. (2007) expanded the application of this technology to patients with aTB and individuals with LTBI in patients with recurrent disease and cured patients with TB using DNA array technology and quantitative reverse-transcriptase polymerase chain reaction (qRT-PCR). Their results demonstrated that a set of nine genes could discriminate the four groups of individuals, including *ATP5G1*, *ASNA1*, *C14orf2*, *KIAA2013*, *LY6G6D*, *NOLA3*, *RIN3*, *SOCS3*, and *TEX264*. Zhang et al. (2007) determined the transcriptomic profiles of exosomal RNAs collected from 30 HCs, 30 patients with aTB, and 30 individuals with LTBI. In comparison with the HCs, five genes were significantly upregulated and highly expressed in individuals with LTBI, but they were downregulated and expressed at low levels in patients with aTB. These included *TTLL10*, *RP11-358N4.3*, *RMRP*, *PPPH1*, and *RN7SK* (Lv et al., 2017), which represent novel biomarkers for the diagnosis of LTBI and aTB. More recently, Bayaa et al. (2021) conducted a multicenter prospective nested case-control study to evaluate the performance of a human blood transcriptomic signature termed *RISK6* in the diagnosis of LTBI and aTB, and their results showed that the sensitivity and specificity of *RISK6* for discriminating aTB from LTBI were 90.9% and 88.5%, respectively.

Transcriptomics is also used to assess the risk of LTBI developing into aTB. In 2010, a study analyzed the genome-wide transcriptional profiles of blood samples obtained from patients with aTB, individuals with LTBI, and HCs and found that the signatures of aTB were observed in 10%–20% of patients with

LTBI, indicating that these identified individuals with LTBI were at risk of developing aTB (Berry et al., 2010).

Proteomics

Proteomics, developed on the basis of genomics, is complementary to studies at the transcriptional level (Betts, 2002). The emergence and development of proteomics have enabled the discovery of new biomarkers at the gene level, which can be used to distinguish LTBI from aTB to be verified at the protein level. Previous studies have identified a large number of biomarkers that are differentially regulated during dormancy and reactivation using proteomics and transcriptomics; for example, the DosR and genes involved in DNA replication are upregulated and downregulated, respectively, during dormancy, but undergo the opposite changes during reactivation (Kundu and Basu, 2021). Cao et al. (2018) performed a proteome microarray assay containing 4,262 antigens to identify potential serum biomarkers for distinguishing between LTBI and aTB, and their results indicated that antigens Rv2031c, Rv1408, and Rv2421c had higher AUCs of 0.8520, 0.8152, and 0.7970, respectively. With the development of high-resolution quantitative proteomics and label-free quantitative proteomics, a growing number of protein signatures that can be used for the differential diagnosis of LTBI and aTB have been discovered. Mateos et al. (2019) performed high-resolution quantitative proteomics using an LTQ-Orbitrap-Elite platform to screen for potential protein signatures in the sputum and saliva of patients with aTB, individuals with LTBI, and HCs. Their findings suggested that a reduction in proteins related to glucose and lipid metabolism was observed in the saliva of patients with TB, while the proteomic signatures of sputum from individuals with LTBI and HCs consisted of proteins related to bitterness perception, pathogen defense, and the innate immune response. Similarly, Sun et al. (2018) performed label-free quantitative proteomics to determine plasma signatures for discriminating PTB from LTBI or HCs and found that a combination of alpha-1-antichymotrypsin (ACT), alpha-1-acid glycoprotein 1 (AGP1), and E-cadherin (CDH1) showed 81.2% sensitivity and 95.2% specificity in discriminating PTB from LTBI and 81.2% sensitivity and 90.1% specificity in discriminating PTB from HCs.

Metabolomics

Metabolomics is a field newly developed after genomics and proteomics, and it is an important part of systems biology. Genomics and proteomics explore the processes of life at the gene and protein levels, respectively. In fact, many life activities in cells occur at the level of metabolites, such as cell signaling, energy transfer, and cell-to-cell communication (Griffiths and Wang, 2009). Since the metabolome is the final downstream product of the genome, transcriptome, and proteome, any interference at these levels will change the metabolome. In 2017, Preez et al. (2017) reviewed and summarized abundant biomarkers related to TB diseases that have been identified in culture (Phillips et al., 2007; Syhre and Chambers, 2008; Olivier and Loots du, 2012; Lau et al., 2015), human sputum (Schoeman et al., 2012; du Preez and Loots, 2013), animal or human blood and tissue (Shin et al., 2011; Somashekar et al., 2012; Weiner et al., 2012; Che et al., 2013; Zhou et al., 2013; Frediani et al., 2014; Feng et al., 2015), human urine (Banday et al., 2011; Das et al., 2015), and human breath (Phillips et al., 2007; Syhre et al., 2009; Phillips et al., 2010; Kolk et al., 2012) using a metabolomics research approach (Preez et al., 2017). However, most of the signatures identified in these studies were obtained by comparing patients with TB and HCs or other diseases, and only one study was performed among patients with TB, individuals with LTBI, and HCs. In this study, Weiner et al. (2012) explored the metabolites in serum collected from three groups of individuals, and their results showed that compared to individuals with LTBI, patients with aTB showed increased indoleamine 2,3 dioxygenase 1 activity, decreased phospholipase activity, increased adenosine metabolite abundance, and increased levels of fibrotic disease indicators. Furthermore, they also found that the abundance of inosine was significantly lower in individuals with LTBI than in patients with TB and HCs (Weiner et al., 2012). More recently, Dutta et al. (2020) analyzed the plasma metabolite profiles of 16 aTB children and 32 household contacts in India using liquid chromatography-mass spectrometry and identified three metabolites (N-acetylneuraminate, quinolinate, and pyridoxate) that could correctly discriminate TB status at distinct times during treatment, with AUCs of 0.66, 0.87, and 0.86, respectively. Although the above studies have used metabolomics techniques to identify abundant biomarkers for distinguishing aTB from individuals with LTBI, they have not linked metabolomics with transcriptomics and proteomics. Integrating metabolomics data with transcriptomics and proteomics data to comprehensively analyze and identify novel biomarkers is a direction for future omics technology development. Saiboonjan et al. (2021) investigated the transcriptomics, proteomics, and metabolomics profiles of three strains of *M. tuberculosis* (including drug-susceptible Beijing strain, multidrug-resistant Beijing strain, and H37Rv strain) cultured under stress conditions to mimic the environment of the host granuloma. They found that NarJ (respiratory nitrate reductase delta chain) was significantly upregulated at the protein and mRNA levels in all three *M. tuberculosis* strains and that NarJ plays an important role in nitrate metabolism during the adaptation of *M. tuberculosis* to stressful and intracellular environments and subsequent establishment of LTBI (Saiboonjan et al., 2021).

Microbiota

Hundreds of millions of microorganisms have coexisted with humans in the respiratory tract and gastrointestinal tract for thousands of years. However, research on them has been recently increasing. A growing number of studies have suggested that the microbiota plays an essential role in maintaining normal health, developing the immune system, and providing protection against pathogens (Khan et al., 2016; Dumas et al., 2018; Gupta et al., 2018; Liu et al., 2021). However, the impact of microbiota on host defense against *M. tuberculosis* infection is poorly understood. A recent review published in PLOS Pathogens summarized 14 microbiome studies performed on animal models of TB and patients with TB (Mori et al., 2021). Among these studies, nine focused on the relationship between microbiota in the intestinal tract and *M. tuberculosis*, including five studies on patients

with TB, three studies on mouse models, and one study on rhesus macaques. Compared with the number of studies on the intestinal tract, only six studies have been performed to explore the correlations between microbiota in the respiratory tract and *M. tuberculosis*, including five studies on patients with TB and one study on rhesus macaques. These studies investigated the impact of *M. tuberculosis* infection on the host microbiome, and all of them found that *M. tuberculosis* infection changed the composition of microbiota, with only four studies reporting the impact of microbiota changes caused by *M. tuberculosis* infection on the immune system. It is important to note that one study compared the changes in the composition of microbiota and its effects on the immune system among patients with TB (n = 25), patients with LTBI (n = 32), and healthy individuals (n = 23) (Huang et al., 2019). The results suggested that dysbiosis with a higher abundance of Bacteroidetes and a low ratio of Firmicutes to Bacteroidetes was related to systemic proinflammation in patients with aTB, while the abundance of Coriobacteriaceae was positively related to the level of IFN-γ and $CD4^+$ T cells in LTBI.

It is becoming increasingly recognized that the composition of the respiratory and gastrointestinal microbiota may affect the systemic immune responses of the host, and that microbiome–immune interactions may affect the susceptibility, manifestation, and progression of *M. tuberculosis* infection (Wipperman et al., 2021). However, the results of most studies are inconsistent and contradictory. This may be due to differences in species, heterogeneity of microbiota between individuals, sample size, detection methods, and experimental design, among others. The current data cannot determine whether microbiota can be used to distinguish between LTBI and aTB, and more high-quality studies with larger sample sizes are urgently needed to clarify this.

CONCLUSION

Tuberculosis is a global infectious disease that threatens human health, and LTBI is the biggest obstacle to achieving the goal of ending the global TB epidemic shared by the UN Sustainable Development Goals and WHO's End TB Strategy. As an ancient test that has been used to diagnose TB for more than 100 years, the TST has made great contributions to the control of TB. However, the TST has several challenges, such as the need for return visits, low specificity and sensitivity, false positives with BCG vaccination, cross-reactivity with NTMs, and false positives in immunosuppression and deficiency. To overcome these shortcomings of the TST, several new detection methods have been developed, such as the Diaskintest, C-Tb skin test, EC-Test, and T-SPOT.TB, QFT-GIT, QFT-Plus, LIAISON QFT-Plus, and LIOFeron TB/LTBI. The application of RD antigens (ESAT-6, CFP-10, TB7.7, and Ala-DH) prevents these novel methods from cross-reacting with BCG inoculation and most NTM infections, with the additional advantages of having higher specificity and sensitivity.

However, these methods cannot distinguish between LTBI and aTB. To investigate the reasons behind this, we believe that the abovementioned methods (1) were only designed based on RD antigens rather than LTBI-RD-associated antigens (Rv1736c, Rv1737c, Rv2031c, Rv2626c, Rv2653c-Rv2660c, Rv1511, Rv1978, Rv1980c, Rv1981c, Rv3872, Rv3873, Rv3878, Rv3879c, Rv3425, and Rv3429), without considering the difference in profiles of antigen expression between latent and active infection of *M. tuberculosis*; (2) only detect the number of IFN-γ-producing T cells and serum concentrations of IFN-γ produced by $CD4^+$ and/or $CD8^+$ T cells, but not of other biomarkers, such as antigen-specific antibodies, IL-2, IL-10, IP-10, and VEGF, nor their combinations; and (3) did not use the latest models and algorithms to improve their diagnosis performance for distinguishing between LTBI and aTB.

Thus, areas for further investigation and development should include (1) understanding the differential expression of various antigens in latent and active infection of *M. tuberculosis* based on omics technologies and studies with larger sample sizes, (2) focusing on multiple cytokines and/or antibodies derived from hosts that have been identified by previous studies, (3) improving the sensitivity and specificity of LTBI differential diagnosis using new models, algorithms, and IS, and (4) exploring the differences in microbiota between patients with LTBI and aTB to find new evidence for improving the diagnostic accuracy of LTBI and aTB.

AUTHOR CONTRIBUTIONS

XW and WG did the conceptualization and wrote–reviewed and edited. WG did the data curation, formal analysis, funding acquisition, methodology, software, and writing–original draft. Both authors contributed to the article and approved the submitted version.

FUNDING

This study was funded by the Beijing Municipal Science & Technology Commission (Grant Nos. 7212103 and Z181100001718005).

ACKNOWLEDGMENTS

We would like to thank Zimeng Yuan from The 8th Medical Center of PLA General Hospital for editing the article for language. We would also like to thank Editage for English language editing. Some elements of figures were obtained from BIORENDER (https://app.biorender.com/).

SUPPLEMENTARY MATERIAL

The Supplementary Material for this article can be found online at: https://www.frontiersin.org/articles/10.3389/fmicb.2021.745592/full#supplementary-material

Supplementary Figure 1 | Twenty-six cytokines were summarized from 34 included publications by Meier, N. R. et al. in a systematic review (Meier et al., 2018). The number of publications related each cytokine was showed as histogram.

REFERENCES

Abedi, S., Moosazadeh, M., Afshari, M., Charati, J. Y., and Nezammahalleh, A. (2019). Determinant factors for mortality during treatment among tuberculosis patients: cox proportional hazards model. *Indian J. Tuberc.* 66, 39–43. doi: 10.1016/j.ijtb.2017.05.001

Acharya, M. P., Pradeep, S. P., Murthy, V. S., Chikkannaiah, P., Kambar, V., Narayanashetty, S., et al. (2021). CD38 +CD27 -TNF-α + on Mtb-specific CD4 + T is a robust biomarker for tuberculosis diagnosis. *Clin. Infect. Dis.* 110, 204–209. doi: 10.1093/cid/ciab144

Achkar, J. M., Chan, J., and Casadevall, A. (2015). B cells and antibodies in the defense against *Mycobacterium tuberculosis* infection. *Immunol. Rev.* 264, 167–181. doi: 10.1111/imr.12276

Aggerbeck, H., Giemza, R., Joshi, P., Tingskov, P. N., Hoff, S. T., Boyle, J., et al. (2013). Randomised clinical trial investigating the specificity of a novel skin test (C-Tb) for diagnosis of *M. tuberculosis* infection. *PLoS One* 8:e64215. doi: 10.1371/journal.pone.0064215

Aggerbeck, H., Ruhwald, M., Hoff, S. T., Borregaard, B., Hellstrom, E., Malahleha, M., et al. (2018). C-Tb skin test to diagnose *Mycobacterium tuberculosis* infection in children and HIV-infected adults: a phase 3 trial. *PLoS One* 13:e0204554. doi: 10.1371/journal.pone.0204554

Agren, D., Stehr, M., Berthold, C. L., Kapoor, S., Oehlmann, W., Singh, M., et al. (2008). Three-dimensional structures of apo- and holo-L-alanine dehydrogenase from *Mycobacterium tuberculosis* reveal conformational changes upon coenzyme binding. *J. Mol. Biol.* 377, 1161–1173. doi: 10.1016/j.jmb.2008.01.091

Al-Khodari, N. Y., Al-Attiyah, R., and Mustafa, A. S. (2011). Identification, diagnostic potential, and natural expression of immunodominant seroreactive peptides encoded by five *Mycobacterium tuberculosis*-specific genomic regions. *Clin. Vaccine Immunol.* 18, 477–482. doi: 10.1128/cvi.00405-10

Allen, M., Bailey, C., Cahatol, I., Dodge, L., Yim, J., Kassissa, C., et al. (2015). Mechanisms of control of *Mycobacterium tuberculosis* by NK cells: role of glutathione. *Front. Immunol.* 6:508. doi: 10.3389/fimmu.2015.00508

Alsleben, N., Ruhwald, M., Rüssmann, H., Marx, F. M., Wahn, U., and Magdorf, K. (2012). Interferon-gamma inducible protein 10 as a biomarker for active tuberculosis and latent tuberculosis infection in children: a case-control study. *Scand. J. Infect. Dis.* 44, 256–262. doi: 10.3109/00365548.2011.632644

Altawallbeh, G., Gabrielson, D., Peters, J. M., and Killeen, A. A. (2021). Performance of an advanced interferon-gamma release assay for *Mycobacterium tuberculosis* detection. *J. Appl. Lab. Med.* 6, 1287–1292. doi: 10.1093/jalm/jfab012

Amiano, N. O., Morelli, M. P., Pellegrini, J. M., Tateosian, N. L., Rolandelli, A., Seery, V., et al. (2020). IFN-gamma and IgG responses to *Mycobacterium tuberculosis* latency antigen Rv2626c differentiate remote from recent tuberculosis infection. *Sci. Rep.* 10:7472. doi: 10.1038/s41598-020-64428-z

Andersen, P., Munk, M. E., Pollock, J. M., and Doherty, T. M. (2000). Specific immune-based diagnosis of tuberculosis. *Lancet* 356, 1099–1104. doi: 10.1016/s0140-6736(00)02742-2

Araujo, L. S., da Silva, N. B. M., da Silva, R. J., Leung, J. A. M., Mello, F. C. Q., and Saad, M. H. F. (2015). Profile of interferon-gamma response to latency-associated and novel in vivo expressed antigens in a cohort of subjects recently exposed to *Mycobacterium tuberculosis*. *Tuberculosis (Edinb)* 95, 751–757. doi: 10.1016/j.tube.2015.08.002

Arroyo, L., Rojas, M., Franken, K. L., Ottenhoff, T. H., and Barrera, L. F. (2016). Multifunctional T cell response to DosR and Rpf antigens is associated with protection in long-term *Mycobacterium tuberculosis*-infected individuals in Colombia. *Clin Vaccine Immunol* 23, 813–824. doi: 10.1128/CVI.00217-16

Ashraf, S., Saqib, M. A., Sharif, M. Z., Khatak, A. A., Khan, S. N., Malik, S. A., et al. (2014). Evaluation of diagnostic potential of Rv3803c and Rv2626c recombinant antigens in TB endemic country Pakistan. *J. Immunoassay Immunochem.* 35, 120–129. doi: 10.1080/15321819.2013.824897

Aspatwar, A., Gong, W., Wang, S., Wu, X., and Parkkila, S. (2021). Tuberculosis vaccine BCG: the magical effect of the old vaccine in the fight against the COVID-19 pandemic. *Int. Rev. Immunol.* 1–14. doi: 10.1080/08830185.2021.1922685 [Epub ahead of print].

ATS (2000). Targeted tuberculin testing and treatment of latent tuberculosis infection. This official statement of the American Thoracic Society was adopted by the ATS Board of Directors, July 1999. This is a Joint Statement of the American Thoracic Society (ATS) and the Centers for Disease Control and Prevention (CDC). This statement was endorsed by the Council of the Infectious Diseases Society of America. (IDSA), September 1999, and the sections of this statement. *Am. J. Respir. Crit. Care Med.* 161(4 Pt 2), S221–S247. doi: 10.1164/ajrccm.161.supplement_3.ats600

Bai, X. (2015). *Preparation of Four Tuberculosis Latent Proteins and the Evaluation of Their Immunological Characteristic*. Doctor. Beijing: Medical School of Chinese PLA.

Banday, K. M., Pasikanti, K. K., Chan, E. C., Singla, R., Rao, K. V., Chauhan, V. S., et al. (2011). Use of urine volatile organic compounds to discriminate tuberculosis patients from healthy subjects. *Anal. Chem.* 83, 5526–5534. doi: 10.1021/ac200265g

Banerjee, U., Baloni, P., Singh, A., and Chandra, N. (2021). Immune subtyping in latent tuberculosis. *Front. Immunol.* 12:595746. doi: 10.3389/fimmu.2021.595746

Bayaa, R., Ndiaye, M. D. B., Chedid, C., Kokhreidze, E., Tukvadze, N., Banu, S., et al. (2021). Multi-country evaluation of RISK6, a 6-gene blood transcriptomic signature, for tuberculosis diagnosis and treatment monitoring. *Sci. Rep.* 11:13646. doi: 10.1038/s41598-021-93059-1

Behr, M. A., Edelstein, P. H., and Ramakrishnan, L. (2018). Revisiting the timetable of tuberculosis. *BMJ* 362:k2738. doi: 10.1136/bmj.k2738

Behr, M. A., Edelstein, P. H., and Ramakrishnan, L. (2019). Is *Mycobacterium tuberculosis* infection life long? *BMJ* 367:l5770. doi: 10.1136/bmj.l5770

Behr, M. A., Kaufmann, E., Duffin, J., Edelstein, P. H., and Ramakrishnan, L. (2021). Latent tuberculosis: two centuries of confusion. *Am. J. Respir. Crit. Care Med.* 204, 142–148. doi: 10.1164/rccm.202011-4239PP

Belay, M., Legesse, M., Mihret, A., Bekele, Y., Ottenhoff, T. H. M., Franken, K. L. M. C., et al. (2015). Pro- and anti-inflammatory cytokines against Rv2031 Are elevated during latent tuberculosis: a study in cohorts of tuberculosis patients, household contacts and community controls in an endemic setting. *PLoS One* 10:e0124134. doi: 10.1371/journal.pone.0124134

Berry, M. P., Graham, C. M., McNab, F. W., Xu, Z., Bloch, S. A., Oni, T., et al. (2010). An interferon-inducible neutrophil-driven blood transcriptional signature in human tuberculosis. *Nature* 466, 973–977. doi: 10.1038/nature09247

Betts, J. C. (2002). Transcriptomics and proteomics: tools for the identification of novel drug targets and vaccine candidates for tuberculosis. *IUBMB Life* 53, 239–242. doi: 10.1080/15216540212651

Bruns, H., Meinken, C., Schauenberg, P., Härter, G., Kern, P., Modlin, R. L., et al. (2009). Anti-TNF immunotherapy reduces CD8+ T cell-mediated antimicrobial activity against *Mycobacterium tuberculosis* in humans. *J. Clin. Invest.* 119, 1167–1177. doi: 10.1172/jci38482

Bui, H. H., Sidney, J., Dinh, K., Southwood, S., Newman, M. J., and Sette, A. (2006). Predicting population coverage of T-cell epitope-based diagnostics and vaccines. *BMC Bioinformatics* 7:153. doi: 10.1186/1471-2105-7-153

Cao, S. H., Chen, Y. Q., Sun, Y., Liu, Y., Zheng, S. H., Zhang, Z. G., et al. (2018). Screening of serum biomarkers for distinguishing between latent and active tuberculosis using proteome microarray. *Biomed. Environ. Sci.* 31, 515–526. doi: 10.3967/bes2018.069

Cao, X. J., Li, Y. P., Wang, J. Y., Zhou, J., and Guo, X. G. (2021). MPT64 assays for the rapid detection of *Mycobacterium tuberculosis*. *BMC Infect Dis* 21:336. doi: 10.1186/s12879-021-06022-w

Chai, Q., Lu, Z., and Liu, C. H. (2020). Host defense mechanisms against *Mycobacterium tuberculosis*. *Cell Mol. Life Sci.* 77, 1859–1878. doi: 10.1007/s00018-019-03353-5

Chaw, L., Chien, L. C., Wong, J., Takahashi, K., Koh, D., and Lin, R. T. (2020). Global trends and gaps in research related to latent tuberculosis infection. *BMC Public Health* 20:352. doi: 10.1186/s12889-020-8419-0

Che, N., Cheng, J., Li, H., Zhang, Z., Zhang, X., Ding, Z., et al. (2013). Decreased serum 5-oxoproline in TB patients is associated with pathological damage of the lung. *Clin. Chim. Acta* 423, 5–9. doi: 10.1016/j.cca.2013.04.010

Chee, C. B. E., Reves, R., Zhang, Y., and Belknap, R. (2018). Latent tuberculosis infection: opportunities and challenges. *Respirology* 23, 893–900. doi: 10.1111/resp.13346

Chegou, N. N., Essone, P. N., Loxton, A. G., Stanley, K., Black, G. F., van der Spuy, G. D., et al. (2012). Potential of host markers produced by infection phase-dependent antigen-stimulated cells for the diagnosis of tuberculosis in a highly endemic area. *PLoS One* 7:e38501. doi: 10.1371/journal.pone.0038501

Chen, F., Zhai, M. X., Zhu, Y. H., Qi, Y. M., Zhai, W. J., and Gao, Y. F. (2012). In vitro and in vivo identification of a novel cytotoxic T lymphocyte epitope from Rv3425 of *Mycobacterium tuberculosis*. *Microbiol. Immunol.* 56, 548–553. doi: 10.1111/j.1348-0421.2012.00470.x

Chen, J., Su, X., Zhang, Y., Wang, S., Shao, L., Wu, J., et al. (2009). Novel recombinant RD2- and RD11-encoded *Mycobacterium tuberculosis* antigens are potential candidates for diagnosis of tuberculosis infections in BCG-vaccinated individuals. *Microbes Infect.* 11, 876–885. doi: 10.1016/j.micinf.2009.05.008

Chinese Antituberculosis Association, Schools and Children Branch of the Chinese Antituberculosis Association, and Editorial Board of Chinese Journal of Antituberculosis (2020). [Expert consensus of clinical application of the recombinant *Mycobacterium tuberculosis* fusion protein (EC)]. *Chin. J. Antituberculosis* 42, 761–768. doi: 10.3969/i.issn.1000-6621.2020.08.001

Cole, S. T., Brosch, R., Parkhill, J., Garnier, T., Churcher, C., Harris, D., et al. (1998). Deciphering the biology of *Mycobacterium tuberculosis* from the complete genome sequence. *Nature* 393, 537–544. doi: 10.1038/31159

Commandeur, S., Lin, M. Y., van Meijgaarden, K. E., Friggen, A. H., Franken, K. L., Drijfhout, J. W., et al. (2011). Double- and monofunctional $CD4^+$ and $CD8^+$ T-cell responses to *Mycobacterium tuberculosis* DosR antigens and peptides in long-term latently infected individuals. *Eur. J. Immunol.* 41, 2925–2936. doi: 10.1002/eji.201141602

Coppola, M., van den Eeden, S. J., Wilson, L., Franken, K. L., Ottenhoff, T. H., and Geluk, A. (2015). Synthetic long peptide derived from *Mycobacterium tuberculosis* latency antigen Rv1733c protects against tuberculosis. *Clin. Vaccine Immunol.* 22, 1060–1069. doi: 10.1128/CVI.00271-15

Cui, X., Gao, L., and Cao, B. (2020). Management of latent tuberculosis infection in China: exploring solutions suitable for high-burden countries. *Int. J. Infect. Dis.* 92S, S37–S40. doi: 10.1016/j.ijid.2020.02.034

da Silva, R. J., da Silva Correa, R., Sardella, I. G., de Paulo Mulinari, A. C., Mafort, T. T., Santos, A. P., et al. (2019). IgA and IgG antibody detection of mycobacterial antigens in pleural fluid and serum from pleural tuberculous patients. *BMC Immunol.* 20:36. doi: 10.1186/s12865-019-0315-y

Das, M. K., Bishwal, S. C., Das, A., Dabral, D., Badireddy, V. K., Pandit, B., et al. (2015). Deregulated tyrosine-phenylalanine metabolism in pulmonary tuberculosis patients. *J. Proteome Res.* 14, 1947–1956. doi: 10.1021/acs.jproteome.5b00016

De Maertelaere, E., Vandendriessche, S., Verhasselt, B., Coorevits, L., Andre, E., Padalko, E., et al. (2020). Evaluation of QuantiFERON-TB gold plus on liaison XL in a low-tuberculosis-incidence setting. *J. Clin. Microbiol.* 58, e00159–e20. doi: 10.1128/JCM.00159-20

Della Bella, C., Spinicci, M., Alnwaisri, H. F. M., Bartalesi, F., Tapinassi, S., Mencarini, J., et al. (2020). LIOFeron(R)TB/LTBI: a novel and reliable test for LTBI and *tuberculosis*. *Int. J. Infect. Dis.* 91, 177–181. doi: 10.1016/j.ijid.2019.12.012

Dong, Y., Demaria, S., Sun, X., Santori, F. R., Jesdale, B. M., De Groot, A. S., et al. (2004). HLA-A2-restricted CD8+-cytotoxic-T-cell responses to novel epitopes in *Mycobacterium tuberculosis* superoxide dismutase, alanine dehydrogenase, and glutamine synthetase. *Infect. Immun.* 72, 2412–2415. doi: 10.1128/iai.72.4.2412-2415.2004

du Preez, I., and Loots, D. T. (2013). New sputum metabolite markers implicating adaptations of the host to *Mycobacterium tuberculosis*, and vice versa. *Tuberculosis (Edinb)* 93, 330–337. doi: 10.1016/j.tube.2013.02.008

Dubois Cauwelaert, N., Baldwin, S. L., Orr, M. T., Desbien, A. L., Gage, E., Hofmeyer, K. A., et al. (2016). Antigen presentation by B cells guides programing of memory CD4(+) T-cell responses to a TLR4-agonist containing vaccine in mice. *Eur. J. Immunol.* 46, 2719–2729. doi: 10.1002/eji.201646399

Dumas, A., Corral, D., Colom, A., Levillain, F., Peixoto, A., Hudrisier, D., et al. (2018). The host microbiota contributes to early protection against lung colonization by *Mycobacterium tuberculosis*. *Front. Immunol.* 9:2656. doi: 10.3389/fimmu.2018.02656

Dutta, N. K., Tornheim, J. A., Fukutani, K. F., Paradkar, M., Tiburcio, R. T., Kinikar, A., et al. (2020). Integration of metabolomics and transcriptomics reveals novel biomarkers in the blood for tuberculosis diagnosis in children. *Sci. Rep.* 10:19527. doi: 10.1038/s41598-020-75513-8

Emery, J. C., Richards, A. S., Dale, K. D., McQuaid, C. F., White, R. G., Denholm, J. T., et al. (2021). Self-clearance of *Mycobacterium tuberculosis* infection: implications for lifetime risk and population at-risk of tuberculosis disease. *Proc. Biol. Sci.* 288:20201635. doi: 10.1098/rspb.2020.1635

Feng, S., Du, Y. Q., Zhang, L., Zhang, L., Feng, R. R., and Liu, S. Y. (2015). Analysis of serum metabolic profile by ultra-performance liquid chromatography-mass spectrometry for biomarkers discovery: application in a pilot study to discriminate patients with tuberculosis. *Chin. Med. J. (Engl)* 128, 159–168. doi: 10.4103/0366-6999.149188

Feng, X., Xiu, B., Chen, K., Yang, X., Zhang, H., Yue, J., et al. (2013). Enhanced serodiagnostic utility of novel *Mycobacterium tuberculosis* polyproteins. *J. Infect.* 66, 366–375. doi: 10.1016/j.jinf.2012.10.029

Floyd, K., Glaziou, P., Zumla, A., and Raviglione, M. (2018). The global tuberculosis epidemic and progress in care, prevention, and research: an overview in year 3 of the End TB era. *Lancet Respir. Med.* 6, 299–314. doi: 10.1016/S2213-2600(18)30057-2

Frediani, J. K., Jones, D. P., Tukvadze, N., Uppal, K., Sanikidze, E., Kipiani, M., et al. (2014). Plasma metabolomics in human pulmonary tuberculosis disease: a pilot study. *PLoS One* 9:e108854. doi: 10.1371/journal.pone.0108854

Geluk, A., Lin, M. Y., van Meijgaarden, K. E., Leyten, E. M., Franken, K. L., Ottenhoff, T. H., et al. (2007). T-cell recognition of the HspX protein of *Mycobacterium tuberculosis* correlates with latent *M. tuberculosis* infection but not with M. bovis BCG vaccination. *Infect. Immun.* 75, 2914–2921. doi: 10.1128/iai.01990-06

Godoy, P. (2021). Guidelines on controlling latent tuberculosis infection to support tuberculosis elimination. *Rev. Esp. Sanid. Penit.* 23, 28–36. doi: 10.18176/resp.00028

Gong, W., Liang, Y., Mi, J., Jia, Z., Xue, Y., Wang, J., et al. (2021). Peptides-based vaccine MP3RT induced protective immunity against *Mycobacterium Tuberculosis* infection in a humanized mouse model. *Front. Immunol.* 12:666290. doi: 10.3389/fimmu.2021.666290

Gong, W., Liang, Y., and Wu, X. (2018). The current status, challenges, and future developments of new tuberculosis vaccines. *Hum. Vaccin Immunother.* 14, 1697–1716. doi: 10.1080/21645515.2018.1458806

Gong, W., and Wu, X. (2020). Is the tuberculosis vaccine BCG an alternative weapon for developing countries to defeat COVID-19? *Indian J. Tuberc.* 68, 401–404.

Gong, W. P., Liang, Y., Ling, Y. B., Zhang, J. X., Yang, Y. R., Wang, L., et al. (2020). Effects of *Mycobacterium vaccae* vaccine in a mouse model of tuberculosis: protective action and differentially expressed genes. *Mil. Med. Res.* 7:25. doi: 10.1186/s40779-020-00258-4

Gordon, S. V., Eiglmeier, K., Garnier, T., Brosch, R., Parkhill, J., Barrell, B., et al. (2001). Genomics of *Mycobacterium bovis*. *Tuberculosis (Edinb)* 81, 157–163. doi: 10.1054/tube.2000.0269

Griffiths, W. J., and Wang, Y. (2009). Mass spectrometry: from proteomics to metabolomics and lipidomics. *Chem. Soc. Rev.* 38, 1882–1896. doi: 10.1039/b618553n

Gupta, N., Kumar, R., and Agrawal, B. (2018). New players in immunity to tuberculosis: the host microbiome, Lung Epithelium, and Innate Immune Cells. *Front. Immunol.* 9:709. doi: 10.3389/fimmu.2018.00709

Hamada, Y., Cirillo, D. M., Matteelli, A., Penn-Nicholson, A., Rangaka, M. X., and Ruhwald, M. (2021). Tests for tuberculosis infection: landscape analysis. *Eur. Respir. J.* 2100167. doi: 10.1183/13993003.00167-2021

Hanif, S. N., Al-Attiyah, R., and Mustafa, A. S. (2011). Cellular immune responses in mice induced by *M. tuberculosis* PE35-DNA vaccine construct. *Scand. J. Immunol.* 74, 554–560. doi: 10.1111/j.1365-3083.2011.02604.x

Hauck, F. R., Neese, B. H., Panchal, A. S., and El-Amin, W. (2009). Identification and management of latent tuberculosis infection. *Am. Fam. Physician* 79, 879–886.

He, H., Yang, H., and Deng, Y. (2015). *Mycobacterium tuberculosis* dormancy-associated antigen of Rv2660c induces stronger immune response in latent *Mycobacterium tuberculosis* infection than that in active tuberculosis in a

Chinese population. *Eur. J. Clin. Microbiol. Infect. Dis.* 34, 1103–1109. doi: 10.1007/s10096-015-2335-8

Hinks, T. S., Dosanjh, D. P., Innes, J. A., Pasvol, G., Hackforth, S., Varia, H., et al. (2009). Frequencies of region of difference 1 antigen-specific but not purified protein derivative-specific gamma interferon-secreting T cells correlate with the presence of tuberculosis disease but do not distinguish recent from remote latent infections. *Infect. Immun.* 77, 5486–5495. doi: 10.1128/iai.01436-08

Hoff, S. T., Peter, J. G., Theron, G., Pascoe, M., Tingskov, P. N., Aggerbeck, H., et al. (2016). Sensitivity of C-Tb: a novel RD-1-specific skin test for the diagnosis of tuberculosis infection. *Eur. Respir. J.* 47, 919–928. doi: 10.1183/13993003.01464-2015

Honaker, R. W., Stewart, A., Schittone, S., Izzo, A., Klein, M. R., and Voskuil, M. I. (2008). *Mycobacterium bovis* BCG vaccine strains lack narK2 and narX induction and exhibit altered phenotypes during dormancy. *Infect. Immun.* 76, 2587–2593. doi: 10.1128/IAI.01235-07

Hong, J. Y., Park, S. Y., Kim, A., Cho, S. N., and Hur, Y. G. (2019). Comparison of QFT-Plus and QFT-GIT tests for diagnosis of *M. tuberculosis* infection in immunocompetent Korean subjects. *J. Thorac. Dis.* 11, 5210–5217. doi: 10.21037/jtd.2019.12.11

Horvati, K., Bosze, S., Gideon, H. P., Bacsa, B., Szabo, T. G., Goliath, R., et al. (2016). Population tailored modification of tuberculosis specific interferon-gamma release assay. *J. Infect.* 72, 179–188. doi: 10.1016/j.jinf.2015.10.012

Houben, R. M., and Dodd, P. J. (2016). The global burden of latent tuberculosis infection: a Re-estimation using mathematical modelling. *PLoS Med* 13:e1002152. doi: 10.1371/journal.pmed.1002152

Huang, S. F., Yang, Y. Y., Chou, K. T., Fung, C. P., Wang, F. D., and Su, W. J. (2019). Systemic proinflammation after *Mycobacterium tuberculosis* infection was correlated to the gut microbiome in HIV-uninfected humans. *Eur. J. Clin. Invest.* 49:e13068. doi: 10.1111/eci.13068

Jacobsen, M., Repsilber, D., Gutschmidt, A., Neher, A., Feldmann, K., Mollenkopf, H. J., et al. (2007). Candidate biomarkers for discrimination between infection and disease caused by *Mycobacterium tuberculosis*. *J. Mol. Med. (Berl)* 85, 613–621. doi: 10.1007/s00109-007-0157-6

Jasenosky, L. D., Scriba, T. J., Hanekom, W. A., and Goldfeld, A. E. (2015). T cells and adaptive immunity to *Mycobacterium tuberculosis* in humans. *Immunol. Rev.* 264, 74–87. doi: 10.1111/imr.12274

Ji, P., Fan, X., Wu, K., and Lu, S. (2015). [Research progress on the antigens associated with latent infection of *Mycobacterium tuberculosis*]. *Chin. J.Microbiol. Immunol.* 35, 59–64. doi: 10.3760/cma.j.issn.0254-5101.2015.01.013

Jia, Z., Gong, W., Liang, Y., Wu, X., and Zhao, W. (2021). Prediction and analyses of HLA-II restricted *Mycobacterium tuberculosis* CD4(+) T cell epitopes in the Chinese population. *Biotechnol. Appl. Biochem.* 2021, 1–13. doi: 10.1002/bab.2171

Jiang, Y., Wei, J., Liu, H., Li, G., Guo, Q., Qiu, Y., et al. (2016). Polymorphisms in the PE35 and PPE68 antigens in *Mycobacterium tuberculosis* strains may affect strain virulence and reflect ongoing immune evasion. *Mol. Med. Rep.* 13, 947–954. doi: 10.3892/mmr.2015.4589

Jungblut, P. R., Schaible, U. E., Mollenkopf, H. J., Zimny-Arndt, U., Raupach, B., Mattow, J., et al. (1999). Comparative proteome analysis of *Mycobacterium tuberculosis* and *Mycobacterium bovis* BCG strains: towards functional genomics of microbial pathogens. *Mol. Microbiol.* 33, 1103–1117. doi: 10.1046/j.1365-2958.1999.01549.x

Kadkhoda, K., Schwichtenberg, G., Dee, M., and Horejsei, R. (2020). Operational usability evaluation of the LIAISON(R) QuantiFERON(R)-TB gold plus solution in a high volume laboratory setting. *Clin. Lab.* 66:11. doi: 10.7754/Clin.Lab.2020.200338

Kanai, K., Kondo, E., and Yasuda, T. (1979). Ultrastructural changes in the alveolar epithelium in response to mycobacterial infection. *Jpn. J. Med. Sci. Biol.* 32, 315–325. doi: 10.7883/yoken1952.32.315

Kasempimolporn, S., Areekul, P., Thaveekarn, W., Sutthisri, R., Boonchang, S., Sawangvaree, A., et al. (2019). Application of transdermal patches with new skin test reagents for detection of latent tuberculosis. *J. Med. Microbiol.* 68, 1314–1319. doi: 10.1099/jmm.0.001037

Khan, N., Vidyarthi, A., Nadeem, S., Negi, S., Nair, G., and Agrewala, J. N. (2016). Alteration in the gut microbiota provokes susceptibility to tuberculosis. *Front. Immunol.* 7:529. doi: 10.3389/fimmu.2016.00529

Kolk, A. H., van Berkel, J. J., Claassens, M. M., Walters, E., Kuijper, S., Dallinga, J. W., et al. (2012). Breath analysis as a potential diagnostic tool for tuberculosis. *Int. J. Tuberc. Lung Dis.* 16, 777–782. doi: 10.5588/ijtld.11.0576

Korma, W., Mihret, A., Chang, Y., Tarekegn, A., Tegegn, M., Tuha, A., et al. (2020). Antigen-specific cytokine and chemokine gene expression for diagnosing latent and active tuberculosis. *Diagnostics (Basel)* 10:716. doi: 10.3390/diagnostics10090716

Kundu, M., and Basu, J. (2021). Applications of transcriptomics and proteomics for understanding dormancy and resuscitation in *Mycobacterium tuberculosis*. *Front. Microbiol.* 12:642487. doi: 10.3389/fmicb.2021.642487

Laennec, R. (1826). *Traite de l'Auscultation Mediate et des Maladies des Poumons et du Coeur*. Paris: Chaude.

Lalvani, A., Pathan, A. A., McShane, H., Wilkinson, R. J., Latif, M., Conlon, C. P., et al. (2001). Rapid detection of *Mycobacterium tuberculosis* infection by enumeration of antigen-specific T cells. *Am. J. Respir. Crit. Care Med.* 163, 824–828. doi: 10.1164/ajrccm.163.4.2009100

Latorre, I., Fernández-Sanmartín, M. A., Muriel-Moreno, B., Villar-Hernández, R., Vila, S., Souza-Galvão, M. L., et al. (2018). Study of CD27 and CCR4 Markers on specific CD4(+) T-cells as immune tools for active and latent tuberculosis management. *Front. Immunol.* 9:3094. doi: 10.3389/fimmu.2018.03094

Lau, S. K., Lam, C. W., Curreem, S. O., Lee, K. C., Lau, C. C., Chow, W. N., et al. (2015). Identification of specific metabolites in culture supernatant of *Mycobacterium tuberculosis* using metabolomics: exploration of potential biomarkers. *Emerg. Microbes Infect.* 4:e6. doi: 10.1038/emi.2015.6

Lewinsohn, D. M., Leonard, M. K., LoBue, P. A., Cohn, D. L., Daley, C. L., Desmond, E., et al. (2017). Official American thoracic society/infectious diseases society of America/Centers for disease control and prevention clinical practice guidelines: diagnosis of tuberculosis in adults and children. *Clin. Infect. Dis.* 64, e1–e33. doi: 10.1093/cid/ciw694

Li, F., Xu, M., Qin, C., Xia, L., Xiong, Y., Xi, X., et al. (2016a). Recombinant fusion ESAT6-CFP10 immunogen as a skin test reagent for tuberculosis diagnosis: an open-label, randomized, two-centre phase 2a clinical trial. *Clin. Microbiol. Infect.* 22, 889.e9–889.e16. doi: 10.1016/j.cmi.2016.07.015

Li, F., Xu, M., Zhou, L., Xiong, Y., Xia, L., Fan, X., et al. (2016b). Safety of Recombinant fusion protein ESAT6-CFP10 as a skin test reagent for tuberculosis diagnosis: an open-label, randomized, single-center phase I clinical trial. *Clin. Vaccine Immunol.* 23, 767–773. doi: 10.1128/CVI.00154-16

Li, G., Yang, F., He, X., Liu, Z., Pi, J., Zhu, Y., et al. (2020). Anti-tuberculosis (TB) chemotherapy dynamically rescues Th1 and CD8+ T effector levels in Han Chinese pulmonary TB patients. *Microbes Infect.* 22, 119–126. doi: 10.1016/j.micinf.2019.10.001

Liang, Y., Gong, W., Wang, X., Zhang, J., Ling, Y., Song, J., et al. (2021). Chinese traditional medicine NiuBeiXiaoHe (NBXH) extracts have the function of antituberculosis and immune recovery in BALB/c Mice. *J. Immunol. Res.* 2021:6234560. doi: 10.1155/2021/6234560

LIONEX (2021). *LIOFeron§TB/LTBI IGRA [Online]. Germany: LIONEX*. Available online at: https://lionex.de/product/lioferon/ (accessed May 17, 2021).

Litvinov, V. I., Shuster, A. M., Slogotskaia, L. V., Sel'tsovskii, P. P., Ovsiankina, E. S., Mushkin, A., et al. (2009). [Effectiveness of new diagnostic drug Diaskintest in children for tuberculosis diagnostic]. *Probl. Tuberk. Bolezn. Legk.* 2009, 19–22.

Liu, Y., Wang, J., and Wu, C. (2021). Microbiota and tuberculosis: a potential role of probiotics, and postbiotics. *Front. Nutr.* 8:626254. doi: 10.3389/fnut.2021.626254

Louis, P. (1825). *Recherches Anatomoco-Pathologiques sur la Phthisie*. Paris: Chez Gabon et Compagnie.

Loxton, A. G., and van Rensburg, I. C. (2021). FasL regulatory B-cells during *Mycobacterium tuberculosis* infection and TB disease. *J. Mol. Biol.* 433:166984. doi: 10.1016/j.jmb.2021.166984

Luabeya, A. K., Kagina, B. M., Tameris, M. D., Geldenhuys, H., Hoff, S. T., Shi, Z., et al. (2015). First-in-human trial of the post-exposure tuberculosis vaccine H56:IC31 in *Mycobacterium tuberculosis* infected and non-infected healthy adults. *Vaccine* 33, 4130–4140. doi: 10.1016/j.vaccine.2015.06.051

Luo, J., Zhang, M., Yan, B., Li, F., Guan, S., Chang, K., et al. (2019). Diagnostic performance of plasma cytokine biosignature combination and MCP-1 as individual biomarkers for differentiating stages *Mycobacterium tuberculosis* infection. *J. Infect.* 78, 281–291. doi: 10.1016/j.jinf.2018.10.017

Luo, L., Zhu, L., Yue, J., Liu, J., Liu, G., Zhang, X., et al. (2017). Antigens Rv0310c and Rv1255c are promising novel biomarkers for the diagnosis of

Mycobacterium tuberculosis infection. *Emerg. Microbes Infect.* 6:e64. doi: 10.1038/emi.2017.54

Luo, W., Qu, Z. L., Xie, Y., Xiang, J., and Zhang, X. L. (2015). Identification of a novel immunodominant antigen Rv2645 from RD13 with potential as a cell-mediated immunity-based TB diagnostic agent. *J. Infect.* 71, 534–543. doi: 10.1016/j.jinf.2015.07.011

Lv, L., Li, C., Zhang, X., Ding, N., Cao, T., Jia, X., et al. (2017). RNA profiling analysis of the serum exosomes derived from patients with active and latent *Mycobacterium tuberculosis* infection. *Front. Microbiol.* 8:1051. doi: 10.3389/fmicb.2017.01051

Mahmoudi, S., Pourakbari, B., and Mamishi, S. (2017). Interferon gamma release assay in response to PE35/PPE68 proteins: a promising diagnostic method for diagnosis of latent tuberculosis. *Eur. Cytokine Netw.* 28, 36–40. doi: 10.1684/ecn.2017.0391

Marino, S., Cilfone, N. A., Mattila, J. T., Linderman, J. J., Flynn, J. L., and Kirschner, D. E. (2015). Macrophage polarization drives granuloma outcome during *Mycobacterium tuberculosis* infection. *Infect. Immun.* 83, 324–338. doi: 10.1128/IAI.02494-14

Martineau, A. R., Newton, S. M., Wilkinson, K. A., Kampmann, B., Hall, B. M., Nawroly, N., et al. (2007). Neutrophil-mediated innate immune resistance to mycobacteria. *J. Clin. Invest.* 117, 1988–1994. doi: 10.1172/jci31097

Mateos, J., Estévez, O., González-Fernández, Á, Anibarro, L., Pallarés, Á, Reljic, R., et al. (2019). High-resolution quantitative proteomics applied to the study of the specific protein signature in the sputum and saliva of active tuberculosis patients and their infected and uninfected contacts. *J. Proteomics* 195, 41–52. doi: 10.1016/j.jprot.2019.01.010

Mayer-Barber, K. D., Andrade, B. B., Barber, D. L., Hieny, S., Feng, C. G., Caspar, P., et al. (2011). Innate and adaptive interferons suppress IL-1α and IL-1β production by distinct pulmonary myeloid subsets during *Mycobacterium tuberculosis* infection. *Immunity* 35, 1023–1034. doi: 10.1016/j.immuni.2011.12.002

Mc, D. W. (1959). Inapparent infection: relation of latent and dormant infections to microbial persistence. *Public Health Rep.* 74, 485–499.

McCune, R. M. Jr., McDermott, W., and Tompsett, R. (1956). The fate of *Mycobacterium tuberculosis* in mouse tissues as determined by the microbial enumeration technique. II. The conversion of tuberculous infection to the latent state by the administration of pyrazinamide and a companion drug. *J. Exp. Med.* 104, 763–802. doi: 10.1084/jem.104.5.763

Meier, N. R., Jacobsen, M., Ottenhoff, T. H. M., and Ritz, N. (2018). A systematic review on Novel *Mycobacterium tuberculosis* antigens and their discriminatory potential for the diagnosis of latent and active tuberculosis. *Front. Immunol.* 9:2476. doi: 10.3389/fimmu.2018.02476

Mistry, R., Cliff, J. M., Clayton, C. L., Beyers, N., Mohamed, Y. S., Wilson, P. A., et al. (2007). Gene-expression patterns in whole blood identify subjects at risk for recurrent tuberculosis. *J. Infect. Dis.* 195, 357–365. doi: 10.1086/510397

Mori, G., Morrison, M., and Blumenthal, A. (2021). Microbiome-immune interactions in tuberculosis. *PLoS Pathog.* 17:e1009377. doi: 10.1371/journal.ppat.1009377

Mosavari, N., Karimi, A., Tadayon, K., Shahhosseini, G., Zavaran Hosseini, A., and Babaie, M. (2021). Evaluation of heating and irradiation methods for production of purified protein derivative (PPD) of *Mycobacterium Tuberculosis*. *Arch. Razi. Inst.* 75, 439–449. doi: 10.22092/ari.2019.123082.1238

Mukherjee, P., Dutta, M., Datta, P., Dasgupta, A., Pradhan, R., Pradhan, M., et al. (2007). The RD1-encoded antigen Rv3872 of *Mycobacterium tuberculosis* as a potential candidate for serodiagnosis of tuberculosis. *Clin. Microbiol. Infect.* 13, 146–152. doi: 10.1111/j.1469-0691.2006.01660.x

Mustafa, A. S., Cockle, P. J., Shaban, F., Hewinson, R. G., and Vordermeier, H. M. (2002). Immunogenicity of *Mycobacterium tuberculosis* RD1 region gene products in infected cattle. *Clin. Exp. Immunol.* 130, 37–42. doi: 10.1046/j.1365-2249.2002.01937.x

Ndzi, E. N., Nkenfou, C. N., Pefura, E. W. Y., Mekue, L. C. M., Guiedem, E., Nguefeu, C. N., et al. (2019). Tuberculosis diagnosis: algorithm that May discriminate latent from active tuberculosis. *Heliyon* 5:e02559. doi: 10.1016/j.heliyon.2019.e02559

Olivier, I., and Loots du, T. (2012). A metabolomics approach to characterise and identify various *Mycobacterium* species. *J. Microbiol. Methods* 88, 419–426. doi: 10.1016/j.mimet.2012.01.012

Pai, M., and Behr, M. (2016). Latent *Mycobacterium tuberculosis* infection and interferon-gamma release assays. *Microbiol. Spectr.* 4, 1–10. doi: 10.1128/microbiolspec.TBTB2-0023-2016

Pan, L., Wei, N., Jia, H., Gao, M., Chen, X., Wei, R., et al. (2017). Genome-wide transcriptional profiling identifies potential signatures in discriminating active tuberculosis from latent infection. *Oncotarget* 8, 112907–112916. doi: 10.18632/oncotarget.22889

Paquin-Proulx, D., Costa, P. R., Terrassani Silveira, C. G., Marmorato, M. P., Cerqueira, N. B., Sutton, M. S., et al. (2018). Latent *Mycobacterium tuberculosis* infection is associated with a higher frequency of mucosal-associated invariant t and invariant natural killer T cells. *Front. Immunol.* 9:1394. doi: 10.3389/fimmu.2018.01394

Pena, D., Rovetta, A. I., Hernandez Del Pino, R. E., Amiano, N. O., Pasquinelli, V., Pellegrini, J. M., et al. (2015). A *Mycobacterium tuberculosis* dormancy antigen differentiates latently infected bacillus calmette-guerin-vaccinated individuals. *EBioMedicine* 2, 884–890. doi: 10.1016/j.ebiom.2015.05.026

Petruccioli, E., Scriba, T. J., Petrone, L., Hatherill, M., Cirillo, D. M., Joosten, S. A., et al. (2016). Correlates of tuberculosis risk: predictive biomarkers for progression to active tuberculosis. *Eur. Respir. J.* 48, 1751–1763. doi: 10.1183/13993003.01012-2016

Phillips, M., Basa-Dalay, V., Bothamley, G., Cataneo, R. N., Lam, P. K., Natividad, M. P., et al. (2010). Breath biomarkers of active pulmonary tuberculosis. *Tuberculosis (Edinb)* 90, 145–151. doi: 10.1016/j.tube.2010.01.003

Phillips, M., Cataneo, R. N., Condos, R., Ring Erickson, G. A., Greenberg, J., La Bombardi, V., et al. (2007). Volatile biomarkers of pulmonary tuberculosis in the breath. *Tuberculosis (Edinb)* 87, 44–52. doi: 10.1016/j.tube.2006.03.004

Pourakbari, B., Mamishi, S., Benvari, S., and Mahmoudi, S. (2019). Comparison of the QuantiFERON-TB Gold Plus and QuantiFERON-TB Gold In-Tube interferon-gamma release assays: a systematic review and meta-analysis. *Adv. Med. Sci.* 64, 437–443. doi: 10.1016/j.advms.2019.09.001

Prabhavathi, M., Pathakumari, B., and Raja, A. (2015). IFN-gamma/TNF-alpha ratio in response to immuno proteomically identified human T-cell antigens of *Mycobacterium tuberculosis* – the most suitable surrogate biomarker for latent TB infection. *J. Infect.* 71, 238–249. doi: 10.1016/j.jinf.2015.04.032

Preez, I. D., Luies, L., and Loots, D. T. (2017). Metabolomics biomarkers for tuberculosis diagnostics: current status and future objectives. *Biomark. Med.* 11, 179–194. doi: 10.2217/bmm-2016-0287

Qiu, B., Liu, Q., Li, Z., Song, H., Xu, D., Ji, Y., et al. (2020). Evaluation of cytokines as a biomarker to distinguish active tuberculosis from latent tuberculosis infection: a diagnostic meta-analysis. *BMJ Open* 10:e039501. doi: 10.1136/bmjopen-2020-039501

Rambaran, S., Naidoo, K., Lewis, L., Hassan-Moosa, R., Govender, D., Samsunder, N., et al. (2021). Effect of inflammatory cytokines/chemokines on pulmonary tuberculosis culture conversion and disease severity in HIV-Infected and -uninfected individuals from South Africa. *Front. Immunol.* 12:641065. doi: 10.3389/fimmu.2021.641065

Ren, N., JinLi, J., Chen, Y., Zhou, X., Wang, J., Ge, P., et al. (2018). Identification of new diagnostic biomarkers for *Mycobacterium tuberculosis* and the potential application in the serodiagnosis of human tuberculosis. *Microb. Biotechnol.* 11, 893–904. doi: 10.1111/1751-7915.13291

Rodrigues, T. S., Conti, B. J., Fraga-Silva, T. F. C., Almeida, F., and Bonato, V. L. D. (2020). Interplay between alveolar epithelial and dendritic cells and *Mycobacterium tuberculosis*. *J. Leukoc. Biol.* 108, 1139–1156. doi: 10.1002/jlb.4mr0520-112r

Rozot, V., Vigano, S., Mazza-Stalder, J., Idrizi, E., Day, C. L., Perreau, M., et al. (2013). *Mycobacterium tuberculosis*-specific CD8+ T cells are functionally and phenotypically different between latent infection and active disease. *Eur. J. Immunol.* 43, 1568–1577. doi: 10.1002/eji.201243262

Ruhwald, M., Aggerbeck, H., Gallardo, R. V., Hoff, S. T., Villate, J. I., Borregaard, B., et al. (2017). Safety and efficacy of the C-Tb skin test to diagnose *Mycobacterium tuberculosis* infection, compared with an interferon gamma release assay and the tuberculin skin test: a phase 3, double-blind, randomised, controlled trial. *Lancet Respir. Med.* 5, 259–268. doi: 10.1016/S2213-2600(16)30436-2

Ruhwald, M., Cayla, J., Aggerbaek, H., Dheda, K., and Andersen, P. L. (2016). Diagnostic accuracy of the novel C-Tb skin test for LTBI, results from two phase III trials. *Eur. Respir. J.* 48:OA3037. doi: 10.1183/13993003.congress-2016.OA3037

Ruibal, P., Voogd, L., Joosten, S. A., and Ottenhoff, T. H. M. (2021). The role of donor-unrestricted T-cells, innate lymphoid cells, and NK cells in anti-mycobacterial immunity. *Immunol. Rev.* 301, 30–47. doi: 10.1111/imr.12948

Saiboonjan, B., Roytrakul, S., Sangka, A., Lulitanond, V., Faksri, K., and Namwat, W. (2021). Proteomic analysis of drug-susceptible and multidrug-resistant nonreplicating Beijing strains of *Mycobacterium tuberculosis* cultured in vitro. *Biochem. Biophys. Rep.* 26:100960. doi: 10.1016/j.bbrep.2021.100960

Sakai, S., Kauffman, K. D., Oh, S., Nelson, C. E., Barry, C. E. III, and Barber, D. L. (2021). MAIT cell-directed therapy of *Mycobacterium tuberculosis* infection. *Mucosal Immunol.* 14, 199–208. doi: 10.1038/s41385-020-0332-4

Saracino, A., Scotto, G., Fornabaio, C., Martinelli, D., Faleo, G., Cibelli, D., et al. (2009). QuantiFERON-TB Gold In-Tube test (QFT-GIT) for the screening of latent tuberculosis in recent immigrants to Italy. *New Microbiol.* 32, 369–376.

Schoeman, J. C., du Preez, I., and Loots du, T. (2012). A comparison of four sputum pre-extraction preparation methods for identifying and characterising *Mycobacterium tuberculosis* using GCxGC-TOFMS metabolomics. *J. Microbiol. Methods* 91, 301–311. doi: 10.1016/j.mimet.2012.09.002

Scordo, J. M., Knoell, D. L., and Torrelles, J. B. (2016). Alveolar epithelial cells in *Mycobacterium tuberculosis* infection: active players or innocent bystanders? *J. Innate Immun.* 8, 3–14. doi: 10.1159/000439275

Shin, J. H., Yang, J. Y., Jeon, B. Y., Yoon, Y. J., Cho, S. N., Kang, Y. H., et al. (2011). (1)H NMR-based metabolomic profiling in mice infected with *Mycobacterium tuberculosis*. *J. Proteome Res.* 10, 2238–2247. doi: 10.1021/pr101054m

Somashekar, B. S., Amin, A. G., Tripathi, P., MacKinnon, N., Rithner, C. D., Shanley, C. A., et al. (2012). Metabolomic signatures in guinea pigs infected with epidemic-associated W-Beijing strains of *Mycobacterium tuberculosis*. *J. Proteome Res.* 11, 4873–4884. doi: 10.1021/pr300345x

Sotgiu, G., Saderi, L., Petruccioli, E., Aliberti, S., Piana, A., Petrone, L., et al. (2019). QuantiFERON TB Gold Plus for the diagnosis of tuberculosis: a systematic review and meta-analysis. *J. Infect.* 79, 444–453. doi: 10.1016/j.jinf.2019.08.018

Starshinova, A., Dovgalyk, I., Malkova, A., Zinchenko, Y., Pavlova, M., Belyaeva, E., et al. (2020). Recombinant tuberculosis allergen (Diaskintest((R))) in tuberculosis diagnostic in Russia (meta-analysis). *Int. J. Mycobacteriol.* 9, 335–346. doi: 10.4103/ijmy.ijmy_131_20

Steffen, R. E., Pinto, M., Kritski, A., and Trajman, A. (2020). Cost-effectiveness of newer technologies for the diagnosis of *Mycobacterium tuberculosis* infection in Brazilian people living with HIV. *Sci. Rep.* 10:21823. doi: 10.1038/s41598-020-78737-w

Stop TB Partnership (2015). *The Global Plan to End TB*. Geneva: Stop TB Partnership.

Sudbury, E. L., Clifford, V., Messina, N. L., Song, R., and Curtis, N. (2020). *Mycobacterium tuberculosis*-specific cytokine biomarkers to differentiate active TB and LTBI: a systematic review. *J. Infect.* 81, 873–881. doi: 10.1016/j.jinf.2020.09.032

Sun, H., Pan, L., Jia, H., Zhang, Z., Gao, M., Huang, M., et al. (2018). Label-free quantitative proteomics identifies novel plasma biomarkers for distinguishing pulmonary tuberculosis and latent infection. *Front. Microbiol.* 9:1267. doi: 10.3389/fmicb.2018.01267

Syhre, M., and Chambers, S. T. (2008). The scent of *Mycobacterium tuberculosis*. *Tuberculosis (Edinb)* 88, 317–323. doi: 10.1016/j.tube.2008.01.002

Syhre, M., Manning, L., Phuanukoonnon, S., Harino, P., and Chambers, S. T. (2009). The scent of *Mycobacterium tuberculosis*–part II breath. *Tuberculosis (Edinb)* 89, 263–266. doi: 10.1016/j.tube.2009.04.003

Tailleux, L., Schwartz, O., Herrmann, J. L., Pivert, E., Jackson, M., Amara, A., et al. (2003). DC-SIGN is the major *Mycobacterium tuberculosis* receptor on human dendritic cells. *J. Exp. Med.* 197, 121–127. doi: 10.1084/jem.20021468

Theel, E. S., Hilgart, H., Breen-Lyles, M., McCoy, K., Flury, R., Breeher, L. E., et al. (2018). Comparison of the QuantiFERON-TB Gold Plus and QuantiFERON-TB Gold In-Tube Interferon Gamma Release Assays in Patients at Risk for Tuberculosis and in Health Care Workers. *J. Clin. Microbiol.* 56, e00614–18. doi: 10.1128/JCM.00614-18

Tolosie, K., and Sharma, M. K. (2014). Application of cox proportional hazards model in case of tuberculosis patients in selected addis ababa health centres, ethiopia. *Tuberc. Res. Treat.* 2014:536976. doi: 10.1155/2014/536976

Venkatappa, T. K., Punnoose, R., Katz, D. J., Higgins, M. P., Banaei, N., Graviss, E. A., et al. (2019). Comparing QuantiFERON-TB gold plus with other tests to diagnose *Mycobacterium tuberculosis* infection. *J. Clin. Microbiol.* 57, e00985–19. doi: 10.1128/JCM.00985-19

Villate, J. I., Ibáñez, B., Cabriada, V., Pijoán, J. I., Taboada, J., and Urkaregi, A. (2006). Analysis of latent tuberculosis and mycobacterium avium infection data using mixture models. *BMC Public Health* 6:240. doi: 10.1186/1471-2458-6-240

Vinuesa, C. G., Toellner, K. M., and Papa, I. (2016). "Extrafollicular antibody responses," in *Encyclopedia of Immunobiology*, ed. M. J. H. Ratcliffe (Oxford: Academic Press), 208–215.

Wang, J., Qie, Y., Zhang, H., Zhu, B., Xu, Y., Liu, W., et al. (2008). PPE protein (Rv3425) from DNA segment RD11 of *Mycobacterium tuberculosis*: a novel immunodominant antigen of *Mycobacterium tuberculosis* induces humoral and cellular immune responses in mice. *Microbiol. Immunol.* 52, 224–230. doi: 10.1111/j.1348-0421.2008.00029.x

Wang, S., Chen, J., Zhang, Y., Diao, N., Zhang, S., Wu, J., et al. (2013). *Mycobacterium tuberculosis* region of difference (RD) 2 antigen Rv1985c and RD11 antigen Rv3425 have the promising potential to distinguish patients with active tuberculosis from M. bovis BCG-vaccinated individuals. *Clin. Vaccine Immunol.* 20, 69–76. doi: 10.1128/cvi.00481-12

Wang, S., Li, Y., Shen, Y., Wu, J., Gao, Y., Zhang, S., et al. (2018). Screening and identification of a six-cytokine biosignature for detecting TB infection and discriminating active from latent TB. *J. Transl. Med.* 16:206. doi: 10.1186/s12967-018-1572-x

Watson, A., Li, H., Ma, B., Weiss, R., Bendayan, D., Abramovitz, L., et al. (2021). Human antibodies targeting a *Mycobacterium* transporter protein mediate protection against tuberculosis. *Nat. Commun.* 12:602. doi: 10.1038/s41467-021-20930-0

Weiner, J. III, Parida, S. K., Maertzdorf, J., Black, G. F., Repsilber, D., Telaar, A., et al. (2012). Biomarkers of inflammation, immunosuppression and stress with active disease are revealed by metabolomic profiling of tuberculosis patients. *PLoS One* 7:e40221. doi: 10.1371/journal.pone.0040221

Westphalen, K., Gusarova, G. A., Islam, M. N., Subramanian, M., Cohen, T. S., Prince, A. S., et al. (2014). Sessile alveolar macrophages communicate with alveolar epithelium to modulate immunity. *Nature* 506, 503–506. doi: 10.1038/nature12902

WHO (2015). *WHO Guidelines Approved by the Guidelines Review Committee," in Guidelines on the Management of Latent Tuberculosis Infection*. Geneva: World Health Organization, 33.

WHO (2018). *Global Tuberculosis Report 2018*. Geneva: World Health Organization.

WHO (2020). *Global Tuberculosis Report 2020*. Geneva: World Health Organization.

Wipperman, M. F., Bhattarai, S. K., Vorkas, C. K., Maringati, V. S., Taur, Y., Mathurin, L., et al. (2021). Gastrointestinal microbiota composition predicts peripheral inflammatory state during treatment of human tuberculosis. *Nat. Commun.* 12:1141. doi: 10.1038/s41467-021-21475-y

Won, E. J., Choi, J. H., Cho, Y. N., Jin, H. M., Kee, H. J., Park, Y. W., et al. (2017). Biomarkers for discrimination between latent tuberculosis infection and active tuberculosis disease. *J. Infect.* 74, 281–293. doi: 10.1016/j.jinf.2016.11.010

Wu, J., Bai, J., Wang, W., Xi, L., Zhang, P., Lan, J., et al. (2019). ATBdiscrimination: an in silico tool for identification of active tuberculosis disease based on routine blood test and T-SPOT.TB detection results. *J. Chem. Inf. Model.* 59, 4561–4568. doi: 10.1021/acs.jcim.9b00678

Yan, Z. H., Yi, L., Wei, P. J., Jia, H. Y., Wang, J., Wang, X. J., et al. (2018). Evaluation of panels of *Mycobacterium tuberculosis* antigens for serodiagnosis of tuberculosis. *Int. J. Tuberc. Lung Dis.* 22, 959–965. doi: 10.5588/ijtld.18.0060

Yang, C. T., Cambier, C. J., Davis, J. M., Hall, C. J., Crosier, P. S., and Ramakrishnan, L. (2012). Neutrophils exert protection in the early tuberculous granuloma by oxidative killing of mycobacteria phagocytosed from infected macrophages. *Cell Host Microbe* 12, 301–312. doi: 10.1016/j.chom.2012.07.009

Yang, D. (2018). *Epitope Prediction, Recombinant Protein Preparation and Immunological Characteristics Of Mycobacterium Tuberculosis* rv2657c. Master. Zhangjiakou: Hebei North University.

Yang, X., Zhang, J., Liang, Q., Pan, L., Duan, H., Yang, Y., et al. (2021). Use of T-SPOT.TB for the diagnosis of unconventional pleural tuberculosis is superior to ADA in high prevalence areas: a prospective analysis of 601 cases. *BMC Infect. Dis.* 21:4. doi: 10.1186/s12879-020-05676-2

Zellweger, J. P., Sotgiu, G., Corradi, M., and Durando, P. (2020). The diagnosis of latent tuberculosis infection (LTBI): currently available tests, future

developments, and perspectives to eliminate tuberculosis (TB). *Med. Lav.* 111, 170–183. doi: 10.23749/mdl.v111i3.9983

Zhang, H., Wang, J., Lei, J., Zhang, M., Yang, Y., Chen, Y., et al. (2007). PPE protein (Rv3425) from DNA segment RD11 of *Mycobacterium tuberculosis*: a potential B-cell antigen used for serological diagnosis to distinguish vaccinated controls from tuberculosis patients. *Clin. Microbiol. Infect.* 13, 139–145. doi: 10.1111/j.1469-0691.2006.01561.x

Zhou, A., Ni, J., Xu, Z., Wang, Y., Lu, S., Sha, W., et al. (2013). Application of (1)h NMR spectroscopy-based metabolomics to sera of tuberculosis patients. *J. Proteome Res.* 12, 4642–4649. doi: 10.1021/pr40k07359

Zhou, Y., Du, J., Hou, H. Y., Lu, Y. F., Yu, J., Mao, L. Y., et al. (2017). Application of immunoscore model for the differentiation between active tuberculosis and latent tuberculosis infection as well as monitoring anti-tuberculosis therapy. *Front. Cell Infect. Microbiol.* 7:457. doi: 10.3389/fcimb.2017.00457

Conflict of Interest: The authors declare that the research was conducted in the absence of any commercial or financial relationships that could be construed as a potential conflict of interest.

Publisher's Note: All claims expressed in this article are solely those of the authors and do not necessarily represent those of their affiliated organizations, or those of the publisher, the editors and the reviewers. Any product that may be evaluated in this article, or claim that may be made by its manufacturer, is not guaranteed or endorsed by the publisher.

frontiers in Microbiology

ORIGINAL RESEARCH
published: 23 December 2021
doi: 10.3389/fmicb.2021.812690

Multiple Cross Displacement Amplification Combined With Real-Time Polymerase Chain Reaction Platform: A Rapid, Sensitive Method to Detect *Mycobacterium tuberculosis*

Wei-wei Jiao[1†], Gui-rong Wang[2†], Lin Sun[1], Jing Xiao[1], Jie-qiong Li[1], Ya-cui Wang[1], Shu-ting Quan[1], Hai-rong Huang[2] and A-dong Shen[1,3]**

[1] Key Laboratory of Major Diseases in Children, Beijing Key Laboratory of Pediatric Respiratory Infection Disease, Ministry of Education, National Key Discipline of Pediatrics (Capital Medical University), National Clinical Research Center for Respiratory Diseases, National Center for Children's Health, Beijing Pediatric Research Institute, Beijing Children's Hospital, Capital Medical University, Beijing, China, [2] National Tuberculosis Clinical Laboratory, Beijing Key Laboratory for Drug Resistance Tuberculosis Research, Beijing Tuberculosis and Thoracic Tumor Research Institute, Beijing Chest Hospital, Capital Medical University, Beijing, China, [3] Children's Hospital Affiliated to Zhengzhou University, Henan Children's Hospital, Zhengzhou Children's Hospital, Zhengzhou, China

In this study, we evaluated the diagnostic accuracy of multiple cross displacement amplification (MCDA) combined with real-time PCR platform in pulmonary tuberculosis (PTB) patients. Total 228 PTB patients and 141 non-TB cases were enrolled. Based on the analysis of the first available sample of all participants, MCDA assay showed a higher overall sensitivity (64.0%), with a difference of more than 10% compared with Xpert MTB/RIF (Xpert) assay (51.8%, $P < 0.05$) and combined liquid and solid culture (47.8%, $P < 0.001$) for PTB diagnosis. In particular, MCDA assay detected 31 probable TB patients, which notably increased the percentage of confirmed TB from 57.9% (132/228) to 71.5% (163/228). The specificities of microscopy, culture, Xpert and MCDA assay were 100% (141/141), 100% (141/141), 100% (141/141), and 98.6% (139/141), respectively. Among the patients with multiple samples, per patient sensitivity of MCDA assay was 60.5% (52/86) when only the first available sputum sample was taken into account, and the sensitivity increased to 75.6% (65/86) when all samples tested by MCDA assay were included into the analysis. Therefore, MCDA assay established in this study is rapid, accurate and affordable, which has the potential in assisting the accurate and rapid diagnosis of PTB and speed up initiation of TB treatment in settings equipped with real-time PCR platform.

Keywords: ***Mycobacterium tuberculosis*, multiple cross displacement amplification, MCDA, diagnosis, pulmonary tuberclosis**

OPEN ACCESS

Edited by:
Tianyu Zhang, Guangzhou Institutes of Biomedicine and Health, Chinese Academy of Sciences (CAS), China

Reviewed by:
Mao-Shui Wang, Shandong Provincial Chest Hospital, China
Mae Newton-Foot, Stellenbosch University, South Africa
Gang Hou, China-Japan Friendship Hospital, China

****Correspondence:***
Hai-rong Huang
huanghairong@tb123.org
A-dong Shen
shenad18@126.com

† These authors have contributed equally to this work

Specialty section:
This article was submitted to Infectious Agents and Disease, a section of the journal Frontiers in Microbiology

Received: *10 November 2021*
Accepted: *07 December 2021*
Published: *23 December 2021*

Citation:
Jiao W-w, Wang G-r, Sun L, Xiao J, Li J-q, Wang Y-c, Quan S-t, Huang H-r and Shen A-d (2021) Multiple Cross Displacement Amplification Combined With Real-Time Polymerase Chain Reaction Platform: A Rapid, Sensitive Method to Detect Mycobacterium tuberculosis. Front. Microbiol. 12:812690. doi: 10.3389/fmicb.2021.812690

INTRODUCTION

Tuberculosis (TB), caused by *Mycobacterium tuberculosis* (MTB), is still a leading cause of mortality worldwide from a single infectious agent, being responsible for 9.9 million new cases and 1.3 million deaths in 2019 (World Health Organization [WHO], 2021). China is one of the high TB burden countries, accounting for 8.5% of all estimated incident cases globally (World Health Organization [WHO], 2021). Thus, much effort should be made to achieve the global END TB targets.

Rapid and accurate diagnosis is essential for TB control, which facilitates the timely initiation of appropriate treatment and further decreases the transmission risk. Current diagnostic tests for TB disease include smear microscopy, culture and rapid molecular tests. Smear microscopy is a routinely available test with low sensitivity. Culture-based methods remain the reference standard. However, it takes up to 8 weeks to provide the results and cannot meet the clinical needs. The Xpert MTB/RIF (Xpert) assay and loop-mediated isothermal amplification test (TB-LAMP) is World Health Organization (WHO) endorsed molecular tests (World Health Organization [WHO], 2011, 2016, 2017). Xpert is an automated real-time polymerase chain reaction (PCR) test with sensitivity comparable to liquid culture (Boehme et al., 2010) and is already widely used. The next-generation test Xpert Ultra has higher sensitivity for MTB detection, but it is not a routine laboratory test in China until now. Both Xpert and Xpert Ultra rely on GeneXpert machines and expensive consumable cartridges, which cannot be affordable in resource-poor settings. TB-LAMP is a promising technique with relatively simple device demand. Even a water bath could meet the needs of nucleic acid amplification. However, the results of TB-LAMP were usually determined by unaided eyes or under ultraviolet light, which is potentially subjective and make ambiguous judgment (Ou et al., 2014; Bojang et al., 2016).

Multiple cross displacement amplification (MCDA) is a novel amplification strategy based on isothermal strand-displacement polymerization reaction (Wang et al., 2015). In MCDA, a set of ten specific primers is designed for each target, with high sensitivity to fg level. In recent years, MCDA has been successfully applied to the detection of various pathogens (Wang et al., 2016a,b). In the previous report, we established an MTB detection method employing MCDA combined with lateral flow biosensor (MCDA-LFB) and preliminarily evaluated its clinical application (Jiao et al., 2019). MCDA-LFB is rapid, sensitive and simple, which is suitable for clinical use and field test. However, the application of LFB needs to open the amplification tube, which might lead to contamination in subsequent experiments. Since late 2019, coronavirus disease 2019 (COVID-19) began to wreak havoc all over the world. Although the COVID-19 pandemic is a setback to TB control, it still brings opportunities. In China, molecular detection platforms, especially techniques based on real-time PCR, are widely used all over the country, which greatly improved the detection ability in basic level hospitals and medical institutions. In this study, we integrated the MCDA assay into real-time PCR platform and assessed its accuracy in clinical pulmonary TB (PTB) cases.

MATERIALS AND METHODS

Study Population

Sputum specimens were prospectively collected from suspected TB patients from January 2019 to March 2019 at the Beijing Chest Hospital. All the enrolled patients had symptoms suggestive of TB and abnormal chest imaging. Each sputum specimen was subjected to smear microscopy, Lowenstein-Jensen (LJ) solid culture, mycobacteria growth indicator tube (MGIT) culture and Xpert (Cepheid, United States) simultaneously. The 1 mL aliquot sputum samples were stored at −80°C for further analysis.

The Ethics Committee approved the study protocol (No. 2020-7). Written informed consent was waived, as the specimens used in this study were leftover sputum samples from the clinical microbiology laboratory.

Patient Categories

Based on composite reference standard (CRS) which comprises clinical examination, microbiological evaluation, radiological imaging and follow-up data, patients were classified into three groups. (1) Bacteriologically confirmed TB: at least one positive result was obtained from the following tests: smear microscopy, culture or Xpert. (2) Probable TB: no bacteriological evidence of TB was found, but active TB diagnosis was made according to clinical findings, radiological images, treatment response and follow-up data. (3) Non-TB: the alternative diagnosis was established and clinical improvement was achieved without antitubercular treatment.

Clinical and Laboratory Procedures

Demographic information and clinical data of the enrolled subjects, including age, gender, treatment status, underlying diseases, were collected according to the medical records. The sputum specimens were usually collected early in the morning. Each specimen was transported to the lab within 4 h of collection. A direct smear was prepared and examined by light microscopy after auramine staining. About 2 mL sputum sample was decontaminated with N-acetyl-L-cysteine-sodium hydroxide (NALC-NaOH). After neutralization with sterile saline phosphate buffer (PBS, pH6.8) and centrifugation, the pellet was then inoculated into solid Lowenstein-Jensen medium (Encode Medical Engineering Co., Ltd) and liquid medium using MGIT 960 system (Becton Dickinson, United States). All positive cultures were further confirmed using MPT64 antigen testing (Genesis Biodetection and Biocontrol Co., Ltd).

Xpert (Cepheid) was performed according to the manufacturer's instructions. In brief, 1–2 mL sputum specimen was mixed with double volumes of Xpert sample processing reagent, and vortexed at 5 min intervals for 15 min. Then 2 mL of the mixture was transferred to the cartridge for Xpert testing.

A glass bead-based kit (CapitalBio Co.) was used to extract the genomic DNA. The defrosted samples were fully digested with 2–4 volumes of 4% NaOH depending on the viscosity of the sputum. After centrifugation, the pellet was washed once using TE buffer and re-suspended with 100 μL DNA extraction buffer. The mixture was transferred to the tube with glass beads and shook for

15 min at a high speed using Extractor 36 (CapitalBio Co.). The tube was heated using a metal rack at 95°C for 5 min. Total 90 μL DNA was obtained after centrifugation at 12, 000 rpm for 5 min and 5 μL of the supernatant was used for MCDA amplification.

The MCDA assay was performed as described previously (Jiao et al., 2019) with some modifications. Two sets of non-labeled primers targeting IS*6110* and IS*1081* were used. To monitor the MCDA reaction, 0.3 μL of EvaGreen dye was added into the reaction mixture to produce the fluorescence signal. The assay was implemented on real-time platform (Agilent AriaMx) using the FAM/SYBR Green channel. The amplification was performed at 67°C for 40 min with plate reading at 30 s intervals. The normalized fluorescence signal no less than 800 and reaction time no more than 35 min were used to determine MCDA positivity. If the normalized fluorescence signal was more than 800 and reaction time more than 35 min, the result was considered to fall in the gray area and the experiment had to be repeated. The result was determined positive if the fluorescence signal remained more than 800 regardless of reaction time and negative if no/less fluorescence signal. The threshold was derived from a preliminary analysis of smear-positive samples and non-TB patients. All laboratory tests were performed with the operator blinded to the clinical information.

Statistical Analysis

Demographic information of the study population was presented as percentages for categorical variables and medians for continuous variables.

Diagnostic accuracy parameters (sensitivity, specificity, positive and negative predictive values) were calculated using bacteriological results and clinical evidence as reference standards. Among the patients providing more than one sample, diagnostic values were calculated in three ways. (1) Per patient/1st sample, including only the first sample tested for each patient. (2) Per patient/all samples, including all samples tested for each patient and considering the patient as positive if any of these samples was positive. (3) Per sample, including all tested samples individually with performed tests. McNemar's test was used to compare the differences in sensitivity and specificity. A *P*-value less than 0.05 was considered statistically significant. SPSS version 23.0 software was used for statistical analysis.

RESULTS

Study Participants Characteristics

Total 377 patients with suspected PTB were enrolled. Eight patients were subsequently excluded due to a lack of adequate samples ($n = 5$) and contaminated cultures ($n = 3$). Thus, 369 patients were included for analysis of MCDA assay diagnostic performance. **Figure 1** shows the flow of participants according to the case definition categories.

Overall, 228 patients (61.8%) were diagnosed with active PTB, including 132 with bacteriologically confirmed TB and 96 with probable TB. The 141 non-TB cases (38.2%) were 17 lung cancer patients and 124 patients with other infectious diseases, including four with non-tuberculous mycobacteria (NTM) caused disease. Among NTM patients, two were culture-positive and two were diagnosed by molecular testing of biopsy tissues. The age of patients was younger in the TB group than that in the non-TB group (48.5 years vs. 65 years, $P < 0.001$). TB group had more male patients (75.0% vs. 61.7%, $P = 0.007$). A higher proportion of TB patients had diabetes mellitus compared to non-TB patients (27.2% vs. 6.4%, $P < 0.001$). All patients were HIV-negative. Detailed demographic and clinical data are presented in **Table 1**.

Performance of Multiple Cross Displacement Amplification Assay in Pulmonary Tuberculosis Diagnosis

In the MCDA detection, six samples corresponding to six patients (three were confirmed TB, the others are probable TB) fell in the gray area. After repeat, four remained the same and two were positive. Thus, all six samples were considered positive in the following analysis.

Diagnostic value was calculated considering the first collected sputum specimen for all enrolled patients (**Table 2**). Generally, MCDA assay exhibited a sensitivity of 64.0% (146/228) in patients with active PTB, which was significantly higher than Xpert (51.8%, 118/228, $P = 0.008$), culture (MGIT and LJ combined, 47.8%, 109/228, $P < 0.001$) and microscopy (21.5%, 49/228, $P < 0.001$). Then we divided the patients into confirmed TB and probable TB according to CRS without referring to MCDA results. Among 132 confirmed TB cases, the high sensitivity of MCDA assay was shown at 87.1% (115/132), similar to that of Xpert (89.4%, 118/132, $P = 0.566$) and culture (82.6%, 109/132, $P = 0.303$). In addition, the MCDA assay detected 31 probable TB patients. When the MCDA results were integrated into the CRS, these 31 patients were reclassified as confirmed TB cases, and the percentage of confirmed TB increased from 57.9% (132/228) to 71.5% (163/228).

A head-to-head comparison of results from all diagnostic methods showed that MCDA assay produced a sensitivity of 89.0% (97/109) in culture-positive patients, 95.9% (47/49) in microscopy-positive cases, and 84.1% in microscopy-negative but culture-positive cases. MCDA assay also identified TB in 35 Xpert-negative cases and 49 culture-negative cases. In microscopy-negative samples, MCDA assay showed a sensitivity of 55.3% (99/179) and Xpert was 40.2% (72/179). MCDA assay was the only positive test in 31 samples, Xpert in 5 samples, and culture in 8 samples (**Figure 2**).

The specificities of microscopy, culture, Xpert and MCDA assay based on the analysis of the first available sample were 100% (141/141), 100% (141/141), 100% (141/141), and 98.6% (139/141), respectively. With regard to the latter, two lung tumor patients were misdiagnosed as PTB by MCDA assay.

Per Patient and Per Sample Analysis in Patients With Multiple Samples

A total of 98 patients provided two or more sputum samples, including 188 sputum samples from 86 TB patients and 26 samples from 12 non-TB patients. Per patient sensitivity and specificity analysis used the CRS as the reference standard.

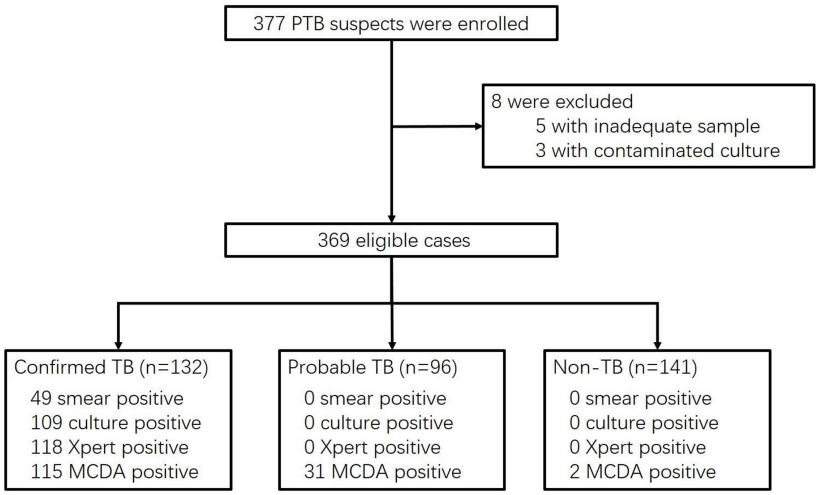

FIGURE 1 | Flow chart of participant recruitment.

TABLE 1 | Demographic and clinical characteristics of the study population.

Characteristic	Total TB (*n* = 228)	Confirmed TB (*n* = 136)	Probable TB (*n* = 92)	Non-TB (*n* = 141)	*P*-value (Total TB vs. Non-TB)
Age, median (range), yr	48.5 (16–88)	48 (17–88)	49 (16–85)	65 (19–97)	<0.001
Gender					
Male, n (%)	171 (75.0)	107 (78.7)	64 (69.6)	87 (61.7)	0.007
Female, n (%)	57 (25.0)	29 (21.3)	28 (30.4)	54 (38.3)	
Treatment status					
New case	174 (76.3)	102 (75.0)	72 (78.3)	/	
Retreated case	54 (23.7)	34 (25.0)	20 (21.7)	/	
Combined extra-pulmonary TB					
Pleural TB	67 (29.4)	32 (23.5)	35 (38.0)	/	
Lymphatic TB	10 (4.4)	5 (3.7)	5 (5.4)	/	
TB meningitis	2 (0.9)	2 (1.5)	0 (0)	/	
Other sites	11 (4.8)	5 (3.7)	6 (6.5)	/	
Underlying diseases					
Diabetes mellitus	62 (27.2)	39 (28.7)	23 (25.0)	9 (6.4)	<0.001
Chronic kidney disease	11 (4.8)	8 (5.9)	3 (3.3)	3 (2.1)	0.188
Autoimmune disease	3 (1.3)	0 (0)	3 (3.3)	2 (1.4)	0.934
Tumor	14 (6.1)	11 (8.1)	3 (3.3)	17 (12.1)	0.046

Values are No. (%) or as indicated.
"/": not applicable.

TABLE 2 | Diagnostic accuracy of different methods in the pulmonary TB patients.

Performance	Microscopy	Culture	Xpert	MCDA	Culture + MCDA
Sensitivity					
Confirmed PTB[a] (*n* = 132)	49/132 (37.1)[b]	109/132 (82.6)	118/132 (89.4)	115/132 (87.1)	127/132 (96.2)[c]
Probable PTB (*n* = 96)	/	/	/	31/96 (32.3)	31/96 (32.3)
PTB total (*n* = 228)	49/228 (21.5)[b]	109/228 (47.8)[b]	118/228 (51.8)[c]	146/228 (64.0)	158/228 (69.3)
Specificity (*n* = 141)	141/141 (100)	141/141 (100)	141/141 (100)	139/141 (98.6)	139/141 (98.6)
PPV total (*n* = 369)	49/49 (100)	109/109 (100)	118/118 (100)	146/148 (98.6)	158/160 (98.8)
NPV total (*n* = 369)	141/320 (44.1)[b]	141/260 (54.2)	141/251 (56.2)	139/221 (62.9)	139/209 (66.5)

Values are No./total No. (%). MCDA, multiple cross displacement amplification; NPV, negative predictive value; PPV, positive predictive value; Xpert, Xpert MTB/RIF.
[a]*Patients were classified according to composite reference standard criteria that does not include MCDA results.*
[b]*Statistically significant (P < 0.001) when compared with MCDA assay.*
[c]*Statistically significant (P < 0.05) when compared with MCDA assay.*

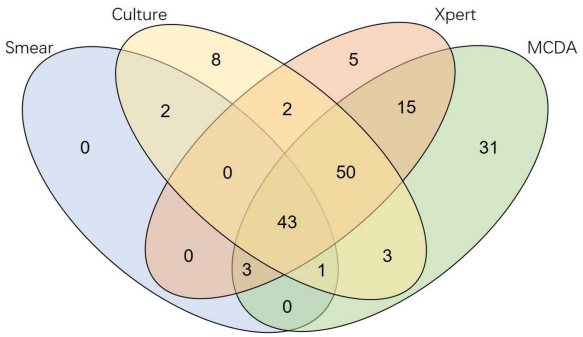

FIGURE 2 | Venn diagram of different diagnostic methods.

Taking only the first available sputum sample into account, the sensitivity of MCDA assay was 60.5% (52/86), while the sensitivity amounted to 75.6% (65/86) when all samples tested by MCDA assay were included in the analysis (**Table 3**). In comparison, the per patient sensitivity of Xpert, culture and microscopy was 46.5% (40/86), 44.2% (38/86) and 25.6% (22/86) for first available sample, respectively, and 50.0% (43/86), 48.8% (42/86) and 30.2% (26/86) for all samples, respectively. When all tested samples were considered individually, per sample sensitivity showed a sensitivity of 58.5% (110/188) for MCDA assay, which was significantly higher than Xpert (47.9%, $P = 0.039$), culture (44.1%, $P = 0.005$) and microscopy (26.1%, $P < 0.001$). None of the patients in the non-TB group was found to be positive using MCDA assay, Xpert, culture or microscopy. Thus the specificity of each method remained high (100%) either per patient or per sample analysis.

DISCUSSION

Early diagnosis is essential for the control of TB. Although there are many available diagnostic methods for TB, only 59% of PTB cases were bacteriologically confirmed according to WHO report (World Health Organization [WHO], 2021). Alternative test that is rapid, sensitive, specific and easy to perform is always the ideal goal to accelerate the process to end TB. In the previous study, we established a promising method for TB detection using MCDA combined with LFB and its limit of detection was 10 fg (Jiao et al., 2019). With the widespread access to real-time PCR techniques, we further moved to monitor the MCDA products using real-time PCR platform and evaluated its diagnostic accuracy in the PTB cases. As a result, MCDA assay showed a higher overall sensitivity (64.0%), with a difference of more than 10% compared with Xpert (51.8%, $P < 0.05$) and combined culture (MGIT and LJ, 47.8%, $P < 0.001$) for PTB diagnosis. In particular, the sensitivity of MCDA assay was 55.3% (99/179) in smear-negative samples and Xpert was 40.2% (72/179). The difference is in line with a previous publication, where 63% of smear-negative patients were detected by Xpert Ultra and 46% detected by Xpert (Dorman et al., 2018). This indicates that MCDA assay has a similar performance with Xpert Ultra in PTB detection.

In this study, the improved diagnostic value of the MCDA assay was especially pronounced in resolving probable PTB cases. 32.3% (31/96) of cases with negative etiological results (including microscopy, culture or Xpert) were positive for TB using MCDA assay, which notably increased the bacteriological confirmation rate from 57.9% (132/228) to 71.5% (163/228). Therefore, MCDA assay might lead to earlier diagnosis and treatment initiation. In contrast with conventional culture (LJ and MGIT), the MCDA assay detected 49 additional PTB cases (**Figure 2**). However, it should be noted that 8 samples were detected as positive only by culture, indicating that MCDA assay can be a promising complementary test for PTB diagnosis, but cannot replace the culture-based algorithms.

Examination of multiple specimens from the same TB patient would improve the detection sensitivity of microscopy, culture and Xpert (Bonnet et al., 2007; Wang G. et al., 2018). Wang et al. (Wang G. et al., 2018) reported that the addition of a second Xpert test increased sensitivity by 4.65% among PTB

TABLE 3 | Per patient diagnostic accuracy in the patients with multiple sputum samples.

	Sensitivity	Samples per patient, mean (SD)	Specificity	Samples per patient, mean (SD)
Microscopy				
First available sample	22/86 (25.6)[a]	1	12/12 (100)	1
All samples	26/86 (30.2)[a]	2.19 (0.45)	12/12 (100)	2.167 (0.39)
Culture				
First available sample	38/86 (44.2)[b]	1	12/12 (100)	1
All samples	42/86 (48.8)[a]	2.19 (0.45)	12/12 (100)	2.167 (0.39)
Xpert				
First available sample	40/86 (46.5)	1	12/12 (100)	1
All samples	43/86 (50.0)[a]	2.19 (0.45)	12/12 (100)	2.167 (0.39)
MCDA				
First available sample	52/86 (60.5)	1	12/12 (100)	1
All samples	65/86 (75.6)	2.19 (0.45)	12/12 (100)	2.167 (0.39)

Values are No./total No. (%). MCDA, multiple cross displacement amplification; NPV, negative predictive value; PPV, positive predictive value; Xpert, Xpert MTB/RIF.
[a]Statistically significant ($P < 0.001$) when compared with MCDA assay.
[b]Statistically significant ($P < 0.05$) when compared with MCDA assay.

patients, which is similar to this study (3.5%). Our data suggested that the overall sensitivity of the MCDA assay increased with the number of sputum samples tested. Compared with Xpert, culture and microscopy, multiple MCDA assays had a higher incremental yield (15.1%) for detection of PTB patients, with a sensitivity of 60.5% for the first available sample to 75.6% for all samples. Thus, multiple MCDA tests will be beneficial for suspected PTB. In the previous study, a second Xpert assay was not recommended for suspected TB patients, especially in smear-negative cases, considering the high cartridge cost (Wang G. et al., 2018). The cost of MCDA assay is much lower, with only about 1/6 of Xpert per test. In this view, using multiple MCDA tests in suspected TB cases presents an affordable and feasible approach, especially for patients with smear-negative results.

The specificity of the MCDA assay compared to the CRS standard was considered acceptable (98.6%). This was due to two patients being misdiagnosed as PTB by MCDA assay with results confirmed after three repeats. One patient is 76 years old with a malignant tumor of the right lung. The other one is 78 years old with pneumonia caused by Klebsiella pneumonia. We assumed that these two patients could have TB comorbidity or a history of TB, as China is a high TB burden country. A similar situation was reported in other studies, especially when using more sensitive methods, such as Xpert Ultra (Dorman et al., 2018; Wang G. et al., 2020). The Xpert Ultra used multi-copy genes IS*6110* and IS*1081* as the targets and showed increased sensitivity in various kinds of specimen types for TB detection. However, the specificity of Xpert Ultra was lower than Xpert, particularly for patients with a history of TB, as Xpert Ultra might have detected MTB DNA as the remnant of a previous active TB episode (Dorman et al., 2018; Theron et al., 2018). MCDA assay employed the same targets as Xpert Ultra and had high sensitivity, which might also lead to the false-positive result in specificity verification. However, cross-contamination or other unknown reasons cannot be excluded.

Different amplification monitoring methods might influence the sensitivity. Compared with our previous study, MCDA assay using real-time platform did not achieve high sensitivity as that with LFB (64.0% vs. 88.2%) (Jiao et al., 2019). The main reason might lie in the different methods of monitoring the assay products. When the LFB was used to detect the MCDA results, the biotin-labeled MCDA amplicons could form a complex with streptavidin-coated polymer nanoparticles (SA-DNPs) *via* biotin-streptavidin interactions at the conjugated pad, which would amplify the signal and increase the sensitivity. Thus, more paucibacillary patients can be detected using MCDA combined with the LFB platform. Nevertheless, the real-time platform has its advantage. One of the essential steps for reporting MCDA results by LFB is to open the amplification tube, which can produce aerosol droplets containing a high concentration of MCDA products (Wang Y. et al., 2018) and possible contamination presents a significant challenge in this case. In contrast, real-time PCR platform permits monitoring of the fluorescence signal through transparent cover of the unopened tube, thus avoiding possible contamination. This approach is more suitable for areas without specialized product testing laboratories.

Compared to the automated Xpert platform, limitations of the developed MCDA assay should be noted. Firstly, the targets of MCDA assay are multi-copy genes IS*6110* and IS*1081*, which ensure high sensitivity and can even detect IS*6110*-absent strains circulating in Southeast Asia. However, it cannot predict drug resistance of MTB simultaneously. Secondly, MCDA assay needs relatively more manual operations, including extraction of genomic DNA, preparation of reaction mixture, etc. Nevertheless, MCDA assay is suitable for labor-intensive and resource-limited areas as the reagents and consumables are affordable.

In conclusion, this study demonstrated a higher sensitivity of the MCDA assay compared with microscopy, culture or Xpert using sputum samples. MCDA assay has the potential in assisting the accurate and rapid diagnosis of PTB and speeds up initiation of TB treatment in settings equipped with real-time PCR platforms.

DATA AVAILABILITY STATEMENT

The raw data supporting the conclusions of this article will be made available by the authors, without undue reservation.

ETHICS STATEMENT

The studies involving human participants were reviewed and approved by Beijing Children's Hospital, Capital Medical University. Written informed consent from the participants' legal guardian/next of kin was not required to participate in this study in accordance with the national legislation and the institutional requirements.

AUTHOR CONTRIBUTIONS

W-WJ conceived and designed the experiments. W-WJ, G-RW, LS, JX, J-QL, Y-CW, and S-TQ performed the experiments. G-RW and H-RH contributed the clinical samples. W-WJ and A-DS contributed the reagents and materials. W-WJ, G-RW, H-RH, and A-DS analyzed the data and wrote the manuscript. All authors have contributed and approved the final version of the manuscript.

FUNDING

This study was funded by Capital's Funds for Health Improvement and Research (2020-2-1142), Beijing Natural Science Foundation (J200005), and Tongzhou Yunhe Project under Grant (YH201905 and YH201917).

REFERENCES

Boehme, C. C., Nabeta, P., Hillemann, D., Nicol, M. P., Shenai, S., Krapp, F., et al. (2010). Rapid molecular detection of tuberculosis and rifampin resistance. *N. Engl. J. Med.* 363, 1005–1015.

Bojang, A. L., Mendy, F. S., Tientcheu, L. D., Otu, J., Antonio, M., Kampmann, B., et al. (2016). Comparison of TB-LAMP, GeneXpert MTB/RIF and culture for diagnosis of pulmonary tuberculosis in The Gambia. *J. Infect.* 72, 332–337. doi: 10.1016/j.jinf.2015.11.011

Bonnet, M., Ramsay, A., Gagnidze, L., Githui, W., Guerin, P. J., and Varaine, F. (2007). Reducing the number of sputum samples examined and thresholds for positivity: an opportunity to optimise smear microscopy. *Int. J. Tuberc. Lung Dis.* 11, 953–958.

Dorman, S. E., Schumacher, S. G., Alland, D., Nabeta, P., Armstrong, D. T., King, B., et al. (2018). Xpert MTB/RIF Ultra for detection of Mycobacterium tuberculosis and rifampicin resistance: a prospective multicentre diagnostic accuracy study. *Lancet Infect. Dis.* 18, 76–84. doi: 10.1016/S1473-3099(17)30691-6

Jiao, W. W., Wang, Y., Wang, G. R., Wang, Y. C., Xiao, J., Sun, L., et al. (2019). Development and clinical validation of multiple cross displacement amplification combined with nanoparticles-based biosensor for detection of mycobacterium tuberculosis: preliminary results. *Front. Microbiol.* 10:2135. doi: 10.3389/fmicb.2019.02135

Ou, X., Li, Q., Xia, H., Pang, Y., Wang, S., Zhao, B., et al. (2014). Diagnostic accuracy of the PURE-LAMP test for pulmonary tuberculosis at the county-level laboratory in China. *PLoS One* 9:e94544.

Theron, G., Venter, R., Smith, L., Esmail, A., Randall, P., Sood, V., et al. (2018). False-Positive xpert mtb/rif results in retested patients with previous tuberculosis: frequency, profile, and prospective clinical outcomes. *J. Clin. Microbiol.* 56:e01696-17. doi: 10.1128/JCM.01696-17

Wang, G., Wang, S., Jiang, G., Fu, Y., Shang, Y., and Huang, H. (2018). Incremental cost-effectiveness of the second Xpert MTB/RIF assay to detect Mycobacterium tuberculosis. *J. Thorac. Dis.* 10, 1689–1695. doi: 10.21037/jtd.2018.02.60

Wang, G., Wang, S., Yang, X., Sun, Q., Jiang, G., Huang, M., et al. (2020). Accuracy of Xpert MTB/RIF ultra for the diagnosis of pleural TB in a multicenter cohort study. *Chest* 157, 268–275. doi: 10.1016/j.chest.2019.07.027

Wang, Y., Li, H., Li, D., Li, K., Wang, Y., Xu, J., et al. (2016a). Multiple cross displacement amplification combined with gold nanoparticle-based lateral flow biosensor for detection of vibrio parahaemolyticus. *Front. Microbiol.* 7:2047. doi: 10.3389/fmicb.2016.02047

Wang, Y., Li, H., Wang, Y., Xu, H., Xu, J., and Ye, C. (2018). Antarctic thermolabile uracil-DNA-glycosylase-supplemented multiple cross displacement amplification using a label-based nanoparticle lateral flow biosensor for the simultaneous detection of nucleic acid sequences and elimination of carryover contamination. *Nano Res.* 11, 2632–2647. doi: 10.1007/s12274-017-1893-z

Wang, Y., Wang, Y., Ma, A. J., Li, D. X., Luo, L. J., Liu, D. X., et al. (2015). Rapid and sensitive isothermal detection of nucleic-acid sequence by multiple cross displacement amplification. *Sci. Rep.* 5:11902.

Wang, Y., Wang, Y., Xu, J., and Ye, C. (2016b). Development of multiple cross displacement amplification label-based gold nanoparticles lateral flow biosensor for detection of *shigella* spp. *Front. Microbiol.* 7:1834. doi: 10.3389/fmicb.2016.01834

World Health Organization [WHO] (2011). *Policy Statement: Automated Real-Time Nucleic Acid Amplification Technology for Rapid and Simultaneous Detection of Tuberculosis and Rifampicin Resistance: Xpert MTB/RIF System*. Geneva: World Health Organization.

World Health Organization [WHO] (2016). *The Use of Loop-Mediated Isothermal Amplification (TB-LAMP) for the Diagnosis of Pulmonary Tuberculosis: Policy Guidance*. Geneva: World Health Organization.

World Health Organization [WHO] (2017). *WHO meeting report of a technical expert consultation: non-inferiority analysis of Xpert MTB/RIF Ultra compared to Xpert MTB/RIF*. Geneva: World Health Organization.

World Health Organization [WHO] (2021). *Global tuberculosis report*. Geneva: World Health Organization.

Conflict of Interest: The authors declare that the research was conducted in the absence of any commercial or financial relationships that could be construed as a potential conflict of interest.

Publisher's Note: All claims expressed in this article are solely those of the authors and do not necessarily represent those of their affiliated organizations, or those of the publisher, the editors and the reviewers. Any product that may be evaluated in this article, or claim that may be made by its manufacturer, is not guaranteed or endorsed by the publisher.

frontiers in Microbiology

ORIGINAL RESEARCH
published: 23 February 2022
doi: 10.3389/fmicb.2022.823324

Computer-Aided Diagnosis of Spinal Tuberculosis From CT Images Based on Deep Learning With Multimodal Feature Fusion

Zhaotong Li[1,2†], Fengliang Wu[3,4†], Fengze Hong[5], Xiaoyan Gai[6], Wenli Cao[7], Zeru Zhang[1,2], Timin Yang[4], Jiu Wang[4], Song Gao[1] and Chao Peng[4*]*

[1] Institute of Medical Technology, Peking University Health Science Center, Beijing, China, [2] School of Health Humanities, Peking University, Beijing, China, [3] Beijing Key Laboratory of Spinal Disease Research, Engineering Research Center of Bone and Joint Precision Medicine, Department of Orthopedics, Peking University Third Hospital, Beijing, China, [4] Department of Orthopedic, People's Hospital of Tibet Autonomous Region, Lhasa, China, [5] Medical College, Tibet University, Lhasa, China, [6] Department of Respiratory and Critical Care Medicine, Peking University Third Hospital, Beijing, China, [7] Tuberculosis Department, Beijing Geriatric Hospital, Beijing, China

OPEN ACCESS

Edited by:
Hairong Huang,
Capital Medical University, China

Reviewed by:
Xiangzhi Bai,
Beihang University, China
Guangming Zhu,
Stanford University, United States
Qingquan Kong,
Sichuan University, China

****Correspondence:***
Song Gao
gaoss@bjmu.edu.cn
Chao Peng
pengchaodedian@163.com

[†] These authors have contributed equally to this work and share first authorship

Specialty section:
This article was submitted to Infectious Agents and Disease, a section of the journal Frontiers in Microbiology

Received: *27 November 2021*
Accepted: *13 January 2022*
Published: *23 February 2022*

Citation:
Li Z, Wu F, Hong F, Gai X, Cao W, Zhang Z, Yang T, Wang J, Gao S and Peng C (2022) Computer-Aided Diagnosis of Spinal Tuberculosis From CT Images Based on Deep Learning With Multimodal Feature Fusion. Front. Microbiol. 13:823324. doi: 10.3389/fmicb.2022.823324

Background: Spinal tuberculosis (TB) has the highest incidence in remote plateau areas, particularly in Tibet, China, due to inadequate local healthcare services, which not only facilitates the transmission of TB bacteria but also increases the burden on grassroots hospitals. Computer-aided diagnosis (CAD) is urgently required to improve the efficiency of clinical diagnosis of TB using computed tomography (CT) images. However, classical machine learning with handcrafted features generally has low accuracy, and deep learning with self-extracting features relies heavily on the size of medical datasets. Therefore, CAD, which effectively fuses multimodal features, is an alternative solution for spinal TB detection.

Methods: A new deep learning method is proposed that fuses four elaborate image features, specifically three handcrafted features and one convolutional neural network (CNN) feature. Spinal TB CT images were collected from 197 patients with spinal TB, from 2013 to 2020, in the People's Hospital of Tibet Autonomous Region, China; 3,000 effective lumbar spine CT images were randomly screened to our dataset, from which two sets of 1,500 images each were classified as tuberculosis (positive) and health (negative). In addition, virtual data augmentation is proposed to enlarge the handcrafted features of the TB dataset. Essentially, the proposed multimodal feature fusion CNN consists of four main sections: matching network, backbone (ResNet-18/50, VGG-11/16, DenseNet-121/161), fallen network, and gated information fusion network. Detailed performance analyses were conducted based on the multimodal features, proposed augmentation, model stability, and model-focused heatmap.

Results: Experimental results showed that the proposed model with VGG-11 and virtual data augmentation exhibited optimal performance in terms of accuracy, specificity, sensitivity, and area under curve. In addition, an inverse relationship existed between

the model size and test accuracy. The model-focused heatmap also shifted from the irrelevant region to the bone destruction caused by TB.

Conclusion: The proposed augmentation effectively simulated the real data distribution in the feature space. More importantly, all the evaluation metrics and analyses demonstrated that the proposed deep learning model exhibits efficient feature fusion for multimodal features. Our study provides a profound insight into the preliminary auxiliary diagnosis of spinal TB from CT images applicable to the Tibetan area.

Keywords: computer-aided diagnosis, spinal tuberculosis, computed tomography, feature fusion, deep learning

INTRODUCTION

Spinal tuberculosis (spinal TB) is secondary to TB of the lung, gastrointestinal tract, or lymphatic tract, and it causes bone TB *via* the blood circulation route (Garg and Somvanshi, 2011; Rasouli et al., 2012; Khanna and Sabharwal, 2019). The insidious onset of spinal TB and the lack of specificity in clinical manifestations can lead to serious symptoms, such as kyphosis, abscess injection, and spinal instability, further causing paraplegia or death (Qian et al., 2018; Vanino et al., 2020). The incidence of TB is significantly higher in underdeveloped plateau regions, particularly in the Tibetan area of China (Du et al., 2017; Zhu et al., 2017); for example, the rate of reported TB cases in the Tibet Autonomous Region was 166.6 per 100,000 in 2017, which was the highest in China. Spinal TB accounts for approximately 2% of pulmonary TB, 15% of extrapulmonary TB, and 50% of bone and joint TB throughout the world (Fuentes Ferrer et al., 2012). Moreover, the CT manifestation of spinal TB is complicated, including typical manifestations (destruction of the vertebral body, collapse of the vertebral space, abscess compression on the spinal cord or nerve roots, etc.) and atypical manifestations (vertebral body osteoid formation, vertebral body disruption in the anterior column, vertebral body endplate worm-like disruption, pus in the paravertebral soft tissue shadow, continuous unilateral bone disruption, and asymmetry between the imaging manifestations and symptoms) (Cremin et al., 1993; Rauf et al., 2015).

Local grassroots hospitals lack experienced specialists and multimodal medical imaging equipment, they have only CT or digital radiography (DR) machines. Therefore, most Tibetan grassroots doctors cannot make expeditious medical decisions. These poor health conditions lead to high rates of misdiagnosis, missed diagnosis, and delays in effective treatment, which result in severe complications that impose serious social burdens on Tibetan herdsmen (Wang et al., 2015). Computer-aided diagnosis (CAD), including classical machine learning (ML) and deep learning (DL), is an effective method for assisting primary care physicians in treating patients with spinal TB; CAD builds mathematical models on computers using fuzzy mathematics, probability statistics, and even artificial intelligence to process patient information and propose diagnostic opinions and treatment plans. To the best of our knowledge, except for a few reports on the simple application of statistical analysis to the clinical diagnosis of spinal TB (Zhang et al., 2019; Liu et al., 2021), there are limited studies on artificial intelligence-aided diagnosis of spinal TB, including diagnostic classification, pathological grading, lesion segmentation, and prognostic analysis.

Radiomics, a typical example of traditional ML, is an automated high-throughput method that extracts a significant amount of quantitative handcrafted features from medical images (Lambin et al., 2012). These handcrafted features are the conversion of digital images into mineable data and the subsequent analyses of these data for decision support (Gillies et al., 2016), such as color, texture, shape, and statistical characteristics, including scale-invariant feature transform (SIFT), speeded-up robust features (SURF), and oriented rotated brief (ORB) (Abdellatef et al., 2020). Currently, although many handcrafted features have been designed for various clinical applications (Moradi et al., 2007; Aerts et al., 2014; Cook et al., 2014; Wang et al., 2014; Li et al., 2018; Tian et al., 2018; Song et al., 2021), classical ML cannot accurately perform ancillary diagnostics of TB owing to its limited accuracy (Goodfellow et al., 2016; Currie et al., 2019). The design of handcrafted features often involves finding the right trade-off between accuracy and computational efficiency based on the subjective understanding of key issues (Nanni et al., 2017); therefore, an inappropriate handcrafted feature typically results in poor generalization ability (Suzuki et al., 2012), which significantly hinders the development of ML diagnostic systems.

Contrastingly, DL based on convolutional neural networks (CNNs) is another medical CAD method that enhances the identification of subtle differences in radiographical characteristics, and it is feasible for integrating multi-omics medical data by harnessing the power of computing (Altaf et al., 2019; Alkhateeb et al., 2021). Unlike traditional ML, the features extracted by DL can be predetermined by a CNN during training, without elaborate design (Anwar et al., 2018). There are various CNN models that are applicable to different medical scenarios, such as common CNN for grading (Yang et al., 2018; Swarnambiga et al., 2019), U-Net for segmentation (Ronneberger et al., 2015; Jackson et al., 2018; Deng et al., 2021), and GAN for the generation of synthetic images (Lei et al., 2019). The technological innovations of CAD show that DL could be a suitable candidate for auxiliary diagnosis in modern healthcare systems. However, a CNN needs the majority of datasets to extract features automatically and requires significant training time to obtain a reliable model (Goodfellow et al., 2016; Currie et al., 2019), both of which are scarce resources

in medical practices. Moreover, the lack of interpretability of DL is another important factor that hinders its development in rigorous clinical work.

Therefore, the effective fusion of the multimodal features extracted from both ML and DL is one of the key directions to further improve the performance of CAD when compared with the counterparts of individuals above. This approach has had several successful applications with medical radiological images, such as in the determination of tumor benignity and malignancy (Antropova et al., 2017; Xie et al., 2018; Khosravi et al., 2021), lesion segmentation (Su et al., 2021), survival prediction (Shboul et al., 2019; Guo et al., 2021), detection of COVID-19 from chest CT images (Wang S.-H. et al., 2021), and cancer diagnosis and prognosis (Chen et al., 2020). By contrast, published studies on spinal TB have mainly focused on the clinical manifestations and surgical protocol of spinal tuberculosis (Garg and Somvanshi, 2011; Zhu et al., 2017; Khanna and Sabharwal, 2019). Different feature fusion methods have been developed for different clinical purposes, such as a Bayesian algorithm-based method that can realize the fusion decision of multiple features (Khaleghi et al., 2013), a sparse representation-based method that can obtain the joint sparse representation of multiple features (Lai and Deng, 2018), and a DL-based method that can strengthen the feature learning process of deep neural networks (Zhang et al., 2021). However, most of the aforementioned fused features are different representations under the same modality owing to the difficulty of multimodal fusion, and in cross-modal learning, it is difficult to implement transfer learning between more than two modalities. Conversely, the gated information fusion network (Arevalo et al., 2017; Kim et al., 2018) ensures that each single modality can work independently and transfer knowledge mutually, and it realizes the effective fusion of multimodal information, including histology images and genomic features (Chen et al., 2020). It adopts the Kronecker product of unimodal feature representations to control the expressiveness of each single feature *via* a gated information attention mechanism.

In this study, a multimodal feature fusion CNN is proposed to classify spinal TB CT images obtained from local grassroots hospitals in the Tibetan area. It provides a breakthrough in the application area of spinal TB auxiliary diagnosis, although it simply implements the classification of tuberculosis-health diagnostic results in spinal TB CT images. Specifically, the proposed network fuses three different elaborate features, namely SIFT, SURF, and ORB, with the DL feature that originates from the convolutional output layer of common CNNs. A new augmentation algorithm for handcrafted features that effectively simulates the data distribution in the feature space is proposed as a substitute for the image augmentation method. Additionally, a model was designed and used to effectively integrate these individual features, which included four different sections: matching network for consistency of different feature dimensions, backbone for sparse representation of features, fallen network for dimensional reduction, and fusion network for hybridizing multimodal features by a gated mechanism. We evaluated the hypothesis that the proposed method can effectively distinguish tubercular cases from healthy images by conducting experiments and performing several analyses. For convenience, from here on, "positive" and "negative" represent tuberculosis and health, respectively. Based on initial hypothesis attempts, further research will be conducted on other auxiliary diagnostics to form a complete auxiliary diagnostic process for spinal TB and solve the long-standing problem of spinal tuberculosis in Tibet.

MATERIALS AND METHODS

Data Collection

A multimodal image dataset was obtained from the People's Hospital of Tibet Autonomous Region, China, and consisted of DR and CT images of 197 patients with spinal TB acquired between 2013 to 2020. They were screened by two physicians based on basic patient information, medical records, and imaging evaluation, all of which were surgically treated as definite spinal tuberculosis pathology according to the corresponding guidelines about the diagnosis of spinal TB (Hoffman et al., 1993; Liu et al., 2021). The inclusion and exclusion criteria for the spinal TB cases were as follows:

Inclusion criteria:

- Diagnosis of spinal tuberculosis was confirmed by puncture biopsy or postoperative pathological examination;
- Preoperative DR and CT examinations were performed;
- Complete case data (e.g., gender, age, medical history, physical examination, imaging, and pathology data);
- Patients who were first examined in primary care hospitals in less developed areas and had CT imaging data were prioritized for inclusion.

Exclusion criteria:

- Cases suspected of having spinal tuberculosis without pathological examination;
- A history of spinal trauma before the diagnosis of spinal tuberculosis;
- Incomplete case information.

Table 1 presents the patients' gender, age, and lesion segment. Some patients had multiple site infections; therefore, the total number of female and male patients is not equal to the total number of cases of cervical, thoracic, lumbar, and sacral vertebral infections. It can be seen that middle-aged people (30–59 years) were the most infected among all age groups, and the number of men infected with spinal TB was higher than that of women. The patients presented in this table are the ones who bear the heaviest social and family pressures. Furthermore, the lumbar vertebrae are the most susceptible to spinal TB infection; therefore, the current research was mainly conducted on the TB of lumbar vertebrae.

Although X-ray examinations are widely used in various primary hospitals, they provide limited information. CT examinations are approximately 20–25 times more sensitive than X-ray-based tissue density tests and are currently one of the most effective clinical bone examination methods. Spiral electron CT provides a high-resolution visualization of the destruction, hyperplasia, sclerosis, and focal boundaries of vertebral bone.

Furthermore, it reveals the position of dead bone, fragmented bone, and their protrusion into the spinal canal, showing paravertebral abscesses and their density. Moreover, the lumbar spine has the highest incidence of tuberculosis as it has the most mobility and bears the heaviest burden along the entire spine, as shown in **Table 1**. For the initial research of spinal TB, a total of 3,000 CT images of the lumbar vertebrae were randomly selected from the abovementioned multimodal image dataset based on slice level, which included a set of 1,500 slices for negative and positive cases. Finally, a small dataset of spinal TB CT images was obtained to explore the flexibility of CAD on spinal TB CT images.

TABLE 1 | Information of patient with spinal TB.

Age	Gender		Lesion segment			
	Female	Male	Cervix	Thorax	Lumbar	Sacrum
10–19	3	7	0	4	4	3
20–29	12	14	0	9	19	1
30–39	18	22	0	19	23	6
40–49	24	19	1	19	24	3
50–59	18	27	1	29	16	4
60–69	10	13	1	13	9	2
70–79	3	6	0	5	4	0
80–89	0	1	0	0	1	0
Sum	88	109	3	98	100	19

Feature Selection

Feature engineering is a key step in the supervised classification of pathology images that directly affects the final classification result. Image feature extraction is the premise of image analysis, which is the most effective way to simplify the expression of high-dimensional image data. Based on the above qualitative diagnostic characteristics from orthopedists, three handcrafted features were extracted from spinal TB CT images, including three types of feature descriptors of the vertebral column in CT slices: SIFT (Lowe, 2004), SURF (Bay et al., 2006), and ORB (Rublee et al., 2011). In addition to the handcrafted features mentioned above, deep features were extracted from the convolutional layers and fully connected layers of CNNs. These elaborate features are required for initial preprocessing to ensure dimensional consistency between different features before extracting the respective image characteristics. To understand the varied descriptions of different features, the meaning of the diverse features is indicated as follows.

Local feature:	Feature vectors of SIFT, SURF, ORB;
Elaborate feature:	Hand-crafted feature and deep learning feature extracted from CT images by classical machine learning and deep learning;
Hand-crafted feature:	Vectors manually extracted from CT images by classical machine learning;
Deep learning feature:	Vectors automatically extracted from convolutional layer of CNN by deep learning;
Extracted feature:	Hand-crafted feature and deep learning feature extracted from CT images by classical machine learning and deep learning;
Individual feature:	Single feature of SIFT, SURF, ORB, and CNN;
Training feature descriptor:	Key point descriptor of SIFT, SURF, ORB calculated from training dataset;
Feature descriptor:	Key point descriptor of SIFT, SURF, ORB;
Clustering feature:	Hand-crafted feature after searching codebook;
Augmented feature:	Hand-crafted feature after augmentation;
Weighted feature:	Hand-crafted feature after TF-IDF, i.e., local feature.

Local Features Described With Scale-Invariant Feature Transform, Speeded-Up Robust Features, and Oriented Rotated Brief

Several key points, such as the points of corners and edges, highlights, and dark spots, in an image do not change with luminance, transformation, and noise. These image feature points, which are typically used for image matching and image recognition, can reflect the essential features of an image. Scale-invariant feature transform (SIFT), speeded-up robust features (SURF), and oriented rotated brief (ORB) are three widespread methods used to describe these local feature points. Speckle and corner are just two typical feature points that can reflect key information that exists in the image. Speckle points usually refer to areas with color and grayscale that are different from the surrounding regions. Corner points are the intersection of two edges in the stable and informative areas of an image, which have certain characteristics, such as rotation invariance, scale invariance, affine invariance, and illumination invariance. These feature descriptors have been applied to various medical scenarios, such as medical image classification (Khan et al., 2015), medical image stitching (Singla and Sharma, 2014; Win and Kitjaidure, 2018), medical image fusion (Wang L. et al., 2021), medical image registration (Lukashevich et al., 2011; Li et al., 2012), and medical image retrieval (Govindaraju and Kumar, 2016).

Scale-invariant feature transform uses the Difference of Gaussian (DoG) matrix, which is a speckle detection method, to detect scale-space extrema, and uses an orientation histogram to extract the key point direction. The essence of the SIFT algorithm is to identify the key points and calculate their directions in different scale-spaces. The key points found by SIFT are almost speckle points that cannot be changed by illumination, affine transformation, or noise, such as highlights in dark areas and dark spots in bright areas.

Speeded-up robust features is a scale and rotation invariant descriptor on based on SIFT. Rather than choosing the difference of a Gaussian matrix to detect scale-space extrema in SIFT, it calculates an approximation of the Laplacian of the Gaussian by a Hessian matrix. Instead of using an orientation histogram in SIFT, Harris wavelet response, a corner detection algorithm, is used to assign key point orientations in SURF. Therefore, the key points found by SURF are significantly different from the speckle points found by SIFT. The number of key points detected by SURF is more than that detected by SIFT, whereas the vector dimension (64) of SURF is less than the length (128) of SIFT.

As a very fast binary descriptor based on two algorithms, Features from Accelerated Segment Test (FAST) (Khan et al., 2015) and Binary Robust Independent Elementary Features (BRIEF) (Calonder et al., 2010), ORB is an improved algorithm that outperforms the SIFT and SURF algorithms in terms of nearest-neighbor matching and description efficiency. FAST was used to extract the corner points whose pixel gray value is obviously different from the pixel gray value in the surrounding fields, and BRIEF was employed to describe the points that were extracted by FAST. It has the least number of feature points and the lowest dimensionality (32) of extracted features. In summary, it is a fast feature extracting and matching algorithm with poor quality compared with SIFT and SURF.

Before extracting feature points, the original spinal TB CT images were enhanced by adjusting the window width and position, and the vertebral region was isolated by watershed segmentation, which had a clear presentation on the centrum and also eliminated noise interference from non-skeletal areas. Subsequently, the feature points of SIFT, SURF, and ORB were transported to the bag of words (BoW) and term frequency–inverse document frequency (TF-IDF) models to obtain fifty-dimension feature vectors, as illustrated in **Figure 1**. The BoW and TF-IDF models with virtual augmentation are explored in section "Feature Preprocessing." Finally, we obtained three eigenvectors, which are the local features of all TB images.

Deep Learning Features

In addition to the above handcrafted features, the DL characteristics extracted from the convolutional layer of the CNN were another critical feature that contained highly abstract image features. It is generally assumed that there is a closer spatial connection between local pixels than the counterparts between pixels at a greater distance. Thus, each neuron only needs to perceive the local areas of the image and not the global image. Consequently, the global information is obtained by combining the local information at a higher level. A variety of CNNs have been applied to various medical image processing tasks, such as ResNet, VGG, and DenseNet, and thus, the DL features also differ from each other. Because of the black box property of DL features (Guidotti et al., 2018), different CNNs were selected to form the backbone of the proposed network to explore the optimal classification performance of spinal TB CT images.

Figure 2 shows the procedure for extracting DL features. Because the TB image dataset was small, the models that had more or fewer parameters tended to overfit or underfit, respectively; that is, the neural networks with different numbers of layers, ResNet-18 and ResNet-50, VGG-11 and VGG-16, DenseNet-121, and DenseNet-161, were selected as the backbone of the proposed network to avoid overfitting or underfitting.

Feature Preprocessing

The elaborate features should be preprocessed for dimensional consistency between different features. The identical handcrafted features of each slice were stacked vertically into one larger characteristic set. Subsequently, we used two algorithms, BoW and TF-IDF, to handle the low-dimension characteristic set extracted from the single-scale image. BoW adopted the K-means clustering method for unsupervised clustering of a large number of extracted SIFT, SURF, and ORB key points. The features with strong similarities were classified into the same clustering category. TF-IDF is the product of term frequency (TF) and IDF; it indicates the weight vector of features, where TF is the frequency of occurrence of a feature among all features, and IDF represents the uniqueness of a feature. **Figure 3** shows a flowchart illustrating the preprocessing of features. First, we used the key points feature descriptor of SIFT, SURF, and ORB from the training sets to build CodeBook using BoW. The clustering features were the statistics on the number of occurrences of each category after clustering in the feature descriptors by searching the CodeBook. The number of categories was set to 50 after several pretraining experiments with individual features. Second, a new data augmentation algorithm was proposed to improve the generalization of small datasets, and the **Algorithm 1** describes the data augmentation methods, which were only applicable to the cluster features processed by the BoW model. Specifically, the clustering information of each feature point was calculated using CodeBook, and the perturbation noise that obeys the normal distribution was used to jitter the clustering information for data augmentation, which increased the generalizability of the dataset. Finally, TF-IDF implemented feature weighting, which counted the frequency information of each feature vector appearing in the augmented feature sets. None of the augmented feature vectors existed in real TB images; that is, only the virtual key points of SIFT, SURF, and ORB existed.

ALGORITHM 1 | Data augmentation.

Input: Cluster Features Set: $C = \{c_1, c_2, \cdots, c_m\}$
Output: Augmented Features Set:
$C = \{a_{11}, \cdots, a_{1n}, a_{21}, \cdots, a_{2n} \cdots a_{m1}, \cdots, a_{mn}\}$
for $i \in [1, 2, \cdots, n]$ **do**
  Initialize $g_{ij} = \{\text{empty}\}$
  for j$\in [1, 2, \cdots, m]$ **do**
    $g_{ij} \cup \lceil temp \rceil \rightarrow g_{ij}, \forall\ temp \sim N(0, 3)$
end
$G_i = g_{ij}C$
end
$C \cup \bigcup_{i=1}^{n} G_i \rightarrow A$

Fusion Convolutional Neural Network Construction

After comprehensively considering the characteristics of vertebral morphology, we extracted four features from slice images, including the SIFT, SURF, and ORB vectors, and CNN features. Although the extracted handcrafted and DL features cover a wide range of valuable information involving both the local tissue and global slice, an

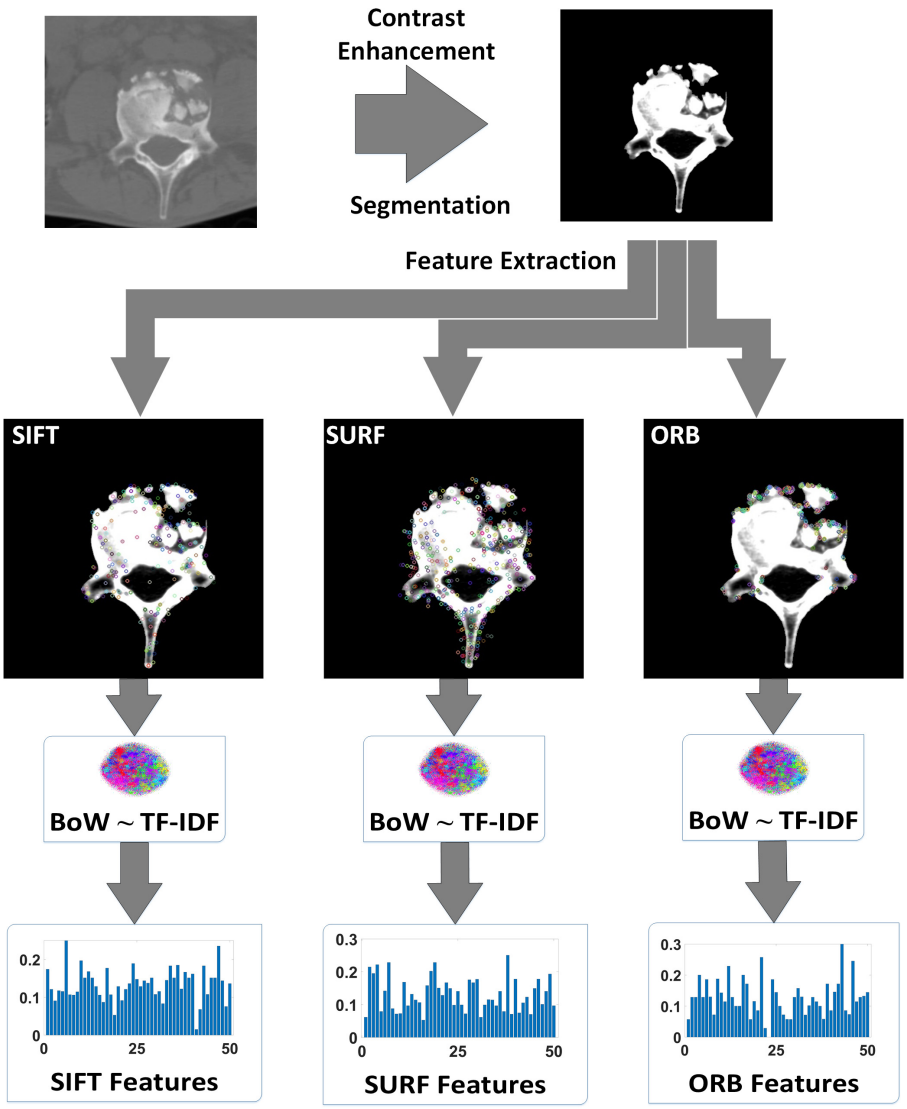

FIGURE 1 | Process of extracting local features of tuberculosis images.

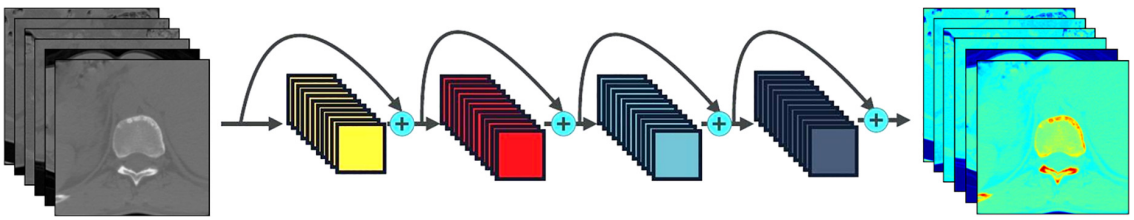

FIGURE 2 | Process of extracting the deep learning features of tuberculosis images. The series of images on the left are the raw CT data, the series of images on the right are the feature maps of the convolution layer of the CNN, and the middle represents the common CNNs.

effective method is imperative to fuse these features from different scales to improve prediction accuracy such that it is superior to the corresponding figures of any single feature.

As shown in **Figure 4**, the proposed network consists of four phases: the matching network that adjusts handcrafted features, backbone (i.e., different common CNNs) for processing all features, fallen network for dimension reduction, and fusion

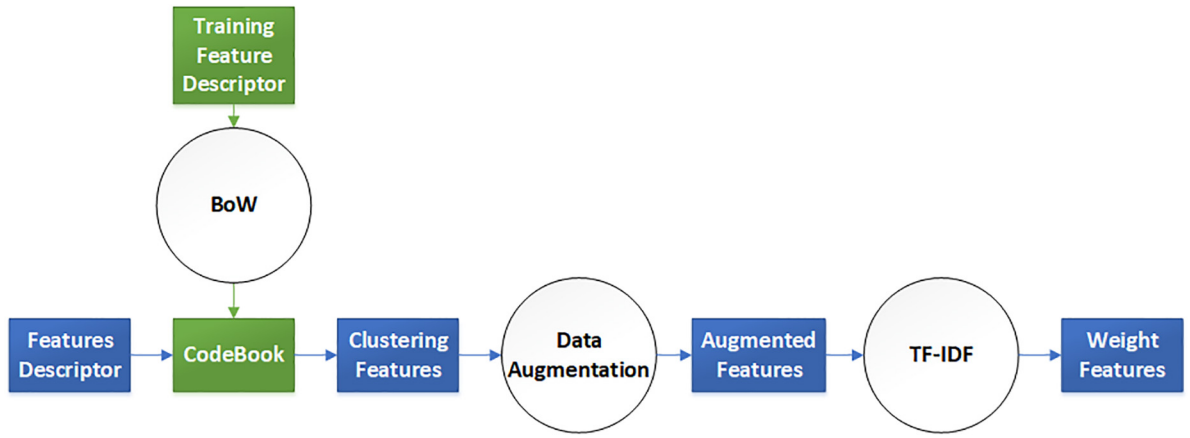

FIGURE 3 | Virtual augmentation model with bag of words (BoW) and term frequency–inverse document frequency (TF-IDF).

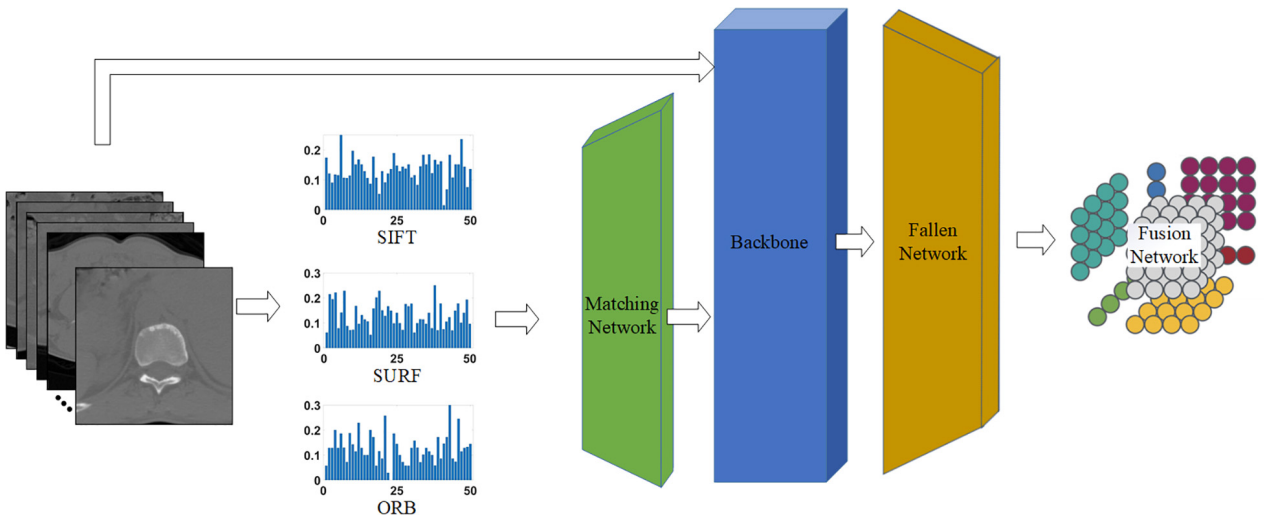

FIGURE 4 | Proposed network for classifying tuberculosis images. The middle three histograms are the SIFT, SURF, ORB vectors with length of 50 extracted from raw CT images, and the green, blue, and orange block represent the matching network, backbone, and fallen network, respectively. The matching network and fallen network are illustrated in **Figures 5A,B**, respectively, and the last block is the fusion network, which is illustrated in **Figure 5C**.

network for blending different characteristics. Each network is explained in the following sections.

Matching Network

Inconsistencies were present in the characteristic dimensions between the handcrafted and the DL features. Specifically, all handcrafted features were stacked into one-dimensional features with a size of 1×50, which was inconsistent with the dimensions of the DL features. Therefore, a matching network was required to reconcile the contradictions in the feature sizes between handcrafted and DL features, that is, to convert one-dimensional vectors into two-dimensional ones.

The matching network consisted of nine convolutional blocks, with each block including a fractionally strided convolution, batch normalization, and ReLU activation function. The detailed architecture of the matching network is shown in **Figure 5A**. The one-dimensional feature with size $1 \times 1 \times 50$ was mapped to a two-dimensional vector of size $224 \times 224 \times 3$, which is similar to the common input size of CNN architectures such as ResNets and to the two-dimensional space of the DL features. Hence, it is easier to tune hyperparameters and fuse handcrafted and DL features.

Fallen Network

After the matching network, the handcrafted image features were transformed into the same dimensional space as that of the DL features. Subsequently, a common network was employed to hybridize these different vectors including handcrafted and DL features. This integrated network includes two foundational networks: a backbone network and fallen network. Various CNNs, such as ResNet (He et al., 2016), DenseNet (Huang et al., 2017), and VGG-Net

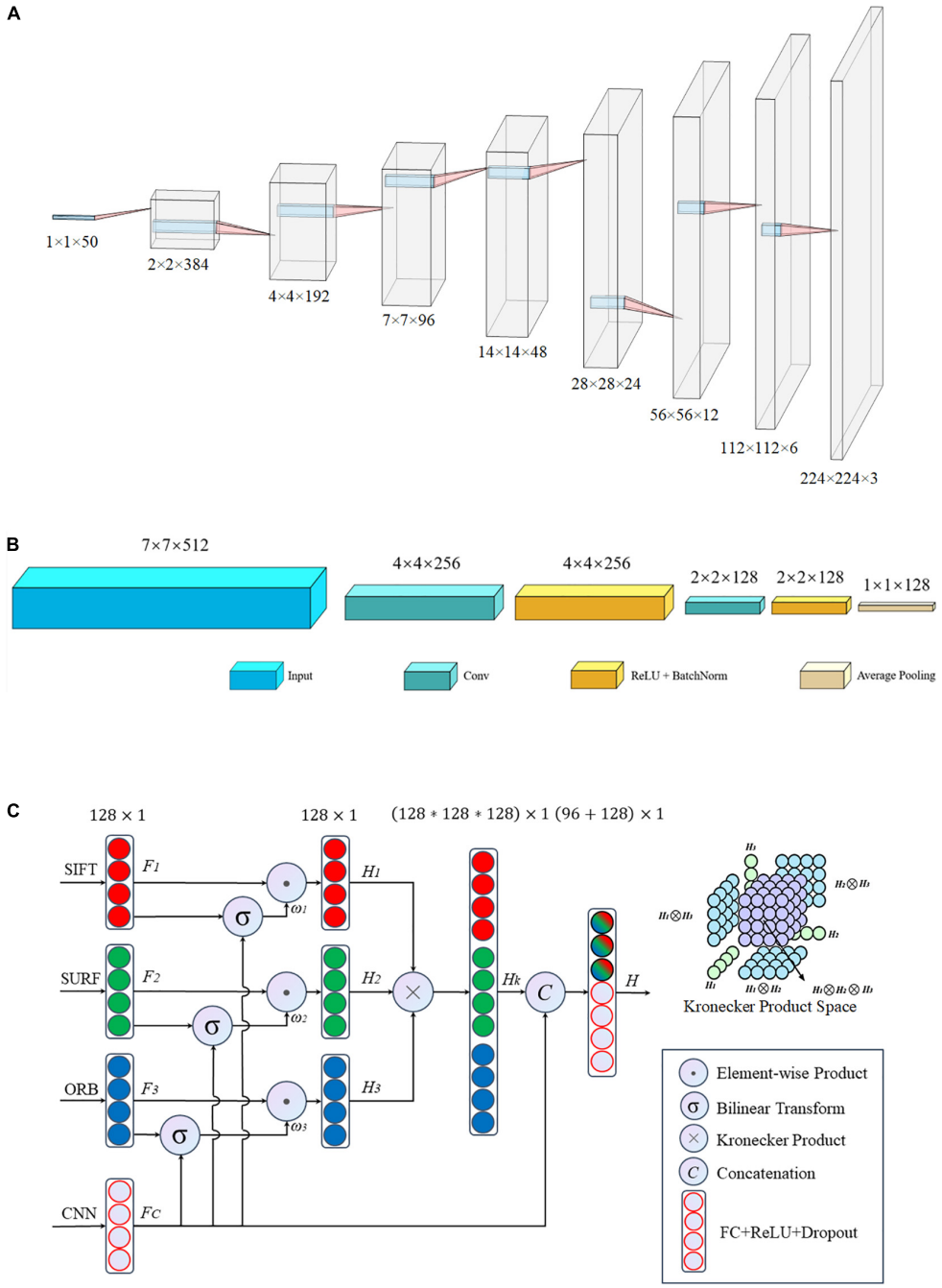

FIGURE 5 | Architecture of the proposed network: **(A)** matching network, **(B)** fallen network, and **(C)** gated information fusion network. The upper right corner of panel **(C)** is the Kronecher space of interactions among three features H_1, H_2, and H_3.

(Simonyan and Zisserman, 2015), serve as the backbone, and they have exhibited outstanding performance in different applications. The fallen network includes two convolutional operations and one average pooling, as shown in **Figure 5B**. It was used to refine the output characteristics of the backbone by mapping the outputs into a low-dimensional space, that is, a two-dimensional space with a size of 7 × 7 fell into a one-dimensional space with a size of 1 × 1 in detail. Essentially, we obtained a series of one-dimensional feature vectors for the subsequent processing of the fusion network.

Gated Information Fusion Network

All image features, including the handcrafted and DL features, were eventually converted into one-dimensional vectors of length 128 after the fallen network was processed. There was high collinearity between the handcrafted and DL characteristics;

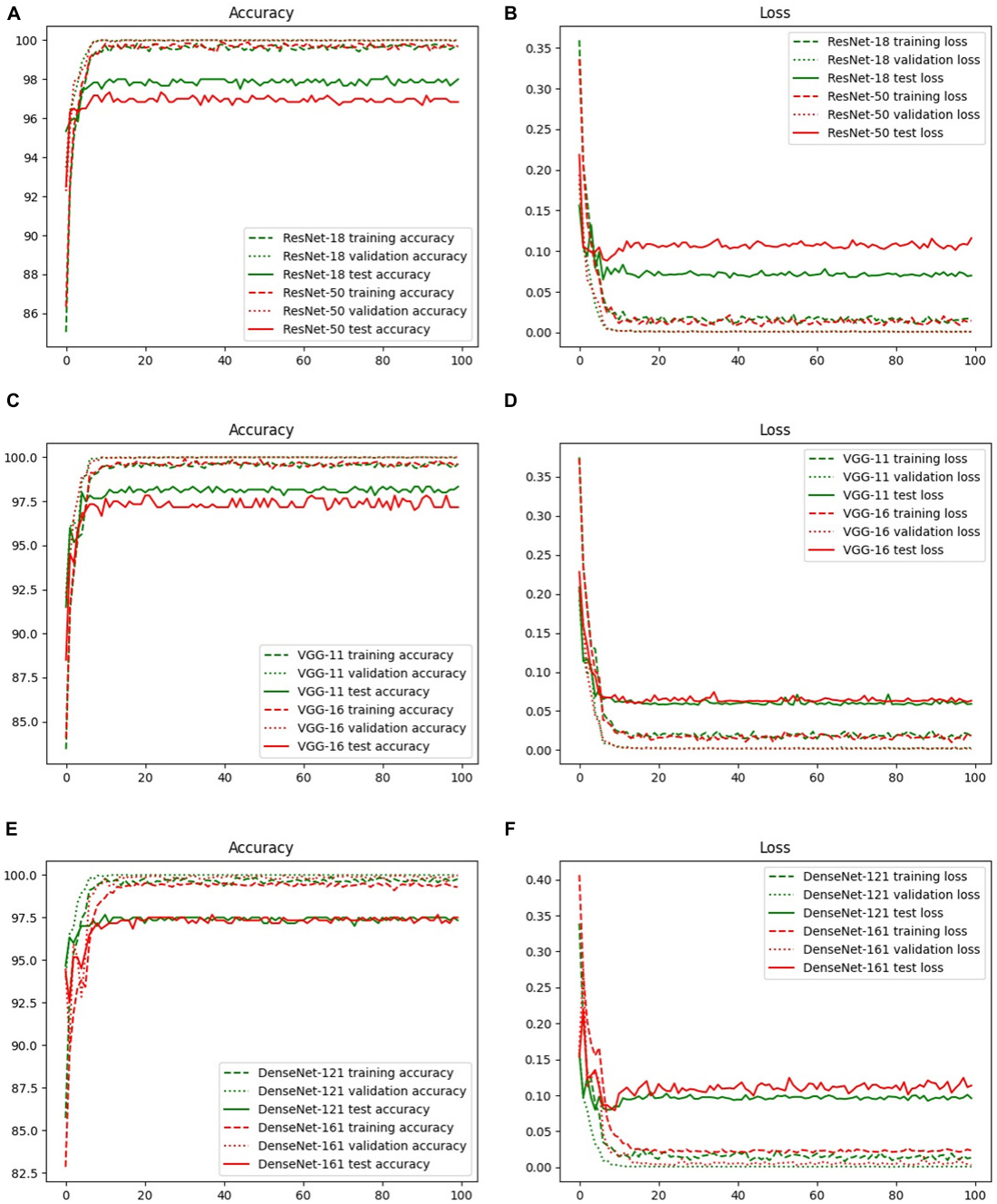

FIGURE 6 | Accuracy and loss curves with different backbones: **(A)** ResNet-18, **(B)** ResNet-50, **(C)** VGG-11, **(D)** VGG-16, **(E)** DenseNet-121, and **(F)** DenseNet-161.

therefore, an early fusion method that gates the weight contribution of the different tensors at the feature level was used to blend the aforementioned four image features before making a pathological diagnostic evaluation for the final classification.

The structure of the gated fusion network is shown in **Figure 5C**. For each feature tensor from SIFT, SURF, ORB, and CNN, the dimensions of the input vectors F_1, F_2, F_3, and F_C, respectively, are gradually reduced through the fully connected layer network with a dropout rate of 0.5. For the same dimension, because of the connection between individual captured features, the feature expressions of each handcrafted tensor are weighted by the gated mechanism *via* a combination with DL features to reduce the size of the feature space. The gated mechanism consists of two pathways: one is a one-dimensional vector F_i with a size of 128 × 1 after the ReLU activation function, and the other vector ω_i of length 128 is the output of the bilinear

TABLE 2 | Performance of the proposed network with different backbones.

Backbone	Accuracy	Specificity	Sensitivity	AUC
ResNet-18	0.9817	0.9800	**0.9833**	0.9960
ResNet-50	0.9733	0.9700	0.9767	0.9967
VGG-11	**0.9833**	0.9833	**0.9833**	**0.9984**
VGG-16	0.9783	0.9833	0.9783	0.9983
DenseNet-121	0.9767	0.9767	0.9767	0.9976
DenseNet-161	0.9767	**0.9867**	0.9667	0.9971

The bold figures represent the maximum value of each evaluation index.

transform between F_i and CNN features F_C, which evaluates the importance of each feature F_i relative to the more precise CNN features by this non-linear correlation. Subsequently, the Kronecher product, which models the interaction of different features across modalities, constructs a threefold Cartesian space defined by H_1, H_2, and H_3, that is, SIFT, SURF, and ORB, respectively. It also captures the trimodal interactions of all possible unimodal combinations, as shown in the upper right corner of **Figure 5C**. Finally, the predicted vectors, with a size of 96, and F_C, with a size of 128, are vertically stacked into a larger one-dimensional vector with a length of 224. Subsequently, the predicted values of classification for the TB images are obtained after the fully connected layer operating on the former concatenated one-dimensional vector.

The detailed operations above are summarized as shown below.

$$\omega_i = \sigma\left(F_i, F_C\right),\ i = 1, 2, 3 \tag{1}$$

$$H_i = \mathrm{RELU}\left(f\left(F_i \bigodot \omega_i\right)\right),\ i = 1, 2, 3 \tag{2}$$

$$H_m = H_1 \bigotimes H_2 \bigotimes H_3 \tag{3}$$

$$H_k = \mathrm{RELU}\left(f\left(H_1 \bigotimes H_2 \bigotimes H_3\right)\right) \tag{4}$$

$$H_C = \mathrm{RELU}\left(f\left(\left[H_k, F_C\right]\right)\right) \tag{5}$$

where, $\left[x, y\right]$ denotes the concatenation of x and y, and

$$\sigma\left(x, y\right) = xAy + b \tag{6}$$

$$f\left(x, y\right) = xA^T + b \tag{7}$$

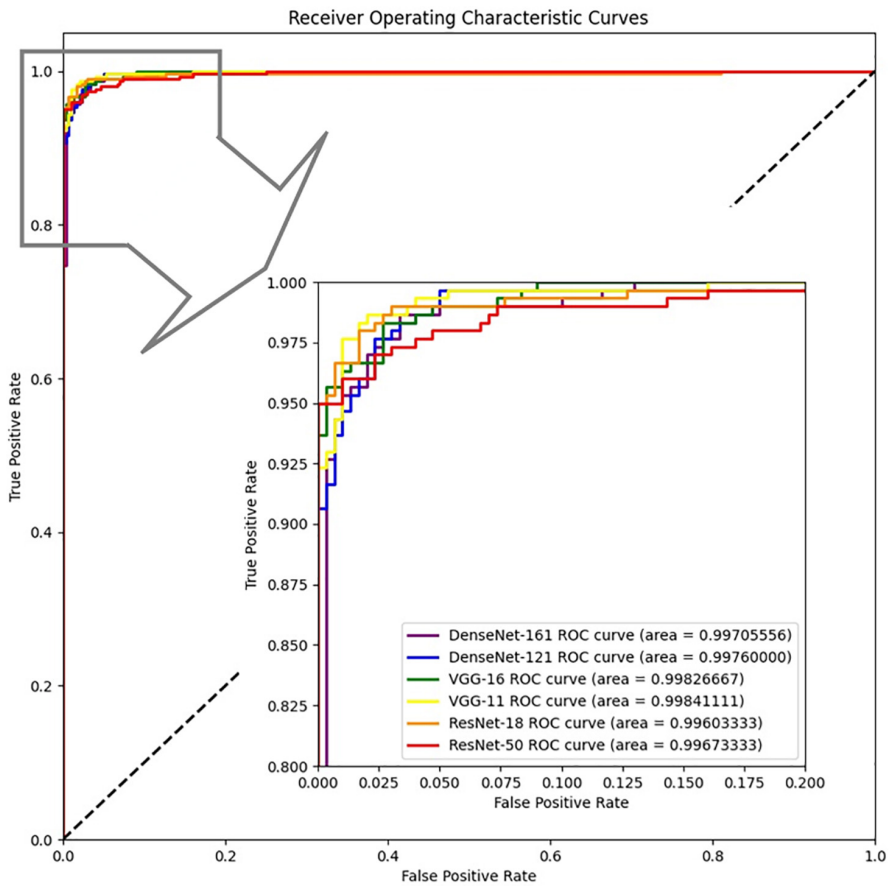

FIGURE 7 | ROCs of the proposed network with different backbones: ResNet-18, ResNet-50, VGG-11, VGG-16, DenseNet-121, and DenseNet-161.

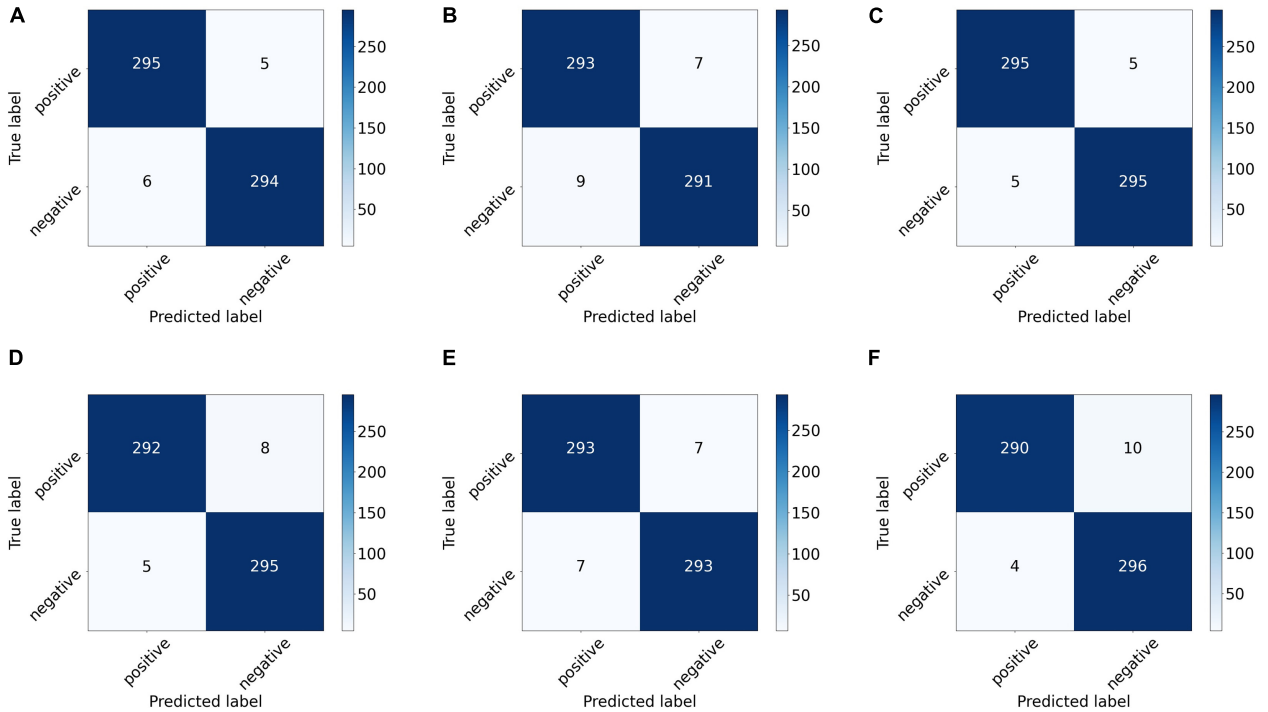

FIGURE 8 | Confusion matrix of the proposed network with different backbones: **(A)** ResNet-18, **(B)** ResNet-50, **(C)** VGG-11, **(D)** VGG-16, **(E)** DenseNet-121, and **(F)** DenseNet-161. The number on each sub-block represents the number of predictions, and the bars on the right of each block represent the heat value chart of the predicted numbers.

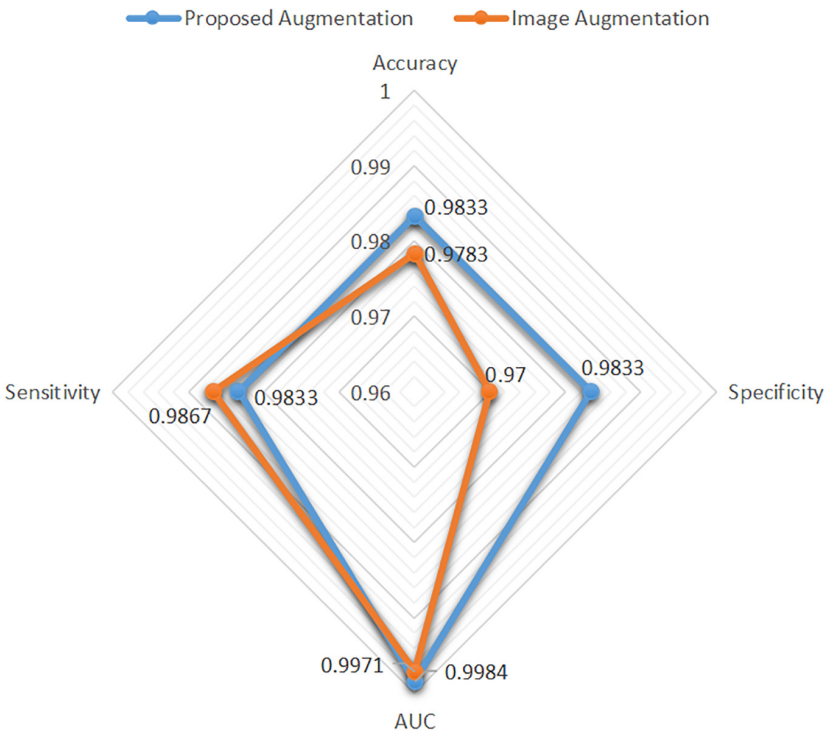

FIGURE 9 | Performance difference between the proposed augmentation and image augmentation.

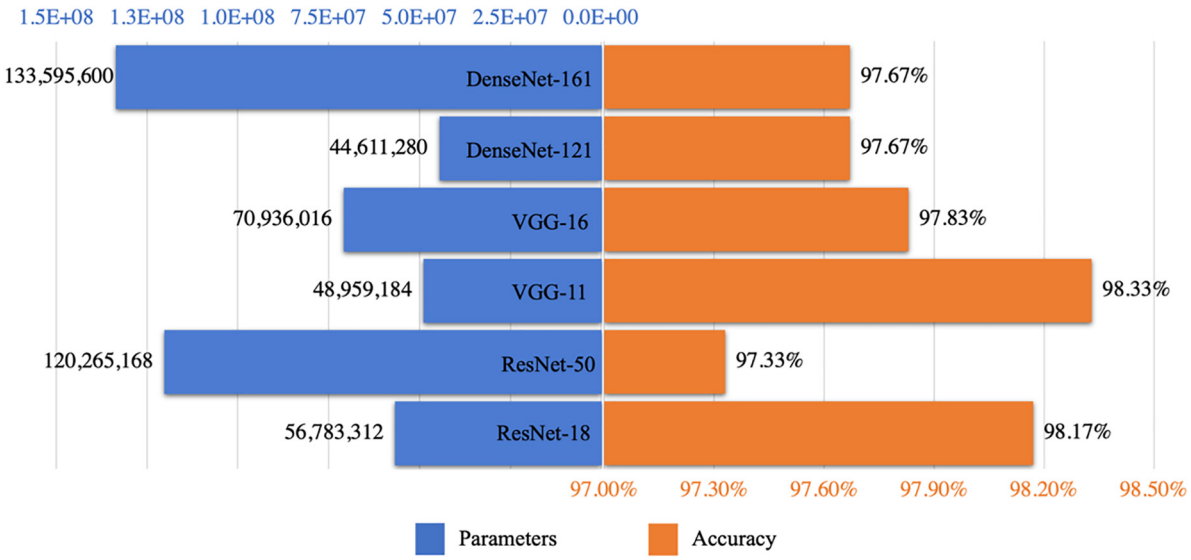

FIGURE 10 | Correlation between model size and training accuracy.

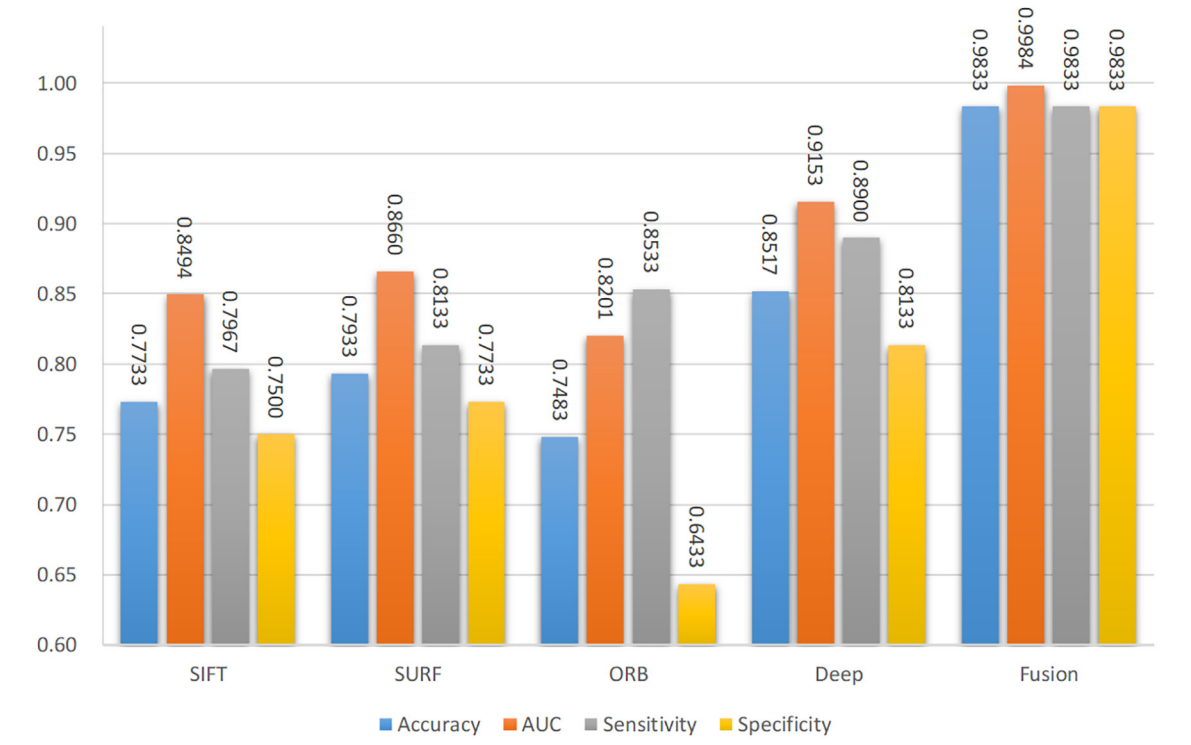

FIGURE 11 | Performance of single features and fusion features.

RESULTS

Convergence of the Proposed Model With Different Backbones

A total of 3,000 spinal TB CT images were obtained and subsequently divided into two 1,500 datasets of positive and negative CT slices. For each type of CT image, 900, 300, and 300 slices were randomly selected as the training, validation, and test sets from the small TB dataset, respectively. In terms of training parameters, the optimizer was stochastic gradient descent (SGD) with a momentum of 0.9 and weight decay of 0.001, the learning rate was set to 0.01, which decayed by 0.1 every 7 epochs, and

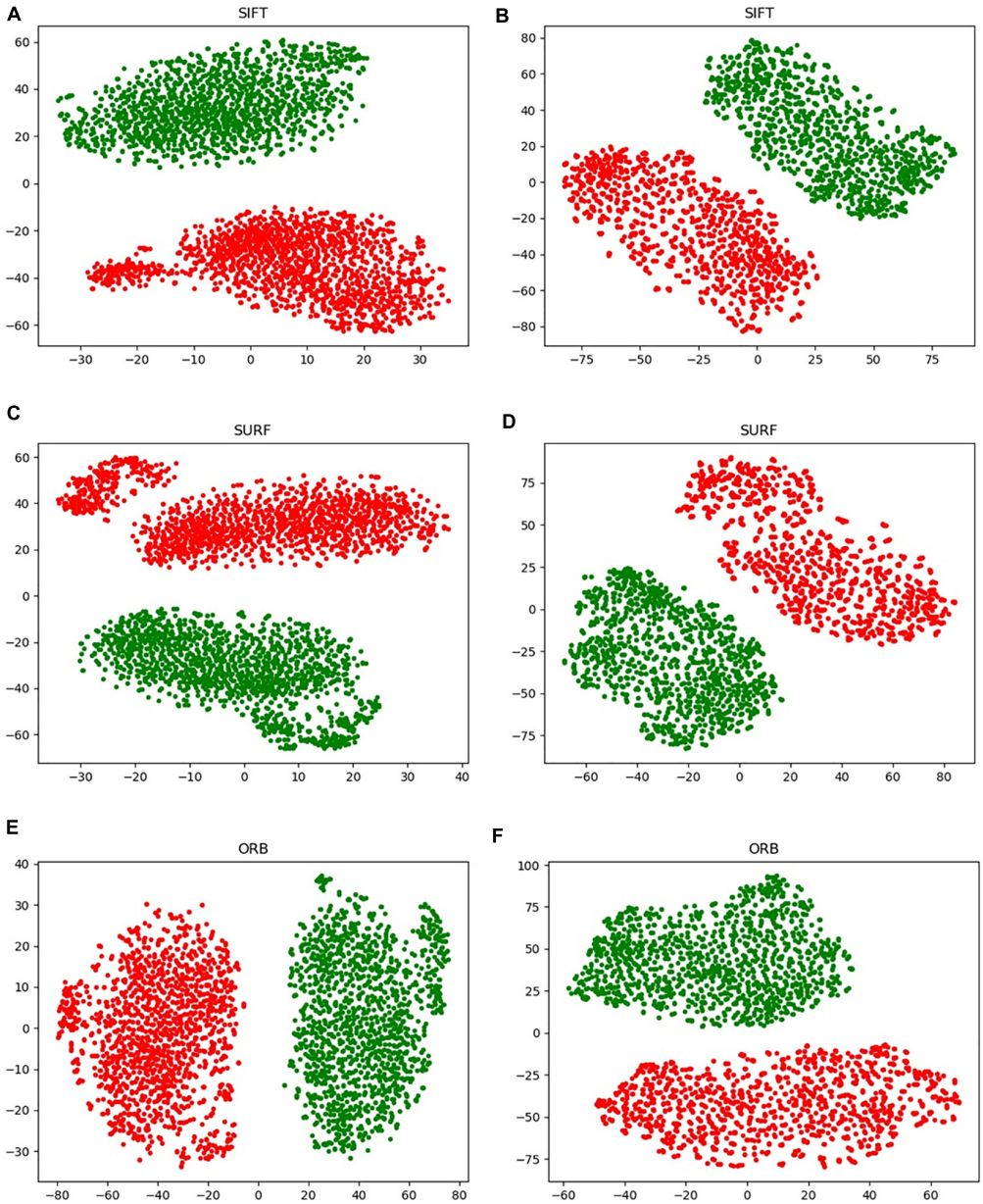

FIGURE 12 | Visualization of the handcrafted features through T-SNE. **(A,C,E)** Virtual data augmentation of SIFT, SURF, and ORB, respectively; **(B,D,F)** real image augmentation of SIFT, SURF, and ORB, respectively.

the loss function was a cross-entropy loss function describing the distance between two probability distributions. In addition, three different common deep CNNs (DCNNs) were used as the backbone: ResNet, VGG, and DenseNet. For each DCNN, two main networks with different numbers of layers were used to train on our small TB dataset to generate different sizes of models: 18 vs. 50 layers for ResNet, 11 vs. 16 layers for VGG, and 121 vs. 161 layers for DenseNet. The running environment was Pytorch 1.8.0, CUDA 11.1, and Python 3.7.1 based on Windows 10 with an advanced hardware configuration in terms of the GPU and CPU, i.e., GeForce RTX 3090 and Intel Xeon W-2255, respectively.

The accuracy and loss curves of the training, validation, and test sets are shown in **Figure 6**. The accuracy curves clearly appear to level off, and the loss curves converge to equilibrium with slight fluctuations starting at epoch 10. Specifically, the test loss curve of ResNet-50 is above the ResNet-18 loss curve, which indicates that the corresponding accuracy curve has a lower position compared with that of ResNet-18. Although there are few differences between the loss curves of VGG-11 and VGG-16, the accuracy is the same as that of ResNet, that is, the more layers in the network, the lower is the test accuracy value. However, there was a slight

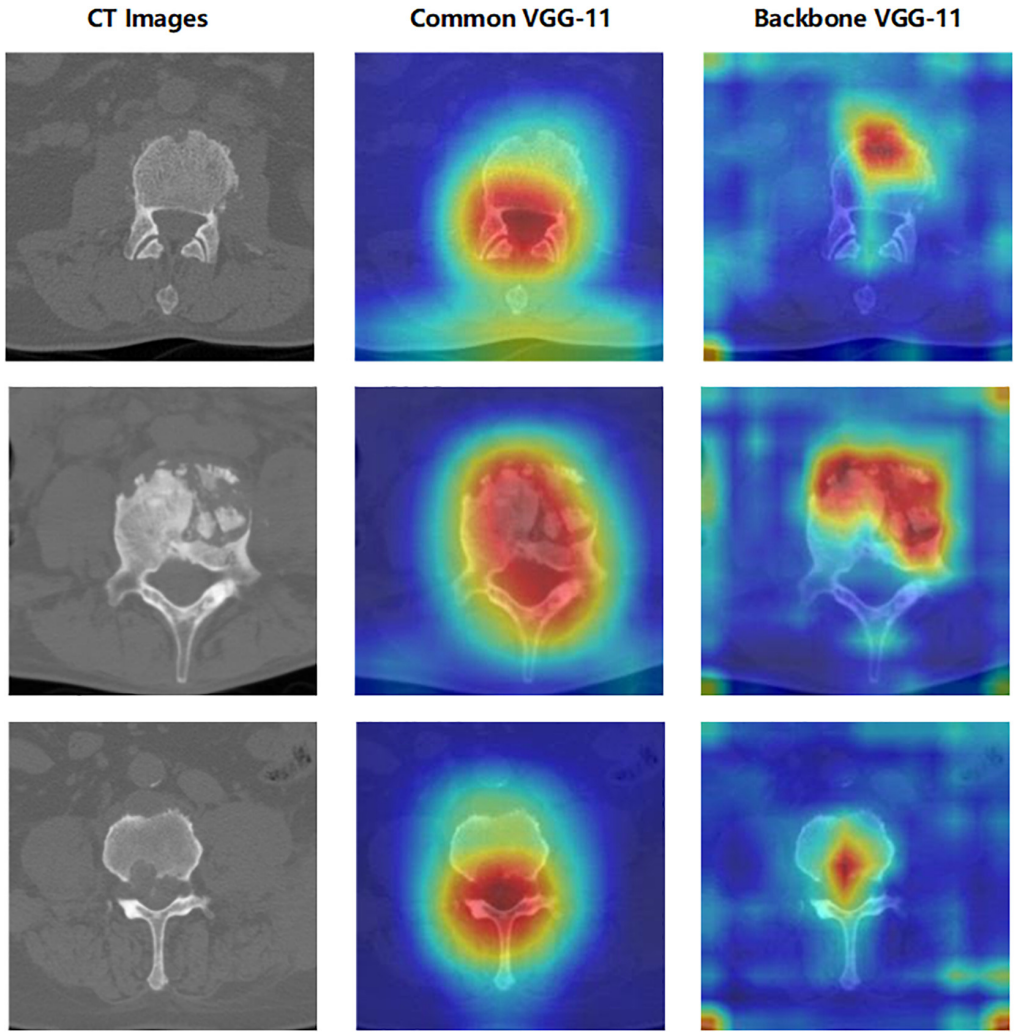

FIGURE 13 | Heatmap of the convolution layer weight visualization based on Grad-CAM++. The left column contains the original CT images, the middle column contains the heatmap generated by common VGG-11, and the right column contains the heatmap generated by backbone VGG-11 of the proposed network.

difference between DenseNet-121 and 161. These phenomena are explained in the Discussion, and the evaluation indicators of these three backbones, including accuracy, specificity, sensitivity, and area under the curve (AUC), are discussed in the next section.

Performance of the Proposed Network With Different Backbones

There are four different quantitative indicators, namely accuracy, specificity, sensitivity, and AUC, that illustrate the predictive performance on 600 test images, as shown in **Table 2**. The variates of accuracy, specificity, and sensitivity reflect the proportion of all samples with correct predictions, all negative samples with correct predictions, and all positive samples with correct predictions for all actual samples, all actual positive samples, and all actual negative samples, respectively. The AUC is the area enclosed by the coordinate axis under the receiver operating characteristic (ROC) curve. The proposed model with the backbone VGG exhibited the best performance compared with the other models, particularly VGG-11 achieved an accuracy of 98.33%, specificity of 98.33%, sensitivity of 98.33%, and AUC of 99.84%. Although the proposed model with ResNet-50 had the worst accuracy compared with the other models, the AUC was higher than that of ResNet-18, which demonstrated the existence of a superior classification threshold value for ResNet-18. For DenseNet, there were few significant differences between DenseNet-121 and DenseNet-161, both of which had an acceptable performance with an accuracy of 97.67%. Specifically, DenseNet-121 effectively predicted positive samples, whereas DenseNet-161 accurately predicted negative samples. This is due to the higher sensitivity of the former and the higher specificity of the latter.

We also drew the ROC curves and calculated the AUC of the proposed model with different backbones, as shown in **Figure 7** in which the above quantitative indices (including specificity,

sensitivity, and AUC) are visualized as the false positive rate, true positive rate, and AUCs. It provides a more intuitive comparison of the differences among these networks when focusing on the upper left area. VGG11 (yellow line) was closest to the perfect classification point in the upper left corner, where the anticipated true positive rate and false positive rate were under different classified threshold values. More importantly, we provide the confusion matrix for each network in **Figure 8**, in which we can observe the number of correct identifications and the number of incorrect identifications for each category in detail. There was a total of 600 CT images, including 300 positive samples and 300 negative samples. 295 true positives (TP) for VGG-11 and ResNet-18 and 296 true negative (TN) for DenseNet-161 were the maximum of all correctly classified sample volumes, which represents the recognition capability for health and disease. Similarly, the five false positives (FP) for VGG-11 and ResNet-18 and four false negatives (FN) for DenseNet-161 were the minimum of all incorrectly classified sample volumes. Overall, VGG-11 had the highest TP and comparatively higher TN and relatively lower FN, and there was a balanced capacity in predicting negative and positive samples, which demonstrated that VGG-11 was the optimal selection.

Overall, we recommend VGG-11 as the backbone of the proposed deep network for the auxiliary diagnosis of TB CT images based on accuracy, stability, and convergence of the loss function among the six backbones. The subsequent section discusses the analysis conducted on VGG-11.

Data Augmentation for Handcrafted Features

The image augmentation was similar to the real data distribution in the feature space. In this study, a new data augmentation method was proposed to simulate a real data distribution. The performance of spinal TB classification with the proposed augmentation and image augmentation is shown in **Figure 9**, highlighting the strength of the proposed augmentation algorithm. The accuracy, specificity, and AUC of the proposed augmentation were all slightly higher than those of image augmentation, and the sensitivity of the former was slightly lower than that of the latter. Generally, the radar map of image augmentation was surrounded by the proposed augmentation; therefore, the proposed method showed significant superiority over direct augmentation on images.

DISCUSSION

Model Size vs. Accuracy

We employed ResNet, VGG, and DenseNet as the backbones. The model layers influenced the classification accuracy, as shown in **Figure 6**. **Figure 10** shows a strong correlation between the number of parameters owned in the selected DCNN models and the prediction accuracy of test sets, which caused underfitting or overfitting when the DL model was too simple or complex to make accurate predictions for unrelated features from the small dataset. For ResNet and VGG, a decline was observed with the increase in parameters, as shown in **Figure 10**, demonstrating that the excessive number of network layers in DCNN leads to model overfitting. By contrast, the model size had no impact on the accuracy of DenseNet, and the short paths from the initial layers to subsequent layers of DenseNet alleviated the vanishing gradient problem, which ensured maximum information transmission between layers in the network. Essentially, VGG exhibited optimal training performance. In particular, VGG-11 had a superior test accuracy of 98.33% compared with others.

Individual Features vs. Fusion Feature

The four main characteristics were extracted from the CT images to identify spinal TB, namely three handcrafted features and one DCNN feature, i.e., SIFT, SURF, ORB of the local features, and deep features. As illustrated in **Table 2**, accurate classification performances were obtained by fusing the four different features based on different backbones, particularly for VGG-11. A thorough investigation was conducted to show the significant influence of individual features on the proposed network. As a comparison of the fusion feature, we analyzed the performance of each feature separately based on the proposed network with backbone VGG-11 in **Figure 11**. Diverse performances were obtained from various characteristics. A common trait was that not all handcrafted features outperformed the deep feature. Furthermore, the four evaluation indicators, namely accuracy, sensitivity, specificity, and AUC, were significantly different in one individual; however, none of them exceeded 90%. This shortcoming was effectively addressed when these different handcrafted features and deep features were fused by the proposed DCNN with the backbone VGG-11, as depicted in the last block of **Figure 11**. Specifically, the accuracy, AUC, sensitivity, and specificity of deep features improved from 85.17%, 91.53%, 89.00%, and 81.33–98.33%, 99.84%, 99.33%, and 98.33%, respectively, with assistance from the other three handcrafted features.

Real Image Augmentation vs. Virtual Data Augmentation

A new data augmentation method for handcrafted features was proposed based on the algorithm, as described in section "Data Augmentation for Handcrafted Features." The direct augmentation of images is a common method of data amplification and can produce an augmented feature dataset after extracting the handcrafted features from augmented images. Moreover, it has an identical data scale as the proposed augmentation algorithm. **Figure 9** illustrates an intuitive comparison of these two augmentation schemes using a radar map from the four indices. In this study, we conducted a visual analysis of the retained original information in a low-dimensional feature space through t-distributed stochastic neighbor embedding (T-SNE), as shown in **Figure 12**. In column b, that is, the T-SNE visualization of image augmentation, there are irregular gaps within the same category and considerable overlap among neighboring data points. This demonstrates that the CT slices obtained from image augmentation do not fully represent the real data distribution. By contrast, the binary data

distribution (i.e., the red and green points) of the proposed augmentation (column a) is more uniform than that of image augmentation (column b), except for several outliers. This proves that the newly generated feature points can effectively fill the missing data in the spatial distribution.

Comparison of Heatmap Between Common Convolutional Neural Networks and the Proposed Network

In **Figure 11**, a significant improvement can be observed when the CNN features from VGG-11 fused three different handcrafted features. The accuracy increased from 85.17% to 98.33%. Compared with the direct classification of VGG-11 on CT images, some changes were observed in the region of interest for the proposed fusion model with VGG-11 as the backbone. To explore the differences in the area of interest between these two models, Grad-CAM++ (Chattopadhay et al., 2018) was used to generate a heatmap++, as shown in **Figure 13**. Significant differences can be observed between these two methods on the heatmap of model concerns. VGG-11 focused on the vertebral foramen region in the TB images, regardless of negative or positive cases, which created a significant distraction for the classified judgment. By contrast, the proposed fusion model focused on the areas of destruction of vertebral bodies, even though some unrelated regions received little attention from the fusion models, which had less of an adverse effect on the final classification.

CONCLUSION

This study proposes a novel DL-based classification model by fusing four image features, including three handcrafted features and one CNN feature—SIFT, SURF, ORB, and the CNN feature. During the feature engineering phase, the BoW and TF-IDF algorithms combined with a new data augmentation algorithm were used to extract the three handcrafted features, and the deep features were extracted from the convolution layers of common DCNNs, including ResNet, VGG, and DenseNet. The proposed network consists of four main sections: matching network, backbone, fallen network, and fusion network. Specifically, the matching network is used to adjust the dimensions of handcrafted features to match the image size, the fallen network integrates and processes each single feature from two-dimensional into one-dimensional vectors, and the fusion network is composed of a gated information fusion network and Kronecher space, which realizes the effective fusion of different characteristics and outputs the final classification results of TB images. Experimental results were obtained using different backbones: ResNet-18/50, VGG-11/16, and DenseNet-121/201. The results demonstrated that VGG-11 achieved the optimal performance in terms of accuracy, AUC, specificity, and sensitivity. Furthermore, we analyzed the performance of the individual features, the proposed augmentation algorithm, the model stability, and the model-focused heatmap to prove the advancement of the proposed network. The proposed method is interpretable in multimodal feature fusion and can be extended to more medical scenarios, which may aid clinical radiologists, particularly grassroots physicians. It has promising potential, although our research was limited to the positive and negative classification of spinal TB CT images. In subsequent studies, the patient clinical data, including gender, age, and medical history, have a strong relationship for the classification of spinal TB, it is worth adding this personal feature into the fusion networks. In addition, we aim to extend the proposed method to CT images that include all types of spines, such as thoracic, sacral, cervical, and lumbar vertebrae. Further exploration will be conducted for DR images based on spinal TB CT images, which can form a more complete auxiliary diagnosis system applicable to grassroots hospitals in Tibet, China.

DATA AVAILABILITY STATEMENT

The original contributions presented in the study are included in the article/supplementary material, further inquiries can be directed to the corresponding author/s.

ETHICS STATEMENT

The studies involving human participants were reviewed and approved by Ethics Committee of People's Hospital of Tibet Autonomous Region, China. The patients/participants provided their written informed consent to participate in this study.

AUTHOR CONTRIBUTIONS

ZL: conceptualization, data curation, software, and writing original draft preparation. FW: conceptualization, data acquisition, and funding acquisition. FH and ZZ: data acquisition. XG, WC, TY, and JW: conceptualization and manuscript revision. SG: conceptualization, supervision, manuscript review and funding acquisition. CP: data acquisition and funding acquisition. All authors contributed to the article and approved the submitted version.

FUNDING

This work was supported by the National Natural Science Foundation of China (Grant Nos. 12075011 and 82071280), Beijing Municipal Natural Science Foundation of China (Grant No. 7202093), and Key Research and Development Program of Science and Technology Planning Project of Tibet Autonomous Region, China (Grant No. XZ202001ZY0005G).

ACKNOWLEDGMENTS

We would like to thank the top journal editing plan service of Editage. English language and grammar were edited, logical presentation of the ideas and structure of the manuscript was checked, and a peer review of the manuscript contents was performed before submitting this manuscript.

REFERENCES

Abdellatef, E., Omran, E. M., Soliman, R. F., Ismail, N. A., Abdelrahman, S. E. S. E., Ismail, K. N., et al. (2020). Fusion of deep-learned and hand-crafted features for cancelable recognition systems. *Soft. Comput.* 24, 15189–15208. doi: 10.1007/s00500-020-04856-1

Aerts, H. J. W. L., Velazquez, E. R., Leijenaar, R. T. H., Parmar, C., Grossmann, P., Carvalho, S., et al. (2014). Decoding tumour phenotype by noninvasive imaging using a quantitative radiomics approach. *Nat. Commun.* 5:4006. doi: 10.1038/ncomms5006

Alkhateeb, A., Tabl, A. A., and Rueda, L. (2021). "Deep learning in multi-omics data integration in cancer diagnostic," in *Deep Learning for Biomedical Data Analysis*, ed. M. Elloumi (Cham: Springer), 255–271.

Altaf, F., Islam, S. M. S., Akhtar, N., and Janjua, N. K. (2019). Going deep in medical image analysis: concepts, methods, challenges, and future directions. *IEEE Access* 7, 99540–99572. doi: 10.1109/access.2019.2929365

Antropova, N., Huynh, B. Q., and Giger, M. L. (2017). A deep feature fusion methodology for breast cancer diagnosis demonstrated on three imaging modality datasets. *Med. Phys.* 44, 5162–5171. doi: 10.1002/mp.12453

Anwar, S. M., Majid, M., Qayyum, A., Awais, M., Alnowami, M., and Khan, M. K. (2018). Medical Image Analysis using Convolutional Neural Networks: a Review. *J. Med. Syst.* 42:226. doi: 10.1007/s10916-018-1088-1

Arevalo, J., Solorio, T., Montes-y-Gómez, M., and González, F. A. (2017). Gated multimodal units for information fusion. *arXiv* [preprint]. Available Online at: https://arxiv.org/abs/1702.01992 (accessed September, 2021).

Bay, H., Tuytelaars, T., and Van Gool, L. (2006). "SURF: speeded up robust features," in *Computer Vision – ECCV 2006*, eds A. Leonardis, H. Bischof, and A. Pinz (Berlin Heidelberg: Springer), 404–417.

Calonder, M., Lepetit, V., Strecha, C., and Fua, P. (2010). "BRIEF: binary robust independent elementary features," in *Proceedings of the 11th European conference on Computer vision: part IV*, (Heraklion, Crete, Greece: Springer-Verlag).

Chattopadhay, A., Sarkar, A., Howlader, P., and Balasubramanian, V. N. (2018). "Grad-CAM++: generalized Gradient-Based Visual Explanations for Deep Convolutional Networks," in *2018 IEEE Winter Conference on Applications of Computer Vision (WACV)*, (Lake Tahoe, NV, USA: IEEE), 839–847.

Chen, R. J., Lu, M. Y., Wang, J., Williamson, D. F. K., Rodig, S. J., Lindeman, N. I., et al. (2020). Pathomic Fusion: an Integrated Framework for Fusing Histopathology and Genomic Features for Cancer Diagnosis and Prognosis. *IEEE Trans. Med. Imaging* 1. doi: 10.1109/TMI.2020.3021387

Cook, G. J. R., Siddique, M., Taylor, B. P., Yip, C., Chicklore, S., and Goh, V. (2014). Radiomics in PET: principles and applications. *Clin. Transl. Imaging* 2, 269–276. doi: 10.1007/s40336-014-0064-0

Cremin, B. J., Jamieson, D. H., and Hoffman, E. B. (1993). CT and MR in the management of advanced spinal tuberculosis. *Pediatr. Radiol.* 23, 298–300. doi: 10.1007/BF02010920

Currie, G., Hawk, K. E., Rohren, E., Vial, A., and Klein, R. (2019). Machine learning and deep learning in medical imaging: intelligent imaging. *J. Med. Imaging Radiat. Sci.* 50, 477–487. doi: 10.1016/j.jmir.2019.09.005

Deng, Y., Wang, C., Hui, Y., Li, Q., Li, J., Luo, S., et al. (2021). CTSpine1K: a large-scale dataset for spinal vertebrae segmentation in computed tomography. *arXiv* [preprint]. Available Online at: https://arxiv.org/abs/2105.14711v3 (accessed September, 2021).

Du, H., Cai, G., Ge, S., Ci, W., and Zhou, L. (2017). Secondary laryngeal tuberculosis in Tibet China: a report of six cases. *Otolaryngol. Case Rep.* 2, 26–28. doi: 10.1016/j.xocr.2017.02.004

Fuentes Ferrer, M., Gutiérrez Torres, L., Ayala Ramírez, O., Rumayor Zarzuelo, M., and del Prado González, N. (2012). Tuberculosis of the spine. A systematic review of case series. *Int. Orthop.* 36, 221–231. doi: 10.1007/s00264-011-1414-4

Garg, R. K., and Somvanshi, D. S. (2011). Spinal tuberculosis: a review. *J. Spinal Cord Med.* 34, 440–454. doi: 10.1179/2045772311y.0000000023

Gillies, R. J., Kinahan, P. E., and Hricak, H. (2016). Radiomics: images are more than pictures, they are data. *Radiology* 278, 563–577. doi: 10.1148/radiol.2015151169

Goodfellow, I., Bengio, Y., and Courville, A. (2016). *Deep Learning*. Cambridge, Massachusetts: MIT Press, 1–20.

Govindaraju, S., and Kumar, G. P. R. (2016). A novel content based medical image retrieval using SURF features. *Indian J. Sci. Technol.* 9, 1–8. doi: 10.17485/ijst/2016

Guidotti, R., Monreale, A., Ruggieri, S., Turini, F., Giannotti, F., and Pedreschi, D. (2018). A survey of methods for explaining black box models. *ACM Comput. Surv.* 51:93. doi: 10.1145/3236009

Guo, W., Liang, W., Deng, Q., and Zou, X. (2021). A multimodal affinity fusion network for predicting the survival of breast cancer patients. *Front. Genet.* 12:709027. doi: 10.3389/fgene.2021.709027

He, K., Zhang, X., Ren, S., and Sun, J. (2016). "Deep residual learning for image recognition," in *2016 IEEE Conference on Computer Vision and Pattern Recognition*, (Las Vegas, NV, USA: IEEE).

Hoffman, E. B., Crosier, J. H., and Cremin, B. J. (1993). Imaging in children with spinal tuberculosis. A comparison of radiography, computed tomography and magnetic resonance imaging. *J. Bone Joint Surg. Br.* 75, 233–239. doi: 10.1302/0301-620x.75b2.8444943

Huang, G., Liu, Z., Van Der Maaten, L., and Weinberger, K. Q. (2017). "Densely connected convolutional networks," in *Proceedings of the IEEE Conference on Computer Vision and Pattern Recognition (CVPR)*, (Honolulu, HI, USA: IEEE), 4700–4708.

Jackson, P., Hardcastle, N., Dawe, N., Kron, T., Hofman, M. S., and Hicks, R. J. (2018). Deep learning renal segmentation for fully automated radiation dose estimation in unsealed source therapy. *Front. Oncol.* 8:215. doi: 10.3389/fonc.2018.00215

Khaleghi, B., Khamis, A., Karray, F. O., and Razavi, S. N. (2013). Multisensor data fusion: a review of the state-of-the-art. *Inf. Fusion* 14, 28–44. doi: 10.1016/j.inffus.2011.08.001

Khan, S., Yong, S., and Deng, J. D. (2015). "Ensemble classification with modified SIFT descriptor for medical image modality," in *2015 International Conference on Image and Vision Computing New Zealand (IVCNZ)*, (Auckland, New Zealand: IEEE), 1–6.

Khanna, K., and Sabharwal, S. (2019). Spinal tuberculosis: a comprehensive review for the modern spine surgeon. *Spine J.* 19, 1858–1870. doi: 10.1016/j.spinee.2019.05.002

Khosravi, P., Lysandrou, M., Eljalby, M., Li, Q., Kazemi, E., Zisimopoulos, P., et al. (2021). A deep learning approach to diagnostic classification of prostate cancer using pathology–radiology fusion. *J. Magn. Reson. Imaging* 54, 462–471. doi: 10.1002/jmri.27599

Kim, J., Koh, J., Kim, Y., Choi, J., Hwang, Y., and Choi, J. (2018). "Robust deep multi-modal learning based on gated information fusion network," in *Asian Conference on Computer Vision*, eds C. Jawahar, H. Li, G. Mori, and K. Schindler (Cham: Springer), 90–106.

Lai, Z., and Deng, H. (2018). Medical image classification based on deep features extracted by deep model and statistic feature fusion with multilayer perceptron. *Comput. Intell. Neurosci.* 2018:2061516. doi: 10.1155/2018/2061516

Lambin, P., Rios-Velazquez, E., Leijenaar, R., Carvalho, S., Van Stiphout, R. G. P. M., Granton, P., et al. (2012). Radiomics: extracting more information from medical images using advanced feature analysis. *Eur. J. Cancer* 48, 441–446. doi: 10.1016/j.ejca.2011.11.036

Lei, Y., Harms, J., Wang, T., Liu, Y., Shu, H. K., Jani, A. B., et al. (2019). MRI-only based synthetic CT generation using dense cycle consistent generative adversarial networks. *Med. Phys.* 46, 3565–3581. doi: 10.1002/mp.13617

Li, S., Jiang, H., Wang, Z., Zhang, G., and Yao, Y.-D. (2018). An effective computer aided diagnosis model for pancreas cancer on PET/CT images. *Comput. Methods Prog. Biomed.* 165, 205–214. doi: 10.1016/j.cmpb.2018.09.001

Li, Z., Kurihara, T., Matsuzaki, K., and Irie, T. (2012). "Evaluation of medical image registration by using 3D SIFT and phase-only correlation," in *international MICCAI Workshop on Computational and Clinical Challenges in Abdominal Imaging*, (Heidelberg: Springer), 255–264.

Liu, X., Zheng, M., Sun, J., and Cui, X. (2021). A diagnostic model for differentiating tuberculous spondylitis from pyogenic spondylitis on computed tomography images. *Eur. Radiol.* 31, 7626–7636. doi: 10.1007/s00330-021-07812-1

Lowe, D. (2004). Distinctive image features from scale-invariant keypoints. *Int. J. Comput. Vis.* 60, 91–110.

Lukashevich, P. V., Zalesky, B. A., and Ablameyko, S. V. (2011). Medical image registration based on SURF detector. *Pattern Recognit. Image Anal.* 21:519. doi: 10.1134/S1054661811020696

Moradi, M., Mousavi, P., and Abolmaesumi, P. (2007). Computer-aided diagnosis of prostate cancer with emphasis on ultrasound-based approaches: a review. *Ultrasound Med. Biol.* 33, 1010–1028. doi: 10.1016/j.ultrasmedbio.2007.01.008

Nanni, L., Ghidoni, S., and Brahnam, S. (2017). Handcrafted vs. non-handcrafted features for computer vision classification. *Pattern Recognit.* 71, 158–172. doi: 10.1016/j.patcog.2017.05.025

Qian, X., Nguyen, D. T., Lyu, J., Albers, A. E., Bi, X., and Graviss, E. A. (2018). Risk factors for extrapulmonary dissemination of tuberculosis and associated mortality during treatment for extrapulmonary tuberculosis. *Emerg. Microbes Infect.* 7:102. doi: 10.1038/s41426-018-0106-1

Rasouli, M. R., Mirkoohi, M., Vaccaro, A. R., Yarandi, K. K., and Rahimi-Movaghar, V. (2012). Spinal tuberculosis: diagnosis and management. *Asian Spine J.* 6, 294–308. doi: 10.4184/asj.2012.6.4.294

Rauf, F., Chaudhry, U. R., Atif, M., and ur Rahaman, M. (2015). Spinal tuberculosis: our experience and a review of imaging methods. *Neuroradiol. J.* 28, 498–503. doi: 10.1177/1971400915609874

Ronneberger, O., Fischer, P., and Brox, T. (2015). "U-Net: convolutional networks for biomedical image segmentation," in *Medical Image Computing and Computer-Assisted Intervention – MICCAI 2015*, eds N. Navab, J. Hornegger, W. M. Wells, and A. F. Frangi (Cham: Springer), 234–241.

Rublee, E., Rabaud, V., Konolige, K., and Bradski, G. (2011). "ORB: an efficient alternative to SIFT or SURF," in *2011 International Conference on Computer Vision*, (Barcelona, Spain: IEEE), 2564–2571.

Shboul, Z. A., Alam, M., Vidyaratne, L., Pei, L., Elbakary, M. I., and Iftekharuddin, K. M. (2019). Feature-guided deep radiomics for glioblastoma patient survival prediction. *Front. Neurosci.* 13:966. doi: 10.3389/fnins.2019.00966

Simonyan, K., and Zisserman, A. (2015). "Very deep convolutional networks for large-scale image recognition," in *The International Conference on Learning Representations*, (La Jolla,CA: ICLR).

Singla, S., and Sharma, R. (2014). Medical image stitching using hybrid of sift & surf techniques. *Int. J. Adv. Res. Electron. Commun. Eng.* 3, 838–842.

Song, Q., Guo, X., Zhang, L., Yang, L., and Lu, X. (2021). New approaches in the classification and prognosis of sign clusters on pulmonary CT images in patients with multidrug-resistant tuberculosis. *Front. Microbiol.* 12:714617. doi: 10.3389/fmicb.2021.714617

Su, H., Lin, B., Huang, X., Li, J., Jiang, K., and Duan, X. (2021). MBFFNet: multi-branch feature fusion network for colonoscopy. *Front. Bioeng. Biotechnol.* 9:696251. doi: 10.3389/fbioe.2021.696251

Suzuki, K., Yan, P., Wang, F., and Shen, D. (2012). Machine learning in medical imaging. *Int. J. Biomed. Imaging* 2012:123727. doi: 10.1155/2012/123727

Swarnambiga, A., Varghese, A., Mahendra, K., and Ganapathy, K. (2019). "Medical image retrieval using Resnet-18," in *Medical Imaging 2019: imaging Informatics for Healthcare, Research, and Applications: international Society for Optics and Photonics*, (New York: ACM), 1095410.

Tian, Q., Yan, L.-F., Zhang, X., Zhang, X., Hu, Y.-C., Han, Y., et al. (2018). Radiomics strategy for glioma grading using texture features from multiparametric MRI. *J. Magn. Reson. Imaging* 48, 1518–1528. doi: 10.1002/jmri.26010

Vanino, E., Tadolini, M., Evangelisti, G., Zamparini, E., Attard, L., Scolz, K., et al. (2020). Spinal tuberculosis: proposed spinal infection multidisciplinary management project (SIMP) flow chart revision. *Eur. Rev. Med. Pharmacol. Sci.* 24, 1428–1434. doi: 10.26355/eurrev_202002_20201

Wang, L., Chang, C., Liu, Z., Huang, J., Liu, C., and Liu, C. (2021). A Medical Image Fusion Method Based on SIFT and Deep Convolutional Neural Network in the SIST Domain. *J. Healthc. Eng.* 2021:9958017.

Wang, S., Burtt, K., Turkbey, B., Choyke, P., and Summers, R. M. (2014). Computer aided-diagnosis of prostate cancer on multiparametric MRI: a technical review of current research. *Biomed Res. Int.* 2014:789561. doi: 10.1155/2014/789561

Wang, S.-H., Govindaraj, V. V., Górriz, J. M., Zhang, X., and Zhang, Y.-D. (2021). Covid-19 classification by FGCNet with deep feature fusion from graph convolutional network and convolutional neural network. *Inf. Fusion* 67, 208–229. doi: 10.1016/j.inffus.2020.10.004

Wang, W., Shi, L., Yin, A., Mao, Z., Maitland, E., Nicholas, S., et al. (2015). Primary care quality among different health care structures in Tibet, China. *Biomed Res. Int.* 2015:206709. doi: 10.1155/2015/206709

Win, K. P., and Kitjaidure, Y. (2018). "Biomedical images stitching using ORB feature based approach," in *2018 International Conference on Intelligent Informatics and Biomedical Sciences (ICIIBMS)*, (Bangkok, Thailand: IEEE), 221–225.

Xie, Y., Zhang, J., Xia, Y., Fulham, M., and Zhang, Y. (2018). Fusing texture, shape and deep model-learned information at decision level for automated classification of lung nodules on chest CT. *Inf. Fusion* 42, 102–110. doi: 10.1016/j.inffus.2017.10.005

Yang, Y., Yan, L.-F., Zhang, X., Han, Y., Nan, H.-Y., Hu, Y.-C., et al. (2018). Glioma grading on conventional MR images: a deep learning study with transfer learning. *Front. Neurosci.* 12:804. doi: 10.3389/fnins.2018.00804

Zhang, H., Xu, H., Tian, X., Jiang, J., and Ma, J. (2021). Image fusion meets deep learning: a survey and perspective. *Inf. Fusion* 76, 323–336. doi: 10.1016/j.inffus.2021.06.008

Zhang, N., Zeng, X., He, L., Liu, Z., Liu, J., Zhang, Z., et al. (2019). The value of MR imaging in comparative analysis of spinal infection in adults: pyogenic versus tuberculous. *World Neurosurg.* 128, 806–813. doi: 10.1016/j.wneu.2019.04.260

Zhu, S., Xia, L., Yu, S., Chen, S., and Zhang, J. (2017). The burden and challenges of tuberculosis in China: findings from the Global Burden of Disease Study 2015. *Sci. Rep.* 7:14601. doi: 10.1038/s41598-017-15024-1

Conflict of Interest: The authors declare that the research was conducted in the absence of any commercial or financial relationships that could be construed as a potential conflict of interest.

Publisher's Note: All claims expressed in this article are solely those of the authors and do not necessarily represent those of their affiliated organizations, or those of the publisher, the editors and the reviewers. Any product that may be evaluated in this article, or claim that may be made by its manufacturer, is not guaranteed or endorsed by the publisher.

frontiers in Microbiology

ORIGINAL RESEARCH
published: 03 March 2022
doi: 10.3389/fmicb.2022.821066

Plasma Concentrations of sTREM-1 as Markers for Systemic Adverse Reactions in Subjects Treated With Weekly Rifapentine and Isoniazid for Latent Tuberculosis Infection

*Tsai-Yu Wang[1,2], Jia-Yih Feng[3,4], Chin-Chung Shu[5], Susan Shin-jung Lee[4,6], Chung-Yu Chen[7], Yu-Feng Wei[8], Chih-Bin Lin[9], Wei-Chang Huang[10,11,12,13,14,15], Wei-Juin Su[3] and Shu-Min Lin[1,2]**

[1] Department of Thoracic Medicine, Chang Gung Memorial Hospital Linkou Main Branch, Taoyuan, Taiwan, [2] School of Medicine, Chang Gung University, Taoyuan, Taiwan, [3] Department of Chest Medicine, Taipei Veterans General Hospital, Taipei, Taiwan, [4] Faculty of Medicine, School of Medicine, National Yang-Ming Chiao-Tung University, Taipei, Taiwan, [5] Department of Internal Medicine, National Taiwan University Hospital, Taipei, Taiwan, [6] Division of Infectious Diseases, Kaohsiung Veterans General Hospital, Kaohsiung, Taiwan, [7] Division of Pulmonary and Critical Care Medicine, Department of Internal Medicine, National Taiwan University Hospital Yunlin Branch, Yunlin, Taiwan, [8] Division of Chest Medicine, Department of Internal Medicine, E-Da Hospital, I-Shou University, Kaohsiung, Taiwan, [9] Division of Chest Medicine, Department of Internal Medicine, Hualien Tzu Chi Hospital, Hualien, Taiwan, [10] Division of Chest Medicine, Department of Internal Medicine, Taichung Veterans General Hospital, Taichung, Taiwan, [11] Department of Post-Baccalaureate Medicine, College of Medicine, National Chung Hsing University, Taichung, Taiwan, [12] Ph.D. Program in Translational Medicine, National Chung Hsing University, Taichung, Taiwan, [13] School of Medicine, Chung Shan Medical University, Taichung, Taiwan, [14] Department of Medical Technology, Jen-Teh Junior College of Medicine, Nursing and Management, Miaoli, Taiwan, [15] Master Program for Health Administration, Department of Industrial Engineering and Enterprise Information, Tunghai University, Taichung, Taiwan

OPEN ACCESS

Edited by:
Xiao-Yong Fan,
Fudan University, China

Reviewed by:
Sandeep Sharma,
Lovely Professional University, India
Yair Molad,
Rabin Medical Center, Israel

***Correspondence:**
Shu-Min Lin
smlin100@gmail.com

Specialty section:
This article was submitted to Infectious Agents and Disease, a section of the journal Frontiers in Microbiology

Received: *23 November 2021*
Accepted: *31 January 2022*
Published: *03 March 2022*

Citation:
Wang T-Y, Feng J-Y, Shu C-C, Lee SS-j, Chen C-Y, Wei Y-F, Lin C-B, Huang W-C, Su W-J and Lin S-M (2022) Plasma Concentrations of sTREM-1 as Markers for Systemic Adverse Reactions in Subjects Treated With Weekly Rifapentine and Isoniazid for Latent Tuberculosis Infection. Front. Microbiol. 13:821066. doi: 10.3389/fmicb.2022.821066

Background: A regimen of once-weekly rifapentine plus isoniazid for 3 months (3HP) is an effective treatment for subjects with latent tuberculosis infection; however, no reliable biomarker exists for predicting systemic adverse reactions (SARs) to 3HP treatment.

Methods: This prospective, multi-center study evaluated the plasma concentrations of soluble triggering receptors expressed on myeloid cells (sTREM)-1 and sTREM-2 in subjects undergoing 3HP treatment and examined the associations between these biomarkers and SARs.

Results: This study enrolled 80 consecutive subjects receiving 3HP treatment, 25 of whom had SARs and 55 of whom did not. Subjects with SARs presented higher concentrations of sTREM-1 at baseline than those without SARs (240.1 ± 19.1 vs. 176.7 ± 9.4 pg/mL, $P = 0.001$). The area under the receiver operating characteristic curves revealed that day 1 plasma levels of sTREM-1 (0.708, 95% CI, 0.584–0.833, $P = 0.003$) and sTREM-2 (0.343, 95% CI, 0.227–0.459, $P = 0.025$) as well as the sTREM-1/sTREM-2 ratio (0.748, 95% CI, 0.638–0.858, $P = 0.001$) had modest discriminative power pertaining to the development of SARs. An sTREM-1 level exceeding the cut-off value (>187.4 pg/mL) (hazard ratio [HR], 6.15; 95% CI 1.67–22.70, $P = 0.006$) and a sTREM-2 below the cut-off value (<237.2 pg/mL) (HR, 4.46;

95% CI 1.41–14.1, $P = 0.011$) were independent predictors of SARs after controlling for other variables.

Conclusions: Plasma sTREM-1 and sTREM-2 levels are useful biomarkers for predicting SARs during 3HP treatment.

Clinical trial government: NCT04655794

Keywords: exacerbation, sTREM-1, sTREM-2, LTBI, tuberculosis

INTRODUCTION

Tuberculosis (TB) is the leading cause of infectious disease-associated death worldwide, with 9 million new cases and nearly 2 million deaths reported annually (Dye et al., 1999). Treating high-risk patients for latent *M. tuberculosis* infection (LTBI) before the disease progresses to the active stage is a crucial strategy for controlling and eliminating TB (Rose, 2000; Cohn et al., 2020). A 9-month regimen of daily isoniazid (9H) has long been used as a treatment; however, it is associated with liver toxicity and high treatment interruption rates (Hirsch-Moverman et al., 2008). A regimen of once-weekly rifapentine plus isoniazid for 3 months (3HP) is an effective treatment for patients with LTBI, as the efficacy is similar to that of the 9H regimen but with a shorter treatment duration as well as higher adherence and treatment completion (Sterling et al., 2011). Nonetheless, recent studies have reported that the 3HP regimen is associated with systemic drug reactions (SDRs), such as flu-like syndrome (Sterling et al., 2015). One study on patients undergoing 3HP treatment reported that 8.2% experienced drug-related adverse events and 4.9% discontinued treatment due to adverse events (Sterling et al., 2011). Due to the shorter treatment duration and higher completion rate, there is a trend in increasing use of 3HP regimen for treatment of LTBI in medical practice. However, the occurrence of adverse reactions has been reported to be the major cause of treatment discontinuation in patients on the 3HP regimen (Sterling et al., 2011).

The mechanisms underlying the development of SDRs have yet to be clearly defined. Recent studies on 3HP as a treatment for LTBI have reported inconsistencies in symptoms upon single and multiple drug rechallenge. Note that many patients completed treatment despite adverse drug reactions (Schechter et al., 2006). This suggests that SDRs and flu-like symptoms are not necessarily immunologically mediated. One study reported that a 3HP regimen in conjunction with antiretroviral agents was correlated with a high incidence of flu-like symptoms and the acute release of inflammatory cytokines, including tumor necrosis factor-α (TNF-α), interferon-γ, and C-reactive protein (CRP) (Brooks et al., 2018). Thus, it appears that the development of SDRs in patients undergoing 3HP treatment may be attributed to inflammatory responses.

Triggering receptors expressed on myeloid cells-1 (TREM-1) is constitutively expressed on human monocytes/macrophages and neutrophils and is up-regulated by stimuli with lipopolysaccharide (LPS) binding to the TLR4. TREM-1 amplify inflammation by increasing the production of inflammatory cytokines (e.g., TNF-α, IL-1β, and IL-6) synergistically with toll-like receptor (TLR) and NOD-like receptor (NLR) signaling (Ornatowska et al., 2007; Dower et al., 2008; Thankam et al., 2016; Cao et al., 2017). Recent studies have also suggested that plasma sTREM-1 levels could potentially be used as a biomarker for disease severity and treatment outcomes in patients with pulmonary TB and latent TB (Shu et al., 2016; Feng et al., 2018). Signaling mediated by TREM-2 and DAP12 promotes phagocytosis and dampens TLR signaling, which reduces the production of proinflammatory cytokines (Thankam et al., 2016). By blocking systemic inflammation, the effects of TREM-2 activation are essentially the opposite of the effects of TREM-1 activation. The TREM-1/TREM-2 ratio has been identified as a reliable indicator of inflammation intensity associated with many diseases (Nguyen et al., 2015; Suchankova et al., 2020). However, researchers have yet to determine whether plasma sTREM-1, sTREM-2, or TNF-α can be used as biomarkers to predict the occurrence of systemic adverse reactions (SARs) during 3HP treatment.

This prospective multicenter observational study measured plasma concentrations of sTREM-1, sTREM-2, sTLR4, and TNF-α in patients undergoing 3HP treatment regimens and examined the independent association between these biomarkers and SARs. These biomarkers were also serially measured to determine their correlation with changes in SARs throughout the course of 3HP treatment.

MATERIALS AND METHODS

This prospective multicenter observational study was performed using data from eight medical centers in Taiwan covering the period from January 2017 to August 2019. The local Ethics Committee of Chang Gung Memorial Hospital approved the research protocol (NCT04655794), and each patient provided written informed consent.

Study Population

Subjects newly identified with LTBI who elected to receive LTBI preventive therapy *via* 3HP were eligible for enrolment. Indications for LTBI screening included close contact with patients with active TB, patients with autoimmune diseases preceding biological therapy, healthcare workers, and subjects with other clinical conditions that increased the risk of LTBI. Diagnosis of LTBI was confirmed using the QuantiFERON-TB Gold In-Tube test (QFT-GIT; Qiagen, Valencia, CA, United States) with a cut-off value of 0.35 IU/mL. Exclusion criteria included age younger than 20 years, pregnancy, obesity,

active TB or suspected of active TB during the clinical evaluation, close contact with a patient with multidrug-resistant TB, and previous instances of severe liver disease, end-stage renal disease (ESRD), or organ transplantation.

Definition

Systemic adverse reactions were defined as adverse reactions of grade 2 or higher (Feng et al., 2020). Grade 2 SARs are defined as moderate, which indicates minimal, local, or non-invasive interventions as well as limiting age-appropriate instrumental activities of daily living (ADL). Grade 3 SARs are defined as severe or medically significant but not immediately life-threatening, which indicates hospitalization or prolongation of hospitalization, disabling, and limiting self-care ADL. Grade 4 SARs are life-threatening consequences in which urgent intervention is indicated. Grade 5 SARs are death related to adverse events. The investigator in charge determined whether SARs developed in relation to the LTBI treatment regimen. Patients visited outpatient clinics at weeks 2, 4, 8, and 12 for clinical evaluations and blood tests. The occurrence of adverse reactions was recorded during every visit throughout the treatment period. SARs severity was graded in accordance with the Cancer Therapy Evaluation Program Common Toxicity Criteria, version 5.0 (Cancer Therapy Evaluation Program, 2020). Hepatotoxicity was defined as an alanine aminotransferase (ALT) level greater than 3 times the upper limit of normal (ULN) with symptoms of nausea, vomiting, fatigue, or jaundice, or ALT levels greater than 5 times the ULN (Bliven-Sizemore et al., 2015).

Study Design

This study assessed whether baseline plasma soluble TREM-1 (R&D, United States), soluble TREM-2 (RayBiotech, United States), soluble TLR4 (MyBioSource, United States), CRP (R&D, United States), and TNF-α (R&D, United States) could be used to predict the occurrence of SARs during 3HP treatment. In Taiwan, the directly observed treatment short-course (DOTS) program was started in 2006 (Lo et al., 2011) All LTBI patients were included in the DOTS program during the study period. All medical expenses related to the 3HP regimen and the DOTS program were paid for by the government. Blood samples obtained on day 1 and day 14 were used for plasma collection to identify instances of SARs side effects of grade 2 or higher. Soluble TREM-1, soluble TREM-2, soluble TLR4, CRP, and TNF-α plasma concentrations were obtained using ELISA in accordance with the manufacturer's instructions. We compared the plasma levels of mediators between subjects with and without SARs (≥grade 2 side effects), between days 1 and 14 as well as at SARs.

Statistical Analysis

Data are expressed as the standard error of the mean (SEM). The student's *t*-test was used to compare continuous variables between the two groups, and the Mann-Whitney *U* test was used to deal with non-normal distributions. Categorical variables were compared using the chi-squared or Fisher's exact test. Univariate analysis was used primarily for the selection of variables based on a *P* value of less than 0.1. Selected variables, including age, sTREM-1, and sTREM-2, were entered into a Cox proportional hazards model to identify the net effects of each individual factor. Hazard ratios (HRs) with 95% confidence intervals (CIs) were used to assess the independent contributions of significant factors. Receiver operating characteristic (ROC) curves were plotted to illustrate the predictive values of day 1 sTREM-1 and sTREM-2 on the development of SARs. We also calculated the respective areas under the curves. A *P* value of less than 0.05 was considered statistically significant. Analysis was conducted using SPSS (version 15.0; SPSS; Chicago, IL, United States).

RESULTS

Clinical Characteristics and Adverse Effects

This study enrolled 80 consecutive subjects receiving 3HP treatment, 25 of whom had SARs and 55 of whom did not. The timing of SARs after the initiation of therapy was 17.2 ± 14.0 days. **Table 1** lists the baseline demographics and clinical characteristics. The mean ages of subjects were as follows: with SARs (57.2 years) and without SARs (48.7 years). The distribution of male subjects was as follows: with SARs (41.7%) and without SARs (48.4%). The two groups were similar in terms of comorbidity frequency. sTREM-1 levels in the non-SARs group differed from those in the SARs group on day 1 (176.7 ± 9.4 vs. 240.1 ± 19.1 pg/mL, $P < 0.001$). The sTREM-1/sTREM-2 ratio was lower in the non-SARs group (0.7 ± 0.1 vs. 1.1 ± 0.1, $P < 0.001$) than in the SARs group; however, sTREM-2 levels were higher (484.9 ± 59.5 vs. 237.4 ± 12.6 pg/mL, $P = 0.007$). The two groups were similar in terms of sTLR4, TNF-α, and CRP levels. In subjects with SARs, the concentration of sTREM-1 on the day of SARs development (348.6 ± 46.5 pg/mL) was significantly higher than on day 1 (251.7 ± 35.3 pg/mL) and day 14 (287.8 ± 55.3 pg/mL vs. $P = 0.006$) (**Figure 1**). By contrast, the concentration of sTREM-1 in the non-SARs group did not differ between day 1 and day 14 (144.2 ± 12.4 pg/mL vs. 146.1 ± 12.5 pg/mL). The concentration of sTREM-2 in the SARs group was not significantly different among on the day of SARs development, day 1, and day 14 (408.6 ± 59.3 pg/mL vs. 328.5 ± 70.1 pg/mL vs. 359.2 ± 38.2 pg/mL, $P = 0.198$). The concentration of sTREM-2 in the non-SARs group did not differ significantly between day 1 and day 14 (450.5 ± 76.7 pg/mL vs. 512.3 ± 83.0 pg/mL) (**Figure 1**). The incidence of autoimmune disease was similar in patients with SARs vs. without SARs (**Table 1**). The baseline levels of sTREM-1, sTREM-2, sTREM-1/sTREM-2, sTLR4, TNF-α, and CRP were similar in patients with and without autoimmune disease (**Supplementary Table 1**).

Table 2 lists data pertaining to adverse events. In the SARs group, the most common adverse events associated with the gastrointestinal system were nausea and vomiting (48%) and anorexia (36%). The most common flu-like symptoms were

TABLE 1 | Demographic and clinical characteristics of patients.

Characteristics	Non-SARs *n* = 55	SARs *n* = 25	*p* value
Age (years)	48.7 ± 2.3	57.2 ± 3.6	0.023
Male	15 (48.4)	5 (41.7)	0.745
BMI (kg/m^2)	24.6 ± 0.5	23.6 ± 0.6	0.836
Smoking	18 (32.7)	12 (48.0)	0.219
Comorbidities			
Asthma	1 (1.8)	0 (0)	0.999
HBV	3 (5.5)	1 (4.0)	0.999
HCV	2 (3.6)	0 (0)	0.999
HIV	1 (1.8)	0 (0)	0.999
Autoimmune disease	4 (7.2)	2 (8.0)	0.999
Laboratory data baseline			
AST, U/L	24.9 ± 2.2	26.0 ± 2.7	0.769
ALT, U/L	23.9 ± 2.9	25.8 ± 4.2	0.713
Total bilirubin, mg/dL	0.6 ± 0.1	0.7 ± 0.1	0.542
Creatinine, mg/dL	0.6 ± 0.1	1.2 ± 0.4	0.899
sTREM-1, pg/ml	176.7 ± 9.4	240.1 ± 19.1	0.001
sTREM-2, pg/ml	484.9 ± 59.5	237.4 ± 12.6	0.007
sTREM-1/sTREM-2	0.7 ± 0.1	1.1 ± 0.1	0.001
sTLR4, ng/ml	1.7 ± 0.5	1.8 ± 0.9	0.917
TNF-α, pg/ml	3.5 ± 0.3	4.2 ± 0.3	0.137
CRP, mg/ml	3.7 ± 2.5	4.3 ± 5.2	0.907

Data are presented as mean (SEM) or n (%). BMI, body mass index; HBV, hepatitis B virus; HCV, hepatitis C virus; HIV, human immunodeficiency virus; SARs, systemic adverse reactions ≥ grade 2; AST, Aspartate aminotransferase; ALT, Alanine aminotransferase.

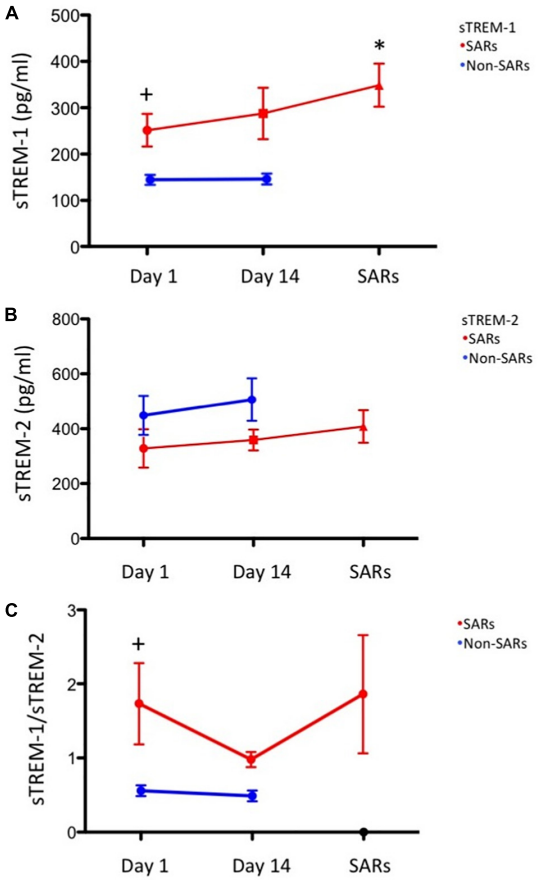

FIGURE 1 | Serial sTREM plasma levels. (*N* = 12: systemic adverse reactions (SARs) group; *N* = 31: non-SARs group): **(A)** Mean sTREM-1 plasma levels were significantly higher in the SARs group (red circle) than in the non-SARs group (blue circle) on day 1 (*P* = 0.006). Mean sTREM-1 plasma levels were significantly higher on the day of SARs development (red circle) than that on day 1 (*P* = 0.003); **(B)** Mean sTREM-2 plasma levels in the SARs group (red circle) were not significantly higher than in the non-SARs group (blue circle) on day 1; **(C)** The sTREM-1/sTREM-2 ratio in the SARs group (red circle) was significantly higher than in the non-SARs group (blue circle) on day 1. $^*P < 0.05$ versus day 1 of SAR group, $^+P < 0.05$ versus day 1 of Non-SAR group.

fatigue (68%) and fever (52%). The percentage of abnormal liver function was similar in both groups.

Area Under the Receiver Operating Characteristic Curve for Predicting Systemic Adverse Reactions

The areas under the ROC curves (AUROCs) revealed that day-1 plasma levels of sTREM-1 (0.708, 95% CI, 0.584–0.833, $P = 0.003$) and sTREM-2 (0.343, 95% CI, 0.227–0.459, $P = 0.025$) as well as the sTREM-1/sTREM-2 ratio (0.748, 95% CI, 0.638–0.858, $P = 0.001$) had modest discriminative power pertaining to the development of SARs (**Table 3**). The cut-off values for sTREM-1, sTREM-2, and the sTREM1/sTREM-2 ratio in predicting SARs were 187.4 pg/mL, 237.2 pg/mL, and 0.698, respectively.

Cox Proportional Hazards Analysis for Predicting Systemic Adverse Reactions

Univariate analysis was used for the selection of variables based on a *P* value of less than 0.1. We entered the variables (age, sTREM-1 levels higher than the cut-off value of >187.4 ng/mL, and sTREM-2 levels less than the cut-off value of <237.2 ng/mL) into a Cox proportional hazard model (**Table 4**). After controlling for other variables, sTREM-1 levels (HR, 6.15; 95% CI 1.67–22.70, $P = 0.006$) and sTREM-2 levels (HR, 4.46; 95% CI 1.41–14.12, $P = 0.011$) remained significant predictors of SARs. Note that after adjusting for the effects of other factors, age was not significantly predictive of SARs occurrence.

Association Between Plasma sTREM-1 and Adverse Reactions

To elucidate the relationship between sTREM-1 and adverse reactions, we compared plasma sTREM-1 levels with several related variables (**Table 5**). Plasma sTREM-1 levels were correlated with nausea and vomiting ($r = 0.269$, $P = 0.016$) and fatigue ($r = 0.278$, $P = 0.013$) but not with abdominal pain, anorexia, dizziness, headache, myalgia, arthralgia, or fever.

TABLE 2 | List of adverse events.

Characteristic	Non-SAR *n* = 55	SAR *n* = 25	*p* value
Adverse event	**Grade 1**	**≥Grade2**	
Gastrointestinal reaction			
Abdominal pain	0 (0)	8 (32.0)	0.001
Nausea/vomiting	2 (3.6)	12 (48.0)	0.001
Anorexia	1 (1.8)	9 (36.0)	0.001
Flu-like symptoms			
Fatigue	3 (5.5)	17 (68.0)	0.001
Dizziness	4 (7.3)	12 (48.0)	0.001
Headache	1 (1.8)	8 (32.0)	0.001
Fever	2 (3.6)	13 (52.0)	0.001
Myalgia/arthralgia	1 (1.8)	9 (36.0)	0.001
Hypersensitivity reaction	1 (1.8)	1 (4.0)	0.037
Elevated liver enzyme levels			
Any	2 (3.6)	1 (4.0)	0.999
1-3 ULN	2 (3.6)	1 (4.0)	0.999
3-5 ULN	0 (0)	0 (0)	0.999
>5 ULN	0 (0)	0 (0)	0.999
Other drug reactions	0 (0)	1 (4.0)	0.168

Data are presented as n (%); SARs, systemic adverse reactions ≥ grade 2.

TABLE 3 | Area under the receiver operating characteristic curves for serum levels of sTREM-1 and sTREM-2 on day 1 for the prediction of SARs.

	Area (95% CI)	*P*-value	Cut-off value	Sensitivity	Specificity
sTREM-1	0.708 (0.584–0.833)	0.003	187.4 pg/ml	0.760	0.618
sTREM-2	0.343 (0.227–0.459)	0.025	237.2 pg/ml	0.680	0.425
sTREM-1/sTREM-2	0.748 (0.638–0.858)	0.001	0.698	0.800	0.636

SARs: systemic adverse reactions ≥ grade 2.

TABLE 4 | Cox proportional hazards analysis of risk factors for SARs.

	Univariate			Multivariate		
Factors	**HR**	**95% CI**	***P* value**	**HR**	**95% CI**	***P* value**
Age	0.96	0.93–0.99	0.027	0.97	0.93–1.01	0.126
sTREM-1 > cut-off value	6.30	1.91–20.79	0.003	6.15	1.67–22.70	0.006
sTREM-2 < cut-off value	2.96	1.09–8.01	0.033	4.46	1.41–14.12	0.011

SARs, systemic adverse reactions ≥ grade 2.

TABLE 5 | Linear regression analysis of day 1 sTREM-1 versus variables of adverse reactions.

Variables	Correlation (r)	*P* value
Gastrointestinal reaction		
Abdominal pain	0.206	0.067
Nausea/vomiting	0.269	0.016
Anorexia	0.088	0.439
Flu-like symptoms		
Fatigue	0.278	0.013
Dizziness	0.038	0.735
Headache	0.126	0.265
Myalgia/arthralgia	0.057	0.618
Fever	0.164	0.146

DISCUSSION

Systemic adverse reactions are common in patients receiving 3HP treatment for LTBI. Baseline sTREM-1 levels and the sTREM-1/sTREM-2 ratio were higher in subjects with SARs than those in subjects without SARs; however, sTREM-2 levels were lower. We also observed significantly higher sTREM-1 concentrations at exacerbation than at baseline. Taken together, sTREM-1 and sTREM-2 plasma levels were independent predictors of SARs development. ROC curves revealed that sTREM-1 and sTREM-2 levels as well as the sTREM-1/sTREM-2 ratio at day 1 had moderate discriminative power in predicting the development of SARs.

A regimen of weekly rifapentine plus isoniazid is as effective as a 9-month regimen of daily isoniazid in treating LTBI in high-risk subjects; however, 3HP treatment regimen commonly leads to the occurrence of SARs. Researchers have yet to elucidate the possible mechanisms underlying SARs development. One recent study examined potential mechanisms underlying SARs development in healthy volunteers undergoing a once-weekly regimen of isoniazid and rifapentine with an antiretroviral medicine, dolutegravir (Brooks et al., 2018). They determined that the SARs symptoms were associated with elevated cytokine plasma levels, including TNF-α, CRP, and IFN-γ. It appears that inflammatory responses may play an important role in mediating SARs in drug-induced adverse reactions. Further studies are required to identify the mechanism underlying the development of SARs in patients undergoing treatment using rifapentine plus isoniazid.

In the current study, patients who developed SARs during the 3HP regimen had higher baseline sTREM-1 and lower sTREM-2 levels than those without SARs. Day-1 sTREM-1 and sTREM-2 levels were independent predictors of SARs development. sTREM-1 levels at the time of exacerbation were significantly higher than those at baseline. TREM-1 amplifies inflammation by increasing inflammatory cytokine levels *via* TLR-4 and NLR signaling (Ornatowska et al., 2007; Dower et al., 2008; Thankam et al., 2016; Cao et al., 2017). This indicates that inflammation associated with TREM-1 may play a key role in the development of SARs in patients receiving 3HP treatment for LTBI. Elevated sTREM-1 levels have been identified in infectious and non-infectious inflammatory diseases (Cao et al., 2017). In fact, plasma sTREM-1 has been identified as a potential biomarker for disease severity and treatment outcomes in patients with pulmonary TB. sTREM-1 levels are associated with TB-related constitutional symptoms, such as poor

appetite (Feng et al., 2018). Plasma sTREM-1 levels are also an independent risk factor for persistent positive readings in interferon-gamma release assays in cases of LTBI (Shu et al., 2016). Note, however, that this is the first study to identify sTREM-1 and sTREM-2 levels as independent predictors of SARs in patients with LTBI.

Our study showed that development of SARs was associated with increased plasma levels of sTREM-1 and sTREM-1/sTREM-2 ratio but not with plasma levels of CRP, sTLR-4, and TNF-α. The possible causes for the different results comparing with previous report may be attributed by distinct study populations. Our study recruited patients receiving 3HP treatment while their study recruited patients receiving combination of 3HP and antiretroviral treatment. In addition, TREM-1 activation was shown to result in a persistent release of cytokines and chemokines (TNF-α, IL-1β, IL-8, and monocyte chemotactic protein [MCP]-1), (Cao et al., 2017). Thus, further studies are required to identify the mechanism underlying TREM-1 associated development of SARs in patients undergoing treatment using rifapentine plus isoniazid.

Evidence revealed that sTREM-1 levels are associated with the disease activity of autoimmune disease (Bassyouni et al., 2017). Our results showed similar incidences of autoimmune disease in SARs and non-SARs groups. The baseline levels of sTREM-1, sTREM-2, and sTREM-1/sTREM-2 were similar in patients with and without autoimmune disease. Therefore, the different levels of sTREM-1, sTREM-2, and sTREM-1/sTREM-2 ratio in SARs vs. non-SARs groups are not affected by comorbidity of autoimmune disease.

We observed elevated plasma sTREM-1 and sTREM-2 levels and a higher sTREM-1/sTREM-2 ratio in patients with LTBI who experienced SARs after 3HP treatment. The corresponding AUROC identified plasma sTREM-1 and sTREM as modest predictors of SARs development after 3HP treatment. If further large-scale prospective studies provide corroborative evidence, these findings could have substantial clinical implications. Patients could have their sTREM-1 and sTREM-2 levels measured prior to undergoing 3HP therapy. In cases where the levels are high, the patient could be monitored more frequently and perhaps treated *via* 3HP to improve compliance and clinical outcomes. Nonetheless, further studies will be required to evaluate the efficacy of this approach.

Emerging evidence suggests that TREM-2 activation inhibits the production of proinflammatory cytokines and promotes phagocytosis in macrophages. This implies that TREM-2 activation has the opposite effect of TREM-1 activation; i.e., blocking the development of systemic inflammation (Ito and Hamerman, 2012). The elevated sTREM-1/sTREM-2 ratio in the blood indicates that enhanced systemic inflammation may play an essential role in the development of SARs during 3HP treatment.

sTREM-1 is released from myeloid cells in response to toll-like receptor-4 (TLR4) activation (Netea et al., 2006). In addition, TREM-1 has the synergistic ability to amplify the signaling of the TLR4, which can recognize components of a variety of microorganisms including bacteria, fungi, and viruses (Netea et al., 2006; Fortin et al., 2007). Therefore, TREM-1 expression is closely linked to TLR4 activity. However, our results showed 3HP treatment related SARs are correlated with sTREM-1 plasma level but not with sTLR4 levels. According to previous studies, these interaction of TREM-1 expression and activation are mediated through the binding of membrane-bound TLR4 molecule. Soluble TLR4 are considered structurally identical to their membrane bound counterparts but do not participate in the TLR pathway. Instead, they reduce inflammatory responses by competing with TLRs for ligands (Hyakushima et al., 2004). The study was designated to measure the potential plasma biomarkers for prediction of SARs in 3HP regimen, thus, we measure the plasm levels of sTLR rather than the expression of membrane-bound TLR4. This may explain the reason why the levels of sTREM-1 but not sTLR4 are predictors for SARs in 3HP treatment.

This study had several limitations that should be considered in the interpretation of our results. First, the sample size was somewhat small, and we recruited only a specific subgroup of subjects with LTBI undergoing 3HP treatment. Previous studies reported higher baseline plasma sTREM-1 levels in patients with liver cirrhosis and ESRD (Shu et al., 2016). Thus, to avoid bias related to elevated baseline sTREM-1 levels in these subgroups, we excluded patients with liver cirrhosis and ESRD. We have yet to determine whether these markers identified in this study provide similar predictive power for other subpopulations receiving 3HP treatment for LTBI. In addition, the single-arm observational study of 3HP treatment in LTBI patients did not measure the role of those inflammatory biomarkers in LTBI patients receiving other treatment regimens. A randomized control study comparing the plasma levels of inflammatory biomarkers in patients receiving 3HP vs. 9H treatment is needed to elucidate the role of these biomarkers in LTBI patients receiving different treatment regimens.

Taken together, plasma sTREM-1 and sTREM-2 appear to be useful biomarkers for predicting the development of SARs during 3HP treatment. Further prospective studies with larger samples will be required to confirm these results. Nonetheless, the results of this study provide a basis for further research into the role of inflammation in adverse reactions associated with 3HP.

DATA AVAILABILITY STATEMENT

The datasets presented in this article are not readily available because of patient confidentiality and participant privacy. Requests to access the datasets should be directed to TYW (wang5531@gmail.com).

ETHICS STATEMENT

The studies involving human participants were reviewed and approved by the Ethics Committee of Chang Gung Memorial Hospital approved the research protocol (NCT04655794).

The patients/participants provided their written informed consent to participate in this study.

AUTHOR CONTRIBUTIONS

TYW and SML are the guarantors taking responsibility for the content of the manuscript and including all data and analysis. TYW, JYF, and CCS contributed directly to the study design and were responsible for the gathering of data. SSJL, CYC, YFW, CBL, WCH, and WJS contributed directly to data management and statistical analysis. All authors were substantially involved in the study design and drafting of the manuscript for intellectual content, and all authors reviewed the final manuscript prior to submission.

FUNDING

This study was supported by a research grant from Chang Gung Memorial Hospital, Taiwan (CMRPG3J0611) and the Taiwan Centers for Disease Control (CB106027). The funders played no role in the design of this study, in the collection, analysis, or interpretation of data, or in the writing of the manuscript.

SUPPLEMENTARY MATERIAL

The Supplementary Material for this article can be found online at: https://www.frontiersin.org/articles/10.3389/fmicb.2022.821066/full#supplementary-material

REFERENCES

Bassyouni, I. H., Fawzi, S., Gheita, T. A., Bassyouni, R. H., Nasr, A. S., El Bakry, S. A., et al. (2017). Clinical association of a soluble triggering receptor expressed on myeloid cells-1 (sTREM-1) in patients with systemic lupus erythematosus. *Immunol. Invest.* 46, 38–47. doi: 10.1080/08820139.2016.1211140

Bliven-Sizemore, E. E., Sterling, T. R., Shang, N., Benator, D., Schwartzman, K., Reves, R., et al. (2015). Three months of weekly rifapentine plus isoniazid is less hepatotoxic than nine months of daily isoniazid for LTBI. *Int. J. Tuberc. Lung Dis.* 19, 1039–1044, i–v. doi: 10.5588/ijtld.14.0829

Brooks, K. M., George, J. M., Pau, A. K., Rupert, A., Mehaffy, C., De, P., et al. (2018). Cytokine-mediated systemic adverse drug reactions in a drug-drug interaction study of Dolutegravir with once-weekly Isoniazid and Rifapentine. *Clin. Infect. Dis.* 67, 193–201. doi: 10.1093/cid/ciy082

Cancer Therapy Evaluation Program (2020). *Common Terminology Criteria for Adverse Events (CTCAE) v5.0*. Available online at: https://ctep.cancer.gov/protocolDevelopment/electronic_applications/docs/CTCAE_v5_Quick_Reference_5x7.pdf (accessed November 27, 2017).

Cao, C., Gu, J., and Zhang, J. (2017). Soluble triggering receptor expressed on myeloid cell-1 (sTREM-1): a potential biomarker for the diagnosis of infectious diseases. *Front. Med.* 11:169–177. doi: 10.1007/s11684-017-0505-z

Cohn, D. L., O'Brien, R. J., Geiter, J., Gordin, F. M., Hershfield, E., Horsburg, C. R. Jr., et al. (2000). Targeted tuberculin testing and treatment of latent tuberculosis infection. This official statement of the American Thoracic Society was adopted by the ATS Board of Directors, July 1999. This is a joint statement of the American Thoracic Society (ATS) and the Centers for disease control and prevention (CDC). This statement was endorsed by the Council of the infectious diseases society of America. (IDSA), September 1999, and the sections of this statement. *Am. J. Respir. Crit. Care Med.* 161, S221–S247. doi: 10.1164/ajrccm.161.supplement_3.ats600

Dower, K., Ellis, D. K., Saraf, K., Jelinsky, S. A., and Lin, L. L. (2008). Innate immune responses to TREM-1 activation: overlap, divergence, and positive and negative cross-talk with bacterial lipopolysaccharide. *J. Immunol.* 180, 3520–3534. doi: 10.4049/jimmunol.180.5.3520

Dye, C., Scheele, S., Dolin, P., Pathania, V., and Raviglione, M. C. (1999). Consensus statement. Global burden of tuberculosis: estimated incidence, prevalence, and mortality by country. WHO Global surveillance and monitoring project. *JAMA* 282, 677–686. doi: 10.1001/jama.282.7.677

Feng, J. Y., Huang, W. C., Lin, S. M., Wang, T. Y., Lee, S. S., Shu, C. C., et al. (2020). Safety and treatment completion of latent tuberculosis infection treatment in the elderly population-a prospective observational study in Taiwan. *Int. J. Infect. Dis.* 96, 550–557. doi: 10.1016/j.ijid.2020.05.009

Feng, J. Y., Su, W. J., Pan, S. W., Yeh, Y. C., Lin, Y. Y., and Chen, N. J. (2018). Role of TREM-1 in pulmonary tuberculosis patients- analysis of serum soluble TREM-1 levels. *Sci. Rep.* 8:8223. doi: 10.1038/s41598-018-26478-2

Fortin, C. F., Lesur, O., Fulop, T. Jr. (2007). Effects of TREM-1 activation in human neutrophils: activation of signaling pathways, recruitment into lipid rafts and association with TLR4. *Int Immunol.* 19, 41–50. doi: 10.1093/intimm/dxl119

Hirsch-Moverman, Y., Daftary, A., Franks, J., and Colson, P. W. (2008). Adherence to treatment for latent tuberculosis infection: systematic review of studies in the US and Canada. *Int. J. Tuberc. Lung Dis.* 12, 1235–1254.

Hyakushima, N., Mitsuzawa, H., Nishitani, C., Sano, H., Kuronuma, K., Konishi, M., et al. (2004). Interaction of soluble form of recombinant extracellular TLR4 domain with MD-2 enables lipopolysaccharide binding and attenuates TLR4-mediated signaling. *J. Immunol.* 173, 6949–6954. doi: 10.4049/jimmunol.173.11.6949

Ito, H., and Hamerman, J. A. (2012). TREM-2, triggering receptor expressed on myeloid cell-2, negatively regulates TLR responses in dendritic cells. *Eur. J. Immunol.* 42, 176–185. doi: 10.1002/eji.201141679

Lo, H. Y., Yang, S. L., Chou, P., Chuang, J. H., and Chiang, C. Y. (2011). Completeness and timeliness of tuberculosis notification in Taiwan. *BMC Public Health* 11:915. doi: 10.1186/1471-2458-11-915

Netea, M. G., Azam, T., Ferwerda, G., Girardin, S. E., Kim, S. H., and Dinarello, C. A. (2006). Triggering receptor expressed on myeloid cells-1 (TREM-1) amplifies the signals induced by the NACHT-LRR (NLR) pattern recognition receptors. *J. Leukoc. Biol.* 80, 1454–1461. doi: 10.1189/jlb.1205758

Nguyen, A. H., Koenck, C., Quirk, S. K., Lim, V. M., Mitkov, M. V., Trowbridge, R. M., et al. (2015). Triggering receptor expressed on myeloid cells in cutaneous melanoma. *Clin. Transl. Sci.* 8, 441–444. doi: 10.1111/cts.12308

Ornatowska, M., Azim, A. C., Wang, X., Christman, J. W., Xiao, L., Joo, M., et al. (2007). Functional genomics of silencing TREM-1 on TLR4 signaling in macrophages. *Am. J. Physiol. Lung Cell Mol. Physiol.* 293, L1377–L1384. doi: 10.1152/ajplung.00140.2007

Rose, D. N. (2000). Benefits of screening for latent Mycobacterium tuberculosis infection. *Arch. Intern. Med.* 160, 1513–1521. doi: 10.1001/archinte.160.10.1513

Schechter, M., Zajdenverg, R., Falco, G., Barnes, G. L., Faulhaber, J. C., Coberly, J. S., et al. (2006). Weekly rifapentine/isoniazid or daily rifampin/pyrazinamide for latent tuberculosis in household contacts. *Am. J. Respir. Crit. Care Med.* 173, 922–926. doi: 10.1164/rccm.200512-1953OC

Shu, C. C., Hsu, C. L., Lee, C. Y., Wu, V. C., Yang, F. J., Wang, J. Y., et al. (2016). Inflammatory markers and clinical characteristics for predicting persistent positivity of interferon gamma release assay in dialysis population. *Sci. Rep.* 6:34577. doi: 10.1038/srep34577

Sterling, T. R., Moro, R. N., Borisov, A. S., Phillips, E., Shepherd, G., Adkinson, N. F., et al. (2015). Flu-like and other systemic drug reactions among persons

receiving weekly Rifapentine Plus Isoniazid or daily Isoniazid for treatment of latent Tuberculosis Infection in the PREVENT Tuberculosis study. *Clin. Infect. Dis.* 61, 527–535. doi: 10.1093/cid/civ323

Sterling, T. R., Villarino, M. E., Borisov, A. S., Shang, N., Gordin, F., Bliven-Sizemore, E., et al. (2011). Three months of rifapentine and isoniazid for latent tuberculosis infection. *N. Engl. J. Med.* 365, 2155–2166. doi: 10.1056/NEJMoa1104875

Suchankova, M., Urban, J., Ganovska, M., Tibenska, E., Szaboova, K., Tedlova, E., et al. (2020). TREM-1 and TREM-2 expression on CD14(+) cells in bronchoalveolar lavage fluid in pulmonary Sarcoidosis and hypersensitivity pneumonitis in the context of t cell immune response. *Mediators Inflamm.* 2020:9501617. doi: 10.1155/2020/9501617

Thankam, F. G., Dilisio, M. F., Dougherty, K. A., Dietz, N. E., and Agrawal, D. K. (2016). Triggering receptor expressed on myeloid cells and 5'adenosine monophosphate-activated protein kinase in the inflammatory response: a potential therapeutic target. *Expert. Rev. Clin. Immunol.* 12, 1239–1249. doi: 10.1080/1744666X.2016.1196138

Conflict of Interest: The authors declare that the research was conducted in the absence of any commercial or financial relationships that could be construed as a potential conflict of interest.

Publisher's Note: All claims expressed in this article are solely those of the authors and do not necessarily represent those of their affiliated organizations, or those of the publisher, the editors and the reviewers. Any product that may be evaluated in this article, or claim that may be made by its manufacturer, is not guaranteed or endorsed by the publisher.

frontiers in Microbiology

ORIGINAL RESEARCH
published: 24 March 2022
doi: 10.3389/fmicb.2022.819654

A Novel Cross-Priming Amplification-Based Assay for Tuberculosis Diagnosis in Children Using Gastric Aspirate

Shuting Quan[1], Tingting Jiang[2], Weiwei Jiao[1], Yu Zhu[3], Qiong Liao[3], Yang Liu[3], Min Fang[4], Yan Shi[4], Li Duan[4], Xiaomei Shi[4], Yacui Wang[1], Xue Tian[1], Chaomin Wan[3], Lin Sun[1]* and Adong Shen[1,2]**

[1]Beijing Key Laboratory of Pediatric Respiratory Infection Diseases, Key Laboratory of Major Diseases in Children, Ministry of Education, National Clinical Research Center for Respiratory Diseases, National Key Discipline of Pediatrics (Capital Medical University), Beijing Pediatric Research Institute, Beijing Children's Hospital, Capital Medical University, National Center for Children's Health, Beijing, China, [2]Baoding Children's Hospital, Baoding, China, [3]West China Second Hospital, Sichuan University, Chengdu, China, [4]The No. 1 People's Hospital of Liangshan Yizu Autonomous Prefecture, Liangshan, China

OPEN ACCESS

Edited by:
Xiao-Yong,
Fudan University, China

Reviewed by:
Guido Vincent Bloemberg,
University of Zurich,
Switzerland
Jun Long,
Southern Medical University, China

***Correspondence:**
Adong Shen
shenad16@hotmail.com
Lin Sun
sunlinbch@163.com
Chaomin Wan
wcm0220@126.com

Specialty section:
This article was submitted to Infectious Agents and Disease, a section of the journal Frontiers in Microbiology

Received: 22 November 2021
Accepted: 02 March 2022
Published: 24 March 2022

Citation:
Quan S, Jiang T, Jiao W, Zhu Y, Liao Q, Liu Y, Fang M, Shi Y, Duan L, Shi X, Wang Y, Tian X, Wan C, Sun L and Shen A (2022) A Novel Cross-Priming Amplification-Based Assay for Tuberculosis Diagnosis in Children Using Gastric Aspirate. Front. Microbiol. 13:819654. doi: 10.3389/fmicb.2022.819654

Low detection rates of *Mycobacterium tuberculosis* (MTB) by culture and smear microscopy prevent early diagnosis of tuberculosis (TB) in children. Therefore, developing rapid and accurate diagnostic techniques are critical to achieving the global aim of minimizing childhood TB. The present study was performed to evaluate the diagnostic effectiveness of the novel cross-priming amplification-based EasyNAT MTB complex assay (EasyNAT) in childhood TB. Five hundred and six children with suspected TB were enrolled from January 2018 to October 2021. Gastric aspirate (GA) samples were tested by bacterial culture, acid-fast bacillus microscopy, EasyNAT, Xpert MTB/RIF (Xpert), or Xpert MTB/RIF Ultra (Xpert Ultra). Among 239 children simultaneously tested by EasyNAT and Xpert methods, both assays showed similar sensitivities in total active TB cases [22.6% (31/137) vs. 26.3% (36/137), $p = 0.441$] and in bacteriologically confirmed TB cases [both 60.0% (9/15)]. The two assays presented similar specificities of 98.0% (100/102) and 99.0% (101/102), respectively ($p = 1.000$). Among 267 children who were simultaneously tested with EasyNAT and Xpert Ultra, Xpert Ultra demonstrated higher sensitivity than EasyNAT in total active TB cases [50.9% (89/175) vs. 30.3% (53/175), $p < 0.001$]. EasyNAT and Xpert Ultra yielded similar specificities, at 97.8% (90/92) and 100.0% (92/92), respectively ($p = 0.155$). These findings indicated that Xpert Ultra was superior to EasyNAT despite its higher cost and EasyNAT was not inferior to Xpert in the diagnosis of childhood TB using GA samples. EasyNAT may therefore be a suitable alternative diagnostic method for childhood TB based on its cost-effectiveness, speed, and accuracy.

Keywords: child, diagnosis, gastric aspirate, tuberculosis, Ustar EasyNAT MTC assay, Xpert MTB/RIF

INTRODUCTION

According to the latest global tuberculosis (TB) report, there were 9.9 million new TB cases in 2020, with children accounting for 11% of these and 16% of TB-associated deaths globally. The higher proportion of child deaths and lower disease detection rate indicates that children have a poorer chance of receiving effective disease prevention and control than adults. In 2020, the estimated number of new TB cases in China was 842,000, but children comprised only 1% (World-Health-Organization, 2021a). The diagnosis and treatment of childhood TB are hampered by the paucibacillary nature of samples and the difficulty in collecting high-quality specimens. Therefore, bacteriological confirmation by *Mycobacterium tuberculosis* (MTB) culture and smear microscopy detects low positivity rates in children, reducing the early diagnosis and treatment of childhood TB. Thus, developing rapid and accurate diagnostic techniques are critical to achieving the global aim of minimizing TB in children.

Xpert MTB/RIF (Xpert) and its next-generation product, Xpert MTB/RIF Ultra (Xpert Ultra), are both recommended by the WHO for use as initial diagnostic tests for TB in children with signs and symptoms of pulmonary TB (PTB; World-Health-Organization, 2021b). Xpert and Xpert Ultra are both automated, cartridge-based molecular tests that permit rapid detection of MTB complex (MTC) and identification of rifampicin resistance (Sun et al., 2019). However, Xpert and Xpert Ultra are expensive and require sophisticated instruments. Thus, these techniques are not suitable for resource-limited areas, many of which may have high incidence of TB.

Isothermal amplification of nucleic acids can rapidly and efficiently amplify nucleic acid sequences at a constant temperature (Zhao et al., 2015). To date, many isothermal amplification technologies, including helicase-dependent amplification (Barreda-Garcia et al., 2016), multiple cross displacement amplification (Jiao et al., 2019), loop-mediated isothermal amplification (Sharma et al., 2020; Dayal et al., 2021), and cross-priming amplification (CPA), have been used to detect MTB. Among these, CPA is a powerful, innovative amplification method and has been used in the detection of various pathogens, such as infectious spleen and kidney necrosis virus, Salmonella enterica serovar Indiana, and *Staphylococcus aureus* (Qiao et al., 2015; Liu et al., 2018; Wang et al., 2018). A novel kit, the EasyNAT MTC assay (EasyNAT, Ustar, Biotechnologies Co. Ltd., China) based on the CPA technique, has been developed to diagnose TB in adults using sputum and has demonstrated good accuracy (Zhang et al., 2021). In this kit, two cross primers targeting the insertion sequence IS*6110* were designed to specifically detect MTC and improve sensitivity. The assay is carried out in a sealed tube to prevent cross-contamination and the DNA extraction, DNA purification, amplification, and detection of the target gene are performed in three separate chambers within the cartridge (Zhang et al., 2021). As a quick point-of-care test, the results can be reported within 2 h, which can provide early diagnosis for TB.

The recently published WHO communication on the management of TB in children and adolescents highlighted that evidence-based evaluations of diagnostic assays are needed in children especially in those younger than 10 years old to overcome the current shortfall in case detection (World-Health-Organization, 2021c). It was also suggested that ideal treatment decision algorithms could be tailored to be highly specific to each country's settings and resources, and should consider different settings with varying access to diagnostic tests (World-Health-Organization, 2011a). Considering the rapid turnaround and low cost when compared with Xpert, the EasyNAT assay may represent a valuable tool for diagnosis of TB in children. This study enrolled children with suspected PTB and aimed to evaluate the diagnostic value of EasyNAT in childhood TB using gastric aspirate (GA) and compare the accuracy of EasyNAT with the established Xpert and Xpert Ultra methods.

MATERIALS AND METHODS

Study Population

From January 2018 to October 2021, children aged 18 years or younger were enrolled in the study if they had (1) symptoms suggestive of TB, including, but not limited to, long-lasting fever, night sweats, and weight loss, and (2) positive chest radiograph changes.

The enrolled children were categorized into three groups (Graham et al., 2012) based on the final diagnosis. (1) Bacteriologically confirmed TB: positive results of MTB culture and/or microscopy; (2) probable TB: at least 1 sign and symptom AND X-ray abnormalities suggestive of tuberculosis AND at least 1 of the following: exposure history of active TB, clinical presentation improvement after anti-TB treatment, positive results of tuberculin skin test, or interferon-γ release assay; and (3) non-TB patients with respiratory tract infections (RTIs): symptomatic but not fitting the above criteria and confirmed evidence of bacterial or viral infection (**Supplementary Table S1**). The respiratory samples were tested by molecular commercial kits and/or bacterial culture. Patients who had previously received anti-TB treatment or being treated for more than 1 week were not included in this study.

This study was approved by the Medical Ethics Committee of Beijing Children's Hospital, Capital Medical University. Written informed consent was obtained from the guardians of the patients.

Procedures

GA samples were collected early in the morning after an overnight fast of at least 4 h. Children without the contraindications (including severe high blood pressure, esophageal stricture, esophageal tumor, heart failure, and upper gastrointestinal bleeding) can be collected GA using nasogastric tube. The nasogastric tube entered the stomach through the nose, and 2–8 ml of GA was drawn with a syringe. Each specimen was transported to the lab within 6 h of collection and stored at −80°C after aliquoting. The samples were then

subjected to mycobacteria growth indicator tube (MGIT) 960 culture, microscopy testing, EasyNAT, Xpert, and Xpert Ultra assays.

According to clinical practice standards, MTB culture and acid-fast bacilli microscopy were tested on three consecutive days, while the molecular tests were performed once using the samples collected on the first day. Therefore, the children with bacteriologically confirmed TB were defined as those who were tested positively by MTB culture or acid-fast bacilli microscopy using the first samples collected.

Culture and Smear

Two milliliters of GA sample were decontaminated with 2 ml N-acetyl-L-cysteine 2% sodium hydroxide for 15–20 min after sufficient vortexing. The mixture was then neutralized with sterile saline phosphate buffer (PBS) to a final volume of 45 ml and centrifuged at 3,000 × *g* for 15 min at 4°C. The pellet was resuspended in 1 ml of PBS and inoculated into the MGIT 960 system (Becton, Dickinson and Company, United States) and Lowenstein-Jensen solid medium.

The pellet was smeared on a slide for Ziehl-Neelsen acid-fast staining and examined by microscopy directly.

Xpert and Xpert Ultra Assays

Two milliliters of GA sample were added to sodium hydroxide (final concentration, 0.75%) and vortexed at 5-min intervals for 15 min, followed by centrifugation at 4,000 × *g* for 15 min. The pellet was resuspended in 2 ml of the sample processing reagent and the mixture was transferred into Xpert or Xpert Ultra cartridges then loaded into the GeneXpert instrument. Both assays presented results in the same semiquantitative categories of high, medium, low, and very low. Additionally, a semiquantitative category of "trace" was introduced in the Xpert Ultra assay, which was designed to identify samples with the lowest number of targets for MTB. Invalid results were repeated. When a valid result was produced, the semiquantitative scale from each test was recorded.

EasyNAT Assay

Two milliliters of GA sample were homogenized and digested using 3–4 ml 4% sodium hydroxide solution for 15 min at room temperature until fully liquified. After centrifugation at 4,000 × *g* for 10 min and then 12,000 rpm for 3 min, the pellet was resuspended with DNA extraction liquid premixed with the internal control before being added to the sample chamber of the cartridge. This assay evaluated the specimens as invalid, negative, positive, and no result. Invalid results were repeated and the valid results (negative or positive) were recorded.

Statistical Analysis

SPSS version 25.0 (IBM, Armonk, NY, United States) was used for statistical analysis. Sensitivity and specificity were compared using the Chi-square test, while concordance between the different diagnostic tests was assessed using the Kappa test. Correlation of the semiquantitative scale of the tests was presented using Spearman's rank correlation coefficients. $p < 0.05$ was considered as statistically significant.

RESULTS

Patient Characteristics

In total, 506 children with suspected PTB were recruited. The median (interquartile range) age was 6.9 (2.4–11.1) years, with 199 (39.3%) cases under 5 years of age, and 328 (64.8%) cases under 10 years of age. All 506 enrolled children were classified into two groups: 239 children (including 137 children with TB and 102 children with RTIs) tested simultaneously with both EasyNAT and Xpert methods were enrolled in group 1 and 267 children (including 175 children with TB and 92 children RTIs) tested simultaneously by both EasyNAT and Xpert Ultra methods were enrolled in group 2. **Figure 1** and **Table 1** show the patient selection and their clinical characteristics.

Comparison of EasyNAT and Xpert

Among 239 children (137 PTB patients and 102 RTI patients) tested simultaneously with EasyNAT and Xpert, similar sensitivities were observed for both methods [22.6% (31/137) vs. 26.3% (36/137), respectively; $p = 0.441$]. Among 137 children with PTB, 15 (10.9%) were classified as bacteriologically confirmed TB and 122 (89.1%) were classified as probable TB. EasyNAT yielded identical sensitivity to Xpert for MTB detection in children with bacteriologically confirmed TB, with both assays demonstrating sensitivity of 60.0% (9/15). In children with probable TB, the sensitivity of Xpert was observed to be similar with that of EasyNAT, the difference was not significant [22.1% (27/122) vs. 18.0% (22/122), respectively; $p = 0.424$]. Both EasyNAT and Xpert methods showed high specificity in children with RTIs, demonstrating 98.0% (100/102) and 99.0% (101/102) specificity, respectively ($p = 1.000$; **Table 2**).

Agreement between EasyNAT and Xpert was moderate ($\kappa = 0.498$) among 239 children (**Figure 2A**). Concordant results were obtained for 209 children (20 cases positive by both tests [EasyNAT+ Xpert+]; 189 negative by both tests [EasyNAT− Xpert−]). Discordant results were found in 27 children with TB (16 EasyNAT− Xpert+ and 11 EasyNAT+ Xpert− results) and 3 children with RTIs (1 EasyNAT− Xpert+ and 2 EasyNAT+ Xpert− results). Among 27 children with TB, the semiquantitative scale of Xpert were low in 10 cases and very low in six cases, the cycle thresholds of EasyNAT were similar in children with EasyNAT+ Xpert− results than those with EasyNAT+ Xpert+ results (19.8 vs. 19.2, $p = 0.844$). Concordance of the semiquantitative scale for EasyNAT and Xpert was further analyzed for the 20 children with double positive results (**Figure 3A**). The results indicated a trend for patients with lower semiquantitative scores in Xpert being more likely to have higher cycle thresholds in EasyNAT, with a correlation coefficient of 0.411.

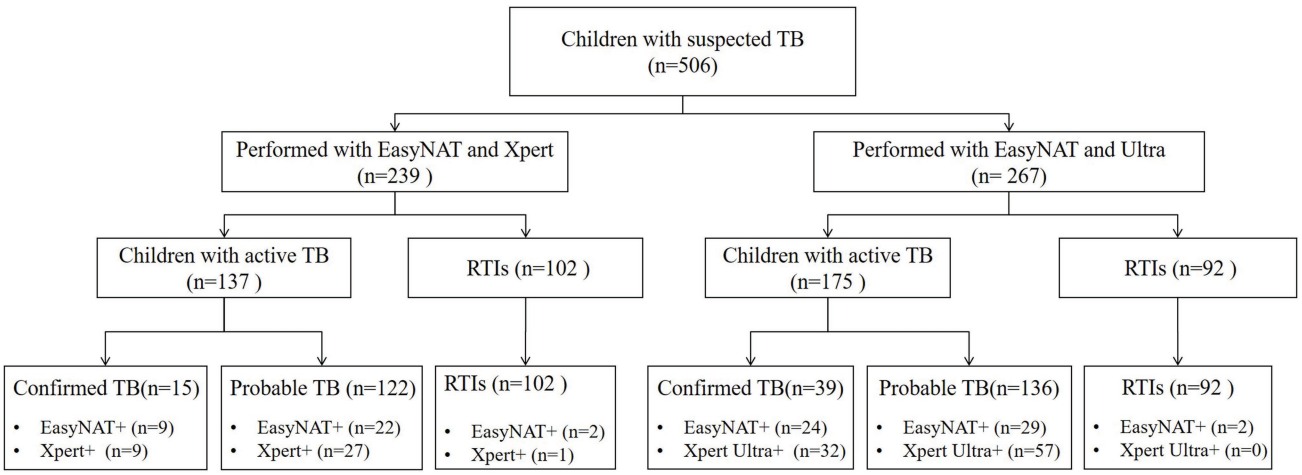

FIGURE 1 | Flow chart of the study population. TB, tuberculosis; RTIs, respiratory tract infections; EasyNAT, EasyNAT MTC assay; Xpert, Xpert MTB/RIF; and Ultra, Xpert MTB/RIF Ultra.

TABLE 1 | Main clinical characteristics of the study population.

Characteristic		Part 1 ($n=239$)			Part 2 ($n=267$)		
	Total ($n=506$), n (%)	Bacteriologically confirmed TB ($n=15$), n (%)	Probable TB ($n=122$), n (%)	RTIs ($n=102$), n (%)	Bacteriologically confirmed TB ($n=39$), n (%)	Probable TB ($n=136$), n (%)	RTIs ($n=92$), n (%)
Age	6.9(2.4–11.1)	2.8(1.4–12.4)	10.0(7.0–12.8)	4.9(0.9–8.0)	7.0(4.4–11.7)	8.5(4.3–11.6)	4.8(0.92–8.0)
Mean (interquartile Range)							
full range	0.0–16.0	0.2–14.0	0.2–15.0	0.0–16.0	0.3–14.0	0.2–15.3	0.0–13.2
Gender							
Male	288(56.9)	8(53.3)	73(59.8)	62(60.8)	18(46.2)	73(53.7)	54(58.7)
Female	218(43.1)	7(46.7)	49(40.2)	40(39.2)	21(53.8)	63(46.3)	38(41.3)
Tuberculin skin test							
Positive	279(55.1)	12(80.0)	107(87.7)	17(16.7)	28(71.8)	106(77.9)	11(12.0)
Negative	138(27.3)	3(20.0)	9(7.4)	45(44.1)	10(25.6)	27(19.9)	42(45.7)
No data	89(17.6)	0(0)	6(4.9)	40(39.2)	1(2.6)	3(2.2)	39(42.4)
Interferon-γ release assay							
Positive	291(57.5)	11(73.3)	106(86.9)	7(6.9)	36(92.3)	120(88.2)	13(14.1)
Negative	112(22.1)	3(20.0)	15(12.3)	46(45.1)	3(7.7)	14(10.3)	30(32.6)
No data	103(20.4)	1(6.7)	1(0.8)	49(48.0)	0(0)	2(1.5)	49(53.3)

RTIs, respiratory tract infections; TB, tuberculosis.

Comparison of EasyNAT and Xpert Ultra

The detection outcomes of EasyNAT and Xpert Ultra assays among 267 children (including 175 children with PTB and 92 with RTIs) are presented in **Table 3**. Among 175 children with PTB, 39 (22.3%) were bacteriologically confirmed TB. Xpert Ultra showed higher sensitivity than EasyNAT, both in the total 175 PTB patients [50.9% (89/175) vs. 30.3% (53/175), respectively; $p<0.001$] and in the 39 children with bacteriologically confirmed TB [82.1% (32/39) vs. 61.5% (24/39), respectively; $p=0.044$], which indicated that Xpert Ultra was superior to EasyNAT despite its higher cost. If "trace" results in Xpert Ultra were not included, then the sensitivities of Xpert Ultra and EasyNAT were similar [34.9% (61/175) vs. 30.3% (53/175), respectively; $p=0.201$]. Furthermore, similar specificities were observed in EasyNAT and Xpert Ultra assays, at 97.8% (90/92) and 100.0% (92/92), respectively ($p=0.155$).

Agreement between EasyNAT and Xpert Ultra was further analyzed among 267 children, and concordant results were obtained for 217 children (47 EasyNAT+ Xpert Ultra+; 170 EasyNAT− Xpert Ultra−). Discordant results were found in 48 children with TB (42 with EasyNAT− Xpert Ultra+ and 6 with EasyNAT+ Xpert Ultra- results) and 2 children with RTIs (2 with EasyNAT+Xpert Ultra- results; **Figure 2B**). Among 48 children with TB, the semiquantitative scale of Xpert Ultra was low in 11 cases, very low in eight cases, and trace in 23 cases, indicating the bacterial load of these samples were low. The cycle thresholds of EasyNAT were higher in children with

TABLE 2 | Comparison of EasyNAT and Xpert in children with TB and RTIs.

Group	Sensitivity, % (*n* of *N*)		*p*	Specificity, % (*n* of *N*)		*p*
	EasyNAT	Xpert		EasyNAT	Xpert	
All enrolled children	22.6 (31of 137)	26.3 (36 of 137)	0.441	98.0 (100 of 102)	99.0 (101 of 102)	1.0
Bacteriologically confirmed	60.0(9 of 15)	60.0 (9 of 15)	1.0			
Probable TB	18.0 (22 of 122)	22.1 (27 of 122)	0.424			

TB, pulmonary tuberculosis; RTIs, respiratory tract infections; EasyNAT, EasyNAT MTC assay; and Xpert, Xpert MTB/RIF.

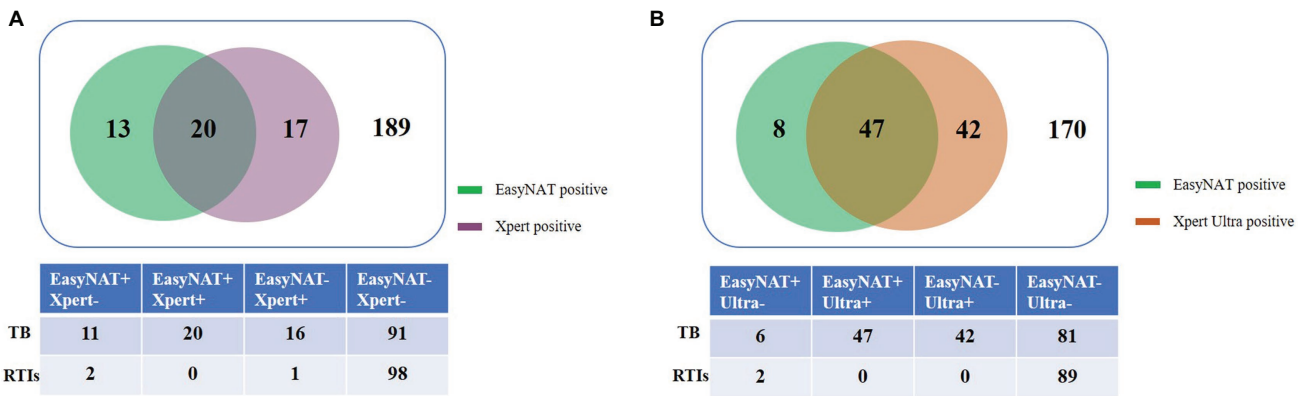

	EasyNAT+ Xpert-	EasyNAT+ Xpert+	EasyNAT- Xpert+	EasyNAT- Xpert-
TB	11	20	16	91
RTIs	2	0	1	98

	EasyNAT+ Ultra-	EasyNAT+ Ultra+	EasyNAT- Ultra+	EasyNAT- Ultra-
TB	6	47	42	81
RTIs	2	0	0	89

FIGURE 2 | Venn diagram of the different diagnostic test results for childhood tuberculosis using gastric aspirate samples. **(A)** EasyNAT MTC and Xpert MTB/RIF. **(B)** EasyNAT MTC and Xpert MTB/RIF Ultra.

EasyNAT+ Xpert Ultra-results than those with EasyNAT+ Xpert Ultra+results (27.0 vs. 15.5, $p = 0.083$). Additionally, we found that among 28 Xpert Ultra trace cases, five were EasyNAT+.

Concordance of the semiquantitative scales for EasyNAT and Xpert Ultra was analyzed in 47 PTB children with both double positive results (**Figure 3B**). The result showed that patients with lower semiquantitative scores in Xpert Ultra tended to have higher cycle thresholds in EasyNAT, with a Spearman's rank correlation coefficient of 0.343 ($p = 0.018$).

Invalid Results From the Assays

Among all the enrolled children, none had an invalid Ultra test result. Three "invalid" results were initially obtained from the EasyNAT test; after repeated testing two were "positive" and one had "negative" results. Two "invalid" results were initially obtained from the Xpert test and the repeated resulted showed "positive" results.

DISCUSSION

Since 2010, the WHO has recommended that national health authorities employ the Xpert MTB/RIF assay in the management of TB, multi-drug resistant TB, and HIV-associated TB (World-Health-Organization, 2011b). The global TB report published in 2018 introduced the EasyNAT assay, which was developed in China as a possible alternative to the GeneXpert platform in primary health care facilities (World-Health-Organization, 2018). EasyNAT has a similar limit of detection (LOD) to Xpert [100 colony forming units (CFU)/ml and 114 CFU/ml, respectively]. However, evidence regarding the performance of EasyNAT is limited. No data indicating its diagnostic value in children have been published. Therefore, the global report highlighted that well-designed validation studies are needed to enable the WHO to review and assess the performance of this assay.

The first aim of the present study was to compare diagnostic accuracy between EasyNAT and Xpert or Xpert Ultra. Similar sensitivities and specificities were observed between the two assays. Furthermore, the semiquantitative scale of Xpert was also concordant with the cycle threshold generated by EasyNAT, indicating an equal detection efficiency in childhood TB using GA specimens. The sensitivities of EasyNAT and Xpert in bacteriologically confirmed TB were both 61.5%, which is similar to previously reported data from a meta-analysis (66.0%; Chakravorty et al., 2017). Considering the low cost of the EasyNAT assay, less than half that of Xpert, it may be a promising diagnostic assay for childhood TB.

The use of Xpert Ultra in GA and stool samples has been suggested for TB diagnosis in children (World-Health-Organization, 2021c). Because of the improved detection efficiency with a LOD of 16 CFU/ml, Xpert Ultra presented a higher sensitivity than EasyNAT (50.9% vs. 30.3%, respectively, $p < 0.001$) and Xpert (50.9% vs. 26.3%, respectively $p < 0.001$).

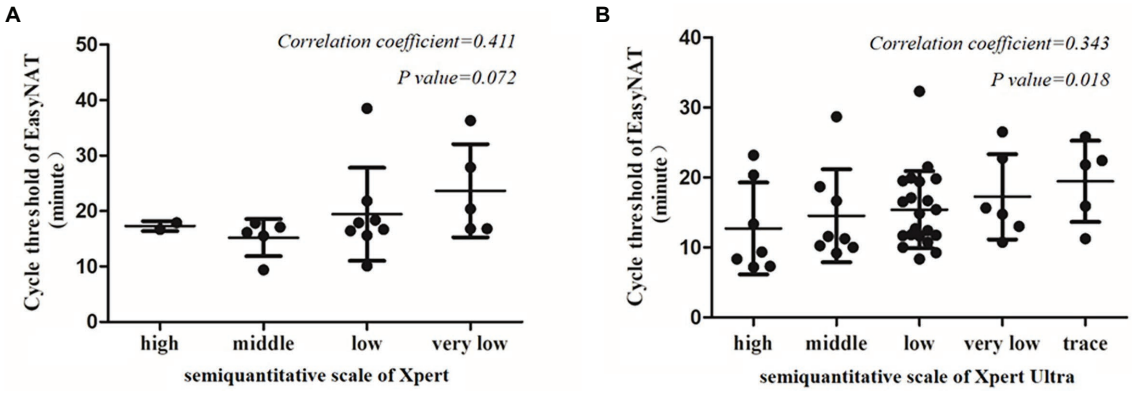

FIGURE 3 | Correlation between the cycle threshold of EasyNAT MTC assay and the semiquantitative scale of Xpert MTB/RIF or Xpert MTB/RIF Ultra. **(A)** Correlation between EasyNAT MTC and Xpert MTB/RIF. **(B)** Correlation between EasyNAT MTC and Xpert MTB/RIF Ultra.

TABLE 3 | Comparison of EasyNAT and Xpert ultra in children with TB and RTIs.

Group	Sensitivity, % (*n* of *N*)		*p*	Specificity, % (*n* of *N*)		*p*
	EasyNAT	Ultra		EasyNAT	Ultra	
All children	30.3 (53 of 175)	50.9 (89 of 175)	<0.001	97.8 (90 of 92)	100.0 (92 of 92)	0.155
Bacteriologically confirmed	61.5 (24 of 39)	82.1 (32 of 39)	0.044			
Probable TB	21.3 (29 of 136)	41.9 (57 of 136)	<0.001			

Comparison of EasyNAT and Xpert Ultra in children with TB and RTIs. TB, pulmonary tuberculosis; RTIs, respiratory tract infections; EasyNAT, EasyNAT MTC assay; and Ultra, Xpert MTB/RIF Ultra.

The relative higher sensitivity of Xpert Ultra compared with Xpert in children has been reported in our previous studies, at 80 and 67%, respectively, using bronchoalveolar lavage fluid (Sun et al., 2019), and 66.7 and 42.9%, respectively, using sputum (Peng et al., 2021). To improve sensitivity for the detection of MTB, an additional two multicopy amplification targets (IS*6110* and IS*1081*) are used in Xpert Ultra. Because of the paucibacillary specimens obtained from children, 31.4% (28/89) of Xpert Ultra positive results were classified as "trace" in the semiquantitative scale in the present study, suggesting the value of Xpert Ultra in samples with low bacillary burden for MTB detection (Chakravorty et al., 2017). It suggested that Xpert Ultra performed better than EasyNAT in children although the current cost of the former hindered its implementation. In addition, we found among 28 cases with an Xpert Ultra trace readout, five were EasyNAT+. This suggested a promising use for EasyNAT in children with low bacterial burden samples.

We also found some discordant results between EasyNAT and the Xpert or Xpert Ultra. In children with RTIs, four with EasyNAT-positive and one with Xpert-positive results presented a very low load of MTB. All five children have no symptoms or signs or X-ray abnormalities suggestive of TB, no contact history of active TB, and positive responded to antibiotic treatment rather than anti-TB treatment. Among them, four children had negative IGRAs results, and one child was diagnosed as latent TB infection and *Mycoplasma pneumonia*. All the children with discordant results were not further tested with a third nucleic acid-based test because of the following reasons: First, some of these TB children (27/75) were confirmed by MTB culture, and the rest of the TB cases (48/75) were clinically diagnosed based their clinical manifestations, chest X-ray results, clinical presentation improvement after anti-TB treatment, and positive results of tuberculin skin test or interferon-γ release assay. Second, Xpert Ultra is considered to be the most sensitive nucleic acid detection test, with the lowest limit of detection of 15.6 CFU/ml. So the negative results of the tests in children with discordant results suggested a underdiagnosis in these cases.

The first generation EasyNAT TB Isothermal Amplification Diagnostic Kit (EasyNAT TB IAD) and the next-generation EasyNAT MTC assay used here have been evaluated in the diagnosis of TB in adults (Ou et al., 2014; Zhang et al., 2021). One study reported that the sensitivity of EasyNAT TB IAD in adults with culture-confirmed TB was 84.1% (Ou et al., 2014). The next-generation EasyNAT MTC assay performed in a clinical setting demonstrated an overall sensitivity of 72.19%, which further increased to 86.84% in cases with confirmed TB using sputum (Zhang et al., 2021). Compared with these findings, the sensitivity of EasyNAT was lower in children. Several reasons may have contributed to the differences in sensitivities between the adult subjects enrolled in previous studies and the present childhood cohort. Firstly, the bacillary burden of bacteria in adult specimens is higher than that in

children, which may lead to a lower bacterial positivity rate in children compared with adults. According to nationwide data reported in Mainland China, the positivity rate of bacteriology in children was 21% (Yang et al., 2020), while the bacteriologically confirmed rate in adults was 37.5% (Pang et al., 2019). Thus, diagnosing TB in children is more difficult than in adults, highlighting the urgent need for high sensitivity nucleic acid amplification tests for diagnosis of childhood TB.

Secondly, the detection rates of molecular tests vary between different specimen types. Sputum, the main specimen type in adult PTB patients, is difficult to obtain in children. However, GA is an invasive but well-tolerated procedure that can be used in children. WHO Guidance for the management of tuberculosis in children suggested to use early-morning GA for pediatric TB diagnosis as children swallow respiratory secretions (World-Health-Organization, 2014). Therefore, GA is an alternative specimen type for children with unavailable sputum samples. Data from the German national notification system showed that GA samples were used in 59% of the children who were diagnosed with pulmonary TB, and GA was the only reported specimen for 34.7% of the bacteriological notified patients (Fiebig et al., 2014). One meta-analysis reported that expectorated sputum was the best sample type for diagnosing adult PTB, with a pooled sensitivity of 90%, while the pooled sensitivity of expectorated sputum in children was only 14%. Although GA specimens were suitable for childhood TB diagnosis, the sensitivity (80%) was slightly lower than that of sputum in adults (Lyu et al., 2020). The pretreatment protocol applied to GA specimens in this study was adapted from that of sputum samples; whether this method is suitable and can affect the detection rate of the EasyNAT MTC assay remains unclear. The processing methods for GA samples should be optimized in future studies.

In conclusion, the EasyNAT assay had a similar diagnostic capacity for MTB in GA samples compared with the Xpert assay in children but demonstrated a lower sensitivity than Xpert Ultra. EasyNAT may therefore be useful as a suitable alternative method of childhood TB diagnosis based on its cost-effectiveness, speed, and accuracy.

DATA AVAILABILITY STATEMENT

The raw data supporting the conclusions of this article will be made available by the authors, without undue reservation.

ETHICS STATEMENT

The studies involving human participants were reviewed and approved by the Medical Ethics Committee of Beijing Children's Hospital. Written informed consent to participate in this study was provided by the participants' legal guardian/next of kin.

AUTHOR CONTRIBUTIONS

SQ, TJ, WJ, YW, and LS performed the tests. YZ, QL, YL, MF, YS, LD, XT, and XS enrolled the subjects and collected data and samples. SQ and LS analyzed the data and drafted the initial manuscript. CW, LS, and AS conceptualized and designed the study and reviewed and revised the manuscript. All authors contributed to the article and approved the submitted version.

FUNDING

This work was partly supported by the Capital's Funds for Health Improvement and Research (2020-1-2091), Key Project of the Department of Science and Technology Beijing, China (D181100000418003), and National Science and Technology Major Project of China (2018ZX10103001-003).

SUPPLEMENTARY MATERIAL

The Supplementary Material for this article can be found online at: https://www.frontiersin.org/articles/10.3389/fmicb.2022.819654/full#supplementary-material

REFERENCES

Barreda-Garcia, S., Miranda-Castro, R., De-Los-Santos-Alvarez, N., Miranda-Ordieres, A. J., and Lobo-Castanon, M. J. (2016). Comparison of isothermal helicase-dependent amplification and PCR for the detection of mycobacterium tuberculosis by an electrochemical genomagnetic assay. *Anal. Bioanal. Chem.* 408, 8603–8610. doi: 10.1007/s00216-016-9514-z

Chakravorty, S., Simmons, A. M., Rowneki, M., Parmar, H., Cao, Y., Ryan, J., et al. (2017). The new xpert MTB/RIF ultra: improving detection of mycobacterium tuberculosis and resistance to rifampin in an assay suitable for Point-of-Care testing. *mBio* 8, e00812–e00817. doi: 10.1128/mBio.00812-17

Dayal, R., Yadav, A., Agarwal, D., Kumar, M., Kamal, R., Singh, D., et al. (2021). Comparison of diagnostic yield of tuberculosis loop-mediated isothermal amplification assay with cartridge-based nucleic acid amplification test, acid-fast bacilli microscopy, and mycobacteria growth indicator tube culture in children with pulmonary tuberculosis. *J. Pediatric. Infect. Dis. Soc.* 10, 83–87. doi: 10.1093/jpids/piaa019

Fiebig, L., Hauer, B., Brodhun, B., Balabanova, Y., and Haas, W. (2014). Bacteriological confirmation of pulmonary tuberculosis in children with gastric aspirates in Germany, 2002-2010. *Int. J. Tuberc. Lung Dis.* 18, 925–930. doi: 10.5588/ijtld.13.0578

Graham, S. M., Ahmed, T., Amanullah, F., Browning, R., Cardenas, V., Casenghi, M., et al. (2012). Evaluation of tuberculosis diagnostics in children: 1. Proposed clinical case definitions for classification of intrathoracic tuberculosis disease. Consensus from an expert panel. *J. Infect. Dis.* 205(Suppl 2), S199–S208. doi: 10.1093/infdis/jis008

Jiao, W. W., Wang, Y., Wang, G. R., Wang, Y. C., Xiao, J., Sun, L., et al. (2019). Development and clinical validation of multiple cross displacement amplification combined with nanoparticles-based biosensor for detection of mycobacterium tuberculosis: preliminary results. *Front. Microbiol.* 10:2135. doi: 10.3389/fmicb.2019.02135

Liu, W., Zhou, Y., Fan, Y., Jiang, N., Cain, K., and Zeng, L. (2018). Development of cross-priming amplification coupled with vertical flow visualization for rapid detection of infectious spleen and kidney necrosis virus (ISKNV) in mandarin fish, Siniperca chuatsi. *J. Virol. Methods* 253, 38–42. doi: 10.1016/j.jviromet.2017.12.008

Lyu, M., Zhou, J., Cheng, Y., Chong, W., Wu, K., Fang, T., et al. (2020). Which sample type is better for Xpert MTB/RIF to diagnose adult and pediatric pulmonary tuberculosis? *Biosci. Rep.* 40:BSR20200308. doi: 10.1042/BSR20200308

Ou, X., Song, Y., Zhao, B., Li, Q., Xia, H., Zhou, Y., et al. (2014). A multicenter study of cross-priming amplification for tuberculosis diagnosis at peripheral level in China. *Tuberculosis* 94, 428–433. doi: 10.1016/j.tube.2014.04.006

Pang, Y., An, J., Shu, W., Huo, F., Chu, N., Gao, M., et al. (2019). Epidemiology of Extrapulmonary tuberculosis among inpatients, China, 2008-2017. *Emerg. Infect. Dis.* 25, 457–464. doi: 10.3201/eid2503.180572

Qiao, B., Cui, J. Y., Sun, L., Yang, S., and Zhao, Y. L. (2015). Cross-priming amplification targeting the coagulase gene for rapid detection of coagulase-positive staphylococci. *J. Appl. Microbiol.* 119, 188–195. doi: 10.1111/jam.12836

Sharma, M., Sinha, S. K., Sharma, M., Singh, A. K., Samanta, J., Sharma, A., et al. (2020). Challenging diagnosis of gastrointestinal tuberculosis made simpler with multi-targeted loop-mediated isothermal amplification assay. *Eur. J. Gastroenterol. Hepatol.* 32, 971–975. doi: 10.1097/MEG.0000000000001765

Sun, L., Qi, X., Liu, F., Wu, X., Yin, Q., Guo, Y., et al. (2019). A test for more accurate diagnosis of pulmonary tuberculosis. *Pediatrics* 144:e20190262. doi: 10.1542/peds.2019-0262

Wang, Y. X., Zhang, A. Y., Yang, Y. Q., Lei, C. W., Cheng, G. Y., Zou, W. C., et al. (2018). Sensitive and rapid detection of salmonella enterica serovar Indiana by cross-priming amplification. *J. Microbiol. Methods* 153, 24–30. doi: 10.1016/j.mimet.2018.08.003

World-Health-Organization (2011a). Policy statement: Automated real-time nucleic acid amplification technology for rapid and simultaneous detection of tuberculosis and rifampicin resistance: Xpert MTB/RIF system. Available at: https://www.who.int/news/item/18-05-2011-xpert-mtb-rif---rapid-tb-test---who-publishes-policy-and-guidance-for-implementers (Accessed November 10, 2021).

World-Health-Organization (2011b). Prerequisites to country implementation of Xpert MTB/RIF and key action points at country level. Available at: https://www.who.int/publications/i/item/WHO-HTM-TB-2011.12 (Accessed November 10, 2021).

World-Health-Organization (2014). Guidance for national tuberculosis programmes on the management of tuberculosis in children (Accessed November 10, 2021). (Reprinted).

World-Health-Organization (2018). Global tuberculosis report 2018.Licence: CC BY-NC-SA 3.0 IGO. Available at: https://apps.who.int/iris/bitstream/handle/10665/274453/9789241565646-eng.pdf (Accessed November 10, 2021).

World-Health-Organization (2021a). Global Tuberculosis Report 2021. Available at: https://www.who.int/teams/global-tuberculosis-programme/tb-reports/global-tuberculosis-report-2021 (Accessed November 9, 2021).

World-Health-Organization (2021b). WHO consolidated guidelines on tuberculosis. Module 3 diagnosis - rapid diagnostics for tuberculosis detection, 2021 update. Available at: https://www.who.int/publications/i/item/9789240029415 (Accessed November 9, 2021).

World-Health-Organization (2021c). Rapid communication on updated guidance on the management of tuberculosis in children and adolescents. Available at: https://www.who.int/publications/i/item/9789240033450 (Accessed November 10, 2021).

Yang, R., Liu, M., Jiang, H., Zhang, Y., Yin, J., Li, Q., et al. (2020). The epidemiology of pulmonary tuberculosis in children in mainland China, 2009-2015. *Arch. Dis. Child.* 105, 319–325. doi: 10.1136/archdischild-2019-317635

Zhang, Z., Du, J., Liu, T., Wang, F., Jia, J., Dong, L., et al. (2021). EasyNAT MTC assay: a simple, rapid, and low-cost cross-priming amplification method for the detection of mycobacterium tuberculosis suitable for point-of-care testing. *Emerg. Microbes Infect.* 10, 1530–1535. doi: 10.1080/22221751.2021.1959271

Zhao, Y., Chen, F., Li, Q., Wang, L., and Fan, C. (2015). Isothermal amplification of nucleic acids. *Chem. Rev.* 115, 12491–12545. doi: 10.1021/acs.chemrev.5b00428

Conflict of Interest: The authors declare that the research was conducted in the absence of any commercial or financial relationships that could be construed as a potential conflict of interest.

Publisher's Note: All claims expressed in this article are solely those of the authors and do not necessarily represent those of their affiliated organizations, or those of the publisher, the editors and the reviewers. Any product that may be evaluated in this article, or claim that may be made by its manufacturer, is not guaranteed or endorsed by the publisher.

frontiers in Microbiology

ORIGINAL RESEARCH
published: 30 March 2022
doi: 10.3389/fmicb.2022.825413

Diagnostic Performance of a Novel *CXCL10* mRNA Release Assay for *Mycobacterium tuberculosis* Infection

Liping Pan[1†], Mailing Huang[2†], Hongyan Jia[1], Guofang Deng[3], Yu Chen[4], Rongrong Wei[1], Mingxia Zhang[5], Xin Li[6], Qi Sun[1], Mutong Fang[3], Pengfei Ren[4], Aiying Xing[1], Qi Chen[5], Xinxin Li[4], Boping Du[1], Tao Chen[3], Mengqiu Gao[2] and Zongde Zhang[1]**

[1] Beijing Chest Hospital, Beijing Key Laboratory for Drug Resistant Tuberculosis Research, Beijing Tuberculosis and Thoracic Tumor Research Institute, Capital Medical University, Beijing, China, [2] Department of Tuberculosis, Beijing Chest Hospital, Beijing Tuberculosis and Thoracic Tumor Research Institute, Capital Medical University, Beijing, China, [3] Department of Pulmonary Medicine, The Third People's Hospital of Shenzhen, Shenzhen, China, [4] Department of Tuberculosis, Henan Provincial Infectious Disease Hospital, Zhengzhou, China, [5] Laboratory Medical Center, The Third People's Hospital of Shenzhen, Guangdong Key Lab of Emerging Infectious Diseases, Shenzhen, China, [6] Laboratory Medical Center, Henan Provincial Infectious Disease Hospital, Zhengzhou, China

OPEN ACCESS

Edited by:
Xiao-Yong Fan,
Fudan University, China

Reviewed by:
Eduard Otto Roos,
Clinomics, South Africa
Jianping Xie,
Southwest University, China

***Correspondence:**
Mengqiu Gao
gaomqwdm@aliyun.com
Zongde Zhang
zzd417@ccmu.edu.cn

† These authors have contributed equally to this work

Specialty section:
This article was submitted to Infectious Agents and Disease, a section of the journal Frontiers in Microbiology

Received: *30 November 2021*
Accepted: *14 February 2022*
Published: *30 March 2022*

Citation:
Pan L, Huang M, Jia H, Deng G, Chen Y, Wei R, Zhang M, Li X, Sun Q, Fang M, Ren P, Xing A, Chen Q, Li X, Du B, Chen T, Gao M and Zhang Z (2022) Diagnostic Performance of a Novel CXCL10 mRNA Release Assay for Mycobacterium tuberculosis Infection. Front. Microbiol. 13:825413. doi: 10.3389/fmicb.2022.825413

One-fourth of the world's population has been infected with *Mycobacterium tuberculosis* (*M.tb*). Although interferon-gamma release assays (IGRAs) have been shown to be valid methods for identifying *M.tb* infection and auxiliary methods for diagnosis of active tuberculosis (TB), lower sensitivity and higher indeterminate rate were often detected among immunosuppressed patients. IP-10 was an alternative biomarker due to the higher expression level after *M.tb* antigen stimulation, but whether *CXCL10* mRNA (the gene that transcribes for the IP-10 protein) can be used as a target for *M.tb* infection diagnosis was limited. Therefore, we aimed to evaluate the performance of a novel *M.tb*-specific *CXCL10* mRNA release assay in diagnosis of *M.tb* infection. Suspected TB patients and healthy controls were prospectively recruited between March 2018 and November 2019 from three hospitals in China. *CXCL10* mRNA release assay and traditional interferon-gamma release assay (T-SPOT.TB) were simultaneously performed on peripheral blood. Of the 1,479 participants enrolled in the study, 352 patients with definite TB and 153 healthy controls were analyzed. *CXCL10* mRNA release assay provided a sensitivity of 93.9% (95% CI = 90.8–96.2%) and a specificity of 98.0% (95% CI = 94.3–99.6%) in the diagnosis of *M.tb* infection, respectively, while T-SPOT.TB gave a sensitivity of 94.5% (95% CI = 91.5–96.6%) and a specificity of 100% (95% CI = 97.6–100.0%) in the diagnosis of *M.tb* infection, respectively. The diagnostic performance of *CXCL10* mRNA release assay was consistent with T-SPOT.TB, with a total coincidence rate of 95.0% (95% CI = 93.0–96.9%) and a Cohen's kappa value of 0.89 (0.84–0.93, $p < 0.001$). However, among TB patients with HIV co-infection ($n = 14$), *CXCL10* mRNA release assay presented significantly higher positive rate [92.9% (66.1–99.8%) *vs*. 61.5% (31.6–86.1%), $p = 0.029$] than those of T-SPOT.TB. These results suggested that *M.tb*-specific *CXCL10* mRNA was a novel and useful target in the diagnosis of *M.tb* infection.

Keywords: tuberculosis, *M.tb* infection, molecular diagnosis, mRNA, T-SPOT.TB, *CXCL10*

INTRODUCTION

Tuberculosis (TB) is an infectious disease that seriously threatens human health, which caused 9.9 million new cases and 1.5 million deaths worldwide in 2020 (World Health Organization [WHO], 2021). Furthermore, one-fourth of the world's population has been infected with *Mycobacterium tuberculosis* (*M.tb*) (Cohen et al., 2019). The global goal of "End TB" would be difficult to achieve due to the high burden of active TB and latent TB infection, unless there are innovations in diagnosis, treatment, and prevention methods.

The World Health Organization has recommended preventive treatment among latent TB infection population to reduce the incidence of active TB (World Health Organization [WHO], 2020). Until now, *M.tb* infection is mainly defined by tuberculin skin test (TST) or interferon-gamma release assays (IGRAs; Diel et al., 2010, 2011; Gao et al., 2015; Getahun et al., 2015). Due to the lower sensitivity of conventional *M.tb* culture or smear, as well as the lack of sputum to do the microbiological or rapid molecular tests in some suspected TB patients (World Health Organization [WHO], 2021), IGRAs have also been becoming an auxiliary method for the diagnosis of active TB. However, the TST is an *in vivo* test, and the specificity of TST is decreased seriously in BCG-vaccinated population (Pai et al., 2008). The diagnostic performance of IGRAs was decreased in immunosuppression patients, such as HIV co-infection, leukopenia, or corticosteroid and immunosuppressant drug treatment, with lower sensitivity and higher indeterminate rate (Cattamanchi et al., 2011; Jung et al., 2012; Pan et al., 2015). Furthermore, due to the longer time of antigen stimulation (18–24 h), the results of IGRA tests will not be available until the next day. In addition, ELISPOT-based IGRAs, such as T-SPOT.TB test, were mostly performed manually, which requires technicians with higher technique and may result in operation bias. Therefore, novel rapid and accurate test for diagnosis of *M.tb* infection should be developed.

Previous studies have identified an alternative biomarker in peripheral blood for *M.tb* infection, namely, interferon-gamma-induced protein 10 (IP-10) (Lu et al., 2011; Ruhwald et al., 2011, 2012; Petrone et al., 2018). IP-10 is a chemokine in CXC family, which can be expressed in a significantly higher level than conventional IFN-γ after *M.tb* antigen stimulation. Recently, IP-10 has been becoming a novel promising biomarker for TB diagnosis. Meta-analyses showed that IP-10 presented a higher sensitivity of 86% (95% CI = 80–90%) and a specificity of 88% (95% CI = 82–92%) in the diagnosis of *M.tb* infection, respectively (Qiu et al., 2019). However, most of the studies detected the expression level of IP-10 protein by ELISA or other protein examination methods, and whether *CXCL10* mRNA (the gene that transcribes for the IP-10 protein) quantification can be used in the diagnosis of *M.tb* infection was not yet elucidated. It is reported that the expression of *CXCL10* mRNA can be upregulated by about 100 times, within 2.5–8 h of *M.tb*-specific antigen stimulation (Blauenfeldt et al., 2014). Therefore, *CXCL10* mRNA as target may enable higher sensitivity in identifying individuals with *M.tb* infection (Aabye et al., 2010; Syed Ahamed Kabeer et al., 2010; Kabeer et al., 2011).

The present study aims to evaluate the diagnostic performance of the novel *M.tb*-specific *CXCL10* mRNA release assay for *M.tb* infection and analyze in accordance with the novel *CXCL10* mRNA release assay and the widely used T-SPOT.TB assay.

MATERIALS AND METHODS

Ethical Approval

This study was performed in accordance with the guidelines of the Helsinki Declaration and was approved by the Ethics Committee of the Beijing Chest Hospital, Capital Medical University (Ethical approval number: BJXK-2017-40-01). A written informed consent was obtained from each participant before blood collection.

Study Design and Participants

This multicenter, prospective study was performed in three hospitals in China, including the Beijing Chest Hospital (North), the Third People's Hospital of Shenzhen (South), and the Henan Provincial Infectious Disease Hospital (Middle). Between March 2018 and November 2019, patients with suspected TB were prospectively enrolled in these three hospitals. Meanwhile, healthy controls were also enrolled. All the participants were tested with *CXCL10* mRNA release assay and T-SPOT.TB assay. The laboratory technicians were blinded to the diagnosis throughout the study, and the clinicians were blinded to the *CXCL10* mRNA release assay and T-SPOT.TB results before the end of the clinical trial enrollment. Furthermore, the laboratory technician who performed the *CXCL10* mRNA release assay was blind to the technician who performed the T-SPOT.TB. Thus, laboratory interpretation and clinical diagnosis were independent.

Categorization of Participants

The final diagnosis was based on clinical manifestation, biochemical examinations, and histopathological, radiological, and microbiological information. All subjects were followed up for at least 6 months and were monitored for changes in their diagnostic categorization. Finally, patients were categorized as (1) Definite TB: Patients who have positive *M.tb* culture, positive Xpert MTB/RIF, positive microscopy, or positive histology were defined as definite TB. (2) Probable TB: Patients who have clinical and radiological findings of TB, and presenting well response to anti-TB treatment, but lacking microbiological or histopathological evidence of *M.tb* infection, were defined as probable TB. (3) Non-TB patients: Patients who were initially suspected of active TB, but ended up not having active TB, due to other diagnoses made, or clinical improvement occurred without recent anti-TB therapy, were defined as non-TB patients. (4) Healthy controls: Individuals who have no clinical symptoms and radiological findings of TB, and with negative TST results, were defined as healthy controls.

Blood Collection

A total of 10 ml of peripheral blood was collected in heparin-containing vacutainer tubes from each participant, and

CXCL10 mRNA Release Assay and T-SPOT.TB Test were further performed.

CXCL10 mRNA Release Assay

The commercial *CXCL10* mRNA Release Assay, including the kit for blood incubation and RNA extraction (CLR001A48, InnowaveDx Co., Ltd., Suzhou, China) and kit for reverse transcription and further qPCR Test (CLR002A48, InnowaveDx Co., Ltd., Suzhou, China), were performed according to the instructions of the manufacturer. Briefly, the blood was divided into three special tubes (1.5 ml per tube): one coated with novel *M.tb*-specific peptides (peptides of ESAT6, CFP-10, and PPE68), one coated with phytohemagglutinins (PHA) as a positive control, and one without antigen coating as a negative control (Nil). The tubes were incubated immediately for 4 h at 37°C. Next, RNA was automatically extracted from the incubated whole blood (100 μl). A total of 10 μl of RNA and 10 μl of reverse transcription solution (including buffer and reverse transcriptase) were mixed and reverse transcribed to cDNA with the following procedure: 50°C for 20 min, 85°C for 2 min. RNA extraction and reverse transcription were performed using the automatic nucleic acid extraction and detection system Innovo-100 (InnowaveDx Co., Ltd., Suzhou, China). All the commercial reagents and kits for RNA extraction and reverse transcription were matched for the instrument. A total of 10 μl of cDNA was then mixed with 15 μl of quantitative real-time PCR (qPCR) mix (including enzyme, buffer, and probe). qPCR was performed on the ABI 7500 Real-time PCR System (Applied Biosystems, Inc., Foster City, CA, United States), with the following procedure: 50°C for 2 min, 95°C for 2 min, and then 40 cycles of 95°C for 10 s and 60°C for 30 s. The cycle threshold (CT) for target gene (*CXCL10*, Gene ID: 3627) and housekeeping gene (CHMP2A, Gene ID: 27243) detector was automatically determined. ΔCT (the CT value for target gene, subtract the CT value for housekeeping gene) was calculated, and this statistic was used to determine relative gene expression (Schmittgen and Livak, 2008). The relative amount of *CXCL10* mRNA in each tube with or without antigens was calculated separately. The test results were determined as indeterminate, negative, or positive according to the criteria (**Supplementary Table 1**).

T-SPOT.TB Test

The T-SPOT.TB test (Oxford Immunotec Ltd., Abingdon, United Kingdom) was performed in accordance with the instructions of the manufacturer. Briefly, peripheral blood mononuclear cells (PBMCs) were isolated, and then 2.5×10^5 PBMCs per well were incubated with AIMV medium (Nil control), PHA antigen (positive control), and two *M.tb*-specific antigens (ESAT-6 and CFP-10). The procedure was performed in the plates precoated with anti-interferon-γ antibodies at 37°C for 16 to 20 h. After application of alkaline phosphatase-conjugated second antibody and chromogenic substrate, the number of spot-forming cells (SFCs) in each well was automatically counted with a CTL ELISPOT system (CTL-ImmunoSpot S5 Versa Analyzer, United States). The test results were determined as indeterminate, negative, or positive according to the criteria (**Supplementary Table 1**).

Statistical Analysis

Data analysis was performed using SPSS for Windows, version 21 (SPSS, Inc.). Categorical variables were compared by Pearson's Chi-square test or Fisher's exact test, while continuous variables were compared by Student's *t*-test or Mann–Whitney *U*-test, as appropriate. Sensitivity and specificity were calculated to evaluate diagnostic performance for the *CXCL10* mRNA release assay and T-SPOT.TB assay. Concordance between *CXCL10* mRNA release assay and T-SPOT.TB assay was calculated using Cohen's kappa test. The expression levels of *CXCL10* mRNA and the number of SFCs in T-SPOT.TB test were converted to lg values, in order to calculate the correlation between these two tests by Pearson's correlation test. The criterion for statistical significance was $p < 0.05$.

RESULTS

Clinical Characteristics of Participants

As shown in **Figure 1**, a total of 1,307 patients with suspected TB were enrolled from the three hospitals. According to the final diagnosis and a follow up of at least 6 months, 352 definite TB patients were included for analysis as definite *M.tb* infection status. A total of 441 probable TB patients, 348 non-TB patients, and 166 patients with inconclusive diagnosis were excluded because there were no definite *M.tb* infection evidence. Furthermore, of 172 healthy controls enrolled, only 153 persons with negative TST results and without radiological findings were included in the analysis. A total of 14 patients with definite TB were HIV positive, and there was no HIV infection among healthy controls. The detailed demographic and clinical characteristics of the participants are shown in **Table 1**.

Indeterminate Results in *CXCL10* mRNA Release Assay and T-SPOT.TB Test

Among the 505 participants in the final analysis, 2 participants (0.39%) presented indeterminate result in *CXCL10* mRNA release assay, due to invalid ΔCT in the mitogen tube (>-1.2), while 7 participants (1.39%) presented an indeterminate result in T-SPOT.TB, due to higher SFCs (>10 spots) in Nil control well or lower SFCs (<20 spots) in positive control well. The proportion of indeterminate results of T-SPOT.TB was higher than that of *CXCL10* mRNA release assay, although the difference did not reach statistical significance ($p = 0.094$). HIV co-infection rate is significantly higher in participants with indeterminate results of *CXCL10* mRNA release assay and T-SPOT.TB test (33.3%, 3/9) than that in participants with valid results of *CXCL10* mRNA release assay and T-SPOT.TB test (2.22%, 11/496) ($p = 0.0013$).

Concordance Between *CXCL10* mRNA Release Assay and T-SPOT.TB Test

Concordance between *CXCL10* mRNA release assay and T-SPOT.TB test was also analyzed in 496 participants with both valid *CXCL10* mRNA release assay and T-SPOT.TB results (**Table 2**). Both *CXCL10* mRNA release assay and T-SPOT.TB were positive in 312 participants and negative in 159 participants,

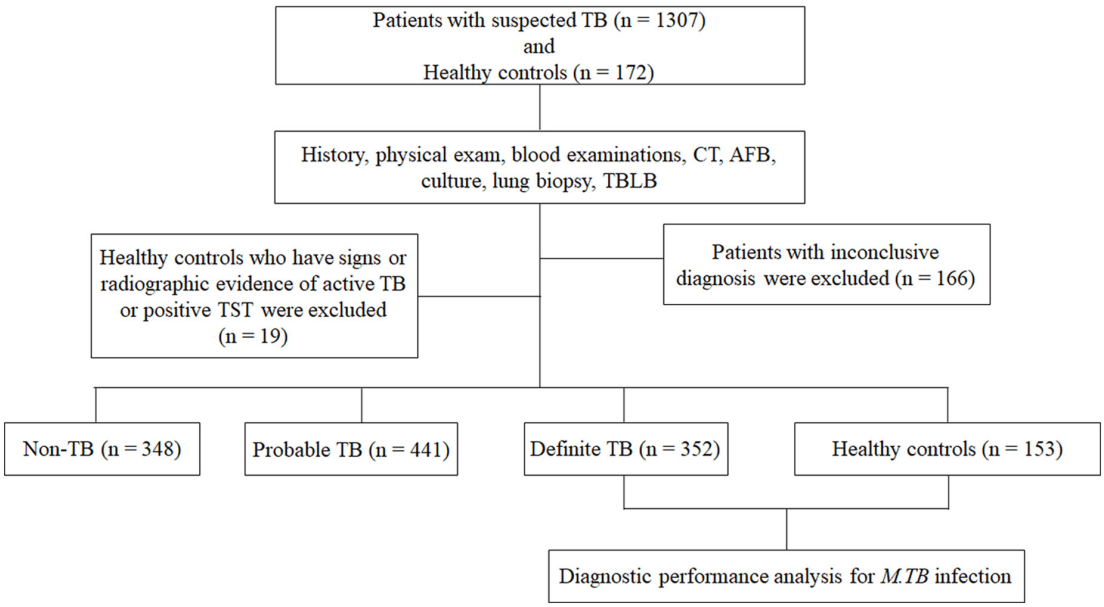

FIGURE 1 | Flow chart of the study participants. Of the 1,307 patients with suspected TB and 172 healthy controls recruited, 352 definite TB patients and 153 healthy controls with lower risk of *Mycobacterium tuberculosis* (*M.tb*) infection were eligible for inclusion in the final analysis. TB, tuberculosis; CT, computed tomography; AFB, acid-fast bacilli; TBLB, transbronchial lung biopsy.

with a good concordance (Kappa value = 0.89, $p < 0.001$). The overall concordance between the two tests was 95.0% (95% CI = 93.0–96.9%), the positive agreement was 96.3% (95% CI = 94.2–98.3%), and the negative agreement was 92.4% (95% CI = 88.5–96.4%), respectively.

We further investigated the association between the number of SFCs in the T-SPOT.TB test and the relative amounts of *CXCL10* mRNA in the *CXCL10* mRNA release assay (**Figure 2**). In most cases, the relative amount of *CXCL10* mRNA was increased when the number of SFCs in the T-SPOT.TB test was increased, indicating a moderate correlation between the expression level of *CXCL10* mRNA and the IFN-γ release in the two tests ($r = 0.6761$, $p < 0.0001$).

TABLE 1 | The demographic and clinical characteristics of subjects ($n = 505$).

	Definite TB	Healthy controls
Number of patients	352	153
Age (years, range)	38 (18–88)	18 (18–22)
Gender		
Male	226	79
Female	126	74
Pulmonary TB	329	–
Extrapulmonary TB	23	–
Skeleton	17	–
Lymph nodes	2	–
Urinary and genital organs	2	–
Abdomen	1	–
Meninges	1	–
HIV infection	14	0

Diagnostic Performance of the *CXCL10* mRNA Release Assay and T-SPOT.TB Assay for *M.tb* Infection

We evaluated the diagnostic performance of *CXCL10* mRNA release assay for *M.tb* infection based on the patients with definite TB and healthy controls (**Table 3**). The diagnostic sensitivity and specificity of *CXCL10* mRNA release assay was 93.9% (95% CI = 90.8–96.2%) and 98.0% (95% CI = 94.3–99.6%), respectively, while the diagnostic sensitivity and specificity of T-SPOT.TB assay were 94.5% (95% CI = 91.5–96.6%) and 100% (95% CI = 97.6–100.0%), respectively. No significant differences were detected in the sensitivity ($p = 0.745$) and specificity ($p = 0.247$) between *CXCL10* mRNA release assay and T-SPOT.TB assay.

The diagnostic performance of the combination of *CXCL10* mRNA release assay and T-SPOT.TB assays was also evaluated, and the positive result was assumed when either test was positive, and a negative result was assumed when both tests were negative (**Table 3**). Based on this standard, the diagnostic performance for *M.tb* infection was enhanced, with a better NPV value [94.3% (89.7–96.9%)].

The Positive Rate of *CXCL10* mRNA Release Assay and T-SPOT.TB Assay Among Tuberculosis Patients With HIV Co-infection

Both the *CXCL10* mRNA release assay and the T-SPOT.TB assay are based on the host immune response to *M.tb*-specific antigens, and previous study identified HIV co-infection as the risk factor for false-negative and indeterminate IGRA results. Therefore, we

TABLE 2 | Concordance analysis between the *CXCL10* mRNA release assay and T-SPOT.TB assay.

		T-SPOT.TB		Agreement (95% CI)	Kappa value (95% CI)
		Positive	Negative		
CXCL10 mRNA release assay	Positive	312	13	95.0 (93.0–96.9)	0.89 (0.84–0.93)
	Negative	12	159		

further compared the diagnostic performance of *CXCL10* mRNA release assay and T-SPOT.TB assay among TB patients with HIV co-infection (**Table 4**). Among the 14 TB patients with HIV co-infection, all presented valid *CXCL10* mRNA release assay results, while 3 patients presented indeterminate results in T-SPOT.TB test. The positive rate of *CXCL10* mRNA release assay and T-SPOT.TB test were 92.9% (95% CI = 66.1–99.8%) and 61.5% (95% CI = 31.6–86.1%), respectively, with a significant difference in sensitivity between these two tests (p = 0.029). These results indicated a promising method for identifying *M.tb* infection among HIV co-infection population, although our sample size was not large enough.

DISCUSSION

In the present study, the concordance between the novel *CXCL10* mRNA release assay and the traditional T-SPOT.TB test was good, and the sensitivity and specificity were similar between these two tests, respectively. These results suggested that the diagnostic performance of the novel *CXCL10* mRNA release assay was consistent with the T-SPOT.TB test, indicating that *CXCL10* mRNA release assay was an alternative test for the diagnosis of *M.tb* infection. The similar performance in *M.tb* infection diagnosis may be related to the fact that the two targets belong to the same immune response signal pathway activated by *M.tb*-specific antigens. IP-10 is mainly released from the monocytes and T lymphocytes and is an IFN-γ inducible chemokine. It was reported that free IFN-γ can activate STAT1 and then amplifies JAK/STAT1 signal to release a large amount of IP-10 (Tsuboi et al., 2011). Previous studies have detected that the expression level of *IFNG* mRNA was only elevated slightly after *M.tb*-specific antigen stimulation and sustained in shorter time duration, which makes the *IFNG* mRNA not the best choice for diagnosis of *M.tb* infection (Kim S. et al., 2013; Savolainen et al., 2016). Gene expression profile identified the mRNA of multiple cytokines, such as *CXCL10*, which can be used as the detection target of the specific T-cell-based immune response to *M.tb* (Kim H. J. et al., 2013). In comparison with *IFNG* mRNA, the expression level of *CXCL10* mRNA was significantly expressed at 100-fold after *M.tb*-specific antigen stimulation, and the higher level of *CXCL10* mRNA could be sustained for a long time (Blauenfeldt et al., 2014). Thus, it is possible to explore a novel T cell based on immune response test targeting the *CXCL10* mRNA.

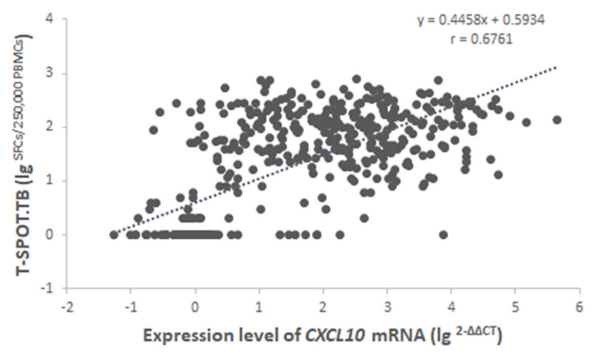

FIGURE 2 | Correlation analysis between the expression level of *CXCL10* mRNA in the *CXCL10* mRNA release assay and the number of SFCs in the T-SPOT.TB assay among 496 subjects with both valid results. Regression analysis was demonstrated by linear correlation (r). SFCs, spot-forming cells.

The diagnostic sensitivity of *CXCL10* mRNA release assay in our study was slightly higher than that in the previous Meta-analysis study [85% (95% CI = 80–88%)] (Qiu et al., 2019). This may be caused by the fact that the highly expressed *CXCL10* mRNA was used as the target. Recently, Ruhwald et al. have provided proof of high technical performance of a molecular assay detecting *CXCL10* mRNA expression, although it was reported that the *CXCL10* mRNA after 8 h of stimulation with *M.tb*-specific antigens in the QFT-IT test showed lower sensitivity than that of IP-10 protein and IFN-γ protein in the diagnosis of *M.tb* infection (Blauenfeldt et al., 2020), which was inconsistent with our results. This may be caused by the fact that the antigens used in our study were modified and could trigger stronger immune response than that in the QFT-IT test, and the appropriate stimulation time was extremely important for the utility of *CXCL10* mRNA as a target.

Interferon-gamma release assay test mainly relies on the ability of host immune response to *M.tb* antigen stimulation. It was reported that IGRA presented lower diagnostic performance in the diagnosis of TB patients with immunosuppression status, such as HIV co-infection (Cho et al., 2012; Santin et al., 2012). HIV patients were easily co-infected with *M.tb* and progressed to active TB patients (Mhango et al., 2021). The risk of HIV and *M.tb* co-infection individuals developing active tuberculosis is 20–30 times than those infected with *M.tb* alone, and the mortality of TB/HIV patients is also higher than that of patients with TB (Pawlowski et al., 2012). Therefore, the development of novel technologies that can increase the positive rate of TB with HIV infection is of great significance for timely identification and intervention of such population. In this study, we analyzed the performance of these two tests in TB patients with HIV co-infection and found that the proportion of indeterminate results of *CXCL10* mRNA release assay was lower than that of T-SPOT.TB test. Furthermore, the positive rate of *CXCL10* mRNA release assay was significantly higher than that of T-SPOT.TB test among TB patients with HIV co-infection,

TABLE 3 | Diagnostic performance of the *CXCL10* mRNA release assay and T-SPOT.TB assay for *Mycobacterium tuberculosis* (*M.tb*) infection.

	Sensitivity% (95% CI)	Specificity% (95% CI)	NPV% (95% CI)	PPV% (95%CI)	LR + (95% CI)	LR- (95% CI)
CXCL10 mRNA release assay	93.9 (90.8–96.2)	98.0 (94.3–99.6)	87.6 (82.4–91.5)	99.1 (97.2–99.7)	47.6 (15.5–145.9)	0.06 (0.04–0.09)
T-SPOT.TB	94.5 (91.5–96.6)	100.0 (97.6–100.0)	88.9 (83.8–92.5)	100.0 (100.0–100.0)	/†	0.05 (0.06–0.09)
CXCL10 or T-SPOT.TB*	97.4 (95.1–98.8)	98.0 (94.3–99.6)	94.3 (89.7–96.9)	99.1 (97.3–99.7)	49.3 (16.1–151.3)	0.03 (0.01–0.05)

NPV, negative predictive value; PPV, positive predictive value; LR+, likelihood ratio for positive test; LR−, likelihood ratio for negative value.
**The positive result was assumed when either test was positive, and a negative result was assumed when both tests were negative.*
†The LR + was unavailable when the diagnostic specificity was 100%.

indicating that the detection of *CXCL10* mRNA may be more suitable than that of T-SPOT.TB for the diagnosis of *M.tb* infection in HIV co-infection patients. The increase in positive rate of *CXCL10* mRNA release assay in HIV co-infection patients may be related to the high expression level of *CXCL10* that was caused by the cascade amplification in signal pathway, and maybe there are other signal pathways involved in the release of *CXCL10* but independent of IFN-γ signal pathway or $CD4^+$ T cells.

CXCL10 mRNA release assay also has some operational advantages. Since the high expression level of *CXCL10* mRNA, the antigen stimulation time was shortened to only 4 h, which saves at least 12 h compared with traditional IGRA test. Therefore, the test result can be issued on the day of blood collection, which leads to better clinical applicability. Furthermore, automated instruments are used throughout the test, and the results are automatically interpreted, which can minimize errors or bias caused by manual operation. These advantages bring more convenience for the clinical application of *CXCL10* mRNA release assay in the diagnosis of TB.

To our knowledge, our study is the largest investigation that prospectively evaluates the diagnostic performance of *CXCL10* mRNA release assay in the diagnosis of *M.tb* infection. However, there were still some limitations in our study. The sample size of TB patients with HIV co-infection was not large enough; thus, the power for evaluating the performance of *CXCL10* mRNA release assay in this population was decreased, and further validation is needed in a larger sample size of HIV co-infected population. Furthermore, no other test was simultaneously performed as a third judge method to validate the inconsistent results between *CXCL10* mRNA release assay and T-SPOT.TB test. In addition, this study did not deeply analyze the diagnostic performance of *CXCL10* mRNA release assay in other special populations, such as patients treated with immunosuppressants, patients with other complications, and children. Further validation in the abovementioned populations should be conducted in the future.

In conclusion, the present study parallelly compared the performance of novel *CXCL10* mRNA release assay and T-SPOT.TB test in the diagnosis of *M.tb* infection. The results suggested that the overall diagnostic performance of the *CXCL10* mRNA release assay was consistent with the T-SPOT.TB test, and it presented a better positive rate in HIV co-infection patients.

TABLE 4 | Performance of the *CXCL10* mRNA release assay and T-SPOT.TB assay among tuberculosis (TB patients) with HIV co-infection.

	Positive rate% (95% CI)	*p*-Value
CXCL10 mRNA release assay	92.9 (66.1–99.8)	0.029
T-SPOT.TB	61.5 (31.6–86.1)	

DATA AVAILABILITY STATEMENT

The raw data supporting the conclusions of this article will be made available by the authors, without undue reservation.

ETHICS STATEMENT

The studies involving human participants were reviewed and approved by the Ethics Committee of Beijing Chest Hospital, Capital Medical University. The patients/participants provided their written informed consent to participate in this study.

AUTHOR CONTRIBUTIONS

LP, MG, and ZZ designed the experiments. HJ, RW, QS, PR, AX, QC, XL, BD, and TC conducted the experiments. MH, GD, YC, MZ, XL, MF, and MG enrolled the subjects. LP and MH analyzed the data. LP wrote the manuscript. All authors contributed to the article and approved the submitted version.

FUNDING

This work was supported by grants from the Beijing Natural Science Foundation (7192038), National Natural Science Foundation (81902024 and 82172279), the "Beijing Municipal Administration of Hospitals" Youth Programme (QML20151501), the National Science and Technology Major Project of China (2017ZX10201301-004), the Tongzhou Yunhe Project (YH201807, YH201921, and YH202001), and the "Beijing Municipal Administration of Hospitals" Ascent Plan (DFL20181601).

ACKNOWLEDGMENTS

We thank the research nurses at the three hospitals for their work in the recruitment of participants.

SUPPLEMENTARY MATERIAL

The Supplementary Material for this article can be found online at: https://www.frontiersin.org/articles/10.3389/fmicb.2022.825413/full#supplementary-material

REFERENCES

Aabye, M. G., Ruhwald, M., Praygod, G., Jeremiah, K., Faurholt-Jepsen, M., Faurholt-Jepsen, D., et al. (2010). Potential of interferon-gamma-inducible protein 10 in improving tuberculosis diagnosis in HIV-infected patients. *Eur. Respir. J.* 36, 1488–1490. doi: 10.1183/09031936.00039010

Blauenfeldt, T., Heyckendorf, J., Graff Jensen, S., Lange, C., Drabe, C., Hermansen, T. S., et al. (2014). Development of a one-step probe based molecular assay for rapid immunodiagnosis of infection with *M. tuberculosis* using dried blood spots. *PLoS One* 9:e105628. doi: 10.1371/journal.pone.0105628

Blauenfeldt, T., Villar-Hernandez, R., Garcia-Garcia, E., Latorre, I., Holm, L. L., Muriel-Moreno, B., et al. (2020). Diagnostic accuracy of interferon gamma-induced protein 10 mRNA release assay for tuberculosis. *J. Clin. Microbiol.* 58:e00848-20. doi: 10.1128/JCM.00848-20

Cattamanchi, A., Smith, R., Steingart, K. R., Metcalfe, J. Z., Date, A., Coleman, C., et al. (2011). Interferon-gamma release assays for the diagnosis of latent tuberculosis infection in HIV-infected individuals: a systematic review and meta-analysis. *J. Acquir. Immune Defic. Syndr.* 56, 230–238. doi: 10.1097/QAI.0b013e31820b07ab

Cho, K., Cho, E., Kwon, S., Im, S., Sohn, I., Song, S., et al. (2012). Factors associated with indeterminate and false negative results of QuantiFERON-TB gold in-tube test in active tuberculosis. *Tuberc. Respir. Dis. (Seoul.)* 72, 416–425. doi: 10.4046/trd.2012.72.5.416

Cohen, A., Mathiasen, V. D., Schon, T., and Wejse, C. (2019). The global prevalence of latent tuberculosis: a systematic review and meta-analysis. *Eur. Respir. J.* 54:1900655. doi: 10.1183/13993003.00655-2019

Diel, R., Goletti, D., Ferrara, G., Bothamley, G., Cirillo, D., Kampmann, B., et al. (2011). Interferon-gamma release assays for the diagnosis of latent *Mycobacterium tuberculosis* infection: a systematic review and meta-analysis. *Eur. Respir. J.* 37, 88–99. doi: 10.1183/09031936.00115110

Diel, R., Loddenkemper, R., and Nienhaus, A. (2010). Evidence-based comparison of commercial interferon-gamma release assays for detecting active TB: a metaanalysis. *Chest* 137, 952–968. doi: 10.1378/chest.09-2350

Gao, L., Lu, W., Bai, L., Wang, X., Xu, J., Catanzaro, A., et al. (2015). Latent tuberculosis infection in rural China: baseline results of a population-based, multicentre, prospective cohort study. *Lancet Infect. Dis.* 15, 310–319. doi: 10.1016/S1473-3099(14)71085-0

Getahun, H., Matteelli, A., Chaisson, R. E., and Raviglione, M. (2015). Latent *Mycobacterium tuberculosis* infection. *N. Engl. J. Med.* 372, 2127–2135. doi: 10.1056/NEJMra1405427

Jung, J. Y., Lim, J. E., Lee, H. J., Kim, Y. M., Cho, S. N., Kim, S. K., et al. (2012). Questionable role of interferon-gamma assays for smear-negative pulmonary TB in immunocompromised patients. *J. Infect.* 64, 188–196. doi: 10.1016/j.jinf.2011.09.008

Kabeer, B. S., Raja, A., Raman, B., Thangaraj, S., Leportier, M., Ippolito, G., et al. (2011). IP-10 response to RD1 antigens might be a useful biomarker for monitoring tuberculosis therapy. *BMC Infect. Dis.* 11:135. doi: 10.1186/1471-2334-11-135

Kim, H. J., Prithiviraj, K., Groathouse, N., Brennan, P. J., and Spencer, J. S. (2013). Gene expression profile and immunological evaluation of unique hypothetical unknown proteins of *Mycobacterium leprae* by using quantitative real-time PCR. *Clin. Vaccine Immunol.* 20, 181–190. doi: 10.1128/CVI.00419-12

Kim, S., Kim, Y. K., Lee, H., Cho, J. E., Kim, H. Y., Uh, Y., et al. (2013). Interferon gamma mRNA quantitative real-time polymerase chain reaction for the diagnosis of latent tuberculosis: a novel interferon gamma release assay. *Diagn. Microbiol. Infect. Dis.* 75, 68–72. doi: 10.1016/j.diagmicrobio.2012.09.015

Lu, C., Wu, J., Wang, H., Wang, S., Diao, N., Wang, F., et al. (2011). Novel biomarkers distinguishing active tuberculosis from latent infection identified by gene expression profile of peripheral blood mononuclear cells. *PLoS One* 6:e24290. doi: 10.1371/journal.pone.0024290

Mhango, D. V., Mzinza, D. T., Jambo, K. C., and Mwandumba, H. C. (2021). New management approaches to tuberculosis in people living with HIV. *Curr. Opin. Infect. Dis.* 34, 25–33. doi: 10.1097/QCO.0000000000000704

Pai, M., Zwerling, A., and Menzies, D. (2008). Systematic review: T-cell-based assays for the diagnosis of latent tuberculosis infection: an update. *Ann. Intern. Med.* 149, 177–184. doi: 10.7326/0003-4819-149-3-200808050-00241

Pan, L., Jia, H., Liu, F., Sun, H., Gao, M., Du, F., et al. (2015). Risk factors for false-negative T-SPOT.TB assay results in patients with pulmonary and extra-pulmonary TB. *J. Infect.* 70, 367–380. doi: 10.1016/j.jinf.2014.12.018

Pawlowski, A., Jansson, M., Skold, M., Rottenberg, M. E., and Kallenius, G. (2012). Tuberculosis and HIV co-infection. *PLoS Pathog.*8:e1002464. doi: 10.1371/journal.ppat.1002464

Petrone, L., Vanini, V., Chiacchio, T., Petruccioli, E., Cuzzi, G., Schinina, V., et al. (2018). Evaluation of IP-10 in Quantiferon-Plus as biomarker for the diagnosis of latent tuberculosis infection. *Tuberculosis (Edinb.)* 111, 147–153. doi: 10.1016/j.tube.2018.06.005

Qiu, X., Xiong, T., Su, X., Qu, Y., Ge, L., Yue, Y., et al. (2019). Accumulate evidence for IP-10 in diagnosing pulmonary tuberculosis. *BMC Infect. Dis.* 19:924. doi: 10.1186/s12879-019-4466-5

Ruhwald, M., Aabye, M. G., and Ravn, P. (2012). IP-10 release assays in the diagnosis of tuberculosis infection: current status and future directions. *Expert Rev. Mol. Diagn.* 12, 175–187. doi: 10.1586/erm.11.97

Ruhwald, M., Dominguez, J., Latorre, I., Losi, M., Richeldi, L., Pasticci, M. B., et al. (2011). A multicentre evaluation of the accuracy and performance of IP-10 for the diagnosis of infection with *M. tuberculosis*. *Tuberculosis (Edinb.)* 91, 260–267. doi: 10.1016/j.tube.2011.01.001

Santin, M., Munoz, L., and Rigau, D. (2012). Interferon-gamma release assays for the diagnosis of tuberculosis and tuberculosis infection in HIV-infected adults: a systematic review and meta-analysis. *PLoS One* 7:e32482. doi: 10.1371/journal.pone.0032482

Savolainen, L. E., Kantele, A., Knuuttila, A., Pusa, L., Karttunen, R., Valleala, H., et al. (2016). Combined expression of IFN-gamma, IL-17, and IL-4 mRNA by Recall PBMCs moderately discriminates active tuberculosis from latent mycobacterium tuberculosis infection in patients with miscellaneous inflammatory underlying conditions. *Front. Immunol.* 7:239. doi: 10.3389/fimmu.2016.00239

Schmittgen, T. D., and Livak, K. J. (2008). Analyzing real-time PCR data by the comparative C(T) method. *Nat. Protoc.* 3, 1101–1108. doi: 10.1038/nprot.2008.73

Syed Ahamed Kabeer, B., Raman, B., Thomas, A., Perumal, V., and Raja, A. (2010). Role of QuantiFERON-TB gold, interferon gamma inducible protein-10 and tuberculin skin test in active tuberculosis diagnosis. *PLoS One* 5:e9051. doi: 10.1371/journal.pone.0009051

Tsuboi, H., Wakamatsu, E., Iizuka, M., Nakamura, Y., Sugihara, M., Suzuki, T., et al. (2011). Importance of serine727 phosphorylated STAT1 in IFNgamma-induced signaling and apoptosis of human salivary gland cells. *Int. J. Rheum. Dis.* 14, 86–91. doi: 10.1111/j.1756-185X.2010.01575.x

World Health Organization [WHO] (2020). *WHO Consolidated Guidelines on Tuberculosis Module 1: Prevention: Tuberculosis Preventive Treatment*. Geneva: World Health Organization.

World Health Organization [WHO] (2021). *World Health Organization: Global Tuberculosis Report 2021*. Geneva: World Health Organization.

Conflict of Interest: The authors declare that the research was conducted in the absence of any commercial or financial relationships that could be construed as a potential conflict of interest.

frontiers | Frontiers in Microbiology

ORIGINAL RESEARCH
published: 08 April 2022
doi: 10.3389/fmicb.2022.825021

QuantiFERON-TB Gold Plus Assay in Patients With Latent vs. Active Tuberculosis in a Low Incidence Setting: Level of IFN-γ, CD4/CD8 Responses, and Release of IL-2, IP-10, and MIG

*Séverine Carrère-Kremer[1], Pratt Kolia-Diafouka[1], Amandine Pisoni[1], Karine Bolloré[1], Marianne Peries[1], Sylvain Godreuil[2], Arnaud Bourdin[3], Philippe Van de Perre[1] and Edouard Tuaillon[1]**

[1] Pathogenesis and Control of Chronic and Emerging Infections, University of Montpellier, INSERM U1058, EFS, Antilles University, Montpellier University Hospital, Montpellier, France, [2] UMR MIVEGEC IRD-Centre National pour la Recherche Scientifique (CNRS), University of Montpellier, Montpellier University Hospital, Montpellier, France, [3] PhyMedExp, INSERM U1046, Centre National pour la Recherche Scientifique (CNRS) UMR 9214, University of Montpellier, Montpellier University Hospital, Montpellier, France

OPEN ACCESS

Edited by:
Axel Cloeckaert,
Institut National de Recherche pour l'Agriculture, l'Alimentation et l'Environnement (INRAE), France

Reviewed by:
Marco Pio La Manna,
University of Palermo, Italy
Piero Valentini,
Agostino Gemelli University Polyclinic (IRCCS), Italy
Danilo Buonsenso,
Catholic University of the Sacred Heart, Italy

***Correspondence:**
Edouard Tuaillon
e-tuaillon@chu-montpellier.fr

Specialty section:
This article was submitted to Infectious Agents and Disease, a section of the journal Frontiers in Microbiology

Received: 29 November 2021
Accepted: 07 March 2022
Published: 08 April 2022

Citation:
Carrère-Kremer S, Kolia-Diafouka P, Pisoni A, Bolloré K, Peries M, Godreuil S, Bourdin A, Van de Perre P and Tuaillon E (2022) QuantiFERON-TB Gold Plus Assay in Patients With Latent vs. Active Tuberculosis in a Low Incidence Setting: Level of IFN-γ, CD4/CD8 Responses, and Release of IL-2, IP-10, and MIG. Front. Microbiol. 13:825021. doi: 10.3389/fmicb.2022.825021

Objectives: We analyzed the results of the QuantiFERON Glod Plus assay (QFT) and cytokine patterns associated with active tuberculosis (ATB) among patients with positive QFT.

Methods: A total of 195 patients are QFT-positive, among which 24 had an ATB and 171 had a latent tuberculosis infection (LTBI). Interferon-gamma (IFN-γ) secretion was analyzed relative to interleukin-2 (IL-2), IFN-γ inducible protein or CXCL-10 (IP-10), and monokine induced by IFN-γ or CXCL-9 (MIG) secretion, and then compared between two sets of peptide antigens [tube 1 - cluster of differentiation 4 ($CD4^+$) T cell stimulation; tube 2 - $CD4^+$/$CD8^+$ T cell response].

Results: Higher IFN-γ responses were measured in the ATB group ($p = 0.0089$). The results showed that there was a lower ratio of tube 1/tube 2 IFN-γ concentrations in the ATB group ($p = 0.0009$), and a median [interquartile ranges (IQR)] difference between the two sets at −0.82 IU/ml (−1.67 to 0.18) vs. −0.07 IU/ml (−0.035 to 0.11, $p < 0.0001$) in the ATB group compared to the LTBI group, respectively. In addition, patients with low ratios of IL-2/IFN-γ, IP-10/IFN-γ, and MIG/IFN-γ were much more likely to have ATB.

Conclusion: High levels of IFN-γ secretion, preferential IFN-γ response in tube 2, and lower secretion of IL-2, IP-10, and MIG release relative to IFN-γ secretion were more likely observed in subjects with ATB. These features of T cell response may be helpful in low prevalence settings to suspect ATB in patients tested positive for IFN-γ release assays (IGRA).

Keywords: tuberculosis, QuantiFERON TB Gold plus®, IL-2, IP-10 (CXCL-10), latent tuberculosis, active tuberculosis, cytokines, interferon-gamma (IFN-γ)

INTRODUCTION

Tuberculosis (TB) remains a major health problem worldwide with 1.5 million deaths per year (World Health Organization [WHO], 2021). Latent TB infections (LTBI) are defined as a state of the persistent immune response against *Mycobacterium tuberculosis* (*Mtb)* without clinically manifested evidence of active TB (ATB). Out of the 1.7 billion people with latent tuberculosis (LTBI), it is estimated 5–15% will progress to ATB (Vynnycky and Fine, 2000). Interferon-gamma (IFN-γ) release assays (IGRAs) have been introduced as an alternative to the tuberculin skin test (TST) to detect the immune response against *Mtb* while avoiding *in vivo* screening tests, cross-reactions with bacille Calmette-Guérin (BCG) vaccination, and non-tuberculous mycobacterial infections (Huebner et al., 1993). Hence IGRAs are frequently preferred to TST in routine practice. The QuantiFERON assay (QFT, Qiagen) quantifies IFN-γ released after incubation of whole blood with a cocktail of peptides derived from 6-kDa Early Secretory Antigenic Target (ESAT-6) (Rv3875) and 10-kDa Culture Filtrate Antigen (CFP-10) (Rv3874) antigens. This assay is increasingly used in Europe for the screening of health care workers and for the diagnosis of those with LTBI who are at risk for progression to ATB, including persons living with HIV, persons recently exposed to ATB, children, and persons who had prior anti-TNF therapy. One of the major restrictions of IGRA is its inability to distinguish between ATB and LTBI. TB diagnosis still remains a major concern having important public health implications. The incidence of ATB is low in West European countries but the prevalence of LTBI remains significant. LTBI prevalence has been recently estimated at 6.3% in France in the general population, i.e., 4,158,000 persons (Houben and Dodd, 2016), of which 15% are health care workers exposed to ATB (Lucet et al., 2015). In comparison, 4,741 ATB were notified in 2015 in France, i.e., 7.1 per 100,000 habitants (Guthmann et al., 2017). Even when the level of clinical suspicion for TB is low, it is sometimes challenging to rule out ATB in patients tested positive for IGRA. In other words, it is a question of how to identify patients needing TB culture and molecular tests when IGRA is positive.

Several studies suggested that the accuracy of IGRA in discriminating ATB vs. LTBI disease can be improved by parallel assessment of the profile of *Mtb*-specific T cells for other cytokines secreted along with IFN-γ. Interleukin-2 (IL-2) was the most extensively investigated alternative immunological biomarker (Hur et al., 2015; Wergeland et al., 2016; Won et al., 2017; La Manna et al., 2018; Lesosky et al., 2019). IFN-γ inducible protein or CXCL-10 (IP-10) (Jeong et al., 2015; Wergeland et al., 2016; Villar-Hernández et al., 2017) and monokine induced by IFN-γ or CXCL-9 (MIG) (Frahm et al., 2011; Carrère-Kremer et al., 2016) have also been highly analyzed. The pattern of T helper cell type 1 (Th1)-pro-inflammatory cytokines could improve the sensitivity for ATB diagnosis alone (Biselli et al., 2010; Borgström et al., 2012; Biraro et al., 2016) or combined with IGRA results (Suter-Riniker et al., 2011; Carrère-Kremer et al., 2016), but the conclusions of the studies were sometimes conflicting. Authors have also suggested that a strong IFN-γ response of cluster of differentiation 8 ($CD8^+$) T cells stimulated by ESAT-6 and CFP-10 may be associated with ATB (Nikolova et al., 2013; Rozot et al., 2013). Qiagen company launched the latest generation of a QFT assay in 2015 (QuantiFERON-TB Gold Plus) including an additional new set of peptides designed to elicit both $CD8^+$ and $CD4^+$ T cell responses (Collins and Kaufmann, 2001; Day et al., 2011).

We previously reported that the detection of a high number of IFN-γ secreting cells using T-SPOT test and an impaired capacity of multi-cytokine release measured by a multiplex microbeads-based method had both appeared as signatures of ATB in a low prevalence setting (Carrère-Kremer et al., 2016). In this study, we assessed the IL-2, IP-10, and MIG response relative to IFN-γ secretion in patients with ATB and LTBI. The IFN-γ secretion in QFT Plus tube 1 containing peptides, which was designed to stimulate $CD4^+$ T cell response, was also compared to tube 2 peptides, which was designed to elicit both $CD4^+$/$CD8^+$ T cell response.

MATERIALS AND METHODS

Patients and Samples

This case-control study was conducted in the Montpellier University Hospital (France) in outpatients and hospitalized adults. Subjects were enrolled based on clinical presentation and their positive IGRA result. Samples were collected at diagnosis, before initiation of any tuberculosis treatment, or no later than 7 days after tuberculosis diagnosis. People living with HIV and immunocompromised subjects were excluded from the study. The status ATB vs. LTBI was established on *Mtb* culture results, CT scan, and after multidisciplinary chart review based on clinical presentations and outcomes. The study was performed in accordance with the guidelines of the Helsinki Declaration and was approved by the local ethics committee (Sud-Méditerrannée-III, France, NCT02898623).

Laboratory Methods

QuantiFERON-Tb Gold Plus Assay

The assay was performed according to the manufacturer's instructions (Qiagen, Darmstadt, Germany). Briefly, 1 ml of whole blood was drawn into the three QFT tubes coated with saline (Nil Control), which were peptide cocktails simulating ESAT-6, CFP-10 (*Mtb* antigens), or phytohemagglutinin (Mitogen Control), and incubated at 37°C. Following 20 h incubation, the plasma was harvested from each tube to determine the IFN-γ concentration. The highest value between the QTF tube 1 (TB1) and tube 2 (TB2) was retained for comparison between LTBI and ATB groups.

Abbreviations: ATB, active tuberculosis infection; AUC, areas under the curve; BCG, bacille Calmette-Guérin; IFN-γ, interferon-gamma; IL-2, interleukin-2; IGRA, interferon-gamma release assays; IP-10, IFN-γ inducible protein or CXCL-10; LTBI, latent tuberculosis Infection; MIG, monokine induced by IFN-γ or CXCL-9; MTB, *Mycobacterium tuberculosis*; QFT, QuantiFERON; TB, tuberculosis; TB1, Tube 1; TB2, Tube 2; TST, tuberculin skin test.

ELISA

Interleukin-2, IP-10, and MIG secretion were quantitated in supernatants of QFT Plus tube 1 and negative control tube (Nil) using Duoset ELISA Development kits for (Bio-Techne, MN, United States). The supernatant was diluted at 1:2 for all cytokines except 1:10 for IP-10 measurement. Levels were obtained by subtracting the Nil from the TB1 levels. Results were expressed in pg/ml.

Statistical Analysis

Results were analyzed using GraphPad Prism 6 (GraphPad Software, La Jolla, CA, United States) and SAS 9.4 (SAS/STAT Software, Cary, NC, United States). The median concentration of IFN-γ in paired TB1 and TB2 was compared using a Wilcoxon signed-rank test. The median cytokine levels [interquartile ranges (IQR)] of the ATB and LTBI groups were compared using the non-parametric Wilcoxon Mann–Whitney test. A p-value < 0.05 was considered significant. The receiver operating characteristics (ROC) curves were constructed by plotting the true positive rate (ATB samples; sensitivity) against the false positive (LTBI samples; 1-specificity). Areas under the curve (AUCs) were calculated along with their 95% CIs. Cut-offs for cytokines were determined using the Youden index, which was defined as sensitivity + specificity-1, and a visual appreciation on scatter plots. With these cut-offs, crude and adjusted odds ratios (ORs) were calculated using logistic regression. Multivariate analysis was not performed since parameters were all generated based on IFN-γ secretion (IFN-γ secretion, cytokines/IFN-γ ratios, and IFN-γ in TB1 vs. TB2).

RESULTS

Patients Characteristics

A total of 195 patients who tested positive with QFT were enrolled, among which 24 (12%) had an ATB and 171 (88%) had an LTBI. Clinical characteristics of the patients are shown in **Table 1**.

TABLE 1 | Patients' characteristics.

Characteristic	ATB	LTBI
Numbers of patients	24*	171
Median age in year (IQR)	38 (29–58)	47 (32–62)
Number of females (%)	10 (42%)	92 (53%)
IFN-g [IU/ml, median (IQR)]	5.34 (1.15–8.9)	1.24 (0.69–4.1)
Smear positive	5	0
Culture positive	24	0

**TB localization: pulmonary localization (n = 15); pulmonary + extra pulmonary (n = 8); 1 extra pulmonary.*

A High Value of IFN-γ Is Associated With an Increased Risk of Active Tuberculosis

Higher levels of IFN-γ secretion were measured in the ATB group, median (IQR): 5.34 IU/ml (1.09–9.15) compared to patients with LTBI 1.24 IU/ml (0.69–4.21), $p = 0.0089$ (**Figure 1A**). ROC curves were established to evaluate the capacity of the IFN-γ secretion in order to distinguish ATB and LTBI in our population (**Figure 1B**). The AUC of IFN-γ secretion was 0.67 (95% CI 0.53–0.79). Based on the Youden index, we determined an optimal cut-off value at 8 IU/ml corresponding to a specificity of 92% and a sensitivity of 38%. By selecting patients with a QFT value greater than 8 IU/ml, 9 out of 24 (37.5%) from the ATB group and 13 out of 171 (7.6%) from the LTBI group had results above this cut-off, which led to OR = 7.8 for ATB (**Table 2**).

A Stronger Response in the Second QTF Antigen Tube Compared to the First Tube Is Associated With Active Tuberculosis

The concentrations of IFN-γ in supernatants were compared after $CD4^+$ peptides stimulation (TB1) and $CD4^+/CD8^+$ peptides stimulation (TB2). The contribution of $CD8^+$ T-cell to IFN-γ secretion was first expressed as a ratio of IFN-γ TB1/TB2 concentration (**Figure 2A**). A lower ratio was observed in the ATB group compared to the LTBI group [median (IQR):0.77

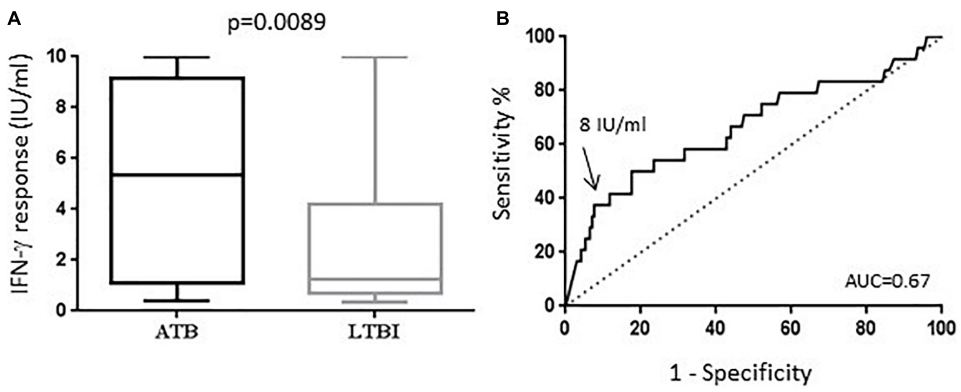

FIGURE 1 | QFT results for discrimination between active and latent tuberculosis. **(A)** The level of IFN-γ in ESAT-6, CFP-10 simulated T cells was quantified by the QFT assay from blood samples of 24 patients with ATB (black boxplot) and 171 patients with LTBI (gray boxplot). The median, IQR, 10th and 90th is shown in boxplots of each group. The p-value was calculated by the Mann–Whiteny U test. **(B)** The ROC curve shows sensitivity vs. specificity for IFN-γ in differentiating the ATB from LTBI group. The AUC and a threshold at 8 IU/ml are indicated in the graph.

TABLE 2 | Concentrations in pg/ml of cytokines secreted by T cells in QuantiFERON (QFT) supernatants after ESAT-6, CFP-10 stimulation in 24 subjects with active tuberculosis (ATB) and 171 with latent TB infection (LTBI).

	ATB pg/ml [median (IQR)]	LTBI pg/ml [median (IQR)]	*p*-value
IL-2	163 (33–456)	85 (10–290)	$p = 0.128$
IP-10	2907 (997–6955)	4416 (2000–6849)	$p = 0.631$
MIG	844 (379–1524)	948 (267–1806)	$p = 0.810$

LOD, the limit of detection; n, number of values above detection level; nsd, non-significantly different. ATB, active tuberculosis; LTBI, latent tuberculosis infection; IQR, interquartile range.

(0.69–0.91) vs. 0.96, (0.82–1.08; $p = 0.0009$), respectively]. The difference was also estimated by subtracting the quantitative value of the TB2 to TB1 (**Figure 2B**). We observed the largest difference between the two sets of peptide antigens in the ATB group compared to LTBI, with a median (IQR) difference of −0.82 IU/ml (−1.67 to 9.18), vs. −0.07 IU/ml (−0.035 to 0.11; $p < 0.0001$), respectively.

Cytokine Association Highlights Active Tuberculosis Risk Groups

QuantiFERON supernatants from the tube containing antigens dedicated to $CD4^+$ T cell stimulation (TB1) were tested by ELISA. IL-2, IP-10, and MIG concentrations were not found significantly different between the two groups (**Table 2**).

The ratios of IL-2, IP-10, and MIG to IFN-γ were significantly lower in the ATB group than in LTBI group (**Figures 3A,C,E**). The indices for ATB and LTBI were respectively 43.6 (26.5–110.3) vs. 66.7 (47.3–115.1) for IL-2 ($p = 0.091$), 1298.6 (572.8–1863.5) vs. 4383.8 (1065.7–4326.7) for IP-10 ($p = 0.00932$), and 201 (112–476) vs. 502 (264–1052) for MIG ($p = 0.00288$).

Using ROC curves, AUC were 0.63, 0.63, and 0.66 for IL-2/IFN-γ, IP-10/IFN-γ, and MIG/IFN-γ ratios, respectively (data not shown). Thresholds were determined using Youden indices to determine ATB risk groups with ORs (**Figure 2C,D, Table 3**).

DISCUSSION

In this study, we observed that the *Mtb*-specific T cell signature associated with ATB is characterized by a higher IFN-γ cell response, a significant $CD8^+$ T cell response detectable in the second QTF-Plus tube, and a preferential IFN-γ production relative to IL-2, IP-10, and MIG secretions. IL-2, IP-10, and MIG responses to peptide antigen stimulation were assessed using ratios of cytokine productions measured by ELISA relative to IFN-γ secretion. We observed that IL-2, IP-10, and MIG indices were lower in the ATB group. Hence, low IL-2/IFN-γ, MIG/IFN-γ, and IP-10/IFN-γ ratios were associated with ATB with ORs

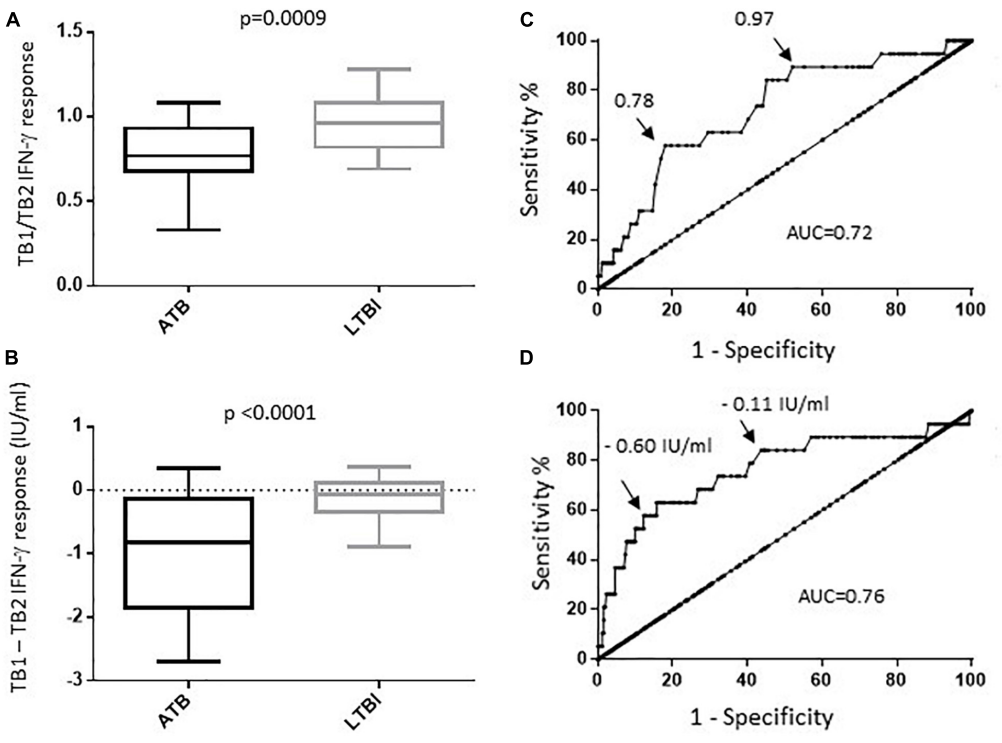

FIGURE 2 | Comparison of IFN-γ response in QTF tube 1 versus tube 2. Tube 1 (TB1) contain ESAT6 and CFP10 peptides designed to stimulated TB specific $CD4^+$ and $CD8^+$ T cell mediated responses. **(A)** Ratio of TB1/TB2 IFN-γ response. The median, IQR, 10th and 90th are shown in boxplots for each group. **(B)** Difference of the IFN-γ response in TB1 minus TB2 in ATB and LTBI. The median, IQR, 10th and 90th are shown in boxplots for each group. **(C)** ROC curve for TB1/TB2 IFN-γ response in differentiating ATB and LTBI. **(D)** ROC curve for TB1 minus TB2 IFN-γ response in differentiating ATB and LTBI. The AUC and tradeoff values are indicated on the ROC curves.

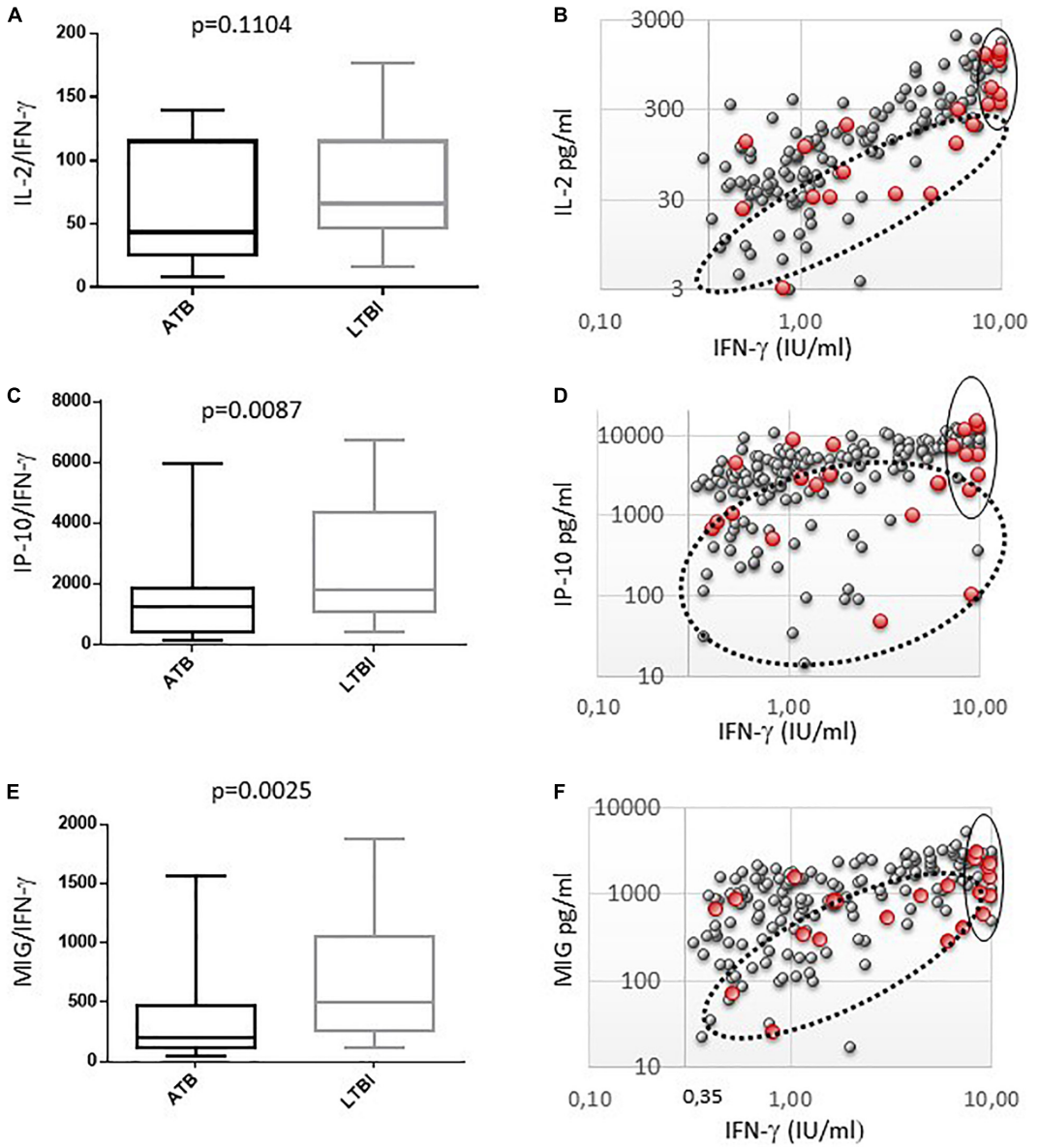

FIGURE 3 | Comparison of cytokine response in QFT supernatant between active (ATB) and latent TB infections (LTBI). **(A,C,E)** IL2, IP10 and MIG indexes (cytokine/IFN-γ) are represented, ATB (black boxplots) and LTBI (gray boxplots). The median, IQR, 10th and 90th are shown in boxplots for each group. *p*-values are calculated with the Mann–Whiteny U test. **(B,D,F)** Biparametric graphs between the levels of IFN-γ (IU/ml) and cytokines (pg/ml) in QFT supernatants. ATB are represented by black circles and LTBI by gray circles. Risk groups are circled, subjects with ATB had more tend to have lower ratios of IL-2/IFN-γ, IP-10/IFN-γ, and MIG/IFN-γ (doted line circles), and high IFN-γ response (solide line circles).

ranging from 3 to 5. The poor secretion of MIG and IP-10 that are Th1-related cytokines induced by IFN-γ may reflect the impairment of the T cell response against TB (Collins and Kaufmann, 2001). These results were in line with previous studies highlighting that IL-2/IFN-γ secretion and a relative IL-2 toward IFN-γ production were determined in ATB compared to LTBI (Suter-Riniker et al., 2011; Jeong et al., 2015; Goyal et al., 2017; Suzukawa et al., 2020). Low secretion of IL-2 compared to IFN-γ production and high frequency of single positive tumor necrosis factor alpha (TNF-α) *Mtb*-specific $CD4^+$ T cells have been associated with the defect in TB infection (Sargentini et al., 2009; Harari et al., 2011; Jenum et al., 2014). Hence, multicytokine *Mtb*-specific $CD4^+$ T cell response is thought to protect against TB, while defects in cytokine may be the hallmark of ATB. Furthermore, IGRA based on other TB antigens, such as heparin-binding hemagglutinin antigen (HBHA), emerged as a promising tool for ATB diagnosis (Sali et al., 2018).

Although commercial IGRA is not intended to provide quantitative results, we previously reported that T-SPOT results over 100 IFN-γ secreting cells per 250,000 PBMC

TABLE 3 | Crude odds ratios identifying associations between ATB and interferon-gamma (IFN-γ) from ESAT-6, CFP-10 stimulated whole blood (QFT).

Cytokines (threshold value)	OR	95% CI	*p*-value
IFN-γ (≥ 8*)	7.2	2.6–19.8	0.0001
IFN-γ TB1/TB2 (≤ 0.78)	6.6	2.5–17.2	0.0001
IFN-γ TB1–TB2 (≤ −0.60*)	8.3	3.1–22.0	<0.0001
IL-2/IFN-γ (≤ 47)	2.9	1.2–7.3	0.026
IP-10/IFN-γ (≤ 2330)	4.2	1.4–12.7	0.012
MIG/IFN-γ (≤ 285)	5.0	2.0–12.7	< 0.0006

*OR, odds ratio; CI, confidence interval; *IU/ml.*

were more frequently observed in subjects with ATB (Carrère-Kremer et al., 2016). In this study, we confirmed that a strong IFN-γ response is more frequently detected in ATB than in LTBI in our patient population. We observed that QTF positive subjects with IFN-γ levels above 8 IU/ml were much more likely to have ATB compared to subjects with IFN-γ levels from 0.35 to 7.99 IU/ml (OR > 7) (**Figure 3B,D,F**). Our results were consistent with other studies performed in low burden TB countries,(Higuchi et al., 2008; Kobashi et al., 2010; Diel et al., 2011) suggesting that levels of IFN-γ response should be taken into account in the diagnostic workup of ATB in this setting. This benefit may be attenuated in high setting countries where strong T cell responses against TB are more frequently observed (Metcalfe et al., 2010; Ling et al., 2011).

In comparison with the prior versions of the assay, the QTF-Plus assay includes a second antigen tube stimulating IFN-γ production by both $CD4^+$ plus $CD8^+$ T cells. A stronger $CD8^+$ T-cells response against ESAT-6 and CFP-10 antigens has been observed in subjects with active TB, high mycobacterial load, and recent exposure to TB compared to LTBI (Lancioni et al., 2012; Rozot et al., 2013; Allen et al., 2018). We observed a higher difference in IFN-γ production between the QFT-Plus tubes 1 and 2 in the ATB compared to LTBI. The median delta IFN-γ value between TB1 and TB2 exceeded 0.8 IU/ml in the ATB group, whereas a difference over 0.6 IU/ml has been considered as technically significant regarding the intrinsic variability of the test (Metcalfe et al., 2013; Barcellini et al., 2016; Lee et al., 2021). On the contrary, in the LTBI group, the level of IFN-γ released in TB1 and TB1 is similar, with a median difference close to zero between the two tubes, suggesting that the peptides designed to elicit immune responses from the $CD8^+$ T cells marginally contribute to IFN-γ production in the second antigen tube.

Although the differences between ATB and LTBI groups were statistically significant, an important overlap between these groups was observed when we closely looked at their differences between the cytokine indices. Our studies were not dedicated to validating methods to distinguish ATB from LTBI in clinical practice. However, our results suggested that a better analysis of cytokine profile of T cell response against *Mtb* could provide valuable information about the equilibrium between host and pathogen and may be helpful to evaluate the risk of TB reactivation of ATB among IGRA positive patients.

In our two studies performed on IGRAs (T-SPOT and QuantiFERON), subjects were enrolled on a positive IGRA result. However, comparison between cytokine results using multiplex assay and ELISA is difficult because the two methods used different capture and reporter antibodies, as well as similar diluents and serum blockers, neither some quantity of biological compounds. In addition, while concordance is generally good when using cell supernatants, it is much less robust when using serum or plasma samples (Prabhakar et al., 2004).

Our study has several limitations which are as follows: (i) nine subjects only had extra-pulmonary TB; (ii) the number of subjects with ATB did not permit us to assess the possible association between TB localization, or delay from symptom onset, and cytokine patterns; (iii) we did not assess QTF response and cytokine patterns throughout TB treatment; (iv) we did not enroll ATB subject who tested negative for QTF when according to a recent meta-analysis, 8.6% (95 CI, 12.5–5.8%) of subjects with ATB tested negative for QTF Gold Plus assay (Oh et al., 2021); (v) our results cannot be extrapolated to the pediatric population (Basu Roy et al., 2020; Buonsenso et al., 2020).

In conclusion, giving attention to the level of IFN-γ response and TB1 vs. TB2 response, as well as analyzing cytokine response based on indices of IL-2, MIG, and IP-10 to IFN-γ in QFT supernatants, allowed to define profiles of T cell response that are more likely observed in ATB. In combination with other biological and clinical parameters, these approaches may be helpful to identify QTF-positive patients in whom microbiological tests and radiological examinations would be requested to rule out or confirm ATB.

DATA AVAILABILITY STATEMENT

The raw data supporting the conclusions of this article will be made available by the authors, without undue reservation.

ETHICS STATEMENT

The studies involving human participants were reviewed and approved by the Sud-Méditerrannée-III, France, NCT02898623. The patients/participants provided their written informed consent to participate in this study.

AUTHOR CONTRIBUTIONS

SC-K, AP, KB, and ET: experimental work-up. MP, SG, and PK-D: data collection and statistical analyses. SC-K, PK-D, PV, ET, and AB: manuscript preparation and review. ET and SC-K: study design. All authors contributed to the article and approved the submitted version.

FUNDING

This research was supported by Institut National de la Santé et de la Recherche Médicale (INSERM) U1058, Montpellier, Montpellier University Hospital.

REFERENCES

Allen, N. P., Swarbrick, G., Cansler, M., Null, M., Salim, H., Miyamasu, M., et al. (2018). Characterization of specific CD4 and CD8 T-cell responses in QuantiFERON TB Gold-Plus TB1 and TB2 tubes. *Tuberculosis* 113, 239–241. doi: 10.1016/j.tube.2018.10.014

Barcellini, L., Borroni, E., Brown, J., Brunetti, E., Codecasa, L., Cugnata, F., et al. (2016). First independent evaluation of QuantiFERON-TB Plus performance. *Eur. Respir. J.* 47, 1587–1590. doi: 10.1183/13993003.02033-2015

Basu Roy, R., Thee, S., Blázquez-Gamero, D., Falcón-Neyra, L., Neth, O., Noguera-Julian, A., et al. (2020). Performance of immune-based and microbiological tests in children with tuberculosis meningitis in Europe: a multicentre Paediatric Tuberculosis Network European Trials Group (ptbnet) study. *Eur. Respir. J.* 56:1902004. doi: 10.1183/13993003.02004-2019

Biraro, I. A., Kimuda, S., Egesa, M., Cose, S., Webb, E. L., Joloba, M., et al. (2016). The Use of Interferon Gamma Inducible Protein 10 as a Potential Biomarker in the Diagnosis of Latent Tuberculosis Infection in Uganda. *PLoS One* 11:e0146098. doi: 10.1371/journal.pone.0146098

Biselli, R., Mariotti, S., Sargentini, V., Sauzullo, I., Lastilla, M., Mengoni, F., et al. (2010). Detection of interleukin-2 in addition to interferon-gamma discriminates active tuberculosis patients, latently infected individuals, and controls. *Clin. Microbiol. Infect.* 16, 1282–1284. doi: 10.1111/j.1469-0691.2009.03104.x

Borgström, E., Andersen, P., Atterfelt, F., Julander, I., Källenius, G., Maeurer, M., et al. (2012). Immune responses to ESAT-6 and CFP-10 by FASCIA and multiplex technology for diagnosis of M. tuberculosis infection; IP-10 is a promising marker. *PLoS One* 7:e43438. doi: 10.1371/journal.pone.0043438

Buonsenso, D., Delogu, G., Perricone, C., Grossi, R., Careddu, A., De Maio, F., et al. (2020). Accuracy of QuantiFERON-TB Gold Plus Test for Diagnosis of Mycobacterium tuberculosis Infection in Children. *J Clin Microbiol.* 58, e272–e220. doi: 10.1128/JCM.00272-20

Carrère-Kremer, S., Rubbo, P.-A., Pisoni, A., Bendriss, S., Marin, G., Peries, M., et al. (2016). High IFN-γ Release and Impaired Capacity of Multi-Cytokine Secretion in IGRA Supernatants Are Associated with Active Tuberculosis. *PLoS One* 11:e0162137. doi: 10.1371/journal.pone.0162137

Collins, H. L., and Kaufmann, S. H. (2001). The many faces of host responses to tuberculosis. *Immunology* 103, 1–9. doi: 10.1046/j.1365-2567.2001.01236.x

Day, C. L., Abrahams, D. A., Lerumo, L., Janse van Rensburg, E., Stone, L., O'rie, T., et al. (2011). Functional capacity of Mycobacterium tuberculosis-specific T cell responses in humans is associated with mycobacterial load. *J. Immunol.* 187, 2222–2232. doi: 10.4049/jimmunol.1101122

Diel, R., Loddenkemper, R., Niemann, S., Meywald-Walter, K., and Nienhaus, A. (2011). Negative and positive predictive value of a whole-blood interferon-γ release assay for developing active tuberculosis: an update. *Am. J. Respir. Crit. Care Med.* 183, 88–95. doi: 10.1164/rccm.201006-0974OC

Frahm, M., Goswami, N. D., Owzar, K., Hecker, E., Mosher, A., Cadogan, E., et al. (2011). Discriminating between latent and active tuberculosis with multiple biomarker responses. *Tuberc. Edinb. Scotl.* 91, 250–256. doi: 10.1016/j.tube.2011.02.006

Goyal, N., Kashyap, B., Singh, N. P., and Kaur, I. R. (2017). Comparative Diagnostic Utility of Neopterin and IFN-γ/IL-2 in Extrapulmonary Tuberculosis. *Indian J. Clin. Biochem.* 32, 453–458. doi: 10.1007/s12291-016-0624-3

Guthmann, J. P., Aït Belghiti, F., and Lévy-Bruhl, D. (2017). Tuberculosis epidemiology in France in 2015: impact of the suspension of BCG mandatory vaccination on child tuberculosis, 2007-2015. *Bull. Epidemiol. Hebd.* 7, 116–126.

Harari, A., Rozot, V., Bellutti Enders, F., Perreau, M., Stalder, J. M., Nicod, L. P., et al. (2011). Dominant TNF-α+ Mycobacterium tuberculosis-specific CD4+ T cell responses discriminate between latent infection and active disease. *Nat. Med.* 17, 372–376. doi: 10.1038/nm.2299

Higuchi, K., Harada, N., Fukazawa, K., and Mori, T. (2008). Relationship between whole-blood interferon-gamma responses and the risk of active tuberculosis. *Tuberc. Edinb. Scotl.* 88, 244–248. doi: 10.1016/j.tube.2007.11.009

Houben, R. M., and Dodd, P. J. (2016). The Global Burden of Latent Tuberculosis Infection: A Re-estimation Using Mathematical Modelling. *PLoS Med.* 13:e1002152. doi: 10.1371/journal.pmed.1002152

Huebner, R. E., Schein, M. F., and Bass, J. B. (1993). The tuberculin skin test. *Clin. Infect. Dis.* 17, 968–975.

Hur, Y. G., Kang, Y. A., Jang, S. H., Hong, J. Y., Kim, A., Lee, S. A., et al. (2015). Adjunctive biomarkers for improving diagnosis of tuberculosis and monitoring therapeutic effects. *J. Infect.* 70, 346–355. doi: 10.1016/j.jinf.2014.10.019

Jenum, S., Grewal, H. M. S., Hokey, D. A., Kenneth, J., Vaz, M., Doherty, T. M., et al. (2014). The frequencies of IFNγ+IL2+TNFα+ PPD-specific CD4+CD45RO+ T-cells correlate with the magnitude of the QuantiFERON® gold in-tube response in a prospective study of healthy indian adolescents. *PLoS One* 9:e101224. doi: 10.1371/journal.pone.0101224

Jeong, Y. H., Hur, Y. G., Lee, H., Kim, S., Cho, J. E., Chang, J., et al. (2015). Discrimination between active and latent tuberculosis based on ratio of antigen-specific to mitogen-induced IP-10 production. *J. Clin. Microbiol.* 53, 504–510. doi: 10.1128/JCM.02758-14

Kobashi, Y., Shimizu, H., Ohue, Y., Mouri, K., Obase, Y., Miyashita, N., et al. (2010). Comparison of T-cell interferon-gamma release assays for Mycobacterium tuberculosis-specific antigens in patients with active and latent tuberculosis. *Lung* 188, 283–287. doi: 10.1007/s00408-010-9238-3

La Manna, M. P., Orlando, V., Li Donni, P., Sireci, G., Di Carlo, P., Cascio, A., et al. (2018). Identification of plasma biomarkers for discrimination between tuberculosis infection/disease and pulmonary non tuberculosis disease. *PLoS One* 13:e0192664. doi: 10.1371/journal.pone.0192664

Lancioni, C., Nyendak, M., Kiguli, S., Zalwango, S., Mori, T., Mayanja-Kizza, H., et al. (2012). CD8+ T cells provide an immunologic signature of tuberculosis in young children. *Am. J. Respir. Crit. Care Med.* 185, 206–212. doi: 10.1164/rccm.201107-1355OC

Lee, J. K., Lee, H. W., Heo, E. Y., Yim, J. J., and Kim, D. K. (2021). Comparison of QuantiFERON-TB Gold Plus and QuantiFERON-TB Gold In-Tube tests for patients with active and latent tuberculosis: A prospective cohort study. *J. Infect. Chemother.* 27, 1694–1699. doi: 10.1016/j.jiac.2021.08.003

Lesosky, M., Rangaka, M. X., Pienaar, C., Coussens, A. K., Goliath, R., Mathee, S., et al. (2019). Plasma Biomarkers to Detect Prevalent or Predict Progressive Tuberculosis Associated With Human Immunodeficiency Virus-1. *Clin. Infect. Dis.* 69, 295–305. doi: 10.1093/cid/ciy823

Ling, D. I., Pai, M., Davids, V., Brunet, L., Lenders, L., Meldau, R., et al. (2011). Are interferon-γ release assays useful for diagnosing active tuberculosis in a high-burden setting? *Eur. Respir. J.* 38, 649–656. doi: 10.1183/09031936.00181610

Lucet, J. C., Abiteboul, D., Estellat, C., Roy, C., Chollet-Martin, S., Tubach, F., et al. (2015). Interferon-γ release assay vs. tuberculin skin test for tuberculosis screening in exposed healthcare workers: a longitudinal multicenter comparative study. *Infect. Control Hosp. Epidemiol.* 36, 569–574. doi: 10.1017/ice.2015.19

Metcalfe, J. Z., Cattamanchi, A., McCulloch, C. E., Lew, J. D., Ha, N. P., Graviss, E. A., et al. (2013). Test variability of the QuantiFERON-TB gold in-tube assay in clinical practice. *Am. J. Respir. Crit. Care Med.* 187, 206–211. doi: 10.1164/rccm.201203-0430OC

Metcalfe, J. Z., Cattamanchi, A., Vittinghoff, E., Ho, C., Grinsdale, J., Hopewell, P. C., et al. (2010). Evaluation of quantitative IFN-gamma response for risk stratification of active tuberculosis suspects. *Am. J. Respir. Crit. Care Med.* 181, 87–93. doi: 10.1164/rccm.200906-0981OC

Nikolova, M., Markova, R., Drenska, R., Muhtarova, M., Todorova, Y., Dimitrov, V., et al. (2013). Antigen-specific CD4- and CD8- positive signatures in different phases of Mycobacterium tuberculosis infection. *Diagn. Microbiol. Infect. Dis.* 75, 277–281. doi: 10.1016/j.diagmicrobio.2012.11.023

Oh, C. E., Ortiz-Brizuela, E., Bastos, M. L., and Menzies, D. (2021). Comparing the Diagnostic Performance of QuantiFERON-TB Gold Plus to Other Tests of Latent Tuberculosis Infection: A Systematic Review and Meta-analysis. *Clin. Infect. Dis.* 73, e1116–e1125. doi: 10.1093/cid/ciaa1822

Prabhakar, U., Eirikis, E., Reddy, M., Silvestro, E., Spitz, S., Pendley, C., et al. (2004). Validation and comparative analysis of a multiplexed assay for the simultaneous quantitative measurement of Th1/Th2 cytokines in human serum and human peripheral blood mononuclear cell culture supernatants. *J. Immunol. Meth.* 291, 27–38. doi: 10.1016/j.jim.2004.04.018

Rozot, V., Vigano, S., Mazza-Stalder, J., Idrizi, E., Day, C. L., Perreau, M., et al. (2013). Mycobacterium tuberculosis-specific CD8+ T cells are functionally and phenotypically different between latent infection and active disease. *Eur. J. Immunol.* 43, 1568–1577. doi: 10.1002/eji.201243262

Sali, M., Buonsenso, D., D'Alfonso, P., De Maio, F., Ceccarelli, M., Battah, B., et al. (2018). Combined use of Quantiferon and HBHA-based IGRA supports tuberculosis diagnosis and therapy management in children. *J. Infect.* 77, 526–533. doi: 10.1016/j.jinf.2018.09.011

Sargentini, V., Mariotti, S., Carrara, S., Gagliardi, M. C., Teloni, R., Goletti, D., et al. (2009). Cytometric detection of antigen-specific IFN-gamma/IL-2 secreting cells in the diagnosis of tuberculosis. *BMC Infect. Dis.* 9:99. doi: 10.1186/1471-2334-9-99

Suter-Riniker, F., Berger, A., Mayor, D., Bittel, P., Iseli, P., and Bodmer, T. (2011). Clinical significance of interleukin-2/gamma interferon ratios in Mycobacterium tuberculosis-specific T-cell signatures. *Clin. Vaccine Immunol.* 18, 1395–1396. doi: 10.1128/CVI.05013-11

Suzukawa, M., Takeda, K., Akashi, S., Asari, I., Kawashima, M., Ohshima, N., et al. (2020). Evaluation of cytokine levels using QuantiFERON-TB Gold Plus in patients with active tuberculosis. *J. Infect.* 80, 547–553. doi: 10.1016/j.jinf.2020.02.007

Villar-Hernández, R., Latorre, I., Mínguez, S., Díaz, J., García-García, E., Muriel-Moreno, B., et al. (2017). Use of IFN-γ and IP-10 detection in the diagnosis of latent tuberculosis infection in patients with inflammatory rheumatic diseases. *J. Infect.* 75, 315–325. doi: 10.1016/j.jinf.2017.07.004

Vynnycky, E., and Fine, P. E. (2000). Lifetime risks, incubation period, and serial interval of tuberculosis. *Am. J. Epidemiol.* 152, 247–263. doi: 10.1093/aje/152.3.247

Wergeland, I., Assmus, J., and Dyrhol-Riise, A. M. (2016). Cytokine Patterns in Tuberculosis Infection; IL-1ra, IL-2 and IP-10 Differentiate Borderline QuantiFERON-TB Samples from Uninfected Controls. *PLoS One* 11:e0163848. doi: 10.1371/journal.pone.0163848

Won, E. J., Choi, J. H., Cho, Y. N., Jin, H. M., Kee, H. J., Park, Y. W., et al. (2017). Biomarkers for discrimination between latent tuberculosis infection and active tuberculosis disease. *J. Infect.* 74, 281–293. doi: 10.1016/j.jinf.2016.11.010

World Health Organization [WHO]. (2021). *Global Tuberculosis Report 2021*. Geneva: World Health Organization.

Conflict of Interest: The authors declare that the research was conducted in the absence of any commercial or financial relationships that could be construed as a potential conflict of interest.

Publisher's Note: All claims expressed in this article are solely those of the authors and do not necessarily represent those of their affiliated organizations, or those of the publisher, the editors and the reviewers. Any product that may be evaluated in this article, or claim that may be made by its manufacturer, is not guaranteed or endorsed by the publisher.

frontiers | Frontiers in Microbiology

ORIGINAL RESEARCH
published: 25 April 2022
doi: 10.3389/fmicb.2022.847479

Effectiveness of Endobronchial Ultrasound-Guided Transbronchial Biopsy Combined With Tissue Culture for the Diagnosis of Sputum Smear-Negative Pulmonary Tuberculosis

*Ching-Kai Lin[1,2,3], Hung-Jen Fan[1,4], Kai-Lun Yu[3], Lih-Yu Chang[3], Yueh-Feng Wen[2,3], Li-Ta Keng[3] and Chao-Chi Ho[2]**

[1] Department of Medicine, National Taiwan University Cancer Center, Taipei City, Taiwan, [2] Department of Internal Medicine, National Taiwan University Hospital, Taipei City, Taiwan, [3] Department of Internal Medicine, National Taiwan University Hsin-Chu Hospital, Hsinchu, Taiwan, [4] Department of Internal Medicine, National Taiwan University Biomedical Park Hospital, Hsinchu, Taiwan

OPEN ACCESS

Edited by:
Xiao-Yong Fan,
Fudan University, China

Reviewed by:
Chih-hsi Kuo,
Chang Gung Memorial Hospital, Taiwan
Daisuke Minami,
Hosoya Hospital, Japan

***Correspondence:**
Chao-Chi Ho
ccho1203@ntu.edu.tw

Specialty section:
This article was submitted to Infectious Agents and Disease, a section of the journal Frontiers in Microbiology

Received: 02 January 2022
Accepted: 24 February 2022
Published: 25 April 2022

Citation:
Lin C-K, Fan H-J, Yu K-L, Chang L-Y, Wen Y-F, Keng L-T and Ho C-C (2022) Effectiveness of Endobronchial Ultrasound-Guided Transbronchial Biopsy Combined With Tissue Culture for the Diagnosis of Sputum Smear-Negative Pulmonary Tuberculosis. Front. Microbiol. 13:847479. doi: 10.3389/fmicb.2022.847479

Background: Microorganisms of tuberculosis (TB) are frequently difficult to identify from the airway specimen; therefore, lung biopsy for further histologic and microbiologic study is required. Endobronchial ultrasound-guided transbronchial biopsy (EBUS-TBB) is used for the diagnosis of pulmonary malignancy, but is rarely in the TB population. The purpose of this study was to verify the effectiveness and safety of EBUS-TBB with histologic study and tissue culture in the diagnosis of sputum smear-negative pulmonary TB.

Methods: Patients who underwent EBUS-TBB with histologic study and TB tissue culture for clinically suspected, but sputum smear-negative pulmonary TB from January 2016 to December 2018, were included. The accuracy of each diagnostic modality was calculated, respectively. Factors that might influence the positive rate of TB culture (washing fluid and tissue specimen) were also evaluated.

Results: One hundred sixty-one patients who underwent EBUS-TBB for clinically suspected, but sputum smear-negative pulmonary TB, were enrolled, and 43 of them were finally diagnosed as having pulmonary TB. The sensitivity of washing fluid (a combination of smear, culture, and polymerase chain reaction for TB) and tissue specimen (a combination of pathology and tissue culture) *via* EBUS-TBB for TB diagnosis were 48.8 and 55.8%, respectively. The sensitivity for TB diagnosis would be elevated to 67.4% when both washing fluid and tissue specimens are used. The positive TB culture rate would not statistically increase with a combination of tissue specimens and washing fluid. Univariate analysis revealed that TB microorganisms

would be more easily cultivated when lesions had an abscess or cavity on the computed tomography (CT) image (presence vs. absence; 62.5 vs. 26.3%, $p = 0.022$), heterogeneous echogenicity on the EBUS finding (heterogeneous vs. homogeneous; 93.3 vs. 21.4%, $p = 0.001$), or a necrotic pattern *via* histologic study (presence vs. absence; 70.6 vs. 30.8%, $p = 0.013$). Heterogeneous echogenicity in the EBUS finding was the independent predictor according to the results of multivariate analysis. None of our patients encountered major adverse events or received further intensive care after EBUS-TBB.

Conclusion: Endobronchial ultrasound-guided transbronchial biopsy is safe and effective for use in diagnosing sputum smear-negative pulmonary TB. EBUS echoic feature is also a predictor of the positive TB culture rate in pulmonary TB. However, tissue culture *via* EBUS-TBB has little effect in improving the positive TB culture rate.

Keywords: echoic feature, endobronchial ultrasound-guided transbronchial biopsy, positive tuberculosis culture rate, sputum smear-negative pulmonary tuberculosis, tissue culture

INTRODUCTION

Tuberculosis (TB) is one of the most prevalent infectious diseases in the world, and lung nodules or lung consolidation are common manifestations (Nachiappan et al., 2017). These representations are also frequently seen in other infectious diseases and pulmonary malignancies; therefore, identifying the microorganism is an essential step in the diagnosis of pulmonary TB and in devising an appropriate treatment plan. Analyzing a smear, culture, or polymerase chain reaction for TB (TB-PCR) of the sputum is the basic diagnostic method (Hopewell et al., 2006). Flexible bronchoscopy for extracting the distal airway specimen can be considered when the patient is unable to produce expectorate. A negative microbiologic result frequently occurs, so lung biopsy for further histologic and microbiologic study is needed (Dhamija et al., 2019; Lin et al., 2020). Besides surgical biopsy, computed tomography (CT)-guided biopsy is the traditional way to perform lung lesion sampling. Due to its high complication rate, which may lead to patient morbidity and mortality, further less invasive and safer procedures are required for confirming sputum smear-negative pulmonary TB (White et al., 2000).

Endobronchial ultrasound (EBUS), a miniature ultrasound probe that is inserted through a flexible bronchoscope to scan the bronchial lumen, was first introduced in 1990 (Hürter and Hanrath, 1992). It not only confirms the location of the pulmonary lesions but also analyze their internal structure and help pulmonologists perform transbronchial biopsy (TBB) for peripheral pulmonary lesion sampling (Kurimoto et al., 2002). Previous studies have reported the high accuracy and low complication rate of EBUS in the diagnosis of pulmonary malignancy (Herth et al., 2002; Yamada et al., 2007). However, there is scant evidence as to the utility of EBUS-guided TBB (EBUS-TBB) in the diagnosis of pulmonary TB. Lung tissue obtained *via* EBUS-TBB is seldom used for tissue culture. Therefore, our aims in this study were to investigate the effectiveness of EBUS-TBB combined with histologic study and tissue culture in the diagnosis of sputum smear-negative pulmonary TB, and to evaluate the safety of EBUS-TBB in this population of patients.

MATERIALS AND METHODS

Participants

This was a retrospective chart review of patients who underwent EBUS-TBB for clinically suspected pulmonary TB, performed by pulmonologists or infectious disease physicians at the Department of Thoracic Medicine, National Taiwan University Hospital and National Taiwan University Hsin—Chu Hospital, from January 2016 to December 2018. Before undergoing EBUS-TBB, all patients with suspected sputum smear-negative pulmonary TB needed to have at least three negative Ziehl–Neelsen smear results from sputum analysis or those patients who were unable to produce expectorate. EBUS-TBB procedures without histologic study or tissue culture were excluded. Patients with an endobronchial lesion that was found during the bronchoscopic exam were also not included. Patient data regarding age, gender, immunocompromised status, and the final diagnosis were collected. The characteristics of the lesions (location, size, and CT image with a cavity/abscess pattern), antibacterial agent use prior to EBUS procedures, EBUS characteristics (echogenicity and probe location), pathologic findings, and procedure-related adverse events were also recorded. Written informed consent was obtained from each patient prior to bronchoscopy. The study was approved by the National Taiwan University Hospital Institutional Review Board (IRB #202109054RINB).

Procedures

All procedures were performed by our pulmonologists, who had at least 2 years of experience in EBUS, or by our senior pulmonary fellow doctors supervised by an experienced pulmonologist. The procedure was performed with a flexible bronchoscopy (BF-Q290; Olympus Co., Tokyo, Japan) combined with a 20 MHz radial-EBUS (UM-S20-20R; Olympus Co., Tokyo, Japan). After

premedication with a lidocaine local anesthesia, with or without intravenous midazolam and fentanyl for conscious sedation, the scope was passed through the nasal route. The EBUS probe was inserted through the working channel of the scope into the suspected target bronchus based on the CT image. After confirming the location of the lesion by EBUS, TBB with forceps was carried out for specimen collection. At least four biopsy sample materials were placed in 10% formalin for routine histologic evaluation. One biopsy specimen was placed in 2–3 ml of sterile normal saline for TB tissue culture. After the EBUS-TBB procedure, 25 ml of sterile normal saline was irrigated into the target bronchus, and then the washing fluid was retaken and sent to our microbiology laboratory for Gram stain, Ziehl–Neelsen smear, culture (bacterial, TB, fungal), and TB-PCR.

The diagnostic criteria of pulmonary TB were established based on pathologic evidence, microbiological analyses, or clinical follow-up. If the culture showed positive for a TB microorganism, or acid-fast bacilli or granulomatous inflammation were present in the histologic finding, or the chest CT image led the pulmonologists or infectious disease physicians to suspect a TB infection, and/or there was a response to anti-TB treatment with improvement in the image follow-up, pulmonary TB would be confirmed. Other etiologies of the pulmonary lesions were also diagnosed based on pathologic or microbiological results. When the culture was positive for bacteria, there was a response to antibacterial agent treatment with improvement in the image follow-up, and contamination or specific infections (fungal and mycobacterial)/inflammation process have been excluded, bacterial pneumonia or lung abscess would be considered.

Statistical Analysis

In our study population, the sensitivity, specificity, positive predictive value (PPV), negative predictive value (NPV), and diagnostic accuracy of each diagnostic modality (pathology, smear, culture, and TB-PCR) were calculated, respectively, *via* standard definitions. The positive TB culture rate (tissue specimen or washing fluid) was assessed for patients who had a final diagnosis of TB infection, and the definition was "a positive result for TB culture class/total TB infection class." Comparisons were made using Student's *t*-test or one-way analysis of variance (ANOVA) for continuous variables, and the χ^2 test or Fisher's exact test for categorical variables. Logistic regression identified the independent variables contributing to statistical significance. Odds ratios (OR) and their 95% confidence intervals [95% confidence (CI)] were determined to assess the contribution of significant factors. A *p*-value of less than 0.05 was considered significant. We used SPSS version 21.0 (IBM, SPSS, Chicago, IL, United States) for statistical analysis.

RESULTS

Patients and Endobronchial Ultrasound Procedures

In all, 307 patients with suspected, but sputum smear-negative pulmonary TB underwent EBUS-TBB procedures during our study period. After excluding 120 patients who had a final diagnosis of malignancy, and 26 patients who were lost to our clinical follow-up without a definite diagnosis, we finally enrolled 161 patients in our study group. About half of the study population (48.4%) was immunocompromised patients. Most of the pulmonary lesions were located at the upper lobe (34.8% in the right upper lobe and 21.1% in the left upper lobe). The mean lesion size was 40.2 mm, and 44.1% had an abscess or cavity within the lesion, as detected in the CT image. The EBUS probe arrived within the lesion in 87% of the study population, and heterogeneous echogenicity was seen in 26.1% of the lesions. Thirty-five patients received antibacterial agents before EBUS-TBB. Fifteen patients had a procedure-related adverse effect after EBUS-TBB, as follows: fever in seven patients; pneumothorax in five patients, but no need for tube drainage; bronchospasm in one patient; transient hypoxia with complete recovery in one patient; and persistent bleeding in one patient who needed instillation of a vasoactive agent and a prolonged scope wedge. None of our patients required further intensive care after the procedure (**Table 1**).

The final diagnosis revealed that 43 of the 161 patients had pulmonary TB, 10 had non-tuberculous mycobacterial infection, 18 had fungal infection, 61 had bacterial pneumonia or lung abscess, and 11 had interstitial lung disease. The remaining 18 patients had no specific pathological or microbiological diagnosis and were classified as having non-specific inflammation (**Table 2**).

Performance of Each Diagnostic Modality for Tuberculosis Diagnosis

For the accuracy of the washing fluid, the Ziehl–Neelsen smear had 2.3% sensitivity, 100% specificity, 100% PPV, 73.8% NPV, and 73.9% diagnostic accuracy. Culture for TB had 41.9% sensitivity, 100% specificity, 100% PPV, 82.5% NPV, and 84.5% diagnostic accuracy. TB-PCR had 30.2% sensitivity, 99.2% specificity, 92.9% PPV, 79.6% NPV, and 80.8% diagnostic accuracy. The combination of Ziehl–Neelsen smear, culture, and TB-PCR had 48.8% sensitivity, 100% specificity, 100% PPV, 84.3% NPV, and 86.3% diagnostic accuracy (**Table 3**).

For tissue specimen analysis, the sensitivity, specificity, PPV, NPV, and diagnostic accuracy of typical histologic findings (positive of acid-fast bacilli or granulomatous inflammation) alone were 41.9, 91.5, 64.3, 81.2, and 78.3%, respectively. The sensitivity, specificity, PPV, NPV, and diagnostic accuracy of tissue culture for TB were 27.9, 100, 100, 79.2, and 80.8%, respectively. Combining the histologic finding and tissue culture, the sensitivity, specificity, PPV, NPV, and diagnostic accuracy were 55.8, 100, 100, 86.1, and 88.2%, respectively. When washing fluid and tissue specimens were combined for the diagnosis of TB infection, the sensitivity, specificity, PPV, NPV, and diagnostic accuracy were 67.4, 100, 100, 89.4, and 91.3%, respectively (**Table 3**).

Subgroup Analysis of Patients Diagnosed With Tuberculosis Infection

Twenty-nine (67.4%) of the 43 patients who had a final diagnosis of TB infection were diagnosed *via* bronchoscopic exam. Only

TABLE 1 | Characteristics of the patients, target lesions, and endobronchial ultrasound (EBUS) procedures.

Characteristics	*N*
Number	161
Age (years old, range)	58.9 (20–93)
Male gender (%)	109 (67.7)
Immunocompromised host (%)	78 (48.4)
Hematologic disease	9 (5.6)
Solid malignancy	18 (11.2)
Other systemic disease	51 (31.7)
Diabetes mellitus with poor control	23 (14.3)
Long-term steroid use	19 (11.8)
End-stage renal disease	4 (2.5)
Liver cirrhosis	5 (3.1)
Lesion location	
Right upper lobe	56 (34.8)
Left upper lobe (left upper division and left lingual lobe)	34 (21.1)
Right middle lobe	18 (11.2)
Right lower lobe	39 (24.2)
Left lower lobe	14 (8.7)
Lesion size (mm, range)	40.2 (4–118.4)
Lesion character with abscess/cavity formation	71 (44.1)
EBUS probe location (within,%)	140 (87.0)
Echogenicity under EBUS (heterogeneous,%)	42 (26.1)
Antibacterial agent used prior to EBUS procedures	35 (21.7)
Procedure-related complications (%)	15 (9.3)
Post-procedure fever	7 (4.3)
Pneumothorax	5 (3.1)
Bronchospasm	1 (0.6)
Hypoxia	1 (0.6)
Bleeding	1 (0.6)

EBUS, endobronchial ultrasound; N, number.

TABLE 2 | Final diagnosis of the 161 patients.

Final diagnosis	*N* (%)
Mycobacterium tuberculosis	43 (26.7)
Non-tuberculous mycobacteria	10 (6.2)
Mycobacterium avium intracellulare complex	4 (2.5)
Mycobacterium kansasii	3 (1.9)
Mycobacterium abscessus	2 (1.2)
Mycobacterium gordonae	1 (0.6)
Fungus	18 (11.2)
Candida	2 (1.2)
Aspergillus	8 (5.0)
Cryptococcosis	7 (4.3)
Mucormycosis	1 (0.6)
Bacterial pneumonia/abscess	61 (37.9)
Klebsiella pneumoniae	32 (19.9)
Pseudomonas aeruginosa	12 (7.5)
Escherichia coli	9 (5.6)
Enterobacter spp.	7 (4.3)
Mycoplasma pneumoniae	1 (0.6)
Interstitial lung disease	11 (6.8)
Organizing pneumonia	7 (4.3)
Connective tissue disease associated with interstitial lung disease	2 (1.2)
Sarcoidosis	1 (0.6)
Pneumoconiosis	1 (0.6)
Non-specific inflammation	18 (11.2)

N, number.

four patients had a procedure-related adverse effect after EBUS-TBB (**Table 4**). The positive TB culture rate of washing fluid and tissue *via* EBUS-TBB were 41.9 and 27.9%, respectively. The positive culture rate of the washing fluid did not statistically improve when combining the tissue specimen for analysis ($p = 0.664$) (**Figure 1**).

We also evaluated some factors that might influence the positive rate of TB culture when using washing fluid and tissue specimens. Univariate analysis revealed that lesions with abscess or cavity patterns on CT imaging had a higher positive TB culture rate (62.5 vs. 26.3%, $p = 0.022$). A superior positive TB culture rate was also seen when heterogeneous echogenicity was detected in the EBUS study (93.3 vs. 21.4%, $p = 0.001$). If a necrotic pattern was disclosed within the histologic specimens, microorganisms would be more easily cultivated (70.6 vs. 30.8%,

TABLE 3 | Performance of diagnostic modalities for TB infection in isolation and in combination.

	Sensitivity (%)	Specificity (%)	PPV (%)	NPV (%)	Accuracy (%)
Washing fluid study					
Ziehl–Neelsen smear	2.3	100	100	73.8	73.9
TB culture	41.9	100	100	82.5	84.5
TB-PCR	30.2	99.2	92.9	79.6	80.8
Smear + culture + PCR	48.8	100	100	84.3	86.3
Tissue specimen study					
Histologic finding	41.9	91.5	64.3	81.2	78.3
TB tissue culture	27.9	100	100	79.2	80.8
Histology + tissue culture	55.8	100	100	86.1	88.2
Fluid + tissue study					
Washing fluid (smear + culture + PCR) + histologic finding + tissue culture	67.4	100	100	89.4	91.3

NPV, negative predictive value; PCR, polymerase chain reaction; PPV, positive predictive value; TB, tuberculosis.

TABLE 4 | Characteristics of the 43 patients with pulmonary TB infection.

Characteristics	*N*
Number	43
Age (years old, range)	54.9 (20–89)
Male gender (%)	32 (74.4)
Procedure-related complications (%)	4 (9.3)
Post-procedure fever	1 (2.3)
Pneumothorax	1 (2.3)
Bronchospasm	1 (2.3)
Bleeding	1 (2.3)
Final diagnostic modalities (%)	
Bronchoscopy	29 (67.4)
Endobronchial ultrasound guided-transbronchial needle aspiration	3 (7.0)
Computed tomography guided-biopsy	2 (4.7)
Image follow-up	9 (20.9)

N, number; TB, tuberculosis.

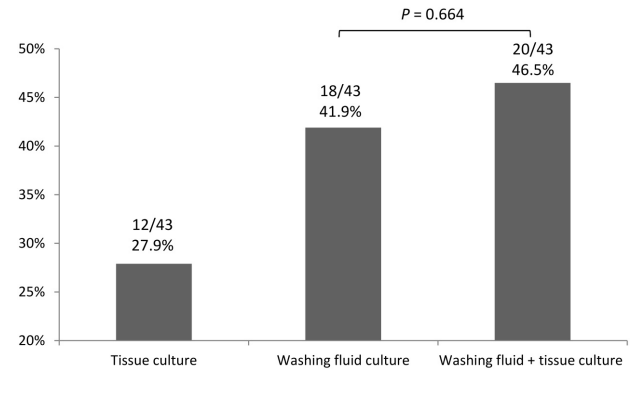

FIGURE 1 | The positive TB culture rate of washing fluid and tissue specimen *via* EBUS–TBB. EBUS–TBB, endobronchial ultrasound-guided transbronchial biopsy; TB, tuberculosis.

$p = 0.013$). We also used abscess or cavity patterns on CT imaging, heterogeneous echogenicity on EBUS study, and necrosis within the histologic specimens for multivariate analysis. Heterogeneous echogenicity was the independent factor, with an OR of 44.33 (95% CI, 3.70–530.93). The patient's immunocompromised status, the location, and size of the lesion, and the position of the probe did not affect the positive TB tissue culture rate *via* EBUS-TBB (**Table 5**).

DISCUSSION

This retrospective study showed that EBUS-TBB, with a low complication rate, improved the diagnostic accuracy of sputum smear-negative pulmonary TB. Also, when the lesions had heterogeneous echogenicity in the EBUS finding, a TB organism would be more easily cultivated.

The diagnosis of pulmonary TB infection is conventionally made *via* sputum or bronchoscopy with bronchoalveolar lavage analysis (Jacomelli et al., 2012). However, the sensitivity of bronchial washing fluid analysis seems to be insufficient for sputum smear-negative pulmonary TB. Even with a combined Ziehl–Neelsen smear, TB culture, and TB-PCR, the sensitivity was only 48.8% in our study. Tissue sampling is still essential to aid diagnostic accuracy in this population (Beck et al., 2019). An endobronchial lesion is uncommon in sputum smear-negative pulmonary TB (Jacomelli et al., 2012), therefore, some bronchoscopic techniques, such as fluoroscopy, bronchoscopic navigation, or EBUS are required to guide the peripheral lung lesion biopsy (Ishida et al., 2011; Boonsarngsuk et al., 2012; Asano et al., 2015). In the present study, we used EBUS to guide the lung biopsy. The sensitivity of tissue specimens (combined histologic and TB culture) *via* EBUS-TBB was higher than with washing fluid analysis alone. The sensitivity was also elevated to nearly 70% when both washing fluid and tissue specimens were used. We confirmed that EBUS-TBB could help increase the sensitivity for sputum smear-negative pulmonary TB diagnosis.

Image-guided procedures, such as CT-guided percutaneous lung biopsy, have a high rate of accuracy for the diagnosis of peripheral pulmonary lesions. However, pulmonary hemorrhage and pneumothorax frequently occur during the procedure, at a rate of 10-40% (White et al., 2000; Yun et al., 2018). Fatal complications, such as systemic air embolism, may even cause patient mortality (Lang et al., 2018; Sakatani et al., 2018). In the present study, less than 10% of all study participants had a procedure-related adverse effect after EBUS-TBB, and none of them needed further intensive care. Pneumothorax occurred in five patients (3.1%), and none of them required tube drainage. In Lin's study, only one patient (1%) developed pneumothorax after the EBUS procedure (Lin et al., 2009). In another study, no adverse effect was found when combining EBUS and electromagnetic navigation for pulmonary TB diagnosis (Gu et al., 2019). Infection is also a common adverse event in many invasive procedures. However, only 4.3% of our study population had new fever episode after EBUS-TBB, and all of them recovered rapidly after a short course of antibacterial agent treatment. In our institution, prophylactic antibacterial agents are not routinely used for all bronchoscopic procedures. Only 35 patients (21.7%) in our study population used antibacterial agents prior to EBUS procedures due to persisting fever and bacterial infection could not be excluded. In addition, image-guided lung sampling can obtain specimens from a single pulmonary lesion only. Unlike bronchoscopic procedures, it is difficult to collect specimens simultaneously from the target lesion and all parts of bronchial tree. We believe EBUS-TBB is safe and has a high degree of efficacy for the diagnosis of pulmonary TB.

The TB culture result not only confirms the presence of a microorganism, but also provides information on drug sensitivity, which may guide clinicians in devising an appropriate treatment plan. Some factors were thought to affect the positive rate for TB culture *via* bronchoscopic procedures. Large lesion size or patients with an immunocompromised status might be considered to have a higher TB organism burden within the lesion. In the present study, the TB culture rate using washing fluid and tissue specimen was not statistically different in these situations. The reason might be that the TB organism is not distributed evenly. In previous studies, higher TB organism burdens were usually found in central, necrotic zones of necrotizing granulomas (Radhika et al., 1989; El-Zammar and Katzenstein, 2007). In the present study, the lesions with abscess

TABLE 5 | Logistic regression analysis of factors influencing the positive TB culture rate of washing fluid and tissue specimen.

Factors	Positive TB tissue culture rate (%)		Univariate		Multivariate	
	Factor presence	Factor absence	OR (95% CI)	*p*-Value	OR (95% CI)	*p*-Value
Patient characteristics						
Immunocompromised hosts	8/20 (40)	12/23 (52.2)	0.61 (0.18–2.05)	0.426	–	–
Lesion characteristics						
Location (upper lobe)	16/35 (45.7)	4/8 (50)	0.84 (0.18–3.92)	0.827	–	–
Size (≥ 3 cm)	13/26 (50)	7/17 (41.2)	1.43 (0.42–4.91)	0.571	–	–
Abscess/cavity patterns	15/24 (62.5)	5/19 (26.3)	6.07 (1.14–32.41)	0.022*	1.07 (0.16–7.26)	0.941
EBUS characteristics						
Heterogeneous echogenicity	14/15 (93.3)	6/28 (21.4)	51.33 (5.57–472.89)	0.001*	44.33 (3.70–530.93)	0.003*
Probe within the lesion	18/37 (48.6)	2/6 (33.3)	1.90 (0.31–11.64)	0.490	–	–
Pathologic finding						
Present necrosis	12/17 (70.6)	8/26 (30.8)	5.40 (1,42–20.52)	0.013*	4.32 (0.71–26.32)	0.113

CI, confidence intervals; EBUS-TBB, endobronchial ultrasound-guided transbronchial biopsy; OR, odds ratio; TB, tuberculosis.
**Statistical significance with p-value < 0.05.*

or cavity patterns on CT imaging also had a higher positive TB culture rate. EBUS-TBB pathology showing a necrosis pattern had a significantly higher positive culture rate than those without a necrotic component (70.6 vs. 30.8%, $p = 0.013$). This result is very similar to that of our previous study, which found that a higher positive microbiologic yield will be obtained using the EBUS-TBNA procedure when the pathologic specimen shows a necrotic tissue component (Lin et al., 2020). TB organisms might be difficult to identify in external or non-necrotic parts of the lesion. Finding a proper site might influence the probability to expose TB organism in the diagnosis of pulmonary TB during bronchoscopy exam.

Tuberculosis organisms would be easier to cultivate when the lung lesions show heterogeneous echogenicity *via* the EBUS image, as in our study result. Heterogeneous echogenicity means that non-unique components, such as necrosis or cavitation, exist in the structure of the lung lesions (Kuo et al., 2011). As such, necrotic components are likely to be obtained in that part of the lung lesion with heterogeneous echogenicity, which retains a higher TB bacterial burden. In the present study, heterogeneous echogenicity in the EBUS finding was the only independent predictor according to the results of multivariate analysis ($p = 0.003$; OR of 44.33; 95% CI, 3.70–530.93). This result shows that the part of the lesion with heterogeneous echogenicity in the EBUS findings should be the better site for discovering TB organisms. To our knowledge, this was the first study to confirm the echoic feature as a predictor of the positive TB culture rate in pulmonary TB. We can even use the EBUS image pattern to guide us to a better site to diagnose pulmonary TB.

Apart from using specimens from the respiratory tract for TB culture, tissue culture *via* EBUS-TBB was also used for pulmonary TB diagnosis in our study. In previous literatures, tissue specimens obtained *via* image-guided percutaneous lung biopsy used for TB tissue culture has improved the diagnosis of pulmonary TB (Park et al., 2010; Zhao et al., 2020). However, there are a few reports on using tissue specimens *via* TBB for TB culture. Several studies have revealed that specimens obtained *via* bronchial washing were more sensitive for culture positivity than specimens obtained *via* TBB; therefore, using TBB for bacterial investigations is of limited diagnostic value (Chan et al., 1992; Sekine et al., 2017). Unlike the traditional transbronchial lung sampling method, which does not use a guiding system in the previous study, utilizing EBUS can help confirm the location of the lesions, and assist the operators in choosing a better site for biopsy. We performed EBUS-TBB for tissue culture, but the positive culture rate of TB tissue culture was relatively low. The positive culture rate of the washing fluid did not statistically improve when combining tissue specimens for analysis ($p = 0.664$). Tissue culture *via* EBUS-TBB has little effect on improving the positive TB culture rate. Moreover, the sensitivity of TB tissue culture alone was even lower than histologic findings *via* EBUS-TBB. It seems that defining granulomatous inflammation from histologic examination, but not tissue TB culture, is the main merit of the EBUS-TBB approach for diagnosing pulmonary TB. Nevertheless, two patients (4.7%) in our TB population had positive TB tissue culture results with negative washing fluid culture. In these circumstances, we believe that tissue culture is still required for clinicians to assist with pulmonary TB treatment.

Our study, however, has several limitations. First, this was a retrospective study, so there might be a risk of selection bias in our study population. For example, patients who did not undergo EBUS-TBB and those for whom specimens were not obtained for tissue culture were not enrolled. Second, the sample size was relatively small. Some special population groups, such as human immunodeficiency virus-infected hosts, who are also at risk of TB infection, were not enrolled. Although rare serious complications such as severe infection, abscess formation, hemodynamic changes, or acute respiratory events were not seen in our small study population, we are unable to determine whether these complications would not occur when the sample size is increased. Third, we did not perform brushing or use guide sheath in our institution when pulmonary infection was suspected because extra cost was needed. Previous publications revealed that TBB combined with these techniques has higher

sensitivity for the diagnosis of peripheral pulmonary lesions (Kovnat et al., 1975; Kikuchi et al., 2004; Kurimoto et al., 2004), so they are performed routinely in many institutions. Therefore, a prospective design with a comprehensive study group and various diagnostic devices is warranted. Finally, not all of our TB patients had a diagnosis based on pathologic or microbiologic evidence. Nine patients (20.9%) had the TB diagnosis based on the clinical criteria. However, all of these nine patients had typical CT image pattern and the image improved after completing the anti-TB treatment course without any antibacterial agent. In endemic areas, clinical physicians consider TB infection if a typical pathologic pattern, positive microbiologic report (Ziehl-Neelsen smear, culture, and TB-PCR), or even a typical CT image pattern is presented. We also used the image response after a complete anti-TB treatment course. We think our results are more easily applied in clinical practice.

In conclusion, EBUS-TBB improves the diagnosis of pulmonary TB. The TB organism is easier to detect in the necrotic part of the lesion; therefore, lesions with abscess/cavity patterns or heterogeneous echogenicity on EBUS findings had a higher positive TB culture rate. We believe that the EBUS image pattern with heterogeneous echogenicity can be used for guidance of TBB and collecting airway specimens when TB infection is highly suspected. However, tissue culture *via* EBUS-TBB has little effect on improving the positive TB culture rate.

DATA AVAILABILITY STATEMENT

The original contributions presented in the study are included in the article/supplementary material, further inquiries can be directed to the corresponding author.

ETHICS STATEMENT

The studies involving human participants were reviewed and approved by the study was approved by the National Taiwan University Hospital Institutional Review Board (IRB #202109054RINB). The patients/participants provided their written informed consent to participate in this study.

AUTHOR CONTRIBUTIONS

C-KL and C-CH contributed to the study concept and design, acquisition, analysis, interpretation of data, and drafting of the manuscript. C-KL, H-JF, K-LY, L-YC, Y-FW, and L-TK contributed to the data collection and manuscript review. C-KL, Y-FW, and C-CH contributed to the study concept and design, analysis and interpretation of data, and critical revision of the manuscript for important intellectual content. C-CH supervised the study. All authors read and approved the final manuscript.

REFERENCES

Asano, F., Shinagawa, N., Ishida, T., Tsuzuku, A., Tachihara, M., Kanazawa, K., et al. (2015). Virtual bronchoscopic navigation improves the diagnostic yield of radial-endobronchial ultrasound for peripheral pulmonary lesions with involved bronchi on CT. *Intern. Med*. 54, 1021–1025. doi: 10.2169/internalmedicine.54.3497

Beck, K. S., Han, D. H., Lee, K. Y., and Kim, S. J. (2019). Role of CT-guided transthoracic biopsy in the diagnosis of mycobacterial infection. *J. Investig. Med.* 67, 850–855. doi: 10.1136/jim-2018-000887

Boonsarngsuk, V., Raweelert, P., and Juthakarn, S. (2012). Endobronchial ultrasound plus fluoroscopy versus fluoroscopy-guided bronchoscopy: a comparison of diagnostic yields in peripheral pulmonary lesions. *Lung* 190, 233–237. doi: 10.1007/s00408-011-9359-3

Chan, C. H., Chan, R. C., Arnold, M., Cheung, H., Cheung, S. W., and Cheng, A. F. (1992). Bronchoscopy and tuberculostearic acid assay in the diagnosis of sputum smear-negative pulmonary tuberculosis: a prospective study with the addition of transbronchial biopsy. *Q. J. Med*. 82, 15–23. doi: 10.1016/0278-2316(90)90014-7

Dhamija, A., Ganga, V. B., Guliani, A., Raveendran, R., Verma, K., and Basu, A. K. (2019). Endobronchial ultrasound for tubercular mediastinal adenopathy and its comparison with traditional tools. *Int. J. Tuberc. Lung. Dis.* 23, 907–912. doi: 10.5588/ijtld.18.0381

El-Zammar, O. A., and Katzenstein, A. L. (2007). Pathological diagnosis of granulomatous lung disease: a review. *Histopathology* 50, 289–310. doi: 10.1111/j.1365-2559.2006.02546.x

Gu, Y., Wu, C. Y., Yu, F. G., Gui, X. W., Ma, J., Cheng, L. P., et al. (2019). Application of endobronchial ultrasonography using a guide sheath and electromagnetic navigation bronchoscopy in the diagnosis of atypical bacteriologically-negative pulmonary tuberculosis. *Ann. Transl. Med.* 7:567. doi: 10.21037/atm.2019.09.37

Herth, F. J. F., Ernst, A., and Becker, H. D. (2002). Endobronchial ultrasound-guided transbronchial lung biopsy in solitary pulmonary nodules and peripheral lesions. *Eur. Respir. J.* 20, 972–974. doi: 10.1183/09031936.02.00032001

Hopewell, P. C., Pai, M., Maher, D., Uplekar, M., and Raviglione, M. C. (2006). International standards for tuberculosis care. *Lancet Infect. Dis.* 6, 710–725. doi: 10.1016/S1473-3099(06)70628-4

Hürter, T., and Hanrath, P. (1992). Endobronchial sonography: feasibility and preliminary results. *Thorax* 47, 565–567. doi: 10.1136/thx.47.7.565

Ishida, T., Asano, F., Yamazaki, K., Shinagawa, N., Oizumi, S., Moriya, H., et al. (2011). Virtual bronchoscopic navigation combined with endobronchial ultrasound to diagnose small peripheral pulmonary lesions: a randomised trial. *Thorax* 66, 1072–1077. doi: 10.1136/thx.2010.145490

Jacomelli, M., Silva, P. R. A. A., Rodrigues, A. J., Demarzo, S. E., Seicento, M., and Figueiredo, V. R. (2012). Bronchoscopy for the diagnosis of pulmonary tuberculosis in patients with negative sputum smear microscopy results. *J. Bras. Pneumol.* 38, 167–173. doi: 10.1590/s1806-37132012000200004

Kikuchi, E., Yamazaki, K., Sukoh, N., Kikuchi, J., Asahina, H., Imura, M., et al. (2004). Endobronchial ultrasonography with guide-sheath for peripheral pulmonary lesions. *Eur. Respir. J.* 24, 533–537. doi: 10.1183/09031936.04.00138603

Kovnat, D. M., Rath, G. S., Anderson, W. M., Siber, F., and Snider, G. L. (1975). Bronchial brushing through the flexible fiberoptic bronchoscope in the diagnosis of peripheral pulmonary lesions. *Chest* 67, 179–184. doi: 10.1378/chest.67.2.179

Kuo, C. H., Lin, S. M., Chung, F. T., Lee, K. Y., Ni, Y. L., Lo, Y. L., et al. (2011). Echoic features as predictors of diagnostic yield of endobronchial ultrasound-guided transbronchial lung biopsy in peripheral pulmonary lesions. *Ultrasound Med. Biol.* 37, 1755–1761. doi: 10.1016/j.ultrasmedbio.2011.07.007

Kurimoto, N., Miyazawa, T., Okimasa, S., Maeda, A., Oiwa, H., Miyazu, Y., et al. (2004). Endobronchial ultrasonography using a guide sheath increases the ability to diagnose peripheral pulmonary lesions endoscopically. *Chest* 126, 959–965. doi: 10.1378/chest.126.3.959

Kurimoto, N., Murayama, M., Yoshioka, S., and Nishisaka, T. (2002). Analysis of the internal structure of peripheral pulmonary lesions using endobronchial ultrasonography. *Chest* 122, 1887–1894. doi: 10.1378/chest.122.6.1887

Lang, D., Reinelt, V., Horner, A., Akbari, K., Fellner, F., Lichtenberger, P., et al. (2018). Complications of CT-guided transthoracic lung biopsy: A short report on current literature and a case of systemic air embolism. *Wien Klin Wochenschr*. 130, 288–292. doi: 10.1007/s00508-018-1317-0

Lin, C. K., Keng, L. T., Lim, C. K., Lin, Y. T., Lin, S. Y., Chen, L. Y., et al. (2020). Diagnosis of mediastinal tuberculous lymphadenitis using endobronchial ultrasound-guided transbronchial needle aspiration with rinse fluid polymerase chain reaction. *J. Formos. Med. Assoc.* 119, 509–515. doi: 10.1016/j.jfma.2019.07.014

Lin, S. M., Chung, F. T., Huang, C. D., Liu, W. T., Kuo, C. H., Wang, C. H., et al. (2009). Diagnostic value of endobronchial ultrasonography for pulmonary tuberculosis. *J. Thorac. Cardiovasc. Surg.* 138, 179–184. doi: 10.1016/j.jtcvs.2009.04.004

Nachiappan, A. C., Rahbar, K., Shi, X., Guy, E. S., Mortani Barbosa, E. J. Jr., Shroff, G. S., et al. (2017). Pulmonary tuberculosis: role of radiology in diagnosis and management. *Radiographics* 37, 52–72. doi: 10.1148/rg.2017160032

Park, J. S., Kang, Y. A., Kwon, S. Y., Yoon, H. I., Chung, J. H., Lee, C. T., et al. (2010). Nested PCR in lung tissue for diagnosis of pulmonary tuberculosis. *Eur. Respir. J.* 35, 851–857. doi: 10.1183/09031936.00067209

Radhika, S., Gupta, S. K., Chakrabarti, A., Rajwanshi, A., and Joshi, K. (1989). Role of culture for mycobacteria in fine-needle aspiration diagnosis of tuberculous lymphadenitis. *Diagn. Cytopathol.* 5, 260–262. doi: 10.1002/dc.2840050306

Sakatani, T., Amano, Y., Sato, J., and Nagase, T. (2018). Air embolism after CT-guided percutaneous lung biopsy. *Jpn. J. Clin. Oncol.* 48, 699–700. doi: 10.1093/jjco/hyy072

Sekine, A., Saito, T., Satoh, H., Morishita, Y., Tsunoda, Y., Tanaka, T., et al. (2017). Limited value of transbronchial lung biopsy for diagnosing Mycobacterium avium complex lung disease. *Clin. Respir. J.* 11, 1018–1023. doi: 10.1111/crj.12459

White, C. S., Weiner, E. A., Patel, P., and Brit, E. J. (2000). Transbronchial needle aspiration: guidance with CT fluoroscopy. *Chest* 118, 1630–1638. doi: 10.1378/chest.118.6.1630

Yamada, N., Yamazaki, K., Kurimoto, N., Asahina, H., Kikuchi, E., Shinagawa, N., et al. (2007). Factors related to diagnostic yield of transbronchial biopsy using endobronchial ultrasonography with a guide sheath in small peripheral pulmonary lesions. *Chest* 132, 603–608. doi: 10.1378/chest.07-0637

Yun, S., Kang, H., Park, S., Kim, B. S., Park, J. G., and Jung, M. J. (2018). Diagnostic accuracy and complications of CT-guided core needle lung biopsy of solid and part-solid lesions. *Br. J. Radiol.* 91:20170946. doi: 10.1259/bjr.20170946

Zhao, Z. L., Peng, L. L., Wei, Y., Li, Y., Wang, G. M., and Yu, M. A. (2020). The accuracy of ultrasound-guided lung biopsy pathology and microbial cultures for peripheral lung lesions. *J. Thorac. Dis.* 12, 858–865. doi: 10.21037/jtd.2019.12.92

Conflict of Interest: The authors declare that the research was conducted in the absence of any commercial or financial relationships that could be construed as a potential conflict of interest.

Publisher's Note: All claims expressed in this article are solely those of the authors and do not necessarily represent those of their affiliated organizations, or those of the publisher, the editors and the reviewers. Any product that may be evaluated in this article, or claim that may be made by its manufacturer, is not guaranteed or endorsed by the publisher.

frontiers | Frontiers in Microbiology

REVIEW
published: 26 April 2022
doi: 10.3389/fmicb.2022.845229

Proteomics in Biomarker Discovery for Tuberculosis: Current Status and Future Perspectives

Jiubiao Guo[1,2], Ximeng Zhang[2], Xinchun Chen[2] and Yi Cai[2]**

[1] College of Pharmacy, Shenzhen Technology University, Shenzhen, China, [2] Guangdong Provincial Key Laboratory of Regional Immunity and Diseases, Department of Pathogen Biology, School of Medicine, Shenzhen University, Shenzhen, China

Tuberculosis (TB) continues to threaten many peoples' health worldwide, regardless of their country of residence or age. The current diagnosis of TB still uses mainly traditional, time-consuming, and/or culture-based techniques. Efforts have focused on discovering new biomarkers with higher efficiency and accuracy for TB diagnosis. Proteomics—the systematic study of protein diversity—is being applied to the discovery of novel protein biomarkers for different types of diseases. Mass spectrometry (MS) technology plays a revolutionary role in proteomics, and its applicability benefits from the development of other technologies, such as matrix-based and immune-based methods. MS and derivative strategies continuously contribute to disease-related discoveries, and some promising proteomic biomarkers for efficient TB diagnosis have been identified, but challenges still exist. For example, there are discrepancies in the biomarkers identified among different reports and the diagnostic accuracy of clinically applied proteomic biomarkers. The present review summarizes the current status and future perspectives of proteomics in the field of TB biomarker discovery and aims to elicit more promising findings for rapid and accurate TB diagnosis.

Keywords: tuberculosis, proteomics, biomarker, diagnosis, mass spectrometry

OPEN ACCESS

Edited by:
Xiao-Yong Fan,
Fudan University, China

Reviewed by:
Suereta Fortuin,
Stellenbosch University, South Africa
Jianping Xie,
Southwest University, China

****Correspondence:***
Yi Cai
caiyi0113@szu.edu.cn
Xinchun Chen
chenxinchun@szu.edu.cn

Specialty section:
This article was submitted to Infectious Agents and Disease, a section of the journal Frontiers in Microbiology

Received: *29 December 2021*
Accepted: *24 February 2022*
Published: *26 April 2022*

Citation:
Guo J, Zhang X, Chen X and Cai Y (2022) Proteomics in Biomarker Discovery for Tuberculosis: Current Status and Future Perspectives. Front. Microbiol. 13:845229. doi: 10.3389/fmicb.2022.845229

INTRODUCTION

Tuberculosis (TB), caused by the pathogenic bacteria *Mycobacterium tuberculosis* (*Mtb*), continues to be a leading public health threat that affects all countries and age groups (Zumla et al., 2013). In 2020, approximately 10 million people developed TB, and 1.3 million people died from the infection worldwide. Of increasing concern, a total of 157,903 drug-resistant cases were reported, with 132,222 cases of multidrug- or rifampicin-resistant TB and 25,681 cases of pre-extensively drug-resistant TB or extensively drug-resistant TB detected, although this was a large fall (of 22%) from the total of 201,997 people detected with drug-resistant TB in 2019 (WHO, 2021). Tuberculosis control strategies aim to reduce the spread of the infection and cure infectious TB patients, who need rapid and accurate diagnosis to facilitate the administration of prompt anti-TB treatment, thereby helping to reduce the transmission of TB and development of drug resistance.

Mtb is an intracellular pathogen that preferentially infects host macrophages and primarily resides within lung granulomas (Brites and Gagneux, 2015; Elkington et al., 2021), making directly detecting *Mtb* in human body fluids, such as blood, saliva, or urine, impossible. A current challenge in TB diagnosis is the development of rapid point-of-care tests. Sputum smear microscopy is the

most common way of diagnosing TB worldwide (Steingart et al., 2006; Molicotti et al., 2014); however, the sensitivity of sputum smear microscopy ranges from 30 to 60% and is largely dependent on the operator and the abundance of *Mtb* in the samples (Molicotti et al., 2014). Microbiological culture is considered a diagnostic gold standard, but it requires several weeks and laboratory containment facilities to culture and identify *Mtb* in samples due to the slow growth rate and biohazard level of the microbe (Lagier et al., 2015). The rapid molecular-based diagnostic test Xpert MTB/RIF has high sensitivity and specificity for the diagnosis of smear-positive sputum TB patients (Steingart et al., 2013); however, Xpert MTB/RIF has a lower sensitivity for smear-negative sputum samples, leaving the diagnosis of a significant proportion of TB-infected cases reliant on diagnostic tests with sub-optimal accuracy.

Recently, many researchers have focused on the discovery of host biomarkers for TB diagnostics. Host immune responses to *Mtb* infection (Dey and Bishai, 2014) leave traceable signals within the host that may prove valuable for the accurate diagnosis and/or prognosis of TB (Parida and Kaufmann, 2010). Increasingly, investigators are validating the feasibility and accuracy of using proteomic signatures for TB diagnosis and prognosis (De Groote et al., 2017b; Penn-Nicholson et al., 2019). For example, our team previously screened for and validated key proteomic TB biomarkers using an antibody-based array for whole-blood samples that were stimulated with pooled *Mtb* peptides (ESAT-6 and CFP-10 derived peptides) (Chen et al., 2009) or mitogen, and we successfully identified an eight-protein bio-signature of I-TAC, I-309, MIG, granulysin, FAP, MEP1B, furin, and LYVE-1. The combination of the eight biomarkers allowed us to distinguish TB from healthy control individuals in a test cohort with a specificity and sensitivity of 83% (95% CI, 71–91%) and 76% (95% CI, 56–90%), respectively (Yang et al., 2020). In this review, we summarize the proteomics research approaches followed over the past several years, focusing on the progress of TB biomarker discovery via proteomics, with the hope of eliciting more promising biomarker discoveries for rapid and accurate TB diagnosis.

PROTEOMICS RESEARCH APPROACHES

Proteomics is the systematic study of the proteome with the aim of uncovering the nature of sophisticated protein-interaction networks with respect to protein expression, structure, function, and control of biological processes within an organism (Patterson and Aebersold, 2003). By comparing different patterns within the proteome, proteomics has continued to provide a powerful method for studying the changes in protein diversity that accompany health and disease processes, making the clinical diagnosis, prognosis, and even treatment of different diseases possible (Kavallaris and Marshall, 2005).

It is the development of technology and informatics that make a new concept achievable, as is the case for proteomics. **Figure 1** illustrates the timeline of proteomic technology and protein database development that has promoted proteomics research. However, the proteome of a particular cell type or tissue is a mixture of all the proteins expressed (Wilkins, 2009); thus, protein separation is a prerequisite for single-protein analysis. As early as 1975, two-dimensional polyacrylamide gel electrophoresis (2D-PAGE), which separates proteins based on their size and surface charge, was first employed to separate ribosomal proteins of *Escherichia coli* (Knopf et al., 1975). Mass spectrometry (MS), which is usually applied to the identification of individual protein spots separated by 2D-PAGE, was first described in 1899. It was not, however, until the development of non-destructive large-biomolecule ionization methods, including matrix-assisted laser desorption/ionization (MALDI) (Karas and Hillenkamp, 1988) and electrospray ionization (Fenn et al., 1989), that the widespread application of MS became feasible. Peptide mass fingerprinting (Henzel et al., 2003) and isotope-coded affinity tag (Gygi et al., 1999) approaches were then combined with different MS strategies for the accurate quantification of concurrent peptides from proteins that are found abundantly or even in trace amounts in complex mixtures.

Benefiting from the rapid development of technology during the 21st century, some classical technologies have helped to further revolutionize proteomics. For example, 2D-PAGE and MS have been developed into techniques such as difference-gel 2D-electrophoresis (Larbi and Jefferies, 2009), surface-enhanced laser desorption/ionization time of flight (SELDI-TOF) MS (Marcos et al., 2013), quantitative chemical cross-linking with MS (Wippel et al., 2021), and immunodepletion techniques for "low-abundance" protein determination (Liu et al., 2021b). Moreover, "protein chips" have been designed and combined with MS approaches for the specific analysis of selected proteins (Zhou et al., 2001). It is important to consider that, coupled with proteomic technologies, proteomics databases, including Swiss-Prot, Entrez, and the Human Proteome Organization, also continue to contribute to the development of proteomics (Kavallaris and Marshall, 2005). Moreover, in addition to other single-cell approaches (Mauger et al., 2021), single-cell proteomics is emerging as a way to identify and quantify the proteins in individual cells (Li et al., 2021). Although there are no high-throughput proteomic "sequencers" available as yet, it is believed that this technology will contribute to the discovery of new aspects of protein and cell biology in the future.

DIAGNOSTIC APPLICATION OF PROTEOMIC BIOMARKERS FOR TUBERCULOSIS

Upon *Mtb* infection, the host cells' response is to produce and secrete certain effectors to deal with the invading bacteria (Dey and Bishai, 2014; Brites and Gagneux, 2015; Llibre et al., 2021). Blood is the primary vehicle for the transport of either host effectors or *Mtb* factors and is usually routinely sampled for clinical testing, making blood samples readily accessible for research purposes and diagnostic tests. The recent advances in proteomics make the simultaneous detection of thousands of proteins possible, facilitating the capture of effectors and

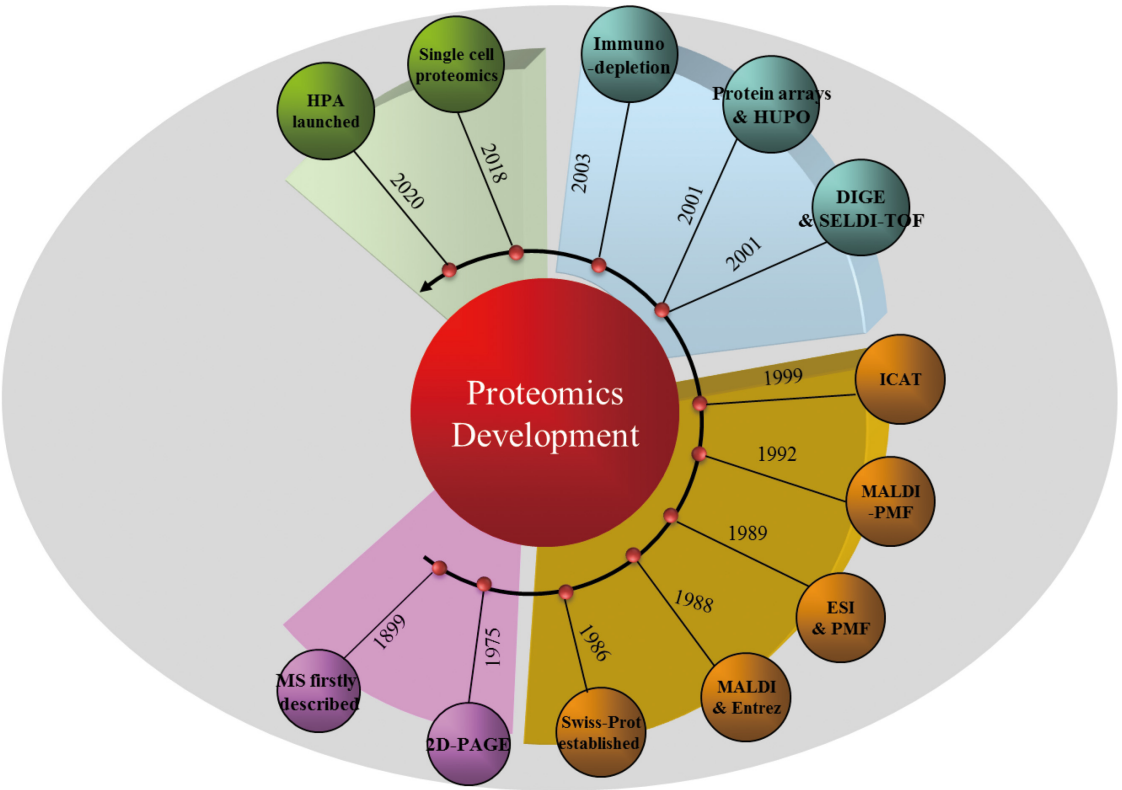

FIGURE 1 | Timeline of proteomic technologies and protein database development. MS, mass spectrometry; 2D-PAGE, two-dimensional polyacrylamide gel electrophoresis; MALDI, matrix-assisted laser desorption/ionization; ESI, electrospray ionization; PMF, peptide mass fingerprinting; ICAT, isotope-coded affinity tag; DIGE, difference-gel 2D-electrophoresis; SELDI-TOF, surface-enhanced laser desorption/ionization time of flight; HUPO, Human Proteome Organization; HPA, Human Protein Atlas.

thus paving the way for alternative and efficient TB biomarker discovery. In this section, we summarize the recent developments in the identification of proteomic biomarkers that can be used for differentiating TB from healthy or other disease status individuals. This has been achieved by categorizing the origin of the biomarkers from either blood samples, urine samples, or other types of human body fluids.

Identification of Tuberculosis Biomarkers in Human Blood Samples

Human blood and derivative samples are ideal for TB diagnosis with respect to convenience, feasibility, and the amount of sample that can be collected. In addition, upon *Mtb* infection, molecules secreted during host immune responses, such as cytokines, are mainly delivered via the blood. The advantages of blood samples make them a priority choice, and most studies of proteomic biomarkers for TB diagnosis are based on blood samples. Some biomarkers, for example, ESAT6 (Chiappini et al., 2012; Liu et al., 2017), IP-10 (Estevez et al., 2020), and CD161 (Yang et al., 2015), are secreted by either *Mtb* or the host and have been verified and validated for the detection of *Mtb* and TB diagnosis. But due to the low chance of detecting *Mtb* traces in blood samples and the reported inconsistencies among different research findings, more intensive investigations are necessary in the search for further potential biomarkers for TB diagnosis.

Agranoff et al. (2006) undertook research to discriminate between TB-infected and control individuals by utilizing SELDI-TOF MS (von Eggeling et al., 2001; Issaq et al., 2002) to search for proteomic biomarkers in serum samples. In the first phase of the study, they recruited 349 individuals and studied 179 confirmed culture-positive TB samples and 170 controls collected at St George's Hospital, United Kingdom; Angola; the Gambia; and Uganda. After profiling all the serum samples with weak cation exchange (CM10) protein chip arrays and supervised machine learning classification methods, the authors chose a Gaussian kernel support vector machine classifier to discriminate the proteomic profile of patients with active TB from that of controls, and the diagnosis sensitivity was 93.5%, specificity was 94.9%, and overall diagnostic accuracy of 94% as the best discriminator for the TB and control groups. A second independent and prospectively collected testing set that included 41 validation samples (18 TB and 23 controls) achieved a sensitivity of 88.9% and specificity of 77.2%. This study was robust but did not clarify the identity of the potential protein biomarkers, which hampered their subsequent application in other sets of samples. In addition, the size of the second testing set was limited, and a larger set of testing samples would have provided a more accurate validation.

Another study (De Groote et al., 2017b) reported the execution of a large multi-center study designed to search for a diagnostic serum protein signature for pulmonary TB. Using the 4,000-plex SOMAscan assay (De Groote et al., 2017a), they performed in-depth proteomic analysis of 1,470 serum samples from seven TB-endemic countries: South Africa, Peru, Zimbabwe, Uganda, Vietnam, Colombia, and Bangladesh. A total of 504 samples (252 non-TB and 252 TB) were tested on SOMAscan for biomarker discovery. The identified HR6 model of host response markers, which included SYWC, kallistatin, complement C9, gelsolin, testican-2, and aldolase C, was subjected to testing with a blinded verification set of 204 samples and reached an area under the curve (AUC) of 0.87 (95% CI, 0.81–0.91). Besides the identified HR6 protein signature, several previously described TB markers, such as IP-10, LBP, FCG3B, and TSP4, were also detected in this study. The reason that IP-10 and other known markers were not included in the HR6 signature may be the statistical methods applied or other reasons. Although there were claims that the 4,000-plex SOMAscan assay is able to simultaneously measure > 4,000 proteins in serum samples, many other proteins, and thus other more promising biomarkers, could have been missed.

Tuberculosis (TB) co-infection is a leading cause of death among people living with HIV, and diagnostic biomarker discovery among this group of people is necessary to reduce mortality (Corbett et al., 2003). Singer et al. (2021) analyzed and compared plasma host proteins from subjects from South Africa (n = 30, representing a region of high TB incidence) and the United States (n = 24, representing a region of low TB incidence), and CD14, A2GL, NID1, SCTM1, and A1AG1 were identified as overlapping between both cohorts. The authors further assessed the diagnostic performance of these host proteins using cross-validation and found that panels of 5–12 proteins had excellent accuracy 0–6 (AUC 0.93) at 6–12 months (AUC 0.86) prior to TB diagnosis for the South African cohort and good accuracy 0–6 (AUC 0.74) at 6–12 months (AUC 0.76) prior to TB diagnosis for the United States cohort. In addition, Shen et al. (2020) analyzed 200 HIV-positive plasma samples using data-independent acquisition MS-based proteomics, and they reported that, in combination, the proteins markers AMACR, LDHB, and RAP1B may serve as TB markers for HIV-infected patients (Shen et al., 2020). Overall, the TB diagnosis of patients co-infected with HIV is difficult due to interference from the HIV infection. Intensive studies of large cohorts with diverse genetic backgrounds are needed to achieve accurate and consistent data.

Recently, an increasing number of investigations have reported new proteomic biomarkers for TB diagnosis using either blood, urine, or other body fluid samples (**Table 1**). It should be noted that discrepancies exist among the different investigation outcomes, even among similar studies (**Table 1**). In addition, most of the proteomic biomarkers identified in various body fluid samples originated from preliminary investigations, and there is still a long journey ahead before these potential biomarkers can be applied in clinical diagnosis. Moreover, due to the intracellular survival and other adaptation features of the bacterium (Brites and Gagneux, 2015), few studies have discovered mycobacterium-derived proteomic biomarkers that have the potential to be used in the diagnosis of active TB (Hendrickson et al., 2000; Chen et al., 2018). Some additional identified blood-based proteomic biomarkers are summarized in **Table 1**.

Identification of Tuberculosis Biomarkers in Human Urine Samples

Besides blood samples, urine samples are another common choice for identifying proteomic biomarkers for human TB diagnosis, and some relevant investigations have been reported. In 2021, Liu et al. (2021a) analyzed and compared the urinary proteomic profiles of TB patients and healthy controls. They first screened for potential biomarkers using the liquid chromatography coupled with tandem mass spectrometry (LC–MS/MS) technique on 20 TB and 20 healthy control samples, then further validated the identified proteomic biomarkers in another 52 TB, 52 latent tuberculosis infection (LTBI), and 52 healthy control samples. Based on the data, they concluded that a combination of glutathione peroxidase 3 (P22352), neurotrimin (Q9P121), poliovirus receptor (P15151), signaling lymphocytic activation molecule family 1 (Q13291), and hemicentin-2 (Q8NDA2) could potentially be applied to the diagnosis of TB, with an 82.7% sensitivity for TB diagnosis and a 92.3% specificity for the diagnosis of TB in the LTBI category. By comparing urine samples from 21 active TB, 24 LTBI, and 18 healthy controls via LC–MS/MS, Young et al. identified IGKC, RBP4, PTGDS, AMBP, ORM1, IGCL2, and SECTM1 as potential protein biomarkers for distinguishing TB from LTBI or healthy control samples. However, they did not validate the group of biomarkers in a second cohort and did not clarify the diagnostic sensitivity or specificity (Young et al., 2014). In addition, a unique 21-mer *Mtb* peptide sequence (VVLGLTVPGGVELLPGVALPR) was identified (Pollock et al., 2018) from urine samples of Zimbabwean patients that showed 95% sequence homology with *Mtb* oxidoreductase (MRGA423_21210) from the clinical isolate MTB423 (identified in Kerala, India), but the relevance of this occasionally identified *Mtb*-originating protein biomarker needs to be verified in further investigations.

Identification of Tuberculosis Biomarkers in Other Human Body Fluids

Saliva and sputum, which contain thousands of proteins, mRNA, and bacterial species, have been used widely for biomarker studies and as samples for disease diagnosis and assessment (Ruhl, 2012; Carpenter, 2013; Kaczor-Urbanowicz et al., 2017; Sun et al., 2017). Collecting a saliva/sputum sample is easy, non-invasive, and more acceptable for repeat testing. Several biomarkers for the diagnosis of TB have been identified in saliva by proteomics approaches. Recently, P01011, Q8NCW5, P28072, A0A2Q2TTZ9, and Q99574 were identified using a QExactive Orbitrap mass spectrometer, with which the combined five-protein bio-signature was shown, after leave-one-out cross validation, to yield an AUC of 1.00 (95% CI, 1.00–1.00), sensitivity of 100% (95% CI, 76.2–100%), and specificity of 90.9% (95% CI, 58.7–99.8%) in TB diagnosis (Mutavhatsindi et al., 2021). Using MS, a signature comprising

TABLE 1 | Proteomic biomarker identification for TB diagnosis.

Sample type/size	Proteomic biomarker	Sensitivity and specificity	Technology employed	References
Total 196 urine samples	Glutathione peroxidase 3, neurotrimin, poliovirus receptor, signaling lymphocytic activation molecule family 1, and hemicentin-2	82.7% sensitivity and 92.3% specificity	LC–MS/MS	Liu et al. (2021a)
Total 342 plasma samples	CFHR5, LRG1, CRP, LBP, and SAA1	AUC of 0.93 (95% CI: 0.89–1.00, $p \leq 0.001$) or 0.81 (95% CI: 0.68–0.94, $p = 0.001$)	High-resolution MS	Garay-Baquero et al. (2020)
Total 120 serum samples	sCD14, PGLYRP2, and FGA	AUC of 0.934, sensitivity of 81.2%, and specificity of 90%	MS strategy	Chen et al. (2020)
Total 6,363 plasma samples	Complement factor 9, IGFBP-2,CD79A, MXRA-7, NrCAM, CK-MB, and C1qTNF3/CTNFF3	AUC of 0.66 (0.56–0.75) or 0.65 (0.55–0.75)	Multiplexed proteomic assay (SOMAscan)	Penn-Nicholson et al. (2019)
1,470 serum samples	SYWC, kallistatin, complement C9, gelsolin, testican-2, and aldolase C	AUC of 0.95 or 0.92 in a blinded verification set	4,000-plex SOMAscan assay	De Groote et al. (2017b)
172 serum and plasma proteins	CLEC3B, ECM1, IGFALS, IGFBP3, SELL, and VWF	AUC > 0.85	MRM-MS assay	Bark et al. (2017)
Total 63 urine samples	IGKC, RBP4, PTGDS, AMBP, ORM1, IGCL2, and SECTM1	Not available	LC–MS/MS	Young et al. (2014)
Total 132 serum samples	Apolipoprotein CII (APOCII), CD5 antigen-like (CD5L), and retinol-binding protein 4 (RBP4)	93.42% sensitivity and 92.86% specificity	iTRAQ-coupled 2D LC–MS/MS technique	Xu et al. (2014)
Total 103 sputum samples	UqhC	Not available	2D-PAGE and MALDI-TOF/TOF MS	Fu et al. (2012)
Two isolated *Mtb* strains	Rv0443, Rv0379, and Rv0147	Not available	2D-PAGE and MS	Hadizadeh Tasbiti et al. (2021)
Total 285 urine samples	miR-625-3p, mannose-binding lectin 2, and inter-α-trypsin inhibitor H4	85.87% sensitivity and 87.50% specificity	2D-PAGE and MALDI-TOF/TOF MS	Wang et al. (2018)
Total 104 saliva samples	Salivary CRP, ferritin, serum amyloid P, MCP-1, alpha-2-macroglobulin, fibrinogen, and tissue plasminogen activator	78.1% sensitivity and 83.3% specificity	Luminex multiplex immunoassay	Jacobs et al. (2016)
Total 141 serum samples	2,024, 8,007, and 8,598 Da identified by biomarker patterns software	Blind test data indicated sensitivity of 80.0% and specificity of 84.2%	SELDI-TOF MS and protein-chip	Liu et al. (2011)
Total 264 serum samples	Three protein peaks at m/z 5,643, 4,486, and 4,360 Da	96.9% sensitivity, 97.8% specificity, and up to 97.3% accuracy	SELDI-TOF MS and protein-chip	Zhang et al. (2012)
Total 630 stimulated blood samples	I-TAC, I-309, MIG, granulysin, FAP, MEP1B, furin, and LYVE-1	For prediction cohort, specificity of 84% (95% CI 74–92%) and sensitivity of 75% (95% CI 57–89%)	Protein arrays	Yang et al. (2020)
Total 160 serum samples	S100A9, SOD3, and MMP9	Sensitivity of 92.5% and specificity of 95% for discriminating between TB and HC	iTRAQ-coupled 2D LC–MS/MS	Xu et al. (2015)
Total 391 serum samples	2,554.6, 4,824.4, 5,325.7, and 8,606.8 Da	Sensitivity of 83.3% and specificity of 84.2%	SELDI-TOF MS	Liu et al. (2013)
Total 390 serum samples	Serum amyloid A and transthyretin	Sensitivity of 88.9% and specificity of 77.2% in test cohort	SELDI-TOF MS and protein chip arrays	Agranoff et al. (2006)

MRM-MS, mass spectrometry coupled with multiple-reaction monitoring; MS, mass spectrometry; LC–MS/MS, liquid chromatography coupled with tandem mass spectrometry; AUC, area under the curve; iTRAQ, isobaric tags for relative and absolute quantification; SELDI-TOF, surface-enhanced laser desorption/ionization time of flight; 2D-PAGE, two-dimensional polyacrylamide gel electrophoresis; MALDI-TOF/TOF MS, matrix-assisted laser desorption/ionization-time of flight tandem mass spectrometry; TB, tuberculosis; HC, healthy controls.

β-integrin, vitamin D-binding protein, uteroglobin, profilin, and cathelicidin antimicrobial peptide in saliva was confirmed to differentiate active TB patients from non-TB patients with an AUC of 0.75 (Bishwal et al., 2019). Mariam and colleagues investigated the sputum proteome of patients with active and latent TB infections as well as community controls using an ultrafast sample-preparation approach (HaileMariam et al., 2018). A 49-protein signature was used to successfully distinguish TB from control subjects; however, this panel of proteins was unable to differentiate LTBI from healthy subjects. In another study, salivary proteomic analysis demonstrated that TB patients exhibit a specific accumulation of proteins related

to complement activation, inflammation, and the modulation of the immune response and a decrease in proteins related to glucose and lipid metabolism. A group of proteins, including haptoglobin, alpha-1-acid glycoprotein 1 and 2, immunoglobulin gamma 4 chain, fibrinogens, dermcidin, protein disulfide isomerase, triosephosphate isomerase, and ras GTPase-activating-like protein, are other potential biomarkers for the diagnosis of TB (Mateos et al., 2019).

CHALLENGES AND FUTURE PERSPECTIVES

Intensive investigations into *Mtb*–host interactions have broadened and deepened our knowledge on the strategies applied by *Mtb* to infect hosts and the host responses upon infection. The development of technologies, especially MS, has facilitated proteomic biomarker identification with high efficiency, but there are still some technical challenges slowing down the application of proteomics to the diagnosis of active TB. Sampling complexities (e.g., the timing of sample collection, small-molecule interference, and the coexistence of TB with other types of disease), differences in protein abundances, the presence of isoforms, and post-translational modifications are barriers preventing the identification of accurate and universal biomarkers with current technologies and strategies. More powerful techniques with improved sensitivity will be required, especially for low-abundance proteins and for differentiating protein isoforms and modifications. In addition, there is a risk of diagnostic bias when using a single protein biomarker, and a group of biomarkers within a panel could be detected simultaneously using current technologies, but discrepancies among different reports are increasing, providing confusing or even misleading evidence for the optimum TB diagnostic markers. One reason for the unsatisfactory reproducibility of the discovered biomarkers is that the studied cohorts have differed with regard to their genomic backgrounds, immune responses, or other factors. Large cohorts of samples from various populations that include a diversity of TB patient statuses may be needed to overcome this problem. Moreover, a combination of different "omics" techniques may be useful for improving TB diagnostic accuracy and consistency, and single-cell proteomics holds particular promise as a method that will advance active TB diagnosis in the future (Petelski et al., 2021).

AUTHOR CONTRIBUTIONS

JG and YC contributed to the conceptualization and design, reviewed the literature, prepared the figures and tables, and wrote the original draft of the manuscript. XZ contributed to literature review and data preparation. XC and YC supervised the data and wrote, reviewed, and edited the manuscript. JG, XC, and YC contributed to the project administration, funding acquisition, and resources. All authors contributed to the article and approved the submitted version.

FUNDING

This study was supported by the National Natural Science Foundation of China (Grant Nos. 31800064 and 82072252), the Science and Technology Project of Shenzhen (Grant No. JCYJ20180507182049853), and Guangdong Provincial Key Laboratory of Regional Immunity and Diseases (2019B030301009).

REFERENCES

Agranoff, D., Fernandez-Reyes, D., Papadopoulos, M. C., Rojas, S. A., Herbster, M., Loosemore, A., et al. (2006). Identification of diagnostic markers for tuberculosis by proteomic fingerprinting of serum. *Lancet* 368, 1012–1021. doi: 10.1016/S0140-6736(06)69342-2

Bark, C. M., Manceur, A. M., Malone, L. L., Nsereko, M., Okware, B., Mayanja, H. K., et al. (2017). Identification of host proteins predictive of early stage *Mycobacterium tuberculosis* infection. *EBioMedicine* 21, 150–157. doi: 10.1016/j.ebiom.2017.06.019

Bishwal, S. C., Das, M. K., Badireddy, V. K., Dabral, D., Das, A., Mahapatra, A. R., et al. (2019). Sputum proteomics reveals a shift in vitamin d-binding protein and antimicrobial protein axis in tuberculosis patients. *Sci. Rep.* 9:1036. doi: 10.1038/s41598-018-37662-37669

Brites, D., and Gagneux, S. (2015). Co-evolution of *Mycobacterium tuberculosis* and *Homo sapiens*. *Immunol. Rev.* 264, 6–24. doi: 10.1111/imr.12264

Carpenter, G. H. (2013). The secretion, components, and properties of saliva. *Annu Rev Food Sci Technol.* 4, 267–276. doi: 10.1146/annurev-food-030212-182700

Chen, J., Han, Y. S., Yi, W. J., Huang, H., Li, Z. B., Shi, L. Y., et al. (2020). Serum sCD14, PGLYRP2 and FGA as potential biomarkers for multidrug-resistant tuberculosis based on data-independent acquisition and targeted proteomics. *J. Cell Mol. Med.* 24, 12537–12549. doi: 10.1111/jcmm.15796

Chen, X., Yang, Q., Zhang, M., Graner, M., Zhu, X., Larmonier, N., et al. (2009). Diagnosis of active tuberculosis in China using an in-house gamma interferon enzyme-linked immunospot assay. *Clin. Vaccine Immunol.* 16, 879–884. doi: 10.1128/CVI.00044-49

Chen, Y., Cao, S., Liu, Y., Zhang, X., Wang, W., and Li, C. (2018). Potential role for Rv2026c- and Rv2421c- specific antibody responses in diagnosing active tuberculosis. *Clin. Chim. Acta* 487, 369–376. doi: 10.1016/j.cca.2018.09.008

Chiappini, E., Della Bella, C., Bonsignori, F., Sollai, S., Amedei, A., Galli, L., et al. (2012). Potential role of *M. tuberculosis* specific IFN-gamma and IL-2 ELISPOT assays in discriminating children with active or latent tuberculosis. *PLoS One* 7:e46041. doi: 10.1371/journal.pone.0046041

Corbett, E. L., Watt, C. J., Walker, N., Maher, D., Williams, B. G., Raviglione, M. C., et al. (2003). The growing burden of tuberculosis: global trends and interactions with the HIV epidemic. *Arch. Intern. Med.* 163, 1009–1021. doi: 10.1001/archinte.163.9.1009

De Groote, M. A., Higgins, M., Hraha, T., Wall, K., Wilson, M. L., Sterling, D. G., et al. (2017a). Highly multiplexed proteomic analysis of quantiferon supernatants to identify biomarkers of latent tuberculosis infection. *J. Clin. Microbiol.* 55, 391–402. doi: 10.1128/JCM.01646-1616

De Groote, M. A., Sterling, D. G., Hraha, T., Russell, T. M., Green, L. S., Wall, K., et al. (2017b). Discovery and validation of a six-marker serum protein signature for the diagnosis of active pulmonary tuberculosis. *J. Clin. Microbiol.* 55, 3057–3071. doi: 10.1128/JCM.00467-417

Dey, B., and Bishai, W. R. (2014). Crosstalk between *Mycobacterium tuberculosis* and the host cell. *Semin. Immunol.* 26, 486–496. doi: 10.1016/j.smim.2014.09.002

Elkington, P., Polak, M. E., Reichmann, M. T., and Leslie, A. (2021). Understanding the tuberculosis granuloma: the matrix revolutions. *Trends Mol. Med.* 28, 143–154. doi: 10.1016/j.molmed.2021.11.004

Estevez, O., Anibarro, L., Garet, E., Pallares, A., Pena, A., Villaverde, C., et al. (2020). Identification of candidate host serum and saliva biomarkers for a better diagnosis of active and latent tuberculosis infection. *PLoS One* 15:e0235859. doi: 10.1371/journal.pone.0235859

Fenn, J. B., Mann, M., Meng, C. K., Wong, S. F., and Whitehouse, C. M. (1989). Electrospray ionization for mass spectrometry of large biomolecules. *Science* 246, 64–71. doi: 10.1126/science.2675315

Fu, Y. R., Yi, Z. J., Guan, S. Z., Zhang, S. Y., and Li, M. (2012). Proteomic analysis of sputum in patients with active pulmonary tuberculosis. *Clin. Microbiol. Infect.* 18, 1241–1247. doi: 10.1111/j.1469-0691.2012.03824.x

Garay-Baquero, D. J., White, C. H., Walker, N. F., Tebruegge, M., Schiff, H. F., Ugarte-Gil, C., et al. (2020). Comprehensive plasma proteomic profiling reveals biomarkers for active tuberculosis. *JCI Insight* 5:e137427. doi: 10.1172/jci.insight.137427

Gygi, S. P., Rist, B., Gerber, S. A., Turecek, F., Gelb, M. H., and Aebersold, R. (1999). Quantitative analysis of complex protein mixtures using isotope-coded affinity tags. *Nat. Biotechnol.* 17, 994–999. doi: 10.1038/13690

Hadizadeh Tasbiti, A., Yari, S., Siadat, S. D., Karimipoor, M., Badmasti, F., Masoumi, M., et al. (2021). Comparing mRNA expression and protein abundance in MDR *Mycobacterium tuberculosis*: novel protein candidates, Rv0443, Rv0379 and Rv0147 as TB potential diagnostic or therapeutic targets. *Biotechnol. Rep. (Amst)* 30:e00641. doi: 10.1016/j.btre.2021.e00641

HaileMariam, M., Eguez, R. V., Singh, H., Bekele, S., Ameni, G., Pieper, R., et al. (2018). S-Trap, an ultrafast sample-preparation approach for shotgun proteomics. *J. Proteome Res.* 17, 2917–2924. doi: 10.1021/acs.jproteome.8b00505

Hendrickson, R. C., Douglass, J. F., Reynolds, L. D., McNeill, P. D., Carter, D., Reed, S. G., et al. (2000). Mass spectrometric identification of mtb81, a novel serological marker for tuberculosis. *J. Clin. Microbiol.* 38, 2354–2361. doi: 10.1128/JCM.38.6.2354-2361.2000

Henzel, W. J., Watanabe, C., and Stults, J. T. (2003). Protein identification: the origins of peptide mass fingerprinting. *J. Am. Soc. Mass Spectrom.* 14, 931–942. doi: 10.1016/S1044-0305(03)00214-219

Issaq, H. J., Veenstra, T. D., Conrads, T. P., and Felschow, D. (2002). The SELDI-TOF MS approach to proteomics: protein profiling and biomarker identification. *Biochem. Biophys. Res. Commun.* 292, 587–592. doi: 10.1006/bbrc.2002.6678

Jacobs, R., Tshehla, E., Malherbe, S., Kriel, M., Loxton, A. G., Stanley, K., et al. (2016). Host biomarkers detected in saliva show promise as markers for the diagnosis of pulmonary tuberculosis disease and monitoring of the response to tuberculosis treatment. *Cytokine* 81, 50–56. doi: 10.1016/j.cyto.2016.02.004

Kaczor-Urbanowicz, K. E., Martin Carreras-Presas, C., Aro, K., Tu, M., Garcia-Godoy, F., and Wong, D. T. (2017). Saliva diagnostics - current views and directions. *Exp. Biol. Med. (Maywood)* 242, 459–472. doi: 10.1177/1535370216681550

Karas, M., and Hillenkamp, F. (1988). Laser desorption ionization of proteins with molecular masses exceeding 10,000 daltons. *Anal. Chem.* 60, 2299–2301. doi: 10.1021/ac00171a028

Kavallaris, M., and Marshall, G. M. (2005). Proteomics and disease: opportunities and challenges. *Med. J. Aust.* 182, 575–579. doi: 10.5694/j.1326-5377.2005.tb06817.x

Knopf, U. C., Sommer, A., Kenny, J., and Traut, R. R. (1975). A new two-dimensional gel electrophoresis system for the analysis of complex protein mixtures: application to the ribosome of *E. coli*. *Mol. Biol. Rep.* 2, 35–40. doi: 10.1007/BF00357295

Lagier, J. C., Edouard, S., Pagnier, I., Mediannikov, O., Drancourt, M., and Raoult, D. (2015). Current and past strategies for bacterial culture in clinical microbiology. *Clin. Microbiol. Rev.* 28, 208–236. doi: 10.1128/CMR.00110-114

Larbi, N. B., and Jefferies, C. (2009). 2D-DIGE: comparative proteomics of cellular signalling pathways. *Methods Mol. Biol.* 517, 105–132. doi: 10.1007/978-1-59745-541-1_8

Li, Y., Li, H., Xie, Y., Chen, S., Qin, R., Dong, H., et al. (2021). An integrated strategy for mass spectrometry-based multiomics analysis of single cells. *Anal. Chem.* 93, 14059–14067. doi: 10.1021/acs.analchem.0c05209

Liu, C., Zhao, Z., Fan, J., Lyon, C. J., Wu, H. J., Nedelkov, D., et al. (2017). Quantification of circulating *Mycobacterium tuberculosis* antigen peptides allows rapid diagnosis of active disease and treatment monitoring. *Proc. Natl. Acad. Sci. U S A.* 114, 3969–3974. doi: 10.1073/pnas.1621360114

Liu, J. Y., Jin, L., Zhao, M. Y., Zhang, X., Liu, C. B., Zhang, Y. X., et al. (2011). New serum biomarkers for detection of tuberculosis using surface-enhanced laser desorption/ionization time-of-flight mass spectrometry. *Clin. Chem. Lab. Med.* 49, 1727–1733. doi: 10.1515/CCLM.2011.634

Liu, J., Jiang, T., Wei, L., Yang, X., Wang, C., Zhang, X., et al. (2013). The discovery and identification of a candidate proteomic biomarker of active tuberculosis. *BMC Infect. Dis.* 13:506. doi: 10.1186/1471-2334-13-506

Liu, L., Deng, J., Yang, Q., Wei, C., Liu, B., Zhang, H., et al. (2021a). Urinary proteomic analysis to identify a potential protein biomarker panel for the diagnosis of tuberculosis. *IUBMB Life* 73, 1073–1083. doi: 10.1002/iub.2509

Liu, L., Kwak, H., Lawton, T. L., Jin, S. X., Meunier, A. L., Dang, Y., et al. (2021b). An ultra-sensitive immunoassay detects and quantifies soluble *Abeta oligomers* in human plasma. *Alzheimers Dement*. doi: 10.1002/alz.12457 [Epub ahead of print].

Llibre, A., Dedicoat, M., Burel, J. G., Demangel, C., O'Shea, M. K., and Mauro, C. (2021). Host immune-metabolic adaptations upon mycobacterial infections and associated co-morbidities. *Front. Immunol.* 12:747387. doi: 10.3389/fimmu.2021.747387

Marcos, B., Gou, P., Guardia, M. D., Hortos, M., Colleo, M., Mach, N., et al. (2013). Surface-enhanced laser desorption/ionisation time-of-flight mass spectrometry: a tool to predict pork quality. *Meat Sci.* 95, 688–693. doi: 10.1016/j.meatsci.2012.10.014

Mateos, J., Estevez, O., Gonzalez-Fernandez, A., Anibarro, L., Pallares, A., Reljic, R., et al. (2019). High-resolution quantitative proteomics applied to the study of the specific protein signature in the sputum and saliva of active tuberculosis patients and their infected and uninfected contacts. *J. Proteomics* 195, 41–52. doi: 10.1016/j.jprot.2019.01.010

Mauger, S., Monard, C., Thion, C., and Vandenkoornhuyse, P. (2021). Contribution of single-cell omics to microbial ecology. *Trends Ecol. Evol.* 37, 67–78. doi: 10.1016/j.tree.2021.09.002

Molicotti, P., Bua, A., and Zanetti, S. (2014). Cost-effectiveness in the diagnosis of tuberculosis: choices in developing countries. *J. Infect. Dev. Ctries* 8, 24–38. doi: 10.3855/jidc.3295

Mutavhatsindi, H., Calder, B., McAnda, S., Malherbe, S. T., Stanley, K., Kidd, M., et al. (2021). Identification of novel salivary candidate protein biomarkers for tuberculosis diagnosis: a preliminary biomarker discovery study. *Tuberculosis (Edinb)* 130:102118. doi: 10.1016/j.tube.2021.102118

Parida, S. K., and Kaufmann, S. H. E. (2010). The quest for biomarkers in tuberculosis. *Drug Discov. Today* 15, 148–157. doi: 10.1016/j.drudis.2009.10.005

Patterson, S. D., and Aebersold, R. H. (2003). Proteomics: the first decade and beyond. *Nat. Genet.* 33(Suppl.), 311–323. doi: 10.1038/ng1106

Penn-Nicholson, A., Hraha, T., Thompson, E. G., Sterling, D., Mbandi, S. K., Wall, K. M., et al. (2019). Discovery and validation of a prognostic proteomic signature for tuberculosis progression: a prospective cohort study. *PLoS Med.* 16:e1002781. doi: 10.1371/journal.pmed.1002781

Petelski, A. A., Emmott, E., Leduc, A., Huffman, R. G., Specht, H., Perlman, D. H., et al. (2021). Multiplexed single-cell proteomics using SCoPE2. *Nat. Protoc.* 16, 5398–5425. doi: 10.1038/s41596-021-00616-z

Pollock, N., Dhiman, R., Daifalla, N., Farhat, M., and Campos-Neto, A. (2018). Discovery of a unique *Mycobacterium tuberculosis* protein through proteomic analysis of urine from patients with active tuberculosis. *Microbes Infect.* 20, 228–235. doi: 10.1016/j.micinf.2017.12.011

Ruhl, S. (2012). The scientific exploration of saliva in the post-proteomic era: from database back to basic function. *Expert Rev. Proteomics* 9, 85–96. doi: 10.1586/epr.11.80

Shen, Y., Xun, J., Song, W., Wang, Z., Wang, J., Liu, L., et al. (2020). Discovery of potential plasma biomarkers for tuberculosis in HIV-Infected patients by data-independent acquisition-based quantitative proteomics. *Infect. Drug Resist.* 13, 1185–1196. doi: 10.2147/IDR.S245460

Singer, S. N., Ndumnego, O. C., Kim, R. S., Ndung'u, T., Anastos, K., French, A., et al. (2021). Plasma host protein biomarkers correlating with increasing *Mycobacterium tuberculosis* infection activity prior to tuberculosis diagnosis in people living with HIV. *EBioMedicine* 75:103787. doi: 10.1016/j.ebiom.2021.103787

Steingart, K. R., Henry, M., Ng, V., Hopewell, P. C., Ramsay, A., Cunningham, J., et al. (2006). Fluorescence versus conventional sputum smear microscopy for tuberculosis: a systematic review. *Lancet Infect. Dis.* 6, 570–581. doi: 10.1016/S1473-3099(06)70578-70573

Steingart, K. R., Sohn, H., Schiller, I., Kloda, L. A., Boehme, C. C., Pai, M., et al. (2013). Xpert(R) MTB/RIF assay for pulmonary tuberculosis and rifampicin resistance in adults. *Cochrane Database Syst. Rev.* 2014:CD009593. doi: 10.1002/14651858.CD009593.pub2

Sun, Y., Liu, S., Qiao, Z., Shang, Z., Xia, Z., Niu, X., et al. (2017). Systematic comparison of exosomal proteomes from human saliva and serum for the detection of lung cancer. *Anal. Chim. Acta* 982, 84–95. doi: 10.1016/j.aca.2017.06.005

von Eggeling, F., Junker, K., Fiedle, W., Wollscheid, V., Durst, M., Claussen, U., et al. (2001). Mass spectrometry meets chip technology: a new proteomic tool in cancer research? *Electrophoresis* 22, 2898–2902. doi: 10.1002/1522-2683(200108)22:14<2898::AID-ELPS2898>3.0.CO;2-A

Wang, J., Zhu, X., Xiong, X., Ge, P., Liu, H., Ren, N., et al. (2018). Identification of potential urine proteins and microRNA biomarkers for the diagnosis of pulmonary tuberculosis patients. *Emerg. Microbes Infect.* 7:63. doi: 10.1038/s41426-018-0066-65

WHO (2021). *Global Tuberculosis Report 2021*. Geneva: WHO.

Wilkins, M. (2009). Proteomics data mining. *Expert Rev. Proteom.* 6, 599–603. doi: 10.1586/epr.09.81

Wippel, H. H., Chavez, J. D., Tang, X., and Bruce, J. E. (2021). Quantitative interactome analysis with chemical cross-linking and mass spectrometry. *Curr. Opin. Chem. Biol.* 66:102076. doi: 10.1016/j.cbpa.2021.06.011

Xu, D. D., Deng, D. F., Li, X., Wei, L. L., Li, Y. Y., Yang, X. Y., et al. (2014). Discovery and identification of serum potential biomarkers for pulmonary tuberculosis using iTRAQ-coupled two-dimensional LC-MS/MS. *Proteomics* 14, 322–331. doi: 10.1002/pmic.201300383

Xu, D., Li, Y., Li, X., Wei, L. L., Pan, Z., Jiang, T. T., et al. (2015). Serum protein S100A9, SOD3, and MMP9 as new diagnostic biomarkers for pulmonary tuberculosis by iTRAQ-coupled two-dimensional LC-MS/MS. *Proteomics* 15, 58–67. doi: 10.1002/pmic.201400366

Yang, Q., Chen, Q., Zhang, M., Cai, Y., Yang, F., Zhang, J., et al. (2020). Identification of eight-protein biosignature for diagnosis of tuberculosis. *Thorax* 75, 576–583. doi: 10.1136/thoraxjnl-2018-213021

Yang, Q., Xu, Q., Chen, Q., Li, J., Zhang, M., Cai, Y., et al. (2015). Discriminating active tuberculosis from latent tuberculosis infection by flow cytometric measurement of CD161-expressing T cells. *Sci. Rep.* 5:17918. doi: 10.1038/srep17918

Young, B. L., Mlamla, Z., Gqamana, P. P., Smit, S., Roberts, T., Peter, J., et al. (2014). The identification of tuberculosis biomarkers in human urine samples. *Eur. Respir. J.* 43, 1719–1729. doi: 10.1183/09031936.00175113

Zhang, J., Wu, X., Shi, L., Liang, Y., Xie, Z., Yang, Y., et al. (2012). Diagnostic serum proteomic analysis in patients with active tuberculosis. *Clin. Chim. Acta* 413, 883–887. doi: 10.1016/j.cca.2012.01.036

Zhou, H., Roy, S., Schulman, H., and Natan, M. J. (2001). Solution and chip arrays in protein profiling. *Trends Biotechnol* 19, S34–S39. doi: 10.1016/S0167-7799(01)01798-X

Zumla, A., Raviglione, M., Hafner, R., and von Reyn, C. F. (2013). Tuberculosis. *N. Engl. J. Med.* 368, 745–755. doi: 10.1056/NEJMra1200894

Conflict of Interest: The authors declare that the research was conducted in the absence of any commercial or financial relationships that could be construed as a potential conflict of interest.

Publisher's Note: All claims expressed in this article are solely those of the authors and do not necessarily represent those of their affiliated organizations, or those of the publisher, the editors and the reviewers. Any product that may be evaluated in this article, or claim that may be made by its manufacturer, is not guaranteed or endorsed by the publisher.

frontiers | Frontiers in Microbiology

ORIGINAL RESEARCH
published: 06 May 2022
doi: 10.3389/fmicb.2022.789725

Statistical Investigation of High Culture Contamination Rates in Mycobacteriology Laboratory

Muatsim Ahmed Mohammed Adam[1], *Rasha Sayed Mohammed Ebraheem*[1] *and Shahinaz Ahmed Bedri*[2]*

[1] National Public Health Laboratory (NPHL), National Tuberculosis Reference Laboratory (NTRL), Khartoum, Sudan,
[2] National Public Health Laboratory (NPHL), DG, Khartoum, Sudan

Background: Culture of *Mycobacterium tuberculosis* remains the gold standard in mycobacteriology laboratories, constrained by the very high risk of contamination; therefore, contamination rate is an important key performance indicator (KPI) for laboratory monitoring and evaluation processes.

Aim: This study aimed to investigate the factors that contribute to elevated contamination rates in the Sudan National Tuberculosis Reference Laboratory.

Method: A laboratory-based retrospective study was applied; a TB culture register-book was carefully reviewed and data from 2 January 2019 to 31 December 2019 were entered, cleaned, and analyzed using IBM SPSS 20. A multivariate logistic regression model was performed to examine two dependent variables, the massive contamination, and the single tube contamination against predictors of reason for cultivation, type of specimen, experiment team, and the quarter of cultivation.

Results: It has been found that in 2019 contamination rates were frequently higher; the highest rates were recorded in January and November, 28.2 and 25.2%, respectively. August is an exception with an accepted contamination rate of 4.6%. Of 1,149 specimens requested for culture, 945 (82.2%) samples were eligible to be included in multivariate logistic regression analysis. The team conducting the experiment was significantly associated with a high single tube contamination *p value* 0.007; adjusted odds ratio AOR 3.570 (1.415–9.005). The correlation between the single tube contamination and the massive contamination is significant; *p value* 0.01.

Conclusion: The study concludes that high culture contamination is the greatest risk to the quality of laboratory service and can end in either the loss of specimens or delay in the decisions of initiating patient treatment. In addition, the low quality or incompleteness of data increases the uncertainty and undermines the measurement of key performance indicators.

Keywords: culture, contamination, management review, continuous improvement, laboratory diagnosis, tuberculosis, quality indicators

OPEN ACCESS

Edited by:
Hairong Huang,
Capital Medical University, China

Reviewed by:
Pooja Vir,
Uniformed Services University of the Health Sciences, United States
Miriam Cordovana,
Bruker Daltonik GmbH, Germany

***Correspondence:**
Shahinaz Ahmed Bedri
shahinazbedri@gmail.com

Specialty section:
This article was submitted to Infectious Agents and Disease, a section of the journal Frontiers in Microbiology

Received: *05 October 2021*
Accepted: *13 January 2022*
Published: *06 May 2022*

Citation:
Mohammed Adam MA, Ebraheem RSM and Bedri SA (2022) Statistical Investigation of High Culture Contamination Rates in Mycobacteriology Laboratory. Front. Microbiol. 13:789725. doi: 10.3389/fmicb.2022.789725

INTRODUCTION

Sudan is a moderately tuberculosis (TB) burdened country. In 2014 the prevalence was 159/100,000; it is higher among adults, in urban settings, and in the male population, although 11–13% of all notified cases are children. In 2017, the estimated TB incidence was 77/100,000, for a total of 31,000 cases and a mortality rate of 12/100,000. Comparatively, TB case notifications remained steady for the last decade in a range of (19,817–22,097). In 2016, the total notification was 21,091 cases. Among them, 19,305 (91.5%) were new, while 1,786 (8.5%) were retreatment cases. Of the new cases, 6,520 (30.9%) were smear-positive, 6,167 (29.2%) were smear-negative, 4,951 (23.5%) were extra-pulmonary, and in 1,667 (7.9%) sputum was not done. Last year there were three presumptive cases of extensively drug resistant tuberculosis (XDR-TB); only one of them was confirmed and the notified multi drug resistant tuberculosis (MDR-TB) cases were 220 (CNCDCD et al., 2018).

In Sudan, the GeneXpert network was designed and consists of three levels; it was managed and supervised centrally by the National Tuberculosis Reference Laboratory (NTRL), connected with 18 state laboratories located in capital cities, equipped with one machine or more. Based on MDR notifications, it was expanded to serve 72 sites in localities. An external quality assessment (EQA) system was planned but not yet implemented. The GeneXpert network was employed as the earliest diagnostic tool in the diagnostic algorithm which prioritizes screening and early identification of rifampicin resistant cases among TB suspect and MDR-TB high-risk groups, such as TB retreatment cases, MDR-TB contact, HIV patients, and prisoners. To scale up the programmatic management of drug resistant tuberculosis; sputum smear microscopy was only dedicated for the monitoring of treatment of first-line anti TB drugs (FLDs). So far, culture is the gold standard diagnostic method in the mycobacteriology laboratory.

Several types of culture systems have been developed, however, Löwenstein–Jensen medium (LJ) is considered the reference mycobacterial growth medium (Rageade et al., 2014). Solid egg-based cultures are cheaper and safer, more specific, and allow better visibility of colonial morphology compared to liquid systems (Kidenya et al., 2013; Ahmad et al., 2017). Cultures are more sensitive and significantly increase the number of notified cases (Asmar and Drancourt, 2015). However, they are time-consuming when compared to molecular techniques and sputum smear microscopy. Additionally, cultures provide the necessary isolates for conventional drug susceptibility testing (DST) to provide a definitive diagnosis, therefore, molecular techniques and sputum smear microscopy are not replacing the culture of *M. tuberculosis* (World Health Organization, 1998; Chihota et al., 2010). Cultivation of mycobacteria is the only method that enables differentiation between viable and dead bacterial cells. This characteristic was frequently recruited to monitor treatment response, to confirm patient sterility and sputum conversion, as well as to ensure the breaking of transmission cycles and to document cure of patients (Su et al., 2011; World Health Organization, 2014; Lawn and Nicol, 2015; Wong et al., 2016).

The accuracy of technical manipulation of analytical and pre-analytical processes either negatively or positively impacts the prone of mycobacterial culture contamination. Soft decontamination procedures due to the constraints of less time or lower concentration might increase the possibility of contamination occurrence. In addition, poor quality of specimens, delay in transportation to the laboratory, as well as poor quality of culture media and incubation conditions might be addressed as possible causes of contamination (World Health Organization, 2011). In this study, we aimed to explore other factors that might contribute to raised contamination rates in the Sudan National Tuberculosis Reference Laboratory.

MATERIALS AND METHODS

Study Setting

Sudan National Tuberculosis Reference Laboratory (NTRL) is the sole reference TB laboratory in the country; it stands at the top of the hierarchical network of four regional TB culture laboratories, 18 smear microscopy quality assurance (EQA) laboratories, and 327 tuberculosis management units (TBMUs). The diagnostic menu includes a variety of conventional laboratory tests: Ziehl–Neelsen (ZN) and Phenolic-Auramine fluorescence microscopy (FM), egg-based cultures, first line, and second-line drug susceptibility testing (DST). In addition, the WHO endorsed molecular techniques Xpert® MTB/RIF assay (Cepheid Inc., Sunnyvale, CA, United States) and Line Probe Assay GenoType MTBDR*plus* for rifampicin and isoniazid resistance (Hain Lifescience GmbH, Nehren, Germany), and GenoType MTBDR*sl* for XDR detection.

Laboratory Culture

Sudan National Tuberculosis Reference Laboratory is adopting the Petroff method for sputum decontamination and homogenization. Standard operating procedure (SOP) describes the addition of an equal volume of 4% sodium hydroxide solution (4% NaOH) to the sputum sample, gentle shaking, and homogenization for 15 min. Neutralization of alkaline solution includes three without-centrifugation options: the use of hydrochloric acid (HCl) with phenol red indicator, use of phosphate buffer saline (PBS) pH 6.8, or direct inoculation onto two tubes of Ogawa acidified medium. Löwenstein-Jensen medium (LJ) Slants were incubated at 37°C for 8 weeks and inspected regularly for the recording of negative results. Culture contamination and the grades of positive results (scanty, +, ++, +++) were recorded immediately when visible mycobacterial growth appear.

Data Collection and Data Management

The culture laboratory register book was carefully reviewed. It includes data about specimens, patients, and results of smear and culture. Data were categorized, double entered onto statistical package for social sciences (IBM SPSS statistics 20), checked, and cleaned. Category "Not recorded" was elaborated for not filled data from the original institution that requested the culture, unknown data, or data not transcribed from the request form inside the reference laboratory. Specimens that were requested and not received or not processed were excluded. Furthermore,

information about sample collection, sample reception, and sample processing dates were not completely filled in the culture register book; therefore, these variables were also excluded from this study. Dried culture tubes indicate ignorance of early inspection of culture slants, undermines the good microbiological technique (GMT), and also ends to the loss of specimen; therefore, dried tubes were considered as contaminated. In case of two different direct and indirect smears positive results from the same specimen, or any other difference between positive results of each single culture tube, the highest grade was considered. For example, if the result was (++) and the result of the other tube was (+) the result of culture was recorded as (++).

Statistical Analysis

In this study, the proposed predictors include the reason for cultivation, type of specimen, the team conducting the experiment, and the quarter of cultivation which referred to three successive months in the year (January to March, April to June, July to September, and October to December); each predictor that had complete data was illegible for statistical analysis. These predictors were examined separately against two dependent variables: the massive contamination (contamination of all three cultivated tubes) and contamination of single tube (contamination of only one or two cultivated tubes). A multivariate logistic regression model was applied to examine statistical associations at 95% confidence intervals, the reference category is first ordered ascending. Odds ratios, upper bound, lower bound, and p values were calculated, and a correlation between both types of contamination was determined.

Ethical Consideration and Publication Approval

This study is based on secondary data, and it did not involve working with any type of human subjects, clinical specimens or interventions, patients' interviews, or clinical trials; however, the proposal has been scientifically and ethically approved by the national public health laboratory ethical committee. The publication permission and approval were obtained from the general directorate of the National Public Health Laboratory (NPHL).

RESULTS

Study Subjects and Study Population

From 2 January 2019 to 31 December 2019, a number of 1,149 specimens were requested for culture in the National Tuberculosis Reference Laboratory, of which 1,125 (97.9%) were received and processed and have had a laboratory culture result. The majority of specimens (881–78.3%) were requested for treatment monitoring, whereas 83 (7.4%) were baseline specimens and the reason for culture request of 161 (14.3%) were not recorded. In addition, 1,040 (92.4%) specimens were sputum, 30 (2.7%) were other than sputum, and 55 (4.9%) were not recorded. Experiments were conducted by five principal operators in six work teams and the range of workload for culture is 51–159 specimens per month. Only 496 (43.2%) of patients' demographic information is complete and shown in **Figure 1**.

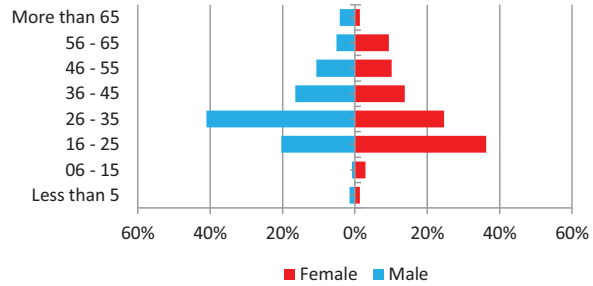

FIGURE 1 | Demographic of TB presumptive and follow-up cases.

Laboratory Culture

After following the exclusion criteria, of the 1,125 registered samples, a total of 945 (84%) samples were eligible to be included in statistical analysis; of them, 656 (73%) were smear-negative, 255 (16.7%) were smear-positive, and the remaining 97 (10.3%) were not recorded. A breakdown of results is shown in **Table 1**.

Culture Contamination

Massive contamination rates were higher in March (13.7%) and in November (8.5%). They decreased to 0.1% in January and did not occur (0%) in February, April, June, and August; Single tube contamination rates were higher in January (28.2%), November (25.2%), and in March (24.5%) (**Figure 2**).

Predictors of High Culture Contamination Rates

Out of 1,125 specimens included in this study, 180 (16%) samples were excluded from the statistical analysis. The remaining 945 samples (84%) had complete data regarding independent variables and are eligible to be included in the statistical analysis; details were shown in **Tables 3**, **4**.

DISCUSSION

The WHO laboratory quality management system LQMS document recommends management reviews of all information gathered in the laboratory records regularly (World Health Organization, 2011); the typical period for conducting a management review is annually to provide useful information about areas for improvement (International Organization for Standardization, 2005, 2012).

The accepted culture contamination rate in Löwenstein–Jensen (LJ) solid medium is 3–5% (European Centre for Disease Prevention Control, 2016). In this report culture contamination rates were higher, up to 28.2%. Inaccuracy

TABLE 1 | Frequency of smear microscopy result, reason of specimen cultivation, and culture result.

Reason for culture			Culture						Total
			Negative	Scanty	1+	2+	3+	Contamination	
Base line	Smear	Negative	28	2	3	0	0	1	34
		1+	4	1	9	6	1	0	21
		2+	1	0	4	1	4	0	10
		3+	0	0	0	1	2	0	3
		Not recorded	4	0	4	1	0	1	10
	Total		37	3	20	9	7	2	78
Follow-up	Smear	Negative	624	8	10	1	0	13	656
		Scanty	10	6	0	0	0	0	16
		1+	57	3	18	7	4	1	90
		2+	2	1	5	3	2	0	13
		3+	2	0	1	2	0	0	5
		Not recorded	73	3	3	0	0	8	87
	Total		768	21	37	13	6	22	867
Total	Smear	Negative	652	10	13	1	0	14	690
		Scanty	10	6	0	0	0	0	16
		1+	61	4	27	13	5	1	111
		2+	3	1	9	4	6	0	23
		3+	2	0	1	3	2	0	8
		Not recorded	77	3	7	1	0	9	97
	Total		805	24	57	22	13	24	945

The majority of the specimens (91.7%) were requested for treatment monitoring reasons while the remaining (8.3%) were requested for diagnosis reasons. One half of the results of smear microscopy for the diagnostic specimens were positive and the other half was negative. Noticeably, (13%) of the data were missing. Of the follow up, (75%) of specimens were smear negative, (10%) of data were missing, and (15%) were smear positive. When all specimens were pooled, 690 of them (73%) were smear negative, 97 (10.3%) of the data were not recorded, and the rest (17%) were smear positive.

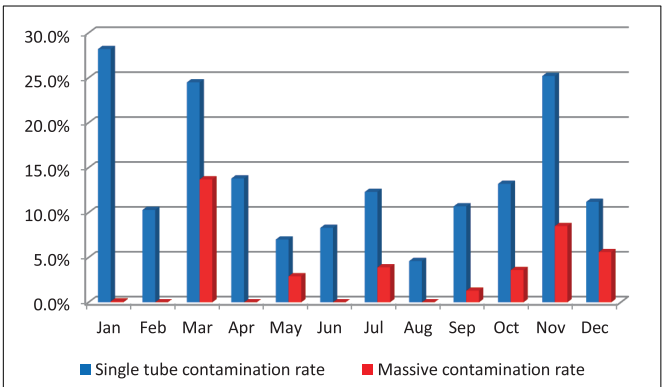

FIGURE 2 | Culture contamination rate, 2019.

of analytical processes are the most likely proposed cause of high contamination rates; however, several other factors are thought to contribute to increasing the contamination rate. High contamination rate in solid egg-based culture media is frequently seen in different settings, such as Kenya (Okumu et al., 2017) and India (Sharma et al., 2017). Further, as in other low-income countries, the laboratories infrastructure was fragile, and this could contribute to additional causes of high contamination rates (Engel et al., 2016). In this study, the team conducting the experiment was significantly associated with single tube high contamination rate; similar findings were perceived in other reports (Reddy et al., 2014). Sudan National Tuberculosis Reference Laboratory was fully staffed with experienced qualified technical personnel; however, this association might be attributed to the uneven level of proficiency or other socioeconomic factors.

Major limitations of this study were due to the missing, not recorded, or not transcribed data; this could increase the uncertainty of generated information rather than the appropriate interpretation of the study findings (Dilraj et al., 2015), as in this study approximately only one-half of data regarding age and gender was completed. However, TB epidemiology of the laboratory attendees was similar to international status (Dodd et al., 2016; Marcoa et al., 2018). Secondly, it could decrease the ability of extracting and assessing other key performance indicators in the TB culture laboratory which could be measured routinely. These indicators were highlighted in several studies. Cultures can increase TB detection by 30–50% (Demers et al., 2012; Kassaza et al., 2014). In this study, due to the negative impact of not recorded data, it was not possible to measure the recovery rate indicator. Other indicators, such as turnaround time, was also reported to affect the quality of the laboratory service (Stapleton and Sammond, 2012). The effect of delay between the collection, dispatching, and processing was seen in Burkina Faso (Kaboré et al., 2014; Reddy et al., 2014). To date, Sudan National Tuberculosis Reference Laboratory relies upon a paper-based recording system, which increases the chances of error. These limitations can partially be fixed by the development of a

TABLE 2 | Correlation between single tube contamination and massive contamination.

		Single tube contamination	Massive contamination
Single tube contamination	Pearson Correlation	1	0.262**
	P value		0.000
	N	945	945
Massive contamination	Pearson Correlation	0.262**	1
	P value	0.000	
	N	945	945

*The computed 2 × 2 table revealed a significant weak correlation between massive contaminations, and single tube contamination at 0.01; correlation coefficient was 0.262. Details are shown in this table. **Correlation is significant at the 0.01 level.*

TABLE 3 | Multivariate logistic regression of single tube contamination.

Predictor	Category	*p* value	AOR*	95% Confidence interval	
				Lower bound	Upper bound
Reason of culture	Base line	0.378	1.289	0.733	2.268
	Follow-up		1		
Type of specimen	Sputum	0.678	0.781	0.242	2.516
	Other		1		
Quarter of cultivation	Q1[a]	0.060	1.671	0.978	2.853
	Q2[b]	0.661	0.883	0.507	1.538
	Q3[c]	0.103	0.650	0.388	1.091
	Q4[d]		1		
Team of work	A	0.492	1.406	0.532	3.718
	B	0.120	2.168	0.817	5.751
	C	0.077	2.373	0.910	6.189
	D	0.289	1.697	0.639	4.509
	E	0.007	3.570	1.415	9.005
	F		1		.

*[a]January to March, [b]April to June, [c]July to September, [d]October to December. Multivariate logistic regression reveals a significant association between experiment team and single tube high contamination rate p value 0.007; AOR 3.570 (1.415–9.005). * Adjusted odds ratio.*

TABLE 4 | Multivariate logistic regression of massive culture contamination.

Predictor	Category	*p* value	AOR*	95% Confidence interval	
				Lower bound	Upper bound
Reason of culture	Base line	0.778	0.778	0.135	4.468
	Follow-up		1		
Type of specimen	Sputum	0.075	0.093	0.007	1.273
	Other		1		
Quarter of cultivation	Q1[a]	0.446	1.579	0.488	5.112
	Q2[b]	0.097	0.230	0.041	1.303
	Q3[c]	0.079	0.274	0.065	1.163
	Q4[d]		1		
Team of work	A	0.200	0.140	0.007	2.830
	B	0.136	0.102	0.005	2.056
	C	0.879	0.832	0.078	8.919
	D	0.167	0.149	0.010	2.215
	E	0.622	1.758	0.187	16.537
	F		1		

*[a]January to March, [b]April to June, [c]July to September, [d]October to December. Multivariate logistic regression reveals there is no significant statistical associations between massive contamination and proposed predictors. * Adjusted odds ratio.*

Laboratory information management system (LIMS); it is an important tool for the management of laboratory data on samples, instruments, results, and quality indicators. The LIMS can also support laboratory performance to acquire accreditation (Parsons et al., 2011).

CONCLUSION

The study concludes that high culture contamination is the greatest risk to the quality of laboratory service and can end in either the loss of specimens or delay in the decisions of initiating patients' treatment. In addition, the low quality of data increases the uncertainty and undermines the measurement of key performance indicators. Furthermore, the team conducting the experiment was found to be associated with high culture contamination rate. Therefore, the study recommends that all culture laboratory staff should be on the same level of knowledge and proficiency according to their role and should be under regular restricted supervision; in addition, laboratory management should have to use regular assessment tools for internal audits.

DATA AVAILABILITY STATEMENT

The original contributions presented in the study are included in the article/supplementary material, further inquiries can be directed to the corresponding author.

AUTHOR CONTRIBUTIONS

MM wrote the preliminary draft. RE contributed to data entry and data cleaning. SB critically reviewed the manuscript. All authors contributed to the article and approved the submitted version.

ACKNOWLEDGMENTS

We acknowledge all National Tuberculosis Reference Lab staff.

REFERENCES

Ahmad, V., Hanif, M., Chopra, K. K., Sidiq, Z., Dwivedi, K. K., and Shrivastsava, D. (2017). Isolation and identification of *Mycobacterium tuberculosis* with mixed growth from positive MGIT 960 cultures by re-decontamination. *J. Biotechnol. Biomater.* 7:3. doi: 10.4172/2155-952X.1000267

Asmar, S., and Drancourt, M. (2015). Rapid culture-based diagnosis of pulmonary tuberculosis in developed and developing countries. *Front. Microbiol.* 6:1184. doi: 10.3389/fmicb.2015.01184

Chihota, V. N., Grant, A. D., Fielding, K., Ndibongo, B., van Zyl, A., Muirhead, D., et al. (2010). Liquid vs. solid culture for tuberculosis: performance and cost in a resource-constrained setting. *Int. J. Tuberc. Lung Dis.* 14, 1024–1031.

CNCDCD, MoH, WHO, and Chest Physician Association (2018). *Sudan National TB Management Guideline*. Available online at: https://www.humanitarianresponse.info/en/operations/sudan/document/sudan-national-tb-manegement-guideline-2018 (accessed July, 2019).

Demers, A., Verver, S., Boulle, A., Warren, R., van Helden, P., Behr, M. A., et al. (2012). High yield of culture-based diagnosis in a TB-endemic setting. *BMC Infect. Dis.* 12:218. doi: 10.1186/1471-2334-12-218

Dilraj, A., Bristow, C. C., Connolly, C., Margot, B., Dlamini, S., and Podewils, L. J. (2015). Validation of sputum smear results in the electronic TB register fot the management of tuberculosis, South Africa. *Int. J. Tuberc. Lung Dis.* 17, 1317–1321. doi: 10.5588/ijtld.12.0904

Dodd, P. J., Looker, C., Plumb, I. D., Bond, V., Schaap, A., Shanaube, K., et al. (2016). Age- and sex-specific social contact patterns and incidence of *Mycobacterium tuberculosis* infection. *Am. J. Epidemiol.* 183, 156–166. doi: 10.1093/aje/kwv160

Engel, N., Wachter, K., Pai, M., Gallarda, J., Boehme, C., Celentano, I., et al. (2016). Addressing the challenges of diagnostics demand and supply: insights from an online global health discussion platform. *Br. Med. J. Glob. Health* 1:e000132. doi: 10.1136/bmjgh-2016-000132

European Centre for Disease Prevention and Control (2016). *Handbook on TB Laboratory Diagnostic Methods for the European Union*. Stockholm: ECDC.

International Organization for Standardization (2005). *ISO/IEC 17025:2005(E) General Requirements for the Competence of Testing and Calibration Laboratories*. Geneva: International Organization for Standardization.

International Organization for Standardization (2012). *Medical Laboratories—Requirements for Quality and Competence, ISO Document 15189*, 3rd Edn. Geneva: International Organization for Standardization.

Kaboré, A., Hien, H., Sanou, A., Zingué, D., Daneau, G., Ganamé, Z., et al. (2014). Impact of pre-analytical factors on mycobacterium cultures contaminations rates in Burkina Faso, West Africa. *Pan Afr. Med. J.* 19:396. doi: 10.11604/pamj.2014.19.396.5551

Kassaza, K., Orikiriza, P., Llosa, A., Bazira, J., Nyehangane, D., Page, A., et al. (2014). Lowenstein-Jensen selective medium for reducing contamination in *Mycobacterium tuberculosis* culture. *J. Clin. Microbiol.* 52, 2671–2673. doi: 10.1128/JCM.00749-14

Kidenya, B. R., Kabangila, R., Peck, R. N., Mshana, S. E., Webster, L. E., Koenig, S. P., et al. (2013). Early and efficient detection of *Mycobacterium tuberculosisin* sputum by microscopic observation of broth cultures. *PLoS One* 8:e57527. doi: 10.1371/journal.pone.0057527

Lawn, S. D., and Nicol, M. P. (2015). Dead or alive: can viability staining predict response to tuberculosis treatment? *Clin. Infect. Dis.* 60, 1196–1198. doi: 10.1093/cid/ciu1156

Marcoa, R., Ribeiro, A. I., Zãoc, I., and Duartea, R. (2018). Tuberculosis and gender — factors influencing the risk of tuberculosis among men and women by age group. *Pulmonology* 24, 199–202. doi: 10.1016/j.pulmoe.2018.03.004

Okumu, A., McCarthy, K., Orwa, J., Williamson, J., Musau, S., Alexander, H., et al. (2017). Comparison of *Mycobacterium tuberculosis* complex yield and contamination rates using Lowenstein-Jensen with and without antibiotics in Western Kenya. *JMSCR* 05, 26503–26511. doi: 10.18535/jmscr/v5i8.86

Parsons, L. M., Somosko, A., Gutierrez, C., Lee, E., Paramasivan, C. N., Abimiku, A., et al. (2011). Laboratory diagnosis of tuberculosis in resource-poor countries: challenges and opportunities. *Clin. Microbiol. Rev.* 24, 314–350. doi: 10.1128/CMR.00059-10

Rageade, F., Picot, N., Blanc-Michaud, A., Chatellier, S., Mirande, C., Fortin, E., et al. (2014). Performance of solid and liquid culture media for the detection of *Mycobacterium tuberculosis* in clinical materials: meta-analysis of recent studies. *Eur. J. Clin. Microbiol. Infect. Dis.* 33, 867–870. doi: 10.1007/s10096-014-2105-z

Reddy, M., Gounder, S., and Reid, S. A. (2014). Tuberculosis diagnostics in Fiji: how reliable is culture? *Public Health Action* 4, 184–188. doi: 10.5588/pha.14.0019

Sharma, S., Chatterjee, B., Bhargava, A., Kotwal, A., and Sindhwani, G. (2017). Comparison of rapid slide culture with culture in L-J medium and MGIT for isolating *Mycobacterium tuberculosis* from Bronchoalveolar Lavage fluid. *Indian J. Microbiol. Res.* 4, 384–387. doi: 10.18231/2394-5478.2017.0085

Stapleton, K., and Sammond, D. (2012). Improved laboratory stat test turnaround time using lean six sigma. *Am. J. Clin. Pathol.* 138:A184.

Su, W. J., Feng, J. Y., Chiu, Y. C., Huang, S. F., and Lee, Y. C. (2011). Role of 2-month sputum smears in predicting culture conversion in pulmonary tuberculosis. *Eur. Respir. J.* 37, 376–383. doi: 10.1183/09031936.00007410

Wong, C., Ngan, P. H., Michal, E., Pawlowski, M. E., Edward, A., Graviss, E. A., et al. (2016). Differentiating between live and dead *Mycobacterium smegmatis* using autofluorescence. *Tuberculosis (Edinb).* 101, S119–S123. doi: 10.1016/j.tube.2016.09.010

World Health Organization (1998). *Laboratory Services in Tuberculosis Control, Part III: Culture*. Geneva: World Health Organization.

World Health Organization (2011). *Laboratory Quality Management System*. Geneva: World Health Organization.

World Health Organization (2014). *Companion Handbook to the WHO Guidelines for the Programmatic Management of Drug-Resistant Tuberculosis*. Geneva: World Health Organization.

Conflict of Interest: The authors declare that the research was conducted in the absence of any commercial or financial relationships that could be construed as a potential conflict of interest.

frontiers | Frontiers in Microbiology

MINI REVIEW
published: 11 May 2022
doi: 10.3389/fmicb.2022.817661

Rapid Molecular Diagnosis of Extra-Pulmonary Tuberculosis by Xpert/RIF Ultra

*Laura Rindi**

Dipartimento di Ricerca Traslazionale e delle Nuove Tecnologie in Medicina e Chirurgia, Università di Pisa, Pisa, Italy

Rapid detection of *Mycobacterium tuberculosis* complex and determination of drug resistance are essential for early diagnosis and treatment of tuberculosis (TB). Xpert MTB/RIF Ultra (Xpert Ultra), a molecular test that can simultaneously identify *M. tuberculosis* complex and resistance to rifampicin directly on clinical samples, is currently used. Xpert Ultra represents a helpful tool for rapid pulmonary TB diagnosis, especially in patients with paucibacillary infection. The aim of this review is to provide an overview of the diagnostic performance of Xpert Ultra in detection of extra-pulmonary tuberculosis.

Keywords: ***Mycobacterium tuberculosis*, diagnosis, Xpert Ultra, extra-pulmonary, tuberculosis**

OPEN ACCESS

Edited by:
Xiao-Yong Fan,
Fudan University, China

Reviewed by:
Guido Vincent Bloemberg,
University of Zurich, Switzerland
Shampa Anupurba,
Banaras Hindu University, India

***Correspondence:**
Laura Rindi
laura.rindi@unipi.it

Specialty section:
This article was submitted to Infectious Agents and Disease, a section of the journal Frontiers in Microbiology

Received: *18 November 2021*
Accepted: *11 April 2022*
Published: *11 May 2022*

Citation:
Rindi L (2022) Rapid Molecular Diagnosis of Extra-Pulmonary Tuberculosis by Xpert/RIF Ultra. Front. Microbiol. 13:817661. doi: 10.3389/fmicb.2022.817661

INTRODUCTION

Tuberculosis (TB) currently represents a major infectious disease worldwide. In 2019, the World Health Organization (WHO) estimated 1.2 million deaths and 7.1 million new cases (World Health Organization [WHO], 2020). Although TB mainly affects the lung parenchyma, *Mycobacterium tuberculosis* can spread to extra-pulmonary sites. On average, extra-pulmonary TB (EPTB) accounted for 16% of active cases of TB reported in 2019 (World Health Organization [WHO], 2020), with the proportion being greater among children and individuals positive for HIV. Pleurae and lymph nodes are the most common sites of involvement in EPTB, while meningeal TB, the most serious form of TB infection, occurs less frequently. EPTB diagnosis remains a great challenge because of the paucibacillary nature of the disease, subclinical or non-specific symptoms, and difficulties in obtaining qualified clinical specimens for *M. tuberculosis* detection.

In 2013 the World Health Organization (WHO) endorsed the use of Xpert MTB/RIF (Xpert) assay (Cepheid, Sunnyvale, CA, United States), a semi-automated cartridge-based molecular test, which allows for rapid TB diagnosis by simultaneous detection of *M. tuberculosis* complex and resistance to rifampicin (Boehme et al., 2010; Lawn et al., 2011; Theron et al., 2014; Detjen et al., 2015). However, the sensitivity of this assay is poor when the load of bacilli is very low and remains variable when tested on different types of extra-pulmonary specimens (Theron et al., 2014). Several systematic reviews and meta-analyses evaluated the performance of Xpert and reported pooled sensitivity ranging from 69 to 83% (Maynard-Smith et al., 2014; Penz et al., 2015; Jiang et al., 2020). Recently, the new version Xpert MTB Ultra (Xpert Ultra) has been developed to overcome the limitations of the Xpert assay (Chakravorty et al., 2017) and has been endorsed by the WHO in 2017. The Xpert Ultra system, based on the amplification of two multicopy sequences and characterized by improved assay chemistry, offers a greater sensitivity given the decreased limit of detection of *M. tuberculosis*. A prospective multicenter diagnostic accuracy study showed the excellent sensitivity of Xpert Ultra for detection of pulmonary TB,

especially for paucibacillary specimens (i.e., from individuals with smear-negative TB or HIV infection) (Dorman et al., 2018). Similar results were found when the diagnostic performance of Xpert Ultra was evaluated for the detection of pediatric pulmonary TB (Sabi et al., 2018). Further studies confirmed that Xpert Ultra represents a useful tool for rapid diagnosis of pulmonary TB (Hodille et al., 2019; Kolia-Diafouka et al., 2019; Opota et al., 2019b; Ssengooba et al., 2020).

The Xpert Ultra assay has different sensitivities and specificities for detecting *M. tuberculosis* complex obtained from lymph nodes, pleural fluid, gastrointestinal tract, genitourinary system, cerebrospinal fluid, and other samples (Opota et al., 2019a; Zhang et al., 2020; Park and Kon, 2021). The aim of this review is to provide an overview of the current knowledge of the diagnostic accuracy of Xpert Ultra for the detection of EPTB, taking into consideration a broad range of different types of extra-pulmonary specimens. Recently, several studies have addressed the performance of Xpert Ultra for the diagnosis of EPTB, evaluating the diagnostic accuracy of Xpert Ultra compared with culture and/or a composite reference standard (CRS) based on clinical, laboratory, histopathologic, and radiological features. **Table 1** summarizes the diagnostic performance of Xpert Ultra on EPTB specimens. The following paragraphs will consider the studies carried out on each of the main EPTB specimens.

Pleural Fluid/Tissue

Pleural TB is the most common type of EPTB in adults (World Health Organization [WHO], 2020). The diagnosis of pleural TB, depending on detection of *M. tuberculosis* in pleural fluids or biopsy tissues, is often challenging given the paucibacillary nature of the disease (Shaw et al., 2018). Recently, several studies have addressed the performance of Xpert Ultra for the diagnosis of pleural TB. In Wang et al. (2019) analyzed 108 pleural fluid specimens and showed an overall sensitivity of Xpert Ultra of 61.1%; the sensitivity was 84.2% vs. culture. In a larger multicenter cohort study, which included pleural fluids from 208 individuals diagnosed with pleural TB, the same authors reported a sensitivity of 44.2% against CRS and a sensitivity of 83.6% among pleural effusion culture-positive cases (Wang et al., 2020). This is in line with a further publication, where 43.7% of 103 pleural fluids were detected by Xpert Ultra (Wu et al., 2019). Perez-Risco et al. (2018) evaluated the diagnostic performance of Xpert Ultra on different types of extra-pulmonary specimens, including pleural fluids and biopsy tissues, demonstrating that 47.6% of culture-positive pleural fluids were detected by Xpert Ultra; this study also included 2 pleural biopsy samples, both detected by Xpert Ultra. A prospective observational study revealed a poor sensitivity (37.5%) of Xpert Ultra for the diagnosis of bacteriologically and/or histopathologically confirmed pleural TB; moreover, the authors demonstrated that pleural fluid concentration did not significantly improve the sensitivity of Xpert Ultra (Meldau et al., 2019). Another study, conducted in a high-resource setting with low TB prevalence, reported a sensitivity of Xpert Ultra compared with culture of 50% on pleural fluid samples, showing the lowest sensitivity among non-respiratory samples (López-Roa et al., 2021); as previously described (Perez-Risco et al., 2018), also in this case, the only 2 culture-positive biopsy tissues were detected by Xpert Ultra (López-Roa et al., 2021). A further study that assessed Xpert Ultra against culture in pleural fluid specimens found a sensitivity of 66.7% (Mekkaoui et al., 2021). Finally, in a most recent study, Xpert Ultra on 27 pleural fluid and 27 biopsy tissue samples yielded a sensitivity of 48.1 and 81.5%, respectively, showing that Xpert Ultra with pleural biopsy alone had a diagnostic capacity equivalent to that of pathological examination for pleural TB diagnosis. Moreover, the "trace" positive outcome of Xpert Ultra was highly supportive of TB diagnosis for both biopsy tissue and pleural fluid examinations (Gao et al., 2021).

For all the studies mentioned above, Xpert Ultra showed a specificity ranging from 95.1% for biopsy and 98.5% for fluid to 100%. When evaluated, rifampicin susceptibility results of Xpert Ultra were fully concordant with phenotypic results.

From the above data, it appears that Xpert Ultra, even if it showed a variable sensitivity in the different studies, has a great potential in the rapid diagnosis of pleural TB. In fact, when its outcomes were integrated into the CRS, an obvious increase in the percentage of patients with defined TB was observed. Moreover, pleural biopsy tissues provided higher yields than pleural fluids; however, the sensitivity of Xpert Ultra in pleural biopsy specimens should be accurately assessed in larger populations.

Lymph Node Aspirate/Tissue

Tuberculosis lymphadenitis is a common extra-pulmonary manifestation of TB, both in low- and high- prevalence TB areas. Cervical lymph nodes are the most typical TB lymphadenopathy site (Qian et al., 2019). Perez-Risco et al. (2018) who evaluated the diagnostic performance of Xpert Ultra on 25 lymph node specimens with culture as the reference standard, showed a sensitivity of 94.1% and a specificity of 100%. Lower sensitivity of 75% vs. culture was reported in a multicenter study in a high-resource setting with low TB prevalence that included 51 lymph node tissues; the specificity was 95.3% (López-Roa et al., 2021). A recent large study, which assessed the performance of Xpert Ultra on 196 lymph node samples, reported a sensitivity of 95.6% and a specificity of 86.1% using a culture reference standard (Mekkaoui et al., 2021). Moreover, the diagnostic accuracy of Xpert Ultra for TB adenitis was prospectively evaluated on 99 adult patients from whom fine-needle aspirates (FNAs) and biopsy tissues were obtained using the CRS. Xpert Ultra sensitivity on FNAs was 70% and on tissues was 67% when compared with culture. Xpert Ultra on FNAs had a sensitivity of 78% and on tissues 90%; the specificity ranged from 96 to 100% using the CRS, and from 78 to 87% using culture as the reference standard. These findings support the use of Xpert Ultra on FNAs as an initial test when TB adenitis is suspected, as Xpert Ultra has a high sensitivity, is minimally invasive, and gives rapid results (Antel et al., 2020). More recently, Xpert Ultra has proved to be highly sensitive for the diagnosis of TB lymphadenitis in an HIV-endemic setting; this study reported sensitivity and a specificity of 91 and 76%, respectively, for 46 FNA biopsies using a culture and cytology reference standard (Minnies et al., 2021). Several other studies, which, however, analyzed a limited

TABLE 1 | Diagnostic performance of Xpert MTB/RIF Ultra (Xpert Ultra) on extra-pulmonary TB (EPTB) specimens.

Specimen type	Sensitivity		Number of specimens		References
	vs Culture	vs CRS	Culture-Positive	Total	
Pleural fluid	84.2%	61.1%	57	108	Wang et al., 2019
	83.6%	44.2%	55	208	Wang et al., 2020
		43.7%		103	Wu et al., 2019
	47.6%		21	24	Perez-Risco et al., 2018
		37.5%		48	Meldau et al., 2019
	50%		6	118	López-Roa et al., 2021
	66.7%		9	77	Mekkaoui et al., 2021
	50%	48.1%	6	27	Gao et al., 2021
Pleural tissue	100%		2	2	Perez-Risco et al., 2018
	100%		2	41	López-Roa et al., 2021
	100%	81.48%	9	27	Gao et al., 2021
Lymph node tissue	94.1%		17	25	Perez-Risco et al., 2018
	75%		8	51	López-Roa et al., 2021
	95.8%		24	196	Mekkaoui et al., 2021
	90%	66.7%	10	24	Antel et al., 2020
		91.3%		46	Minnies et al., 2021
	50%		10	10	Bisognin et al., 2018
	100%	40%	1	5	Hoel et al., 2020
		33.3%		3	Piersimoni et al., 2019
Lymph node aspirate	77.8%	70%	9	30	Antel et al., 2020
	100%	26.7%	4	15	Hoel et al., 2020
CSF		44.2%		43	Wang et al., 2019
		33.3%		6	Piersimoni et al., 2019
	90%	95.4%	10	22	Bahr et al., 2018
	80%	63.6%	5	11	Chin et al., 2019a
		92.9%		42	Cresswell et al., 2020b
	90.9%	59.5%	22	42	Donovan et al., 2020
	96.4%	72%	56	204	Sharma et al., 2020
		46.7%		60	Shao et al., 2020
	71.4%	45%	14	76	| Huang et al., 2021
Joint fluid	87.5%		8	9	Perez-Risco et al., 2018
Osteoarticular pus	62.5%		8	8	Perez-Risco et al., 2018
	96.1%	90.9%	52	132	Sun et al., 2019
Osteoarticular biopsy	100%		2	21	Perez-Risco et al., 2018
	100%		3	27	Mekkaoui et al., 2021
Urine	100%		12	24	Perez-Risco et al., 2018
	100%		2	6	López-Roa et al., 2021
		18%[a]		84[a]	Minnies et al., 2021[a]
		17.2%[b]		203[b]	Andama et al., 2020[b]
		33.9%[c]		56[c]	Cresswell et al., 2020a[c]
Gastric aspirate	75%		4	5	Perez-Risco et al., 2018
	50%		2	2	Bisognin et al., 2018
		60%		5	Piersimoni et al., 2019
	87.5%	60.5%	48	129	Sun et al., 2020
	85.4%	52.5%	48	141	Sun et al., 2021
Stool	80%		5	8	Perez-Risco et al., 2018
		60.3%		141	Sun et al., 2021
	83.3%		72	111	Kabir et al., 2021
		45.5%		126	Liu et al., 2021

[a] *TB lymphadenitis;* [b] *pulmonary TB;* [c] *TB meningitis.*

number of lymph node samples, demonstrated a significant diagnostic performance of Xpert Ultra in the detection of *M. tuberculosis* on lymph node specimens, supporting its use for the diagnosis of TB lymphadenitis, at least as an early test (Bisognin et al., 2018; Piersimoni et al., 2019; Hoel et al., 2020; Menichini et al., 2020).

TABLE 2 | Correlation between sensitivity of Xpert Ultra and cerebrospinal fluid (CSF) testing protocol.

Sensitivity		CSF protocol			References
vs Culture	vs CRS	Volume (ml)	Fresh/Frozen	Centrifugation step	
	44.2%	1	Fresh	No	Wang et al., 2019
90%	95.4%	0.5	Frozen	Yes (10 ml centrifugated and resuspended in 2 ml)	Bahr et al., 2018
80%	63.6%	2	Fresh	No	Chin et al., 2019a
	92.9%	0.5	Fresh	Yes (unknown ml centrifugated and resuspended in 2 ml)	Cresswell et al., 2020b
90.9%	59.5%	0.2	Fresh	Yes (6 ml centrifugated and resuspended in 0.5 ml)	Donovan et al., 2020
96.4%	72%	1	Fresh	No	Sharma et al., 2020
	46.7%	1	Fresh	No	Shao et al., 2020
71.4%	45%	1	Fresh	No	Huang et al., 2021

Cerebrospinal Fluid

Tuberculosis meningitis is the most serious type of EPTB, determining high mortality and severe disabilities (Manyelo et al., 2021). Among individuals positive for HIV, TB meningitis causes mortality of over 50% (Wilkinson et al., 2017). Rapid diagnosis, hampered by the paucibacillary nature of the disease and small volume of CSF, and adequate treatment are essential for the control of meningeal TB. Xpert Ultra is recommended as the initial diagnostic test for suspected TB meningitis, as confirmed in a prospective cohort study aimed to evaluate the performance of Xpert Ultra in 129 adults positive for HIV in Uganda: Xpert Ultra sensitivity was 70% for probable or definite TB meningitis, and it increased to 95% against CRS (Bahr et al., 2018). A further evaluation of Xpert Ultra sensitivity in meningeal TB by Wang et al. tested 43 CSF specimens and showed a sensitivity of 44.4% and 86.36, using the CRS and bacteriological positivity as reference standards, respectively (Wang et al., 2019). In another study performed on 11 patients with TB meningitis, the sensitivity of Xpert Ultra was 63.6% (Chin et al., 2019a). In a following prospective validation study, including 51 participants with probable or definite TB meningitis, Xpert Ultra had 75.5% sensitivity; against the composite microbiological reference standard, Xpert Ultra had a sensitivity of 92.9%. The authors concluded that, despite the high sensitivity, Xpert Ultra cannot be used as a rule-out test given the negative predictive value of 93% (Cresswell et al., 2020b). Similar conclusions were reported by Donovan et al. (2020), who, however, described a lower overall sensitivity of 59.5% in diagnosing meningeal TB; in this prospective, randomized, diagnostic accuracy study, the sensitivity of Xpert Ultra against a reference standard of definite, probable, and possible TB meningitis was 47.2%. In particular, in patients negative for HIV, the sensitivity was 38.9%, while in patients co-infected with HIV, the sensitivity was 64.3%. A diagnostic accuracy study from India that assessed the performance of Xpert Ultra on 204 CSF samples reported an overall sensitivity of 72.05% (96.42 and 62.83% for definite and probable TB meningitis, respectively, where definite TB indicates cases in which *M. tuberculosis* was isolated from CSF culture and probable TB indicates cases that were culture/smearnegative but had a diagnostic score of >10), and a specificity of 100% (Sharma et al., 2020). A further prospective multicenter study was conducted in China on 60 individuals with symptoms suggestive of TB meningitis; using microbiological evidence as a reference, the sensitivity of Xpert Ultra was 93.3%. Xpert correctly identified 28 cases of TB meningitis, indicating an overall sensitivity of 46.7% (Shao et al., 2020). More recently, Xpert Ultra on 160 CSF specimens yielded a sensitivity of 45% for definite, probable, and possible TB meningitis and 81% for definite TB meningitis, thus suggesting that Xpert Ultra, outperforming culture, may speed up the diagnosis and appropriate treatment of patients (Huang et al., 2021).

The studies described above show variability in the sensitivity values of Xpert Ultra, probably also due to the different protocols used, such as volume of CSF specimens, fresh or frozen samples, and centrifugation or not of the sample. As shown in **Table 2**, the sensitivity of Xpert Ultra increases with the centrifugation step; on the other hand, sample volume does not affect the performance of Xpert Ultra. The identification of a standardized procedure should be a priority to improve the management of TB meningitis. A recent study described optimal procedures for the detection of *M. tuberculosis* in CSF using Xpert Ultra, recommending careful attention to the collection, handling, and processing of CSF to maximize the performance of Xpert Ultra (Chin et al., 2019b). However, the contribution of Xpert Ultra is extremely valuable for rapid diagnosis of TB meningitis, and its application as an initial test on CSF could represent an excellent diagnostic tool.

Bone and Joint Fluid/Tissue

Diagnosis of osteoarticular TB is quite challenging given the low bacterial load present in joint and bone specimens and difficulty in obtaining specimens, since tubercle bacilli are present deep inside tissues. In Perez-Risco et al. (2018) analyzed several kinds of osteoarticular specimens, including 9 joint fluids, 3 paravertebral abscess aspirates, 5 osteitis abscess aspirates, 2 intervertebral disc biopsies, 4 bone biopsies, 3 synovial tissues, and 18 joint biopsies; the sensitivity of Xpert Ultra vs. culture ranged from 60% for osteitis abscess aspirates to 100% for the disc, bone, and synovial biopsies. In a study aimed at analyzing the diagnostic value of Xpert Ultra for osteoarticular TB in a high-burden setting, which included 132 osteoarticular pus specimens, sensitivities of 90.91 and 96.15 against the CRS and culture, respectively, were reported; when Xpert Ultra outcomes were integrated, the percentage of confirmed osteoarticular

TB cases increased from 84 to 94%. Xpert Ultra showed a specificity of 100% and full concordance with the phenotypic test for the detection of rifampicin resistance (Sun et al., 2019). A recent study, which assessed the performance of Xpert Ultra on 27 osteoarticular samples, reported a sensitivity of 100% and a specificity of 87.5% using a culture reference standard (Mekkaoui et al., 2021). Therefore, Xpert Ultra was proved capable of detecting significantly more osteoarticular TB cases than culture, making it a helpful tool for rapid diagnosis of osteoarticular TB.

Urine

Urogenital TB, responsible for 15– 40% of EPTB cases, is one of the most common forms of EPTB in both less and more developed regions (Figueiredo et al., 2017). The disease is often associated with delayed diagnosis and treatment, leading to serious consequences, such as renal failure. To date, only a few studies, which included urine in the analysis of extra-pulmonary samples, have evaluated the performance of Xpert Ultra on urine specimens for the rapid diagnosis of urinary tract TB. Perez-Risco et al. (2018) who evaluated the diagnostic performance of Xpert Ultra on 24 urine specimens with culture as the reference standard, showed a sensitivity of 100% and a specificity of 100%. A further study, which analyzed a small number of urine samples, again reported a 100% sensitivity of Xpert Ultra against culture (López-Roa et al., 2021).

Recently, there has been a growing interest in using Xpert Ultra on urine specimens to diagnose non-genitourinary TB. A first study aimed to evaluate the performance of urine Xpert Ultra for pulmonary TB reported low sensitivity (17.2%) but high specificity (98.1%), in reference to sputum-based testing. However, the sensitivity of Xpert Ultra was higher than TB-lipoarabinomannan (TB-LAM) assay and reached 50% in patients positive for HIV, with CD4 <100 cells/ml, thus suggesting that Xpert Ultra on urine samples could be an alternative approach for individuals with advanced HIV infection and unable to produce sputum samples (Andama et al., 2020). Moreover, urine Xpert Ultra has been used to diagnose disseminated TB in a case report, showing to be a useful adjunctive diagnostic tool for HIV-associated TB (Atherton et al., 2018). A further study determined the prevalence of disseminated TB by testing urine specimens with Xpert Ultra in adults positive for HIV with suspected meningitis. Urine Xpert Ultra was positive in 12% of the tested cohort, and in 41% of patients with definite TB meningitis, demonstrating that urine is an additional viable clinical specimen for use with Xpert Ultra. Despite the lack of concordance between Xpert Ultra and TB-LAM assay, which needs further investigation, the use of Xpert Ultra with urine could represent a rapid and non-invasive test for suspected TB meningitis and a prognostic tool in individuals positive for HIV with TB meningitis (Cresswell et al., 2020a). A recent study by Minnies et al. assessed the performance of Xpert Ultra on urine samples for the diagnosis of TB lymphadenitis: Xpert Ultra had a low sensitivity (18%) and a high specificity (98%) when tested on urine specimens compared to FNA biopsies; none of the patients negative for HIV had any positive urine Xpert Ultra, while 12% of the patients positive for HIV were urine Xpert Ultra-positive, thus indicating that the use of Xpert Ultra on urine from patients positive for HIV with presumptive TB lymphadenitis could reduce invasive sampling (Minnies et al., 2021). Therefore, urine Xpert Ultra as a tool to diagnose pulmonary or disseminated TB seems to offer good diagnostic usefulness for patients infected with HIV.

Gastric Aspirate

Gastric aspirates represent an alternative type of specimen for the diagnosis of pulmonary TB in patients, especially children, who have difficulty producing sputum. Perez-Risco et al. (2018) found Xpert Ultra to be 75% sensitive for 4 culture-positive gastric aspirate specimens in adults. A multicenter accuracy study performed to evaluate the value of testing gastric aspirate with Xpert Ultra for diagnosis of childhood TB reported a sensitivity of 87.5 and 60.5% in bacteriologically confirmed TB and in total TB cases, respectively; in particular, the sensitivity was 80% in children aged <4 years, which is significantly higher than that in older children (48.1%). The specificity of Xpert ultra was 99.4%. In conclusion, the study showed that Xpert Ultra on gastric aspirate samples had a diagnostic value for the early and accurate diagnosis of TB, especially in younger children (Sun et al., 2020). More recently, the same authors analyzed the performance of Xpert Ultra on gastric aspirate specimens for the diagnosis of pediatric pulmonary TB in a high-burden area in China and reported an overall sensitivity of 52.5% and a sensitivity of 85.4% for 48 children with confirmed TB, concluding that gastric aspirate Xpert Ultra is an appropriate test for bacteriological TB confirmation in children (Sun et al., 2021).

Stool

Microbiological confirmation of pulmonary TB in children with sputum is often difficult given the low volume and poor quality of specimens; induced sputa and gastric aspirates, obtained by invasive procedures, have a low diagnostic yield and may be inaccessible in low-resource settings. Stool samples are easily obtainable and represent promising alternatives to respiratory specimens for childhood TB. Recently, some stool processing methods for Xpert Ultra have been developed (Lounnas et al., 2020; Jasumback et al., 2021). Perez-Risco et al. (2018) found Xpert Ultra to be 80% sensitive for 5 culture-positive stool specimens in adults. A cross-sectional study on children aged <15 years from Bangladesh that assessed the performance of Xpert Ultra on stool to diagnose pulmonary TB in children reported a sensitivity of 83.3% (60 were positive out of 72 bacteriologically confirmed cases); a high proportion of Xpert Ultra positive assays had trace results (Kabir et al., 2021). More recently, Sun et al. (2021) analyzed the performance of Xpert Ultra on stool specimens for the diagnosis of pediatric pulmonary TB in a high-TB burden and resource-limited area in China, and reported an overall sensitivity of 60.3%. Among 48 children with confirmed TB, Xpert Ultra testing was equally sensitive on stool and gastric aspirate specimens (85.4%); however, the agreement between Xpert on stool and on gastric aspirate was moderate in children with active TB (Sun et al., 2021). A prospective cohort study revealed a 45.5% sensitivity of Xpert Ultra using stool specimens for the diagnosis of

pulmonary TB in children; moreover, the authors demonstrated that stool sample-based Xpert Ultra was a comparable alternative to *M. tuberculosis* culture on respiratory samples (Liu et al., 2021). In conclusion, testing stool specimens with Xpert Ultra may provide a useful diagnostic tool for detecting pediatric pulmonary TB.

CONCLUSION

Xpert Ultra represents the most recent advancement in the rapid molecular diagnosis of TB. Many studies have shown a potential for the use of Xpert Ultra in extra-pulmonary specimens. Xpert Ultra sensitivity differs by specimen type, with higher sensitivity among specimens obtained from lymph nodes (ranging from 50 to 100%) and CSF (ranging from 71.4 to 96.4%), and lower sensitivity when using pleural fluids (ranging from 47.6 to 84.2%). Moreover, the performance of Xpert Ultra proved to be particularly high in special populations, such as pediatric TB and HIV co-infected TB. In addition, the use of Xpert Ultra on extra-pulmonary samples, i.e., gastric aspirate and stool, has been demonstrated to be helpful for detecting pulmonary TB.

Although negative Xpert Ultra results are not sufficient to rule out TB, positive Xpert Ultra results may be useful in rapidly identifying EPTB cases, thus suggesting that Xpert Ultra is a useful rule-in rapid diagnostic test that can improve the definitive diagnosis of EPTB.

AUTHOR CONTRIBUTIONS

LR reviewed the literature and wrote the manuscript.

REFERENCES

Andama, A., Jaganath, D., Crowder, R., Asege, L., Nakaye, M., Katumba, D., et al. (2020). Accuracy and incremental yield of urine Xpert MTB/RIF Ultra versus determine TB-LAM for diagnosis of pulmonary tuberculosis. *Diagn. Microbiol. Infect. Dis.* 96:114892. doi: 10.1016/j.diagmicrobio.2019.114892

Antel, K., Oosthuizen, J., Malherbe, F., Louw, V. J., Nicol, M. P., Maartens, G., et al. (2020). Diagnostic accuracy of the Xpert MTB/Rif Ultra for tuberculosis adenitis. *BMC Infect. Dis.* 20:33. doi: 10.1186/s12879-019-4749-x

Atherton, R. R., Cresswell, F. V., Ellis, J., Skipper, C., Tadeo, K. K., Mugumya, G., et al. (2018). Detection of *Mycobacterium tuberculosis* in urine by Xpert MTB/RIF Ultra: a useful adjunctive diagnostic tool in HIV-associated tuberculosis. *Int. J. Infect. Dis.* 75, 92–94. doi: 10.1016/j.ijid.2018.07.007

Bahr, N. C., Nuwagira, E., Evans, E. E., Cresswell, F. V., Bystrom, P. V., Byamukama, A., et al. (2018). Diagnostic accuracy of XpertMTB/RIF Ultra for tuberculous meningitis in HIV-infected adults: a prospective cohort study. *Lancet Infect. Dis.* 18, 68–75. doi: 10.1016/S1473-3099(17)30474-7

Bisognin, F., Lombardi, G., Lombardo, D., Re, M. C., and Dal Monte, P. (2018). Improvement of *Mycobacterium tuberculosis* detection by Xpert MTB/RIF Ultra: a head-to-head comparison on Xpert-negative samples. *PLoS One* 13:e0201934. doi: 10.1371/journal.pone.0201934

Boehme, C., Nabeta, P., Hillemann, D., Nicol, M., Shenai, S., Krapp, F., et al. (2010). Rapid molecular detection of tuberculosis and rifampicin resistance. *N. Engl. J. Med.* 363, 1005–1015. doi: 10.1056/NEJMoa0907847

Chakravorty, S., Simmons, A. M., Rowneki, M., Parmar, H., Cao, Y., Ryan, J., et al. (2017). The new Xpert MTB/RIF Ultra: improving detection of *Mycobacterium tuberculosis* and resistance to rifampin in an assay suitable for point-of-care testing. *mBio* 8:e00812-17. doi: 10.1128/mBio.00812-17

Chin, J. H., Musubire, A. K., Morgan, N., Pellinen, J., Grossman, S., Bhatt, J. M., et al. (2019a). Xpert MTB/RIF Ultra for detection of *Mycobacterium tuberculosis* in cerebrospinal fluid. *J. Clin. Microbiol.* 57:e00249-19. doi: 10.1128/JCM.00249-19

Chin, J. H., Ssengooba, W., Grossman, S., Pellinen, J., and Wadda, V. (2019b). Xpert MTB/RIF Ultra: optimal procedures for the detection of *Mycobacterium tuberculosis* in cerebrospinal fluid. *J. Clin. Tuberc. Other Mycobact. Dis.* 14, 16–18. doi: 10.1016/j.jctube.2019.01.002

Cresswell, F. V., Tugume, L., Bahr, N. C., Kwizera, R., Bangdiwala, A. S., Musubire, A. K., et al. (2020b). Xpert MTB/RIF Ultra for the diagnosis of HIV-associated tuberculous meningitis: a prospective validation study. *Lancet Infect. Dis.* 20, 308–317. doi: 10.1016/S1473-3099(19)30550-X

Cresswell, F. V., Ellis, J., Kagimu, E., Bangdiwala, A. S., Okirwoth, M., Mugumya, G., et al. (2020a). Standardized urine-based tuberculosis (TB) screening with TB-lipoarabinomannan and Xpert MTB/RIF Ultra in ugandan adults with advanced human immunodeficiency virus disease and suspected meningitis. *Open Forum Infect. Dis.* 7:ofaa100. doi: 10.1093/ofid/ofaa100

Detjen, A. K., DiNardo, A. R., Leyden, J., Steingart, K. R., Menzies, D., Schiller, I., et al. (2015). Xpert MTB/RIF assay for the diagnosis of pulmonary tuberculosis in children: a systematic review and meta-analysis. *Lancet Respir. Med.* 3, 451–461. doi: 10.1016/S2213-2600(15)00095-8

Donovan, J., Thu, D. D. A., Phu, N. H., Dung, V. T. M., Quang, T. P., and Nghia, H. D. T. (2020). Xpert MTB/RIF Ultra versus Xpert MTB/RIF for the diagnosis of tuberculous meningitis: a prospective, randomised, diagnostic accuracy study. *Lancet Infect. Dis.* 20, 299–307.

Dorman, S. E., Schumacher, S. G., Alland, D., Nabeta, P., Armstrong, D. T., King, B., et al. (2018). Xpert MTB/RIF Ultra for detection of *Mycobacterium tuberculosis* and rifampicin resistance: a prospective multicentre diagnostic accuracy study. *Lancet Infect. Dis.* 18, 76–84.

Figueiredo, A. A., Lucon, A. M., and Srougi, M. (2017). Urogenital tuberculosis. *Microbiolspectr* 5. doi: 10.1128/microbiolspec.TNMI7-0015-2016

Gao, S., Wang, C., Yu, X., Teng, T., Shang, Y., Jia, J., et al. (2021). Xpert MTB/RIF Ultra enhanced tuberculous pleurisy diagnosis for patients with unexplained exudative pleural effusion who underwent a pleural biopsy via thoracoscopy: a prospective cohort study. *Int. J. Infect. Dis.* 106, 370–375. doi: 10.1016/j.ijid.2021.04.011

Hodille, E., Maisson, A., Charlet, L., Bauduin, C., Genestet, C., Fredenucci, I., et al. (2019). Evaluation of Xpert MTB/RIF Ultra performance for pulmonary tuberculosis diagnosis on smear-negative respiratory samples in a French centre. *Eur. J. Clin. Microbiol. Infect. Dis.* 38, 601–605. doi: 10.1007/s10096-018-03463-1

Hoel, I. M., Syre, H., Skarstein, I., and Mustafa, T. (2020). Xpert MTB/RIF Ultra for rapid diagnosis of extrapulmonary tuberculosis in a high-income low-tuberculosis prevalence setting. *Sci. Rep.* 10:13959. doi: 10.1038/s41598-020-70613-x

Huang, M., Wang, G., Sun, Q., Jiang, G., Li, W., Ding, Z., et al. (2021). Diagnostic accuracy of Xpert MTB/RIF Ultra for tuberculous meningitis in a clinical practice setting of China. *Diagn. Microbiol. Infect. Dis.* 100:115306. doi: 10.1016/j.diagmicrobio.2020.115306

Jasumback, C. L., Dlamini, Q., Kahari, J., Maphalala, G., Dlamini, M. G., Dube, G. S., et al. (2021). Laboratory comparison of stool processing methods for Xpert® Ultra. *Public Health Action*. 11, 55–57. doi: 10.5588/pha.20.0079

Jiang, J., Yang, J., Shi, Y., Jin, Y., Tang, S., Zhang, N., et al. (2020). Head-to-head comparison of the diagnostic accuracy of Xpert MTB/RIF and Xpert MTB/RIF Ultra for tuberculosis: a meta-analysis. *Infect. Dis.* 52, 763–775. doi: 10.1080/23744235.2020.1788222

Kabir, S., Rahman, S. M. M., Ahmed, S., Islam, M. S., Banu, R. S., Shewade, H. D., et al. (2021). Xpert Ultra assay on stool to diagnose pulmonary tuberculosis in children. *Clin. Infect. Dis.* 73, 226–234. doi: 10.1093/cid/ciaa583

Kolia-Diafouka, P., Carrère-Kremer, S., Lounnas, M., Bourdin, A., Kremer, L., Van de Perre, P., et al. (2019). Detection of *Mycobacterium tuberculosis* in paucibacillary sputum: performances of the Xpert MTB/RIF Ultra compared to the Xpert MTB/RIF, and IS6110 PCR. *Diagn. Microbiol. Infect. Dis.* 94, 365–370. doi: 10.1016/j.diagmicrobio.2019.02.008

Lawn, S. D., Brooks, S. V., Kranzer, K., Nicol, M. P., Whitelaw, A., Vogt, M., et al. (2011). Screening for HIV-associated tuberculosis and rifampicin resistance

before antiretroviral therapy using the Xpert MTB/RIF assay: a prospective study. *PLoS Med.* 8:e1001067. doi: 10.1371/journal.pmed.1001067

Liu, X. H., Xia, L., Song, B., Wang, H., Qian, X. Q., Wei, J. H., et al. (2021). Stool-based Xpert MTB/RIF Ultra assay as a tool for detecting pulmonary tuberculosis in children with abnormal chest imaging: a prospective cohort study. *J. Infect.* 82, 84–89. doi: 10.1016/j.jinf.2020.10.036

López-Roa, P., Martin-Higuera, C., Ruiz-Serrano, M. J., Toro, C., Tato, M., Simon, M., et al. (2021). Performance of Xpert MTB/RIF Ultra assay on respiratory and extra-respiratory samples in a high-resource setting with a low tuberculosis prevalence. *Diagn. Microbiol. Infect. Dis.* 99:115235. doi: 10.1016/j.diagmicrobio.2020.115235

Lounnas, M., Diack, A., Nicol, M. P., Eyangoh, S., Wobudeya, E., Marcy, O., et al. (2020). Laboratory development of a simple stool sample processing method diagnosis of pediatric tuberculosis using Xpert Ultra. *Tuberculosis* 125:102002. doi: 10.1016/j.tube.2020.102002

Manyelo, C. M., Solomons, R. S., Walzl, G., and Chegou, N. N. (2021). Tuberculous meningitis: pathogenesis, immune responses, diagnostic challenges, and the potential of biomarker-based approaches. *J. Clin. Microbiol.* 59:e01771-20. doi: 10.1128/JCM.01771-20

Maynard-Smith, L., Larke, N., Peters, J. A., and Lawn, S. D. (2014). Diagnosticaccuracy of the Xpert MTB/RIF assay for extrapulmonary and pulmonarytuberculosiswhen testing non-respiratory samples: a systematic review. *BMC Infect. Dis.* 14:709. doi: 10.1186/s12879-014-0709-7

Mekkaoui, L., Hallin, M., Mouchet, F., Payen, M. C., Maillart, E., Clevenbergh, P., et al. (2021). Performance of Xpert MTB/RIF Ultra for diagnosis of pulmonary and extra-pulmonary tuberculosis, one year of use in a multi-centric hospital laboratory in Brussels. Belgium. *PLoS One* 16:e0249734. doi: 10.1371/journal.pone.0249734

Meldau, R., Randall, P., Pooran, A., Limberis, J., Makambwa, E., Dhansay, M., et al. (2019). Same-day tools, including Xpert Ultra and IRISA-TB, for rapid diagnosis of pleural tuberculosis: a prospective observational study. *J. Clin. Microbiol.* 57:e00614-19. doi: 10.1128/JCM.00614-19

Menichini, M., Lari, N., Lupetti, A., and Rindi, L. (2020). Evaluation of Xpert MTB/RIF Ultra assay for rapid diagnosis of pulmonary and extra-pulmonary tuberculosis in an Italian center. *Eur. J. Clin. Microbiol. Infect. Dis.* 39, 1597–1600. doi: 10.1007/s10096-020-03867-y

Minnies, S., Reeve, B. W. P., Rockman, L., Nyawo, G., Naidoo, C. C., Kitchin, N., et al. (2021). Xpert MTB/RIF Ultra is highly sensitive for the diagnosis of tuberculosis lymphadenitis in an HIV-endemic setting. *J. Clin. Microbiol.* 59:e0131621. doi: 10.1128/JCM.01316-21

Opota, O., Zakham, F., Mazza-Stalder, J., Nicod, L., Greub, G., and Jaton, K. (2019b). Added value of Xpert MTB/RIF Ultra for diagnosis of pulmonary tuberculosis in a low-prevalence setting. *J. Clin. Microbiol.* 57:e01717-18. doi: 10.1128/JCM.01717-18

Opota, O., Mazza-Stalder, J., Greub, G., and Jaton, K. (2019a). The rapid molecular test Xpert MTB/RIF Ultra: towards improved tuberculosis diagnosis and rifampicin resistance detection. *Clin. Microbiol. Infect.* 25, 1370–1376. doi: 10.1016/j.cmi.2019.03.021

Park, M., and Kon, O. M. (2021). Use of Xpert MTB/RIF and Xpert Ultra in extrapulmonary tuberculosis. *Expert Rev. Anti. Infect. Ther.* 19, 65–77. doi: 10.1080/14787210.2020.1810565

Penz, E., Boffa, J., Roberts, D. J., Fisher, D., Cooper, R., Ronksley, P. E., et al. (2015). Diagnosticaccuracy of the Xpert MTB/RIF assay for extra-pulmonarytuberculosis: a meta-analysis. *Int. J. Tuberc. Lung. Dis.* 19, 278–284. doi: 10.5588/ijtld.14.0262

Perez-Risco, D., Rodriguez-Temporal, D., Valledor-Sanchez, I., and Alcaide, F. (2018). Evaluation of the Xpert MTB/RIF Ultra assay for direct detection of *Mycobacterium tuberculosis* complex in smear-negative extrapulmonary samples. *J. Clin. Microbiol.* 56:e00659-18. doi: 10.1128/JCM.00659-18

Piersimoni, C., Gherardi, G., Gracciotti, N., and Pocognoli, A. (2019). Comparative evaluation of Xpert MTB/RIF and the new Xpert MTB/RIF Ultra with respiratory and extra-pulmonary specimens for tuberculosis case detection in a low incidence setting. *J. Clin. Tuberc. Other Mycobact. Dis.* 15:100094. doi: 10.1016/j.jctube.2019.100094

Qian, X., Albers, A. E., Nguyen, D. T. M., Dong, Y., Zhang, Y., Schreiber, F., et al. (2019). Head and neck tuberculosis: literature review and meta-analysis. *Tuberculosis* 116S, S78–S88. doi: 10.1016/j.tube.2019.04.014

Sabi, I., Rachow, A., Mapamba, D., Clowes, P., Ntinginya, N. E., Sasamalo, M., et al. (2018). Xpert MTB/RIF Ultra assay for the diagnosis of pulmonary tuberculosis in children: a multicentre comparative accuracy study. *J. Infect.* 77, 321–327. doi: 10.1016/j.jinf.2018.07.002

Shao, L., Qiu, C., Zheng, L., Yang, Y., Yang, X., Liang, Q., et al. (2020). Comparison of diagnostic accuracy of the GeneXpert Ultra and cell-free nucleic acid assay for tuberculous meningitis: a multicentre prospective study. *Int. J. Infect. Dis.* 98, 441–446. doi: 10.1016/j.ijid.2020.06.076

Sharma, K., Sharma, M., Shree, R., Modi, M., Goyal, M., Narang, D., et al. (2020). Xpert MTB/RIF Ultra for the diagnosis of tuberculous meningitis: a diagnostic accuracy study from India. *Tuberculosis* 125:101990. doi: 10.1016/j.tube.2020.101990

Shaw, J. A., Irusen, E. M., Diacon, A. H., and Koegelenberg, C. F. (2018). Pleural tuberculosis: a concise clinical review. *Clin. Respir. J.* 12, 1779–1786. doi: 10.1111/crj.12900

Ssengooba, W., Iragena, J. D., Nakiyingi, L., Mujumbi, S., Wobudeya, E., Mboizi, R., et al. (2020). Accuracy of Xpert Ultra in diagnosis of pulmonary tuberculosis among children in uganda: a substudy from the SHINE Trial. *J. Clin. Microbiol.* 58:e00410-20. doi: 10.1128/JCM.00410-20

Sun, L., Liu, Y., Fang, M., Chen, Y., Zhu, Y., Xia, C., et al. (2021). Use of Xpert MTB/RIF Ultra assay on stool and gastric aspirate samples to diagnose pulmonary tuberculosis in children in a high-tuberculosis burden but resource-limited area of China: diagnosis of childhood TB using stool. *Int. J. Infect. Dis.* S1201–9712, 858–864. doi: 10.1016/j.ijid.2021.11.012

Sun, L., Zhu, Y., Fang, M., Shi, Y., Peng, X., Liao, Q., et al. (2020). Evaluation of Xpert MTB/RIF Ultra assay for diagnosis of childhood tuberculosis: a multicenter accuracy study. *J. Clin. Microbiol.* 58, e00702-20. doi: 10.1128/JCM.00702-20

Sun, Q., Wang, S., Dong, W., Jiang, G., Huo, F., Ma, Y., et al. (2019). Diagnostic value of Xpert MTB/RIF Ultra for osteoarticular tuberculosis. *J. Infect.* 79, 153–158. doi: 10.1016/j.jinf.2019.06.006

Theron, G., Peter, J., Calligaro, G., Meldau, R., Hanrahan, C., Khalfey, H., et al. (2014). Determinants of PCR performance (Xpert MTB/RIF), including bacterial load and inhibition, for TB diagnosis using specimens from different body compartments. *Sci. Rep.* 4:5658. doi: 10.1038/srep05658

Wang, G., Wang, S., Jiang, G., Yang, X., Huang, M., Huo, F., et al. (2019). Xpert MTB/RIF Ultra improved the diagnosis of paucibacillary tuberculosis: a prospective cohort study. *J. Infect.* 78, 311–316. doi: 10.1016/j.jinf.2019.02.010

Wang, G., Wang, S., Yang, X., Sun, Q., Jiang, G., Huang, M., et al. (2020). Accuracy of Xpert MTB/RIF Ultra for the diagnosis of pleural TB in a multicenter cohort study. *Chest* 157, 268–275. doi: 10.1016/j.chest.2019.07.027

Wilkinson, R. J., Rohlwink, U., Misra, U. K., van Crevel, R., Mai, N. T. H., Dooley, K. E., et al. (2017). Tuberculous meningitis. *Nat. Rev. Neurol.* 13, 581–598. doi: 10.1038/nrneurol.2017.120

World Health Organization [WHO] (2020). *Global Tuberculosis Report 2020: Executive Summary*. Geneva: WHO.

Wu, X., Tan, G., Gao, R., Yao, L., Bi, D., Guo, Y., et al. (2019). Assessment of the Xpert MTB/RIF Ultra assay on rapid diagnosis of extrapulmonary tuberculosis. *Int. J. Infect. Dis.* 81, 91–96. doi: 10.1016/j.ijid.2019.01.050

Zhang, M., Xue, M., and He, J. Q. (2020). Diagnostic accuracy of the new Xpert MTB/RIF Ultra for tuberculosis disease: a preliminary systematic review and meta-analysis. *Int. J. Infect. Dis.* 90, 35–45. doi: 10.1016/j.ijid.2019.09.016

Conflict of Interest: The author declares that the research was conducted in the absence of any commercial or financial relationships that could be construed as a potential conflict of interest.

frontiers | Frontiers in Microbiology

TYPE Original Research
PUBLISHED 22 July 2022
DOI 10.3389/fmicb.2022.885312

OPEN ACCESS

EDITED BY
Xiao-Yong Fan,
Fudan University, China

REVIEWED BY
Damien Portevin,
Swiss Tropical and Public Health Institute (Swiss TPH), Switzerland
Margarida Correia-Neves,
University of Minho, Portugal
Santhi Devasundaram,
National Cancer Institute at Frederick (NIH), United States
Elisa Petruccioli,
National Institute for Infectious Diseases Lazzaro Spallanzani (IRCCS), Italy
Christopher Sundling,
Karolinska Institutet (KI), Sweden
Delia Goletti,
National Institute for Infectious Diseases Lazzaro Spallanzani (IRCCS), Italy

*CORRESPONDENCE
Irene Latorre
ilatorre@igtp.cat

†These authors have contributed equally to this work and share first authorship

‡These authors have contributed equally to this work and share senior authorship

SPECIALTY SECTION
This article was submitted to Infectious Agents and Disease, a section of the journal Frontiers in Microbiology

RECEIVED 27 February 2022
ACCEPTED 28 June 2022
PUBLISHED 22 July 2022

CITATION
Díaz-Fernández S, Villar-Hernández R, Stojanovic Z, Fernández M, Galvão MLDS, Tolosa G, Sánchez-Montalva A, Abad J, Jiménez-Fuentes MÁ, Safont G, Romero I, Sabrià J, Prat C, Domínguez J and Latorre I (2022) Study of CD27, CD38, HLA-DR and Ki-67 immune profiles for the characterization of active tuberculosis, latent infection and end of treatment. *Front. Microbiol.* 13:885312. doi: 10.3389/fmicb.2022.885312

Study of CD27, CD38, HLA-DR and Ki-67 immune profiles for the characterization of active tuberculosis, latent infection and end of treatment

Sergio Díaz-Fernández[1,2,3†], Raquel Villar-Hernández[1,2,3†], Zoran Stojanovic[2,3,4†], Marco Fernández[5], Maria Luiza De Souza Galvão[6], Guillermo Tolosa[7], Adrián Sánchez-Montalva[8,9], Jorge Abad[2,4], María Ángeles Jiménez-Fuentes[6], Guillem Safont[1,2,3], Iris Romero[3], Josefina Sabrià[10], Cristina Prat[1,2,3,11], Jose Domínguez[1,2,3‡] and Irene Latorre[1,2,3*‡]

[1]Institut d'Investigació Germans Trias i Pujol, Barcelona, Spain, [2]CIBER Enfermedades Respiratorias, CIBERES, Instituto de Salud Carlos III, Madrid, Spain, [3]Departament de Genètica i Microbiologia, Universitat Autònoma de Barcelona, Barcelona, Spain, [4]Servei de Pneumologia, Hospital Universitari Germans Trias i Pujol, Barcelona, Spain, [5]Plataforma de Citometría, Institut d'Investigació Germans Trias i Pujol, Barcelona, Spain, [6]Unitat de Tuberculosi de Drassanes, Hospital Universitari Vall d'Hebron, Barcelona, Spain, [7]Universidad de la Frontera (UFRO), Temuco, Chile, [8]Infectious Diseases Department, Vall d'Hebron University Hospital, PROSICS Barcelona, Universitat Autònoma de Barcelona, Barcelona, Spain, [9]Grupo de Estudio de micobacterias (GEIM), Sociedad Española de Enfermedades Infecciosas y Microbiología Clínica (SEIMC), Madrid, Spain, [10]Hospital de Sant Joan Despí Moisès Broggi, Barcelona, Spain, [11]Julius Center for Health Sciences and Primary Care, University Medical Center Utrecht, Utrecht University, Utrecht, Netherlands

Background: Current blood-based diagnostic tools for TB are insufficient to properly characterize the distinct stages of TB, from the latent infection (LTBI) to its active form (aTB); nor can they assess treatment efficacy. Several immune cell biomarkers have been proposed as potential candidates for the development of improved diagnostic tools.

Objective: To compare the capacity of CD27, HLA-DR, CD38 and Ki-67 markers to characterize LTBI, active TB and patients who ended treatment and resolved TB.

Methods: Blood was collected from 45 patients defined according to clinical and microbiological criteria as: LTBI, aTB with less than 1 month of treatment and aTB after completing treatment. Peripheral blood mononuclear cells were stimulated with ESAT-6/CFP-10 or PPD antigens and acquired for flow cytometry after labelling with conjugated antibodies against CD3, CD4, CD8, CD27, IFN-γ, TNF-α, CD38, HLA-DR, and Ki-67. Conventional and multiparametric analyses were done with FlowJo and OMIQ, respectively.

Results: The expression of CD27, CD38, HLA-DR and Ki-67 markers was analyzed in $CD4^+$ T-cells producing IFN-γ and/or TNF-α cytokines after ESAT-6/CFP-10 or PPD stimulation. Within antigen-responsive $CD4^+$ T-cells,

CD27$^-$ and CD38$^+$ (ESAT-6/CFP-10-specific), and HLA-DR$^+$ and Ki-67$^+$ (PPD- and ESAT-6/CFP-10-specific) populations were significantly increased in aTB compared to LTBI. Ki-67 demonstrated the best discriminative performance as evaluated by ROC analyses (AUC>0.9 after PPD stimulation). Data also points to a significant change in the expression of CD38 (ESAT-6/CFP-10-specific) and Ki-67 (PPD- and ESAT-6/CFP-10-specific) after ending the anti-TB treatment regimen. Furthermore, ratio based on the CD27 median fluorescence intensity in CD4$^+$ T-cells over *Mtb*-specific CD4$^+$ T-cells showed a positive association with aTB over LTBI (ESAT-6/CFP-10-specific). Additionally, multiparametric FlowSOM analyses revealed an increase in CD27 cell clusters and a decrease in HLA-DR cell clusters within *Mtb*-specific populations after the end of treatment.

Conclusion: Our study independently confirms that CD27$^-$, CD38$^+$, HLA-DR$^+$ and Ki-67$^+$ populations on *Mtb*-specific CD4$^+$ T-cells are increased during active TB disease. Multiparametric analyses unbiasedly identify clusters based on CD27 or HLA-DR whose abundance can be related to treatment efficacy. Further studies are necessary to pinpoint the convergence between conventional and multiparametric approaches.

KEYWORDS

***Mycobacterium tuberculosis*, T-cells, immune response, activation markers, treatment, flow cytometry, multiparametric analysis, cluster**

Introduction

To date, tuberculosis (TB) is still a major global health threat, with approximately 10 million new *Mycobacterium tuberculosis* (*Mtb*) infections and 1.5 million deaths reported only in 2020. Moreover, the COVID-19 pandemic has set back several years of progress in TB control, and the target of ending the epidemic by 2030 set by the WHO's End TB Strategy seems even more implausible now (Global Tuberculosis Report, 2021). From a pathophysiological setting, TB represents a dynamic spectrum from infection to clinical disease (Furin et al., 2019); however, for pragmatic reasons, patients are usually categorized as having either active TB (aTB) or latent TB infection (LTBI). Defining the latent TB condition has been a matter of discussion over the last decades, since it encompasses a wide array of situations, from individuals with quiescent *Mtb* to individuals with controlled bacterial growth for months (Pai et al., 2016). Updated definitions of LTBI added the concept of host immunity to the clinical picture, and now it is considered as "a state of persistent immunoreactivity to *Mtb* antigenic stimulation with no evidence of clinically manifest active TB" (Drain et al., 2018). Around a quarter of the world's population is estimated to be infected with *Mtb,* from which 5%–10% will develop aTB (Houben and Dodd, 2016). Individuals with LTBI constitute the principal reservoir for the bacilli, which is the reason why accurate diagnosis is essential for halting TB worldwide. Correct characterization of the TB spectrum is, therefore, a priority in the development of novel diagnostic tools.

The immune response to *Mtb* infection is still not fully understood, but CD4$^+$ T-cells arguably play a pivotal role (Gallegos et al., 2011; O'Garra et al., 2013). Depletion of this T-cell subset and/or Th1 responses (Filipe-Santos et al., 2006) result in extreme susceptibility to the disease. In fact, immune response to *Mtb* is so connected to T-cell activity that its measurement is the basis for the main culture-free diagnostic assays (Lalvani and Pareek, 2010), such as the Tuberculin Skin Test (TST) and the interferon (IFN)-gamma (γ) release assays (IGRAs). The TST consists in the intradermal injection of a mixture of mycobacterial antigens, the Purified Protein Derivative (PPD), that causes a skin reaction if there is an immunological memory to *Mycobacterium* spp. (Seddon et al., 2016). Despite being widely used, the TST has a rather low specificity, and false positives are common. This is mainly due to the fact that the PPD antigens are not unique to *Mtb* and are detected by T-cells from patients with the Bacille Calmette-Guérin vaccine and/or infected with nontuberculous mycobacteria (Domínguez et al., 2008; Latorre et al., 2010). These limitations were partly overcome thanks to the introduction of the IGRAs. These assays are based on the detection of specific T-cell responses against *Mtb*, represented by the release of IFN-γ after stimulation with *Mtb*-specific antigens (ESAT-6 and CFP-10; Andersen et al., 2000). The IGRAs have demonstrated better performance than the TST for the diagnosis of *Mtb* infection (Metcalfe et al., 2013); nevertheless, both tests fail to discriminate active disease from latent infection and other status associated to higher risks of developing the disease (Goletti et al., 2022). Moreover, neither of the assays can be used to monitor therapy

efficacy, which would be of great value to shorten treatment regimen and to accelerate the drug evaluation in the clinical trials. Given the fact that T-cells change their activation status and cytokine expression after *Mtb* challenge, the evaluation of their immune profile is an attractive option for the improvement of TB diagnostics.

The study of immunological biomarkers *via* flow cytometry has already been demonstrated to be a useful tool to evaluate host response in TB infection and aTB disease (Pollock et al., 2013; Coppola et al., 2020). Most studies focus the analysis of these disease markers in specific subsets of cells defined by the expression of pro-inflammatory cytokines following antigen stimulation, linking production of TNF-α (Harari et al., 2011; Halliday et al., 2017) and IFN-γ (Petruccioli et al., 2015; Ahmed et al., 2019) with infection. Among these cells, several surface and intracellular proteins have been described as potential biomarkers for aTB (Walzl et al., 2018). The present research explores the role of four of them; namely, CD27, CD38, HLA-DR and Ki-67. CD27 is a maturation marker and its downregulation has already been associated with active disease and tissue destruction in TB (Portevin et al., 2014; Latorre et al., 2019). CD38 is a transmembrane receptor expressed in many immune cell types (Hartman et al., 2010), more recently linked to TB studies because of its strong expression in activated T-cells. HLA-DR is an MHC cell receptor highly present on APCs (Saraiva et al., 2018), but also with robust expression on activated T-cells (Tippalagama et al., 2021). Ki-67, the only intracellular marker from the group, is a nuclear protein commonly associated with cell proliferation (Soares et al., 2010). The latter three proteins are associated with antigenic stimulation; therefore, their expression is likely to be increased in active forms of the disease, where mycobacterial load is higher (Mpande et al., 2021). In this paper, we aim to study the expression of the CD27, CD38, HLA-DR and Ki-67 markers in *Mtb*-specific $CD4^+$ T-cells by performing a side by side comparison of their performance on characterizing active disease and latent infection. Furthermore, we intend to evaluate the capacity of these biomarkers to assess treatment efficacy after its completion. Deeper knowledge on such immune biomarkers could allow the development of new strategies for diagnosis and management of LTBI individuals and aTB patients.

Materials and methods

Study population and inclusion criteria

The patients included in this study ($n = 45$) attended one of the following centers in Barcelona, Spain: Hospital Germans Trias i Pujol, Unitat de Tuberculosi Vall d'Hebron-Drassanes, Sant Joan Despí Moisés Broggi, and Hospital Universitari Vall d'Hebrón. They were classified as follows: (i) twenty-three patients ($n = 23$) with pulmonary aTB, microbiologically confirmed with a positive culture and/or PCR, with less than 1 month of anti-TB treatment; (ii) twenty-two individuals ($n = 22$) with LTBI based on positive TST and/or IGRAs and absence of clinical symptoms and radiological signs, detected by contact-tracing or screening studies, and with less than 1 month of chemoprophylaxis; and (iii) nine ($n = 9$) former aTB patients from group (i) after successfully completing the standard treatment regimen with anti-TB drugs and being considered as cured (eTrt). Overall, 37% were women, and the mean age (years) ± standard deviation (SD) was 42.7 ± 13.5. Clinical and study information is detailed in Table 1.

PBMCs isolation, preservation, and thawing

Approximately 16 ml of whole blood were collected from each patient in cell preparation tubes (CPT tubes; BD Biosciences, San Jose, CA, United States) containing Sodium Citrate and Ficoll for peripheral blood mononuclear cells (PBMCs) isolation. Briefly, following a centrifugation of 1,600 g for 30 min, PBMCs were harvested from the interface and washed with RPMI medium (ThermoFisher, Waltham, MA, United States) supplemented with 10% FBS (BioWest, Miami, Fla., United States). Cells were counted with Trypan Blue staining and were resuspended in heat-inactivated FBS supplemented with 10% Dimethyl Sulfoxide (DMSO) for cryopreservation in liquid nitrogen (Cossarizza et al., 2019). To perform our immunological studies, frozen PBMCs were thawed and incubated for 2 h at 37°C with 5% CO2 in AIM-V medium (Thermo Fisher) with benzonase (Sigma, St. Louis, MO, United States; final concentration 10 U/ml) to avoid cell clumping.

PBMCs stimulation with mycobacterial antigen

Samples included in the study were stimulated for 16 h separately with two mycobacterial antigen mixes: (i) recombinant proteins ESAT-6/CFP-10 (Lionex Diagnostics and Therapeutics, Braunschweig, Germany; final concentration 2 μg/ml each) and (ii) PPD (AJVaccines, Copenhagen, Denmark; final concentration 10 μg/ml). A positive control consisting of staphylococcal enterotoxin B (SEB, Sigma, final concentration of 2 μg/ml) and a negative control without stimulation were also included for each sample. One million (10^6) PBMCs were used in each stimulation condition, adding as co-stimulators anti-CD28 and anti-CD49d monoclonal antibodies (BD Bioscience; final concentration 1 μg/ml each). After a 2 h incubation at 37°C in a 5% CO_2 atmosphere, Brefeldin A (BFA; Sigma; final concentration 3 μg/ml) and Monensin (BioLegend, San Diego, USA, final concentration 1X) were added to inhibit intracellular vesicular transport. Cells were then incubated overnight before starting the staining procedure.

TABLE 1 Demographic and clinical characteristics of the participants in each study group.

Variables	aTB	LTBI	eTrt
Participants, *n*	23	22	9
Mean age[1], years ± SD	43.91 ± 15.47	42.59 ± 12.17	50 ± 14.02
Male gender, *n*(%)	18 (78.3)	16 (72.7)	9 (100)
Disease form, N(%)			
Pulmonary	22 (95.7)	–	9 (100)
Pleural	1 (4.3)	–	–
Reported LTBI enrolment, N(%)			
Contact-tracing	–	14 (63.6)	
LTBI screening	–	7 (31.8)	
Not reported	–	1 (4.5)	
Chemoprofilaxis, N(%)			
Before starting chemoprophylaxis	-	1 (4.5)	-
After starting chemoprophylaxis (<1 month)	22 (95.7)	21 (95.5)	9 (100)
Not prescribed	-	-	-
Mean time of chemoprophylaxis[2], days ± SD	-	20.90 ± 6.32	-
Regimen 3RH	-	19 (86.4)	-
Regimen 6H	-	3 (13.6)	
Anti-TB treatment, N(%)			
Before starting treatment[3]	2 (8.7)	–	–
After starting treatment (<1 month)	21 (91.3)	–	–
Ended treatment[4]	-		9 (100)
Not prescribed	-	22 (100)	–
Mean time of treatment[2], days ± SD	12.95 ± 9.94	–	229.55 ± 91.48
Regimen 2HRZE/4RH	21 (91.3)	–	8 (88.9)
Others[5]	2 (8.7)	–	1 (11.1)
Comorbidities, N(%)			
Other respiratory disorders (asthma, PCD, COPD)	2 (8.7)	2 (9.1)	2 (22.2)
Neoplasies (lung, prostate)	2 (8.7)	–	1 (11.1)
Autoimmune diseases (diabetes, psoriasis, Löfgren Syndrome)	2 (8.7)	2 (9.1)	–
Cardiovascular diseases (AHT, cardiomyopathy)	1 (4.3)	–	1 (11.1)
Hepatitis C	1 (4.3)	2 (9.1)	–
Bacille Calmette-Guérin vaccine, N(%)			
BCG-vaccinated	12 (52.2)	12 (54.5)	3 (33.3)
Not BCG-vaccinated	9 (39.1)	10 (45.5)	5 (55.5)
Not reported	2 (8.7)	–	1 (11.1)
Other information, N(%)			
Reported smokers	9 (39.1)	5 (22.7)	4 (44.44)
Reported drug abuse	5 (21.7)	0 (0)	0 (0)

aTB, active tuberculosis; LTBI, latent tuberculosis infection; eTrt, aTB patients after anti-TB treatment; SD, standard deviation; PCD, primary ciliary dyskinesia; COPD, chronic obstructive pulmonary disease; AHT, arterial hypertension; SEB, staphylococcal enterotoxin B.
[1]Patients in the study are aged 20–73.
[2]Range of time between starting chemoprophylaxis and anti-TB treatment and sample collection was from 0 to 30 days in all participants in both groups.
[3]Both patients were prescribed with RIMSTAR on the day of sample collection.
[4]One of the participants was recruited after 5 months of anti-TB treatment, six of the participants between 6 and 7.5 months and one of the participants after 16 months.
[5]One patient was prescribed with HRZ regimen, and one patient was prescribed with Lzd/Mfx/Cfz/Z/E regimen.

Extracellular and intracellular staining and acquisition in flow cytometer

After stimulation, PBMCs were labeled with viability marker LIVE/DEAD Near-IR fluorescent reactive dye (Thermo Fisher) for 30 min and subsequently stained for 20 min with the following surface markers: anti-CD3-PerCP (BioLegend), anti-CD4-BV786, anti-CD8-BV510, anti-CD27-BV605, anti-CD38-PE, and anti-HLA-DR-BV421 (BD Bioscience). Cells were then fixed and permeabilized with the Foxp3 Transcription Factor Staining

Buffer Set (Thermo Fisher) and stained for 30 min with intracellular markers: anti-IFNγ-APC, anti-TNFα-PE-Cy7 and anti-Ki-67-FITC (BD Bioscience). The complete list of antibodies, conjugated proteins and dilutions can be found in Supplementary Table 1. All incubation processes were performed at room temperature in darkness. Fluorescence Minus One (FMO) controls of the four analyzed cell markers (CD27, CD38, HLA-DR, and Ki-67) were included in each run to accurately distinguish negative from positive populations. Samples were resuspended in 100 µl of PBS-0.1%BSA (Bovine Serum Albumin, Sigma Aldrich) and acquired in a BD LSRFortessa flow cytometer (BD Bioscience) using FACSDiva software (BD Biosciences) with compensated parameters.

Flow cytometry data analysis

For gate-driven analyses, flow cytometry data was analyzed using FlowJo™ (Tree Star, Ashland, OR, United States) and plotted with GraphPad Prism (GraphPad Software, La Jolla, CA). Lymphocytes were gated based on their size (FSC) and complexity (SSC). After exclusion of doublet events, $CD4^+$ T cells were selected from $CD3^+$ alive events. TNF-α^+ and/or IFN-γ^+ populations were selected for the study of *Mtb*-specific responses. To avoid inadequate assessment of population percentages, *Mtb*-specific populations under 100 events were not considered valid for analysis (this meant that out of 54 samples, six PPD-stimulated and eight ESAT-6/CFP-10-stimulated were excluded). CD27 Median Fluorescence Intensity (MFI) ratio

$$\left[\frac{\text{CD27 MFI on total CD4}^+\text{ T}-\text{cells}}{\text{CD27 MFI on } \textit{Mtb}-\text{specific CD4}^+\text{ T}-\text{cells}}\right]$$

$$\text{and } \Delta\text{HLA-DR MFI}\left(\begin{matrix}\text{HLADR MFI on IFNy}^+\\ \text{TNF}^+\text{CD3}^+\text{ cells}\end{matrix}\right)-\left(\begin{matrix}\text{HLADR MFI on}\\ \text{total CD3}^+\text{ cells}\end{matrix}\right)$$

were calculated according to published reports led by Portevin et al. (2014) and Mpande et al. (2021), respectively.

For multiparametric analyses, dimensional reduction and clustering were done using OMIQ data analysis software (OMIQ, Inc. Santa Clara, CA) after preliminary cleaning of data with FlowJo of aggregates, dead cells and debris. All CD3 positive events from all samples were selected for subsequent analysis on the OMIQ platform. flowCut algorithm was run to check and exclude for any aberrant regions of all files analyzed. Subsequently, a UMAP analysis was performed to visualize the different CD3 subsets in groups. FlowSOM was run to cluster the data using metaclustering with $k = 50$. After the FlowSOM analysis, the metaclusters were grouped into commonly recognized biological populations. All clusters were plotted on traditional dot plots for phenotype confirmation as for the standard manual gating analysis.

Statistics

Results comparing variables between LTBI and aTB participants were analyzed using the two-tailed Mann–Whitney test for unpaired comparisons. Paired data from patients followed over time was analyzed using the Wilcoxon-matched pairs test. Comparisons between before and after treatment groups where data was partially paired (combining paired and unpaired observations) were analyzed using a mixed statistical model controlling repeated measures on logit-transformed data. Correlation between variables was calculated using the two-tailed non-parametric Spearman test. Diagnostic accuracy was evaluated *via* the Receiver operating characteristic (ROC) and Area Under the Curve (AUC) analyses. Differences were regarded as statistically significant when the value of p or the False Discovery Rate (FDR) value were below 0.05.

Results

Expression of CD27, CD38, HLA-DR and Ki-67 markers on *Mtb*-specific $CD4^+$ T-cells differs in LTBI individuals and anti-TB treated patients compared to aTB patients

To specifically study the T-cell response against *Mtb*, TNF-α and/or IFN-γ cytokines were analyzed on $CD4^+$ T-cells after stimulation with ESAT-6/CFP-10 or PPD antigens (complete gating strategy can be found in Supplementary Figure 1). From this *Mtb*-specific population, the percentage of $CD27^-$, $CD38^+$, $HLA\text{-}DR^+$ and $Ki\text{-}67^+$ populations were compared between LTBI individuals and aTB patients at the beginning and end of the treatment. To control that the length of the treatment within the 1-month range of the aTB group did not interfere with the marker's expression, we performed a Spearman Correlation Test that showed no correlation between the days of treatment in month 1 and our variables (Supplementary Figure 2).

As shown in Figures 1A–D, the percentage of all populations studied ($CD27^-$, $CD38^+$, $HLA\text{-}DR^+$ and $Ki\text{-}67^+$) within *Mtb*-specific $CD4^+$ T-cells was increased in aTB compared to LTBI in response to ESAT-6/CFP-10 recombinant proteins ($p = 0.0092$ for $CD27^-$, $p = 0.0162$ for $CD38^+$, $p = 0.001$ for $HLA\text{-}DR^+$ and $p < 0.0001$ for $Ki\text{-}67^+$). Additionally, the $HLA\text{-}DR^+$ and $Ki\text{-}67^+$ populations were also associated with aTB patients after stimulation with PPD ($p = 0.0008$ and $p < 0.0001$, respectively). The trends observed in individuals who finished the anti-TB regimen were comparable to those in LTBI individuals. As seen again in Figure 1, following treatment, a decrease in the percentages of all the phenotypes was observed, with significance for the CD38 ($p = 0.0384$ for ESAT-6/CFP-10) and Ki-67 ($p = 0.0293$ for ESAT-6/CFP-10,

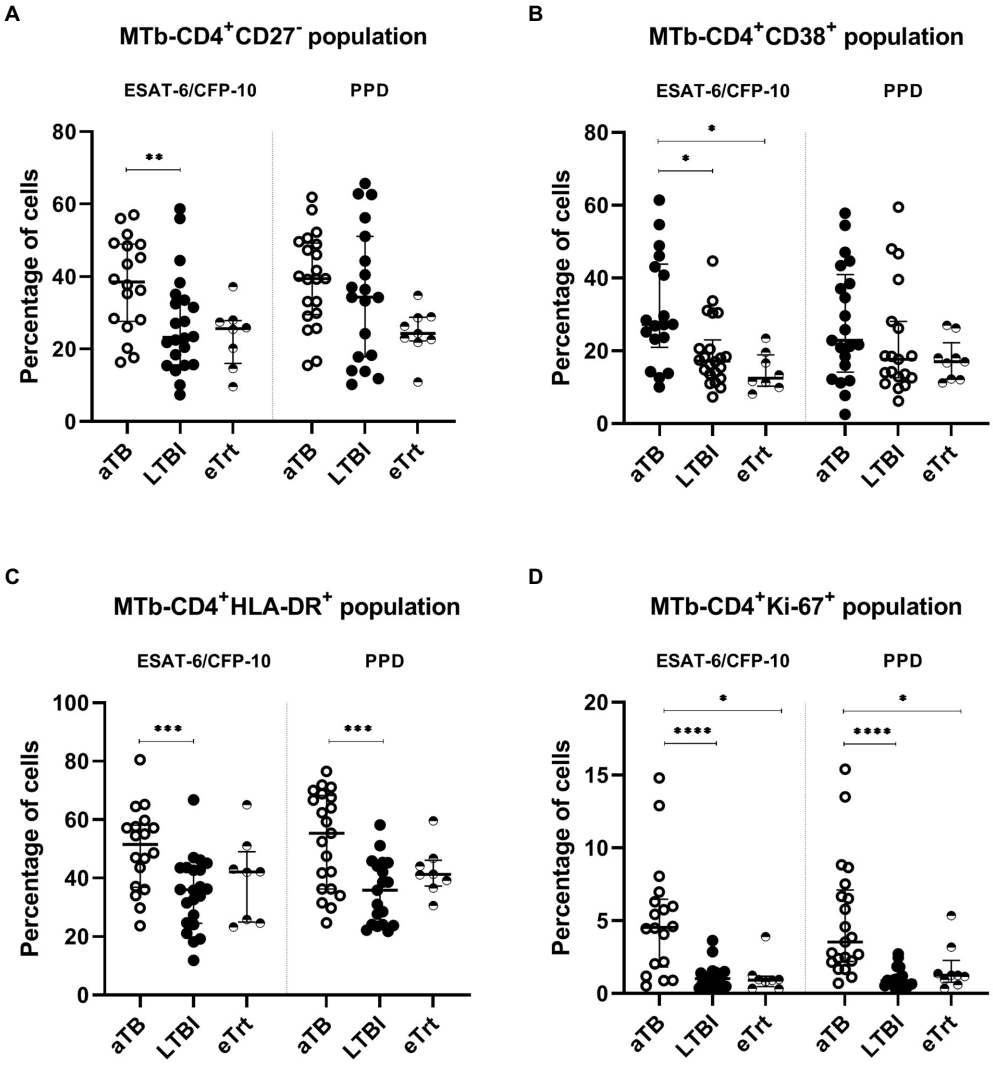

FIGURE 1
CD27⁻, CD38⁺, HLA-DR⁺, and Ki67⁺ phenotype from Mtb-specific CD4⁺ T-cells of each patient group. Percentage of CD27⁻ **(A)**, CD38⁺ **(B)**, HLA-DR⁺ **(C)**, and Ki67⁺ **(D)** within TNF-α⁺ and/or IFN-γ⁺ CD4⁺ T-cells after stimulation with ESAT-6/CFP-10 or PPD (left and right half of graph, respectively) in patients with active TB in the beginning and end of treatment, as well as LTBI individuals. Data plotted with median and interquartile range. Differences between aTB and LTBI conditions were calculated using the two-tailed Mann–Whitney *U*-test. Differences between aTB and eTrt groups were calculated using a mixed statistical model controlling repeated measures on logit-transformed data. *p<0.05, **p<0.01, ***p<0.001, ****p<0.0001. No indication of p value implies non significance. aTB, active TB; LTBI, latent tuberculosis infection; eTrt, aTB patients after anti-TB treatment.

$p = 0.022$ for PPD) markers. Reduction of CD27⁻ and HLA-DR⁺ populations in activated CD4⁺ T-cells was statistically significant only when performing a Mann–Whitney unpaired analysis excluding the matched samples (for CD27⁻, $p = 0.0016$ and $p = 0.0001$ and for HLA-DR⁺, $p = 0.0482$ and $p = 0.0649$ after stimulation with ESAT-6/CFP-10 and PPD, respectively). No differences were detected on any of the markers' expression regarding BCG-status after PPD stimulation (Supplementary Figure 3). When analyzing only the patients monitored at the beginning and at the end of treatment, inter-individual variation of the marker's expression was observed (Supplementary Figure 4).

CD27 MFI ratio provides a useful tool to characterize aTB

We also evaluated an alternative approach based on the ratio between the CD27 MFI in total CD4⁺ T-cells and the MFI of CD27 in *Mtb*-specific CD4⁺ T-cells. An increase of this ratio is a direct consequence of a decrease of the CD27⁺ *Mtb*-specific CD4⁺ T-cells phenotype associated with active disease. Overall, our data shows a reverse trend of the CD27 MFI ratio with aTB to that observed in the percentage of CD27⁻ cells among the *Mtb*-specific CD4⁺ cells. As seen in Figure 2A, the ratio of CD27 MFI was increased in aTB patients compared to LTBI individuals after

10.3389/fmicb.2022.885312

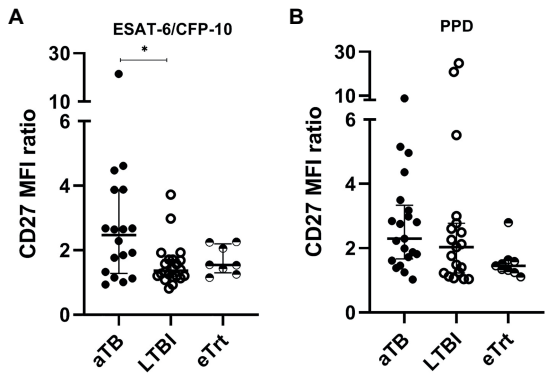

FIGURE 2
CD27 MFI ratio is increased in aTB patients over LTBI individuals (ESAT-6/CFP-10-specific) and patients after anti-TB treatment (PPD-specific). A ratio of CD27 MFI was calculated as suggested by Portevin et al. The numbers result from the division of the MFI of CD27 in $CD4^+$ T-cells over MFI of CD27 in TNF-α^+ and/or IFN-γ^+ $CD4^+$ T-cells. **(A)** CD27 MFI ratio after ESAT-6/CFP-10 or **(B)** PPD stimulation in patients with active TB in the beginning and end of treatment, as well as LTBI individuals. Data plotted with median and interquartile range. Differences between aTB and LTBI conditions were calculated using the two-tailed Mann–Whitney *U*-test. Differences between aTB and eTrt groups were calculated using a mixed statistical model controlling repeated measures on logit-transformed data. *$p<0.05$. aTB, active TB; LTBI, latent tuberculosis infection; eTrt, aTB patients after anti-TB treatment.

ESAT-6/CFP-10 stimulation of T-cells ($p=0.0162$) (Figure 2B). A difference was found when comparing aTB and eTrt groups after PPD stimulation when performing a Mann–Whitney unpaired analysis excluding the matched samples ($p=0.0044$). In order to demonstrate the association between the proportion of $CD27^-$ *Mtb*-specific $CD4^+$ T-cells and the CD27 MFI ratio, we performed a Spearman's correlation test (Supplementary Figure 5). A positive interdependence between the two variables was detected in T-cells responding to both ESAT-6/CFP-10 and PPD, supported by a strong correlation coefficient (for ESAT-6/CFP-10: Spearman's rho = 0.8143, $p<0.0001$; for PPD: Spearman's rho = 0.8766, $p<0.0001$).

Additionally, we calculated the ΔHLA-DR MFI (difference in MFI of HLA-DR between total T-cells and *Mtb*-specific T-cells) to assess its performance in discriminating the three study groups. An increase of this value was observed on aTB patients over LTBI individuals after stimulation with ESAT-6/CFP-10 ($p=0.0341$; Supplementary Figure 6). MFI ratios of CD38 and Ki-67 were also analyzed but showed no difference between study groups (data not shown).

Ki-67$^+$ and HLA-DR$^+$ populations yield the highest discriminative performance

ROC curve analyses were performed for both ESAT-6/CFP-10 and PPD stimulations for each marker in order to explore their diagnostic accuracy of aTB patients over the LTBI condition (Table 2). As expected, highest AUC values (95% confidence interval, CI) corresponded to the marker which provided the highest significant discrimination between aTB and LTBI, Ki-67 [for ESAT-6/CFP-10, AUC 0.87 (0.75–0.99), $p<0.0001$; for PPD, AUC 0.92 (0.83–1.00), $p<0.0001$]. Albeit lower, good AUC values were also obtained for HLA-DR marker with strong significance [for ESAT-6/CFP-10, AUC 0.80 (0.65-0.94), $p=0.0014$; for PPD, AUC 0.80 (0.67–0.94), $p=0.0007$]. All ROC Curves, as well as sensitivity and specificity cut-off values, can be found in Supplementary Figure 7.

TABLE 2 ROC curve analysis of each marker used in the study.

Marker	AUC (95% CI), *p*	
	ESAT-6/CFP-10	PPD
$CD27^-$ Mtb-specific $CD4^+$ T-cells	0.7386 (0.5805-0.8968), 0.0120	0.5714 (0.3841-0.7588), 0.4402
$CD38^+$ Mtb-specific $CD4^+$ T-cells	0.7222 (0.5563-0.8881), 0.0167	0.6078 (0.4268-0.7888), 0.2442
HLA-DR^+ Mtb-specific $CD4^+$ T-cells	0.7967 (0.6514-0.9421), 0.0140	0.8020 (0.6679-0.9361), 0.0011
$Ki67^+$ Mtb-specific $CD4^+$ T-cells	0.8699 (0.7533-0.9866), <0.0001	0.9198 (0.8380-1.0000), <0.0001
CD27 ratio MFI	0.7222 (0.5473-0.8972), 0.0167	0.6015 (0.4199-0.7831), 0.2727

AUC, area under the curve; CI, confidence interval.

Multiparametric analyses reveal the presence of cell subsets with significant differences in abundance in aTB patients before and after treatment

To avoid the analytical bottleneck produced by manual gating, we aimed to explore the same cytometry data in an unbiased manner using a multiparametric analysis. This approach offered the possibility of defining complex cell phenotypes that cannot be revealed using traditional biaxial data presentation. We imported the data on $CD3^+$ populations after ESAT-6/CFP-10 or PPD stimulations into OMIQ and analyzed the data using Uniform Manifold Approximation and Projection for Dimension Reduction (UMAP) and FlowSOM for clustering populations. In total, 50 different cell clusters were defined, being 11 of them positive for TNF-α and/or IFN-γ. Within this subset, at least seven clusters displayed significant changes in expression between the three study groups (Figure 3A). Some of these clusters presented similar features and could broadly be classified into a "maturation phenotype" [$CD4^+$ $CD27^+$ cells with expression of TNF-α (cluster #15_16) or IFN-γ (cluster #20)] or an "activation phenotype" [$CD4^+$ $HLA\text{-}DR^{int}$ cells with expression of TNF-α (cluster #11) or both TNF-α and IFN-γ (clusters #8, #12)]. One of the clusters did not show our markers of interest and just presented low expression of cytokines TNF-α and IFN-γ (cluster #13).

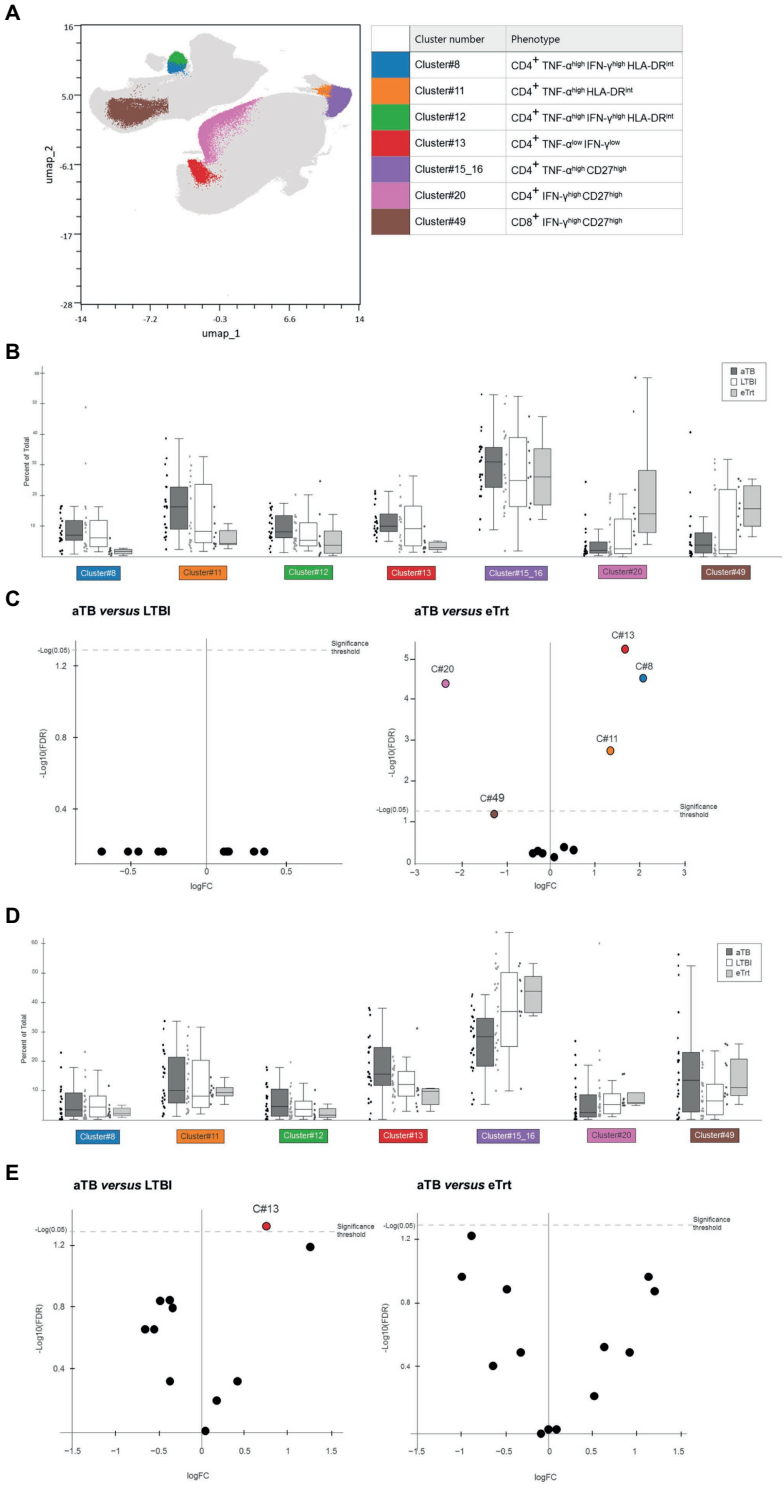

FIGURE 3
Results from multiparametric analyses of the samples. **(A)** UMAP based on the expression of CD4, CD8, TNF-α, IFN-γ, CD27, CD38, HLA-DR and Ki-67 markers in CD3⁺ cells from our dataset containing LTBI individuals and aTB patients before and after treatment, after stimulation with ESAT-6/CFP-10 or PPD. Colored clusters indicate populations with difference in abundance depending on disease status, obtained with FlowSOM and analyzed within TNF-α⁺ and/or IFN-γ⁺ subsets. In background, all 50 cell clusters defined. **(B,D)** Box and dot plots showing percentage (Y axis) of each cluster of interest in each respective group [**(B)** for samples after PPD stimulation, **(D)** for samples after ESAT-6/CFP-10 stimulation. Data plotted with median and interquartile range. **(C,E)** Volcano plot displaying logarithm scale of fold-change of percentage ratio of sample from aTB patients over LTBI individuals (left) and patients who completed treatment (right; **C**) for samples after PPD stimulation, **(E)** for samples after ESAT-6/CFP-10 stimulation]. Positive values (logFC>1) show clusters whose proportion is increased in aTB, while negative values (logFC<−1) show clusters whose proportion is decreased in aTB. Significant samples are represented above the threshold (q<0.05). Volcano plots were automatically produced by the OMIQ software. aTB, active TB; LTBI, latent tuberculosis infection; eTrt, aTB patients after anti-TB treatment, UMAP: uniform manifold approximation; FDR: false discovery rate.

Figures 3B,C show the results obtained for samples stimulated with PPD. As it can be seen, the percentage of population of each cluster was compared between the aTB, LTBI and eTrt groups (Figure 3B). No differences were found between the aTB and LTBI groups for any cluster. However, as evidenced by median $\log_2$ fold-changes [$\log_2$FC(aTB/eTrt) > 1 or < −1 when increased or decreased in aTB samples, respectively] and confirmed by FDR analyses ($q < 0.05$), clusters #8, #11, and #13 were significantly increased in aTB patients, whereas cluster #20 was significantly increased in patients who completed treatment (Figure 3C). An additional cluster of CD8$^+$IFN-γ$^+$CD27$^+$ cells (cluster #49) was also identified with a positive association with cured patients ($q = 0.059$). The same analysis was performed for samples stimulated with ESAT-6/CFP-10 antigens, showing that cluster #13 was more prominent in active TB patients than in LTBI individuals (Figures 3D,E). Together, data from multiparametric analyses show a potential role of CD27 and HLA-DR clusters in differentiating aTB patients before and after treatment, and warrant more research using unbiased analyses.

Discussion

Recently, the field of TB diagnosis and management has seen a rise in the development of tools based on the evaluation of the host immune features. In this study, we have analyzed the expression profile of different biomarkers in specific T-cell subsets stimulated with *Mtb* antigens. We have reported modulations on the expression of the four cell markers in *Mtb*-specific CD4$^+$ T-cells, dependent on the presence of clinical disease or infection alone, and that also reflect therapy efficacy. Additionally, we have provided data from unbiased multiparametric analyses showing the presence of several cell clusters with potential to characterize different disease status.

The results of our conventional analyses show the performance of CD27, CD38, HLA-DR and Ki-67 to discriminate active disease from latent infection. Regarding CD27 receptor, our data suggests that its expression on *Mtb*-specific CD4$^+$ T-cells is down-regulated during active disease. These results are in line with most of the published data; in fact, CD27 is, out of the four proteins of our study, the one with more extensive literature, both in mice (Lyadova et al., 2004) and human (Petruccioli et al., 2016; Riou et al., 2017; Acharya et al., 2021; Xu et al., 2021). CD27 is a maturation marker expressed by lymphocytes associated with lack of responsiveness toward different antigens (Schiött et al., 2004), and downregulated in effector differentiated T-cells (Nikitina et al., 2012). Therefore, it can be expected that CD27$^-$ populations are increased in aTB patients. The rationale behind the discriminative power of the other three markers is simple: they are related to the activation and/or enhancement of immune responses, which commonly follow pathogenic infections. Our data gathered on these also confirms what has been published on the topic: CD38 expression on activated CD4$^+$ T-cells was increased in aTB patients after ESAT-6/CFP-10 stimulation (Luo et al., 2021), but HLA-DR$^+$ and Ki-67$^+$ populations showed the most significant association with active disease in all conditions. These findings are consistent with most of the previous research in the field (Adekambi et al., 2015; Silveira-Mattos et al., 2020). AUC values obtained for the discriminating performance of these two proteins, especially Ki-67, greatly surpass those from CD27, indicating that activation markers might have more potential than maturation markers on conventional analyses.

In this paper we also evaluated the ratio of CD27 MFI as an alternative way to measure the expression of the biomarkers. This method, proposed by Portevin et al. (2014), added a technique to discriminate aTB from LTBI similar to measuring CD27$^-$ populations but allowing normalization of results, thus preventing discrepancies raised by positive or negative gating. Here, we show that CD27 MFI quantification mirrors the data obtained by the analysis of percentage of CD27$^-$. This was further supported using Spearman's Correlation test, which shows positive interdependence between both variables. We also performed an analysis on the ΔHLA-DR median fluorescence intensity biomarker following recent work in South Africa (Mpande et al., 2021), and it provided an even additional technique for distinguishing latent from active infection. These findings warrant further studies on this approach, either for validation with the same biomarkers or implementation on other ones.

Another objective of this research was to study the efficacy of the markers in evaluating anti-TB treatment efficacy. The hypothesis followed was that participants with a successful response to treatment developed similar immunophenotypes to individuals without clinical manifestations. Despite the fact that data on treatment monitoring is sparse, some studies have shown that T cell activation markers are reduced after treatment (Vickers et al., 2020), and that the same markers can be used to identify both LTBI and cured individuals (Ahmed et al., 2018) or predict relapse (Goletti et al., 2018). In our study, a small cohort of patients who completed treatment showed a significant decrease on the expression CD38$^+$, and Ki-67$^+$ phenotypes, compared to those at the beginning of treatment. Despite the size difference between the groups, our results agree with what has been published on the matter (Hiza et al., 2022). We did not find statistical significance differences in our mixed model for the HLA-DR and CD27 expression after anti-TB treatment; however, this can be explained by the relatively small sample size of the group of patients who completed therapy. This limitation was also present when analyzing each patient monitored individually. We expect to carry out future studies with the necessary population size to state robust conclusions.

The unbiased, multiparametric analysis provides an additional approach that is in line with literature on the

evaluation of therapy efficacy *via* manually gated analyses. The abundance of clusters expressing CD27 was increased after treatment, as commonly do the $CD27^+$ populations in conventional analysis; and so occurred with HLA-DR^+ clusters and populations in the case of patients with aTB. It should be noted that Ki-67, the most discriminative marker, was not defined in any of our 50 clusters. However, given that most clustering techniques are more accurate when the number of data points is high, it might be possible that the low cell count in $Ki67^+$ populations posed a difficulty in the identification of such subsets. It seems that the multiparametric analyses might open the door for investigating unique combinations of biomarkers, but much further work is required to establish and standardize this technique.

There are limitations in this study that should be addressed. First, the strategy chosen for the definition of *Mtb*-specific cells relies on the measurement of IFN-γ and TNF-α, since we already showed that CD27 profile was similar in populations positive for one or both cytokines (Latorre et al., 2019). However, not all *Mtb*-specific $CD4^+$ T-cells express these cytokines (Morgan et al., 2021). Other approaches for the characterization of this subset (e.g., measurement of other cytokines or multimeric tetramer staining) should be considered. And second, the immune status of each patient depends on multiple parameters, involving not only host and pathogen genetics but also the age of the host (Veneri et al., 2009), the length and type of antibiotic treatment and the recency of infection (Amiano et al., 2020), among others. Therefore, it is necessary to take into account the inherent heterogeneity of the patients when translating potential biomarkers into clinical applications. The use of healthy controls in future work could help establish the baseline expression of these markers and highlight their diagnostic potential. Another issue to address in future studies is the miniaturization of the assay for its implementation as point of care testing. Although flow cytometry studies are generally unwieldy, they can be simplified as evidenced by recent work on HLA-DR-based (Musvosvi et al., 2018) and CD38-based (Hiza et al., 2021) rapid assays. Reducing diagnostic waiting times, test difficulty and costs, among others, is of utmost importance to make the test deployable in areas with high LTBI burden.

In conclusion, our findings on maturation and activation markers CD27, CD38, HLA-DR and Ki-67 on *Mtb*-specific $CD4^+$ T-cells confirm their promising role as potential TB biomarkers for the characterization of LTBI and aTB. Moreover, we provide data showing that after finishing therapy, the immune profile of these markers resembles that of LTBI individuals. It is crucial to evaluate these results in larger cohorts of patients to validate its performance and to study the possibilities of implementation with other clinical signs and microbiology tests. We also show how multiparametric profiling of *Mtb*-specific cell subsets can lead to the discovery of unique cell clusters with different expression across study groups of aTB, LTBI and cured patients. More research on the topic is necessary in order to pinpoint the link between the immune phenotype and the different stages of the disease.

Data availability statement

The raw data supporting the conclusions of this article will be made available by the authors, without undue reservation.

Ethics statement

The studies involving human participants were reviewed and approved by the Hospital Germans Trias i Pujol (reference number PI-19-149). The patients/participants provided their written informed consent to participate in this study.

Author contributions

IL and RV-H designed the study. IL, MF, RV-H, and SD-F designed the experiments. GT, GS, IR, IL, RV-H, and SD-F performed the experiments. AS-M, CP, MG, MJ-F, JS, JA, and ZS contributed with resources. IL, MF, and SD-F analyzed the data. IL and JD supervised the study. SD-F wrote the paper. All authors contributed to the article and approved the submitted version.

Funding

This research was supported by a grant from the Instituto de Salud Carlos III (PI18/00411, PI19/01408 and CP20/00070), integrated in the Plan Nacional de I+D+I and cofunded by the ISCIII Subdirección General de Evaluación and the Fondo Europeo de Desarrollo Regional (FEDER); a grant from the Sociedad Española de Neumología y Cirugía Torácica (project 25/2016; SEPAR; Barcelona, Spain); and from the European Union's Horizon 2020 Research and Innovation Programme under the Marie Skłodowska-Curie grant agreement no. 823854 (INNOVA4TB). JD and IL are researchers from the Miguel Servet programme. AS-M is supported by a Juan Rodés (JR18/00022) postdoctoral fellowship from ISCIII.

Acknowledgments

The authors thank Ester Boixadera and Ana Vázquez from the Servei d'Estadística Aplicada de la UAB for their help through the data analysis process. The authors also thank all the participants of the study and the clinicians and nurses from the Pneumology Department of Hospital Germans Trias i Pujol for their implication especially to Alan Jhunior Solis Solis for his involvement in patient recruitment and classification.

Conflict of interest

The authors declare that the research was conducted in the absence of any commercial or financial relationships that could be construed as a potential conflict of interest.

Publisher's note

Supplementary material

The Supplementary material for this article can be found online at: https://www.frontiersin.org/articles/10.3389/fmicb.2022.885312/full#supplementary-material

SUPPLEMENTARY FIGURE 1
Gating strategy used for $CD4^+$ T-cells cytokine secretion and markers analysis. **(A)** After rough selection of lymphocytes, aggregated cells were taken off by gating on the diagonal that appears with Forward-Scatter (height; FSC-H) vs. Forward-Scatter (area; FSC-A) dot plot. $CD4^+$ T-cells were gated from a parent population of alive $CD3^+$ T-cells. **(B)** *Mtb*-specific population were selected from parent population $CD4^+$ T-cells and gated based on the expression of TNF-α^+ and/or IFN-γ^+, from which CD27/CD38/HLA-DR/Ki67 expression was studied. The panels are representative of populations found without stimulation (left) and after PPD (middle) and ESAT-6/CFP-10 (right) stimulation. (**C**) Panels showing representative examples of cell distribution according to each marker of the study (sample shown is from an LTBI individual after PPD stimulation). The gates were decided according to FMO (Fluorescence Minus One) controls.

SUPPLEMENTARY FIGURE 2
Expression of markers in aTB patients according to the day of treatment within the first month. Correlation between the percentage of $CD27^-$, $CD38^+$, $HLA\text{-}DR^+$ and $Ki\text{-}67^+$ within TNF-α^+ and/or IFN-γ^+ $CD4^+$T-cells and the days after the start of the treatment during the first month in patients from the aTB group.

SUPPLEMENTARY FIGURE 3
BCG vaccination had no effect in the outcome measures of the analysis in PPD-stimulated samples. Percentage of $CD27^-$, $CD38^+$, $HLA\text{-}DR^+$, and $Ki67^+$ within TNF-α^+ and/or IFN-γ^+ $CD4^+$ T-cells after stimulation with PPD. aTB patients (up) and LTBI individuals (down) are separated by their vaccination status of BCG. Differences between conditions were calculated using the Mann–Whitney U test. No indication of p value implies no significance.

SUPPLEMENTARY FIGURE 4
Changes in $CD27^-$, $CD38^+$, $HLA\text{-}DR^+$, and $Ki67^+$ phenotypes of each monitored individual before and after treatment. Percentage of $CD27^-$, $CD38^+$, $HLA\text{-}DR^+$, and $Ki67^+$ within TNF-α^+ and/or IFN-γ^+ $CD4^+$ T-cells after stimulation with ESAT-6/CFP-10 (left) or PPD (right) exclusively for the aTB patients that were monitored before (≤1month) and after (≥6months) anti-TB therapy. Because of exclusion from one of the points from both ends due to analysis restrictions, only patients with both samples positive for the stimulants are shown. Differences between conditions were calculated using the Wilcoxon signed rank paired test. *p<0.05. No indication of p value implies non significance.

SUPPLEMENTARY FIGURE 5
Strong correlation between the percentage of $CD27^-$ in TNF-α^+ and/or IFN-γ^+ $CD4^+$T-cells and the CD27 MFI ratio after ESAT-6/CFP-10 (left) and PPD (right) stimulation. Correlation was calculated using the two-tailed non-parametric Spearman test. *p<0.05, **p<0.01, ****p<0.0001. aTB, active TB; LTBI, latent tuberculosis infection; eTrt, aTB patients after anti-TB treatment.

SUPPLEMENTARY FIGURE 6
ΔHLA-DR MFI of each respective group. ΔHLA-DR median fluorescent intensity (MFI) was calculated as suggested by Mpande et al. The numbers result from subtracting the HLA-DR MFI on IFN-γ+ and/or TNF+ CD3+ cells to the HLA-DR MFI on total CD3+ cells. **(A)** ΔHLA-DR MFI after ESAT-6/CFP10 or **(B)** PPD stimulation in patients with active TB in the beginning and end of treatment as well as LTBI individuals. Data plotted with median and interquartile range. Differences between aTB and LTBI conditions were calculated using the two-tailed Mann–Whitney U-test. Differences between aTB and eTrt groups were calculated using a mixed statistical model controlling repeated measures on logit-transformed data. *p<0.05.

SUPPLEMENTARY FIGURE 7
Area under the receiver operating characteristic curve (AUROC) showing performance of CFP-10/ESAT-6–specific (left) and PPD-specific (right) TNF-α+ and/or IFN-γ+ CD4+ T-cells to discriminate between aTB and LTBI individuals for every marker studied in the paper. Se, sensitivity; Sp, specificity.

References

Acharya, M. P., Pradeep, S. P., Murthy, V. S., Chikkannaiah, P., Kambar, V., Narayanashetty, S., et al. (2021). CD38+CD27-TNF-α+on Mtb-specific CD4+T cells is a robust biomarker for tuberculosis diagnosis. *Clin. Infect. Dis.* 73, 793–801. doi: 10.1093/cid/ciab144

Adekambi, T., Ibegbu, C. C., Cagle, S., Kalokhe, A. S., Wang, Y. F., Hu, Y., et al. (2015). Biomarkers on patient T cells diagnose active tuberculosis and monitor treatment response. *J. Clin. Invest.* 125:3723. doi: 10.1172/JCI77990

Ahmed, M. I. M., Ntinginya, N. E., Kibiki, G., Mtafya, B. A., Semvua, H., Mpagama, S., et al. (2018). Phenotypic changes on *mycobacterium tuberculosis*-specific CD4 T cells as surrogate markers for tuberculosis treatment efficacy. *Front. Immunol.* 9:2247. doi: 10.3389/fimmu.2018.02247

Ahmed, M. I. M., Ziegler, C., Held, K., Dubinski, I., Ley-Zaporozhan, J., Geldmacher, C., et al. (2019). The TAM-TB assay-A promising TB immune-diagnostic test with a potential for treatment monitoring. *Front. Pediatr.* 7, 27. doi: 10.3389/fped.2019.00027

Amiano, N. O., Morelli, M. P., Pellegrini, J. M., Tateosian, N. L., Rolandelli, A., Seery, V., et al. (2020). IFN-γ and IgG responses to *Mycobacterium tuberculosis* latency antigen Rv2626c differentiate remote from recent tuberculosis infection. *Sci. Rep.* 10:7472. doi: 10.1038/s41598-020-64428-z

Andersen, P., Munk, M. E., Pollock, J. M., and Doherty, T. M. (2000). Specific immune-based diagnosis of tuberculosis. *Lancet* 356, 1099–1104. doi: 10.1016/S0140-6736(00)02742-2

Coppola, M., Villar-Hernández, R., van Meijgaarden, K. E., Latorre, I., Muriel Moreno, B., Garcia-Garcia, E., et al. (2020). Cell-mediated immune responses to *in vivo*-expressed and stage-specific *Mycobacterium tuberculosis* antigens in latent and active tuberculosis across different age groups. *Front. Immunol.* 11:103. doi: 10.3389/fimmu.2020.00103

Cossarizza, A., Chang, H. D., Radbruch, A., Acs, A., Adam, D., Adam-Klages, S., et al. (2019). Guidelines for the use of flow cytometry and cell sorting in immunological studies (second edition). *Eur. J. Immunol.* 49, 1457–1973. doi: 10.1002/eji.201970107

Domínguez, J., Ruiz-Manzano, J., De Souza-Galvão, M., Latorre, I., Milà, C., Blanco, S., et al. (2008). Comparison of two commercially available gamma interferon blood tests for immunodiagnosis of tuberculosis. *Clin. Vaccine Immunol.* 15, 168–171. doi: 10.1128/CVI.00364-07

Drain, P. K., Bajema, K. L., Dowdy, D., Dheda, K., Naidoo, K., Schumacher, S. G., et al. (2018). Incipient and subclinical tuberculosis: A clinical review of early stages and progression of infection. *Clin. Microbiol. Rev.* 31, e00021–e000218. doi: 10.1128/CMR.00021-18

Filipe-Santos, O., Bustamante, J., Chapgier, A., Vogt, G., de Beaucoudrey, L., Feinberg, J., et al. (2006). Inborn errors of IL-12/23- and IFN-γ-mediated immunity: molecular, cellular, and clinical features. *Semin. Immunol.* 18, 347–361. doi: 10.1016/j.smim.2006.07.010

Furin, J., Cox, H., and Pai, M. (2019). Tuberculosis. *Lancet* 393, 1642–1656. doi: 10.1016/S0140-6736(19)30308-3

Gallegos, A. M., van Heijst, J. W. J., Samstein, M., Su, X., Pamer, E. G., and Glickman, M. S. (2011). A gamma interferon independent mechanism of CD4 T cell mediated control of *M. tuberculosis* infection in vivo. *PLoS Pathog.* 7:e1002052. doi: 10.1371/journal.ppat.1002052

Global Tuberculosis Report (2021). Geneva: World Health Organization.

Goletti, D., Delogu, G., Matteelli, A., and Migliori, G. B. (2022). The role of IGRA in the diagnosis of tuberculosis infection, differentiating from active tuberculosis, and decision making for initiating treatment or preventive therapy of tuberculosis infection. *Int. J. Infect. Dis.* doi: 10.1016/j.ijid.2022.02.047 [Epub ahead of print].

Goletti, D., Lindestam Arlehamn, C. S., Scriba, T. J., Anthony, R., Cirillo, D. M., Alonzi, T., et al. (2018). Can we predict tuberculosis cure? What tools are available? *Eur. Respir. J.* 52:1801089. doi: 10.1183/13993003.01089-2018

Halliday, A., Whitworth, H., Kottoor, S. H., Niazi, U., Menzies, S., Kunst, H., et al. (2017). Stratification of latent *mycobacterium tuberculosis* infection by cellular immune profiling. *J. Infect. Dis.* 215, 1480–1487. doi: 10.1093/infdis/jix107

Harari, A., Rozot, V., Enders, F. B., Perreau, M., Stalder, J. M., Nicod, L. P., et al. (2011). Dominant TNF-α+ *Mycobacterium tuberculosis*-specific CD4+ T cell responses discriminate between latent infection and active disease. *Nat. Med.* 17, 372–376. doi: 10.1038/nm.2299

Hartman, W. R., Pelleymounter, L. L., Moon, I., Kalari, K., Liu, M., Wu, T.-Y., et al. (2010). CD38 expression, function, and gene resequencing in a human lymphoblastoid cell line-based model system. *Leuk. Lymphoma* 51, 1315–1325. doi: 10.3109/10428194.2010.483299

Hiza, H., Hella, J., Arbués, A., Magani, B., Sasamalo, M., Gagneux, S., et al. (2021). Case–control diagnostic accuracy study of a non-sputum CD38-based TAM-TB test from a single milliliter of blood. *Sci. Rep.* 11, 13190. doi: 10.1038/s41598-021-92596-z

Hiza, H., Hella, J., Arbués, A., Sasamalo, M., Misana, V., Fellay, J., et al. (2022). CD38 expression by antigen-specific CD4 T cells is significantly restored 5 months after treatment initiation independently of sputum bacterial load at the time of tuberculosis diagnosis. *Front. Med.* 9:821776. doi: 10.3389/fmed.2022.821776

Houben, R. M. G. J., and Dodd, P. J. (2016). The global burden of latent tuberculosis infection: A re-estimation using mathematical modelling. *PLoS Med.* 13:e1002152. doi: 10.1371/journal.pmed.1002152

Lalvani, A., and Pareek, M. (2010). A 100 year update on diagnosis of tuberculosis infection. *Br. Med. Bull.* 93, 69–84. doi: 10.1093/bmb/ldp039

Latorre, I., De Souza-Galvão, M., Ruiz-Manzano, J., Lacoma, A., Prat, C., Altet, N., et al. (2010). Evaluating the non-tuberculous mycobacteria effect in the tuberculosis infection diagnosis. *Eur. Respir. J.* 35, 338–342. doi: 10.1183/09031936.00196608

Latorre, I., Fernández-Sanmartín, M. A., Muriel-Moreno, B., Villar-Hernández, R., Vila, S., De Souza-Galvão, M. L., et al. (2019). Study of CD27 and CCR4 markers on specific CD4+ T-cells as immune tools for active and latent tuberculosis management. *Front. Immunol.* 9:3094. doi: 10.3389/fimmu.2018.03094

Luo, Y., Xue, Y., Mao, L., Lin, Q., Tang, G., Song, H., et al. (2021). Activation phenotype of *Mycobacterium tuberculosis*-specific CD4+ T cells promoting the discrimination between active tuberculosis and latent tuberculosis infection. *Front. Immunol.* 12, 721013. doi: 10.3389/fimmu.2021.721013

Lyadova, I. V., Oberdorf, S., Kapina, M. A., Apt, A. S., Swain, S. L., and Sayles, P. C. (2004). CD4 T cells producing IFN-γ in the lungs of mice challenged with mycobacteria express a CD27-negative phenotype. *Clin. Exp. Immunol.* 138, 21–29. doi: 10.1111/j.1365-2249.2004.02573.x

Metcalfe, J. Z., Cattamanchi, A., McCulloch, C. E., Lew, J. D., Ha, N. P., and Graviss, E. A. (2013). Test variability of the QuantiFERON-TB gold in-tube assay in clinical practice. *Am. J. Respir. Crit. Care Med.* 187, 206–211. doi: 10.1164/rccm.201203-0430OC

Morgan, J., Muskat, K., Tippalagama, R., Sette, A., Burel, J., and Lindestam Arlehamn, C. S. (2021). Classical CD4 T cells as the cornerstone of antimycobacterial immunity. *Immunol. Rev.* 301, 10–29. doi: 10.1111/imr.12963

Mpande, C. A. M., Musvosvi, M., Rozot, V., Mosito, B., Reid, T. D., Schreuder, C., et al. (2021). Antigen-specific T-cell activation distinguishes between recent and remote tuberculosis infection. *Am. J. Respir. Crit. Care Med.* 203, 1556–1565. doi: 10.1164/rccm.202007-2686OC

Musvosvi, M., Duffy, D., Filander, E., Africa, H., Mabwe, S., Jaxa, L., et al. (2018). T-cell biomarkers for diagnosis of tuberculosis: candidate evaluation by a simple whole blood assay for clinical translation. *Eur. Respir. J.* 51, 1800153. doi: 10.1183/13993003.00153-2018

Nikitina, I. Y., Kondratuk, N. A., Kosmiadi, G. A., Amansahedov, R. B., Vasilyeva, I. A., Ganusov, V. V., et al. (2012). Mtb-specific CD27 low CD4 t cells as markers of lung tissue destruction during pulmonary tuberculosis in humans. *PLoS One* 7:e43733. doi: 10.1371/journal.pone.0043733

O'Garra, A., Redford, P. S., McNab, F. W., Bloom, C. I., Wilkinson, R. J., and Berry, M. P. R. (2013). The immune response in tuberculosis. *Annu. Rev. Immunol.* 31, 475–527. doi: 10.1146/annurev-immunol-032712-095939

Pai, M., Behr, M. A., Dowdy, D., Dheda, K., Divangahi, M., Boehme, C. C., et al. (2016). Tuberculosis. *Nat. Rev. Dis. Primers.* 2, 16076. doi: 10.1038/nrdp.2016.76

Petruccioli, E., Navarra, A., Petrone, L., Vanini, V., Cuzzi, G., Gualano, G., et al. (2016). Use of several immunological markers to model the probability of active tuberculosis. *Diagn. Microbiol. Infect. Dis.* 86, 169–171. doi: 10.1016/j.diagmicrobio.2016.06.007

Petruccioli, E., Petrone, L., Vanini, V., Cuzzi, G., Navarra, A., Gualano, G., et al. (2015). Assessment of CD27 expression as a tool for active and latent tuberculosis diagnosis. *J. Infect.* 71, 526–533. doi: 10.1016/j.jinf.2015.07.009

Pollock, K. M., Whitworth, H. S., Montamat-Sicotte, D. J., Grass, L., Cooke, G. S., Kapembwa, M. S., et al. (2013). T-cell immunophenotyping distinguishes active from latent tuberculosis. *J Infect Dis* 208, 952–968. doi: 10.1093/infdis/jit265

Portevin, D., Moukambi, F., Clowes, P., Bauer, A., Chachage, M., Ntinginya, N. E., et al. (2014). Assessment of the novel T-cell activation marker-tuberculosis assay for diagnosis of active tuberculosis in children: A prospective proof-of-concept study. *Lancet Infect. Dis.* 14, 931–938. doi: 10.1016/S1473-3099(14)70884-9

Riou, C., Berkowitz, N., Goliath, R., Burgers, W. A., and Wilkinson, R. J. (2017). Analysis of the phenotype of *Mycobacterium tuberculosis*-specific CD+ T cells to discriminate latent from active tuberculosis in HIV-uninfected and HIV-infected individuals. *Front. Immunol.* 8:968. doi: 10.3389/fimmu.2017.00968

Saraiva, D. P., Jacinto, A., Borralho, P., Braga, S., and Cabral, M. G. (2018). HLA-DR in cytotoxic T lymphocytes predicts breast cancer patients' response to neoadjuvant chemotherapy. *Front Immunol.* 9:2605. doi: 10.3389/fimmu.2018.02605

Schiött, Å., Lindstedt, M., Johansson-Lindbom, B., Roggen, E., and Borrebaeck, C. A. K. (2004). CD27- CD4+ memory T cells define a differentiated memory population at both the functional and transcriptional levels. *Immunology* 113, 363–370. doi: 10.1111/j.1365-2567.2004.01974.x

Seddon, J. A., Paton, J., Nademi, Z., Keane, D., Williams, B., Williams, A., et al. (2016). The impact of BCG vaccination on tuberculin skin test responses in children is age dependent: evidence to be considered when screening children for tuberculosis infection. *Thorax* 71, 932–939. doi: 10.1136/thoraxjnl-2015-207687

Silveira-Mattos, P. S., Barreto-Duarte, B., Vasconcelos, B., Fukutani, K. F., Vinhaes, C. L., Oliveira-De-Souza, D., et al. (2020). Differential expression of activation markers by *Mycobacterium tuberculosis*-specific CD4+T cell distinguishes extrapulmonary from pulmonary tuberculosis and latent infection. *Clin. Infect. Dis.* 71, 1905–1911. doi: 10.1093/cid/ciz1070

Soares, A., Govender, L., Hughes, J., Mavakla, W., de Kock, M., Barnard, C., et al. (2010). Novel application of Ki67 to quantify antigen-specific *in vitro* lymphoproliferation. *J. Immunol. Methods* 362, 43–50. doi: 10.1016/j.jim.2010.08.007

Tippalagama, R., Singhania, A., Dubelko, P., Lindestam Arlehamn, C. S., Crinklaw, A., Pomaznoy, M., et al. (2021). HLA-DR marks recently divided antigen-specific effector CD4 T cells in active tuberculosis patients. *J. Immunol.* 207, 523–533. doi: 10.4049/jimmunol.2100011

Veneri, D., Ortolani, R., Franchini, M., Tridente, G., Pizzolo, G., and Vella, A. (2009). Expression of CD27 and CD23 on peripheral blood B lymphocytes in humans of different ages. *Blood Transfus.* 7, 29–34. doi: 10.2450/2008.0007-08

Vickers, M. A., Darboe, F., Muefong, C. N., Mbayo, G., Barry, A., Gindeh, A., et al. (2020). Monitoring anti-tuberculosis treatment response using analysis of whole blood *Mycobacterium tuberculosis* specific T cell activation and functional markers. *Front. Immunol.* 11:572620. doi: 10.3389/fimmu.2020.572620

Walzl, R., McNerney, R., du Plessis, N., Bates, M., McHugh, T. D., Chegou, N. N., et al. (2018). Tuberculosis: advances and challenges in development of new diagnostics and biomarkers. *Lancet Infect. Dis.* 18, e199–e210. doi: 10.1016/S1473-3099(18)30111-7

Xu, F., Zhang, H., Si, X., Chen, J., Chen, Y., Cui, X., et al. (2021). Assessment of CD27 expression on T-cells as a diagnostic and therapeutic tool for patients with smear-negative pulmonary tuberculosis. *BMC Immunol.* 22, 41. doi: 10.1186/s12865-021-00430-y

Advantages of publishing in Frontiers

OPEN ACCESS
Articles are free to read for greatest visibility and readership

FAST PUBLICATION
Around 90 days from submission to decision

HIGH QUALITY PEER-REVIEW
Rigorous, collaborative, and constructive peer-review

TRANSPARENT PEER-REVIEW
Editors and reviewers acknowledged by name on published articles

Frontiers
Avenue du Tribunal-Fédéral 34
1005 Lausanne | Switzerland

Visit us: www.frontiersin.org
Contact us: frontiersin.org/about/contact

REPRODUCIBILITY OF RESEARCH
Support open data and methods to enhance research reproducibility

DIGITAL PUBLISHING
Articles designed for optimal readership across devices

FOLLOW US
@frontiersin

IMPACT METRICS
Advanced article metrics track visibility across digital media

EXTENSIVE PROMOTION
Marketing and promotion of impactful research

LOOP RESEARCH NETWORK
Our network increases your article's readership